

Regulation of Nitrate and Nitrite
Assimilation in *Paracoccus denitrificans* at
the Level of RNA

Benjamin James Pinchbeck

University of East Anglia

September 2016

This thesis is submitted in partial fulfilment of the requirements of the degree of
Doctor of Philosophy at the University of East Anglia

©This copy of the thesis has been supplied on condition that anyone who consults it is understood to recognise that its copyright rests with the author and that use of any information derived there from must be in accordance with current UK Copyright Law. In addition, any quotation or extract must include full attribution.

Statement

The work submitted in this thesis is my own work, except where due reference is made to other authors, and has not been submitted to this or any other University for any degree.

Abstract

Paracoccus denitrificans, a model Alphaproteobacteria soil denitrifier, can grow solely on nitrate or nitrite as inorganic nitrogen sources using a specialised cytoplasmic assimilatory nitrate/nitrite reducing pathway; Nas. This growth capability is phylogenetically represented throughout heterotrophic and autotrophic bacteria, plants and fungi. Whilst this metabolism has been extensively studied in the latter two, the regulatory mechanisms by which organoheterotrophic bacteria govern this nitrate-dependant metabolism are less understood. The work conducted here primarily investigated genetic regulation of Nas expression in *P. denitrificans*.

In Gram-negative bacteria, transcription of proteins required to import and reduce nitrate/nitrite to ammonium, for nitrogen assimilation, are subject to dual control; promotion in the absence of ammonium by the general nitrogen regulatory system, NtrBC, and nitrate-induced transcriptional anti-termination by the two-component, NasT-NasS complex. Here, a hypothetical gene, *nifR3*, conserved with the *ntr* cluster throughout Alphaproteobacteria, was shown to regulate Nas biosynthesis.

We report *nifR3* encodes a nitrogen-responsive, tRNA-dihydrouridine synthase required for *nasABGHC* translation. Genomic deletion of *nifR3* from *P. denitrificans* resulted in the lethal loss of nitrate assimilation and severe deficiency of dihydrouridine in tRNA, restored by genetic complementation of *nifR3* in trans. Pure NifR3 harboured an FMN cofactor and reversibly catalysed NADH-dependant reduction of uridine, a physiological important post-transcriptional modification. Native band-shift assays using an isolated tRNA fraction of *P. denitrificans* identified specific targets of NifR3: mature tRNA transcripts encoding Phe_{GAA}, Lys_{UUU} and Trp_{CCA}. This novel regulatory role of bacterial NifR3 and tRNA-dihydrouridine formation concerning post-transcriptional fine-tuning of protein expression will be discussed throughout this thesis, in addition to the function of several other nitrogen-responsive proteins explored here.

Separately, we demonstrated that NarJ, the molybdenum-chaperone for biogenesis of respiratory nitrate reductase, NarG, performs an unprecedented wide-spread maturation role of non-Nar nitrate reductases. Here, we found NarJ is solely responsible for fully assembling the functional assimilatory nitrate reductase, NasC, complete with cofactors, even under aerobic conditions.

Acknowledgements

Firstly, I would like to thank my supervisors, David Richardson and Andrew Gates, for the guidance you both have given me over the last four years. Your patience and support has been key in my development throughout my PhD and your advice on all aspects of my project, from experimental work to the writing of this thesis, was invaluable and gratefully received.

Further thanks to everyone in BIO who taught me how to use various pieces of equipment and provided advice on methodologies. A special mention goes to Zoë Waller (CAP, UEA) and Elise Wright for looking after me when I had to briefly work in the scary Chemistry department. Additionally, thank you to Matthew Sullivan and Marcus Edwards, two outstanding Postdoctoral researchers, for putting up and dealing with my everyday basic questions. Thanks in advance to Tom Clarke and David Kelly, my *viva voce* examiners, for taking the time to read through and discuss my thesis with me.

To all members of Lab 2.30, past and present, and all other friends within UEA, thank you for keeping me sane and giving plenty of stress relief with many nights out and coffee time with all the home made cakes! I could not have asked for a better group of colleagues to enjoy 4 years of work with, I wish you all the luck in the world with your futures and I hope our paths cross again soon.

I would also like to thank my friends outside of science, both back in Sleaford and in Norwich, for providing much needed breaks during the weekends or when I have gone home for the holidays. A special shout out goes to Alistair Walsham for all the countless hours spent on Fifa, eating flapjack and drinking milkshakes, to forget about our problems. These times, and the weekly Sunday roasts you cooked for me are majorly appreciated and helped keep me going!!

To my sister and brother, Laura and Thomas, thank you for being there when I grew up and for still being around when I need nowadays, you are pretty awesome siblings! Finally, to my parents, Alan and Beverly, you have always been my role models and there are no better mums or dads, even when you try to palm off your unwanted items on me! Thank you for always believing in me and being there when I needed throughout my life, and thus, this thesis is dedicated to you.

Table of Contents

Statement	II
Abstract	III
Acknowledgements	IV
Table of Contents	V
Chapter 1: General Introduction	1
1.1 The Global Biogeochemical Nitrogen Cycle	1
1.1.1 The nitrogen cycle overview	1
1.1.2 Denitrification/respiratory nitrate reduction	4
1.1.3 Periplasmic nitrate reduction	6
1.1.4 Assimilatory nitrate reduction	7
1.2 Genetic Regulation of Nitrogen Response Proteins in Heterotrophic	
Bacteria	9
1.2.1 Nitrogen stress-response sigma factor: Sigma 54	10
1.2.2 General nitrogen regulators: Ntr system and P _{II} proteins	10
1.3 <i>Paracoccus denitrificans</i>	11
1.3.1 Biochemical and physiological characteristics	11
1.3.2 <i>P. denitrificans</i> encodes three independent nitrate reductases	13
1.4 The <i>nas</i> Gene Cluster for Microbial Nitrate Assimilation	16
1.4.1 Phylogenetic distribution of <i>nas</i> in bacterial species	16
1.4.2 Uptake and reduction of nitrate and nitrite by structural NasABGHC	16
1.4.3 Transcriptional activation of <i>nasABGHC</i> during ammonium starvation	20
1.4.4 Complete synthesis of <i>nas</i> mRNA requires NasTS	20
1.5 Carbon/Nitrogen Interface for Assimilating Inorganic Nitrogen	23
1.5.1 The GS/GOGAT cycle	25
1.5.2 The microbial GDH pathway	27
1.6 Global Transcriptomic Analysis of Nitrate Assimilation in <i>Paracoccus</i>	
<i>Denitrificans</i>	27
1.7 The Impact of Carbon Towards Growth During the Assimilation of Nitrate	29
1.8 Chaperones Responsible for Maturation of Nitrate Reductases	29
1.8.1 NarJ as the respiratory nitrate reductase chaperone	31
1.8.2 NarJ as the candidate for maturation of the assimilatory nitrate reductase	32

1.9 NifR3 - a Putative, Nitrogen-Responsive, tRNA Dihydrouridine Synthase ...	34
1.9.1 The tRNA dihydrouridine synthase protein superfamily	36
1.9.1.1 Phylogenetic conservation of dihydrouridine synthases	36
1.9.1.2 Protein structure and catalytic mechanism	39
1.9.1.3 Physiological function of tRNA-dihydrouridine synthases	41
1.9.2 Phylogenetic distribution and conservation of bacterial <i>nifR3</i>	43
1.9.3 NifR3 as a potential regulator of the bacterial nitrogen-response	46
1.10 Aims and Objectives	46
Chapter 2: Materials and Methods	47
2.1 Media and Growth Conditions	47
2.1.1 Luria-Bertani (LB) medium	47
2.1.2 Minimal salt medium	47
2.2 Bacterial Strains and Plasmids	49
2.3 Oligonucleotide Design and Primers Used	53
2.4 Preparation of Nucleic acid	59
2.4.1 Mini-preparation of plasmid DNA using QIAGEN spin columns	59
2.4.2 Midi-preparation of plasmid DNA using QIAGEN Midi kit	59
2.4.3 Phenol-chloroform extraction of plasmid DNA	59
2.4.4 Preparation of Genomic DNA using Promega spin columns	60
2.4.5 Quantifying DNA/RNA concentrations	60
2.5 Polymerase Chain Reaction (PCR) Amplification of DNA	60
2.5.1 PCR of DNA using Hi-Fidelity Phusion Enzyme	60
2.5.2 PCR of DNA using MyTaq master-mix	61
2.5.3 Colony PCR using MyTaq master-mix	62
2.5.4 Purification of PCR amplified DNA	62
2.6 Agarose Gel Electrophoresis of DNA	62
2.6.1 Visualisation of DNA using Ethidium Bromide	62
2.6.2 Recovery of DNA from agarose gels via QIAGEN gel extraction kit	62
2.7 Restriction Enzyme Digestion of Plasmid DNA	62
2.8 Dephosphorylation of Digested Plasmid DNA	63
2.9 Ligation of DNA Fragments	63
2.10 Transformation of Plasmid DNA into <i>Escherichia coli</i>	63
2.10.1 Preparation of Competent Cells	63

2.10.2 Transformation of Competent Cells	64
2.11 Sequencing DNA	64
2.12 Colony Forming Units (CFU) Cell Culture Count	64
2.13 <i>in vivo</i> Plasmid Conjugations	65
2.13.1 Conjugation via patch crosses	65
2.13.2 Conjugation via filter crosses	65
2.14 High Pressure Liquid Chromatography Quantification of Nitrate and Nitrite	65
2.15 Determination of Ammonium Concentrations	66
2.16 Construction of <i>Paracoccus denitrificans</i> Gene Deleted Mutant Strains ...	66
2.17 β-Galactosidase Gene-Reporter Fusion Assay	68
2.18 RNA Extraction from <i>Paracoccus denitrificans</i>	72
2.18.1 Harvesting cells for RNA extraction	72
2.18.2 Extracting whole cell RNA	72
2.18.3 Experion analysis of RNA integrity	72
2.19 Synthesis of cDNA by Reverse Transcription	73
2.20 Quantitative real-time Reverse Transcriptase PCR (qRT-PCR)	73
2.21 Type II Microarray Analysis	74
2.21.1 Direct Labelling of RNA	74
2.21.2 Direct labelling of DNA	75
2.21.3 Hybridisation to microarray slides	76
2.22 Overexpression and Purification of Proteins	75
2.22.1 6His_NifR3	76
2.22.2 NarJ_6His	76
2.22.3 Concentration of proteins	77
2.23 Bovine Serum Albumin (BSA) Bradford Assay	77
2.24 Poly-Acrylamide Gel Electrophoresis (PAGE)	78
2.24.1 SDS-PAGE separation of proteins	78
2.24.2 Urea-PAGE separation of RNA	78
2.24.3 Native-PAGE separation of RNA	79
2.25 Western-Blot Identification of 6His-tagged Proteins	79
2.26 Mass Spectrometry of Proteins	80
2.27 Spectrophotometry	81

2.27.1 UV-Visible Spectrophotometry	81
2.27.2 Fluorescence Spectrophotometry	81
2.28 Quantification of FMN in Protein Samples	81
2.29 Chemical Synthesis of Dihydrouridine	81
2.29.1 Synthesis of dihydrouridine via hydrogenation of uridine	82
2.29.2 Analysing reaction mixture with thin-layer chromatography (TLC)	82
2.30 Dihydrouridine Quantification Assay	82
2.31 Preparation of <i>Paracoccus denitrificans</i> Cell lysate for Assays	84
2.32 Catalytic Colourimetric Assays	84
2.32.1 NADH Assay	84
2.32.2 Methyl-Viologen Assay	84
2.33 tRNA Extraction from <i>Paracoccus denitrificans</i>	85
2.34 Northern-Blot Identification of RNA	86
2.35 Band Shift Assay for Protein:RNA Interactions	86
2.36 Protein Pull Down Assay to Isolate Binding Partners	87
2.37 Protein X-Ray Crystallography	88
Chapter 3: The Impact of Carbon and Cellular Redox Status on Assimilation of Inorganic Nitrogen Compounds	89
3.1 Introduction	89
3.2 Growth of <i>Paracoccus denitrificans</i> on Different Inorganic Nitrogen Sources	94
3.3 Dependence of <i>Paracoccus denitrificans</i> on Supplemented Carbon During Nitrate Assimilation	100
3.3.1 Succinate	100
3.3.2 Malate	103
3.3.3 Pyruvate	105
3.3.4 Butyrate	105
3.3.5 The Oxidation State of the Carbon Source Influences the Ability of <i>P.</i> <i>denitrificans</i> to Assimilate Nitrate	109
3.4 β-Galactosidase Assays highlights the Regulation of the Carbon:Nitrogen Interface by Ntr Proteins	112
3.5 Investigating Sigma 54 as a Regulator of the Nitrogen Status in <i>Paracoccus</i> <i>Denitrificans</i>	116
3.6 Exploring the Regulatory Role of NtrBC in Nitrogen-Metabolism	120

3.7 Growth of ΔntrBC on Various Carbon Substrates Exhibits an Altered Dependence	128
3.8 Discussion	134
3.8.1 The influence of external carbon compounds upon microbial growth	134
3.8.2 Regulating transcriptional activation of nitrogen-responsive genes	136
3.8.2.1 The nitrogen-responsive sigma 54 factor	136
3.8.2.2 General nitrogen regulatory complex – NtrBC	137
Chapter 4: Establishing the Role of <i>dusN</i> for Nitrogen Assimilation in <i>Paracoccus denitrificans</i>	140
4.1 Introduction	140
4.2 Construction and Phenotypic Characterisation of a <i>P. denitrificans</i> mutant deficient in <i>dusN</i>	142
4.2.1 Constructing a suicide vector for genomic deletion of <i>dusN</i>	142
4.2.2 Phenotypic characterisation of a Δ <i>dusN</i> strain	142
4.3 Genetic Restoration of Wild-Type Phenotype in Δ<i>dusN</i>	150
4.4 Global Transcriptomic Analysis of WT vs Δ<i>dusN</i> during Nitrate-Induced Growth	153
4.5 Deciphering the Physiological Function of DusN using qRT-PCR and Gene-Reporter Fusion Assays	159
4.5.1 qRT-PCR analysis of the <i>nas</i> gene cluster	159
4.5.2 Transcriptional and translation β -galactosidase gene reporter fusion assays	159
4.6 Multiple Nitrogen-Responsive Regulators are Required for Complete <i>nasABGHC</i> Expression	163
4.7 Discussion	166
4.7.1 DusN is involved in regulating a multitude of nitrogen-responsive genes	166
4.7.2 Nas expression requires the effort of multiple regulatory proteins	168
Chapter 5: Characterisation of DusN as a Nitrogen-Responsive tRNA-Dihydrouridine Synthase	171
5.1 Introduction	171
5.2 Construction of an Overexpression and Purification System for DusN	171
5.2.1 Overexpression trials for various tagged forms of recombinant DusN	172
5.2.2 Purification of 6His_DusN for downstream analysis	179
5.3 Identification and Quantification of FMN as a Cofactor of DusN	181
5.3.1 Fluorescence spectroscopy identification of FMN	181

5.3.2 Quantification of FMN:DusN stoichiometry	183
5.4 Chemical Synthesis of Dihydrouridine for DUS-based Experiments	185
5.5 Probing the Catalytic Properties of DusN	185
5.6 Site-Directed Mutagenesis Identified Key Catalytic Residues	192
5.7 Purifying tRNA from <i>Paracoccus denitrificans</i> for Interaction Studies	194
5.7.1 Monitoring purity and integrity using an Experion bioanalyser	194
5.7.2 Identification of tRNA via Northern-blot analysis	196
5.8 Contribution of tRNA-Dihydrouridine Modification by DusN	196
5.8.1 Designing an assay to specifically calculate dihydrouridine concentrations .	196
5.8.2 Quantifying the dihydrouridine content of <i>P. denitrificans</i> RNA	197
5.8.3 Activity of DusA, a housekeeping dihydrouridine synthase	202
5.9 Isolation of Physiological tRNA Targets of DusN	207
5.9.1 <i>In vitro</i> catalytic DusN activity with pure tRNA substrate	207
5.9.2 Band shift assays to visualise DusN:tRNA interactions	209
5.9.3 Kinetic parameters of DusN with its target consensus RNA sequence	211
5.10 Discussion	214
5.10.1 Exploring the dihydrouridine synthases of <i>P. denitrificans</i>	214
5.10.1.1 Purification and biochemical analysis of DusN catalysis	214
5.10.1.2 Cellular function of a housekeeping DusA protein	216
5.10.2 DusN binds specific tRNA transcripts to catalyse dihydrouridine formation	217
Chapter 6: Investigating NarJ as a Chaperone for Nitrate Reductases ...	222
6.1 Introduction	222
6.2 Nitrate and Nitrite Reduction Capacity of <i>Paracoccus denitrificans</i> in Molybdenum-deplete Media	224
6.3 Expression of the <i>nar</i> Gene Cluster during Nitrate-Dependent Growth	225
6.4 Construction of a <i>Paracoccus denitrificans</i> strain deficient in <i>narJ</i>	228
6.4.1 Assembling a suicide vector for gene deletion	228
6.4.2 Nitrate- and nitrite-dependent respiratory growth of $\Delta narJ$	228
6.4.3 Phenotyping $\Delta narJ$ growth during aerobic nitrate assimilation	233
6.5 Genetic Restoration of the $\Delta narJ$ Mutant Strain	235
6.5.1 Constructing a NarJ expression system for $\Delta narJ$ complementation	235
6.5.2 Restoration of nitrate-dependent growth in $\Delta narJ$	235
6.6 Catalytic <i>in vitro</i> Nitrate and Nitrite Reductase Assays	238
6.6.1 Methyl-Viologen enzyme assays to measure NarG catalysis	238
6.6.2 NADH catalytic assays for monitoring NasC activity	239

6.7 Overexpression and Purification of Recombinant NarJ	242
6.8 NarJ Pull-Down Assays to Isolate and Identify Binding Partners	243
6.9 Discussion	248
Chapter 7: General Discussion	250
7.1 Nitrate Assimilation Provides a Biomass-Linked Reductant Vent during Carbon Rich Conditions	250
7.2 Exploring Regulators Required for Expression of Nitrogen-Responsive Genes	252
7.3 Bacterial DusN is a Post-Transcriptional Regulator of Protein Biosynthesis	253
7.3.1 DusN controls expression of a multitude of nitrogen-responsive proteins ...	253
7.3.2 Characterising DusN as a tRNA-dihydrouridine synthase	255
7.3.3 Hypothetical models for DusN regulation over Nas translation	258
7.4 NarJ is the Chaperone Responsible for Maturation of Respiratory and Assimilatory Nitrate Reductases	261
7.5 Concluding Remarks	263
References	265

Chapter 1: General Introduction

1.1 The Global Biogeochemical Nitrogen Cycle

1.1.1 *The nitrogen cycle overview*

Molecular dinitrogen, N_2 , is the most abundant gaseous constituent of Earth's atmosphere, comprising ~78 % (Francis et al. 2007). Nitrogen is a fundamental building block for a vast scope of key biochemical structures, such as nucleotides and proteins. Nitrogen exists in the global biosphere in a range of oxidation states, +V to -III (Castillo, 1999), the biochemical interconversion of which are catalysed by a diverse array of metalloenzymes found in both marine and terrestrial microorganisms (Ferguson 1998; Richardson & Watmough 1999). The various independent redox reactions of these inorganic nitrogenous compounds, both by geological and microbial processes, constitutes a global biogeochemical nitrogen cycle (Figure 1.1). Natural ecosystems contain an assortment of microorganisms capable of catalysing various processes within the nitrogen cycle, utilising each other's nitrogen subproducts for their own metabolism. This can lead to small-scale local nitrogen cycling which allows their syntrophic co-existence within a local community (Handley et al. 2013).

Though dinitrogen is atmospherically abundant, it is a relatively inert gas due to its highly stable triple bond (Postgate 2012), meaning the bioavailability of an otherwise abundant nitrogen source is often limiting for microbial populations (Canfield et al. 2010). To make inorganic nitrogen available for integration with organic compounds, it must exist in the form of ammonia (NH_3), found as the ammonium cation at pH 7 (NH_4^+), $pK_a = 9.4$. This does not pose a problem for organisms which obtain organic nitrogen compounds using uptake transporters or through their diet. However, it creates a significant metabolic obstacle for prokaryotic bacteria and archaea reliant upon their ability to produce ammonium during nitrogen limitation. Assimilation, discussed later, is one way to accomplish this using nitrate. A second method is performed by soil-dwelling diazotrophic organisms; bacteria capable of biological dinitrogen fixation to ammonium (Burns & Hardy 1975). These microbes can form symbiotic relationships with crop legumes, residing in plant nodules to supply ammonium for the plant, in return gaining shelter from the harsh environmental stresses (Postgate 1998). Diazotrophs harbour a copy of genes necessary to fully synthesise the cytoplasmic nitrogenase metalloprotein complex which reduces dinitrogen to two ammonium molecules via a vast input of energy, creating a useable nitrogen source for biomass production (Seefeldt et al. 2009).

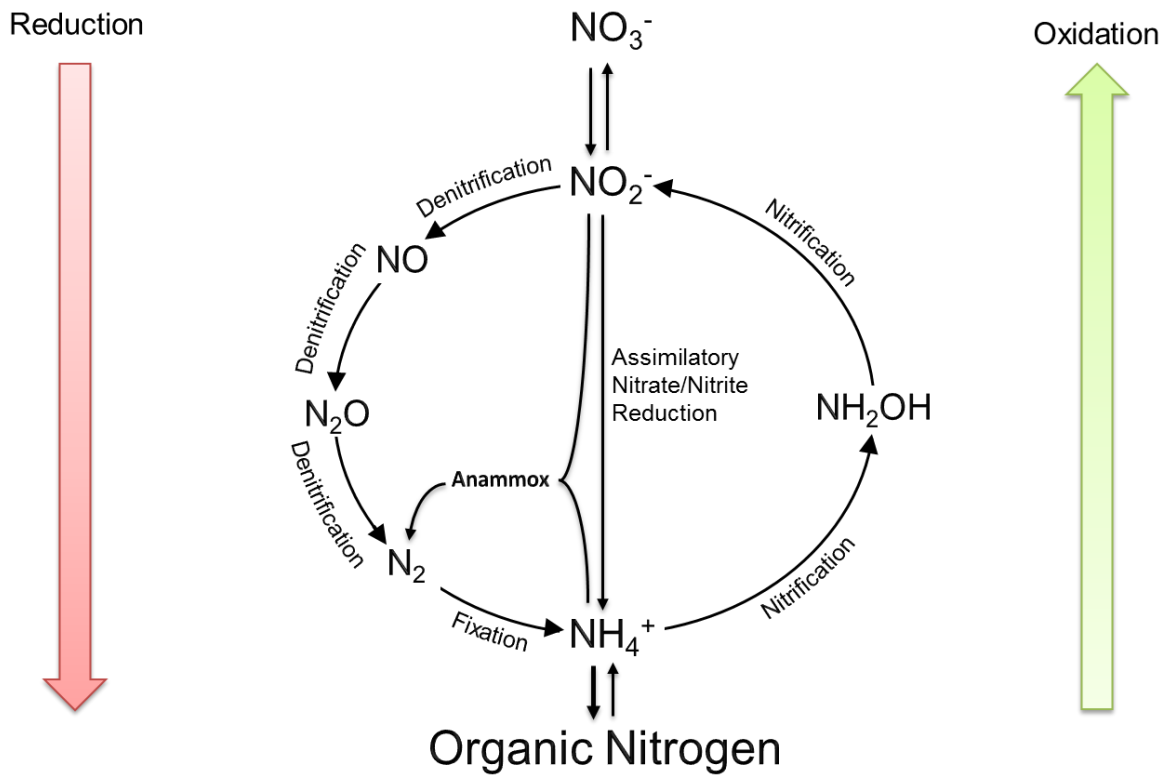


Figure 1.1. The global biogeochemical nitrogen cycle. An overview encompassing the range of redox reactions which comprise the microbial nitrogen cycle. The left side shows the reductive processes: denitrification, assimilation and dissimilation, all stemming from nitrate (NO_3^-), in addition to dinitrogen (N_2) fixation to ammonium (NH_4^+). Oxidative nitrification recycles ammonium to nitrite (NO_2^-) via hydroxylamine (NH_2OH). Ammonium is the bioavailable inorganic nitrogen source for microbes, integrating into organic nitrogen-containing structures to produce biomass.

Fixation and assimilation represent major entry points of nitrogen into the food chain and are key non-respiratory pathways within the nitrogen cycle (Oron 2001). Alternatively, the denitrification, dissimilation, anammox, and nitrification pathways are involved with respiration. This structural arrangement enables microbes to exploit inorganic nitrogen to fuel metabolism and regulate the cellular redox status for appropriate growth (Ferguson 1998; Cabello et al. 2004).

Nitrate reductases belong to the dimethyl sulfoxide (DMSO) reductase family of complex molybdoenzymes and are segregated into three structurally distinct systems to reduce soluble, anionic nitrate (NO_3^-): respiration; NAR, dissimilation; NAP and assimilation; NAS. The denitrification and dissimilation pathways (Figure 1.1) couple nitrate reduction with quinone-linked respiration whereas assimilation produces a useable ammonium source for biomass production during nitrogen limitation. These pathways are all present within the organism used in this study, *Paracoccus denitrificans*, and will be discussed later in greater detail (Richardson 2008; Lin & Stewart 1998).

Denitrification is the major biological pathway through which nitrogen is returned from the soil to the atmosphere. Another microbial driver accountable for large levels of environmental dinitrogen is anaerobic ammonium oxidation (anammox), performed by aquatic planctomycetes (Hu et al. 2011). Here, nitrite acts as an electron donor for ammonium oxidation which produces dinitrogen gas in an energy yielding reaction coupled simultaneously with fixation of carbon dioxide to reduced sugars during autotrophic growth (Kuenen 2008; Fuerst & Sagulenko 2011).

Lastly, the two-step aerobic nitrification of ammonium to nitrite via a hydroxylamine (NH_2OH) intermediate completes the nitrogen cycle and is present throughout various archaea and bacteria such as the *Nitrosomonas* genus (Di et al. 2009). Cytoplasmic oxidation of inorganic ammonium cations liberates energy which these chemolithotrophic organisms harness for growth by coupling with carbon dioxide fixation, rather than solar energy via photosynthesis, to produce organic structures (De Boer & Kowalchuk 2001).

Global microbial cycling of inorganic nitrogen compounds leads to the formation of a range of chemicals, where several have dire environmental consequences when released to the biosphere (US EPA 2011). Nitrous oxide, a by-product of truncated denitrification, is a potent greenhouse gas with global warming potential, molecule for molecule, almost 300 times greater than carbon dioxide (Crutzen et al. 2008; Ravishankara et al. 2009). A major driver for production and emission of anthropogenic nitrous oxide is bacterial denitrification resulting from excess nitrogenous agricultural fertiliser (Bremner & Blackmer 1978; Richardson et al. 2009). Furthermore, if not taken

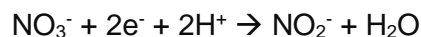
up by organisms, nitrate and nitrite leach through soil until they arrive at an underground water supply, imposing a vast problem due to human toxicity (Addiscott & Benjamin 2006).

The use of inorganic nitrogen fertilisers has risen ~800 % within the last five decades due to the necessity for increased crop yields to sustain an expanding human population, causing drastic exacerbation of both nitrate leaching and nitrous oxide emissions (Canfield et al. 2010). In conjunction with this, a rapidly increasing population is placing greater pressure upon biotechnological industries to instigate superior methods of purifying reliable water sources (Cabello et al. 2004). The microbial denitrification and anammox pathways have potential with aiding the removal nitrate, nitrite and ammonium from water sources. Hence, the nitrogen cycle has received a great deal of interest due to the prospective beneficial effects in bioremediation (Richardson & Watmough 1999; Moreno-Vivián et al. 1999).

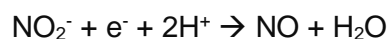
1.1.2 Denitrification/respiratory nitrate reduction

Denitrification is the respiratory reduction of nitrate to dinitrogen via a series of gaseous intermediates used as end terminal electron acceptors during anaerobic respiration (Kuenen & Robertson 1994). Denitrification is characteristically a heterotrophic, bacterial growth-linked process which couples to proton translocation. This generates the proton motive force through the sequential reduction of nitrate, nitrite (NO_2^-), nitric oxide (NO) and nitrous oxide (N_2O) to dinitrogen to enable anaerobic respiration (Hochstein & Tomlinson 1988). Complete denitrification requires four respiratory, membrane-associated metallo-enzymes; Nar, Nir, Nor and Nos (Firestone 1982). Electrons generated via oxidation of carbon compounds are alleviated from the UQH_2 pool to the subsequent nitrogen oxyanions to power ATP production (Betlach 1982). The denitrification apparatus of *P. denitrificans* is outlined below:

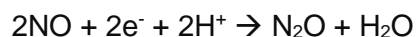
NarG; Respiratory nitrate reductase molybdoenzyme



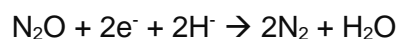
NirS; Cytochrome *cd1* nitrite reductase



NorB; Heme-containing nitric oxide reductase



NosZ; Copper-dependant nitrous oxide reductase



Denitrification initiates at the respiratory nitrate reductase complex, NarGHI, with quinol oxidation at the first heme group of the biheme cytochrome *b* NarI (ubiquinol dehydrogenase), embedded in the inner-membrane. Liberated electrons flow via the second heme *b*, through the four [Fe-S] clusters of NarH and an [Fe-S] cluster of NarG, terminating at the cytoplasmic molybdenum-containing molybdopterin guanine-dinucleotide (Mo[MGD]₂) cofactor of NarG for nitrate reduction (Bertero et al. 2003).

Nitrate generated by NarGHI in the cytoplasm is translocated into the periplasm by the NarK antiporter, where homodimeric NirS, the multiheme cytochrome *cd1* nitrite reductase, is localised. External electrons are donated to the heme *c* structure and pass across the subunit interface to the cytochrome *d1* active site for the one electron reduction yielding nitric oxide (Li et al. 2013).

Membrane anchored nitric oxide reductase, NorBC, reduces two molecules of nitric oxide to nitrous oxide at its periplasmic-facing active site. Electrons are received by cytochrome *c* of NorC and pass via a cytochrome *b* of NorB to the binuclear active center comprising a second cytochrome *b* and non-heme iron (Shiro 2012).

Finally, nitrous oxide is reduced to dinitrogen by the periplasmic, homodimeric NosZ; a copper-dependant nitrous oxide reductase comprising two multi-copper centres (Pomowski et al. 2011). External electrons are donated to a bicopper Cu_A site before transferring across the subunit interface to the tetranuclear copper-sulphide cluster, Cu_Z, the active site of reduction, comprising four copper atoms (Zumft & Kroneck 2007). Environmental copper depletion has been linked to an increase of microbial nitrous oxide emissions by stalling at NosZ catalysis (Sullivan et al. 2013). Gaseous dinitrogen is liberated to the biosphere through the outer-membrane.

Whilst Nar contains an intrinsic ubiquinol oxidising site, the downstream enzymes acquire electrons from external physiological protein donors such as periplasmic pseudoazurin and membrane bound cytochrome *c*-550 (Tolman 2010), which receive their electrons from the cytochrome *bc1* complex.

Most organisms containing a NarG are facultative anaerobes, such as *P. denitrificans* and enteric *Escherichia coli*, located in the soil and mammalian-hosts, respectively, where oxygen levels are limiting (Carlson & Ingraham 1983; Takaya et al. 2003). The capacity for denitrification is represented across many bacterial phylogenetic groups, found in a diverse array of both terrestrial and aquatic ecosystems (Zumft 1997; Seitzinger et al. 2006). Denitrification is well studied and reviewed due to its

environmental implications and bioremediation role (Richardson 2008; Uden & Bongaerts 1997).

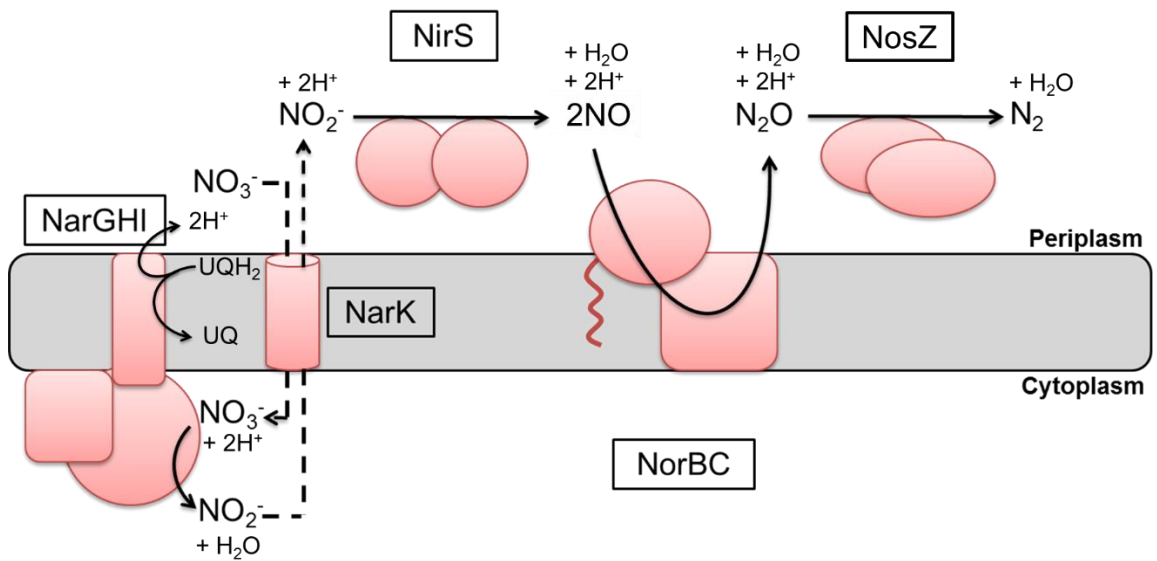
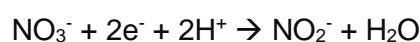


Figure 1.2. The membrane-associated metabolic pathway required for complete bacterial denitrification. A simplified topological perspective outlining the four catalytic steps comprising anaerobic nitrate-respiration. Cytoplasmic nitrate is reduced by the heterotrimeric NarGHI complex with liberated nitrite anions transported into the periplasm via NarK. Cytochrome *cd1* nitrite reductase, NirS, produces nitric oxide which is further reduced to nitrous oxide by the multiheme NorBC complex. Lastly, nitrous oxide is reduced to gaseous dinitrogen by the copper-dependant periplasmic NosZ.

1.1.3 Periplasmic nitrate reduction

The second membrane-associated nitrate reductase is the periplasmic nitrate reductase Nap, which, like Nar, couples nitrate reduction with quinol oxidation, but is not a site for proton translocation (Richardson 2000). This system is non-electrogenic and dissipates excess energy during accumulation of surplus reducing equivalents to balance the cellular redox status (Moreno-Vivián & Ferguson 1998; Berks, Page, et al. 1995). Nap is typically, but not exclusively, synthesised during energy-rich aerobic growth to allow oxidation of excess reducing equivalents to turnover respiration. This effect is enhanced when grown with a highly reduced carbon source, such as butyrate, during chemoheterotrophic conditions (Stewart et al. 2002; Sears et al. 2000). The dissimilatory nitrate reduction catalysed by *P. denitrificans* is outlined below:

NapA; Molybdopterin-dependant nitrate reductase



Dissimilation of nitrate requires the periplasmic associated ubiquinol/nitrate oxidoreductase complex, NapABC, comprising a similar biochemical arrangement as NarGHI. The membrane-anchored, quinol dehydrogenase, tetraheme cytochrome *c* NapC mediates electron transfer between UQH₂ and periplasmic NapAB (Roldan et al. 1998). NapC oxidises UQH₂ and electrons are passed through the two *c*-type hemes of periplasmic NapB and an [Fe-S] cluster of NapA to reach the Mo[MGD]₂ catalytic cofactor of NapA for nitrate reduction. (Wang & Gunsalus 2000; Li et al. 2012).

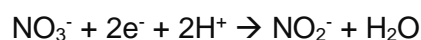
The capacity for nitrate dissimilation is wide-spread across Gram-negative bacteria, offering maintenance of an appropriate redox status to sustain optimal microbial growth under many physiological conditions (Bedzyk et al. 1999; Berks et al. 1994).

1.1.4 Assimilatory nitrate reduction

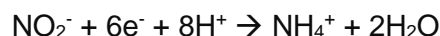
Assimilatory nitrate reduction forms the focus of this research and will be discussed later in greater detail for *P. denitrificans*. Whilst the respiratory-linked processes discussed above employ UQH₂-loops coupling energetic metabolism with nitrate reduction, cytoplasmic assimilation produces a bioavailable inorganic nitrogen source for cell growth during nitrogen-limitation (Pino et al. 2006; Ramos et al. 1993). Nitrate assimilation uses cytoplasmic NAD(P)H (nicotinamide adenine dinucleotide phosphate) (heterotrophic bacteria) or photosynthetically reduced ferredoxin (plants and cyanobacteria) to fully reduce nitrate and nitrite to bioavailable ammonium for incorporation into key organic compounds (Cali et al. 1989; Galloway 2003; Rodríguez et al. 1998).

Reduction of nitrate to ammonium proceeds in two steps and requires the cytoplasmic metalloenzymes; molybdenum-dependant nitrate reductase and the cytochrome nitrite reductase.

Molybdopterin-dependent nitrate reductase



Siroheme-containing nitrite reductase



This 2 and 6 electron sequential catalysis forms the assimilatory pathway at conserved molybdopterin and siroheme active sites. However, biochemical flexibility of the structural proteins involved in nitrate assimilation exists between heterotrophic and photosynthetic bacteria, demonstrated below (Figure 1.3).

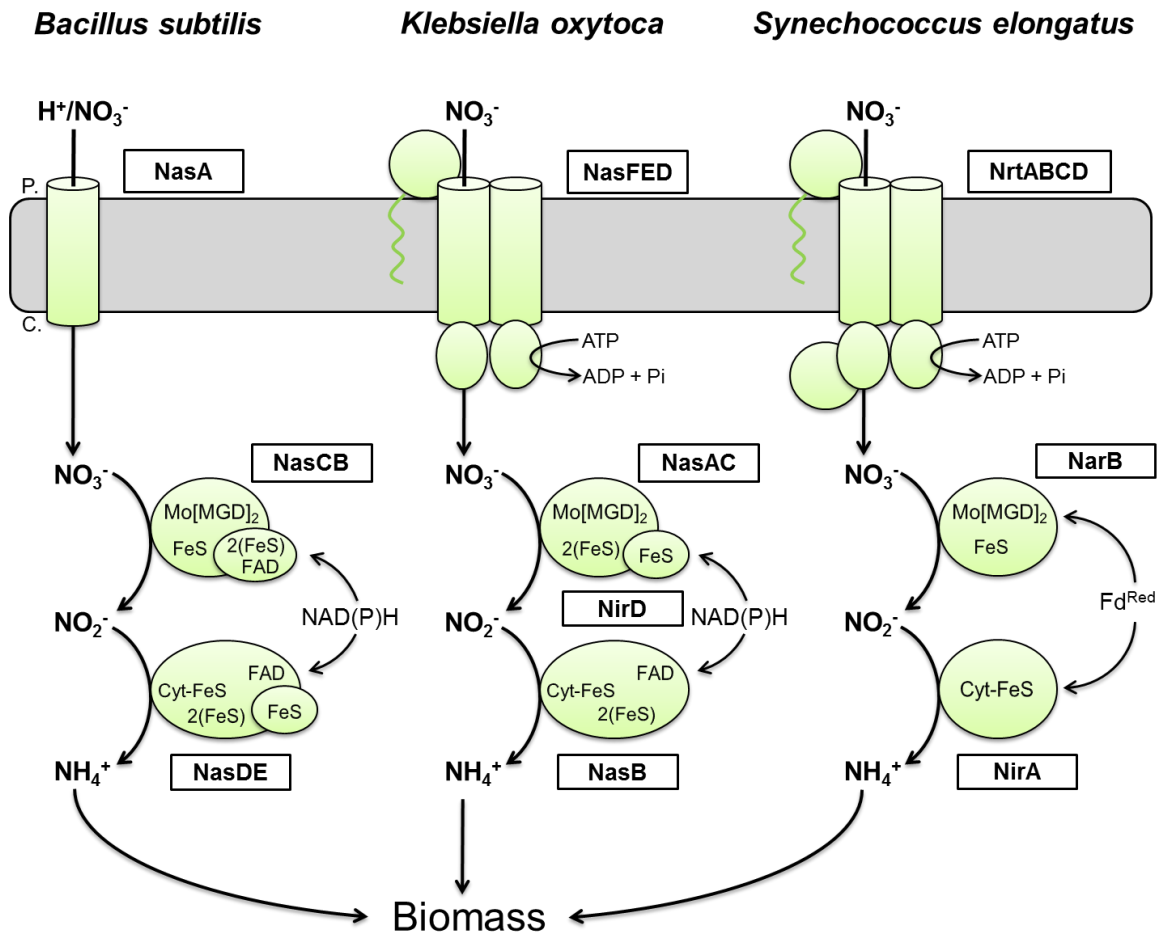


Figure 1.3. Plasticity of structural Nas system across various bacterial assimilatory systems. Schematic representing the physiological variation between structural genes required for assimilatory uptake and reduction of nitrate to ammonium in various bacteria. Periplasmic nitrate may be imported to the cytoplasm by either ATP-dependant primary active transport (*Klebsiella oxytoca* and *Synechococcus elongatus*) or secondary transport utilising the proton-motif force (*Bacillus subtilis*). Autotrophic organisms such as cyanobacteria use photosynthetically reduced ferredoxin compounds (Fd^{Red}) as the physiological electron donor for nitrate and nitrite reduction. In contrast, heterotrophic bacteria oxidise cytoplasmic NAD(P)H at an FAD-domain on the nitrite reductase to provide required electrons, subsequently passed to the separate active sites by an associated Fe-S transfer protein.

Bacillus subtilis utilises the transmembrane proton-motive force to import nitrate to the cell using the transmembrane secondary active-transporter, NasA. In heterotrophic bacteria, reduced pyridine-nucleotide oxidation at flavin-domains of the assimilatory apparatus generates the necessary electrons for reduction of nitrate and nitrite. Here, NAD(P)H is oxidised at FAD (flavin adenine dinucleotide) centres of NasB and NasD to supply electrons, via an associated ferredoxin NasE, to the molybdopterin active site of NasC and heme cofactor of NasD (Glaser et al. 1995; Shi et al. 2014).

Klebsiella oxytoca expresses NasFED which, in contrast to proton-linked transport, forms a periplasmic ABC-transporter system facilitating cytoplasmic import of nitrate through homodimeric NasE, coupled with ATP hydrolysis at the cytoplasmic domain of NasD (Wu & Stewart 1998). NAD(P)H oxidation at a flavin-dependant domain of NasB supplies electrons to the necessary active sites of NasAC and NasB via an associated Rieske-type FeS ferredoxin.

Structural components of cyanobacterial assimilation, such as *Synechococcus elongatus*, are extensively reviewed (Flores et al. 2005), with *nrtABCD* encoding an ABC-type permease coupling ATP hydrolysis to the primary active transport of nitrate across cell membranes (Omata 1991). Photosynthetically reduced ferredoxin and flavodoxin act as physiological electron donors to the catalytic centres of both nitrate and nitrite reductases (Candau et al. 1976; Manzano et al. 1976).

Nitrate assimilation impacts heavily on the biosphere, accounting for a sizeable portion of total inorganic nitrogen uptake within natural communities (Guerrero et al. 1981; Wawrik et al. 2012). Detrimentally, it causes significant environmental impacts by supporting accelerated microbial biomass formation within nitrate-rich communities in the presence of a carbon sink (Malm et al. 2009). This poses a vast agricultural problem when nitrate and nitrite containing fertilisers are applied to fields for crop growth, as free-living soil bacterial communities use this nutrition. Investigations into this pathway and its regulation are key for identifying methods of increasing crop yield whilst blocking artificially induced microbial growth.

1.2 Genetic Regulation of Nitrogen Response Proteins in Heterotrophic Bacteria

In heterotrophic bacteria, the general nitrogen regulatory system, Ntr, is responsible for activating gene expression of most proteins implicated in the nitrogen stress response. During nitrogen-limitation, the NtrC protein, once activated by its cognate partner NtrB, binds to upstream DNA sequences of gene promoters which in turn is recognized by the

nitrogen-responsive sigma factor, RpoN (sigma 54), which transiently associates with RNA polymerase to guide the enzyme to a promoter and catalyse formation of the active isoform (Merrick & Edwards 1995). Therefore, the combined function of the NtrBC system and sigma 54 are typically required for the activation of genes eliciting an appropriate response to govern the nitrogen status of the cell.

1.2.1 Nitrogen stress-response sigma factor: Sigma 54

Sigma factors (sigma factors) are prokaryotic transcription factors essential for initiating gene expression by forming a dissociable complex with core RNA polymerase, guiding the holoenzyme to a promoter region of DNA (Chandrangsu & Helmann 2014; Paget & Helmann 2003). DNA binding domains of sigma factors recognise specific nucleotide consensus sequences thus conferring specificity of the associated RNA polymerase (Mauri & Klumpp 2014; Feklistov & Darst 2009). Bacteria synthesise a variety of sigma factors which respond to various environmental stimuli to coordinate necessary gene expression (Gruber & Gross 2003). As each sigma factor recognises a specific nucleotide sequence, association of independent sigma factors with RNA polymerase orchestrates differential regulation of proteins required for distinct cellular functions (Kazmierczak et al. 2005).

Whilst sigma 70 is the housekeeping sigma factor performing the majority of transcriptional activity during growth under standard physiological conditions (Sharma & Chatterji 2010; Kapanidis et al. 2005), sigma 54 (sigma N) is involved with expression of most target genes associated with nitrogen stress (Buck et al. 2000; Morett & Segovia 1993). Sigma 54 is structurally and functionally distinct from sigma 70 and is widespread amongst proteobacteria where it positively upregulates proteins, for example, amino acid transporters to scavenge external nitrogen, and apparatus necessary for utilisation of nitrogen such as the GS-GOGAT system: Glutamine Synthetase – Glutamate Synthase (GOGAT - glutamine oxoglutarat aminotransferase) (Merrick 1993; Bender 1991). It has been demonstrated to regulate the genes involved in respiratory and assimilatory nitrate-reduction in several organisms such as *E. coli* and *A. vinelandii*, respectively, as well as dinitrogen fixation amongst diazotrophs (Studholme & Buck 2000; Kustu et al. 1989).

1.2.2 General nitrogen regulators: Ntr system and P_{II} proteins

The P_{II} regulatory protein, ubiquitous throughout prokaryotes, fungi and plants, is responsible for initiating signal transductions in response to nitrogen, carbon and energy levels (Durand & Merrick 2006; Forchhammer 2008). The activity of P_{II} proteins is

notoriously controlled by cytoplasmic 2-oxoglutarate and glutamine levels to regulate expression, via a downstream regulatory cascade, of around 100 genes encoding products linked to a multitude of processes concerning nitrogen metabolism (Conroy et al. 2007; Ohashi et al. 2011).

The rationale is as follows: during ammonium starvation, a high intracellular ratio of the carbon compound 2-oxoglutarate to glutamine builds up (Radchenko et al. 2013). These conditions are detected by uridylyltransferase, causing its activation. This subsequently uridylylates P_{II} at a conserved tyrosine residue to result in P_{II}-UMP, the active conformer, which stimulates the two-component Ntr system (Ninfa & Magasanik 1986). Two-component systems require a sensor-kinase protein (NtrB) which modulates the activity of a cognate response-regulator partner (NtrC) (Swanson et al. 1994; Senior 1975).

P_{II}-UMP activation of NtrB causes conformational changes leading to C-terminal ATP binding and histidine-kinase activity, resulting in trans-autophosphorylation between the NtrB dimers (Merrick 1992; Dixon & Kahn 2004). Phosphorylated NtrB transfers the phosphoryl group to a conserved aspartate residue on an N-terminal receiver domain of NtrC (Sanders et al. 1992; Weiss & Magasanik 1988). This phosphorylation event triggers structural changes to expose a C-terminal DNA-binding domain of NtrC (Yang et al. 2004). Active NtrC homodimers exert transcriptional activation by binding to a consensus sequence on DNA using a helix-turn-helix motif (Patriarca et al. 1993; Nakano et al. 1995; Cullen et al. 1998). NtrBC has been demonstrated to upregulate genes such as nitrogenase and the GS-GOGAT system (Stadtman 2001; Reitzer 2004; Merrick & Edwards 1995).

Historically, NtrC is known to function in tandem with sigma 54, stimulating transcription by catalysing the formation of active sigma 54-RNA polymerase holoenzyme (Austin & Dixon 1992). Importantly, however, recent work has emerged to demonstrate NtrC is capable of functioning separately in a sigma 54-independent manner to monitor various genes, e.g. in *R. capsulatus* (Foster-Hartnett et al. 1994).

1.3 *Paracoccus denitrificans*

1.3.1 Biochemical and physiological characteristics

P. denitrificans is a Gram-negative, α -proteobacteria of the Rhodobacteraceae family and typically found in soil as a free-living, facultative anaerobe with vast biochemical flexibility (Richardson 2008). It is a coccoid, non-motile bacterium capable of aerobic

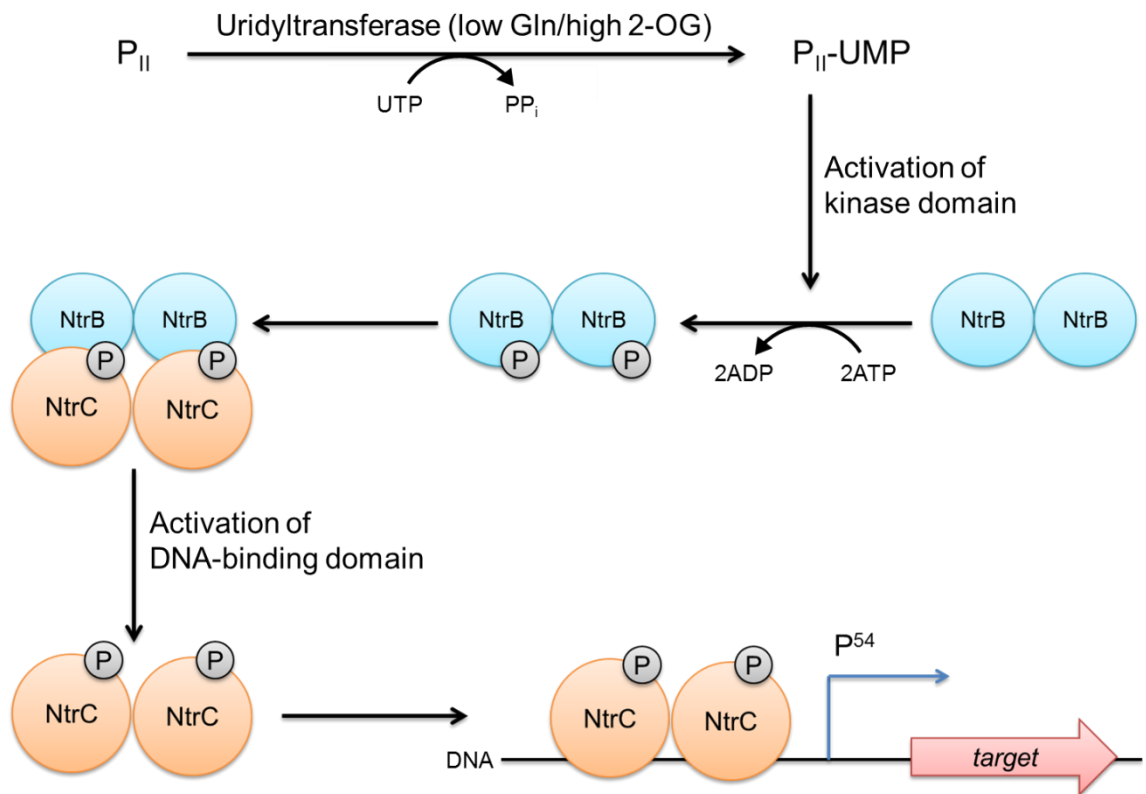


Figure 1.4. Regulatory cascade of the P_{II}/Ntr system in response to nitrogen-limitation in Gram-negative bacteria. During nitrogen limitation, a high intracellular ratio of 2-oxoglutarate (2-OG) to L-glutamine (Gln) accumulates, stimulating uridylyltransferase which targets the P_{II} regulatory protein. P_{II}-UMP activates NtrB kinase domains causing dimerisation and trans-autophosphorylation. Phosphorylated NtrB binds and transfers the phosphate group onto a cognate NtrC partner which causing conformational changes ultimately forming the DNA-binding domain of the response regulator. Functional dimeric NtrC recognises consensus nucleotide sequences at a target genes promoter, typically at sigma⁵⁴-dependant promoters, resulting in gene expression.

heterotrophic growth on a multitude of carbon substrates as well as chemolithotrophic growth via denitrification during anoxic conditions (Martienssen & Schöps 1999). *P. denitrificans* contains great metabolic versatility, such as the aerobic respiratory complexes, β -oxidation pathways, TCA (tricarboxylic acid) enzymes and the glycolysis apparatus (John & Whatley 1975) thus making it a model study organism, largely as a paradigm denitrifier.

1.3.2 *P. denitrificans* encodes three independent nitrate reductases

The bacterium was chosen for this study as it actively synthesises the two heterotrimeric respiratory ubiquinol/nitrate oxidoreductases, Nar and Nap (Gates et al. 2011). In addition, it has recently been demonstrated to actively express the gene cluster responsible for cytoplasmic nitrate assimilation (Figure 1.5) (Sears et al. 1997; Allen et al. 2001).

Each of the three nitrate reductases contain an active site Mo[MGD]₂ cofactor for nitrate reduction, yet perform distinct physiological roles under appropriate environmental conditions and are differentially regulated. Nar generates energy by substituting nitrate as a terminal electron acceptor, thus providing anaerobic ATP production and is regulated by the oxygen-sensitive Fnr (fumarate nitrate reductase) regulatory protein (Li & DeMoss 1988). The DNA-binding FNR-family regulates expression of genes during anoxic growth as a functional homodimeric protein where each monomer contains a [4Fe-4S]²⁺ cluster (Hutchings et al. 2002; Uden et al. 2002). Exposure to oxygen rapidly converts the cluster to a [2Fe-2S]²⁺ form stimulating protein monomerisation which leads to apoFNR (Khoroshilova et al. 1997; Kiley & Beinert 1998). Nap serves to dissipate excess energy to balance the cellular redox status and appears insensitive to both oxygen and ammonium levels. Nas produces biomass during nitrogen limitation in the presence of nitrate or nitrite and is subsequently repressed by cytoplasmic ammonium levels, discussed later in Section 1.4.3 (Luque-Almagro et al. 2011).

Though functioning in separate capacities, the catalytic subunits of each system shares in common motifs for [Fe-S] ligation and Mo[MGD]₂ coordination. The [Fe-S] cluster is covalently bound by four highly conserved cysteines offering covalent thiol bonds (three cysteines and a histidine in NarG). The coordination sphere of Mo generally comprises 6 ligands; two molybdopterin guanine dinucleotide dithiolenes, a protein-derived cysteinyl group (Nap and Nas) or aspartate (Nar), and an oxygen atom from a proximal water molecule to produce a stable oxo-Mo⁵⁺ species, which interconverts with Mo⁶⁺ during catalysis. The MGD molecules themselves form a multitude of hydrogen-bonds and hydrophobic interactions with residues from the core region of the protein. A

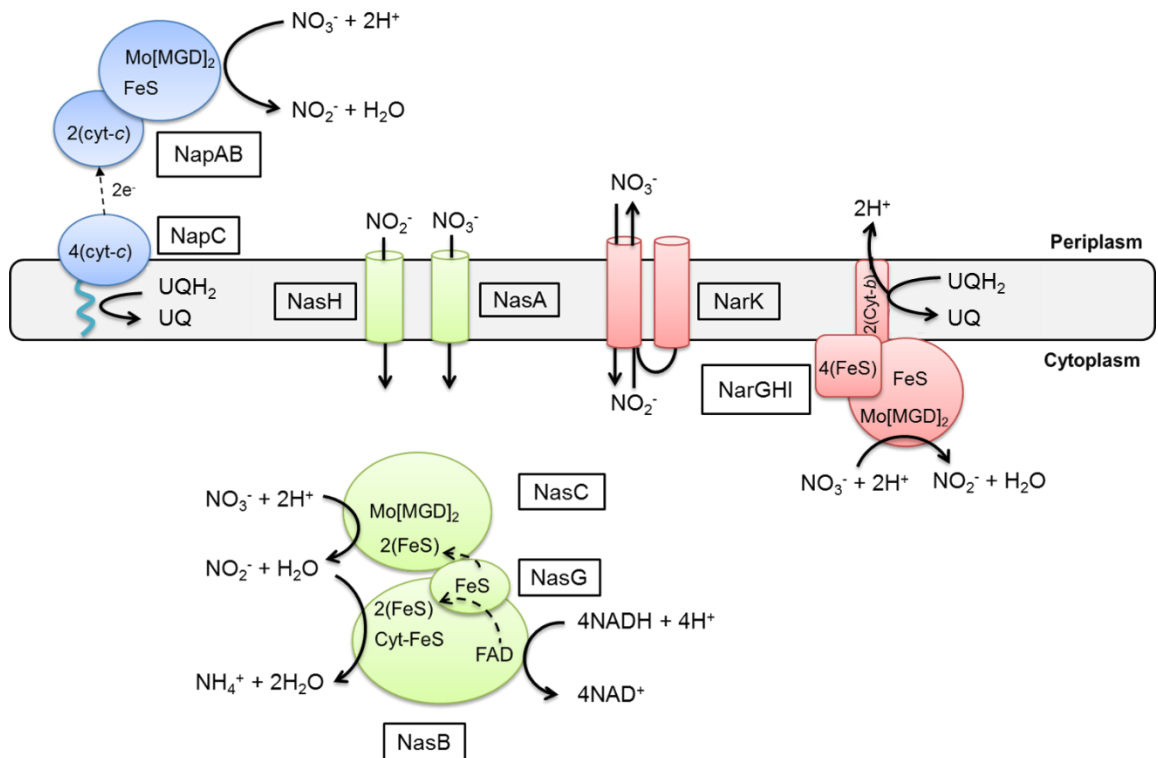
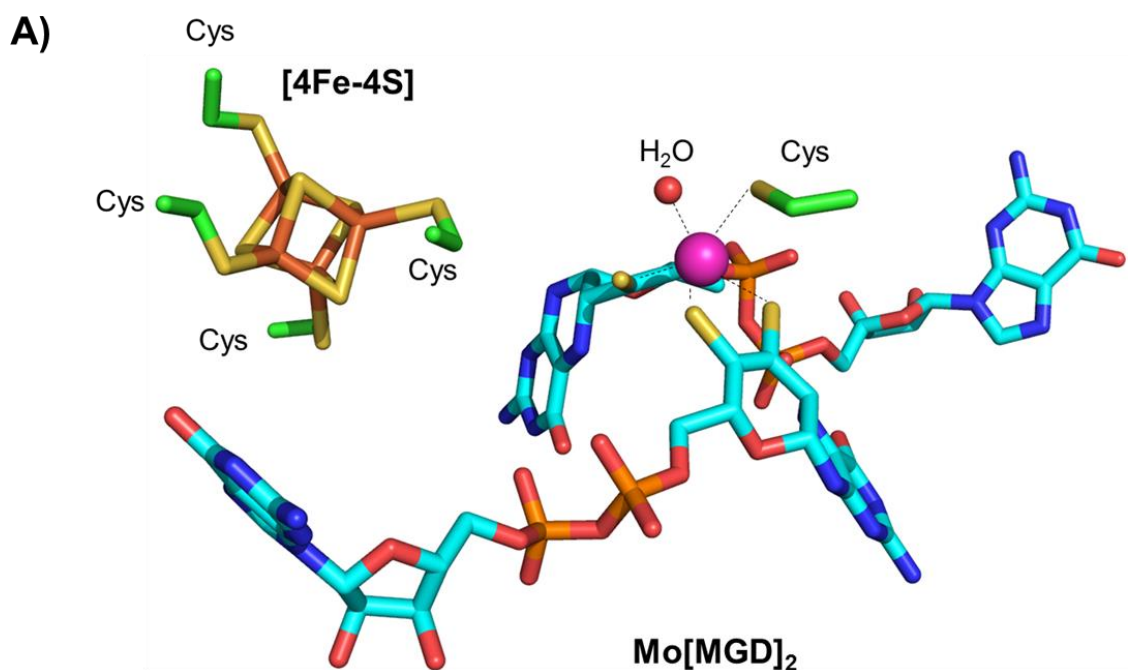


Figure 1.5. Functional and structural organisation of the three individual nitrate reductases of *P. denitrificans*. Non-electrogenic nitrate dissimilation (blue), nitrate assimilation (green) and nitrate respiration (red) are all performed by *P. denitrificans*. Nap couples membrane-bound ubiquinol oxidation of NapC with the nitrate reductase capacity of NapA within the periplasm to dissipate excess energy. Heterotrimeric Nar links ubiquinol oxidation at NarK with cytoplasmic nitrate reduction at NarG to translocate protons across the inner-membrane generating the proton motif force during anoxic growth. The assimilatory three-component Nas complex couples NADH oxidation with the reduction of nitrate to nitrite to ammonium. A rieske-type ferredoxin, NasG, transfers electrons from the FAD-dependant NADH oxidase domain of NasB to the active sites of both NasC and NasB. Image was adapted from Gates (Gates et al. 2011).



NarG	1	MSHLLDRLNFLKPTRKDVFSEGHGQTT-TEN---RDWEDTYRSRWR	DKIVRST	HGVNCT	**	*
NasC	1	-----MQTIR-----	TTC	CPYCG		
NapA	1	--MTISRRLKKAQAAGIAAMAANIPLSADAQVPVGGVESLQITWSK	-----	APCRFCG		
NarG	57	GSCSWKIYVKSGIVTWETQQTDYPRTRPDLPNHEPRGCAR	GASYSWY	LYSANR	KTPLIR	
NasC	13	VGCGVLATPDGKGGGL-----GIAGDPDHPANRGR	CVKGSALGETV	GHGGR	LAPRIH	
NapA	53	TGCGVMVGVKEGRVV-----ATHGDLAEVNRGLNCV	KCYFLSKI	YGQDR	TQPLLR	
NarG	117	GRLMKLWREKRKTMTPIQAWTAIQNDPQARES	YTRIRGKGGFVRATW	DEATE	ITAAANAY	
NasC	66	G-----	REAGW	DEALDLVA	HRRFRD	
NapA	106	KKDGV-----	YAKDGEFTPVS	WEAF	DTMAQAKR	
NarG	177	TARTYGFDRVFGFSPIPAMSMISYAAGTRY-----	ISLLGGT	CMSFYDWY	CDLPPAS	
NasC	85	TIAEHGPDVGFYVSGQLLTEDYVANKLMKGF	IGSAN	DTNSRL	CMSA-----VAGH	
NapA	136	VLKDKGPTAVGMFGSGQWTIFEGYAATKLMRAGFRSNN	DPNARH	CMSA-----	AYAF	
NarG	229	PQTWGEQTDVPESADWYNAGYLLWGSNVPQTR	TPDAHFYTEARY--	RGT	SAVTCPDYS	
NasC	139	RRAFGTDTVPGLYEDLELADTVVLLVGSNLAWCH	PVLYQRLAAAREARG-	TRVVV	DPRA	
NapA	190	MRTFGMDEPMGCYDDFEAADAFVLLWGSNMAEM	PILWTRVADRRL	LGHPHV	VAVLSTFTH	

Figure 1.6. Conservation of key residues required for cofactor coordination in bacterial nitrate reductases. A) Crystal structure of NapA from *E. coli* to give insights the cofactor environments. The [4Fe-4S] cluster is ligated by four thiol bonds donated by protein-derived cysteines (green). The core molybdenum atom (pink sphere) is coordinated twice by each molybdopterin guanine nucleotides (blue), a conserved cysteine residue and an adjacent water molecule (red sphere). PDB 2NYA, manipulated using PyMOL (Jepson et al. 2007). B) Primary sequence alignment of the N-terminal regions of the distinct nitrate reductases of *P. denitrificans* via Clustal Omega (*EMBL-EBI*) and BoxShade (*ExPASy*). Asterisks denote conserved residues required for cofactor coordination in each distinct nitrate reductases.

hydrogen bond network lies between the [4Fe-4S] cluster and the pterin ring of the Mo[MGD]₂ cofactor to allow electron transfer (Jepson et al. 2007).

1.4 The *nas* Gene Cluster for Microbial Nitrate Assimilation

The genetics of nitrate assimilation have been extensively studied and reviewed within fungi and plants (Beevers & Hageman 1969; Crawford & Arst 1993; Shao et al. 2011), whilst work performed in heterotrophic bacteria has been restricted to *Rhodobacter capsulatus*, *K. oxytoca*, *A. vinelandii* and *B. subtilis* (Pino et al. 2006; Lin et al. 1994; Gutierrez et al. 1995; Ogawa et al. 1995). The research performed in this current study focused on the assimilatory nitrate/nitrite reductase pathway of the heterotrophic soil bacterium, *P. denitrificans*.

1.4.1 Phylogenetic distribution of *nas* in bacterial species

The genes encoding cytoplasmic nitrate assimilation are typically clustered together within the genome to comprise a *nas* operon (Figure 1.7) (Luque-Almagro et al. 2011). The two major genes involved are those translating to the assimilatory nitrate reductase and nitrite reductase. Additional required participants are; a rieske-type ferredoxin – a key component in heterotrophs, as well as a nitrate/nitrite uptake system. In Gram-negative bacteria, the *nas* operon is under dual regulation, activation in the absence of ammonia by the general nitrogen regulatory system (*ntr*), and induction specifically by nitrate/nitrite using a novel regulatory system coded by the *nasR* and *nasTS* genes (reviewed in Section 1.4.4) (Gutierrez et al. 1995; Shao et al. 2011).

1.4.2 Uptake and reduction of nitrate and nitrite by structural *NasABGHC*

The *nas* gene cluster of *P. denitrificans* is contained within a 9.5 Kb region on chromosome II (accession number: NC_008687) of the published genome (Pden_4455 – 4449). The *nasABGHC* section codes for the structural proteins responsible for uptake and reduction of the nitrogen oxyanions to ammonium. Approximately 300 bases upstream lies the *nasTS* two-component regulatory system, the products of which control the expression of downstream *nasABGHC* (Figure 1.8).

The *P. denitrificans nas* gene cluster encodes two inner-membrane transporters; NasA and NasH (Gates et al. 2011). NasA is a 12-helix transmembrane (TM) protein belonging to the Major Facilitator Superfamily (MFS); secondary carriers capable of translocating small solutes in response to chemiosmotic ion gradients (Pao et al. 1998). NasA couples the import of either nitrate or nitrite into the cell via symport of protons, exploiting the periplasmic proton motif force (Moir & Wood 2001). NasH shows greater substrate

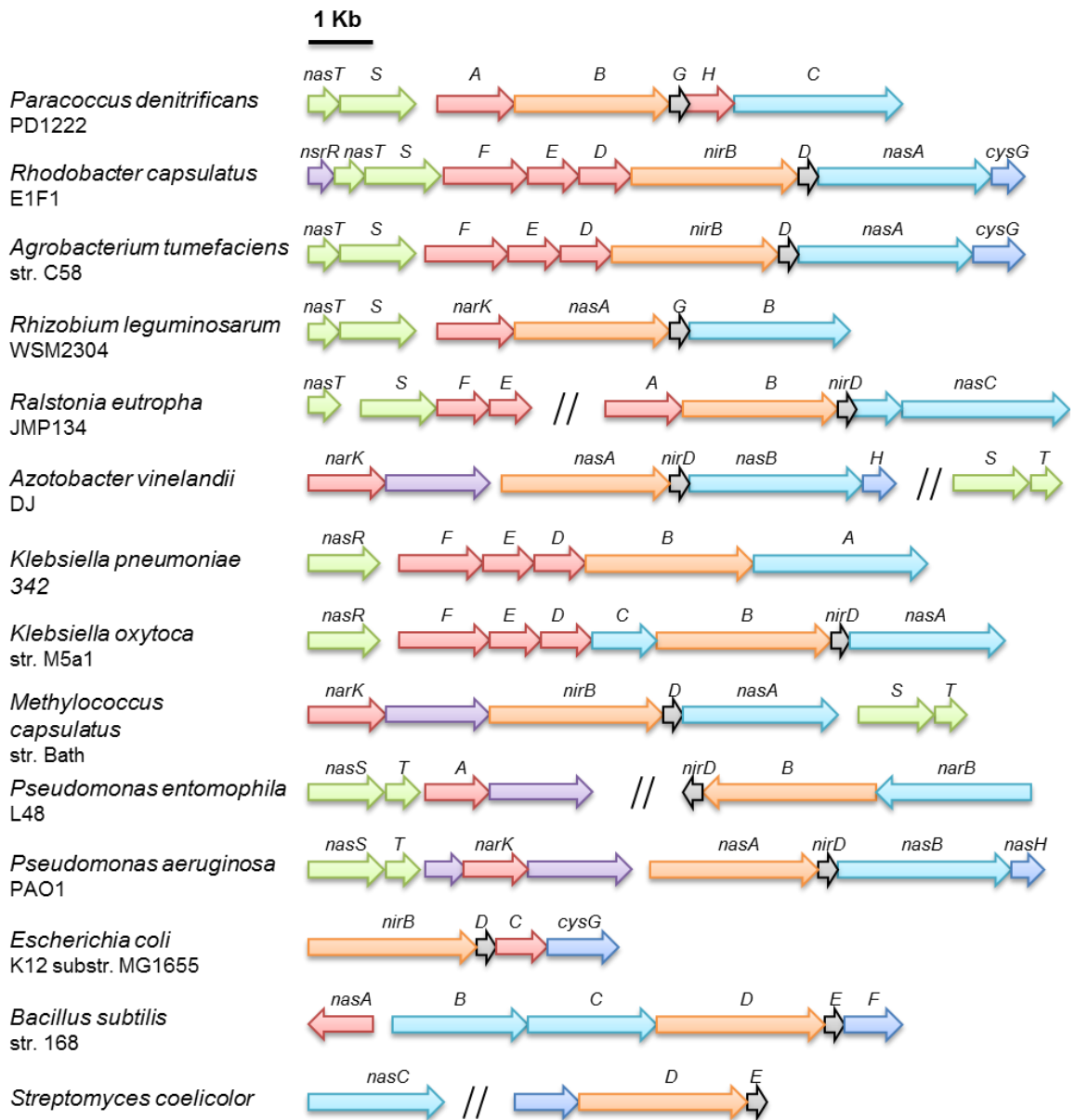


Figure 1.7. Genomic arrangement of *nas* gene clusters from various bacteria. Comparative analysis of open reading frames that confer nitrate assimilation in a widespread range of bacterial species. Open reading frames that encode the following products are coloured as follows: green; nitrate/nitrite-specific regulators, red; nitrate/nitrite transporters, orange; nitrite reductase, black; Rieske-type ferredoxin, blue; nitrate reductase, dark blue; uroporphyrin-III C-methyltransferase, purple; hypothetical genes. Figure adapted from Luque-Almagro (Luque-Almagro et al. 2011).

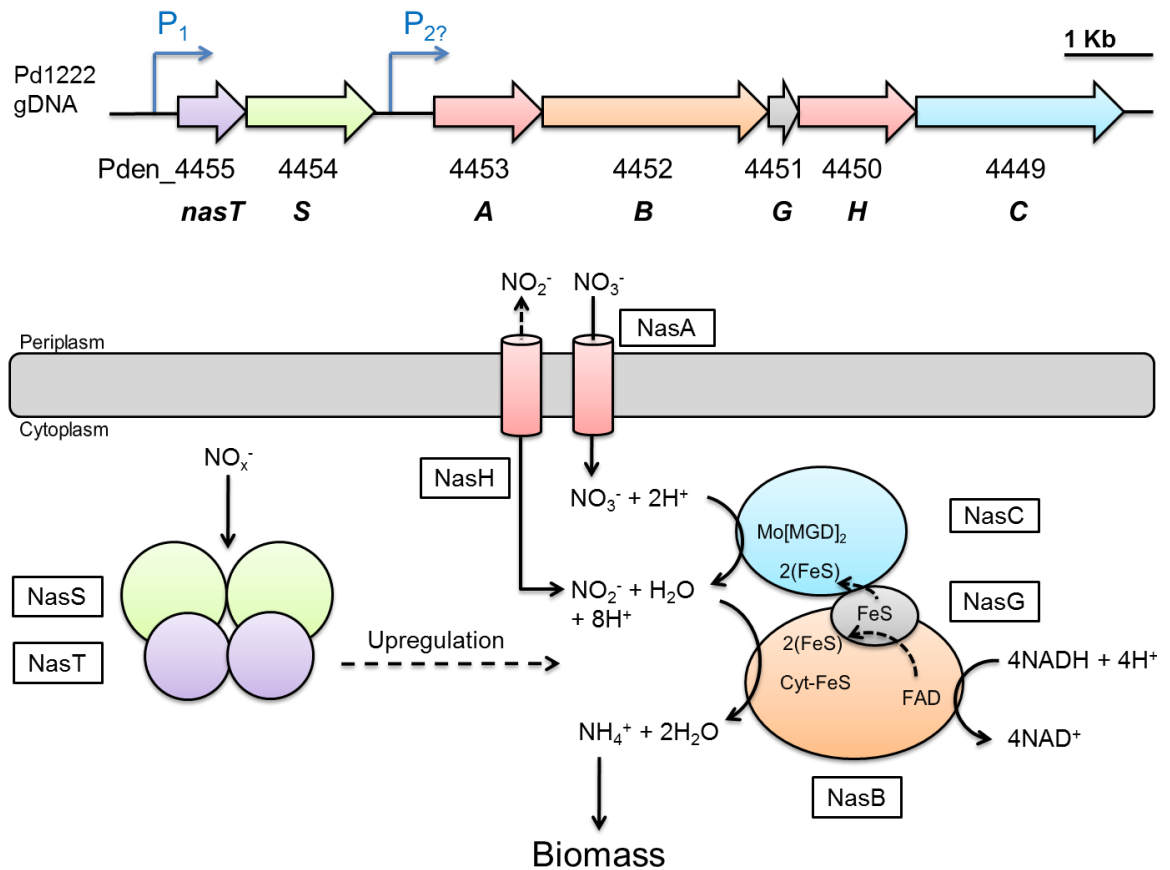


Figure 1.8. Complete uptake and cytoplasmic assimilation of nitrate to ammonium in *Paracoccus denitrificans*. Homodimeric NasT induces gene expression of *nasABGHC* following binding of nitrate/nitrite to its inhibitory cognate partner, NasS. Nitrogen oxyanions accumulate within the cell via transmembrane transporters NasA and NasH. The three component nitrate reductase-nitrite reductase-ferredoxin couples oxidation of the reduced cellular NADH pool with reduction of nitrate and nitrite at complex metal centres of NasC and NasB, respectively. Yielded ammonium is used to accumulate organic cellular material.

specificity as it transports solely nitrite across the inner membrane as a member of the formate-nitrite transporter family. These proteins typically span the membrane with 6-8 TM-helices as pentameric cationic channels to facilitate the bidirectional movement of anions across a membrane (Beckham et al. 2010; Lü et al. 2013).

Cytoplasmic NasC is a 92 kDa metal-dependant assimilatory nitrate reductase, harbouring one [4Fe-4S] cluster and one [2Fe-2S] cluster, which transport electrons to an Mo[MGD]₂ active site cofactor (Jepson et al. 2004; González et al. 2006; Bender & Friedrich 1990). Two externally supplied electrons are utilised in a reductive reaction with a previously reported V_{max} of 111 nmol.min⁻¹.mg protein⁻¹, following which nitrite and water are released (Gates et al. 2011; Bertero et al. 2003).

NasB is a globular 99 kDa assimilatory nitrite reductase. The single polypeptide comprises an N-terminal FAD-dependant NADH oxidase domain necessary to oxidise cytoplasmic reduced nucleotide-pyridines for electrons to supply active sites of both NasB and NasC (Cammack et al. 1982; Thomas & Surdin-Kerjan 1997; Gates et al. 2011). In addition, NasB contains a conserved core and C-terminal region containing the key cysteine residues to coordinate two [4Fe-4S] clusters and a siroheme active site (Nakano et al. 2012). Siroheme cofactors are heme-like prosthetic groups (iron tetra-hydroporphyrin) capable of accomplishing a one step, six electron biological reduction of sulphite and nitrite compounds (Tripathy et al. 2010). The coordination sphere of the central iron atom in the heme cofactor comprises four equatorial bonds, contributed by nitrogens of the porphyrin ring and axial interactions with a conserved protein-derived cysteinyl-thiol bond and a hydrogen bond of a distal water. *cysG* codes for uroporphyrin-III C-methyltransferase, an enzyme involved in synthesising the siroheme cofactor from uroporphyrinogen, a heme group and a vitamin B₁₂ precursor (Murphy et al. 1974) and is often located within the *nas* cluster as demonstrated in Figure 1.8 (Tate et al. 1997). The iron atom of the siroheme ligates and reduces nitrite directly to ammonium, with no free nitrogen compound intermediate detected, functioning with a reported V_{max} of 302 nmol.min⁻¹.mg protein⁻¹ (Gates et al. 2011).

NasB and NasC form a stable, cytosolic three-component complex with NasG, a 12 kDa Rieske-type [2Fe-2S] ferredoxin critical for coupling NADH oxidation to nitrate and nitrite reduction (Gates et al. 2011). Sequence analysis demonstrates bacterial NasC contains no intrinsic NADH oxidising domain which is ubiquitous to the assimilatory nitrate reductases of plants and fungi (Lin & Stewart 1998). This is unimportant to photoautotrophic bacteria which use photosynthetically reduced ferredoxin to donate electrons directly to the active sites during transient interactions (Flores et al. 2005).

However, organoheterotrophic bacteria need to couple reduced pyridine-nucleotides from oxidative metabolism of organic substrates with nitrate reduction. NasG mediates electron transfer from the NADH oxidising domain of NasB to the active sites of both NasB and NasC, perhaps by forming a heterotrimeric complex where the [Fe-S] clusters reside close enough to facilitate electron transfer (Gates et al. 2011).

Complete nitrate assimilation proceeds as follows: NADH is oxidised at the FAD-dependant NADH oxidising domain of NasB. Liberated electrons pass to the [Fe-S] cluster of the NasG ferredoxin which donates them to the Mo[MGD]₂ cofactor of NasC via its two [Fe-S] clusters, reducing nitrate to nitrite (Solomonson & Barber 1990; Richardson et al. 2001). In addition, NasG passes electrons to the siroheme catalytic center of NasB via two [Fe-S] clusters to reduce the oxidised nitrite species to ammonium. Resulting cytoplasmic ammonium cations are integrated with carbon compounds to produce key organic structures, by the GS-GOGAT cycle discussed later.

Expression of the structural components required to assimilate nitrate is under dual control, ammonium repression by the NtrBC system and nitrate induction by the NasTS complex.

1.4.3 Transcriptional activation of nitrate assimilation by NtrBC during ammonium starvation

Complete assimilation of each nitrate requires 8 electrons and 4 NADH compounds, in addition to transport of nitrate into the cell, making it an energetically expensive process. If nitrogen is readily available within the environment, e.g. ammonium or organic compounds such as amino acids, *nas* is not expressed (Motohara et al. 1976). Control of *nasABGHC* transcriptional activation in Gram-negative bacteria is regulated by the Ntr system and P_{II} proteins (Cole & Brown 1980; Caballero et al. 2005) and has been demonstrated previously for several organisms such as *K. oxytoca* (Wu et al. 1999), *A. vinelandii* (Toukdarian & Kennedy 1986), *Rhizobium meliloti* (Szeto et al. 1987), *Pseudomonas aeruginosa* (Li & Lu 2007), *Azorhizobium caulinodans* (Pawlowski et al. 1991) and *Azospirillum brasilense* (Ishida et al. 2002). This system functions as discussed above in Section 1.2.2 where detection of ammonium limitation through 2-oxoglutarate/glutamine levels activates P_{II} to initiate the cascade resulting in NtrC activation of *nasABGHC*.

1.4.4 Complete synthesis of nas mRNA requires NasTS

Successful transcription of *nasABGHC* mRNA following NtrC initiation requires the nitrogen-responsive NasTS/NasR regulators, due to the formation of an inhibitory hairpin secondary structure in the 5'-UTR of the nascent mRNA causing Rho-independent termination (Luque-Almagro et al. 2013; Wilson & von Hippel 1995).

Hairpin structures consist of: an RNA stem loop rich in GC dyad symmetry followed by a stretch of uridines at the 3' end which results in a polynucleotide complex disrupting RNA polymerase binding thus stalling elongation (Farnham & Platt 1981). Formation of an antiterminator stem loop negates this inhibitory effect in a mode of gene regulation termed transcriptional anti-termination. Antiterminators are constructed via the mechanism of a class of signal-responsive RNA-binding proteins containing an ANTAR domain (AmiR and NasR Transcriptional Antiterminator Regulator) (Stewart & van Tilbeurgh 2012; Ramesh et al. 2012). ANTAR domains are unique to bacteria and involved in stimulus-response pathways to alter expression accordingly. Following activation, they dimerise to form a coiled-coil tertiary structure capable of binding a specific ssRNA substrate at inhibitory hairpins to form antiterminators, stabilising the RNA and allowing uninterrupted transcription (Shu & Zhulin 2002).

NasR and the two-component NasTS use a nitrate/nitrite binding function in conjunction with an ANTAR domain programmed to recognise hairpins in the 5'-UTR of *nas* mRNA to act as an antiterminator of transcription specifically activated by nitrate (Goldman et al. 1994). NasR, is abundant in γ -proteobacteria and has been studied previously in *K. pneumoniae* where it was shown to alleviate the inhibitory hairpin allowing nitrate induction of the *nasFEDCBA* operon (Lin & Stewart 1996; Boudes et al. 2012). NasTS is phylogenetically widespread in Gram-negative α -proteobacteria and β -proteobacteria but less studied (Luque-Almagro et al. 2011).

Whilst no crystal structure for NasTS currently exists, the solved crystal structures of the two studied ANTAR proteins NasR and AmiC-AmiR provide detail into the structure and function (Figure 1.9). Both heterotetrameric NasTS and AmiCR segregate their molecule sensing and ANTAR RNA-binding domains between cognate partners in a two-component system governed by protein-protein interaction. Alternatively, homodimeric NasR fuses the functions into a single polypeptide regulated by allosteric shifts (Boudes et al. 2012).

NasS belongs to the super-family of periplasmic binding proteins usually operating as the receptor domain in ABC-type transporters. It shares high sequence similarity to cyanobacterial NrtA nitrate-binding protein found abundantly within the *Synechocystis* membrane and contain a conserved nitrate binding site (Koropatkin et al. 2006).

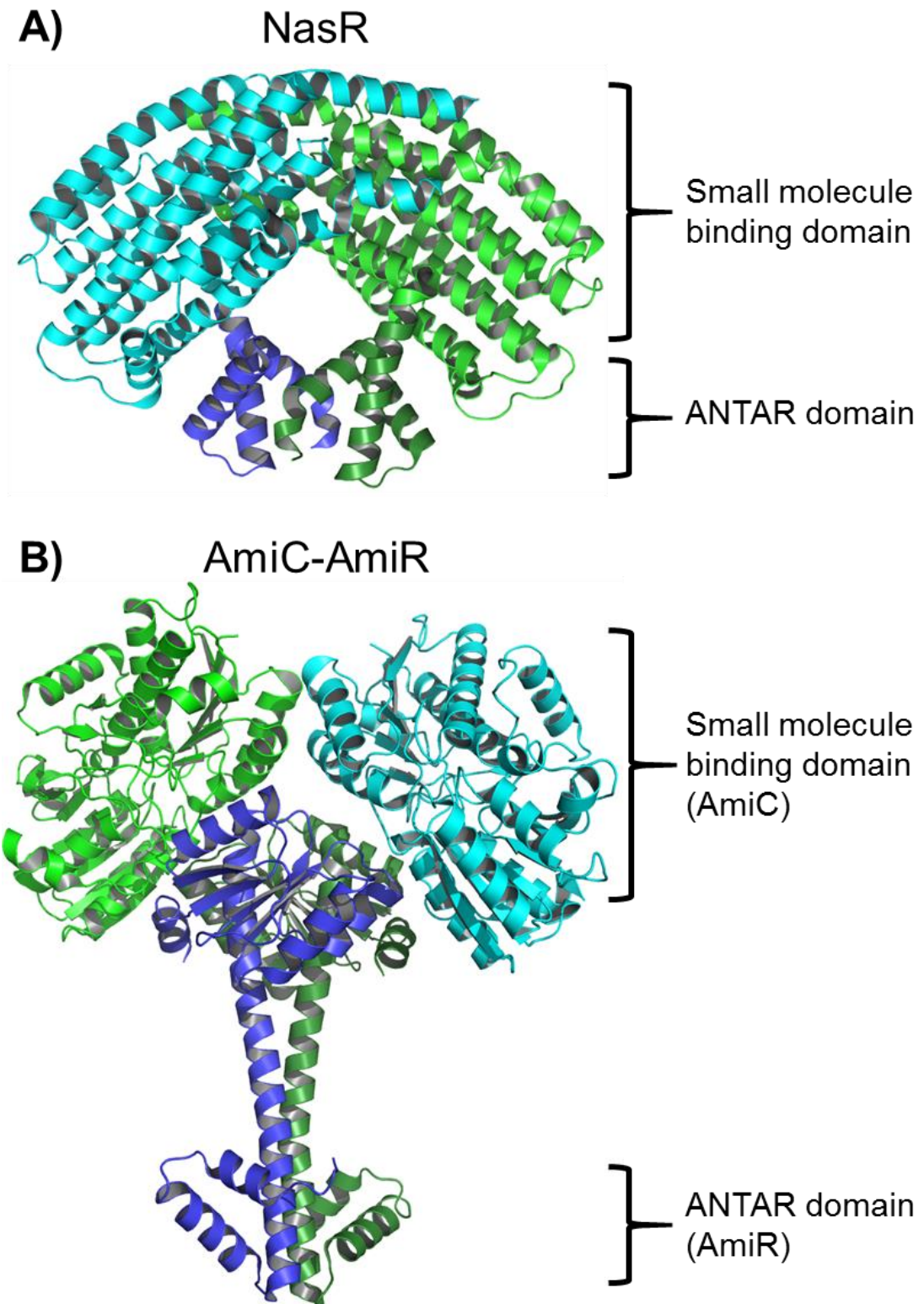


Figure 1.9. Comparison of crystal structures for two regulatory ANTAR proteins: NasR and AmiR. Solved X-ray quaternary structures of A) homodimeric NasR from *K. oxytoca* (Boudes et al. 2012) and B) the AmiC-AmiR heterotetrameric complex of *P. aeruginosa* (O'Hara et al. 1999). Individual polypeptide subunits are coloured green and blue; the lighter being the nitrate sensing domain and darker shade forming the ANTAR RNA-binding region. PDB 4AKK and 1QO0, respectively, illustrated using PyMOL.

However, NasS lacks the N-terminal TM helix thus confining the protein to the cytoplasm where it functions to bind nitrate /nitrite. A previous study by Luque-Almagro and coworkers confirmed NasS holds NasT in a heterooligomeric inactive state and subsequently releases NasT following ligand binding (Luque-Almagro et al. 2013).

Following release from the inhibitory complex with NasS, active NasT homodimers target a *cis*-acting regulatory element: the inhibitory hairpin formed in the leader region of *nasABGHC* mRNA. The RNA-binding motif contains positively charged arginine and lysine residues for interactions with the negative phosphate backbone of RNA, suppressing premature termination to enable positive regulation of *nas* expression. This mode of pre-translation regulation was recently demonstrated for *P. denitrificans* where the purified NasT was shown to interact with the leader mRNA of *nasA* (Luque-Almagro et al. 2013). Figure 1.10 below provides a schematic depicting nitrate-induced expression of *nasABGHC* by NasTS control to allow nitrate assimilation during appropriate conditions for biomass formation.

1.5 Carbon/Nitrogen Interface for Integrating Inorganic Nitrogen into Biomass

Cellular production or uptake of ammonium by microorganisms is followed by a cytoplasmic anabolic pathway integrating carbon and nitrogen in the biosynthesis of key structures. This ubiquitous bacterial combinatory pathway is known as the GS-GOGAT system; Glutamine Synthetase – Glutamate Synthase (GOGAT - glutamine oxoglutarate aminotransferase) (Gunka & Commichau 2012; Tyler 1978). Due to the high affinity for ammonium, and requirement of ATP for catalysis by GS, this mechanism is the dominant pathway of biomass accumulation during energy rich, nitrogen limiting growth (Helling 1998; Mikes et al. 1991). The low K_m of GS allows the assimilation of ammonium into organic material in concentrations lower than 0.1 mM (in *E. coli*) or derived enzymatically from other nitrogen sources, such as nitrate assimilation (Magasanik 1982; Eisenberg et al. 1987). The GS-GOGAT system has been demonstrated to be under NtrBC activation during nitrogen-limiting conditions in heterotrophic bacteria (Reitzer 2004; Stadtman 2001).

Some bacteria, such as *P. denitrificans*, have the capacity to incorporate ammonium into organic structures in an additional manner using glutamate dehydrogenase (GDH). This enzyme exhibits much lower affinity for ammonium but requires no ATP input, only reduced nucleotide pyridines. Due to this, GDH functions at the carbon/nitrogen interface as the primary mechanism to produce organic nitrogen-containing compounds during

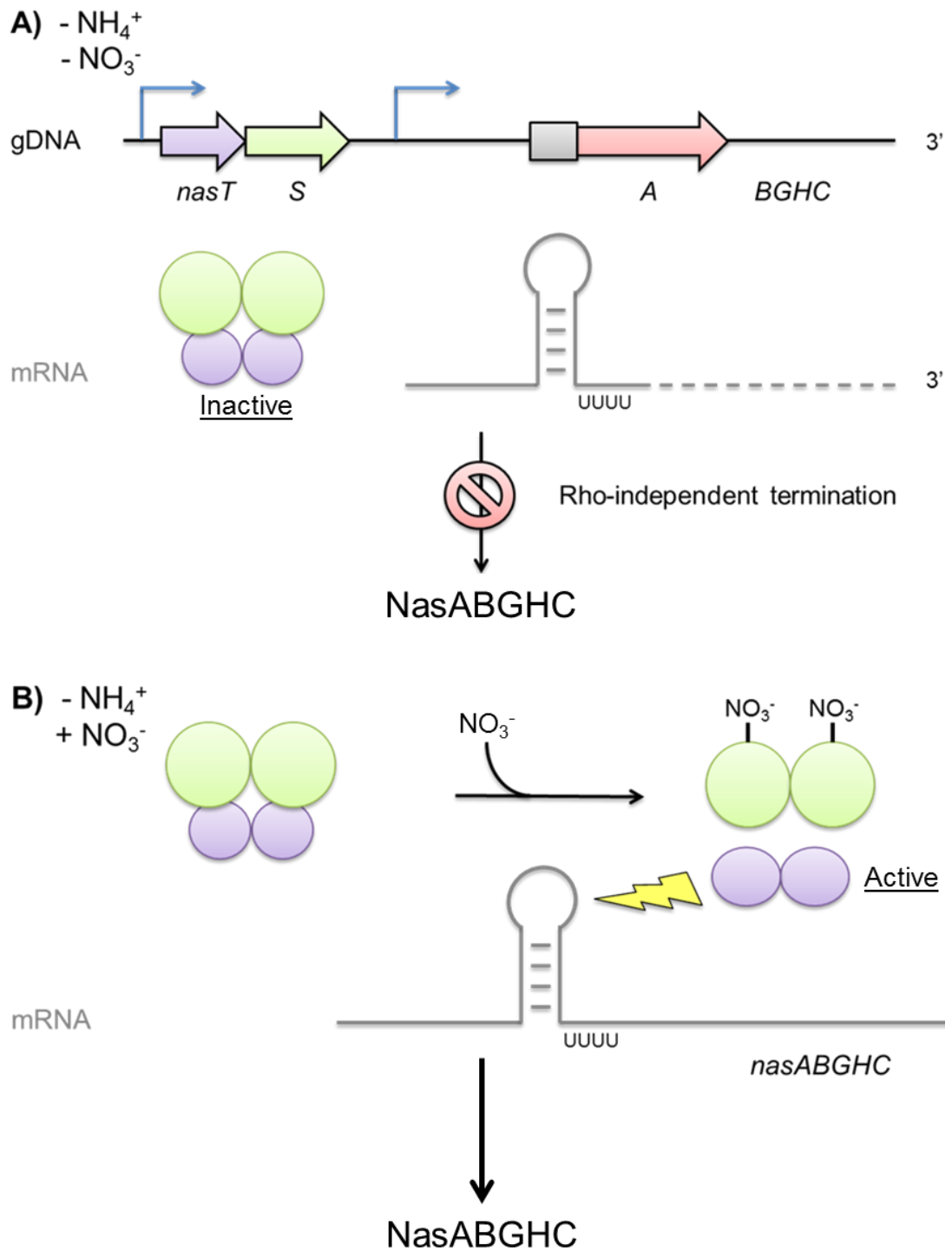


Figure 1.10. Model demonstrating nitrate-specific induction of *nasABGHC* in *P. denitrificans*. A) Following transcription initiation of *nasABGHC* by NtrC in the absence of ammonium, an inhibitory hairpin forms in the leader region of nascent mRNA which disrupts RNA polymerase binding. B) In the presence of nitrate, NasS coordinates these anions thus releasing NasT from the inactive heterotetrameric complex. The ANTAR domains of homodimeric NasT recognises and binds the RNA hairpin and forms an anti-terminator structure. This alleviates its repressive effect to give transcriptional antitermination, resulting in expression of *nasABGHC* under appropriate conditions.

ammonium abundant conditions, typically at a concentration over 0.1 mM (in *E. coli*) (Chavez et al. 1999; Magasanik 1982). Low intracellular nitrogen stimulates the NtrBC system to regulate appropriate transcriptional responses, one of which is the activation of *nac* (nitrogen assimilation control). The Nac regulatory protein binds to the DNA upstream of *gdh* and represses transcription to ensure that during nitrogen-limitation, the GS-GOGAT system is the functional mode at the carbon/nitrogen interface (Tempest et al. 1970; Bird & Wyman 2003; Schwacha & Bender 1993; Camarena et al. 1998).

Both these anabolic pathways catalyse reductive amination to ultimately incorporate ammonium with the carbon compound (and TCA intermediate), 2-oxoglutarate (α -ketoglutarate) to produce glutamate, hence the ratio of these compounds regulates P_{II} proteins to signal the nitrogen status (Figure 1.11). Glutamate and glutamine are widely accepted as being the key nitrogen donors and pivotal metabolic precursors for biosynthetic reactions in most cells (Ebner et al. 1970). Glutamate serves as the primary amino group donor in transamination reactions, accountable for around 88 % of total organic-nitrogen production (Bennett et al. 2009; Ruiz 1998). The side chain amide group of glutamine operates as the direct nitrogen donor for steps in the biosynthesis of amino acids requiring side chain amines (Kanamori et al. 1989).

1.5.1 The GS/GOGAT cycle

GS and GOGAT are ubiquitously found in the cytoplasm of bacteria for assimilating bioavailable ammonium cations into cellular material. The GS enzyme is further conserved throughout the other domains of life for glutamine production in the absence of a dietary source. Due to its metabolic importance, GS activity is heavily regulated at the post-transcriptional level through allosteric inhibition feedback through products of glutamine metabolism, such as tryptophan, histidine and carbamoyl phosphate. Furthermore, adenylation at a conserved tyrosine residue reduces activity. Deadenylation is achieved when active P_{II}-UMP stimulates ATase, thus activating GS during nitrogen limiting conditions through the P_{II} regulation (Shapiro, 1969).

Ammonium is received by homododecameric GS, with each monomer harbouring an individual magnesium-containing active site, which combines it with the side chain carboxyl group of glutamate in an ATP consuming ligation producing glutamine (Liaw et al. 1995; Murray et al. 2013). This subsequently donates its newly received amine group to the α -carbon of an accepting 2-oxoglutarate, produced through the TCA cycle, in an NAD(P)H-dependant transamination. This second step is catalysed by the heterodimeric, metal-dependant GOGAT enzyme at a flavin- and FeS-containing active site, yielding two molecules of glutamate (Miller 1974; van den Heuvel et al. 2003). One

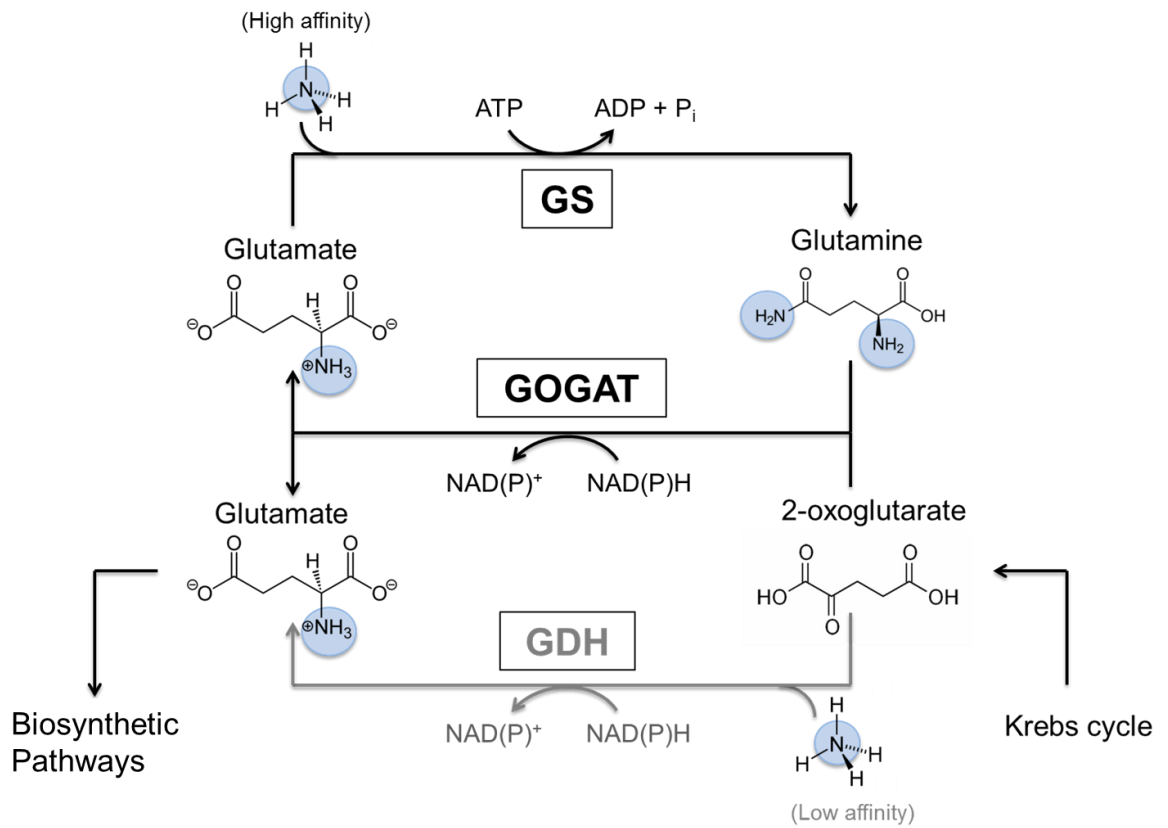


Figure 1.11. The GS-GOGAT cycle and GDH pathway for integrating carbon with inorganic nitrogen in bacteria. A representation of the cytoplasmic carbon/nitrogen interface governing ammonium assimilation into cellular organic structures. The GS-GOGAT pathway (black) combines ammonium with the amino acid glutamate giving glutamine. This subsequently donates an amine group to an accepting 2-oxoglutarate, formed during the Krebs cycle, yielding two molecules of glutamate, where one feeds into biosynthesis for amine donation whilst the other repeats the cycle. GDH (grey) catalyses NAD(P)H-dependant ligation of ammonium directly with 2-oxoglutarate to produce a glutamate compound which serves as an amine-donor to accepting organic precursors.

glutamate molecule is recycled whilst the other feeds into biosynthetic pathways to deliver an activated nitrogen group to accepting organic precursor compounds.

1.5.2 The microbial GDH pathway

Glutamate dehydrogenase is a cytoplasmic enzyme ubiquitous in microbes and governs an important pathway at the carbon/nitrogen interface by incorporating ammonium into biomass in the abundance of environmental ammonium. GDH chelates an NAD(P)H cofactor to catalyse reversible ligation of ammonium directly with 2-oxoglutarate producing glutamate (Frieden 1959; Botman et al. 2014).

Additionally, GDH is present in the mitochondria of eukaryotes where it serves as a key link between catabolic and anabolic pathways. Here, it is necessary for glutamate production but also is needed for ammonium detoxification in organisms, and importantly, ammonium homeostasis in mammalian brains (Spanaki & Plaitakis 2012).

1.6 Global Transcriptomic Analysis of Nitrate Assimilation in *Paracoccus denitrificans*

A recent transcriptomic study comparing whole-genome expression of *P. denitrificans* cultured under ammonium-dependent and nitrate-dependent conditions was performed by microarray analysis (Unpublished data, Gates and coworkers). This transcriptomic analysis highlighted a multitude of genes encoding proteins implicated in nitrogen-metabolising pathways underwent a significant upregulation during nitrate assimilation (Figure 1.12).

The heatmap shown below represents the \log_2 normalised gene expression values as colour, with a greater red signalling higher expression. The selected genes presented all undergo markedly increased transcription when cultures assimilate nitrate as opposed to being supplied with ammonium. As expected, the *nasTSABGHC* cluster (Pden_4449-4455) and GS-GOGAT (4462 and 448) genes are upregulated to produce biomass from nitrate, as is the *ntrBC* system (4129-4131) and *glnB* (P_{II} protein – 4461) to initiate transcription of nitrogen-responsive genes. Most gene products significantly upregulated correspond to transporters importing organic nitrogen compounds to scavenge environmental sources. However, several unprecedented genes interestingly exhibited increased expression during nitrate assimilation and were subsequently investigated throughout this study.

Pden_4619-4621 code for TRAP (Tripartite ATP-independent periplasmic transporters) proteins, a large family of transmembrane ATP-independent transporters which uptake

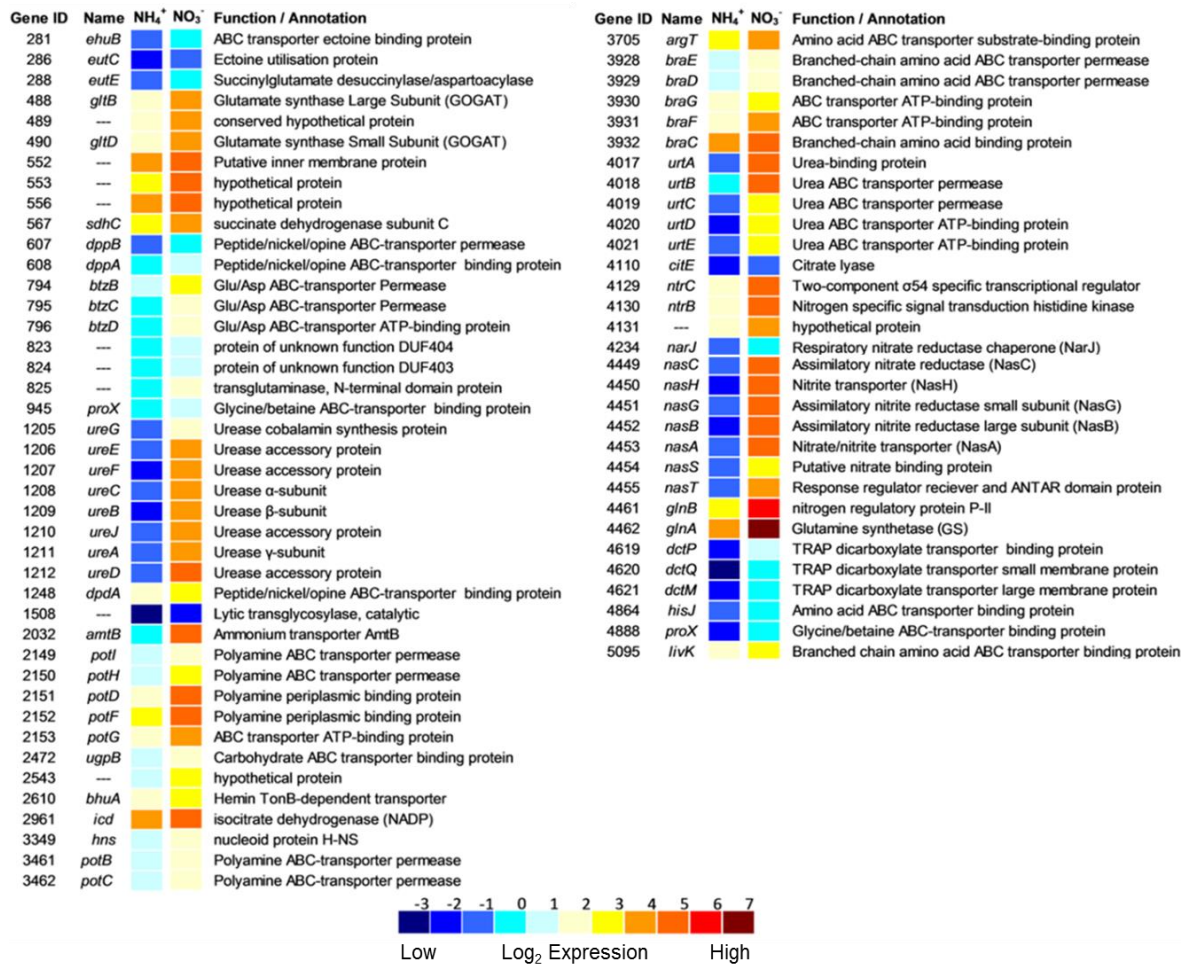


Figure 1.12. Microarray analysis comparing gene expression of *P. denitrificans* during ammonium-dependent versus nitrate-dependent aerobic growth. Heatmap depicting expression levels of significantly upregulated genes from *P. denitrificans* grown aerobically in minimal salt media at 30 °C with 30 mM succinate using either 10 mM ammonium (left column) or nitrate (right column) as a sole nitrogen source. RNA was harvested at a mid-exponential phase and subject to a type-II microarray. Colours indicate average log₂ normalised expression values between three biological replicates. ID represents unique locus tag of each gene in the *P. denitrificans* genome (Accession: NC_008686–008688). Figure adapted from Gates *et al.* (unpublished data).

environmental organic acids and short-chain dicarboxylates into the cell (Forward et al. 1997), discussed further in Section 1.7.

Perhaps most surprising is the upregulation of Pden_4234, *narJ*, a molybdenum chaperone found in the gene cluster coding for NarGHI, the respiratory nitrate reductase typically expressed under anoxia. This is an unprecedented observation for *nar* expression during aerobic heterotrophic growth and will be further covered in Section 1.8. The final upregulated gene examined during this study is encoded by Pden_4131, a hypothetical protein clustered with the NtrBC system. Based upon amino acid composition gene is predicted to code for a tRNA-dihydrouridine synthase (DUS) (Xing et al. 2002), explored in Section 1.9.

1.7 The Impact of Carbon Towards Growth During Assimilation of Nitrate

TRAP proteins are periplasmic transporters ubiquitous to prokaryotes, which exhibit a broad range of specificity for importing various dicarboxylic acids and short chain carbon compounds (Kelly & Thomas 2001; Mulligan et al. 2009). These proteins typically use the transmembrane proton motive force, or sodium gradient, to drive unidirectional active transport of organic acids, such as succinate, into the cytoplasm for respiration (Mulligan et al. 2011; Mulligan et al. 2007).

The necessity for increased uptake of respiratory carbon substrates during nitrate assimilation is likely due to the energetics of the Nas system. Complete reduction of nitrate to ammonium during bacterial heterotrophic growth requires 4 NADH compounds thus forcing the bacterium to be reliant upon cytoplasmic reduced nucleotide-pyridines. The cellular NADH pool is maintained, largely, by oxidation of reduced carbon compounds and organic acids in the TCA cycle. Given that ammonium doesn't require this processing prior to anabolism, cultures assimilating nitrate as a sole nitrogen source are possibly more dependent upon the quantity of carbon sources to fuel NADH production and ultimately drive nitrate reduction. The molecular basis of *P. denitrificans* dependence upon the quantity of organic acid and NADH yield per molecule respired of the compound, whilst growing with nitrate will be explored in Chapter 3.

1.8 Chaperones Responsible for Maturation of Nitrate Reductases

As mentioned previously, *P. denitrificans* contains three distinct nitrate reductases: NarG, NapA and NasC. Whilst segregated into separate cellular pathways, they all comprise an [Fe-S] cluster and a Mo[MGD]₂ cofactor making them large, complex molybdoenzymes (Figure 1.13). NasC is predicted to coordinate an additional [Fe-S]

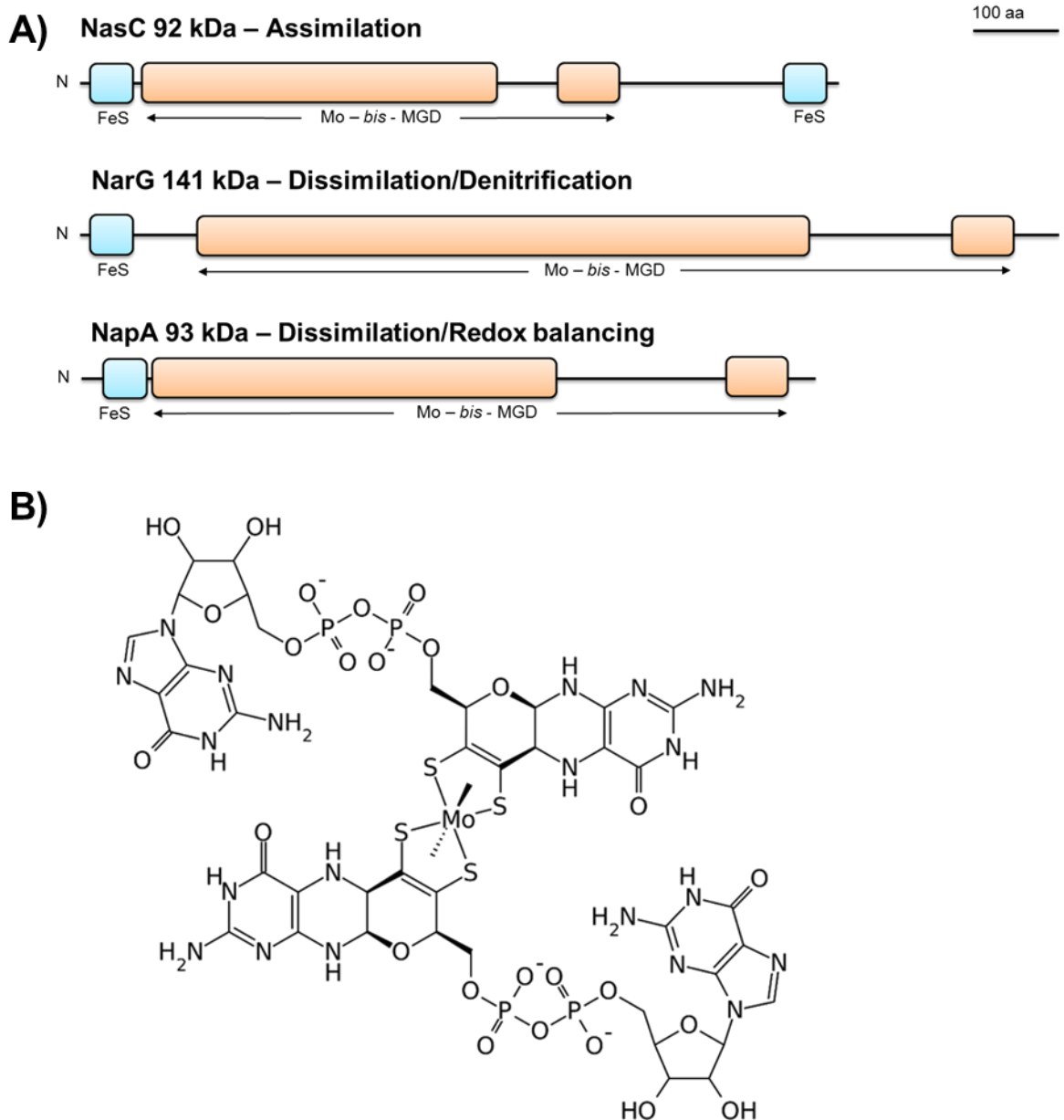


Figure 1.13. Domain overview to highlight required cofactors coordinated by the nitrate reductases of *P. denitrificans*. A) Representation of domain architecture for NasC, NarG and NapA; the assimilatory, respiratory and dissimilatory nitrate reductases respectively. Blue boxes represent [Fe-S] binding domains and orange indicates Mo[MGD]₂ regions. B) Skeletal structure of the molybdenum-containing molybdopterin guanine dinucleotide (Mo[MGD]₂) cofactor which forms the active site for two electron nitrate reduction to nitrite.

cluster at the C-terminus to participate in delivery of electrons to the active site, whereas NarG and NapA have NarH and NapB, respectively, to facilitate this electron transport.

Post-translational insertion of cofactors, covalent folding of proteins and successful maturation of complete quaternary structure is accomplished by cytoplasmic molecular chaperone proteins which recognise epitopes on the unfolded structure of their target protein to assist folding (Ellis 2006). Chaperones which mature complex iron sulfur proteins, typically involved in respiration, are termed redox enzyme maturation proteins (REMP) (Turner et al. 2004). Correct maturation of the dissimilatory NapABC ubiquinol:nitrate oxidoreductase complex is known to require the chaperone activity of NapD (Pden_4722) (Berks et al., 1995). Additionally the molybdenum chaperone NarJ (Pden_4234) is the REMP for NarG during denitrification in bacteria (Turner et al. 2004).

1.8.1 NarJ as the respiratory nitrate reductase chaperone

In *P. denitrificans* and most bacteria containing a Nar system, *narJ* is located within the *narKGHJI* gene cluster coding for the structural machinery necessary for respiratory nitrate reduction. NarJ has been well characterised in the context of denitrification as a molybdenum chaperone required for the maturation of the respiratory nitrate reductase, NarG (Blasco et al. 1998; Dubourdieu & DeMoss 1992).

NarJ belongs to a family of chaperones dedicated in biogenesis of complex iron sulfur molybdoenzymes. Every REMP is responsible for the maturation of a specific enzyme complex by coordinating tasks such as; cofactor insertion, folding, protection against proteolysis during maturation, and targeting the holoenzyme to the twin-arginine translocase (TAT) system (Bay et al. 2015). REMP's mature their cognate redox enzyme in tandem with general molecular chaperones, and the molybdopterin and Fe-S synthesis machinery (Chan et al. 2014). Following cytoplasmic biogenesis, the REMP guides the holoenzyme to the TAT apparatus for secretion across the cytoplasmic membrane (Natale et al. 2008).

Bacterial NarJ belongs to the TorD subfamily of REMP's which comprises NarJ/NarW, DmsD, TorD and YcdY members dedicated to molybdoenzyme biogenesis (Chan et al. 2014; Redelberger et al. 2011). Recent bioinformatic analyses of this taxonomically diverse subfamily has revealed that a close association exists between the specific chaperone and a specific complex iron sulfur molybdoenzyme respiratory system (Turner et al. 2004). This group is believed to have arisen through evolutionary divergence of the dimethylsulfoxide (DMSO) reductase and its maturation factor, DmsD,

i.e. nitrate reductase is a member of the DMSO reductase protein family (Ilbert et al. 2004; McDevitt et al. 2002).

NarJ is a small cytoplasmic protein (Figure 1.14) crucial for biogenesis of the NarGHI apparatus, but is not present within purified samples of the active complex, indicating a transient interaction prior to enzyme function (Sodergren et al. 1988). Deletion studies of *narJ* in *E. coli* observed the accumulation of cytosolic NarGH lacking molybdenum, characteristic of incorrectly folded protein (Blasco et al. 1992). Furthermore, NarJ has been shown to recognise and interact *in vitro* with NarG and the NarGH heterodimer to assist their formation (Blasco et al. 1998). These results conclude a chaperone capacity of NarJ required to assemble active NarGH within the cytoplasm prior to its association with NarI at the membrane (Liu & DeMoss 1997). Though inconclusive as to the mode of NarJ function - whether it coordinates and inserts molybdenum or folds the protein following cofactor biosynthesis and insertion by other factors, it is established as the maturation factor for the respiratory NarG (Li & Turner 2009; Zakian et al. 2010) and is genetically conserved across bacterial denitrifiers (Palmer et al. 1996).

1.8.2 *NarJ* as the candidate for maturation of the assimilatory nitrate reductase

Whilst the *nar* gene cluster contains an intrinsic molybdenum chaperone, the *nasTSABGHC* gene locus contains no such maturation factor and *P. denitrificans* contains no other predicted copy of a molybdenum chaperone type protein within its genome. Interestingly, the earlier microarray analysis (Figure 1.12) observed that when *P. denitrificans* is grown aerobically by nitrate assimilation, solely *narJ* is upregulated from the *nar* gene cluster. This is unprecedented as *nar* is believed to comprise one transcriptional unit, typically induced by the oxygen-responsive, Fe-S-dependant transcriptional activator, Fnr: a DNA binding protein involved in regulating various anoxic pathways in bacteria (Li & DeMoss 1988; Takahashi et al. 1994). However, the transcriptomic data suggests a novel regulatory-mode for *narJ* expression during aerobic growth with nitrate as a sole nitrogen source.

This indicates it may be possible that the NarJ chaperone acts as a dual-function REMP which is necessary for biogenesis of both NasC and NarG, performing an unprecedented maturation role of non-Nar nitrate reductases. The involvement of NarJ with formation of active assimilatory nitrate reductase during appropriate physiological conditions will be explored in Chapter 6.

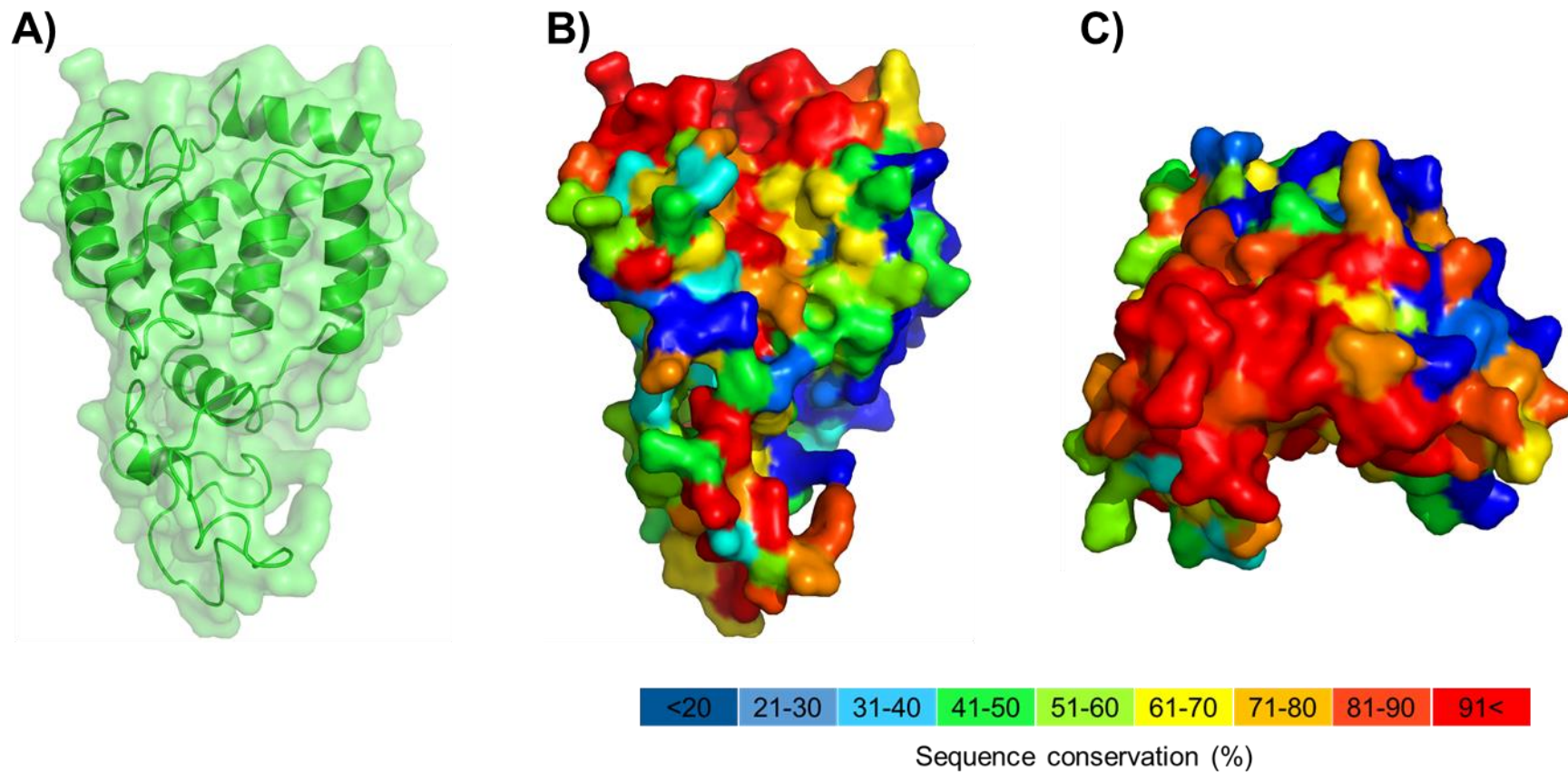


Figure 1.14. Tertiary structure and sequence conservation of NarJ from *P. denitrificans*. A) Predicted structure of NarJ from *P. denitrificans* built with Phyre 2 software based upon solved crystal structures of highly similar proteins (Kelley et al. 2015). B) Surface representation of the protein coloured by percentage conservation of each residue as judged by alignment of the top 50 identical primary sequences (*BLAST*). The ConSurf Server (Ashkenazy et al., 2010) rendered each amino acid based on conservation strength and mapped this onto the predicted 3D protein model. C) View from above. Structure manipulated using PyMOL.

1.9 NifR3 - a Putative, Nitrogen-Responsive, tRNA Dihydrouridine Synthase

The last protein explored in this study is encoded by the open reading frame Pden_4131, observed in the earlier microarray transcriptomic analysis (Figure 1.12) as undergoing a markedly increased expression during nitrate assimilation. This hypothetical gene in *P. denitrificans* is located on chromosome II (accession number: NC_008687) of the published genome, clustered immediately upstream of the key bacterial nitrogen-regulators, *ntrBC* and *ntrYX* and believed to comprise one transcriptional unit (Foster-Hartnett et al. 1993). The gene is predicted to encode a NifR3 protein due to high primary sequence similarity with other bacterial NifR3 proteins – a nitrogen responsive class of the tRNA-dihydrouridine synthase (DUS) superfamily. DUS are ubiquitous, NAD(P)H-dependant, oxidoreductase flavoproteins involved in the post-transcriptional modification of RNA (Xing et al. 2002).

A defining feature of cytoplasmic tRNA is the large quantity of biochemically distinct nucleotides: around 100 characterised so far (Gustilo et al. 2008). Each unique modification contributes towards the physiological role of tRNA as the link between mRNA transcripts and protein polypeptides. Modified nucleotides offer diverse roles such as altering or stabilising tRNA structure, quaternary structure of tRNA:rRNA complexes, modulating anticodon recognition of codons and ultimately increasing translation fidelity (Rozenski et al. 1999). Deficiency of required modifications in tRNA transcripts has been linked with “translation frameshifting” where subtle conformational changes produces mutant tRNA prone to errors in reading the standard genetic code (Urbonavicius et al. 2003).

The introduction of dihydrouridine in tRNA compounds by reduction of the carbon-carbon 5,6 double bond of the pyrimidine ring in uridine is attributable to DUS (Figure 1.15). Dihydrouridine formation is one of the most abundant post-transcriptional modifications of RNA, found widely in tRNA of bacteria, archaea and eukaryotes where it performs a ubiquitous housekeeping function to regulate protein biosynthesis (Sprinzl et al. 1998; Griffiths et al. 2012).

1.9.1 The tRNA dihydrouridine synthase protein superfamily

The DUS superfamily comprises cytoplasmic, flavin-dependant proteins which reduce the base pair uridine (U) to the modified nucleotide dihydrouridine (UH₂/D) at defined positions in the D-loop of intact tRNA. The typical candidates are uridine 16, 17, 20, 21 and 22, with 20 being the most predominately targeted (Xing et al. 2004). Dihydrouridine

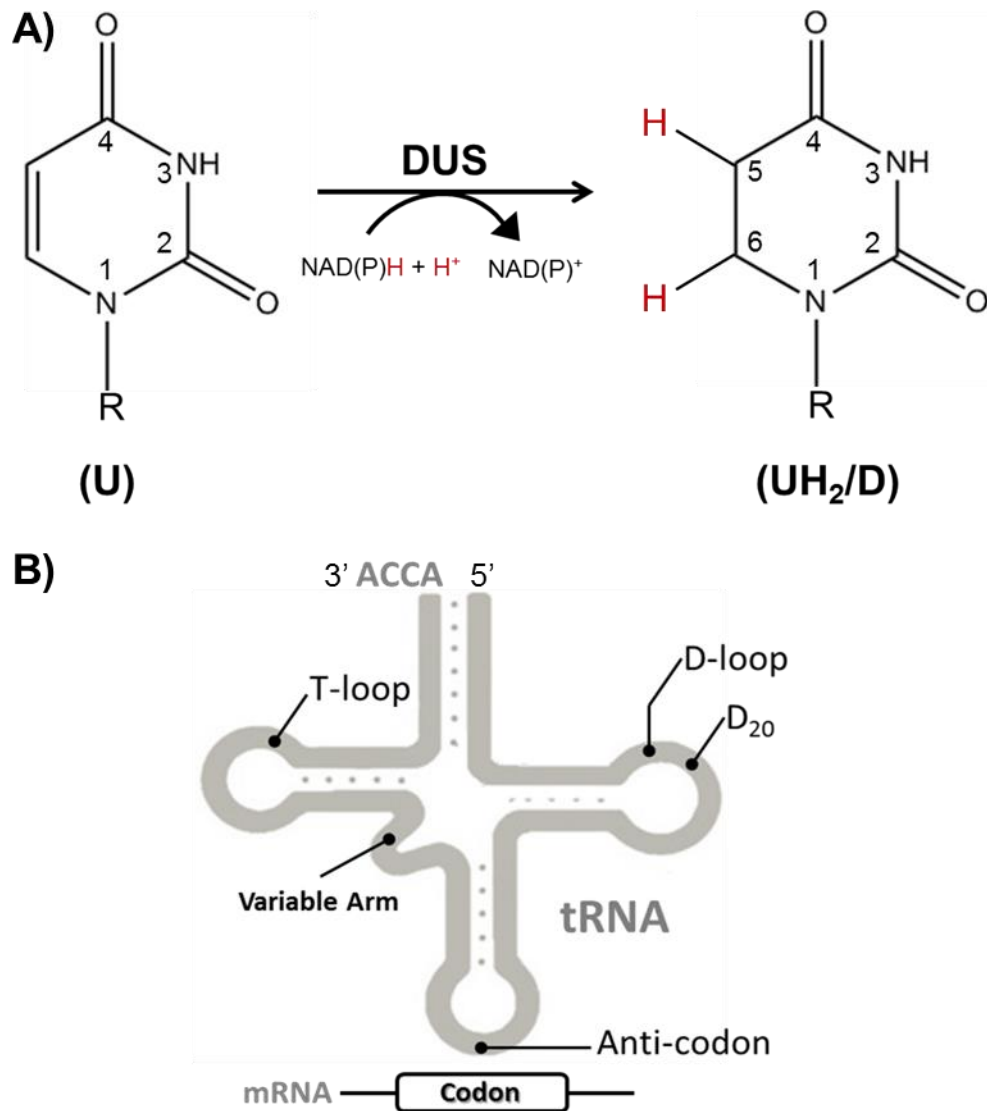


Figure 1.15. The formation and location of dihydrouridine in mature tRNA transcripts. A) The mechanism of the flavin-dependant redox reaction catalysed by DUS family members. NAD(P)H is used as the physiological electron donor to add two hydrogen atoms across the 5,6 C-C double bond of the pyrimidine producing dihydrouridine. B) Backbone structure representing a typical, mature tRNA. tRNA compounds typically contain; a D-loop rich in dihydrouridine (D) nucleotides, an anti-codon pairing an amino acid to a codon, a variable loop, a T-loop and an ACCA acceptor stem to which amino acids are ligated.

has also been reportedly found within rRNA in small quantities (O'Connor et al. 2001). These ubiquitous proteins contain a conserved structural core TIM-barrel motif (8 α /8 β fold) harbouring key residues necessary for FMN (flavin mononucleotide) cofactor coordination. DUS reversibly reduce the 5,6 double bond in uridine using cytoplasmic NAD(P)H as the physiological electron donor to add two hydrogens across the bond in the pyrimidine ring: $\text{NAD(P)H} + \text{H}^+ + \text{U} \rightarrow \text{NAD(P)}^+ + \text{UH}_2$ (Bishop et al. 2002).

1.9.1.1 Phylogenetic conservation of dihydrouridine synthases

DUS proteins demonstrate complete evolutionary conservation throughout bacteria, archaea and eukaryotes, as every organism encodes a DUS protein. Several key residues in the core domain are strictly conserved due to involvement with catalysis either by aiding FMN binding through hydrophobic or planar interactions, or by assisting coordination of tRNA and the target uridine. Cysteine 110, lysine 150 and histidine 180 residues are indispensable for turnover activity as recently demonstrated by Yu and coworkers (Figure 1.16) (Yu et al. 2011).

A previous study in *Saccharomyces cerevisiae* found that distinct subclasses of DUS exist, denoted as DusA, B and C in bacterial species. Construction of genomic deletion mutants and *in vitro* analysis of extracted tRNA demonstrated these individual subfamilies recognise and modify uridine base pairs at different specific positions within tRNA. (Xing et al. 2004). Furthermore, DUS are capable of differentiating between tRNA-aminoacyl compounds to act upon its specific target, with the tRNA coding for phenylalanine being the most reported as most heavily modified (Yu et al. 2011). This specificity results in individual tRNA transcripts containing differing quantities of dihydrouridine at different positions. It can therefore be postulated that the independent classes of DUS may be segregated based upon substrate specificity sites and affinities for both tertiary tRNA structure and a nucleotide consensus sequence. However, these various specificities between the classes are yet to be fully characterised.

Phylogenetic distribution shows DusA is relatively consistent amongst α -proteobacteria whilst DusC is primarily located within species from β - and γ -proteobacteria. DusB is far more diverse and widespread throughout the bacterial kingdom, distributed in proteobacteria, firmicutes, cyanobacteria and actinobacteria (Kasprzak et al. 2012). Every organism encodes atleast one *dus* within its genome, with bioinformatic analysis demonstrating that organisms may contain a variety of the subclasses. For example, *E. coli* contains *dusA*, *dusB* and *dusC* whilst the genome of *P. denitrificans* only contains *dusA* in addition to the recently identified *nifR3*. Each subclass of DUS varies greatly

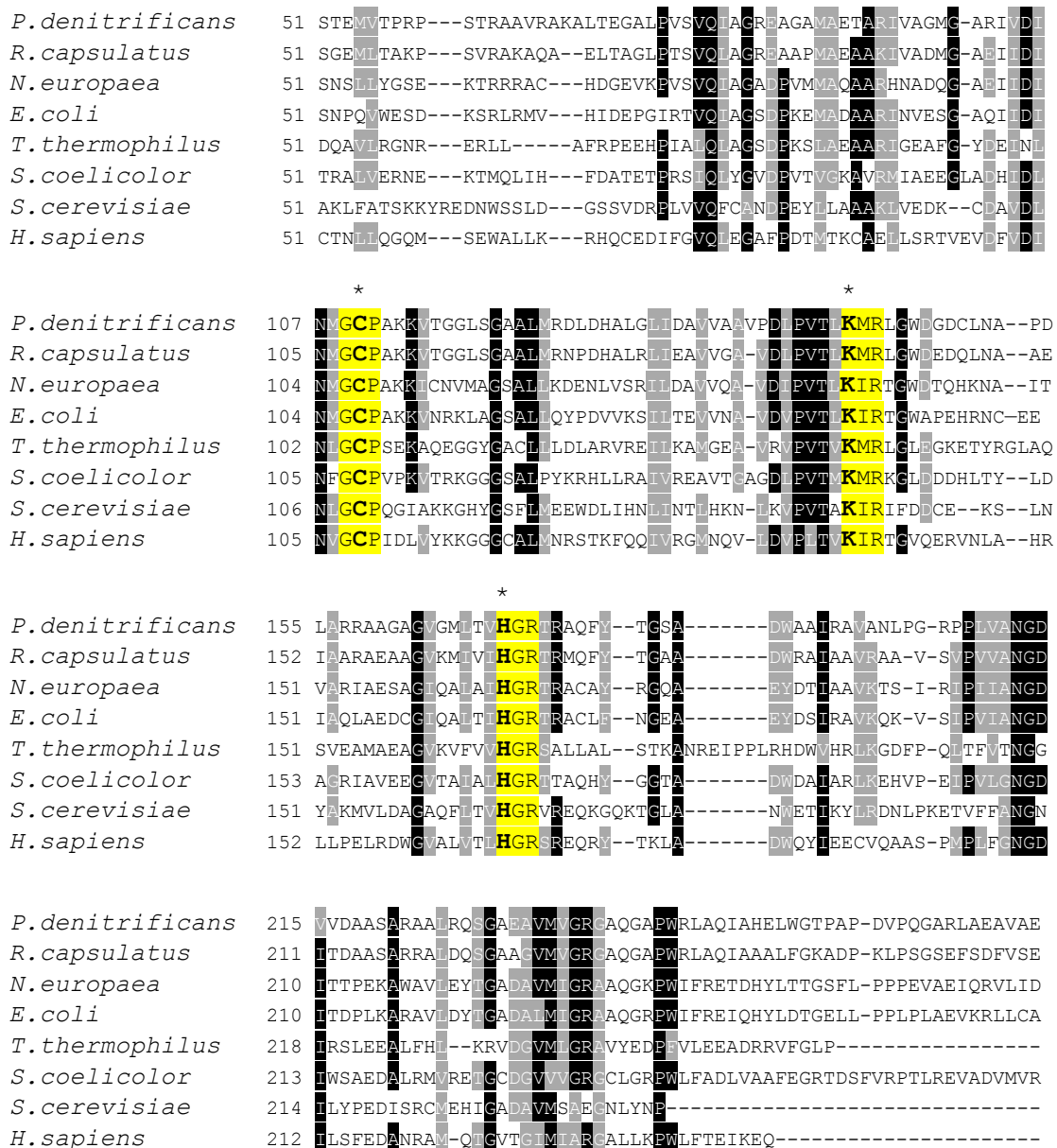


Figure 1.16. Primary sequence alignment demonstrating evolutionary conservation of dihydrouridine synthases. Bioinformatic analysis of NifR3 from *P. denitrificans* using BLAST (NCBI) retrieved primary sequences for DUS from selected organisms, aligned via Clustal Omega (EMBL-EBI) and shaded using BoxShade Server (ExPASy). Alignment depicts the conservation of the tRNA-DUS superfamily between a closely related α -proteobacteria; *Rhodobacter capsulatus*, β -proteobacteria; *Nitrosomonas europaea*, γ -proteobacteria; *Escherichia coli*, a deinococci; *Thermus thermophilus*, the Gram-positive actinobacteria; *Streptomyces coelicolor*, a fungus; *Saccharomyces cerevisiae*, and the significantly distant eukaryote; *Homo Sapiens*. The conserved catalytic motifs are shaded yellow and the three key catalytic residues are marked with asterisks: C110, K150 and H180. Adapted from Kasprzak (Kasprzak et al. 2012).

```

DusA 1 -----
DusB 1 -----
DusC 1 VLLAPMEGVLDLSDLVRELLTEVNDYDLCITEFVRVVDQLLPVKVFHRCPELQNASRTPSG

DusA 1 ----LQLGGSDDPAALAQCAKLAEARGYDEININVCPSDRVQNGMFGACLMGNAQLVADC
DusB 1 ---TVQIAGSDPKEMADAARINVESGAQITDINMGCPAKKVMRKLASALIQYPDVVKSI
DusC 61 TLVRVQLLGQFPQWLAENARAVELGSWGVDTNCGCPSKTVNGSGGGATLLKDPPELLYQG

DusA 57 VKAMR--DVVSIPTVVKTRIGIDDQDSYEFLCDFFINTVSGKGECEMFIHARKAWLSGLS
DusB 58 LTEVV--NAVDPVTIKIRITGWAPENR---NCEETIAQLAEDCGIQALTIHGRTRAC----
DusC 121 AKAMREAVPAHLPVSVKVRILGWDSDEK---KFE--IADAVQQAGATELVVHGRTRKEQ----

DusA 115 PKENREIPPLDYPRVYQLKRDFPHITMSINGGIKSLEEAKA--HLQHMDGVMVGREAYQN
DusB 109 ---LFNG-EAEYDSTRAVKQK-VSTPVIANGDITAPLKKARAVLDYTGADAIMIGRAAQGR
DusC 173 ---GYRAEHIHWQATGEIRQR-LNIPVIANGETWQWQSAQQCIAISGCDAVMIGRGALNI

DusA 173 PGILAAVDREIFGSSDT-----
DusB 164 PWIFREIQHYLDTGELLPLPLAEVKRLLCAHVRELHDFYGPAKGYRIARKHVSWYLQEH
DusC 229 P-----

```

Figure 1.17. Primary sequence alignment of the individual DUS classes from *Escherichia coli*. Amino acid sequences for DusA, B and C from *E. coli* were aligned via Clustal Omega (*EMBL-EBI*) and shaded based on sequence conservation using BoxShade Server (*ExPASy*). The three key catalytic residues are marked with asterisks; C110, K150 and H180. Adapted from Kasprzak (Kasprzak et al. 2012).

with ~30 % identity observed for the primary amino acid sequence between A, B and C from the same organism (Figure 1.17).

Additional domains are observed on the N-terminus of DusC and the C-terminus of DusB, whilst the core sequence exhibits large degrees of variation. This primary sequence flexibility may account for the different nucleotide consensus sequences and recognition of individual aminoacyl-tRNA molecules. It has also been experimentally demonstrated by construction of *dus* mutants that the individual classes do not compensate for each other, thus conferring strict specificity (Xing et al. 2004).

1.9.1.2 Protein structure and catalytic mechanism

DUS are relatively small (~35 kDa), monomeric, hydrophilic proteins localised to the cytoplasm where their RNA substrates are located. They contain a core TIM-barrel motif fold which coordinates the FMN cofactor close to the surface of the protein ensuring accessibility as an active site during tRNA docking (Figure 1.18). DUS typically comprise an N-terminal catalytic domain harbouring the flavin cofactor, a central tRNA-recognition domain and a C-terminal dsRNA binding domain (Whelan et al. 2015). Sequence alignment of various DUS in Figure 1.16 clearly demonstrates large degrees of variation in the C-terminal region which contains the dsRNA binding domain, possibly serving to accurately discriminate between tRNA structures for specific targeting.

Transient association of the tRNA transcript with a DUS is largely achieved by interactions contributed from both the D- and T-loops, most likely at a recognisable nucleotide consensus sequence surrounding the target uridine. In addition, it is observed the C-terminal dsRNA binding-domain clearly interacts with the tRNA at a distant site to the catalytic center. Once bound, the uridine substrate is rotated out of the helical tRNA structure, via large conformational changes, and protrudes out into the surface-exposed active site where FMN is placed within close proximity to catalyse electron transfer.

The active site spatial arrangement (Figure 1.18C) demonstrates the role of FMN and cysteine 110 in stable complex formation during catalysis. The pyrimidine ring exhibits π -stacking interactions with the isoalloxazine ring of FMN, whilst cysteine 110 coordinates uridine by temporarily forming a covalent thioether bond between its side chain sulfur and carbon 5 of the base ring. In addition, lysine 150 and histidine 180 reside close enough to the active site to participate in catalysis, possibly by coordinating FMN.

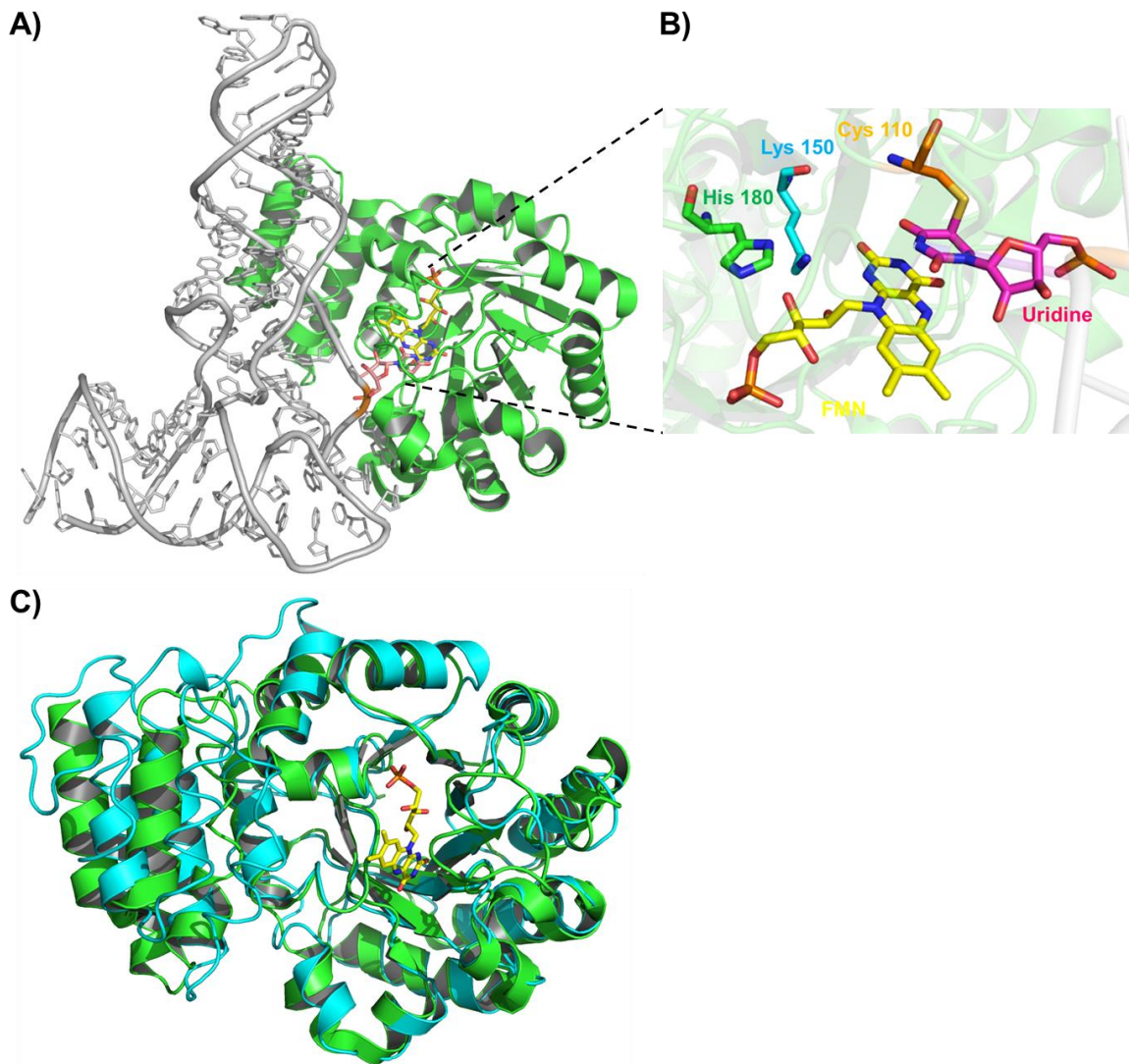


Figure 1.18. Quaternary structure of a dihydrouridine synthase in complex with tRNA. The X-ray crystal structure of dihydrouridine synthase (green) in complex with tRNA^{Phe} (grey) from *Thermus thermophilus*, PDB 3B0V (Yu et al. 2011). A) The flavin mononucleotide (FMN) cofactor (yellow) and uridine 20 (pink) are displayed as sticks. B) Close-up depiction of the active site configuration. The three conserved catalytic residues are highlighted as sticks: Cysteine 110 (orange), lysine 150 (blue) and histidine 180 (green). C) A predicted 3D model of NifR3 from *P. denitrificans* was produced using Phyre 2 software using its amino acid sequence and solved structures of highly identical proteins (Kelley et al. 2015). The predicted structure of NifR3 (blue) was aligned to the solved structure of *T. thermophilus* DUS (green). Figures were manipulated using PyMOL.

Once this transient complex is stable, two hydrogen atoms, arising from NAD(P)H which is proposed to reduce DUS prior to tRNA docking (Rider et al. 2009), are transferred from DUS-FMN to the C5 and C6 atoms of the uracil ring. The hydrogens are believed to be sequentially provided by FMN and cysteine 110, both laying within 4 Å thus being feasible for transfer, with a mechanism proposed by Yu and coworkers outlined below:

A hydride is initially transferred from N5 of FMNH₂ to the weakly electrophilic C6 of the pyrimidine ring, which breaks the double bond. Electrons move to C5 and this newly formed nucleophilic lone pair now attacks the thiol group of cysteine 110, removing the distal hydrogen atom to produce dihydrouridine lacking the initial double bond. This second step appears to form the transient covalent bond captured in the crystal structure between cysteine and uridine, forming a structural analogue reaction intermediate. The result of catalysis is a change in configuration from planar uridine to a more distorted shape that leads to product release (Yu et al. 2011). The reduction potentials of NAD(P)⁺/NAD(P)H and FMNH₂ are -320 and -110 mV, respectively (subject to change in the protein environment), which supports NAD(P)H reduction of the FMN cofactor prior to catalysis (Hillard et al. 2008; Oprian & Coon 1982).

1.9.1.3 Physiological function of tRNA-dihydrouridine synthases

The persistent occurrence of dihydrouridine in the D-loop of each organism underscores a clear important biochemical role during protein synthesis. Despite this, very few studies have been conducted into the physiological role its formation contributes in tRNA and, more broadly, cellular responses. As a result, the precise function of dihydrouridine towards regulating protein synthesis is still elusive. Furthermore, the differential dihydrouridine modification at various positions within the D-loop, and between independent aminoacyl-tRNA by the different DUS classes is also unstudied.

What is known is that the D-loop in the tertiary structure of folded tRNA primarily acts as a recognition site for aminoacyl-tRNA synthetases (AATS) (Hardt et al. 1993; Smith & Yarus 1989). AATS catalyse the loading of their specific amino acid onto their target tRNA compound via esterification, giving the aminoacyl-tRNA structure necessary for protein translation (Woese et al. 2000). As individual AATS recognise their specific tRNA transcript to load with an amino acid, perhaps dihydrouridine formation at specific positions of the D-loop provides fine-tuning of the recognition site stereochemistry for matching amino acids with correct tRNA compounds.

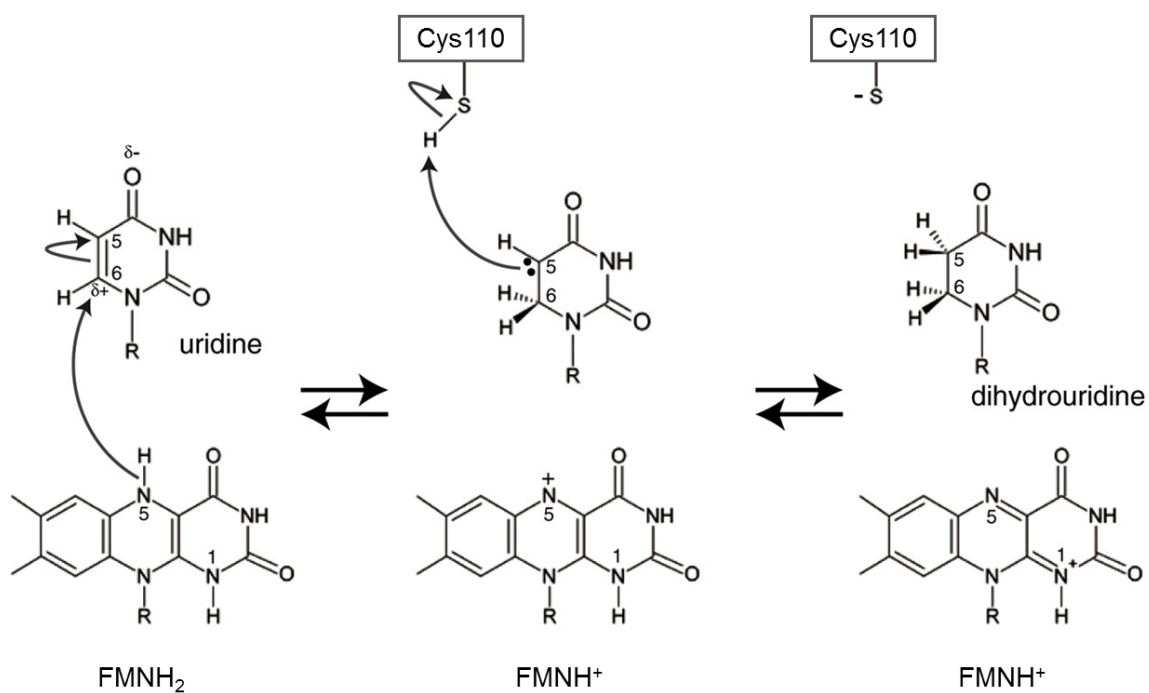


Figure 1.19. Catalytic mechanism for flavin-dependant dihydrouridine synthesis. The proposed reaction mechanism for the DUS-catalysed NAD(P)H-dependant reduction of the 5,6 C-C double bond in the pyrimidine ring of uridine. A hydride species from FMNH₂ first attacks the mildly electrophilic C6 of uridine, breaking the double bond and generating a lone electron pair on C5. This nucleophilic group subsequently takes a proton from the distal thiol group of the conserved cysteine residue to produce reduced dihydrouridine. Figure Adapted from Yu, 2011 (Yu et al. 2011).

The introduction of dihydrouridine promotes conformational flexibility and dynamic motion of the tRNA compound due to the loss of the 5,6 double bond and planar structure (Suck et al. 1971). This results in the resistance of base-pair stacking with adjacent nucleotides due to a lack of π -interactions (Quigley & Rich 1976). Dihydrouridine puckers out of the plane, hampering the ability to form rigidly ordered strands of RNA thus increasing conformational flexibility of tertiary structure.

A previous study by Dalluge and coworkers investigated the structural implications of dihydrouridine formation from a thermodynamic perspective. The research concluded that the modified base adopts a C2'-endo sugar conformation as opposed to the typical C3'-endo form adopted by ribose moieties. The C2'-endo conformer is inherently more flexible due to its ability to accommodate a large range of glycosyl torsion angles (Dalluge et al. 1996). Whilst C3'-endo helps increase regional stability of nucleotide polymers via ordered base-stacking, introduction of C2'-endo nucleotides increases the dynamic motion of polynucleotides. Emerson and Sundaralingam proposed this contributes to the formation of the D-loop structure by increasing molecular flexibility in the local area, and thus lowering the energy required for loop folding (Emerson & Sundaralingam 1980). Dihydrouridine has also been identified in loop-domains of the 23s rRNA of *E. coli*, implicating a potentially more universal biochemical role in RNA maturation than initially thought (Kowalak et al. 1995). Furthermore, an investigation into psychrophilic bacteria brought to light an abundance of dihydrouridine in cytoplasmic tRNA, around 50% higher than those recorded in mesophiles. Due to the compromise of thermal energy in their extreme cold environments, increased levels of dihydrouridine would likely compensate for the lack of dynamic motion by maintaining the necessary level of conformational flexibility required in tRNA (Dalluge et al. 1997).

Whilst the precise intricacies of how formation at various positions differentially regulates target protein biosynthesis are currently unknown, it can be hypothesised that the modification increases tRNA flexibility, possibly promoting the folding of the D-loop to help recognise AATS to load the tRNA with the correct amino acid.

1.9.2 Phylogenetic distribution and conservation of bacterial *nifR3*

NifR3 appears to be an unprecedented nitrogen-responsive class of the DUS superfamily, upregulated in *P. denitrificans* when grown with nitrate as a sole source. The *nifR3* gene is located immediately upstream of the general nitrogen regulators *ntrB* (*nifR2*) and *ntrC* (*nifR1*), believed to comprise an operon with the downstream *ntrYX* genes and expressed during nitrogen stress to mediate a regulatory response.

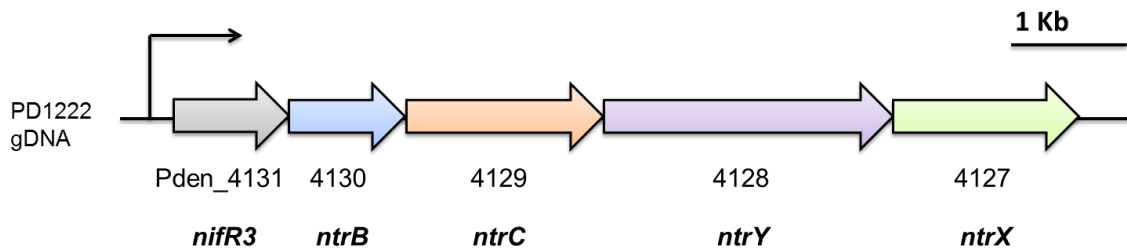


Figure 1.20. Genetic organisation of the nitrogen-responsive *nifR3-ntrBCYX* operon in *P. denitrificans*. Representation of the open reading frames coding for the hypothetical NifR3 and the two-component, general nitrogen regulatory systems NtrBC and NtrYX, on chromosome II of *P. denitrificans* genome.

Using bioinformatic analysis, *nifR3* has so far been identified solely in bacteria. The *nifR3-ntrBC* organisation is tightly conserved across α -proteobacteria where Ntr acts as the general nitrogen regulatory system. However, in some cases within databases, such as *Azospirillum brasilense*, it is annotated as *dusB*. In various β - and γ -proteobacteria, an alternative yet similar gene cluster is present, *dus-fis*, where Fis is a broad gene regulator believed to have arisen from NtrC via horizontal gene transfer during evolutionary divergence (Xu & Johnson 1995). However, no studies have investigated the nitrogen-responsiveness of this operon and thus we cannot conclude if these Dus proteins behave in a similar manner as NifR3, despite in some cases they're annotated as "NifR3-like". Furthermore, "NifR3-like" proteins were identified in several organisms outside the proteobacteria class such as *S. elongatus* and *Chamaesiphon minutus*. These bacteria lack the *ntr* system and thus make it difficult to speculate whether these genes are functional homologues of NifR3 or incorrect annotations for DUS proteins.

The distribution of *nifR3* within bacteria does not appear to be consistent with the capacity to assimilate nitrate. For example, the actinobacteria *Streptomyces coelicolor* contains an assimilatory nitrate reductase but no identifiable *nifR3*, whilst the Alphaproteobacteria *Rhodobacter sphaeroides* contains a copy of genomic *nifR3* yet lacks a Nas system. Furthermore, all Alphaproteobacteria contain a *nifR3* but there exists great divergence between species in terms of nitrogen-metabolic pathways they can perform, giving no clear correlation between the gene and the physiological role.

A phylogenetic tree for several DusA, B and C proteins from various bacteria is shown below in Figure 1.21 (Kasprzak et al. 2012). It is clearly seen that both DusA and DusC are clustered individually and form distinct clades of the superfamily despite the taxonomy of the organism with DusA appearing to be the most distantly related of the classes based upon branch length. Interestingly, the selected NifR3 proteins integrated

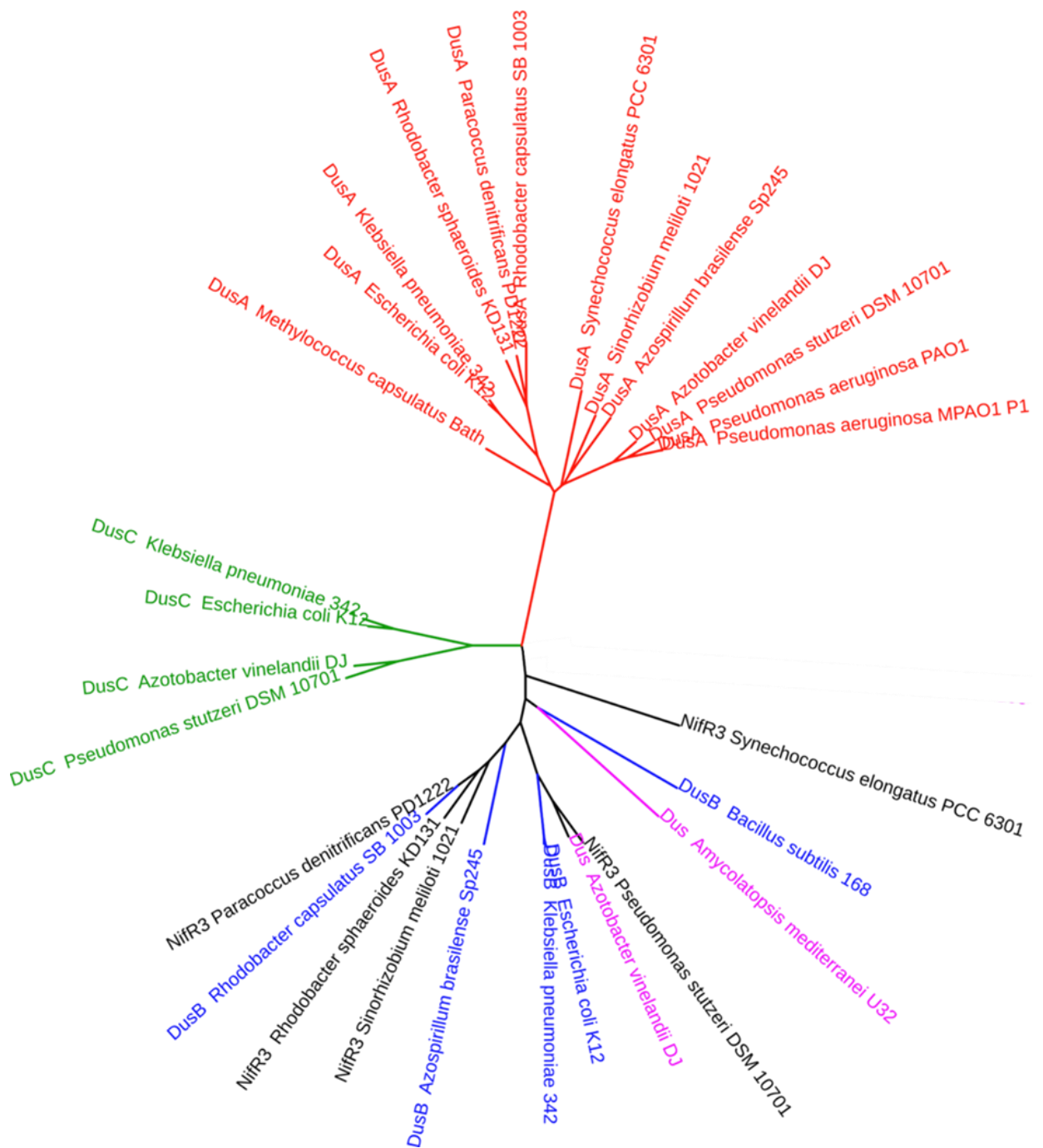


Figure 1.21. Phylogenetic tree for the individual clades of the dihydrouridine synthase superfamily from select bacteria. Examples of DusA (red), DusB (blue), DusC (green), unannotated Dus (pink) and NifR3 (black) were selected from a diverse range of bacteria following BLAST (NCBI) of the NifR3 protein from *P. denitrificans*. The retrieved amino acid sequences were used to construct a phylogenetic tree using Interactive Tree of Life (Letunic & Bork 2007) which depicts the relatedness of the proteins by organising them based upon sequence conservation. Figure adapted from Kasprzak (Kasprzak et al. 2012).

within the DusB branch, rather than occupying a separate distinct space of the tree. This could imply NifR3 behaves as a nitrogen-responsive form of the DusB class, or, as the gene upstream of *ntrB* is sometimes annotated as *dusB*, perhaps all DusB proteins are NifR3 members. Additionally, the “NifR3-like” protein expressed by the cyanobacteria *S. elongatus* is more distinct from those of the proteobacteria, adding evidence for the case of incorrect annotations and we must be careful when identifying “true” NifR3 proteins.

1.9.3 NifR3 as a potential regulator of the bacterial nitrogen-response

The genetic organisation and co-transcription of *nifR3-ntrBC* in tandem with its strong evolutionary conservation hints towards a regulatory role in the nitrogen-response of a widespread range of microorganisms. *P. denitrificans* additionally encodes a *dusA* on Chromosome I which presumably acts as the housekeeping DUS to modulate required basal levels of dihydrouridine within transcribed RNA. However, there have been no previous reports for a regulatory response governed by rapid formation of tRNA-dihydrouridine in response to environmental stimuli. NifR3 may represent a novel regulatory mode for cellular response and alteration of gene/protein expression via the modification and processing of RNA. Initial studies were performed by Foster-Hartnett and coworkers in *R. capsulatus* who demonstrated the cotranscription of *nifR3-ntrBC* during dinitrogen fixation (Foster-Hartnett et al. 1994). However, the study was unable to conclude a clearly defined function for NifR3 under these conditions. We postulate that NifR3 may contribute to the expression and biosynthesis of the NasABGHC structural proteins during nitrate-dependent growth of *P. denitrificans* and this hypothesis will be tested in this study.

1.10 Aims and Objectives

There were four primary aims for the study conducted here which were addressed using a combination of microbiology, molecular biology and protein biochemistry. We aimed to establish whether a clear link could be defined between the availability and redox state of a carbon source and the ability to assimilate nitrate during heterotrophic growth (Chapter 3). In addition, we explored the biochemical nature of NifR3 and investigated potential post-transcriptional regulatory roles and physiological functions it may perform through alteration of tRNA compounds (Chapter 4 and 5). To further elucidate the regulation of *nasABGHC*, the typical candidates for controlling expression of nitrogen-responsive genes, NtrBC and sigma54, were studied. Finally, the involvement of NarJ in the biogenesis of fully functional assimilatory nitrate reductase during aerobic nitrate-dependent growth was investigated (Chapter 6).

Chapter 2: Materials and Methods

2.1 Media and Growth Conditions

Media and buffers used during this work were prepared with analytical grade water, conductivity = 0.4 microsieme (*Fisher Scientific*). Growth media was sterilised at 121 °C for 15 min using an autoclave (*LTE Scientific*) and growth media additions were filtered using a vacuum pump and 0.22 µm nitrocellulose filter paper (*Sartorius Stedim*).

Bacterial batch cultures were routinely grown in either of the two media presented below. *E. coli* strains were grown at 37 °C and agitated in a rotary shaker at 200 rpm. *P. denitrificans* was cultured at 30 °C either with agitation or without to ensure anaerobicity. Growth was measured spectrophotometrically by recording the Optical Density (OD_{600 nm}) of a culture in a 1 cm polystyrene cuvette (*Sarstedt*) using a BioPhotometre (*Eppendorf*). Batch cultures were inoculated with 1 % (v/v) of stationary cells pre-cultured in appropriate conditions. Solid media contained 1.5 % Agar (*Formedium Ltd.*).

Aerobic growth was achieved by growing 50 mL cultures in 250 mL conical flasks. Anaerobic cultures were grown as 400 mL samples in 500 mL Duran bottles with screw tight lids and gas-tight silicone septa for sampling of liquid (for optical density and HPLC analysis). Atmosphere was evacuated by sparging with N₂ for 20 min (Compressed nitrogen (oxygen-free), *BOC*).

The dry mass of cell cultures was obtained by placing the harvested cell pellet, of a culture grown to stationary phase, in a desiccator attached to a vacuum freeze dryer (*Modulyo*). This was left for 24 h at -40 °C with a pressure of 0.05 mbar, and the final measured weight of the desiccated pellet was converted to mg cells/mL culture.

2.1.1 Luria-Bertani (LB) medium

Luria-Bertani (LB) medium (Maniatis *et al.*, 1982) was used to culture both *E. coli*, *P. denitrificans*, and all derivative strains which contained, per litre dH₂O:

Tryptone **10 g**, NaCl **10 g**, Yeast extract **5 g**

The following antibiotics and supplements were used according to Table 2.1.

2.1.2 Minimal salt medium

A defined minimal medium was used for batch culture of *P. denitrificans* under controlled conditions. It contained, per litre dH₂O:

Na₂HPO₄ **4.1 g** (29 mM), KH₂PO₄ **1.5 g** (11 mM), MgSO₄.7H₂O **98 mg** (0.4 mM), pH 7.5

Table 2.1. Antibiotics and supplements used throughout this thesis

Antibiotics	Solvent	[Stock] (mg/mL)	[Final] (µg/mL)	Storage
Carbenicillin	dH ₂ O	100	100	4 °C
Kanamycin	dH ₂ O	50	50	4 °C
Streptomycin	dH ₂ O	60	60	4 °C
Tetracycline	100% Ethanol	5	5	-20 °C, tinfoil
Gentamycin	dH ₂ O	25	25	4 °C
Rifampicin	100% Methanol	50	50	4 °C, tinfoil
Supplement	Solvent	[Stock] (M)	[Final] (mM)	Storage
IPTG	dH ₂ O	1	0.1-1	4 °C
X-gal	2,2- dimethylformamide	0.1	0.1	-20 °C, tinfoil
Taurine	dH ₂ O	0.5	1-10	Room temp.

Throughout this study a variety of carbon and nitrogen sources were used in a range of concentrations to supplement growth. Unless stated otherwise, typical growth was achieved with 30 mM sodium succinate as a carbon source. Aerobic cultures were grown with either 10 mM NH₄Cl, NaNO₃ or NaNO₂ as sole nitrogen sources. Anaerobic growth was achieved with 10 mM NH₄Cl for nitrogen and 20 mM NaNO₃ as a terminal electron acceptor.

Cultures were supplemented with 2 mL/L of Vishniac-Santer trace elements (Vishniac & Santer 1957) which was composed as outlined in Table 2.2. The Vishniac-Santer trace element solution was adjusted to pH 7.5 using 10 M NaOH and stored at 4 °C in a glass container that was treated with 35 % (v/v) nitric acid prior to use to remove metal contamination and rinsed with analytical grade water. Solution was filtered with 0.20 µM nitrocellulose filters (*Sartorius Stedim*) prior to use.

Table 2.2. Composition of Vishniac-Santer trace elements solution.

Compound	Grams/Litre	[Initial] (mM)	[Final] (µM)
EDTA	38	130	260
ZnSO ₄ .7H ₂ O	2.19	7.64	15.28
MnCl ₂ .4H ₂ O	4.95	25	50

FeSO ₄ .7H ₂ O	5.14	18.5	37
Na ₂ MoO ₄ .2H ₂ O	0.22	0.89	1.78
CuSO ₄ .5H ₂ O	1.6	6.4	12.8
CoCl ₂ .6H ₂ O	1.6	6.72	13.4
CaCl ₂ .2H ₂ O	5.5	37.4	74.8

2.2 Bacterial Strains and Plasmids

Strains were routinely stored as 25 % (v/v) glycerol stocks by adding 1 mL of culture, grown to stationary phase in LB media, to 1 mL of sterile, 50 % (v/v) glycerol in a pre-sterilised screw-cap tube. Samples were snap-frozen in liquid nitrogen and stored at -80 °C. The strains used in this thesis are detailed in Table 2.3.

Table 2.3. Bacterial strains used during this thesis.

Bacteria	Characteristics	Source
<i>Escherichia coli</i>		
JM101	Used as a host for small plasmids, <i>recA</i> ⁺	(Messing 1979)
803	Used as a host for large plasmids, Met ⁻	(Wood 1966)
DH5α	Used for transformation of pGEMT-Easy-based plasmids	(Hanahan 1983)
BL21 (DE3)	Used as a protein expression strain for pET derived plasmids, T7 RNA polymerase	(Studier et al. 1990)
<i>P. denitrificans</i>		
Pd1222 (PdWT)	Wild-type strain, enhanced conjugation frequencies, Rif ^r , Spec ^r	(de Vries et al. 1989)
PdΔ <i>ntrBC</i>	<i>ntrBC</i> deletion mutant of Pd1222, Rif ^r , Spec ^r	Donated by M.J.Sullivan
Pd <i>ntrBY</i> Δ::Km,Str	Non-polar Km ^r and Str ^r mutant of Pd1222, deficient in <i>ntrB</i> and <i>ntrY</i> , Rif ^r , Spec ^r	Donated by V. Luque-Almagro
Pd <i>nasT</i> Δ::Str	Non-polar Str ^r mutant of Pd1222, deficient in <i>nasT</i> , Rif ^r , Spec ^r	(Luque-Almagro et al. 2013)
PdΔ <i>nifR3</i>	<i>nifR3</i> deletion mutant of Pd1222, Rif ^r , Spec ^r	This work
PdΔ <i>narJ</i>	<i>narJ</i> deletion mutant of Pd1222, Rif ^r , Spec ^r	This work

Pd Δ <i>dusA</i>	<i>dusA</i> deletion mutant of Pd1222, Rif ^r , Spec ^r	This work
Pd Δ <i>sigma54</i>	<i>sigma54</i> deletion mutant of Pd1222, Rif ^r , Spec ^r	This work
<i>P. pantotrophus</i>		
Pp Δ <i>napD</i>	<i>napD</i> deletion mutant of <i>P. pantotrophus</i>	(Wood et al. 2002)

Table 2.4. Vectors used and constructed in this thesis.

Plasmid	Characteristics	Source
pGEMT-Easy	<i>lacZ</i> , sub-cloning vector, Amp ^r	Promega
pBluescript	M13 phagemid, <i>lacZ</i> , Amp ^r	(Short et al. 1988)
pJET1.2	<i>Eco47IR</i> , sub-cloning vector, Amp ^r	Thermo Scientific
pUC57	<i>lacZ</i> , sub-cloning vector, Amp ^r	GenScript
pRK2013	Mobilising plasmid in tri-parental crosses, Km ^r	(Figurski & Helinski 1979)
pK18 <i>mobsacB</i>	<i>mob</i> ⁺ , allelic exchange suicide vector, sucrose-sensitive, Km ^r	(Schäfer et al. 1994)
pLMB509	<i>mob</i> ⁺ , expression plasmid, <i>tauP</i> , Gm ^r	(Tett et al. 2012)
pET-24a	Expression plasmid, T7 promoter, <i>lacI</i> , Km ^r	Novagen
pET-28a	Expression plasmid, T7 promoter, <i>lacI</i> , Km ^r	Novagen
pMP220	<i>mob</i> ⁺ , transcriptional <i>lacZ</i> -protein fusion vector, Tet ^r	(Spaink et al. 1987)
pIJ1363	<i>mob</i> ⁺ , translational <i>lacZ</i> -protein fusion vector, Tet ^r	(Rossen et al. 1985)
pBP001	pGEMT-Easy-derivative containing 681 bp <i>EcoRI</i> - <i>XbaI</i> fragment used to construct pBP003, Amp ^r	This work
pBP002	pGEMT-Easy-derivative containing 646 bp <i>XbaI</i> - <i>PstI</i> fragment used to construct pBP003, Amp ^r	This work
pBP003	pGEMT-Easy-derivative containing 1227 bp <i>EcoRI</i> - <i>PstI</i> fragment used to construct pBP005, Amp ^r	This work
pBP004	pGEMT-Easy-derivative containing 1103 bp <i>NdeI</i> - <i>NdeI</i> fragment used to construct pBP006, Amp ^r	This work

pBP005	pK18 <i>mobsacB</i> -derivative, construct for PdΔ <i>nifR3</i> , Km ^r	This work
pBP006	pLMB509-derivative containing intact <i>nifR3</i> , Gm ^r	This work
pBP007	pJET1.2-derivative containing 761 bp <i>EcoRI-XbaI</i> fragment used to construct pBP009, Amp ^r	This work
pBP008	pJET1.2-derivative containing 751 bp <i>XbaI-PstI</i> fragment used to construct pBP009, Amp ^r	This work
pBP009	pJET1.2-derivative containing 1512 bp <i>EcoRI-PstI</i> fragment used to construct pBP011, Amp ^r	This work
pBP010	pJET1.2-derivative containing 699 bp <i>NdeI-NdeI</i> fragment used to construct pBP012, Amp ^r	This work
pBP011	pK18 <i>mobsacB</i> -derivative, construct for PdΔ <i>narJ</i> , Km ^r	This work
pBP012	pLMB509-derivative containing intact <i>narJ</i> , Gm ^r	This work
pBP013	pJET1.2-derivative containing 718 bp <i>EcoRI-XbaI</i> fragment used to construct pBP015, Amp ^r	This work
pBP014	pJET1.2-derivative containing 608 bp <i>XbaI-PstI</i> fragment used to construct pBP015, Amp ^r	This work
pBP015	pJET1.2-derivative containing 1326 bp <i>EcoRI-PstI</i> fragment used to construct pBP016, Amp ^r	This work
pBP016	pK18 <i>mobsacB</i> -derivative, construct for PdΔ <i>dusA</i> , Km ^r	This work
pBP017	pJET1.2-derivative containing 628 bp <i>EcoRI-XbaI</i> fragment used to construct pBP015, Amp ^r	This work
pBP018	pJET1.2-derivative containing 653 bp <i>XbaI-PstI</i> fragment used to construct pBP015, Amp ^r	This work
pBP019	pJET1.2-derivative containing 1281 bp <i>EcoRI-PstI</i> fragment used to construct pBP016, Amp ^r	This work
pBP020	pK18 <i>mobsacB</i> -derivative, construct for PdΔ <i>sigma54</i> , Km ^r	This work
pBP021	pUC57-derivative containing 1065 bp <i>NdeI-XhoI</i> fragment used to construct pBP022, 23, 24, Amp ^r	This work
pBP022	pE-T24a-derivative, expression construct for NifR3_6His, Km ^r	This work
pBP023	pE-T24a-derivative, expression construct for NifR3, Km ^r	This work

pBP024	pET-28a-derivative, expression construct for 6His_NifR3, Km ^r	This work
pBP025	pBP006-derivative, with <i>nifR3</i> stop codon altered to CAT, expression construct for NifR3_6His, Gm ^r	This work
pBP026	pBP006-derivative, NifR3 C110G mutant, Gm ^r	This work
pBP027	pBP006-derivative, NifR3 K150M mutant, Gm ^r	This work
pBP028	pBP006-derivative, NifR3 H180L mutant, Gm ^r	This work
pBP029	pJET1.2-derivative containing 711 bp <i>NdeI-NdeI</i> fragment used to construct pBP030, Amp ^r	This work
pBP030	pLMB509-derivative, expression construct for NarJ_6His, Gm ^r	This work
pBP031	pJET1.2-derivative containing 553 bp <i>EcoRI-PstI</i> fragment used to construct pBP042, Amp ^r	This work
pBP032	pJET1.2-derivative containing 527 bp <i>EcoRI-PstI</i> fragment used to construct pBP043, Amp ^r	This work
pBP033	pJET1.2-derivative containing 553 bp <i>BamHI-BamHI</i> fragment used to construct pBP044, Amp ^r	This work
pBP034	pJET1.2-derivative containing 527 bp <i>BamHI-BamHI</i> fragment used to construct pBP045, Amp ^r	This work
pBP035	pJET1.2-derivative containing 791 bp <i>EcoRI-PstI</i> fragment used to construct pBP046, Amp ^r	This work
pBP036	pJET1.2-derivative containing 666 bp <i>EcoRI-PstI</i> fragment used to construct pBP047, Amp ^r	This work
pBP037	pJET1.2-derivative containing 639 bp <i>EcoRI-PstI</i> fragment used to construct pBP048, Amp ^r	This work
pBP038	pJET1.2-derivative containing 666 bp <i>EcoRI-XhoI</i> fragment used to construct pBP049, Amp ^r	This work
pBP039	pJET1.2-derivative containing 760 bp <i>EcoRI-PstI</i> fragment used to construct pBP050, Amp ^r	This work
pBP040	pJET1.2-derivative containing 817 bp <i>EcoRI-PstI</i> fragment used to construct pBP051, Amp ^r	This work
pBP041	pJET1.2-derivative containing 753 bp <i>EcoRI-PstI</i> fragment used to construct pBP052, Amp ^r	This work
pBP042	pMP220-based transcriptional fusion of <i>nasA-lacZ</i> , Tet ^r	This work
pBP043	pMP220-based transcriptional fusion of <i>nasT-lacZ</i> , Tet ^r	This work

pBP044	pIJ1363-based translational fusion of <i>nasA-lacZ</i> , Tet ^r	This work
pBP045	pIJ1363-based translational fusion of <i>nasT-lacZ</i> , Tet ^r	This work
pBP046	pMP220-based transcriptional fusion of <i>nifR3-lacZ</i> , Tet ^r	This work
pBP047	pMP220-based transcriptional fusion of <i>glnA-lacZ</i> , Tet ^r	This work
pBP048	pMP220-based transcriptional fusion of <i>gltD-lacZ</i> , Tet ^r	This work
pBP049	pMP220-based transcriptional fusion of <i>gdhA-lacZ</i> , Tet ^r	This work
pBP050	pMP220-based transcriptional fusion of <i>dnaN-lacZ</i> , Tet ^r	This work

2.3 Oligonucleotide Design and Primers Used

DNA oligonucleotides were ordered from MWG Eurofins Genomic (Ebersberg, Germany) and designed using Primer 3 Plus software alongside Artemis Genome Browser (*Sanger*). PCR primer pairs were chosen with high similarity of melting temperature (T_m), optimum T_m of ~60 °C, and length of 18-22 bases. Oligonucleotides incorporating artificial restriction sites were added onto the 5' end of the primer, with appropriate bases upstream to ensure maximum cutting efficiency. For qRT-PCR, oligonucleotide probes were designed to choose sites lacking in secondary structure and to create ~150 bp fragment. Probes for Northern Blot analysis were designed with an optimum length of 30 bp to ensure specific DNA:RNA hybridisation, and labelled at the 3' end with digoxigenin. Primer sequences and use are listed in Table 2.5.

Table 2.5. Primers used in this study.

Name	Sequence	Usage
Cloning		
5F_nifR3	AC GAATTC CCGCCGATCGAGTAATAGAC	For cloning fragment used in pBP001, <i>EcoRI</i>
5R_nifR3	CAT TCTAGA GCAGTGTCATGGGAGAACT	For cloning fragment used in pBP001, <i>XbaI</i>
3F_nifR3	ACT TCTAGA AATGGCGACGTGGTGGAT	For cloning fragment used in pBP002 <i>XbaI</i>
3R_nifR3	CAC TGCAG AGCCGCTTGAGCATCTCG	For cloning fragment used in pBP002, <i>PstI</i>

F_compnifR3	CA CATATG ACACTGCCCGAACCCAT	For cloning fragment used in pBP004, <i>NdeI</i>
R_compnifR3	GAC CATATG ATCTCGGGATCGGGCAGCATG	For cloning fragment used in pBP004, <i>NdeI</i>
nifR3_FCheck	TGAAGATGTCGAAGACGGAAA	PCR check of <i>nifR3</i>
nifR3_RCheck	CATACCAGCCCAGGTGCTT	PCR check of <i>nifR3</i>
5F_narJ	GAG GAATTC AACCTGCGTCGGCCGCATCC	For cloning fragment used in pBP007, <i>EcoRI</i>
5R_narJ	GAT TCTAGA CTCGGAAGCTTTTCATGCGA	For cloning fragment used in pBP007, <i>XbaI</i>
3F_narJ	GAT TCTAGA GCCGTCTGGGAAGAGGCGCA	For cloning fragment used in pBP008 <i>XbaI</i>
3R_narJ	GAC TGCAG GCCGAGATCATGTGGACAAG	For cloning fragment used in pBP008, <i>PstI</i>
F_compnarJ	GAC CATATG AAAAGCTTCCGAGCCCTTTC	For cloning fragment used in pBP010 & 029 <i>NdeI</i>
R_compnarJ	GAC CATATG TCATTGCGCCGGGTTGGCGA	For cloning fragment used in pBP010, <i>NdeI</i>
narJ_FCheck	GCAGCAGATCGACGAGATGT	PCR check of <i>narJ</i>
narJ_RCheck	GCCCAAGCCGTCGAATAC	PCR check of <i>narJ</i>
5F_dusA	GAG GAATTC GGATGAGCAGCATTTTG	For cloning fragment used in pBP013, <i>EcoRI</i>
5R_dusA	GAT TCTAGA TGCACACATAGAGCACA	For cloning fragment used in pBP013, <i>XbaI</i>
3F_dusA	GAT TCTAGA CGCTGTCGAGATAATAG	For cloning fragment used in pBP014, <i>XbaI</i>
3R_dusA	GAC TGCAG CGAACGGGGCATTCTGA	For cloning fragment used in pBP014, <i>PstI</i>
dusA_FCheck	CTACGGGGATGAACTGTCGT	PCR check of <i>dusA</i>
dusA_RCheck	CTTCCTGATCGGAGAGGTGA	PCR check of <i>dusA</i>
5F_sigma54	GAG GAATTC GGGAACGCATTGTTGGT	For cloning fragment used in pBP017, <i>EcoRI</i>

5R_sigma54	GAT CTAGA AGCTGCATCTTCTGGCT	For cloning fragment used in pBP017, <i>Xba</i> I
3F_sigma54	GAT CTAGA CCAAGTATCGGCTGGGA	For cloning fragment used in pBP018, <i>Xba</i> I
3R_sigma54	GAT CTCAG GCACATCATGCAGAAAT	For cloning fragment used in pBP018, <i>Pst</i> I
sigma54_F	GGGAACGCATTGTTGGTG	PCR check of <i>sigma54</i>
sigma54_R	TTAAAGACGTACTACACG	PCR check of <i>sigma54</i>
FnifR3_6his	GACCGAGGTGCCTTCACATATGCATCATC ACCAT	3 bp transversion of TGA to CAT in pBP006 to make pBP025
RnifR3_6his	ATGGTGATGATCCATATGTGAGGCACCTC GGT	3 bp transversion of TGA to CAT in pBP006 to make pBP025
F_C110G	AACATGGGCGGCCCGGCGAAGAA	1 bp transversion of T to G in pBP006 to make pBP026
R_C110G	TTCTTCGCCGGGCCCGCCCATGTT	1 bp transversion of T to G in pBP006 to make pBP026
F_K150M	GTGACGCTGATGATGCGGCTGG	1 bp transversion of A to T in pBP006 to make pBP027
R_K150M	CCAGCCGCATCATCAGCGTCAC	1 bp transversion of A to T in pBP006 to make pBP027
F_H180L	GACCGTGCTTGGCCGCACG	1 bp transversion of A to T

		T in pBP006 to make pBP028
R_H180L	CGTGCGGCCAAGCACGGTC	1 bp transversion of A to T in pBP006 to make pBP028
R_narJ6His	GAC CATATG TTGCGCCGGGTTGGCGA	For cloning fragment used in pBP029, <i>NdeI</i>
F_nasAtsc	GAG GAATTC CATTTCCGCACCGATCTTTA	For cloning fragment used in pBP031, <i>EcoRI</i>
R_nasAtsc	GAC CTGCAG AGCAGATGGTAAAGGCGAAG	For cloning fragment used in pBP031, <i>PstI</i>
F_nasTtsc	GAG GAATTC GATAGTGATGCACGGCCTTT	For cloning fragment used in pBP032, <i>EcoRI</i>
R_nasTtsc	GAC CTGCAG GGTTTCTTCCGAGATGATGC	For cloning fragment used in pBP032, <i>PstI</i>
F_nasAtl	GAG GATCC CATTTCCGCACCGATCTTTA	For cloning fragment used in pBP033, <i>BamHI</i>
R_nasAtl	GAG GATCC ACGTCCTTGCTGAGCAGCCA	For cloning fragment used in pBP033, <i>BamHI</i>
F_nasTtl	GAG GATCC GATAGTGATGCACGGCCTTT	For cloning fragment used in pBP034, <i>BamHI</i>
R_nasTtl	GAG GATCC GAGCGGTCCACGAACA	For cloning fragment used in pBP034, <i>BamHI</i>
F_nifR3tsc	GAG GAATTC ATCTTCGTCTCGCGGTTTTT	For cloning fragment used in pBP035, <i>EcoRI</i>
R_nifR3tsc	GAC CTGCAG ACCATCTCGCTGACCATCA	For cloning fragment used in pBP035, <i>PstI</i>

F_GStsc	GAG GAATTC CCCTTCAAACCTGGACGATGT	For cloning fragment used in pBP038, <i>EcoRI</i>
R_GStsc	GAC CTCGAG AGCGTCTTTTCGGCATAGAA	For cloning fragment used in pBP038, <i>XhoI</i>
F_GOGATtsc	GAG GAATTC GCGCTTTCGTCTATGACCTC	For cloning fragment used in pBP039, <i>EcoRI</i>
R_GOGATtsc	GAC CTGCAG GCGGTGTCGGTGATGTATTT	For cloning fragment used in pBP039, <i>PstI</i>
F_GDHtsc	GAG GAATTC TTTCGCACATCTGAAACAGG	For cloning fragment used in pBP040, <i>EcoRI</i>
R_GDHtsc	GAC CTGCAG AGCCGAGGAACTTGATGATG	For cloning fragment used in pBP040, <i>PstI</i>
F_dnaNtsc	GAG GAATTC GATGCAGTTCTATAGCGA	For cloning fragment used in pBP041, <i>EcoRI</i>
R_dnaNtsc	GAC CTGCAG CCGCAGCTTGTCGTTTCAG	For cloning fragment used in pBP041, <i>PstI</i>
F_pJET	CGACTCACTATAGGGAGAGCGGC	Sequencing pJET 1.2
F_pK18	TTCGCTTGGTGGTCGAATGGGCA	Sequencing pK18 <i>mobsacB</i>
R_pET24a	TGTGGCGCCGGTGATGCCGG	Sequencing pET-24a
R_pET28a	CAATTCCCCTATAGTGAGTC	Sequencing pET-28a
F_pLMB509	CGCCCAACTGGACTCATCTA	Sequencing pLMB509
qRT-PCR		
dnaN_qF	CATGTCGTGGTGGTCACCATAC	qRT-PCR
dnaN_qR	CTCGCGACCATGCATATAGA	qRT-PCR
nasA_qF	CCTGACGCAGGTCTATGGTT	qRT-PCR
nasA_qR	GACGATGAAGGTCGCATACA	qRT-PCR
nasT_qF	GGATATCGGCCTATGTTCGTG	qRT-PCR
nasT_qR	GATCACCTTGCGCTCCTC	qRT-PCR
nifR3_qF	CGCGATCTGGACCGAAAC	qRT-PCR
nifR3_qR	TGATGGTCAGCGAGATGGT	qRT-PCR

ntrB_qF	AGATCGAGATCGAGGACGAC	qRT-PCR
ntrB_qR	GGTGACGATCTTCGAGACCA	qRT-PCR
ntrC_qF	AACGCTATTTTCGACCTGCAT	qRT-PCR
ntrC_qR	GGTTTATGCCCAGAAGATCG	qRT-PCR
ntrY_qF	CCGATCGCTACCTTTACGTC	qRT-PCR
ntrY_qR	AAGCAGGGAAAACCTCGAACA	qRT-PCR
ntrX_qF	ACGGGATCGACATTCTCAAG	qRT-PCR
ntrX_qR	TCGATGTTGAAGGGCTTCTC	qRT-PCR
narK_qF	TATCCGCCGACCGACTATAC	qRT-PCR
narK_qR	GACCGGGATATGCTTGAAGA	qRT-PCR
narG_qF	GTATGCCCATACCGACCAGT	qRT-PCR
narG_qR	CCGGATGTTGTAGTCGATCA	qRT-PCR
narH_qF	GGAAAAATGCATCCTGTGCT	qRT-PCR
narH_qR	AAGCATCACGCCAGATAAC	qRT-PCR
narJ_qF	GGCGACCTCTACGATCTTCA	qRT-PCR
narJ_qR	CGATAGGTCTCCAGCAGGTC	qRT-PCR
narI_qF	ATGACCATCCTGGTCTCGAT	qRT-PCR
narI_qR	ATGCAGCTTGAAGAGCCAAT	qRT-PCR
Defining gene clusters		
F1_ntrOperon	GACCGAGGTGCCTTCATGAA	<i>nifR3-ntrB</i>
R1_ntrOperon	CCTGTGCGTCCAGGATGATC	<i>nifR3-ntrB</i>
F2_ntrOperon	GGTCTCCAAGATCGTCACCG	<i>ntrB-ntrC</i>
R2_ntrOperon	TCGTCAGCGATCAGAACGG	<i>ntrB-ntrC</i>
F3_ntrOperon	GGGCATAAACCGCAATACGC	<i>ntrC-ntrY</i>
R3_ntrOperon	GCGTTGCGGTATTGCGATAG	<i>ntrC-ntrY</i>
F4_ntrOperon	CATGGCCGAGATCCGTCTG	<i>ntrY-ntrX</i>
R4_ntrOperon	TCGGAAATCAGTTCGCGGAT	<i>ntrY-ntrX</i>
F1_nasOperon	CGACCGCGCCAAGGCCGT	<i>nasT-nasS</i>
R1_nasOperon	CATGTGCGGGCCTGCGC	<i>nasT-nasS</i>
F2_nasOperon	AAAAGGGCCAGATGATTCT	<i>nasS-nasA</i>
R2_nasOperon	GTCGAGAGGCCAGCGCGCG	<i>nasS-nasA</i>
F3_nasOperon	CGGCTTTGCCTTGCCGCTG	<i>nasA-nasB</i>
R3_nasOperon	GGCTCGGCGTTGAACAGGG	<i>nasA-nasB</i>

F4_nasOperon	GGACGTGCCACCCGCCGC	<i>nasB-nasG</i>
R4_nasOperon	CCGGTCGTCCATGGTGCG	<i>nasB-nasG</i>
F5_nasOperon	CGACATGAACTCGGGCAC	<i>nasG-nasH</i>
R5_nasOperon	CGGATCAGCGTGTCCCTTG	<i>nasG-nasH</i>
F6_nasOperon	CGGCGGGCTGACCTTTGT	<i>nasH-nasC</i>
R6_nasOperon	CTCGCCAAGCGCCGAGCC	<i>nasH-nasC</i>
Northern-Blot		
tRNA_Probe	CAGTGGCCACTACGATGTCAACGTA	Northern blot

2.4 Preparation of Nucleic acid

2.4.1 Mini-preparation of plasmid DNA using QIAGEN spin columns

Plasmid Miniprep spin column kits (*QIAGEN*) were used for isolation of highly pure, small scale (<5 µg) plasmids for restriction digest analysis, sequencing and transformation. Centrifugation steps were performed at 20,000 x *g* using a 5424 microcentrifuge (*Eppendorf*) unless stated otherwise. Spin columns and buffers were supplied with the kit and the procedure was performed according to the manufacturer's instructions, except DNA was eluted with 50 µL pre-autoclaved dH₂O.

2.4.2 Midi-preparation of plasmid DNA using QIAGEN Midi kit

For isolation of large amounts (>5 µg) of high purity plasmid DNA, plasmid Midi kits (*QIAGEN*) were used. Centrifugation steps were performed at 20,000 x *g* using a 5424 microcentrifuge (*Eppendorf*) unless stated otherwise. The procedure was performed according to the manufacturer's instructions, except DNA was eluted with 100 µL pre-autoclaved dH₂O.

2.4.3 Phenol-chloroform extraction of plasmid DNA

For isolation of low copy-number plasmids, a phenol-chloroform extraction was used. This procedure followed the same initial steps and reagents as a *QIAGEN* Mini-prep (2.4.1), but uses phenol-chloroform to isolate DNA instead of a silicagel matrix spin-column. Centrifugation steps were performed at 20,000 x *g* using a 5424 microcentrifuge (*Eppendorf*) unless stated otherwise. The procedure was as follows:

- A single colony of bacteria containing the desired plasmid was picked from the LB agar plate into 10 mL LB liquid containing appropriate antibiotics and incubated overnight.
- Cultures were pelleted in 15 mL falcon tubes (*Corning*) for 10 mins, 6,000 x *g*, using an Allegra 25R centrifuge (*Beckman Coulter*).

- Cell pellets were resuspended in 250 μL of resuspension buffer (stored at 4 $^{\circ}\text{C}$, containing 100 $\mu\text{g mL}^{-1}$ RNase A) and transferred to 1.5 mL microfuge tubes.
- 250 μL lysis buffer was added and left for 5 mins at room temperature.
- 350 μL acidic neutralisation buffer was added and samples were centrifuged for 10 mins.
- Supernatant was transferred to a fresh 1.5 mL microfuge tube containing 400 μL phenol-chloroform (phenol:chloroform:isoamyl alcohol 25:24:1, *Sigma*).
- Samples were mixed by vortexing for 10 seconds before centrifugation for 4 mins.
- The upper aqueous layer was transferred to a fresh 1.5 mL tube containing 750 μL 100 % (v/v) ethanol.
- Samples were centrifuged for 10 mins to pellet precipitated DNA.
- DNA pellet was washed with 500 μL of 70 % (v/v) ethanol and centrifuged for 2 mins.
- Supernatant was removed using a micropipette and the pellet was air dried for 15 mins.
- Plasmid DNA was resuspended in 50 μL of pre-autoclaved dH_2O and stored at -20°C .

2.4.4 Preparation of Genomic DNA using Promega spin columns

Wizard genomic DNA purification kits (*Promega*) were used for isolation of genomic DNA for use in PCR amplification, sequencing gene deletion mutants and microarrays. All buffers were provided with the kit and centrifugation steps were performed at 20,000 $\times g$ using a 5424 microcentrifuge (*Eppendorf*). The protocol was carried out according to the manufacturer's instructions for gram negative cells, except DNA was dissolved in 100 μL pre-autoclaved dH_2O .

2.4.5 Quantifying DNA/RNA concentrations

Nucleic acid samples were quantified using a NanoDrop 2000 UV-Vis Spectrophotometer (*Thermo Scientific*). 1 μL of sample was placed on the pedestal and scanned at 260 nm to give the DNA/RNA concentration in $\text{ng}/\mu\text{L}$.

2.5 Polymerase Chain Reaction (PCR) Amplification of DNA

Polymerase Chain Reactions performed during this study were carried out in a TC-512 Thermal Cycler (*Techne*) using pre-autoclaved 0.2 mL PCR tubes. Cycle conditions were calculated based upon polymerase manufacturer's instructions and the annealing temperature of individual primer pairs.

2.5.1 PCR of DNA using High-Fidelity Phusion Enzyme

Phusion High-Fidelity DNA polymerase (*Thermo Scientific*) was used for amplification of fragments for use in cloning procedures. The enzyme was used with the reagents supplied, appropriate concentration of DMSO (*Sigma-Aldrich*) and deoxyribonucleotide triphosphates (dNTP's, *Roche*). Each 50 μL reaction contained the following:

5 x HiFidelity Buffer	10 μL
dNTP's (10 mM)	1 μL
Forward primer (20 μM)	1 μL
Reverse primer (20 μM)	1 μL
Template DNA (~100 ng/ μL)	1 μL
DMSO	x μL
H ₂ O	35.5 – x μL
Phusion Polymerase	0.5 μL

Table 2.6. Standard Phusion HiFidelity PCR cycle.

Stage	Temperature ($^{\circ}\text{C}$)	Time (s)	Cycles
Initial Denaturation	98	120	1
Denaturation	98	15	
Annealing	Variable	20	35
Extension	72	30 s/kb	
Final extension	72	600	1

2.5.2 PCR of DNA using MyTaq master-mix

MyTaq DNA polymerase (*BioLine*) was used for the low-fidelity, fast and efficient PCR of vast quantities of samples. Each 20 μL reaction contained the following:

2 x MyTaq master mix	10 μL
H ₂ O	8.2 μL
Forward primer (20 μM)	0.4 μL
Reverse primer (20 μM)	0.4 μL
Template DNA (~100 ng/ μL)	1 μL

Table 2.7. Standard MyTaq DNA PCR cycle.

Stage	Temperature ($^{\circ}\text{C}$)	Time (s)	Cycles
Initial Denaturation	95	60	1

Denaturation	95	15	
Annealing	Variable	15	35
Extension	72	10 s/kb	
Final extension	72	600	1

2.5.3 Colony PCR using MyTaq master-mix

Single colonies were resuspended in 20 μ L dH₂O and lysed for 10 mins at 95 °C before being recovered on ice for 2 mins. Cell debris was pelleted at 20,000 x g for 2 mins and 1 μ L of supernatant was used as the template in the MyTaq PCR above.

2.5.4 Purification of PCR amplified DNA

DNA was purified using QIAquick PCR purification kit (QIAGEN) following PCR amplification of fragments. Reagents were provided and all centrifugation steps were performed at 20,000 x g using a 5424 microcentrifuge (Eppendorf). Protocol was carried out according to the manufacturer's instructions, except DNA was eluted with 50 μ L pre-autoclaved dH₂O.

2.6 Agarose Gel Electrophoresis of DNA

2.6.1 Visualisation of DNA using Ethidium Bromide

DNA was routinely separated by electrophoresis on 1 % (w/v) agarose gels by dissolving 1.2 g of agarose in 120 mL TAE buffer (45 mM Tris-acetate, 1 mM EDTA, pH 8.0) and adding 2 μ M (final) ethidium bromide (Sigma-Aldrich). DNA samples were mixed with 0.1 volumes of 10 x loading dye (40 % sucrose (w/v), 20 % orange G (w/v)) prior to loading. Gels were submerged and ran in TAE buffer at 120 mA using 1 Kb Hyperladder (Bioline) as a marker and visualised using a Gel Doc XR UV-transilluminator (BioRad).

2.6.2 Recovery of DNA from agarose gels via QIAGEN gel extraction kit

DNA fragments were excised from agarose gels and purified using a QIAquick Gel Extraction kit (QIAGEN). All centrifugation steps were performed at 20,000 x g using a 5424 microcentrifuge (Eppendorf) and the procedure was performed according to the manufacturer's instructions, except DNA was eluted with 35 μ L pre-autoclaved dH₂O.

2.7 Restriction Enzyme Digestion of Plasmid DNA

DNA digestions were carried out using fast-digest restriction enzymes supplied by *Thermo Fisher Scientific* according to the manufacturer's instructions with the supplied buffer. Digests routinely contained 1 µg DNA in a 20 µL reaction with 2 µL of 10 x reaction buffer, 1 µL of enzyme and dH₂O. Reactions were incubated at 37 °C for up to 2 h and stopped either by adding agarose gel loading buffer or heating at 75 °C for 10 mins.

2.8 Dephosphorylation of Digested plasmid DNA

Self-ligation of digested DNA was prevented using Alkaline Phosphatase rAPID (*Roche*) according to the manufacturer's instructions, with the supplied buffers. This step removed 5' phosphate groups from plasmid DNA digested with one enzyme prior to ligations. To the heat inactivated digest, 2 µL of 10 x buffer and 1 µL of enzyme were added and incubated at 37 °C for 1 h before heat inactivation.

2.9 Ligation of DNA Fragments

Recombinant plasmids were constructed by ligating appropriately digested fragments into a target plasmid using T4 DNA ligase (*Roche*) overnight at 4 °C. A 3:1 molar ratio of plasmid to insert was achieved using the following calculation:

$$((\text{ng plasmid} \times \text{Kb insert}) / \text{Kb vector}) \times 3 = \text{ng of insert required}$$

A typical ligation contained:

Plasmid	1 µL
Insert	x µL
H ₂ O	7 – x µL
10 x ligation buffer	1 µL
T4 DNA ligase	1 µL

2.10 Transformation of Plasmid DNA into *Escherichia coli*

2.10.1 Preparation of Competent Cells

E. coli cells were made competent for transformation using ice-cold 0.1 M CaCl₂ (Maniatis *et al.*, 1982). Centrifugation was carried out at 6,000 x g, 4 °C using an Allegra 25R centrifuge (*Beckman Coulter*).

- A single colony of *E. coli* was inoculated to 10 mL LB media and incubated overnight.
- The following day, 1 mL was used to inoculate 100 mL LB media and incubated for ~2 h until OD_{600 nm} = 0.3 – 0.5.

- The culture was split into two pre-chilled 50 mL centrifuge tubes and centrifuged for 10 mins. The supernatant was discarded.
- Both pellets were resuspended in 15 mL CaCl₂ and incubated for 30 mins on ice.
- Cells were pelleted as before and the supernatant was discarded.
- Pelleted cells were resuspended in 2mL CaCl₂ and incubated on ice for a minimum of 2 hours prior to use.

2.10.2 Transformation of Competent Cells

E. coli strain JM101 was routinely used to facilitate cloning procedures of recombinant DNA plasmids used throughout this study. *E. coli* NEB 5-alpha Competent cells™ (New England Biolabs) was used for the transformation of pIJ1363-derived plasmid clones.

- 200 µL competent cells were added to a DNA sample and incubated on ice for 30 mins.
- Cells were heat shocked at 42 °C for 50 s before recovery on ice for 1 min.
- 500 µL LB media was added to the mixture and agitated at 37 °C for 1 h.
- Cells were pelleted at 7,000 x *g* for 2 mins using a 5424 microcentrifuge (*Eppendorf*).
- Cell pellets were resuspended in 150 µL of residual supernatant and plated on LB agar containing appropriate antibiotics and supplements.
- Plates were incubated at 37 °C for 1 day.

2.11 Sequencing DNA

Sequencing of plasmid DNA was carried out by MWG Eurofins Genomics (Ebersberg, Germany) with the provision of 2 µg of DNA and 150 pmol of custom primers.

2.12 Colony Forming Units (CFU) Cell Culture Count

- A single colony of *P. denitrificans* was inoculated from an LB agar plate to 10 mL LB medium containing appropriate antibiotics and incubated for one day.
- Cells were diluted 10⁻² into 5 mL minimal salt media starter cultures containing appropriate carbon and nitrogen.
- Once in stationary phase, cells were used to inoculate 50 mL minimal salt media batch cultures containing appropriate carbon and nitrogen.
- Cultures were incubated at 30 °C with 200 µL aliquots withdrawn at specific time points throughout growth.
- Using this aliquot, serial dilutions were made using fresh minimal media.

- 100 μ L of each sample was plated onto an LB agar plate containing appropriate antibiotics and grown for 2 days.
- Individual colonies were assumed to have initiated from one single ancestor and counted as one CFU.

2.13 *In vivo* Plasmid Conjugations

Recombinant DNA plasmids were transferred to *P. denitrificans* (acceptor) by tri-parental mating with *E. coli* strains containing the desired plasmid (donor) and with *E. coli* 803 containing the plasmid pRK2013 (helper) to mobilise non self-transmissible plasmids. Patch crosses (Johnston et al. 1978) were carried out for protein expression plasmids whilst the filter cross (Beringer & Hopwood 1976) was performed for plasmids used for genomic deletions.

2.13.1 Conjugation via patch crosses

Single colonies of acceptor, donor and helper strains were picked from their respective LB agar plate and placed onto a fresh LB agar plate. The three strains were mixed together in a patch using a sterile toothpick and incubated at 30 °C for 3 days. Cells were then streaked onto LB agar plates containing appropriate antibiotics to recover successful single colony transconjugants of *P. denitrificans*.

2.13.2 Conjugation via filter crosses

P. denitrificans was inoculated to 50 mL LB medium and grown overnight at 30 °C to stationary phase. *E. coli* strains were inoculated the following morning to 50 mL LB medium and cultured at 37 °C until a mid-exponential phase. The three strains were pelleted sequentially in a 50 mL centrifuge tube at 6,000 x *g* using an Allegra 25R centrifuge (*Beckman Coulter*). Combined pellet was resuspended in 1 mL LB and transferred onto a sterile 47 mm nitrocellulose filter (*Whatman*) on an LB agar plate and incubated at 30 °C for 2 days.

Cells were resuspended with 50 % glycerol (v/v) and a serial dilution was created using LB. 100 μ L of each sample was spread on an LB agar plate with appropriate antibiotics and cultured at 30 °C for 3 days to isolate successful *P. denitrificans* transconjugants.

2.14 High Pressure Liquid Chromatography Quantification of Nitrate and Nitrite

Extracellular nitrate and nitrite concentrations of cell media were quantified using an ICS-900 HPLC system fitted with an IonPac AS9-SC carbonate eluent anion-exchange column, a DS5 conductivity detector and an AS40 automated sampler (*Dionex*). Analytical grade water (*Fisher Scientific*) was used for sample and buffer preparation, with all solutions being filtered with 0.20 μM nitrocellulose filters (*Sartorius Stedim*). Supernatant samples were harvested from batch cultures throughout the course of growth and were diluted 10 fold with water. The HPLC/eluent buffer consisted of 1.8 mM Na_2CO_3 , 1.7 mM NaHCO_3 , and the regenerant used was 9.5 mM H_2SO_4 . HPLC flow rate was consistently 250 $\mu\text{L min}^{-1}$ with a 20 μL injection volume.

2.15 Determination of Ammonium Concentrations

Batch culture ammonium concentrations were quantified using an Ammonium Assay Kit (*Sigma*) with the supplied buffers and reagents, according to manufacturer's instructions.

- The supplied vial of α -ketoglutarate and NADPH was reconstituted with 10 mL dH_2O and inverted gently to mix (ammonium assay reagent).
- 1 mL of culture was placed in a 1.5 mL microfuge tube and pelleted at 20,000 $\times g$ using a 5424 microcentrifuge (*Eppendorf*).
- Supernatant was transferred to a fresh 1.5 mL microfuge tube.
- 1 mL of ammonium assay reagent was placed in a 1 cm polystyrene cuvette (*Sarstedt*).
- 50 μL of sample was added and incubated at room temperature for 5 mins; the initial $A_{340\text{ nm}}$ was subsequently read.
- 10 μL of glutamate dehydrogenase was added and inverted to mix.
- The sample was incubated as before, following which the final $A_{340\text{ nm}}$ was taken.
- Ammonium consumption was determined indirectly by monitoring NADPH consumption which was calculated using An $\epsilon_{340\text{ nm}}$ NADPH of 6220 $\text{M}^{-1}\text{ cm}^{-1}$ and assuming a 1:1 stoichiometry of reaction catalysed by GDH.

2.16 Construction of *Paracoccus denitrificans* Gene Deleted Mutant Strains

During this study, unmarked genomic deletion mutants defective for *nifR3*, *dusA*, *sigma54* and *narJ* were constructed by allelic replacement using pK18*mobsacB* which was used to insert regions, flanking the target gene, into the genome via homologous recombination. pK18*mobsacB* is a wide host range plasmid which can be mobilised from *E. coli* to many proteobacteria, but which fails to replicate in them, resulting in the loss of gene expression (Figure 2.1).

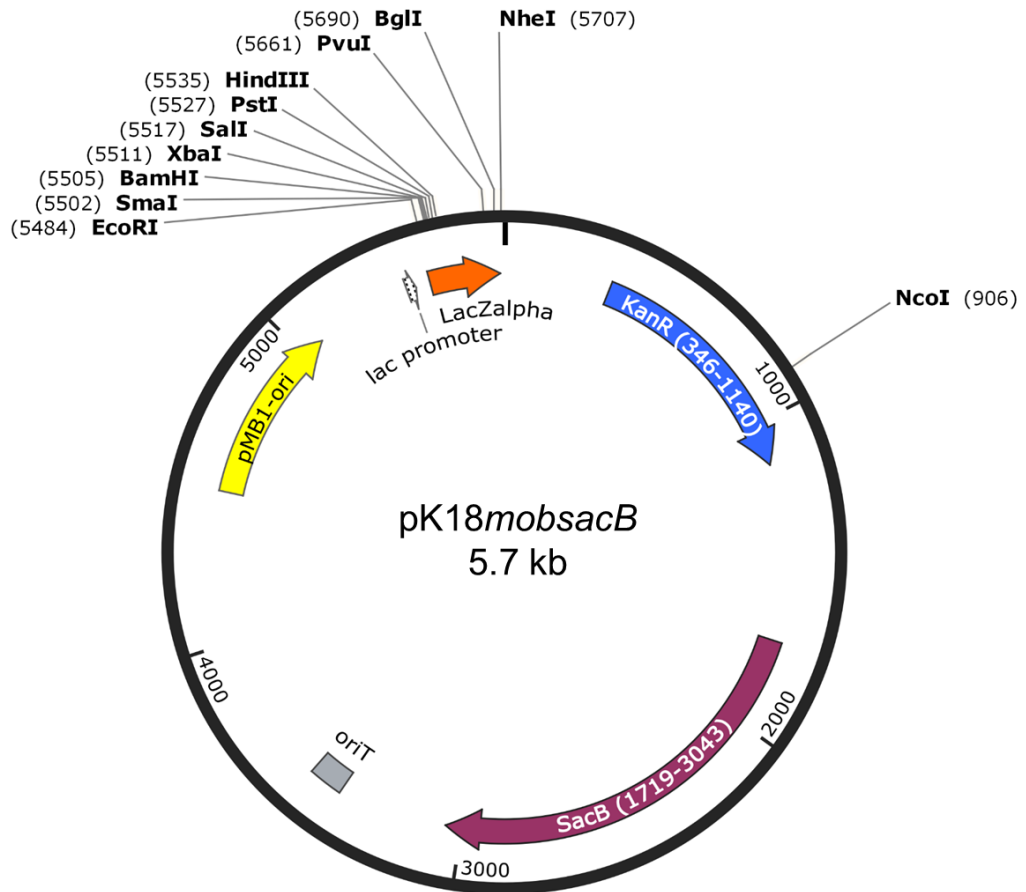


Figure 2.1. Vector map of pK18mobsacB used for constructing deletion mutants. Plasmid diagram highlighting the key features of suicide vector pK18mobsacB: the MCS within the *lacZα*, kanamycin resistance (KanR), RP4-derived *oriT* (mobilisable genes), pMB-origin replication and *sacB* (coding for levansucrase, suicide gene). Vector map drawn using SnapGene Viewer software.

The homologous recombination molecular events which occur for this gene deletion process are outlined in Figure 2.2. To construct a pK18*mobsacB*-derived suicide vector for the deletion of a target gene, fragments ~700 bp homologous to the upstream (5') and downstream (3') region of the gene were cloned from genomic DNA using appropriate primer pairs, containing *EcoRI*, *XbaI*, *XbaI* and *PstI* cut sites, respectively (Figure 2.2A). PCR products were cloned into separate pJET1.2 plasmids. The 3' fragment was digested out the vector with *XbaI/PstI* and inserted into pJET1.2/5' *yfg* cut identically to produce the pJET1.2 derived vector containing the assembled 5' and 3' sections of the gene. The whole fragment was digested out with *EcoRI/PstI* and ligated into pK18*mobsacB* to construct the suicide vector (Figure 2.2B) which was conjugated into *P. denitrificans* 1222 using the filter cross technique (Section 2.13.2).

Single cross-over recombinants were selected for using kanamycin resistance due to the integration of pK18*mobsacB* into the genome (Figure 2.2C and D). Following isolation, transconjugants were incubated in LB media to allow a second recombination event which would result in gene deletion (Figure 2.2E and F). Cultures were plated onto modified LB agar: Tryptone 10 g/L, yeast extract 5 g/L, NaCl 4 g/L, sucrose 60 g/L. The presence of genomic *sacB* leads to expression of levansucrase, an enzyme which breaks down sucrose into a lethal compound, therefore acting as a suicide mechanism to remove single-cross over isolates. Successful colonies were selected from these plates and picked to fresh LB agar master plates of rifampicin, and another of rifampicin and kanamycin. Colonies lacking kanamycin resistance were screened for the deletion using MyTaq colony PCR (Section 2.5.3) with appropriate primer pairs.

2.17 β -Galactosidase Gene-Reporter Fusion Assay

Transcriptional and translational activity of various target genes was measured by fusing the gene to a *lacZ* reporter in pMP220 or pIJ1363, respectively. O-nitrophenyl- β -D-galactopyranoside (ONPG, *Sigma*) was prepared fresh. Z buffer contained: 60 mM Na₂HPO₄, 40 mM NaH₂PO₄, 10 mM KCl, 1 mM MgSO₄, 0.3 % (v/v) β -mercaptoethanol. Assays were performed as outlined by Miller, with minor modifications (Miller 1972).

- *P. denitrificans* was inoculated from a single colony to 10 mL LB medium with appropriate antibiotics and grown for 1 day.
- Cells were diluted 10⁻² into 5 mL minimal salt media containing appropriate carbon and nitrogen sources.
- Once at stationary phase, this culture was used to inoculate a fresh minimal media culture containing appropriate carbon and nitrogen.

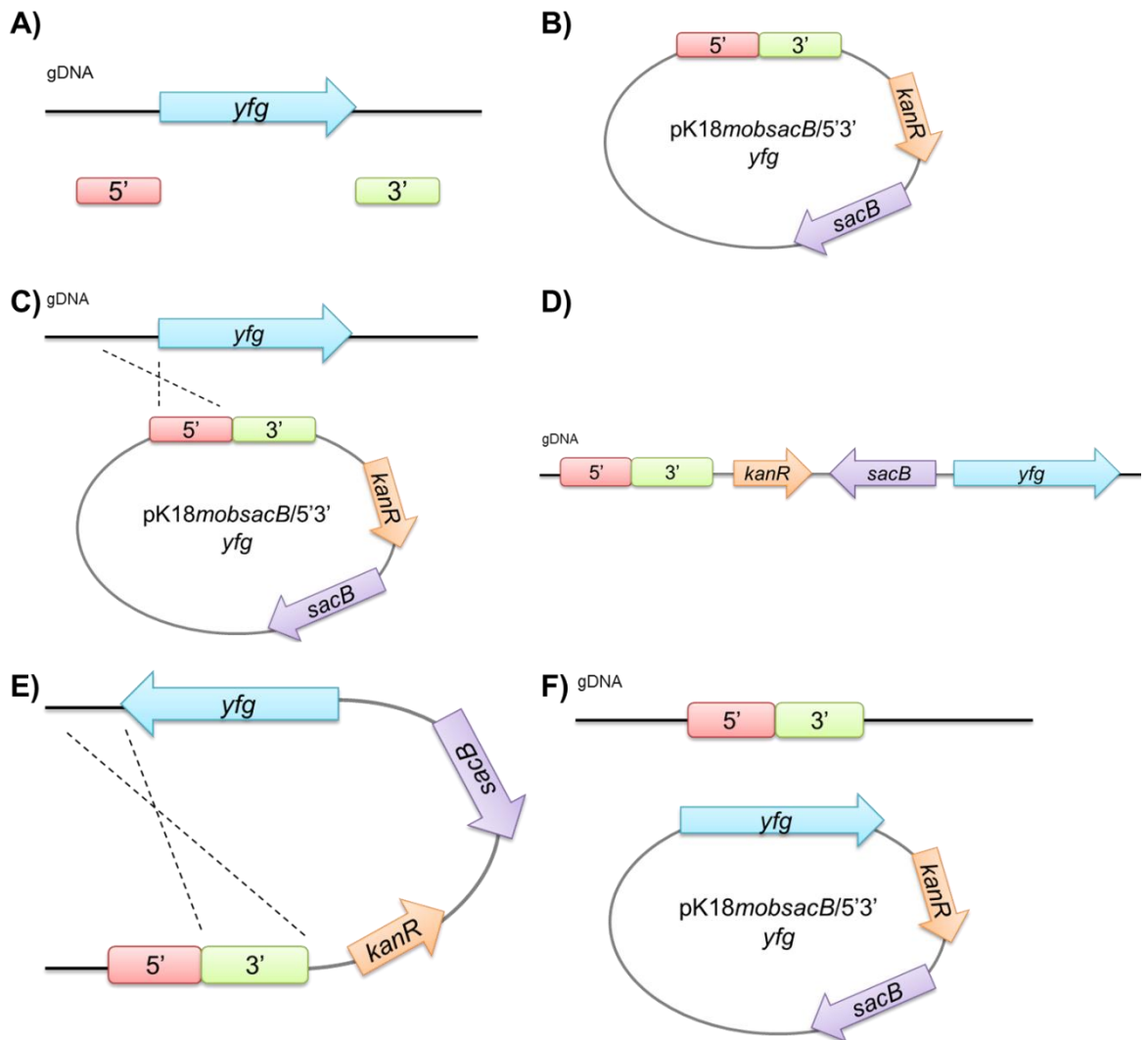


Figure 2.2. Homologous Recombination Events Occuring for Genomic Deletion. Schematic overview representing molecular events allowing allelic replacement to generate genomic deletion mutants. A) Flanking regions around the target gene were PCR amplified and B) cloned into pK18*mobsacB* to produce a suicide construct. C) The recombinant plasmid was conjugated into *P. denitrificans* where upon a single cross-over would occur, D) integrating the plasmid within the genome. E) A second recombination event generates the gene deleted mutant strain F).

- Cells were incubated until $OD_{600\text{ nm}} \sim 0.3 - 1.0$.
- An aliquot (100 - 500 μL , depending upon expected activity) of cell culture was placed into a 2 mL microfuge tube and made up to 1 mL with Z buffer.
- 2 drops of chloroform and 1 drop of 0.1 % SDS (w/v) were added to the cells using a Pasteur pipette.
- Samples were vortex-mixed for 10 s before 5 min incubation at 30 °C
- 200 μL 4 mg/mL ONPG was added and samples were placed at 30 °C with a timer started immediately.
- Once a yellow colour developed, 500 μL of 1 M NaHCO_3 was added to stop the reaction.
- Samples were centrifuged for 5 mins at 20,000 x g to pellet cell debris.
- 1 mL of supernatant was transferred to a polystyrene cuvette and $OD_{420\text{ nm}}$ values were recorded against blank Z buffer.

The breakdown of ONPG to ONP and galactose by β -Galactosidase produces a yellow colour due to a peak absorbance of ONP at 420 nm. The intensity is dependent upon the quantity of enzyme present which correlates with transcription/translation of the inserted promoter. This allows calculation of promoter activity, in Miller units, as follows:

t = time in minutes to develop yellow colour V = volume of culture used

$$\text{Miller units} = \frac{(1000 \times OD_{420\text{ nm}})}{(t \times V \times OD_{600\text{ nm}})}$$

To construct transcription gene-reporter fusions, the promoter region of a gene was cloned into pMP220 directly upstream of *lacZ* as an *EcoRI/PstI* fragment. This plasmid contains a ribosome binding site (RBS) and +1 transcription start site upstream of the cloning region which ensures transcription of *lacZ* correlates directly to the activity of the inserted promoter. pIJ1363 is a similar broad-host range plasmid but lacks an RBS or +1 transcription start site upstream of the *lacZ* gene. Cloning a target promoter with *BamHI* into this vector directly fuses it into the gene sequence of *lacZ* at the eighth codon. The result is a pIJ1363-derived plasmid which expresses in-frame target protein fusions with β -galactosidase, where monitored enzyme activity is directly proportional to translation of the inserted promoter region, as opposed to transcription in pMP220. However, these two plasmids vary greatly in their copy numbers, and therefore direct comparison between transcription and translation can not be accurately assumed by these systems.

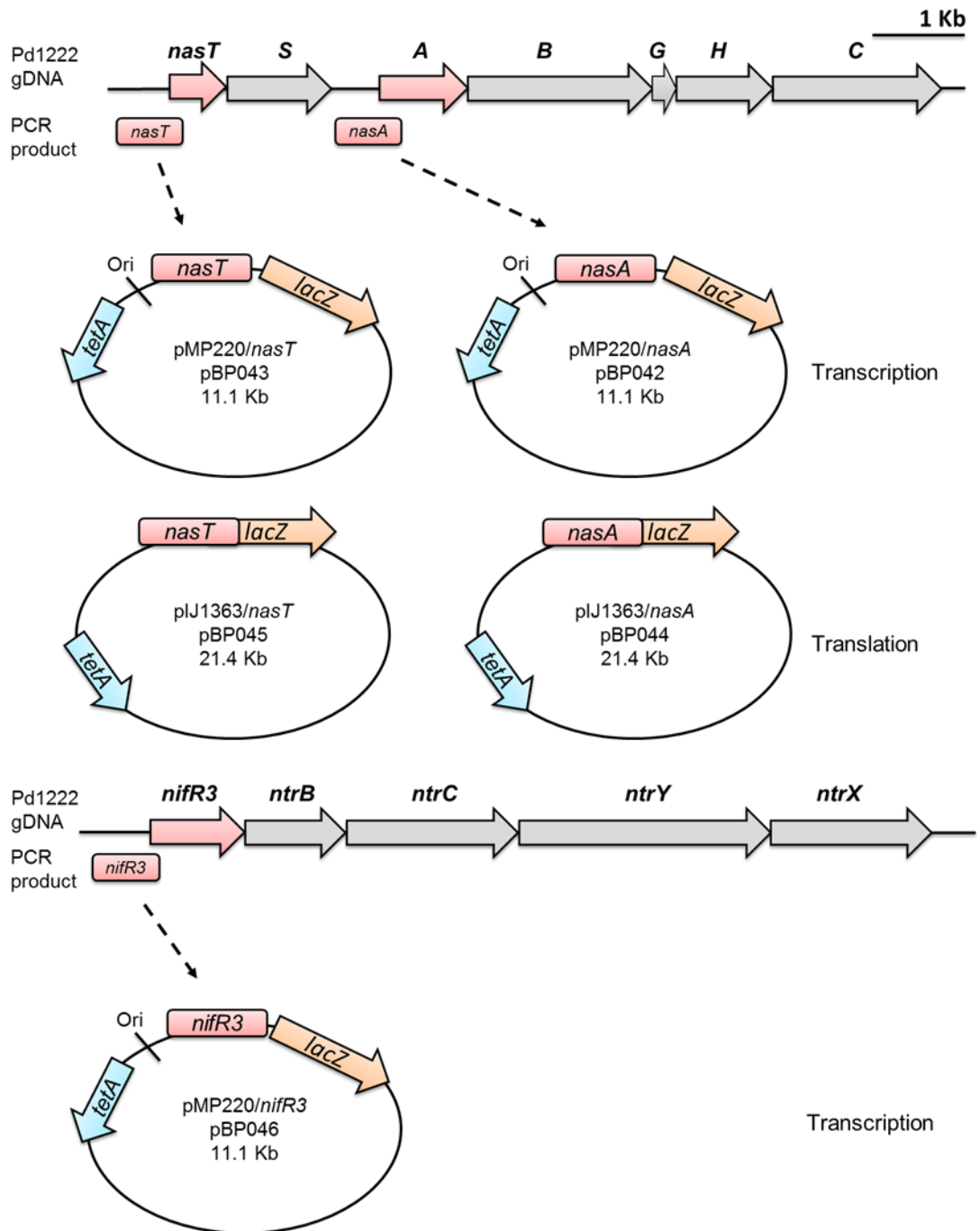


Figure 2.3. Construction of gene-reporter fusion plasmids to enable β -galactosidase measurement proportional to promoter activity. Promoter regions of target genes were PCR-amplified and cloned into pMP220 upstream of *lacZ* as an *EcoRI/PstI* fragment. Resulting plasmids monitored transcriptional activity of the inserted promoter. Target genes cloned into pJ1363 with *Bam*HI were fused directly with the *lacZ* sequence where observed enzyme activity is proportional to translation of the target promoter.

2.18 RNA Extraction from *Paracoccus denitrificans*

For the isolation of RNA suitable for qRT-PCR and microarray analysis, SV Total RNA Isolation Kits (*Promega*) were used. Analytical grade ethanol 96 % (v/v) (Cat. No. 24106 *Sigma*) and phenol pH 4.3 (*Sigma*) were used along with TipOne® RNase-free filter tips (*StarLab*). All plastics were autoclaved prior to use and importantly, equipment (bench-top, gloves, eppendorf racks, micropipettes) was treated with RNaseZAP® (*Ambion*) to ensure the area was contamination free. These measures were ensured for each downstream protocol with RNA in this research. Centrifuge steps were performed at 20,000 x g, 1 min, using a 5424 microcentrifuge unless stated otherwise.

2.18.1 Harvesting cells for RNA extraction

- A single colony was inoculated from an LB agar plate to 10 mL LB medium containing appropriate antibiotics and grown for 1 day.
- Cells were diluted 10⁻² into 5 mL minimal media containing appropriate carbon and nitrogen sources.
- Once grown to stationary phase, these cultures were used to inoculate 50 mL batch cultures of minimal media containing appropriate conditions.
- Cultures were incubated until OD_{600 nm} ~0.4 – 0.6.
- 30 mL of sample was transferred to a 50 mL centrifuge tube, pre-chilled on ice, containing 12 mL of 5 % phenol:95 % ethanol (stored at -20 °C).
- Samples were incubated on ice for 1 h before centrifugation at 6,000 x g, 10 mins, 4 °C.
- Supernatants were discarded and pellets were resuspended in residual supernatant.
- Samples were transferred to a 1.5 mL microfuge tube and pelleted for 2 mins at 4 °C.
- Supernatant was completely removed using a micropipette and cell pellets were snap frozen in liquid nitrogen and stored at -80 °C until use.

2.18.2 Extracting whole cell RNA

For the isolation of RNA SV Total RNA Isolation Kits (*Promega*) were used according to the manufacturer's specifications with supplied reagents on cell pellets harvested as outlined above. RNA was frozen in liquid nitrogen and stored at -80 °C for up to one month.

2.18.3 Experion analysis of RNA integrity

To ensure purity and quality of RNA samples, an Experion Automated Electrophoresis platform (*BioRad*) and StdSens chips (*BioRad*) were used according to manufacturer's

instructions, with the Experion RNA StdSens Analysis kit (*BioRad*). 1 μL of sample was loaded into each well on the chip alongside a ssRNA ladder. Integrity was assumed upon visualisation of clearly defined 23s and 16s rRNA at 2600 and 1400 bp respectively.

2.19 Synthesis of cDNA by Reverse Transcription

Once obtained, RNA was reverse transcribed to cDNA using SuperScript® II Reverse Transcriptase (*Invitrogen*) according to the manufacturer's specifications, with the supplied reagents and buffers.

- ~2 μg RNA was placed in a 1.5 mL microfuge tube, made up to 11 μL with ddH₂O.
- 1 μL 10 mM dNTP's and 1 μL random primers (100 ng/ μL) were added.
- Samples were incubated at 65 °C for 5 mins and recovered 1 min on ice.
- 4 μL 5 x First Strand buffer and 2 μL 0.1 mM DTT were added.
- 1 μL of Reverse Transcriptase was mixed in before incubation at 25 °C for 12 mins.
- Samples were subsequently incubated at 42 °C for 50 mins to transcribe cDNA and then left at 70 °C for 10 mins to heat inactive enzyme.
- 180 μL ddH₂O was added to the resulting product which was stored at -20 °C.

2.20 Quantitative real-time Reverse Transcriptase PCR (qRT-PCR)

qRT-PCR allows the quantification of specific RNA species in *real-time* by incorporation of a fluorescent dye into newly formed dsDNA. SYBR® Green I (*BioRad*) was used throughout this study to monitor levels of certain RNA, against the reference gene *dnaN* (DNA polymerase III, ubiquitously expressed). The RNA concentrations were further quantified using a standard dilution of genomic DNA in the qRT-PCR cycle.

SensiFAST SYBR® No-ROX Kit (*Bioline*) was used according to the manufacturer's specifications. A C1000 Thermal cycler equipped with a CFX96 Real-time PCR detection system (*BioRad*) was used to monitor the qRT-PCR.

- RNA was diluted to 100 ng/ μL using ddH₂O, and dilutions of genomic DNA at 1, 0.1 and 0.01 ng/ μL were prepared.
- qRT-PCR reactions were prepared in the wells of a Hard-Shell® 96-well thin wall PCR plate (*BioRad*) as follows:

2 x SensiFAST mix	10 μL
20 μM Forward primer	0.4 μL
20 μM Reverse primer	0.4 μL

Template (cDNA/gDNA)	1 μ l
H ₂ O	8.2 μ l

- Once in place, the plate was sealed using a Microseal® Adhesive lid (*BioRad*).

Table 2.8. Standard qRT-PCR cycle parameters.

Stage	Temperature (°C)	Time (s)	Cycles
Initial Denaturation	95	180	1
Denaturation	95	5	
Annealing	58	10	40
Extension	72	5	

The relative expression ratio (R) was calculated using the real-time PCR efficiencies of the target and reference *dnaN* gene, (E_{target}) and (E_{ref}) respectively and the recorded change in the threshold cycle ($C(t)$) between the RNA sample and DNA control.

$$R = \frac{(E_{\text{target}})^{\Delta C(t) \text{ (control-sample)}}}{(E_{\text{ref}})^{\Delta C(t) \text{ (control-sample)}}$$

2.21 Type II Microarray Analysis

All buffers were filtered with 0.20 μ M nitrocellulose filter paper (*Sartorius Stedim*). Reagents were used according to respective manufacturer's specifications. Compliant microarrays were performed using intact RNA harvested from three independent replicates, and a genomic DNA control, using custom designed tiled 4 x 44 K oligonucleotide microarray slides (*Agilent*).

2.21.1 Direct Labelling of RNA

- 10 μ g RNA was placed in a 1.5 mL microfuge tube, made to 7 μ L with ddH₂O (*Sigma*).
- 5 μ g random hexamers (*Invitrogen*) was added and the mixture was incubated at 70 °C for 5 mins before ice for 10 mins.
- 2 μ L 0.1 M DTT, 0.6 μ L 25 mM dNTP's and 2 μ L 10 x reaction buffer (*Agilent*) was added.
- 2 μ L 1 mM Cy5-dCTP (*Amersham Pharmacia*) was added to fluorescently label the RNA.
- 4 μ L of AffinityScript Reverse Transcriptase (*Agilent*) was added and incubated at 25 °C for 10 mins to initiate the reaction.
- Samples were left overnight at 42 °C in the dark to complete reverse transcription.

- 15 μL 0.1 M NaOH was added to degrade RNA at 70 °C for 10 mins.
- Hydrolysis was neutralised with 15 μL 0.1 M HCl and samples were cleaned up with a PCR-purification kit (Section 2.5.4).

2.21.2 Direct labelling of DNA

Genomic DNA was labelled using the reagents and buffers supplied by the BioPrime labelling system (*Invitrogen*) according to the manufacturer's specifications.

- 2 μg of chromosomal DNA (isolated as outlined in Section 2.4.5) was placed in a 1.5 mL microfuge tube, made to 20 μL with ddH₂O (*Sigma*).
- 20 μL 2.5 x random primer/reaction buffer mix was added and mixed gently by pipetting.
- Samples were boiled for 5 mins at 95 °C and cooled on ice for a further 5 mins.
- 5 μL 1.2 mM dNTP's was added and 3 μL 1 mM Cy3-dCTP (*Amersham Pharmacia*).
- 1 μL of Klenow enzyme (40 U/ μL) was added and samples were left overnight at 37 °C in the dark to synthesise fluorescently labelled DNA.
- DNA was cleaned up using the PCR-purification kit (Section 2.5.4).

2.21.3 Hybridisation to microarray slides

- DNA was mixed 1:5 with cDNA in a fresh 1.5 mL microfuge tube and made up to 43 μL with ddH₂O.
- Samples were heated at 95 °C for 2 mins and recovered at room temperature for 1 min.
- 50 μL hybridisation buffer was added (50 mM MES pH 6.5, 5 M NaCl, 20 % (v/v) formamide, 0.5 M EDTA, 10 % (v/v) Triton X-100) and mixed gently.
- The mixture was carefully pipetted onto an Agilent SureHyb GASKET slide (*Agilent*).
- An array slide was placed gently on top to seal in the sample.
- Hybridisation occurred in a dark, rotary oven at 55 °C, 8 rpm over 60 h.
- Post-hybridisation, slides were washed in a microscope-slide chamber with 6 x SSPE buffer (10 mM NaH₂PO₄, 150 mM NaCl, 10 mM EDTA, pH 7.4) supplemented with 4 % (v/v) N-Lauroylsarcosine for 5 mins.
- The slide was washed for an additional 5 mins in 0.6 x SSPE buffer supplemented with 0.18 % (v/v) polyethylene glycol and subsequently dried for 30 s by centrifugation.

The microarray slides were scanned using a GenePix 4000B scanner (*Axon Instruments*) using wavelengths of 532 and 635 nm. GenePix Pro software (*Axon Instruments*) quantified the fluorescent signals and filtered out those which were not 2-fold higher than those of the background signal. The red/green (Cy5/Cy3 – RNA/DNA)

ratios were calculated and analysed using GeneSpring 7.3 (*Agilent*) to identify genes which were consistently twofold higher or lower expressed across the three replicates.

2.22 Overexpression and Purification of Proteins

Protein purification steps were performed at 4 °C where possible and samples were kept on ice between procedures. Buffers were filtered with 0.45 µM nitrocellulose filter paper (*Sartorius Stedim*). HisTrap High Performance sepharose columns (*GE Healthcare*) charged with Ni²⁺ were used for Immobilised Metal-Ion Affinity Chromatography (IMAC) of 6His-tagged proteins. Protein purification was achieved using an ÄKTA FPLC system fitted with a UPC-900 high precision monitor (*GE Healthcare*) at a flow of 1 mL/min.

2.22.1 6His_NifR3

The *nifR3* gene of *P. denitrificans* was cloned into pET28a downstream of a 6 histidine sequence to produce an N-terminal 6His tag when overexpressed in *E. coli* BL21 (DE3), discussed in detail in Section 5.2.

- *E. coli* BL21 (DE3) pET28a/6his_*nifR3* was inoculated to 100 mL LB medium containing appropriate antibiotics and grown until OD_{600 nm} ~ 0.7.
- Protein expression was stimulated by the addition of 0.3 mM isopropyl β-D-1-thiogalactopyranoside (IPTG) final concentration.
- Cultures were left to grow for a further 18 h at 25 °C before being harvested at 6,000 x g using an Avanti™ J-20 centrifuge (*Beckman Coulter*).
- Pellets were resuspended in buffer A, 20 mL/L of culture, (20 mM HEPES, 150 mM NaCl, 25 mM imidazole, pH 7.5) containing a Complete EDTA-free protease-inhibitor (*Roche*).
- Cells were lysed via sonication with an ultrasonic processor (*Cole Palmer*) and cell debris was removed using an Optima X100-K ultracentrifuge (*Beckman Coulter*) at 80,000 x g for 1 h.
- Cell lysate was loaded onto a HisTrap sepharose column charged with Ni²⁺ and equilibrated with buffer A
- NifR3 was eluted using buffer B (same composition as buffer A but containing 500 mM imidazole) as a stepped imidazole gradient, running two column volumes of 25 % buffer B and a further two for 100 %. Peak fractions were immediately pooled together and supplemented with glycerol to a final concentration of 10 % (v/v).
- Sample was loaded onto a PD-10 desalting column (*GE Healthcare*) equilibrated with 20 mM HEPES, 150 mM NaCl, 10 % glycerol (v/v), pH 7.5.

- Size exclusion chromatography was performed with 1 column volume of equilibration buffer, via gravity flow, to remove imidazole.

2.22.2 NarJ_6His

The *narJ* gene of *P. denitrificans* was cloned into pLMB509 upstream of a 6 histidine sequence and downstream of a taurine inducible promoter. The recombinant plasmid was conjugated into *P. denitrificans* for overexpression of NarJ_6His.

- *P. denitrificans* pLMB509/*narJ*_6His was grown in minimal salt medium, supplemented with 30 mM succinate, 25 mM nitrate, 15 mM ammonium and 10 mM taurine.
- Cultures were grown anaerobically for 1 day at 30 °C before harvesting at 6,000 x *g* using an Avanti™ J-20 centrifuge (*Beckman Coulter*).
- Pellets were resuspended in buffer A, 20 mL/L of culture, (20 mM HEPES, 150 mM NaCl, 25 mM imidazole, pH 7.5) containing a Complete EDTA-free protease-inhibitor (*Roche*).
- Appropriate amounts of lysozyme (chicken egg white, *Sigma*) and deoxyribonuclease I (bovine pancreas, *Sigma*) were added and agitated for 30 mins, 4 °C, to initiate cell lysis.
- Lysis was completed via sonication and cell debris was removed using an Optima X100-K ultracentrifuge (*Beckman Coulter*) at 80,000 x *g* for 1 h.
- Cell lysate was loaded onto a HisTrap sepharose column charged with Ni²⁺ and equilibrated with resuspension buffer.
- The protein was eluted using a 25-500 mM imidazole gradient and fractions containing NarJ were dialysed overnight at 4 °C against 20 mM HEPES, 150 mM NaCl, pH 7.5, using BioDesign dialysis tubing, 8 kDa cut off (*Thermo Scientific*).

2.22.3 Concentration of proteins

Proteins were concentrated using Amicon Ultra Centrifugal Filters with the appropriate size cut off point (*Merck Millipore*). The sample was placed into the reservoir of the tube and centrifuged at 3,500 x *g*, 4 °C, until the protein had reached its desired concentration.

2.23 Bovine Serum Albumin (BSA) Bradford Assay

Protein concentrations were quantified using the Bradford assay (Bradford 1976). Bradford reagent was prepared by mixing 200 µL of Protein Assay Dye Reagent (*BioRad*) with 780 µL of analytical grade water in a 1 cm polystyrene cuvette. 20 µL of protein sample was added and incubated at room temperature for 5 mins before taking the absorbance at 595 nm. Values were quantified by comparison with a standard calibration curve made using known quantities of bovine serum albumin (*Sigma*).

2.24 Poly-Acrylamide Gel Electrophoresis (PAGE)

2.24.1 SDS-PAGE separation of proteins

Protein samples were denatured and separated by their molecular weight via sodium dodecyl sulphate poly-acrylamide gel electrophoresis (SDS-PAGE). Standard SDS gels were cast using the following recipe:

Table 2.9. Composition of a standard 12.5 % SDS-PAGE gel.

Component	Resolving Gel	Stacking Gel
Polyacrylamide (37.5:1 acrylamide:bis)	12.5 % (v/v)	4 % (v/v)
Tris-HCl pH 8.8	375 mM	-
Tris-HCl pH 6.8	-	125 mM
SDS	0.1 % (w/v)	0.1 % (w/v)
Ammonium persulphate (APS)	0.05 % (w/v)	0.05 % (w/v)
Tetramethylethylenediamine (TEMED)	0.03 % (v/v)	0.03 % (v/v)

Protein samples were prepared by addition of 0.2 volume of 5 x sample buffer (250 mM Tris-HCl pH 6.8, 10 % SDS (w/v), 50 % glycerol (v/v), 5 % β -mercaptoethanol (v/v), 0.1 % bromophenol blue (w/v)) and boiled at 95 °C for 5 mins. Samples were loaded alongside 5 μ L Precision Plus Protein™ Prestained Standards (*BioRad*) as a marker. Gels were run using a Mini-Protean II electrophoresis system (*BioRad*) partially submerged in running buffer (25 mM Tris-HCl, 192 mM glycine, 0.1 % SDS (w/v)) at a constant current of 35 mA for ~1 h 15 mins at room temperature. Gels were stained with InstantBlue Coomassie stain (*Expedeon*) for 30 mins.

2.24.2 Urea-PAGE separation of RNA

RNA samples were too small to be effectively separated via agarose gel electrophoresis, so were resolved by denaturing urea-PAGE. Glass slides used to cast the gel were treated with RNaseZAP® (*Ambion*) and washed thoroughly with ddH₂O to remove contamination. TBE buffer (90 mM Tris-HCl pH 8.3, 90 mM Boric acid, 2 mM EDTA) was filtered with a 0.20 μ M nitrocellulose filter and autoclaved to ensure sterility of RNases.

Table 2.10. Composition of a standard 12 % urea-PAGE gel.

Component	Resolving Gel
Polyacrylamide (37.5:1 acrylamide:bis)	12 % (v/v)

Urea	4 M
10 x TBE buffer	10 % (v/v)
Ammonium persulphate (APS)	0.1 % (w/v)
Tetramethylethylenediamine (TEMED)	0.075 % (v/v)

RNA samples were prepared by the addition of an equal volume of 2 x sample buffer (80 % (v/v) deionized formamide, 10 mM EDTA, 0.01 % (w/v) bromophenol blue) and heating at 70 °C for 2 mins. Gels were ran partially submerged in TBE buffer at a constant current of 30 mA for 20 mins before samples were loaded, to preheat gels. Gels were stained by soaking in TBE buffer supplemented with 2 µM ethidium bromide for 30 mins before visualisation using a Gel Doc XR UV-transilluminator (*BioRad*).

2.24.3 Native-PAGE separation of RNA

Native-PAGE RNA was performed for band-shift assays to visualise protein:RNA interactions. RNase sterility was assured as above.

Table 2.11. Composition of a standard 12 % native-PAGE gel.

Component	Resolving Gel
Polyacrylamide (37.5:1 acrylamide:bis)	12 % (v/v)
10 x TBE buffer	5 % (v/v)
Ammonium persulphate (APS)	0.1 % (w/v)
Tetramethylethylenediamine (TEMED)	0.04 % (v/v)

RNA samples were prepared by the addition of an equal volume of 2 x sample buffer (80 % (v/v) deionized formamide, 10 mM EDTA, 0.01 % (w/v) bromophenol blue). Prepared RNA samples were loaded and gels were ran partially submerged in TBE running buffer at a constant current of 20 mA at 4 °C. Gels were subsequently stained by soaking in TBE buffer supplemented with 2 µM ethidium bromide for 30 mins before visualisation using a Gel Doc XR UV-transilluminator (*BioRad*).

2.25 Western-Blot Identification of 6His-tagged Proteins

Semi-dry Western Blot analysis was used for chemiluminescent detection of target proteins using Monoclonal Anti-polyHistidine-Peroxidase Antibody (*Sigma*) as follows:

- After SDS-PAGE had been performed, the gel was moved to a clean tank and submerged for 5 mins in anode buffer 1: 0.3 M Tris, 20 % (v/v) methanol.

- PVDF membrane (Amersham Hybond™-P, *GE Healthcare*) was activated in 100 % methanol for 1 min before submerging in anode buffer 2: 25 mM Tris, 20 % (v/v) methanol.
- 3 10 x 8 cm segments of blotting paper (*Fisher Scientific*) were submerged in anode buffer 1 and another 3 in anode buffer 2.
- 6 10 x 8 cm segments of blotting paper were equilibrated in cathode buffer: 40 mM ϵ -aminocaproic acid, 0.01 % (w/v) SDS, 20 % (v/v) methanol.
- Blots were ran in a Trans-Blot SD cell by placing, on the anode, blotting paper soaked in anode buffer 2 followed by those from 1. Then the PVDF membrane, SDS-gel and finally blotting papers immersed in cathode solution.
- The cathode was placed on top and the transfer was performed for 1 h at 90 mA / 12 V.
- Next, the membrane was placed in a clean tank containing 5 % (w/v) skimmed milk powder in PBS: 137 mM NaCl, 2.7 mM KCl, 10 mM Na₂HPO₄, 1.8 mM KH₂PO₄.
- Membrane was left for 1 h to block non-specific interactions before the antibody was added to a final concentration of 250 ng/mL. This was shaken for 16 h, 4 °C, in the dark.
- Membranes were washed with 4 x 10 min washes of PBST (PBS with 0.1 % (v/v) TWEEN20) and 2 x 10 min washes of PBS to remove excess antibody.
- Super Signal® West Pico Chemiluminescent Substrate Kit (*Thermo Scientific*) was used according to the manufacturer's instructions.
- Membrane was agitated with chemiluminescent substrates for 4 mins before exposure to Kodak Bio max XAR film (*Sigma*) in a dark room.
- The film was developed using an exograph film developer.

2.26 Mass Spectrometry of Proteins

Protein bands of interest were excised from an SDS gel using a clean scalpel and placed in a fresh microfuge tube. Samples were sent to the John Innes Centre Proteomics Facility (Norwich Research Park) for subsequent trypsin digestion. Peptides were analysed using Matrix-Assisted Laser Desorption / Ionization-Time of Flight (MALDI-TOF) Mass Spectrometry. The resulting peak lists were used for a database search using an in-house Mascot® 2.4 server (Matrix Science, London, United Kingdom). The search was performed on the UniProt Swiss-Prot/TrEMBL database (release 20121031) with taxonomy set to bacteria and on a common contaminants database using the trypsin/P enzyme with a maximum of one missed cleavage, a peptide mass tolerance of 50 ppm, carbamidomethylation as fixed, and oxidation and acetylation (protein N terminus) as variable modifications. Using those parameters, Mascot protein scores greater than 85 were judged to be significant ($p < 0.05$).

Table 2.12. Mass spectrometry results and mascot scores for identification of excised bands of relevant proteins

Protein	Significance Score	Sequence Coverage	Expect Value
NifR3	196	64 %	4.1×10^{-11}
NarJ	183	67 %	6.2×10^{-12}
NarG	154	45 %	2.3×10^{-9}
NasC	139	49 %	3.4×10^{-10}

2.27 Spectrophotometry

2.27.1 UV-Visible spectrophotometry

UV-Visible spectrophotometric analysis was performed for colourimetric enzyme assays and identification of proteins and their cofactors. A U-3310 Hitachi UV-Visible spectrophotometer, equipped with a deuterium and tungsten iodide lamp, was used with reduced volume UV quartz cuvettes and a 1cm pathlength.

2.27.2 Fluorescence spectrophotometry

Identification of FMN in protein samples was achieved using fluorescence spectrophotometry to detect the flavin ring moiety. A Varian Cary Eclipse Fluorescence Spectrophotometer, equipped with a xenon lamp, was used with a high precision quartz fluorescence cuvette (*Hellma Analytics*).

2.28 Quantification of FMN in Protein Samples

To calculate FMN present in a pure 6His_NifR3 sample, the protein was denatured to release the quenched cofactor. The reaction was followed at $\text{Abs}_{444 \text{ nm}}$, which in conjunction with $\epsilon_{444 \text{ nm}} \text{ FMN} = 12,200 \text{ M}^{-1} \text{ cm}^{-1}$, allowed quantification.

- 1 mL of NifR3, at a known concentration, was placed in a reduced volume quartz cuvette.
- 20 μL 10 % (w/v) SDS was added to denature the protein and mixed in.
- The reaction was left for 10 mins in the UV-Visible spectrophotometer.
- The final $\text{Abs}_{444 \text{ nm}}$ was used to calculate the concentration of FMN.

2.29 Chemical Synthesis of Dihydrouridine

Due to the unavailability of commercial dihydrouridine, the compound was chemically synthesised, essentially as described previously, using *Sigma* reagents (Hanze 1967).

2.29.1 Synthesis of dihydrouridine via hydrogenation of uridine

- 100 mg uridine was dissolved in 3.125 mL of H₂O in a 10 mL round bottomed flask.
- 21 mg 5 % rhodium on activated alumina was added as the catalyst.
- The flask was made anaerobic by placing an air-tight subseal on the lid, sealing with parafilm and evacuating the atmosphere with a vacuum pump.
- A balloon was filled with hydrogen gas and attached to a syringe fixed with a needle.
- The needle was placed through the subseal, allowing the slow release of hydrogen gas into the reaction chamber. The mixture was stirred at room temperature for 24 h.
- Once done, the mixture was vacuum filtered through celite dampened with acetone.
- Dihydrouridine was dried using a rotary evaporator (*Buchi*) at 40 °C in synchronisation with a dry ice trap for 2 hours. Drying was completed overnight in a desiccator with CaCl₂.
- Final pure product was dissolved in an appropriate volume of dH₂O.

2.29.2 Analysing reaction mixture with thin-layer chromatography (TLC)

- Glass capillary tubes were used to spot a small amount of uridine, dissolved in methanol, and the reaction mixture onto a starting line on a silica coated TLC-slide.
- The slide was placed in a lidded beaker containing a small amount of solvent: 25 % (v/v) methanol in dichloromethane.
- Left for 2-3 mins until the solvent approached the top of the TLC slide.
- Loss of uridine was visualised with 2 techniques: a UV lamp, or by staining with vanillin (95 mL ethanol, 1.5 mL H₂SO₄, 1 g vanillin) followed by heating for 10 s.

2.30 Dihydrouridine Quantification Assay

Dihydrouridine was quantified as described previously, with minor modifications (Jacobson & Hedgcoth 1970). Compounds were purchased from *Sigma* and prepared as follows: 2,3-batanedione 2-oxime was dissolved 3 % (w/v) in H₂O and stored at 4 °C in tinfoil. 0.2 % (w/v) N-phenyl-p-phenylenediamine was dissolved in 10 % (v/v) ethanol. 1 mM FeCl₃ was prepared in 1 M H₂SO₄.

- 25 – 100 µg RNA sample was made up to 1 mL using ddH₂O.
- 100 µL 1 M KOH was added to hydrolyse the pyrimidine ring structure.
- Reactions proceeded at 37 °C for 30 mins before quenching with 500 µL 1 M H₂SO₄.
- 500 µL 2,3-batanedione 2-oxime and 500 µL N-phenyl-p-phenylenediamine was added
- Samples were boiled at 95 °C for 5 mins followed by room temperature for 5 mins.
- 1 mL 1mM FeCl₃ was added and samples were left for 1 h to develop.

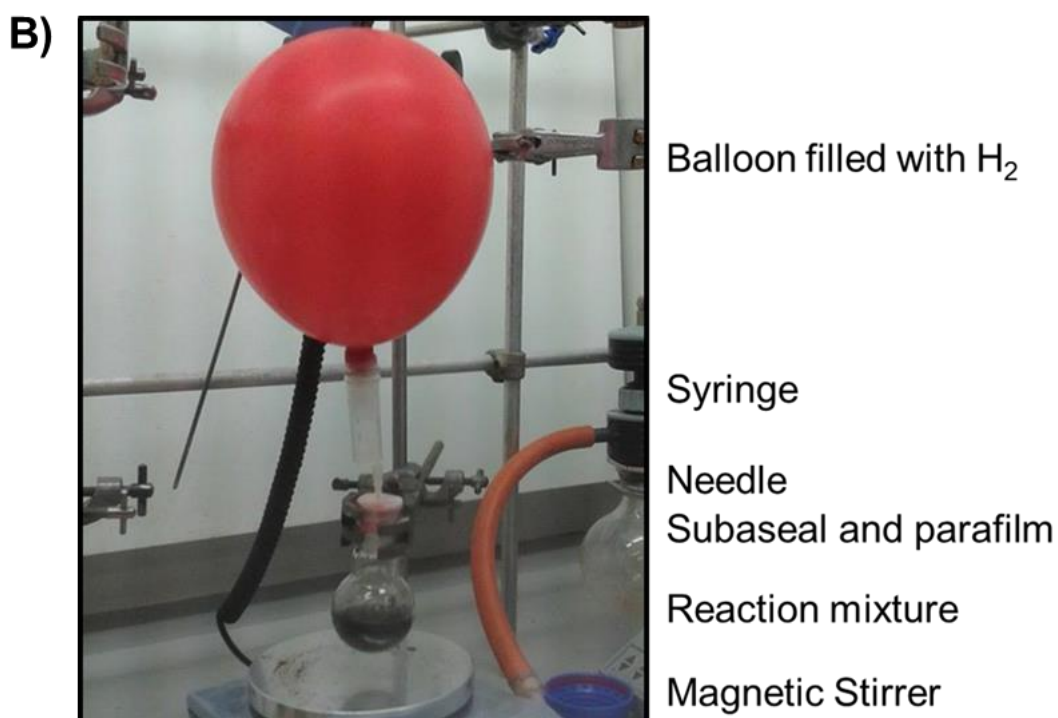
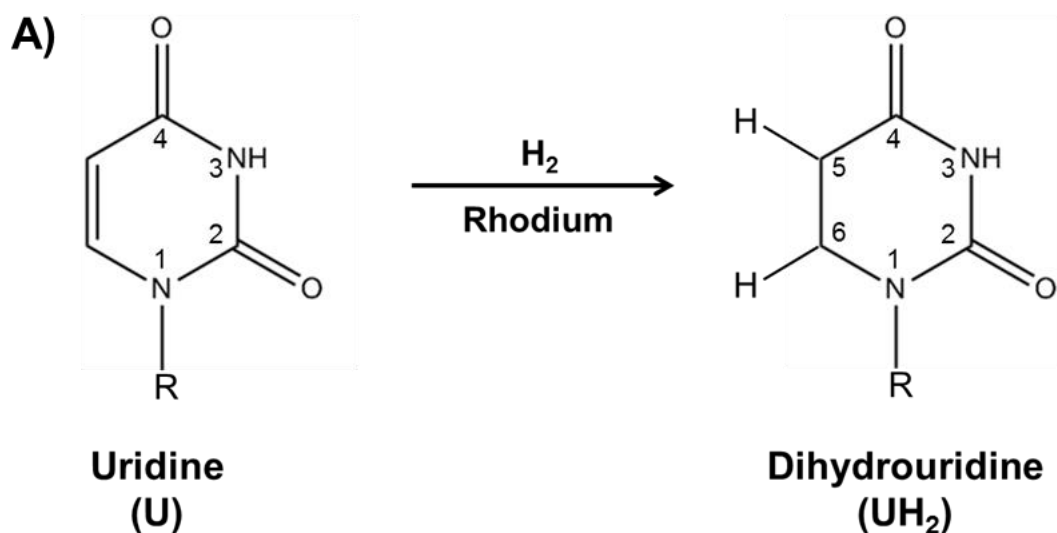


Figure 2.4. Chemical synthesis of dihydrouridine by hydrogenation of uridine. A) Addition of dihydrogen across the C5-C6 double bond of the pyrimidine group in the presence of rhodium produces dihydrouridine. B) Reaction setup; a balloon filled with hydrogen gas was attached to an anaerobic reaction chamber, via a syringe and needle, containing uridine and rhodium on activated alumina. The mixture was left to stir for 24 h before contents were recovered.

- Absorbance at 489 nm was taken and used to calculate concentrations.

2.31 Preparation of *Paracoccus denitrificans* Cell Lysate for Assays

- *P. denitrificans* was inoculated from a single colony on an LB plate to 10 mL LB medium with appropriate antibiotics and grown for 1 day.
- Cells were diluted 10^{-2} into 5 mL starter minimal salt media cultures.
- Once grown, these were used to inoculate 50 mL batch cultures of minimal media containing appropriate carbon and nitrogen sources.
- Cultures were incubated until $OD_{600\text{ nm}} \sim 0.4 - 0.7$, at which point they were harvested at $5,500 \times g$ for 10 mins.
- Cell pellets were resuspended in 1 mL buffer: 20 mM HEPES, 150 mM NaCl, pH 7.5.
- Appropriate amounts of lysozyme (chicken egg white, *Sigma*) and Complete EDTA-free protease-inhibitor cocktail (*Roche*) were added and agitated at 4 °C for 30.
- Cell lysis was completed via sonication (*Cole Palmer*).
- Cell debris was removed by centrifugation at $20,000 \times g$ for 20 mins and cell lysate was transferred to a clean 1.5 mL microfuge tube and stored at 4 °C until further use.

2.32 Catalytic Colourimetric Assays

Throughout this study, various redox enzymes were assayed for activity using spectrophotometric techniques. The *in vitro* electron donors NADH and methyl-viologen (MV) were used due to changes in their UV-Visible spectra upon alteration of redox state.

2.32.1 NADH Assay

- 1 mL sample in a cuvette was placed in a spectrophotometer recording the $Abs_{340\text{ nm}}$.
- After ensuring a steady baseline, an appropriate volume of 100 mM NADH or NAD^+ was added to give the desired concentration and inverted to mix.
- Once the trace was steady, the appropriate enzyme substrate was added to the cuvette and mixed gently by inversion.
- The cuvette was placed back into the spectrophotometer and the reaction was followed.

2.32.2 Methyl-Viologen Assay

Due to the ability of oxygen to oxidise MV and interfere with spectrophotometric readings, all reagents and samples were made anoxic prior to the experiment by sealing with air tight subseals and flushing the atmosphere with compressed dinitrogen gas. Gas-tight Hamilton Microlitre™ syringes (*Sigma*) were used for the transfer of reagents.

- 10 μL 100 mM sodium dithionite was used to fully reduce 1 mL of 100 mM MV^{2+} to MV^{1+} .
- 1 mL cell lysate samples prepared anaerobically in a reduced-volume glass cuvette were placed into the spectrophotometer recording at 600 nm.
- After observing a flat baseline, 10 μL of MV^{1+} was added (1 mM final concentration), mixed gently by inversion and the trace was left to plateau.
- An appropriate volume of enzyme substrate was mixed in and the reaction was left to proceed for 10 mins whilst being monitored.

2.33 tRNA Extraction from *Paracoccus denitrificans*

Sterility against RNase's was ensured as outlined in Section 2.18.1. All steps were performed at 4 °C where possible. Lithium chloride (LiCl) was used to separate tRNA as this salt precipitates the majority of RNA, but does not affect tRNA due to its great degree of secondary structure (Walker 2013; Cathala et al. 1983).

- A single colony of *P. denitrificans* was picked from an LB plate to 10 mL LB medium with appropriate antibiotics and grown for 1 day.
- Cells were diluted 10^{-2} into a 5 mL minimal salt media starter culture.
- Once grown, this was used to inoculate 50 mL batch cultures of minimal salt media containing appropriate carbon and nitrogen sources.
- Cultures were incubated until $\text{OD}_{600 \text{ nm}} \sim 0.4 - 0.7$, at which point they were harvested at $5,500 \times g$ for 10 mins using an Allegra 25R centrifuge (*Beckman Coulter*).
- Cells were resuspended in 2.5 mL of 0.3 M sodium acetate pH 4.5, 10 mM EDTA.
- 2.5 mL phenol, equilibrated in resuspension buffer, was added and vortexed for 2 mins.
- Samples were centrifuged as before and the upper aqueous layer was transferred to a fresh 15 mL falcon tube (Corning) containing 2.5 mL phenol.
- The mixture was vortexed for 1 min before centrifugation as before.
- The upper aqueous layer was carefully moved using a micropipette to a clean 50 mL tube containing 5 mL ethanol (stored at -20 °C) and incubated for 1 h at 4 °C.
- Samples were centrifuged for 15 mins at $20,000 \times g$ to pellet nucleic acids and supernatant was completely removed.
- Pellet was resuspended in 750 μL of 10 mM sodium acetate pH 4.5, 0.8 M LiCl and transferred to a fresh 1.5 mL microfuge tube.
- Nucleic acids were separated using the LiCl gradient for 10 min $20,000 \times g$.
- tRNA remained in the supernatant which was transferred to a clean 1.5 mL microfuge tube containing 750 μL 100 % (v/v) ethanol.

- Samples were centrifuged as before to pellet tRNA which was then washed with 500 μ L 70 % (v/v) ethanol and centrifuged for 2 min 20,000 x g.
- Supernatant was carefully removed and pellets were air dried for 10 mins before resuspension in 100 μ L pre-autoclaved ddH₂O and storage at -80 °C.

2.34 Northern-Blot Identification of RNA

Northern-Blot was used to identify RNA of interest using a complimentary DNA probe labelled with digoxigenin (DIG) and an anti-DIG Alkaline Phosphatase antibody supplied with a Luminescence Detection Kit (*Roche*).

- Following completion of Urea-PAGE, the gel was placed in a gel tank containing TBE buffer alongside 6 10 x 8 cm segments of blotting paper.
- Nitrocellulose membrane (*BioRad*) was submerged in TBE buffer.
- Blots were ran using a Trans-Blot SD cell by placing on the anode, 3 x blotting paper, nitrocellulose membrane, Urea-PAGE gel and finally the last 3 blotting papers.
- The cathode was placed on top and ran for 1 h, 4 °C at a constant of 200 mA.
- The membrane was transferred to a clean gel tank containing PerfectHyb™ Plus Hybridization Buffer (*Sigma*) and blocked for 1 h at 37 °C.
- dsDNA probe/DIG was denatured for 5 mins at 95 °C before addition to the hybridisation buffer at 20 nM final concentration and left overnight at 42 °C.
- Membrane was washed 4 x 20 min washes at 37 °C with 30 mM NaCl, 3 mM Na citrate, 0.1 % (w/v) SDS, pH 7.
- Lastly, washed with washing buffer: 0.1 M maleic acid, 0.15 M NaCl, 0.3 % Tween 20 (v/v), pH 7.5 for 5 min at room temperature.
- 20 mL blocking solution (*Roche*, diluted 10 fold in 0.1 M maleic acid, 0.15 M NaCl, pH 7.5) was added, followed by 4 μ L of Anti-DIG Antibody
- Solution was incubated for 30 mins before 2 x 15 min washes with washing buffer to remove excess antibody.
- Membrane was equilibrated 5 min in detection buffer (0.1 M Tris, 0.1 M NaCl, pH 9.5).
- This was discarded and 10 mL fresh detection buffer was added alongside 200 μ L of NBT/BCIP (*Roche*, substrate for alkaline phosphatase).
- Mixture was left at room temperature to develop colour, which upon reaching desired intensity, was stopped by flushing with cold H₂O.

2.35 Band Shift Assay for Protein:RNA Interactions

- 10 μL of protein, $\sim 150 \mu\text{M}$, (in 20 mM HEPES, 150 mM NaCl, 0.1 mM dithiothreitol (DTT), pH 7.5) was placed in a 1.5 mL microfuge tube.
- Desired amounts of harvested tRNA sample was added and reactions were left at room temperature for 15 mins.
- Equal volume of 2 x sample buffer was added and the sample was subject to native-PAGE (Section 2.24.3).
- Once visualised, the band of interest was excised using a clean scalpel and placed into a fresh 1.5 mL microfuge tube for identification of RNA.
- Gel fragment was finely sliced using the scalpel before 200 μL of 500 mM NaCl, 100 mM Tris, 100 mM MgCl_2 , 10 mM DTT, pH 7.9 was added.
- The mixture was agitated overnight at 4 $^\circ\text{C}$ to solubilise the gel.
- Sample was centrifuged for 1 min, 20,000 x g at 4 $^\circ\text{C}$ and supernatant was transferred to a 1.5 mL microfuge tube containing 750 μL 100 % ethanol.
- Incubated on ice for 30 mins before centrifugation at 20,000 x g for 10 mins.
- Supernatant was discarded and RNA pellet washed with 500 μL 70 % (v/v) ethanol.
- Samples were centrifuged for 2 mins at 20,000 x g and supernatant was removed.
- RNA pellet was air dried for 10 mins before dissolving in 50 μL H_2O .
- The sample was subsequently reverse transcribed to cDNA (Section 2.19) and cloned into pJET/1.2 for sequencing.

2.36 Protein Pull Down Assay to Isolate Binding Partners

His Mag Sepharose[®] Ni (*GE Healthcare*) are molecular magnetic beads charged with Ni^{2+} used to immobilise His-tagged proteins. These were used in conjunction with a 12-Tube Magnetic Separation Rack (*New England Biolabs*) to identify protein interactions.

- 50 μL of resuspended magnetic bead slurry was placed in a 1.5 mL microfuge tube, washed once with 100 μL H_2O and again with buffer A (20 mM HEPES, 150 mM NaCl, 25 mM imidazole, pH 7.5).
- Appropriate amount of pure protein (stated in individual results) was added and the mixture was agitated at 4 $^\circ\text{C}$ for 10 mins.
- Unbound protein was removed with 2 x 100 μL washes of buffer A.
- *P. denitrificans* cell lysate was added to the sample and agitated for 30 mins.
- Beads were thoroughly washed with 4 x 100 μL washes of buffer A.
- Bound protein was removed using 30 μL buffer B (buffer A with 500 mM imidazole), and the sample was subsequently size-resolved on SDS-PAGE for analysis.

2.37 Protein X-Ray Crystallography

Protein crystallisation was performed by vapour diffusion in a sitting-drop format, using 96-well MRC, 2 drop plates (*Molecular Dimensions*). Trials were set up using a variety of commercially available screens (*Qiagen*) and dispensed using an Oryx Nano protein crystallography robot (*Douglas Instruments*). Drops contained a total volume of 0.6 μL consisting of either 1:1 or 2:1 protein:precipitant solution with a reservoir volume of 50 μL . Crystallisation screens routinely used 5-10 mg/mL protein and were incubated at 16 $^{\circ}\text{C}$ once sealed with SureSeal™ DWB plastic coverslips (*Molecular Dimensions*). Crystals were visualised with an SZX9 stereo zoom microscope (*Olympus*) and prepared for X-ray data collection by storing in a solution consisting of: 75 % (v/v) screen condition and 25 % (v/v) cryoprotectant (i.e. ethylene glycol or glycerol), prior to being mounted using CryoLoops (*Hampton Research*). Crystals were flash-cooled in liquid nitrogen and stored in a dewar for transport to Diamond Light Source (UK) for X-ray diffraction experiments on beamline I02.

Initial yellow (consistent with flavin) crystal hits were obtained for 6His_NifR3 (7 mg/mL) in a protein buffer of 20 mM HEPES, 150 mM NaCl, and 10 % (v/v) glycerol with the screen condition 0.2 M CaCl_2 and 30 % (v/v) isopropanol. No detectable diffraction pattern was recorded when these crystals were subject to an X-ray beam, indicating they were not salt, but disordered protein crystals. Optimisation of crystallisation hits was performed by screening a range of conditions similar to the hit.

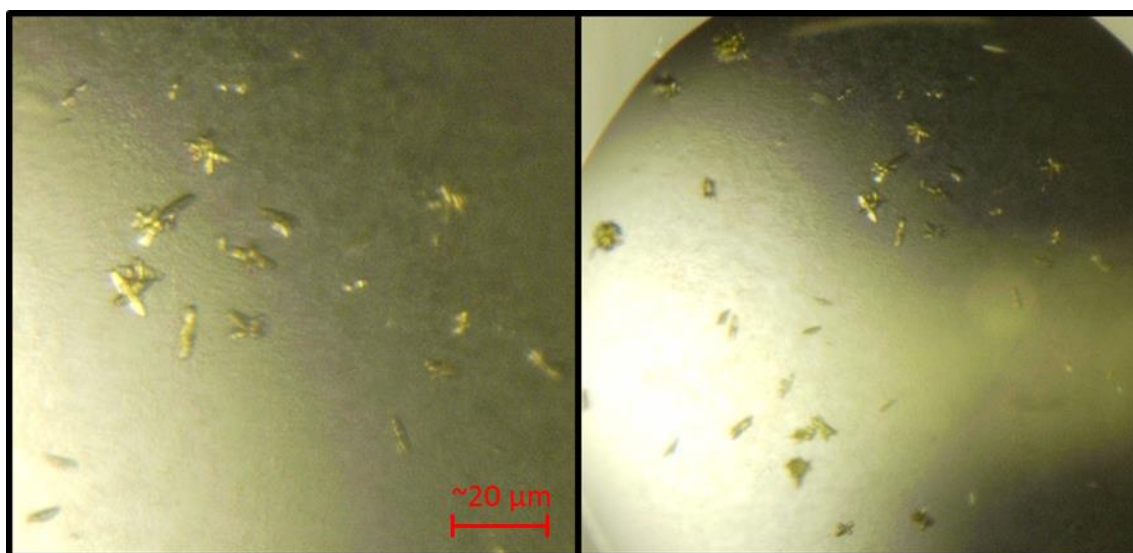


Figure 2.5. Initial crystals obtained for NifR3. Yellow crystals formed after 48 h incubation at 16 $^{\circ}\text{C}$ for 6His_NifR3 (7 mg/mL) in a buffer of 20 mM HEPES, 150 mM NaCl and 10 % (v/v) glycerol. The crystal screen contained 0.2 M CaCl_2 and 30 % (v/v) isopropanol.

Chapter 3: The Impact of Carbon and Cellular Redox Status on Assimilation of Inorganic Nitrogen Compounds

3.1 Introduction

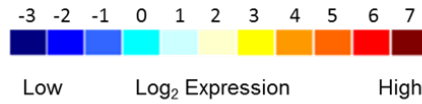
P. denitrificans is a metabolically versatile α -proteobacterium that can express three distinct nitrate reductases. Two of these systems are respiratory ubiquinol/nitrate oxidoreductases that reduce nitrate to nitrite. The membrane-bound enzyme (Nar) performs the first step in denitrification (Craske & Ferguson 1986). Nar is expressed during nitrate-dependant anaerobic growth and generates a proton motive force by employing a ubiquinol (UQH₂)-linked redox loop mechanism (Simon et al. 2008). In contrast, dissimilatory nitrate reduction by the periplasmic nitrate reductase (Nap) oxidizes excess reducing equivalents in UQH₂, but this process does not result in proton translocation, instead the activity of this enzyme dissipates energy (Stewart et al. 2002). Expression of Nap is enhanced during growth on long-chain fatty acids where high levels of excess cellular reductant are generated (Richardson et al. 1988).

In addition to Nar and Nap, another nitrate reductase is encoded in *Paracoccus* sp. that is present during ammonium-limited growth (Sears et al. 1997). In *P. denitrificans*, this cytoplasmic system comprises an NADH/nitrate oxidoreductase (NasC) and NADH/nitrite oxidoreductase (NasBG) that collectively perform the assimilatory reduction of nitrate to ammonium for incorporation of nitrogen into biosynthetic cellular pathways (Gates et al. 2011). During heterotrophic bacterial growth, this ammonium-forming nitrate reductase pathway consumes four equivalents of the physiological electron donor NADH per nitrate molecule assimilated, rendering it an energetically expensive process. For this reason, perhaps, nitrate assimilation is repressed in a wide range of bacteria when cellular ammonium is abundant (Luque-Almagro et al. 2013).

Recent transcriptomic analyses (Section 1.6) to investigate comparative global gene expression of *P. denitrificans* during aerobic growth with ammonium or nitrate as sole nitrogen sources revealed that genes encoding the bacterial Tripartite ATP-independent periplasmic (TRAP) transporters for dicarboxylic acids were upregulated during nitrate-dependant growth (Figure 3.1) (Gates and coworkers, unpublished data). In bacteria, TRAP transporters are characteristically composed of three subunits; a periplasmic soluble binding protein (DctP), a small membrane protein (DctQ) and a larger membrane

A) Gene ID Name $\text{NH}_4^+/\text{NO}_3^-$ Function / Annotation

Gene ID	Name	NH_4^+	NO_3^-	Function / Annotation
4619	<i>dctP</i>	Blue	Light Blue	TRAP dicarboxylate transporter binding protein
4620	<i>dctQ</i>	Dark Blue	Cyan	TRAP dicarboxylate transporter small membrane protein
4621	<i>dctM</i>	Blue	Light Blue	TRAP dicarboxylate transporter large membrane protein



B)

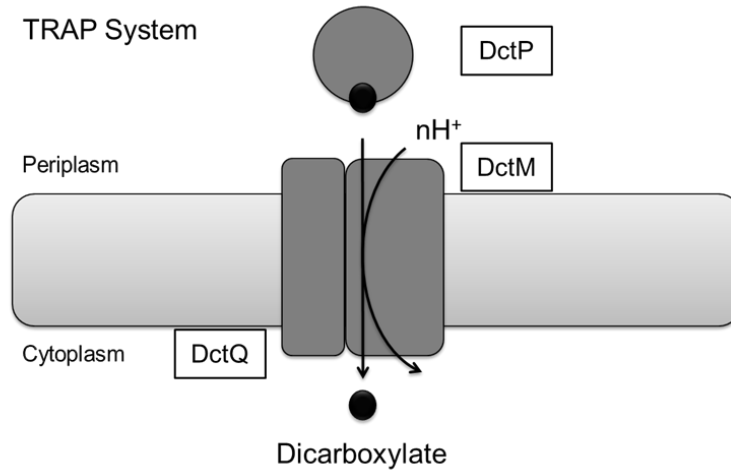


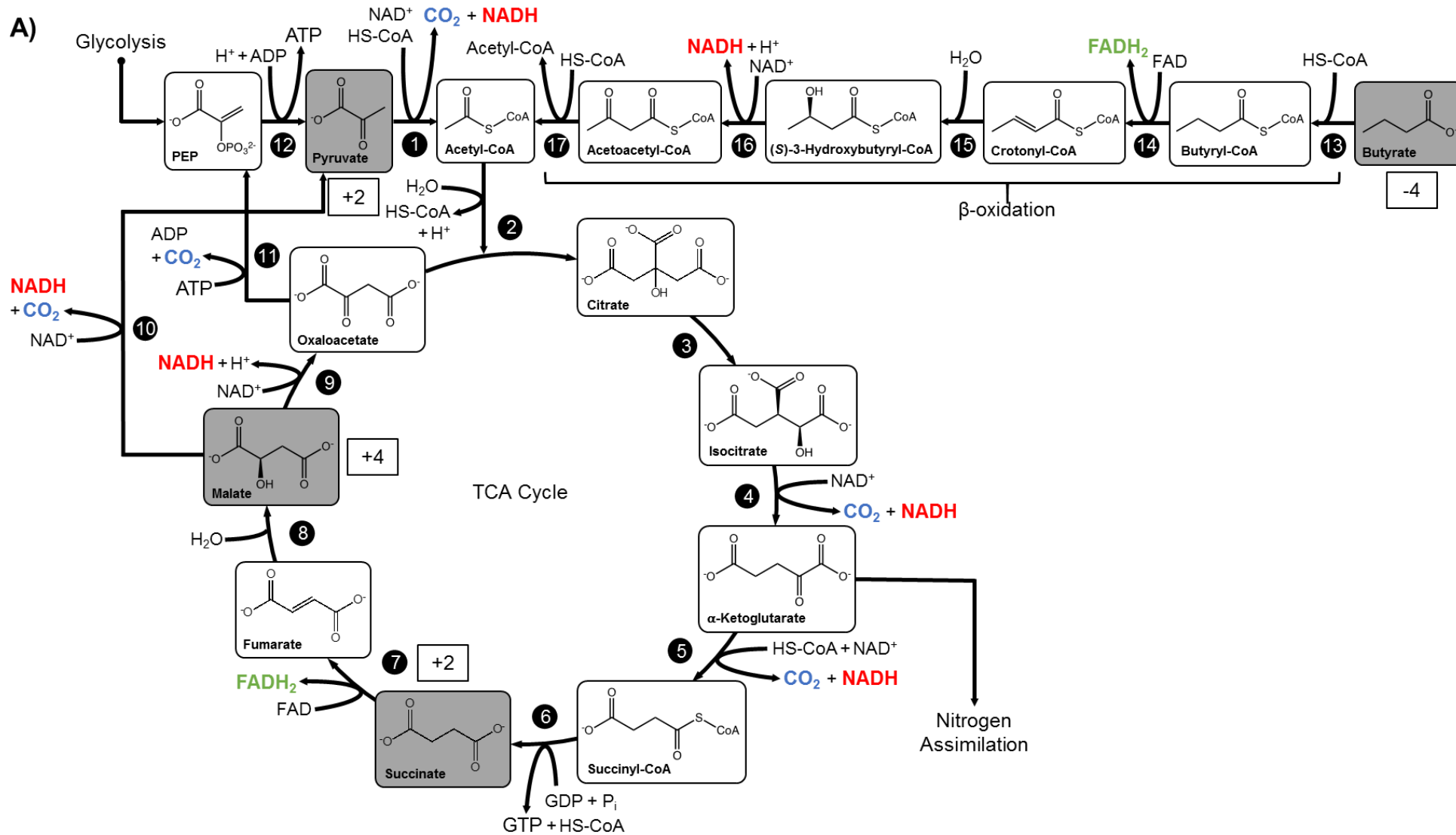
Figure 3.1. Microarray analysis of *P. denitrificans* comparing expression of the tripartite ATP-independent periplasmic transporter subunits during ammonium-dependant versus nitrate-dependant growth. A) Heatmap depicting expression levels of TRAP transporter genes from *P. denitrificans* grown aerobically in minimal salt media at 30 °C with 30 mM succinate using either 10 mM ammonium (left column) or nitrate (right column) as sole nitrogen sources. RNA was harvested at a mid-exponential phase and subject to a type-II microarray analysis. Colours indicate average \log_2 normalised expression values between three independent biological replicates. ID represents unique locus tag of each gene in the *P. denitrificans* genome (Accession: NC_008686–008688). Panel A was adapted from Gates *et al.* (unpublished data). B) Illustration of subunit topology for membrane-bound TRAP transporters as exemplified by *R. capsulatus*, where the image was adapted from Kelly and Thomas (Kelly & Thomas 2001).

protein (DctM) (Forward et al. 1997), all of which are upregulated during nitrate-dependant growth in *P. denitrificans*. This inner-membrane system has been extensively studied in *R. capsulatus* (Kelly & Thomas 2001), where the individual subunits share ~34% sequence identity to those in *P. denitrificans*, and are represented in Figure 3.1B.

Upregulation of the dicarboxylate uptake system enhances import of short-chain organic acids, such as succinate and malate (Kelly & Thomas 2001). Their subsequent entry into the TCA cycle may provide the intracellular electron reservoir, i.e. NADH, necessary to support bacterial nitrate assimilation (discussed in Section 1.7). By contrast, since ammonium is a reduced inorganic nitrogen compound (where nitrogen is -3), relative to nitrate (where nitrogen is +5) (Richardson & Watmough 1999), it can be used directly to fuel anabolic pathways without the need for excess cellular NADH provision over and above the respiratory budget to drive anabolic metabolism (see Figure 3.2A).

The main routes to cellular NADH formation required for bacterial respiration and nitrate assimilation are shown in Figure 3.2. Growth of *Paracoccus* sp. on different carbon compounds during aerobic nitrate respiration has been explored in detail, and butyrate has been shown to alter the redox balance of intracellular electron carrier pools (Ellington et al. 2003; Richardson & Ferguson 1992). These studies have demonstrated a role for the ubiquinol/nitrate oxidoreductase Nap in cellular redox balancing during growth on highly reduced carbon substrates compared with more oxidised carbon sources such as succinate (Richardson et al. 1988). Here, nitrate is proposed to act as an oxidant to alleviate excess reductant in the membrane-confined quinol pool. This is particularly important in cytochrome-*bc₁* dependant organisms, as a balance of ubiquinone and ubiquinol are required for the respiratory electron chain to function optimally.

In the context of Nas, given that NADH is required for nitrate-dependant, but not ammonium-dependant growth, it is proposed that higher cellular NADH levels may indeed favour bacterial growth on nitrate as a sole nitrogen source. Here, the use of nitrogen oxyanions may provide an alternative route for redox balancing in cells that encounter excess cellular reductant in cytoplasmic NADH through generation of biomass. At the outset of this study, we envisaged that Nas functions as a nitrate assimilation pathway, which may simultaneously act as a vent for excess reductant at the level of NADH, and that higher levels of reduced carbon would favour nitrate-dependant over ammonium-dependant growth. This hypothesis was tested by culturing *P. denitrificans* cells on various carbon sources (highlighted in Figure 3.2) with different redox states, which yield different quantities of NADH per molecule oxidised, over a range of concentrations in minimal growth media.



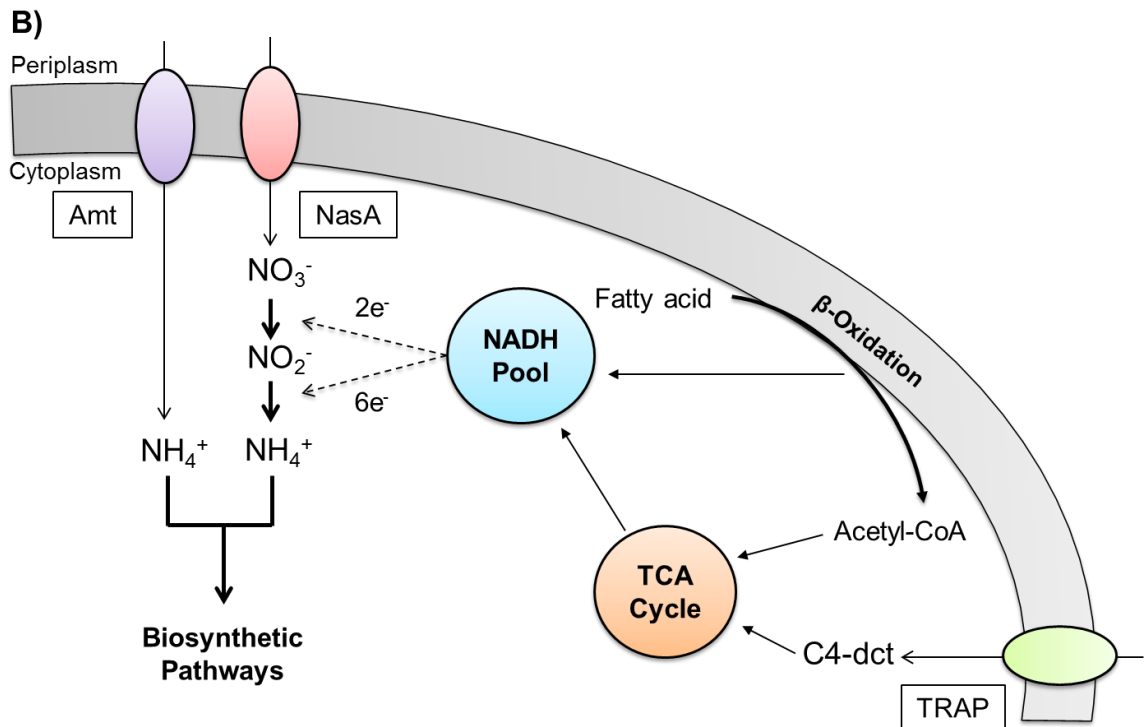


Figure 3.2. Representation of the link between carbon respiration and nitrogen assimilation in *P. denitrificans*. A) Overview of reduced nucleotide pyrimidine production through the TCA/Krebs cycle oxidation of organic acids and β -oxidation of butyrate. Enzymes and Pden_ numbers are as follows: 1; pyruvate dehydrogenase (3892), 2; citrate synthase (3716), 3; aconitase (3071), 4; isocitrate dehydrogenase (2961), 5; α -ketoglutarate dehydrogenase (0555), 6; Succinyl-CoA synthetase (0558), 7; succinate dehydrogenase (0569), 8; fumarase (1908), 9; malate dehydrogenase (0561), 10; malic enzyme (decarboxylating) (2224), 11; PEP carboxykinase (2852), 12; pyruvate kinase (2276), 13; butyryl-CoA synthetase (4213), 14; butyryl-CoA dehydrogenase (0714), 15; crotonyl-CoA hydratase (4513), 16; 3-hydroxybutyryl-CoA dehydrogenase (0197), 17; acetyl-CoA acetyltransferase (2026). Carbon compounds tested here to investigate *P. denitrificans* are shaded grey, with their average carbon oxidation state highlighted. B) Schematic depicting how oxidation of carbon substrates links with the cytoplasmic assimilation of nitrate and nitrite in *P. denitrificans*. The following abbreviations are used for key systems: Amt; high-affinity ammonium transporter, NasA; nitrate/nitrite transporter, TRAP; Tripartite ATP-independent periplasmic transporters (organic acid transporter).

3.2 Growth of *Paracoccus denitrificans* on Different Inorganic Nitrogen Sources

P. denitrificans can use a range of inorganic and organic nitrogen sources for heterotrophic growth. Examples of organic nitrogen compounds include amino acids such as alanine, serine, glutamate and glutamine (Luque-Almagro et al. 2013; Ahmadian et al. 1993). By contrast, inorganic nitrogen compounds include ammonium (which can be directly assimilated into organic nitrogen by the GS-GOGAT and GDH pathways, see Chapter 1) and nitrate/nitrite (which generate ammonium via the Nas pathway). Throughout this study, bacterial cells were cultured in minimal salts medium supplemented with 30 mM succinate and 10 mM of either ammonium, nitrate or nitrite as sole nitrogen source, unless otherwise stated.

Figure 3.3 shows ammonium, nitrate or nitrite can be used effectively and individually as sole inorganic nitrogen sources by *P. denitrificans* to support biosynthesis of essential cellular compounds and growth. Apparent maximal specific growth rates for each condition were determined from semi-log plots of bacterial growth versus time (see Figure 3.3). Cell yields are presented throughout this study as dry weight of cells in mg/mL, where 1 OD₆₀₀ unit contained 1.03 g/L of *P. denitrificans*. Values for μ_{max} (app.) of 0.19, 0.12 and 0.13 h⁻¹ were calculated for the growth rates for ammonium, nitrate and nitrite-dependant growth respectively. Judging by these values, the maximum OD observed at 600 nm (i.e., OD_{max}) achieved by cultures, and growth yield (i.e. dry weight), ammonium is the preferential inorganic nitrogen source as it can be used directly by cellular metabolism for biomass production (Table 3.1). Cultures supplemented solely with nitrate and nitrite have similar growth rates, which are ~65% that of ammonium-dependant growth, as both require the Nas pathway for reduction to ammonium prior to biomass formation. Furthermore, the OD_{max} values and growth yields of these cultures is ~75% compared to ammonium-supplemented cells, possibly as the NADH pool is additionally required for NasBGC function during nitrate or nitrite-dependant growth.

Table 3.1. Summary of relevant growth parameters derived from Figure 3.3.

Nitrogen Source	OD _{max} (600 nm)	Dry weight (mg/mL)	μ_{max} (app.) (h ⁻¹)
10 mM NH ₄ ⁺	1.09 ± 0.04	1.23 ± 0.03	0.19 ± 0.02
10 mM NO ₃ ⁻	0.85 ± 0.03	0.96 ± 0.02	0.12 ± 0.01
10 mM NO ₂ ⁻	0.85 ± 0.04	0.96 ± 0.03	0.13 ± 0.01
5 mM NH ₄ ⁺ 5 mM NO ₃ ⁻	0.87 ± 0.03	0.98 ± 0.02	0.15 ± 0.02

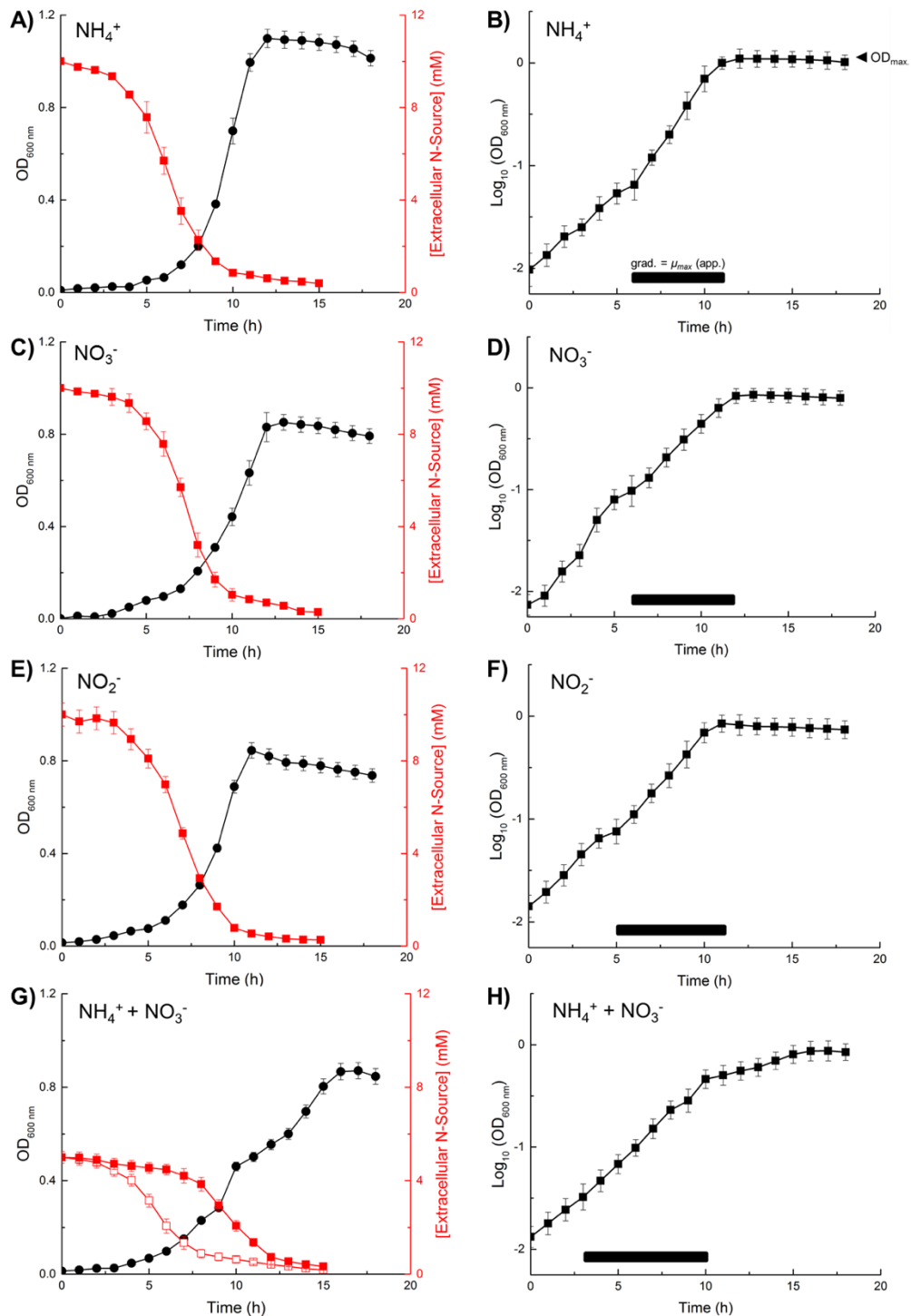


Figure 3.3. Growth analysis of *P. denitrificans* using various nitrogen sources. Aerobic growth of *P. denitrificans* in minimal media, 30 °C, with 30 mM succinate. Cell growth was followed by measuring optical density at 600 nm (black) and extracellular nitrogen concentration was measured by ion-exchange chromatography (red). Cultures were supplemented with 10 mM ammonium, nitrate, nitrite or 5 mM of both ammonium and nitrate. Where a mixture of nitrogen sources were used, open symbols represent ammonium and closed symbols represent nitrate. Corresponding semi-log plots used to calculate $\mu_{\text{max}}(\text{app.})$ values are shown on the right. The regions over which $\mu_{\text{max}}(\text{app.})$ was calculated for each experiment is highlighted by the black box.

Interestingly, when both ammonium and nitrate were supplemented, diauxic growth profiles were observed, where a second lag phase was apparent at ~10 h (Figure 3.3G). Analysis of external nitrogen concentrations revealed ammonium was taken up first, consistent with being the preferred bacterial nitrogen source, followed by nitrate. Ammonium consumption initiates ~4 h, immediately before the exponential phase and nitrate consumption begins ~8 h, prior to the second exponential phase. This additional lag phase may be attributed to cells switching to a nitrate assimilation proteome where the Nas system requires time for expression and protein translation. The apparent maximal specific growth rate here, for the first phase of growth, is ~0.15 h⁻¹, that is intermediate between cultures supplemented solely with ammonium or nitrate (Table 3.1). Given that the growth parameters are not the same as those obtained for solely ammonium-dependant growth, despite ammonium-dependent growth being favoured by bacteria, these observations suggest that for *P. denitrificans* there is mixed growth occurring where cells may be using both inorganic nitrogen sources simultaneously. Many previous studies imply that expression of the structural genes for Nas (i.e., *nasABGHC*) requires the total absence of ammonium (Sears et al. 1997). However, these observations suggest that the regulation of *nas* expression may be more complex as assimilatory nitrate consumption commences whilst residual ammonium, at ~1 mM, is still present within the media.

To investigate the molecular basis of nitrate-dependant growth, particularly with the view to understanding the diauxic growth of *P. denitrificans* on mixed inorganic nitrogen compounds, expression of regulatory and structural genes for *nas* were monitored using β -galactosidase gene-reporter fusion assays.

Transcriptional gene-reporter fusion construction is complex and requires prior knowledge of the transcriptional architecture of the gene cluster under investigation, and preferably promotor locations. With the *P. denitrificans nas* gene cluster, experimental data was not available but *nasTS* and *nasABGHC* were believed to be expressed as two distinct transcriptional units due to distinct expression levels observed in the microarray of Gates and co-workers (unpublished data). Therefore, a detailed analysis of the transcriptional architecture of *nas* using RT-PCR was performed to determine whether *nasTS* and *nasABGHC* formed distinct transcriptional units (Figure 3.4). Here, cDNA was obtained by reverse-transcription of RNA isolated during nitrate-dependent growth of *P. denitrificans*, where *nas* mRNA is abundant.

Selected primer pairs for amplification of the following regions: 1, *nasT-S*; 2, *nas S-A*; 3, *nasA-B*; 4, *nasB-G*; 5, *nasG-H*; and 6, *nasH-C* were used to determine whether they lay

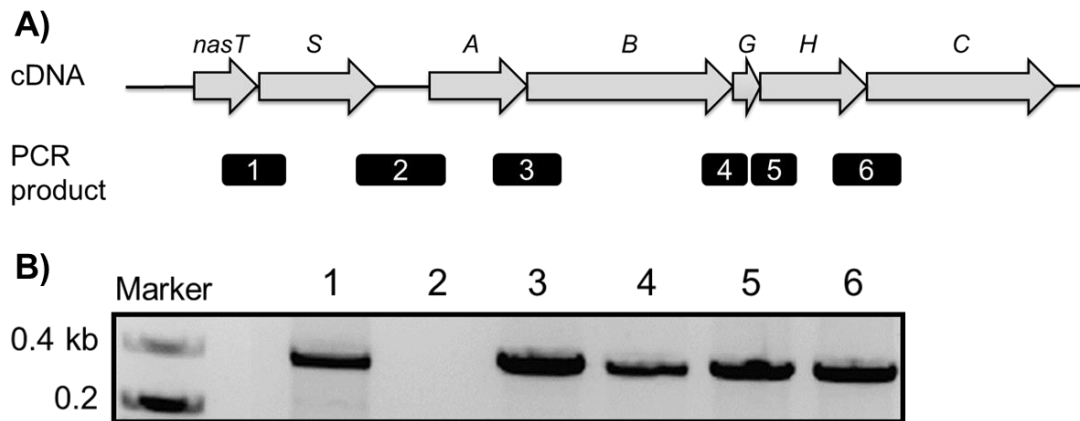


Figure 3.4. Defining the transcriptional architecture of the *nasTSABGHC* gene cluster of *P. denitrificans*. RNA was harvested at a mid-exponential phase from *P. denitrificans* cultures grown aerobically at 30 °C in minimal media with 30 mM succinate and 10 mM nitrate as a sole nitrogen source. RNA was reverse-transcribed to cDNA and set up in separate RT-PCR reactions containing the appropriate primer pairs. A) The *nasTSABGHC* gene cluster of *P. denitrificans*, where PCR-generated fragments spanning adjacent genes are represented as black boxes. B) Agarose gel analysis of the PCR. Lanes 1-6 correspond to the appropriate fragments and the sizes (bp) are as follows: 1; 297, 3; 285, 4; 255, 5; 243, 6; 277. Marker indicates 1 kb Hyperladder.

in the same transcript. Should adjacent genes be co-transcribed, then a band will be present when PCR products were visualised on an agarose gel.

As PCR products were formed using the primer pair for region 1 (i.e., the interface of *nasT* and *nasS*), it is clear that *nasTS* form a transcriptional unit. Similarly, PCR products were generated using separate primer pairs for regions 3, 4, 5 and 6, demonstrating that *nasABGHC* also comprise a single transcriptional unit. However, the absence of a PCR product for region 2 (i.e., between *nasS* and *nasA*) concludes *nasS* and *nasA* are not present together on the same mRNA. Accordingly, *nasTS* and *nasABGHC* form individual operons. Importantly, in constructing *nasT-lacZ* and *nasA-lacZ* gene-reporter fusions, expression levels for of *nasT* and *nasA* will also be representative of the downstream genes in their distinct operons.

For investigation of of *nasT* and *nasA* transcription, *lacZ* gene-reporter fusion constructs were produced in the wide host-range plasmid pMP220 to give the *nasA-lacZ* (pBP042) and *nasT-lacZ* (pBP043) constructs (See Section 2.17 for details), which were mobilised into *P. denitrificans* for experiments. These strains were grown under defined conditions to quantify expression of *nasTS* and *nasABGHC* over the course of growth on various nitrogen sources.

Figure 3.5 shows expression profiles for the regulatory and structural genes for Nas, exemplified by the *nasT* and *nasA* genes respectively, during growth with different nitrogen sources. In the presence of ammonium, at ~100 (*nasT-lacZ*) and ~50 (*nasA-lacZ*) Miller units (Mu), expression of the *nas* genes is low (Figure 3.5A), and consistent with studies that show the activity of the assimilatory nitrate reductase is relatively low in *P. denitrificans* cells grown with ammonium as the sole nitrogen source (Gates et al. 2011). However, despite the low levels of β -galactosidase activity observed for ammonium grown cells, expression of *nasT-lacZ* and *nasA-lacZ* is clearly not absent when compared to the vector control. By contrast, transcription of *nasT* and *nasA* is drastically increased when *P. denitrificans* is grown solely with nitrate as sole nitrogen source. In this case, ~4000 and ~2500 Mu were observed for *nasT-lacZ* and *nasA-lacZ*, respectively (Figure 3.5B), which represent between a 40-fold and 50-fold increase in *nas* expression during growth on nitrate compared with cells using ammonium as sole nitrogen source. The transcription of both genes remains relatively steady over the course of growth. Interestingly, cultures supplemented with both ammonium and nitrate exhibit a clear transcriptional phenotype. Under these growth conditions, both *nasT-lacZ* and *nasA-lacZ* expression is at low background levels, i.e. ~100-200 Mu, similar to those observed for cultures supplemented solely with ammonium. However, following ~8-10 h

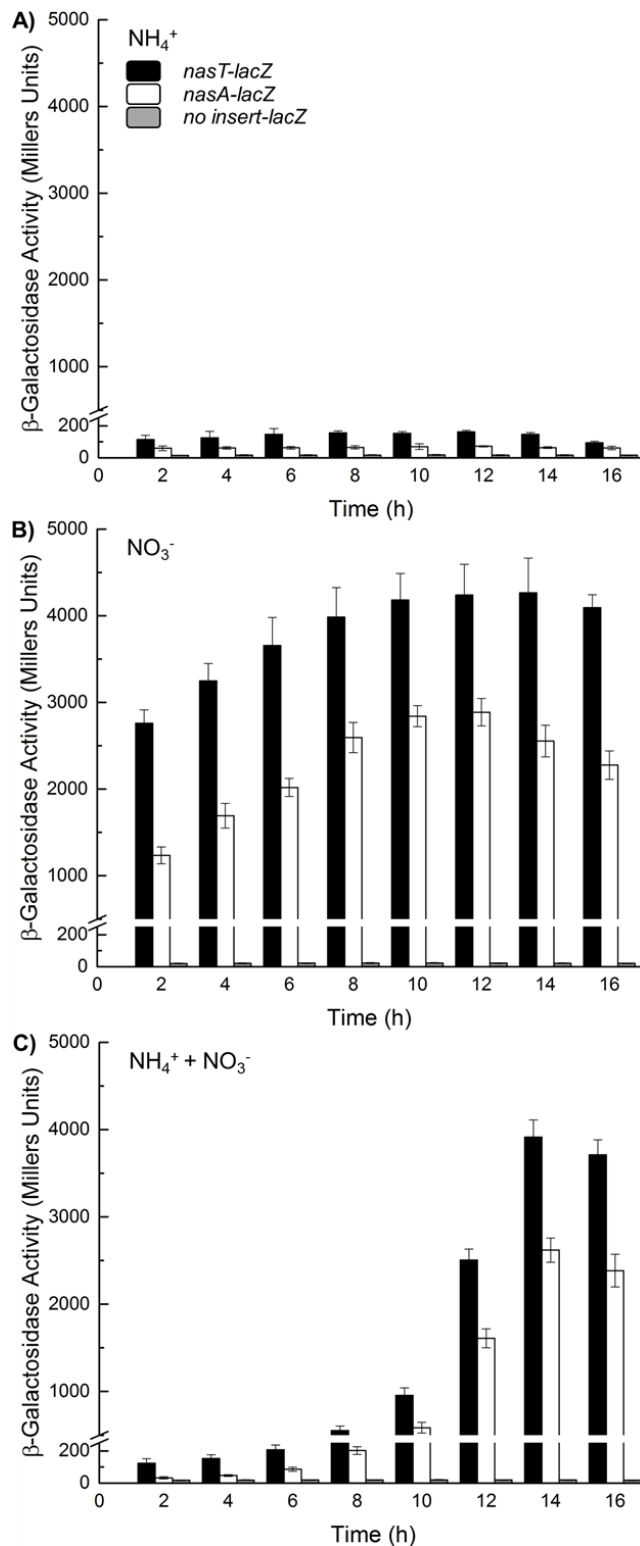


Figure 3.5. Expression of *nasT* and *nasA* in *P. denitrificans* during ammonium-dependent and nitrate-dependent growth. β -galactosidase activities were measured in cells containing plasmid-borne *nasT-lacZ* (black) and *nasA-lacZ* (white) gene-reporter fusions during growth of *P. denitrificans* with an empty vector control containing no promoter (grey). Cultures were grown aerobically in minimal media at 30 °C with 30 mM succinate and either 10 mM ammonium, 10 mM nitrate or 5 mM ammonium and 5 mM nitrate.

of growth, transcription of both *nasT* and *nasA* increases in cells by an order of magnitude. By 14 h, expression of *nasT-lacZ* (~4000 Mu) and *nasA-lacZ* (~2500 Mu) reaches similar levels to those observed in cells grown solely with nitrate. These gene expression studies correlate well with the diauxic growth data presented in Figure 3.3 G, where ammonium is consumed first during the initial growth phase, followed by a switch to nitrate-utilisation at ~10 h, where the onset of extracellular nitrate uptake and the second nitrate-dependent growth phase latter mode of growth requires *nas* expression.

The expression data described above fits well with the mainstream view that heterotrophic bacteria prefer to use ammonium as an inorganic nitrogen source over nitrate. However, in laboratory studies, experiments are often conducted with relatively oxidised carbon substrates and low carbon:nitrogen ratios. Therefore, impact of the availability of carbon substrates with different oxidation states (to alter cellular redox status) was explored to determine the metabolic consequences of NADH-linked nitrate assimilation in *P. denitrificans*.

3.3 The Influence of Carbon on Nitrate-Dependent and Ammonium-Dependent Growth of *Paracoccus denitrificans*

3.3.1 Succinate

Succinate is the most common dicarboxylic acid carbon substrate used for heterotrophic growth of *Paracoccus* sp. in laboratory studies. The acidic form of this 4-carbon containing substrate contains two distinct functional groups: 2(R¹COOH) and 2(R¹CH₂R²) in which the oxidation state of carbon is +3 and -2, respectively (Figure 3.6A) (Hanson 1990). Therefore, the total oxidation number of carbon is +2 and an average oxidation number for carbon of +1/2 can be assigned in this molecule. Succinate is a key intermediate of the TCA cycle where it is oxidised to fumarate by the membrane-bound succinate dehydrogenase, which also participates in the respiratory chain. Conceptually, two molecules of succinate enter the TCA cycle to yield two molecules of malate. One goes on to form oxaloacetate, and the second is used to produce acetyl-CoA by the sequential reactions of Malic enzyme (Figure 1, step 2) and Pyruvate kinase (Figure 1, step 3). Further metabolism of the oxaloacetate and acetyl-CoA produced regenerates a single molecule of succinate (Figure 1). Therefore, the net catabolic oxidation of succinic acid (C₄H₆O₄) generates 14 electrons:



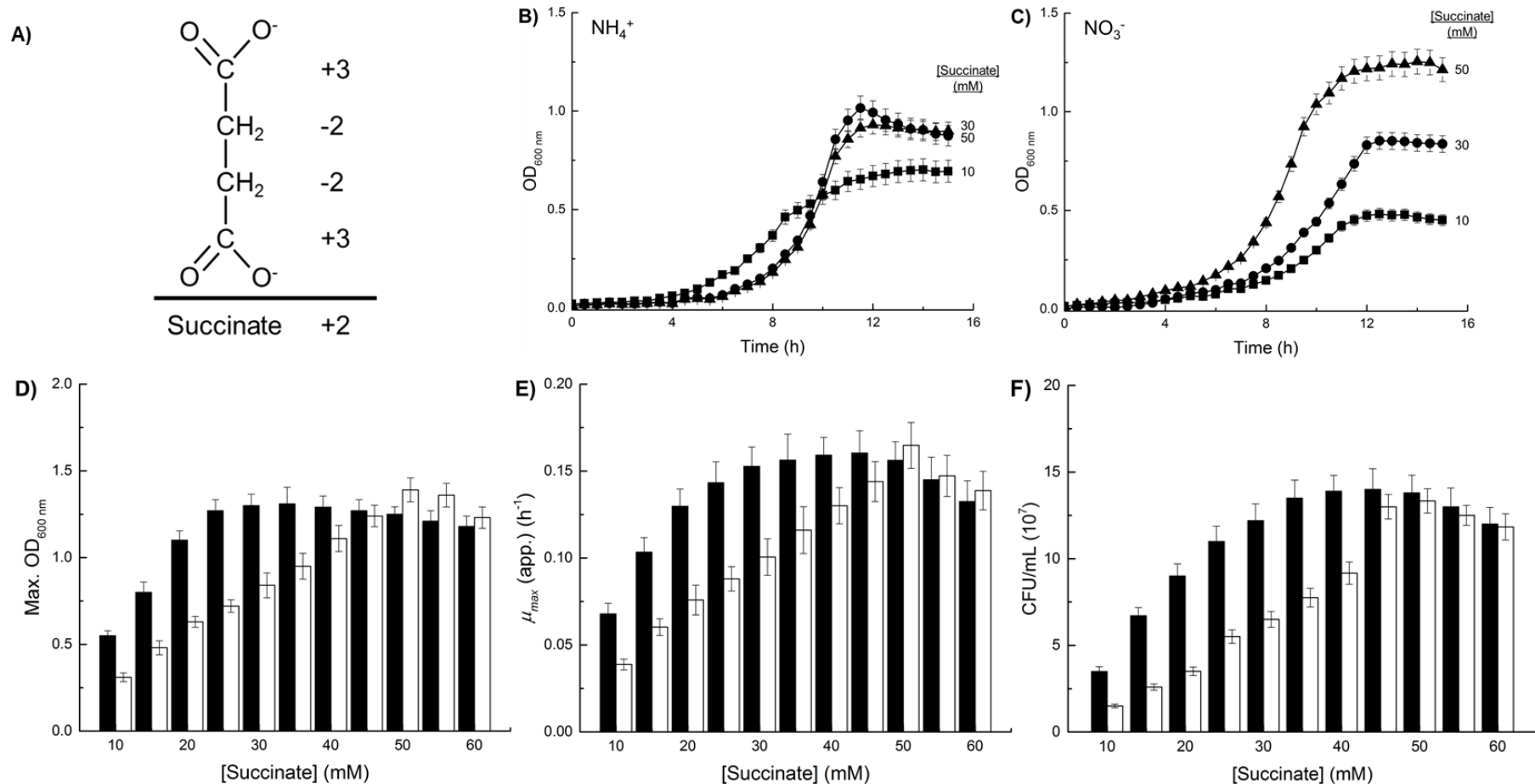


Figure 3.6. Growth of *P. denitrificans* on various concentrations of succinate. A) Skeletal representation of succinate showing oxidation numbers of each carbon atom. Aerobic growth of *P. denitrificans* in minimal media, 30 °C, with 10 mM B) ammonium or C) nitrate as a sole nitrogen source. Squares; 10 mM succinate, circles; 30 mM succinate, triangles; 50 mM succinate. D) Maximum OD_{600 nm}, E) μ_{max} (app.) and F) CFU/mL (at the maximum OD_{600 nm}) of cultures grown with various succinate concentrations with 10 mM ammonium (black) or nitrate (white).

Figure 3.6 shows the effect of succinate availability on the growth of *P. denitrificans* during ammonium-dependent and nitrate-dependant growth. Bacterial cell growth was followed by measuring the optical density of cultures at 600 nm ($OD_{600\text{ nm}}$), as described above, but also by measuring colony forming units per mL (CFU/mL) at the max. $OD_{600\text{ nm}}$ to ensure growth measurements were not subject to interference by possible accumulation of intracellular carbon-storage polymers, e.g. polyhydroxybutyrate (PHB), which may be formed by *P. denitrificans* under carbon-rich growth conditions (Mothes et al. 2004).

Growth curves for *P. denitrificans* using either ammonium or nitrate as sole nitrogen sources show a clear dependence on succinate concentration, as illustrated by Figure 3.6A and 3.6B. With ammonium as a sole nitrogen source, maximal growth was achieved between 25 and 40 mM succinate (Figure 3.6, panels B-F). At 40 mM, the max. $OD_{600\text{ nm}}$ was ~ 1.3 AU, μ_{max} (app.) for the bacterium was $\sim 0.16\text{ h}^{-1}$ and cultures contained $\sim 14 \times 10^7$ cells per mL. In comparison, with nitrate and 40 mM succinate, the max. $OD_{600\text{ nm}}$ was ~ 1.1 AU, μ_{max} (app.) for the bacterium was $\sim 0.13\text{ h}^{-1}$ and cultures contained $\sim 9 \times 10^7$ cells per mL. Nitrate-dependant cultures required higher levels of carbon substrate to reach maximum growth, which was achieved above 50 mM succinate. Interestingly, between 50 and 60 mM succinate both the max. $OD_{600\text{ nm}}$ and μ_{max} (app.) of nitrate-dependant [e.g., max. $OD_{600\text{ nm}} = \sim 1.4$ AU; μ_{max} (app.) = $\sim 0.17\text{ h}^{-1}$ at 50 mM succinate] cultures matches if not exceeds those for ammonium-dependent [e.g., max. $OD_{600\text{ nm}} = \sim 1.3$ AU; μ_{max} (app.) = $\sim 0.16\text{ h}^{-1}$ at 50 mM succinate] growth by $\sim 5\text{-}10\%$. However, similar cell counts of $\sim 13 \times 10^7$ per mL were observed for both growth conditions, which may suggest the bacterium could be storing a small population of carbon that would influence culture OD measurements at 600 nm, from which max. $OD_{600\text{ nm}}$ and μ_{max} (app.) were derived. Having said that, when compared with ammonium, it is strikingly clear that assimilation of nitrate requires substantially more carbon to achieve maximal cell growth, consistent with the need to generate extra NADH to drive assimilatory nitrate reduction.

Given that assimilatory nitrate reduction requires NADH-derived from carbon oxidation and respiratory bacterial nitrate-utilisation pathways (e.g. Nap) may also be used for redox balancing in *Paracoccus* sp., a link between the bioavailability and redox states of alternative carbon sources and nitrate-dependent growth of *P. denitrificans* was tested. Here, aerobic growth using the different carbon sources: malate, pyruvate and butyrate (in order of most oxidised to most reduced) was analysed in minimal salts media. In analogous experiments to that described above for succinate, the concentration of the

different carbon sources was varied between 5 and 60 mM except for butyrate, which was toxic at high-millimolar levels.

3.3.2 Malate

Malate is a highly oxidised 4-carbon containing dicarboxylic acid that participates in the last step of the TCA cycle where it is oxidised to oxaloacetate by malate dehydrogenase. Malic acid contains three distinct functional groups: $2(R^1COOH)$, $R^1CH(OH)R^2$ and $R^1CH_2R^2$ in which the oxidation state of carbon is +3, 0 and -2, respectively (Figure 3.7A) (Hanson 1990). Therefore, the total oxidation number of carbon is +4 and an average oxidation number for carbon of +1 can be assigned in this molecule. Complete catabolic oxidation of malic acid ($C_4H_6O_5$) proceeds in a similar manner to that described above for succinic acid, but instead generates 12 electrons:



Figure 3.9 shows the effect of malate on the growth of *P. denitrificans* with either ammonium or nitrate as sole nitrogen source. With malate as carbon source, there is a clear difference between the ammonium-dependent and nitrate-dependent growth over the concentration range of carbon tested. Significantly lower biomass and μ_{max} (app.) values were observed for cultures using nitrate [i.e., max. $OD_{600\text{ nm}} = \sim 0.6$ AU, μ_{max} (app.) = $\sim 0.09\text{ h}^{-1}$] compared to ammonium [i.e., max. $OD_{600\text{ nm}} = \sim 1.3$ AU, μ_{max} (app.) = $\sim 0.16\text{ h}^{-1}$] as sole nitrogen source (Figure 3.7, panels B-E). This represents a decrease of $\sim 50\%$ and $\sim 40\%$ in terms of max. $OD_{600\text{ nm}}$ and μ_{max} (app.), respectively for nitrate-dependent versus ammonium-dependent growth. However, during ammonium-dependent growth with 50 mM malate, similar values for the max. $OD_{600\text{ nm}}$, μ_{max} (app.) and cell counts, of ~ 1.3 AU, $\sim 0.16\text{ h}^{-1}$ and $\sim 14 \times 10^7$ cells per mL, were observed compared to those determined with 50 mM succinate (see section 3.3.3 above). Similarly, with malate, nitrate-dependent growth gave lower cell counts of $\sim 5 \times 10^7$ cells per mL (compared to $\sim 14 \times 10^7$ cells per mL during ammonium-dependent growth, see Figure 3.7F), which remains relatively constant above 30 mM malate, representing a decrease of $\sim 60\%$.

These clear differences highlight how important the carbon source is for assimilatory nitrate reduction in *P. denitrificans*. As malate yields one $FADH_2$, both respiration and nitrate assimilation are more reliant on the same source of reductant, the NADH pool. Competition between respiration and nitrate assimilation for NADH may provide an explanation as to why nitrate-dependent cell growth with malate is so poor in comparison with ammonium-dependent growth.

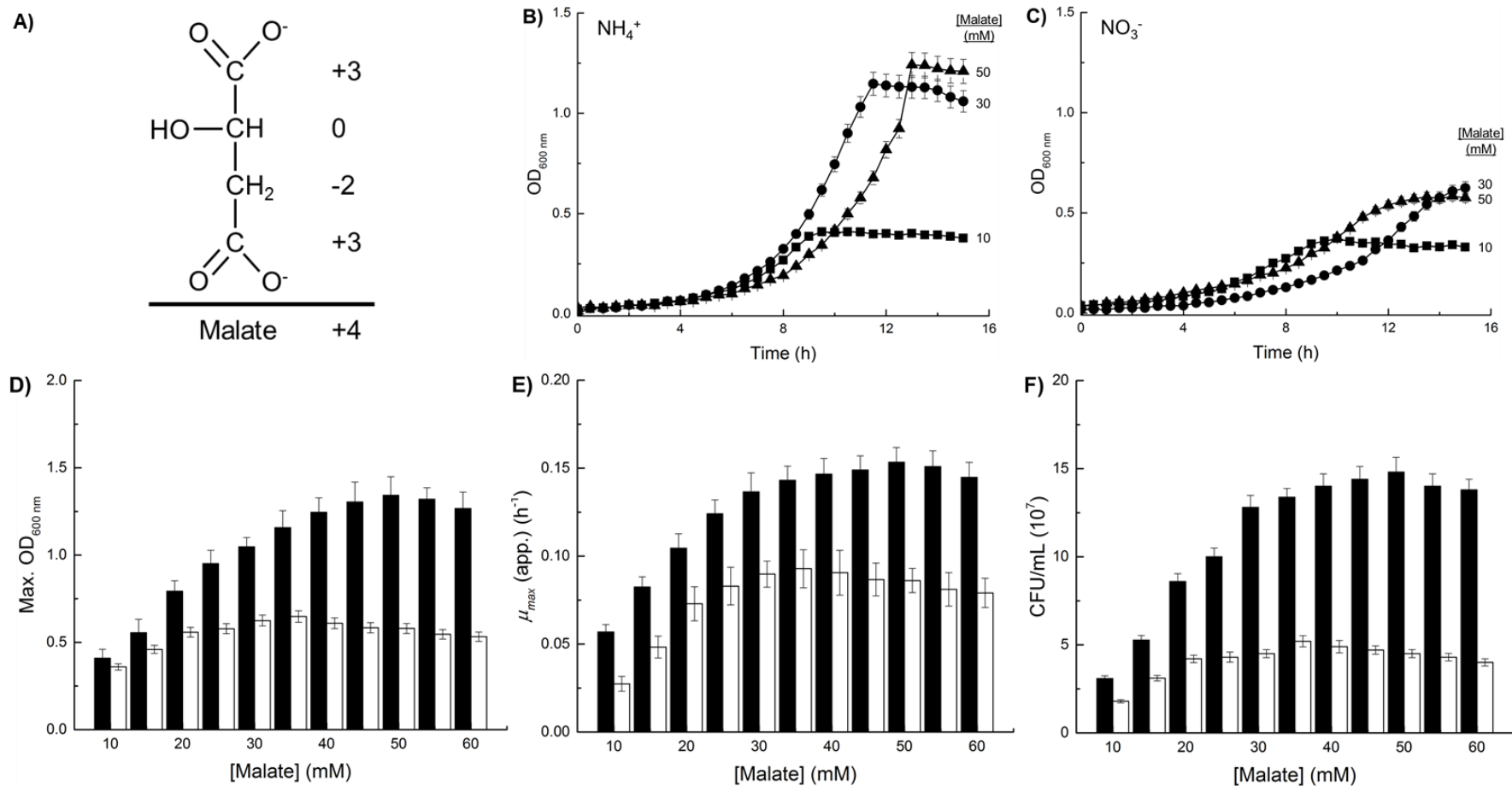


Figure 3.7. Growth of *P. denitrificans* with various concentrations of malate. A) Skeletal representation of malate showing oxidation numbers of each carbon atom. Aerobic growth of *P. denitrificans* in minimal media, 30 °C, with 10 mM B) ammonium or C) nitrate as a sole nitrogen source. Squares; 10 mM malate, circles; 30 mM malate, triangles; 50 mM malate. D) Maximum OD_{600 nm}, E) μ_{max} (app.) values and F) CFU/mL (at the maximum OD_{600 nm}) of cultures grown with various malate concentrations with 10 mM ammonium (black) or nitrate (white).

3.3.3 Pyruvate

Pyruvate is a 3-carbon containing keto-acid that is converted to acetyl-CoA for use in the TCA cycle (Figure 1). The acidic form, pyruvic acid, contains three distinct functional groups: R^1COOH , $R^1R^2C=O$ and R^1-CH_3 in which the oxidation state of carbon is +3, +2 and -3, respectively (Figure 3.8A) (Hanson 1990). Therefore, the total oxidation number of carbon in pyruvate is +2 and an average oxidation number for carbon of +2/3 can be assigned in this molecule. Complete oxidation of a single pyruvic acid ($C_3H_4O_3$) molecule generates 10 electrons:

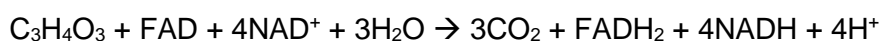


Figure 3.8 demonstrates that *P. denitrificans* can effectively metabolise pyruvate as sole carbon and energy source during either ammonium-dependent or nitrate-dependent growth. With increasing availability of pyruvate, max. $OD_{600\text{ nm}}$ and μ_{max} (app.) increased linearly between 5-25 mM and 5-50 mM carbon during ammonium-dependent and nitrate ammonium and nitrate-dependent growth, respectively. Again, comparatively higher carbon levels were required to achieve maximal growth with nitrate compared to ammonium as sole nitrogen source, a pattern consistent with other carbon sources reported above. Maximum growth for ammonium-dependent cultures was achieved at 25 mM pyruvate, above which it plateaus [max. $OD_{600\text{ nm}} = \sim 1.6$ AU, μ_{max} (app.) = ~ 0.16 h⁻¹] (Figure 3.8, panels D and E). Here, a cell count of $\sim 16 \times 10^7$ per mL was observed (Figure 3.8F). By contrast, when assimilating nitrate, more pyruvate is required for cells to reach similar levels of growth. In this case, cells did not reach their maximum growth until supplemented with 50 mM pyruvate where max. $OD_{600\text{ nm}} = \sim 1.8$ AU, μ_{max} (app.) = ~ 0.18 h⁻¹ and a colony count of $\sim 17 \times 10^7$ per mL was observed (Figure 3.8, panels B-F). Above 50 mM pyruvate, nitrate-dependent growth shows a slight but consistent increase compared with that observed for cells grown with ammonium.

Given that the growth output of *P. denitrificans* exhibits such a greater dependence on the concentration of pyruvate as a carbon (and energy source) when assimilating nitrate, compared to ammonium, it suggests assimilatory nitrate reduction may be a substantial sink for electrons.

3.3.4 Butyrate

Butyrate is a 4-carbon containing short chain fatty acid with three different functional groups: R^1COOH , $2(R^1CH_2R^2)$ and $3(R^1-CH_3)$ in which the oxidation state of carbon is +3, -2 and -3, respectively (Figure 3.8A) (Hanson 1990). Therefore, the total oxidation

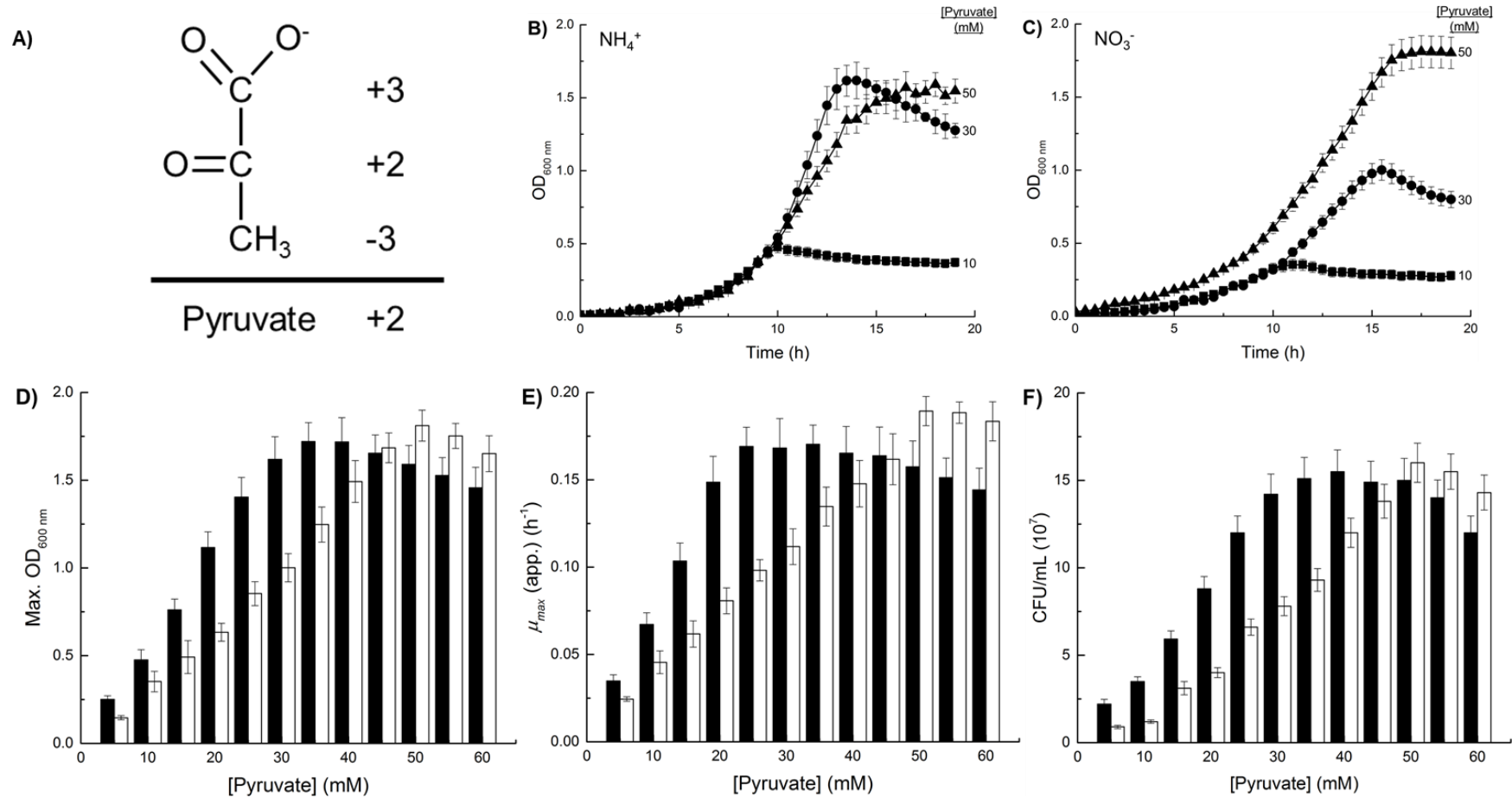
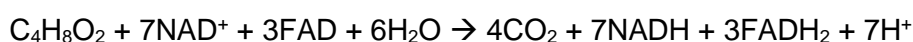


Figure 3.8. Growth of *P. denitrificans* with various concentrations of pyruvate. A) Skeletal representation of pyruvate showing oxidation numbers of each carbon atom. Aerobic growth of *P. denitrificans* in minimal media, 30 °C, with 10 mM B) ammonium or C) nitrate as a sole nitrogen source. Squares; 10 mM pyruvate, circles; 30 mM pyruvate, triangles; 50 mM pyruvate. D) Maximum OD_{600 nm}, E) μ_{max} (app.) and F) CFU/mL (at the maximum OD_{600 nm}) of cultures grown with various pyruvate concentrations with 10 mM ammonium (black) or nitrate (white).

number of carbon in butyrate is -4 and an average oxidation number for carbon of -1 can be assigned in this molecule. Therefore, butyrate is highly reduced compared to succinate, malate and pyruvate described above. Butyrate undergoes β -oxidation at the inner membrane in *P. denitrificans* to form one molecule of FADH₂ and NADH. This produces two molecules of acetyl-CoA, which enter the TCA cycle to yield a further two FADH₂ and six NADH molecules. Hence, complete catabolic oxidation of butyrate produces a total of three FADH₂ molecules and seven NADH molecules for use in cellular respiration:



Butyrate has been shown to alter the intracellular redox balance of *Paracoccus* sp. via production of QH₂ and induces systems such as the QH₂-oxidase cytochrome *bo*₃ and QH₂/nitrate oxidoreductase Nap to vent excess cellular reductant to electron sinks, i.e. oxygen and nitrate respectively, in the periplasm (Gates et al. 2008). The NADH formed may also be used to drive nitrate assimilation.

Figure 3.9 shows that butyrate can be used by *P. denitrificans* as a carbon and energy source under aerobic conditions during either ammonium-dependant or nitrate-dependent growth. Here, similar profiles were observed for growth on ammonium or nitrate with respect to carbon concentration, whereby maximal growth was observed at 10 mM butyrate, above which growth was inhibited by additional levels of carbon. Most strikingly, growth with nitrate was consistently favoured relative to ammonium and at 10 mM the difference was significant where growth on nitrate [max. OD_{600 nm} = ~1.3 AU, μ_{max} (app.) = ~0.16 h⁻¹] was enhanced by ~20% relative to that observed with ammonium [max. OD_{600 nm} = ~1.0 AU, μ_{max} (app.) = ~0.13 h⁻¹]. This behaviour was also reflected by colony counts, where ~16 x 10⁷ or ~13 x 10⁷ per mL were determined for cultures using nitrate or ammonium as sole nitrogen source, respectively (i.e. an increase of ~19% with nitrate versus ammonium).

Although, at this stage, the contribution of Nap to enhanced growth with nitrate could not be excluded, it is possible that Nas offers the major route for the excess energy produced by cellular metabolism of butyrate by coupling NADH oxidation to nitrate reduction and biomass production. Notably, it is not unusual that cells experience difficulty in growing at high levels of fatty acids, which can transport protons across the cytoplasmic membrane and thus act like classical uncoupling molecules of oxidative phosphorylation (Kadenbach 2003). This may explain the apparent toxicity of butyrate above ~15 mM. A previous study on *Paracoccus pantotrophus* investigating growth with butyrate reported similar findings, but concluded that cultures were unable to maintain a suitable redox

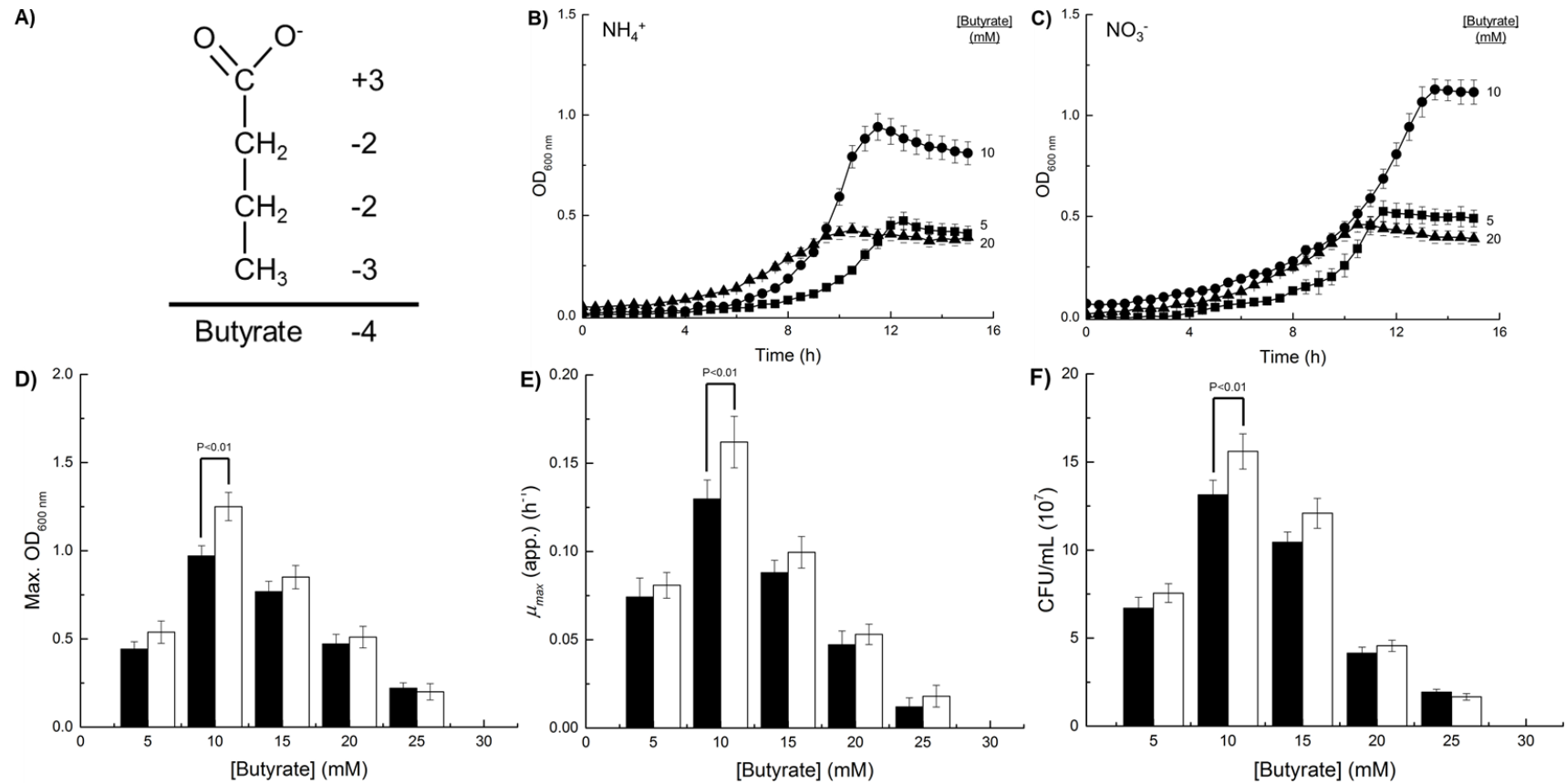


Figure 3.9. Growth of *P. denitrificans* with various concentrations of butyrate. A) Skeletal representation of pyruvate showing oxidation numbers of each carbon atom. Aerobic growth of *P. denitrificans* in minimal media at 30 °C with B) 10 mM ammonium or C) 10 mM nitrate as a sole nitrogen source. Squares; 5 mM butyrate, circles; 10 mM butyrate, triangles; 20 mM butyrate. D) Maximum OD_{600 nm}, E) μ_{max} (app.) values and F) CFU/mL (at the maximum OD_{600 nm}) of cultures grown with various butyrate concentrations with 10 mM ammonium (black) or nitrate (white). Where given, P values were calculated from three independent biological replicates.

status and balance of reducing equivalents (Ellington et al. 2002).

3.3.5 The Oxidation State of the Carbon Source Influences the Ability of *P. denitrificans* to Assimilate Nitrate

To determine whether the ability to assimilate nitrate is dependent upon the cytoplasmic NADH pool and thus can be influenced by the oxidation state of carbon substrates used for growth, the data described above was analysed in terms of carbon:nitrogen (C:N) ratios. Figure 3.10 below shows the maximum growth yields of *P. denitrificans* when cultured on different carbon substrates using a C:N ratio of 4:1 and 16:1 when using either ammonium or nitrate as sole inorganic nitrogen source for growth.

The more reduced the carbon substrate, the more FADH₂ and NADH are typically produced per molecule during cellular respiration (Table 3.2). Butyrate being the most reduced compound tested yields twenty electrons when fully oxidised, of which fourteen may contribute to nitrate/nitrite assimilation. *P. denitrificans* shows preference for growth under butyrate conditions when using a 4:1 C:N ratio irrespective of inorganic nitrogen source, having a cell count of $\sim 15 \times 10^7$ CFU/mL (also supported by growth rates, see Table 3.2) which is around 7-fold higher than those using pyruvate, succinate or malate, presumably as the reducing equivalents produced are sufficient to achieve efficient metabolism and biomass production (Figure 3.10A). Furthermore, it actually appears preferential for cells to assimilate nitrate instead of using ammonium with butyrate at this ratio as the cell count and growth rate was significantly higher. This is likely due to inability of ammonium-dependant growth to dispose of the excess energy produced as a result of butyrate whilst Nas offers an anabolic-linked energy vent for the reducing equivalents generated.

Figure 3.10B shows more distinguished features when cultures are grown at a higher carbon concentration as opposed to Figure 3.10A. At this 16:1 C:N ratio *P. denitrificans* supplemented with ammonium reaches consistent levels of $\sim 14 \times 10^7$ CFU/mL and growth rates of $\sim 0.15 \text{ h}^{-1}$ independent of the carbon substrate. This shows that carbon respiration is no longer limiting growth output during ammonium-dependant growth and it is not dependent upon the concentration or oxidation state. However, when assimilating nitrate, growth becomes much more resolved and distinct between the carbon compounds. Maximum cell counts were recorded of 15.5×10^7 CFU/mL, 9×10^7 CFU/mL and 5×10^7 CFU for pyruvate, succinate and malate respectively, which correlates with the most reduced to most oxidised carbon compound and is also a trend present with the growth rates (Table 3.2). This demonstrates that the growth capability of *P. denitrificans* during nitrate-dependant growth is highly dependent upon the redox

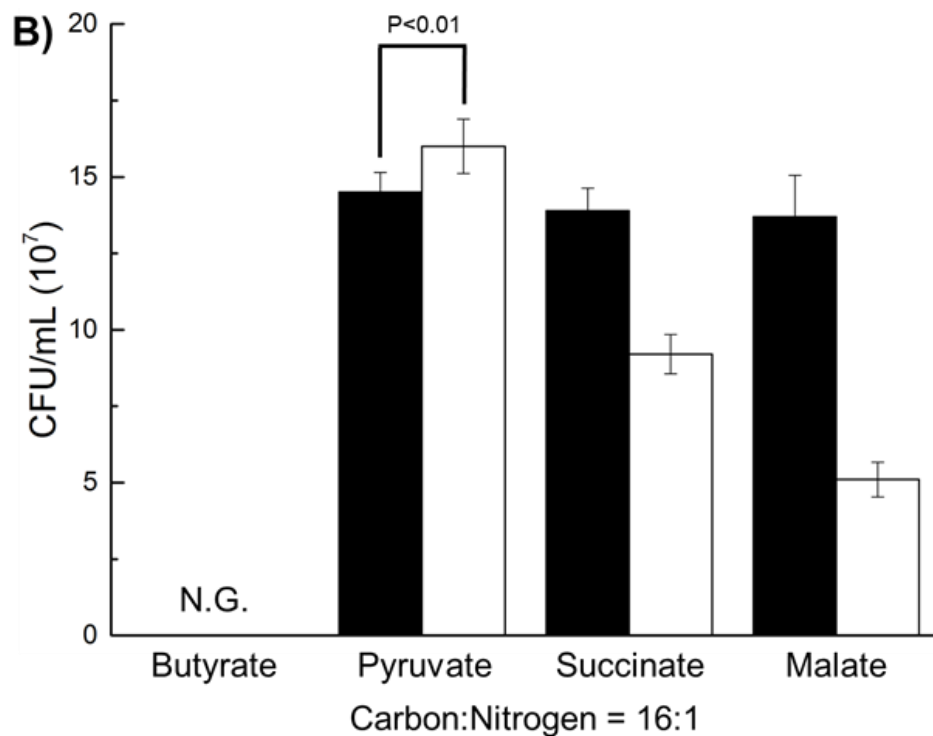
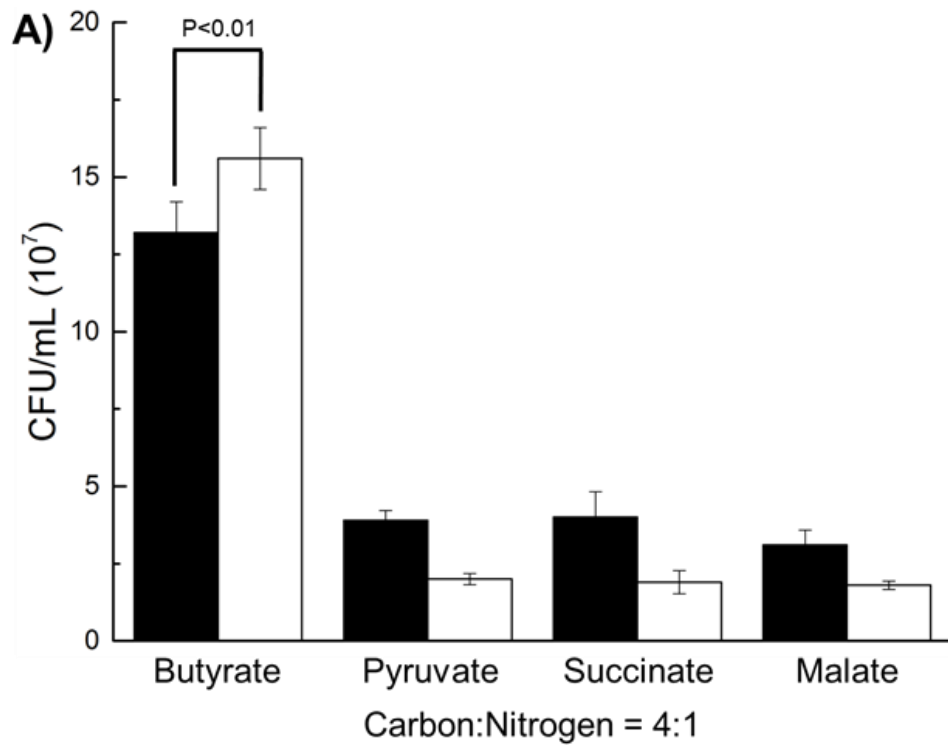


Figure 3.10. Maximum growth of *P. denitrificans* using different carbon substrates at defined carbon:nitrogen ratios. *P. denitrificans* was grown aerobically in minimal media, 30 °C, with 10 mM ammonium (black) or nitrate (white) as sole nitrogen sources. The maximum CFU of cultures grown using butyrate, pyruvate, succinate or malate at A) 4:1 and B) 16:1 carbon:nitrogen ratio are shown. N.G. represents no growth. P values were calculated from three independent biological replicates.

Table 3.2. Relevant growth parameters for *P. denitrificans* cultured with different carbon substrates at defined carbon:nitrogen ratios.

Compound	Total Carbon Oxidation Number	NADH/molecule FADH ₂ /molecule	NADH/carbon FADH ₂ /carbon	C:N	mM	<i>μ</i> _{max} (app.) (h ⁻¹)			Dry Mass (mg/mL)	C:N	mM	<i>μ</i> _{max} (app.) (h ⁻¹)			Dry Mass (mg/mL)
						NH ₄ ⁺	NO ₃ ⁻					NH ₄ ⁺	NO ₃ ⁻		
Butyrate	-4	7	1.75	4:1	10	0.13	13.2	1.08	16:1	40	N.G.	N.G.	N.G.	N.G.	
		3	0.75			0.16	15.6	1.41				.			
Pyruvate	+2	4	1.33	4:1	13.3	0.07	3.9	0.83	16:1	53.3	0.15	14.5	1.70		
		1	0.33			0.04	2.0	0.55				0.17	16.1	1.95	
Succinate	+2	5	1.25	4:1	10	0.07	4.0	0.63	16:1	40	0.16	13.9	1.45		
		2	0.5			0.03	1.9	0.32				0.13	9.2	1.28	
Malate	+4	5	1.25	4:1	10	0.05	3.1	0.53	16:1	40	0.15	13.8	1.33		
		1	0.25			0.03	1.8	0.43				0.08	5.1	0.70	

state of the available environmental carbon substrates. Though pyruvate and succinate are highly comparable in terms of reductant generated, succinate requires two compounds for complete respiration (Figure 3.2A) meaning overall, pyruvate generates greater quantities of NADH and FADH₂ per molecule oxidised. Furthermore, growth output at this ratio for pyruvate was statistically higher in cultures supplemented with nitrate (Figure 3.10B), possibly due to the same effect discussed for butyrate above. Malate generates the least molecules of NADH/FADH₂ per molecule oxidised and as seen in Figure 3.10B this is insufficient to fuel nitrate assimilation for biomass production to the levels observed in ammonium conditions. However, we cannot rule out potential differences in uptake rates between these carbon sources, as the transport systems for dicarboxylates may harbour differing affinities for the distinct compounds. This may account for the poor use of malate as a carbon and energy source.

This informs that heterotrophic nitrate-assimilation is dependent upon not just the concentration of carbon source, but also its redox state and quantities of reducing equivalents it may generate as nitrate/nitrite reduction for synthesis of cellular material is dependent upon this cytoplasmic pool of reduced nucleotide pyridines. Finally, this data shows Nas, the NADH:nitrate/nitrite oxidoreductase, is acting as a reductant vent coupled to nitrate anabolism which is preferential for cells to use under energy-rich conditions. This leads to increased biomass per carbon supplemented to cells, as opposed to the Nap system which is uncoupled to growth and energy production, dissipating excess energy at the inner membrane.

3.4 β -Galactosidase Assays Highlights the Regulation of the Carbon:Nitrogen Interface by Ntr Proteins

To further explore the link between supplemented nitrogen and carbon sources, the GS-GOGAT cycle and GDH pathway was examined: the interface where ammonium is integrated with carbon skeletons to produce organic nitrogen compounds for pivotal cellular structures (see Section 1.5 for review). GDH has low affinity for ammonium but requires little energy input (1 NADH compound) making it ideal for nitrogen rich environments. In contrast, the GS-GOGAT cycle requires ATP and NADH but has a much greater affinity for ammonium, therefore it is typically expressed under nitrogen limited conditions, i.e. nitrate assimilation (Helling 1998).

2-oxoglutarate (α -ketoglutarate) is the pivotal metabolic precursor used to produce glutamine via ammonium ligation, and it is itself a component of the TCA cycle. Therefore, not only is the supplemented carbon responsible for NADH production to assimilate nitrate, it is also required as a substrate to integrate it into organic structures.

The genes encoding GS (*glnA*), GOGAT (*gltD* – small subunit) and GDH (*gdhA*) were fused into the transcriptional *lacZ* plasmid, pMP220, as outlined in Section 2.17. The plasmids were conjugated into *P. denitrificans* to monitor gene expression over the course of growth with various inorganic nitrogen sources (Figure 3.11).

At millimolar levels of ammonium, GDH is the predominant system for biosynthesis of organic nitrogenous compounds due to the high levels of gene expression, ~1000 Millers units, as opposed to basal transcription of GS-GOGAT (Figure 3.11A). Towards the end of growth when ammonium becomes limiting, i.e. stationary phase, GDH transcription decreases whilst GS-GOGAT is upregulated to ~400 Millers units, possibly in an attempt to scavenge residual cytoplasmic ammonium. When cultured by nitrate assimilation where ammonium is limiting, the GS-GOGAT system is upregulated to a high extent, ~1100 Millers Units, whilst GDH is constitutively switched off, consistent with the literature (Figure 3.11B). When grown with both ammonium and nitrate, GDH is transcribed initially to equal levels as seen in just ammonium alone, ~1000 Millers units. However, this expression decreases after cultures enter the exponential phase, ~8 hours, at which point the GS-GOGAT genes are upregulated, reaching ~800 Millers units by late exponential phase, which is 100% greater than the levels they reach in solely ammonium-dependant growth. This correlates with the data shown in Figure 3.3 and 3.4 where ammonium was consumed first, requiring GDH as seen here, followed by nitrate through the GS-GOGAT system, coinciding with *nas* upregulation ~8 h.

The GS-GOGAT cycle and GDH pathway are under strict Ntr regulation; low intracellular ammonium leads to activation of NtrBC (see Section 1.2.2) which positively upregulates the genes necessary for the GS-GOGAT system (Tempest et al. 1970; Bird & Wyman 2003). Furthermore, the Ntr system has been shown to activate the regulatory protein Nac, which in turn represses GDH transcription in ammonium-limitation (Schwacha & Bender 1993; Camarena et al. 1998). The effect NtrBC has upon the carbon/nitrogen interface was investigated by conjugating the gene-reporter plasmids into a *P. denitrificans* mutant strain lacking genomic *ntrBC*; $\Delta ntrBC$ (donated by Sullivan, M. J.). Cultures were grown to $OD_{600\text{ nm}} \sim 0.7$ and the β -galactosidase activity was quantified (Figure 3.12).

GDH is the predominant system for nitrogen incorporation with carbon during WT growth with ammonium whilst the GS-GOGAT cycle operates during nitrate-dependant growth, both systems reaching similar levels of transcription, ~1200 Millers units (Figure 3.12A

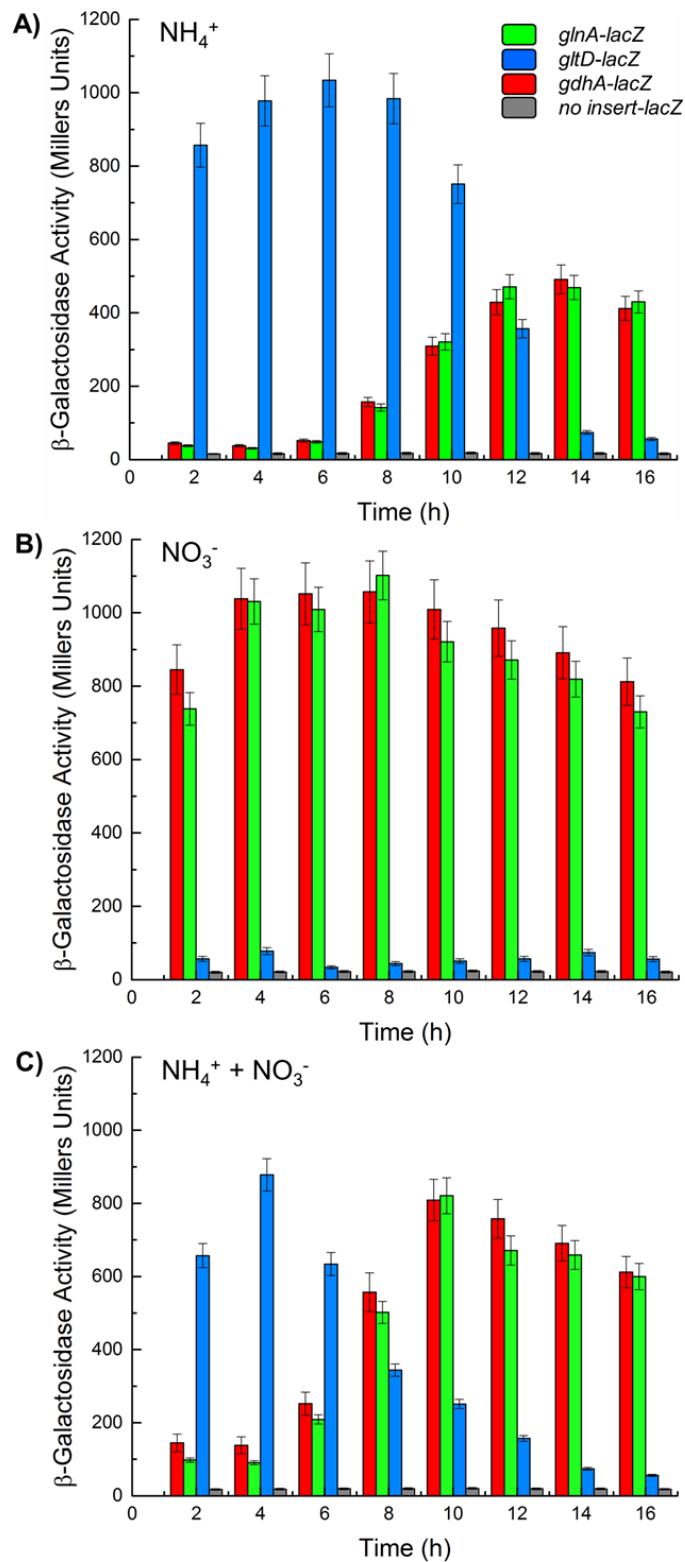


Figure 3.11. β -galactosidase activities of the *glnA-lacZ*, *glnD-lacZ* and *gdhA-lacZ* fusion plasmids during growth. *P. denitrificans* was grown aerobically in minimal media at 30 °C supplemented with 30 mM succinate. The transcriptional activity of *glnA* (red), *glnD* (green), *gdhA* (blue) and pMP220 containing no promoter (grey) is shown throughout the course of growth. Cultures were grown with nitrogen sources of A) 10 mM ammonium, B) 10 mM nitrate and C) 5 mM ammonium and 5 mM nitrate.

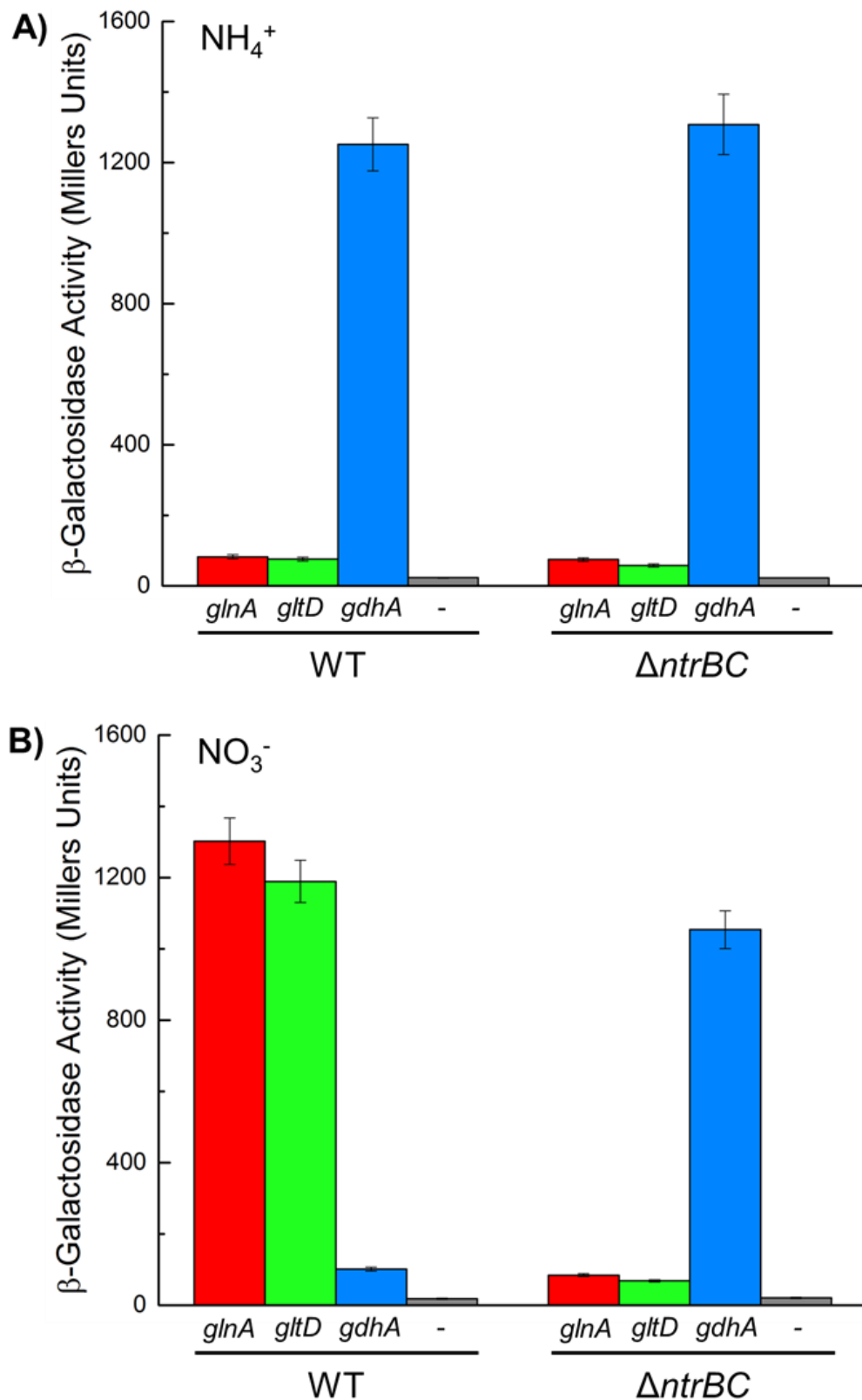


Figure 3.12. β -galactosidase activities of the *glnA-lacZ*, *gltD-lacZ* and *gdhA-lacZ* gene-reporter fusions in *P. denitrificans* strains. Transcriptional activity of *glnA* (red), *gltD* (green), *gdhA* (blue) and a plasmid containing no promoter (grey) measured at a mid-exponential phase in WT and $\Delta ntrBC$ grown aerobically at 30 °C aerobic growth, 30 °C, with 10 mM A) ammonium or B) nitrate as a sole nitrogen source.

and B). However, when *ntrBC* is deleted from the genome, the GS and GOGAT genes are not transcribed during nitrate assimilation as NtrC is not present to activate their expression (Figure 3.12B). Furthermore, NtrC upregulates Nac which in turn represses GDH transcription during nitrogen-limiting conditions. Therefore, in the $\Delta ntrBC$ strain, Nac will not be present and so GDH is constitutively expressed, even under nitrate-dependant growth, upregulated to similar levels as in ammonium conditions, ~1200 Millers units (Figure 3.12B). This data demonstrates the carbon:nitrogen interface is under NtrBC control, as found previously in other gram-negative bacteria, which typically functions in coordination with sigma 54 to regulate nitrogen-responses in bacteria.

3.5 Investigating Sigma 54 as a Regulator of the Nitrogen Status in *Paracoccus denitrificans*

Sigma 54, RpoN, is the typical nitrogen-responsive sigma factor in bacteria and the most probable candidate for initiating *Nas* and GS-GOGAT gene expression by guiding RNA polymerase to the promoter region, in coordination with NtrC. To characterise its regulatory role in *P. denitrificans*, a deletion strain deficient for *rpoN* was constructed.

The genomic deletion of *rpoN* was achieved as outlined in Section 2.16, by PCR-amplifying a pair of fragments identical to the forward and reverse region of *rpoN* and cloning them into pK18*mobsacB* to construct suicide vector pBP020 (Figure 3.13). This plasmid was conjugated into *P. denitrificans* where a double homologous recombinant event would produce $\Delta rpoN$ which was confirmed by sequencing the relevant section of the genome. Initially, the deletion strain was tested for its ability to assimilate and denitrify nitrate (Figure 3.14).

The deletion of sigma 54 has no apparent impact on *P. denitrificans* ability to use nitrate for biomass production or as an end terminal electron acceptor, as the mutant strain exhibited no clear phenotype or lack of nitrate-dependent growth. Should this sigma factor play a role in upregulating expression of *nas* and *nar* genes, it would be expected that $\Delta rpoN$ would be unable to grow under these conditions or exhibit serious attenuation in growth rates and OD_{max}. However, both of these values were similar between the WT and $\Delta rpoN$ strains indicating there was no impact.

This initial growth data indicated sigma 54 is not involved in regulating these gene clusters in *P. denitrificans* and so qRT-PCR analysis was employed on *nas* and *ntr* to identify any genetic phenotype. Cultures were grown under aerobic nitrate assimilation and RNA was harvested at a mid-exponential phase for subsequent analysis (Figure 3.15).

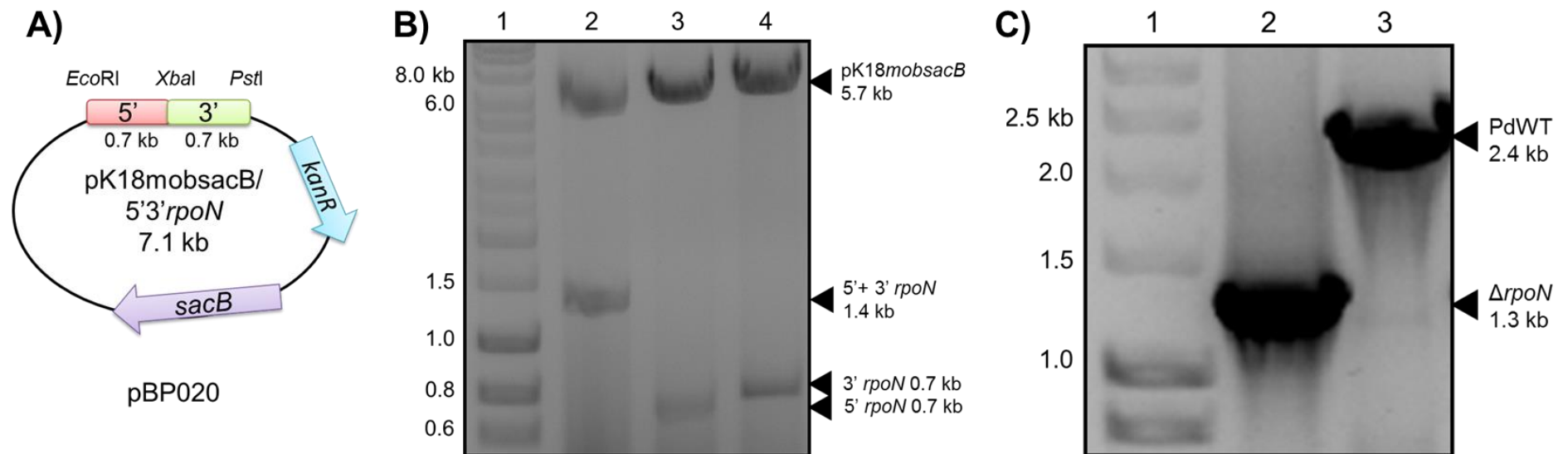


Figure 3.13. Cloning procedure for the deletion of genomic *rpoN* from *P. denitrificans*. A) Suicide-vector pBP020, a *pK18mobsacB* derivative harbouring 5' and 3' fragments of *rpoN* used for deletion. B) Digestion analysis of pBP020, lane 1; 1 kb Hyperladder, 2; *EcoRI/PstI* digestion of the 5'3' fragment, 3; *EcoRI/XbaI* digestion of the 5' fragment, 4; *XbaI/PstI* digestion of the 3' fragment. C) Colony MyTaq PCR confirmation for the removal of ~1 kb section of genomic DNA coding for *rpoN*. Lane 1; 1 kb Hyperladder, 2; $\Delta rpoN$, 3; WT.

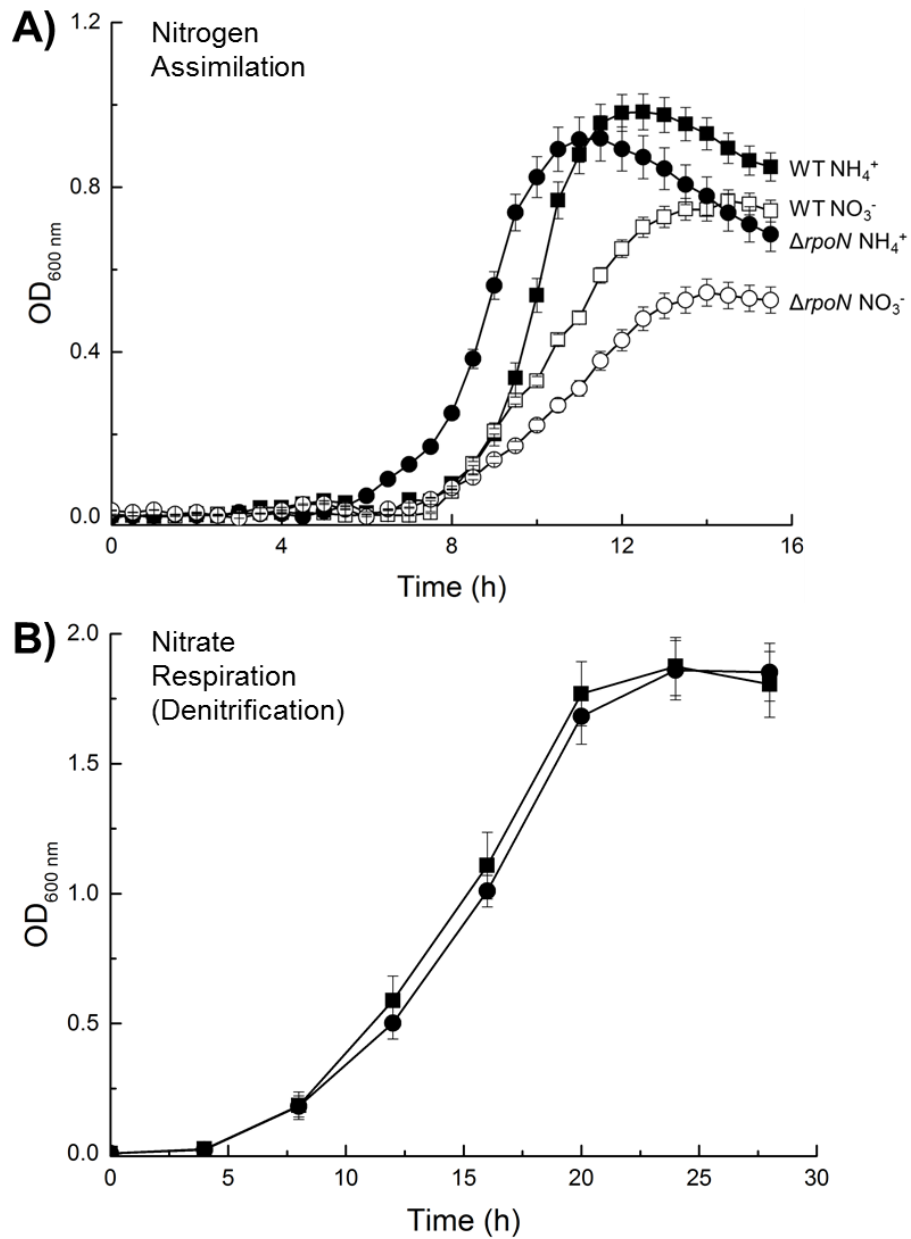


Figure 3.14. Growth phenotype of *P. denitrificans* deficient in genomic sigma 54. WT (squares) and *ΔrpoN* (circles) were grown at 30 °C in batch minimal media cultures supplemented with 30 mM succinate as a carbon source. A) Aerobic growth with either 10 mM ammonium (black) or nitrate (white) as a sole nitrogen source. B) Anaerobic denitrification with 20 mM nitrate as an electron acceptor and 10 mM ammonium as a nitrogen source.

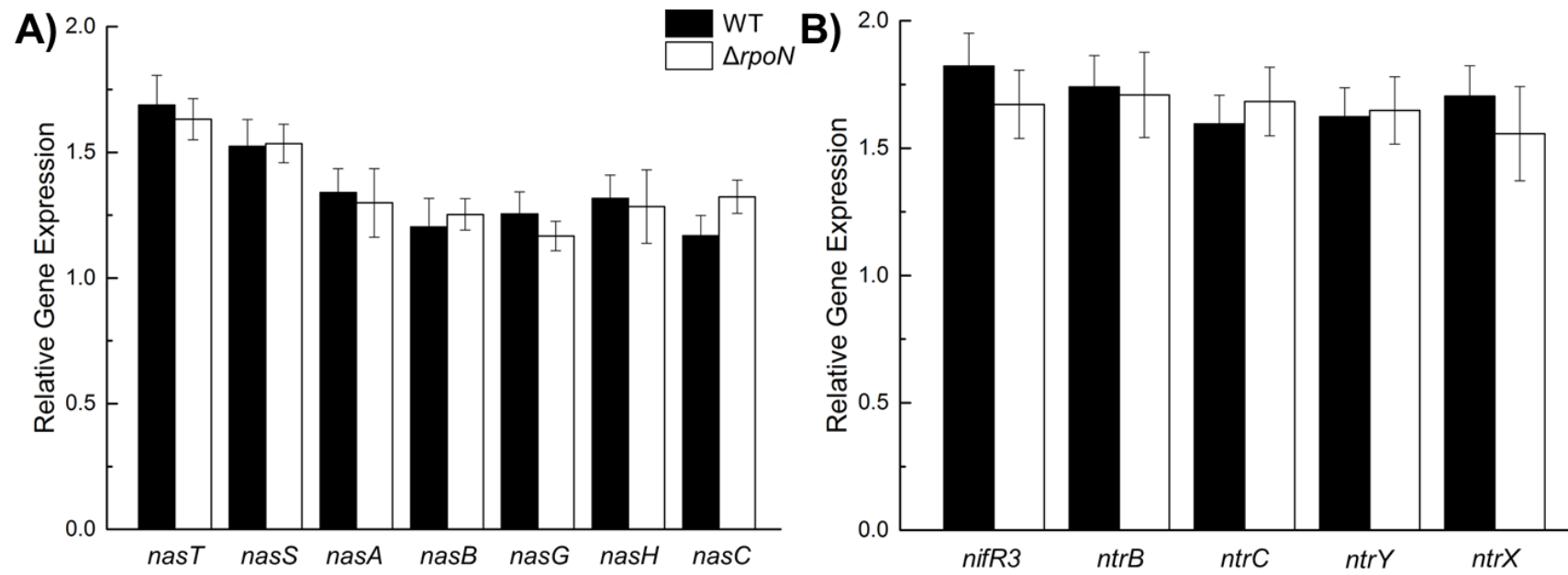


Figure 3.15. qRT-PCR analysis of the *nas* and *ntr* gene clusters in *P. denitrificans* strains during nitrate assimilation. qRT-PCR data representing expression of the A) *nas* and B) *ntr* genes in WT (black) and $\Delta rpoN$ (white) during assimilation of nitrate. Cells were grown aerobically in minimal salt media batch cultures at 30 °C supplemented with 30 mM succinate and 10 mM nitrate as a sole nitrogen source. RNA samples were harvested at a mid-exponential phase and gene expression was normalised to *dnaN*, a housekeeping gene.

As for the growth, no detrimental effects or attenuated expression were observed for the *nas* or *ntr* gene clusters when the sigma 54 gene was deleted from the genome of *P. denitrificans*. During aerobic nitrate-dependent growth, *nasTSABGHC* reached an expression value of ~ 1.5 and the *ntr* operon recorded ~ 1.6. No statistical difference was calculated in these values in the deletion strain. This data concludes the lack of a regulatory role undertaken by sigma 54 in transcriptional activation of the NtrBC system or genes encoding the Nar and Nas pathways in *P. denitrificans*.

Finally, *glnA*, encoding glutamine synthetase, has been previously demonstrated to be under sigma 54 regulation in enteric bacteria such as *E. coli* and *Salmonella* (Garcia et al. 1977). In Figure 3.12, we showed here that NtrBC is critical in regulation of the GS-GOGAT and GDH pathways, and as such, the gene-reporter fusion plasmids for these genes were conjugated into $\Delta rpoN$ to monitor transcription as before (Figure 3.16).

Contrary to previous studies in separate organisms, sigma 54 played no role in upregulation of genes involved in the GS-GOGAT cycle. During nitrate-dependant growth, both *glnA* and *gltD* were transcribed to ~1200 Millers units irrespective of the deletion (Figure 3.16B). We postulated the next likeliest candidate sigma factor for regulating transcription of nitrate assimilation and denitrification was sigma 32, *rpoH*, the heat-shock sigma factor. Following this data, an $\Delta rpoH$ deletion strain was constructed and investigated, but again no impaired growth or transcription of tested genes was observed (data not shown). Furthermore, a double deletion mutant for both sigma 54 and 32 was capable of assimilation and denitrification (data not shown). This implies that in *P. denitrificans*, NtrBC possibly functions in a sigma 54-independent manner to coordinate nitrogen-responsive pathways.

3.6 Exploring the Regulatory Role of NtrBC in Nitrogen-Metabolism

The NtrBC two-component complex is involved in regulating the nitrogen stress response in Gram-negative bacteria and plays a crucial role in maintaining the carbon/nitrogen interface as seen in Section 3.4. An $\Delta ntrBC$ mutant strain was grown aerobically in minimal media using various sole inorganic nitrogen sources (Figure 3.17). The $\Delta ntrBC$ strain exhibits attenuated growth on all inorganic nitrogen sources tested when compared to the WT strain, reaching consistently lower growth yields and taking ~5 h longer to begin the exponential phase, as reflected by the μ_{max} (app.) values (Table 3.3). The WT strain could grow solely on either nitrate or nitrite to reach an OD_{max} value of 0.85, but strains deficient for NtrBC only reached ~70% of this value, with a similar pattern observed for the growth rates. This suggests that nitrate assimilation was not

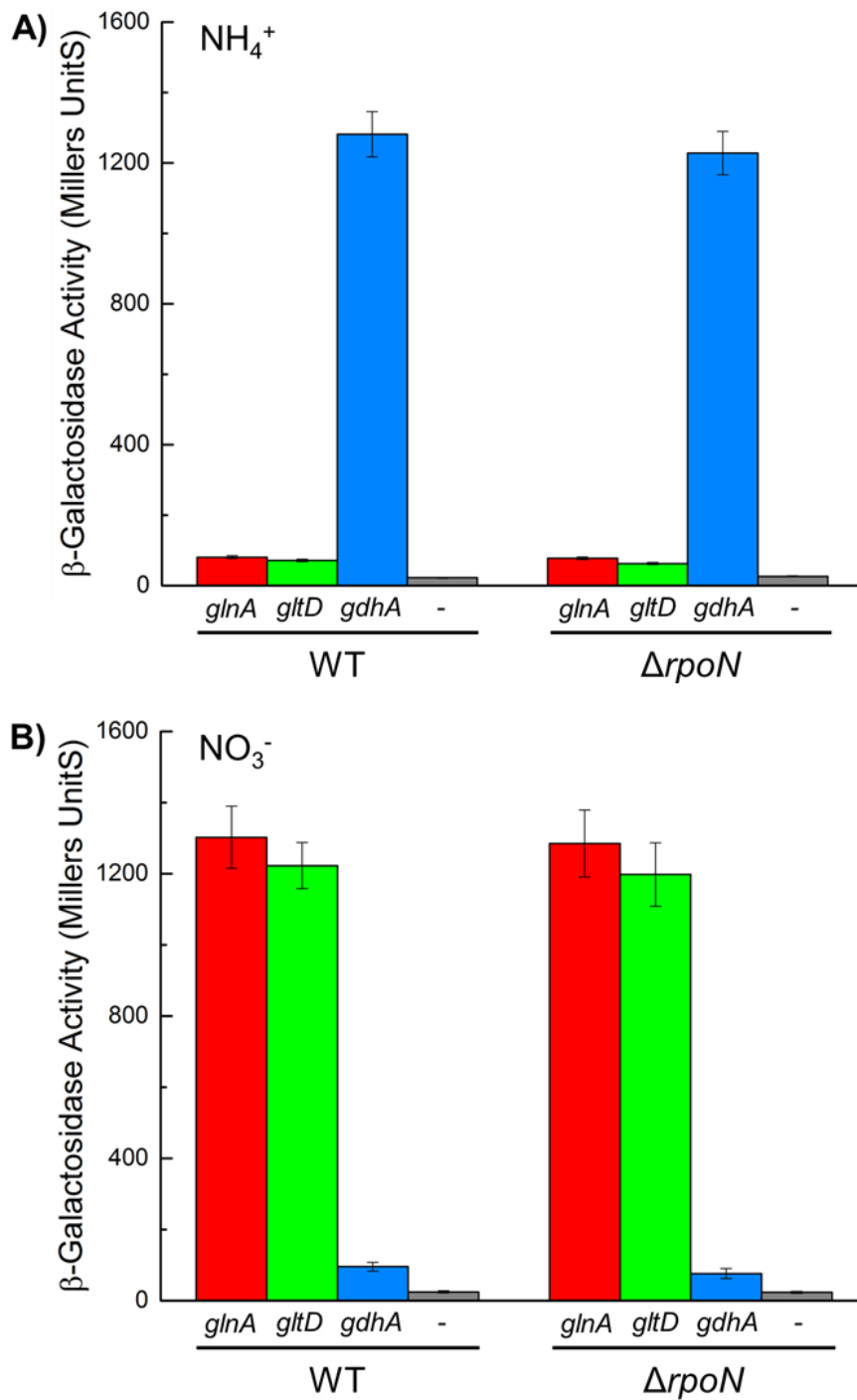


Figure 3.16. β -galactosidase activities of the *glnA-lacZ*, *gltD-lacZ* and *gdhA-lacZ* gene-reporter fusions in *P. denitrificans* strains. Transcriptional activity of *glnA* (red), *gltD* (green), *gdhA* (blue) and a plasmid containing no promoter (grey) measured at a mid-exponential phase in WT and $\Delta rpoN$ grown aerobically at 30 °C aerobic growth, 30 °C, with 10 mM A) ammonium or B) nitrate as a sole nitrogen source.

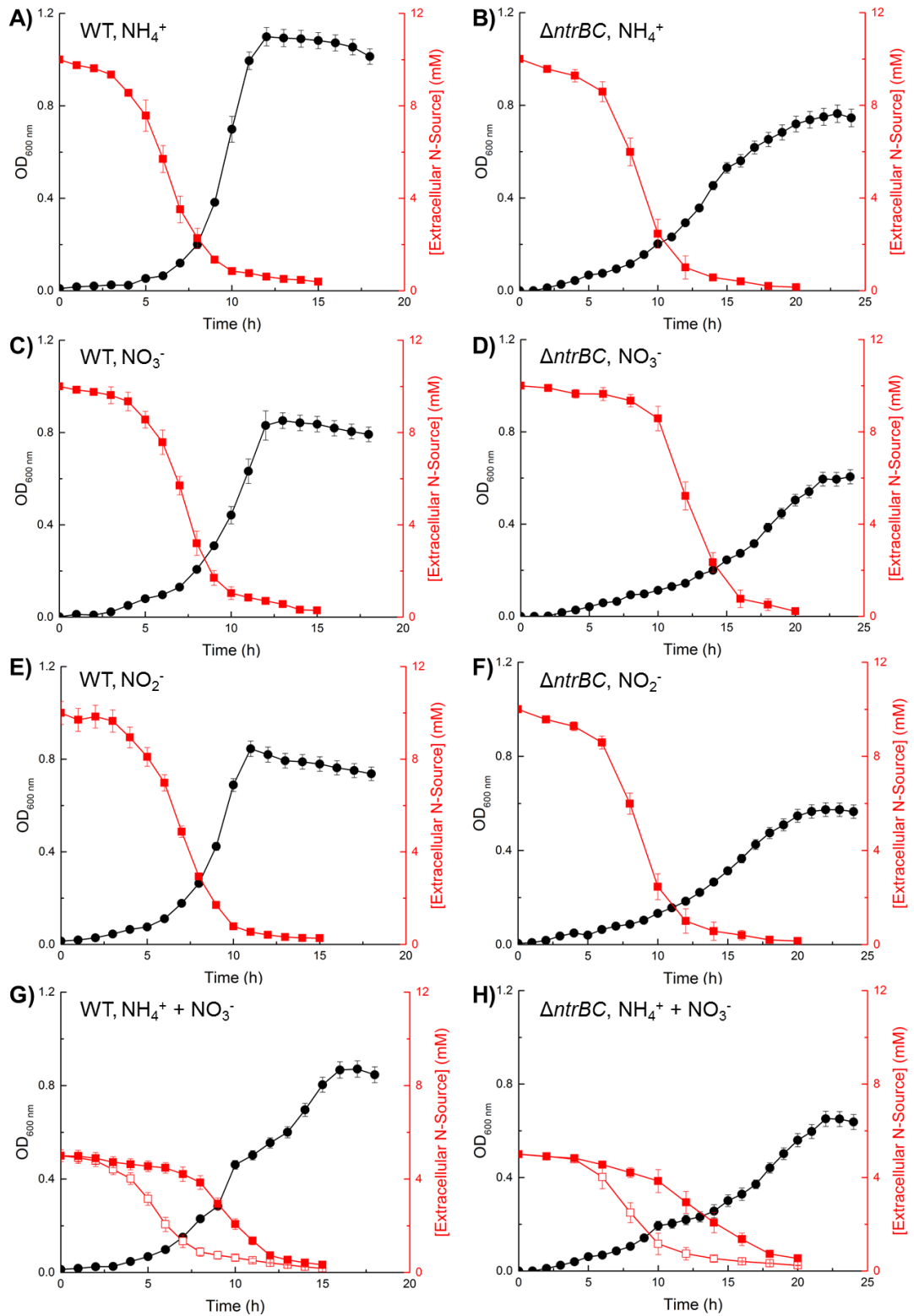


Figure 3.17. Comparative growth of *P. denitrificans* WT and $\Delta ntrBC$ strains with various inorganic nitrogen sources. Aerobic growth of WT and $\Delta ntrBC$ in batch cultures of minimal media at 30 °C with 30 mM succinate. Black; OD_{600 nm}, red; extracellular nitrogen concentration. Cultures were supplemented with 10 mM ammonium, nitrate, nitrite or 5 mM of both ammonium and nitrate. Red open symbols represent ammonium and red closed symbols represent nitrate in the condition with both sources.

Table 3.3. Summary of relevant growth parameters derived from Figure 3.17.

Nitrogen Source	OD _{max.} (at 600 nm)		μ_{max} (app.) (h ⁻¹)	
	WT	$\Delta ntrBC$	WT	$\Delta ntrBC$
10 mM NH ₄ ⁺	1.09 ± 0.04	0.76 ± 0.04	0.19 ± 0.02	0.13 ± 0.02
10 mM NO ₃ ⁻	0.85 ± 0.03	0.61 ± 0.03	0.12 ± 0.01	0.08 ± 0.01
10 mM NO ₂ ⁻	0.85 ± 0.04	0.57 ± 0.03	0.13 ± 0.01	0.07 ± 0.01
5 mM NH ₄ ⁺ 5 mM NO ₃ ⁻	0.87 ± 0.03	0.65 ± 0.03	0.15 ± 0.02	0.09 ± 0.01

functioning efficiently in the mutant strain, possibly due too attenuated Nas expression, studied later.

However, ammonium-dependant cultures also observed diminished growth and rates in $\Delta ntrBC$, where the values were ~65% that calculated for WT. This phenotype suggested that NtrBC may regulate other general nitrogen pathways and thus inefficient metabolism may be causing reduced biomass production. Gene-reporter data in Figure 3.12 showed that NtrBC is required for activation of the GS-GOGAT genes which harbour a high affinity for ammonium to enable maximum biomass production when low levels of cytoplasmic ammonium remain, below the K_m of GDH. The absence of this system in $\Delta ntrBC$ results in the GDH pathway being the integrator for ammonium into organic structures. It's low affinity for the inorganic cation may be why WT growth yield was not reached, as it is unable to completely incorporate this nitrogen source into biomass, despite the external nitrogen concentrations reporting complete uptake of ammonium, nitrate and nitrite in each culture.

Following this aerobic phenotype, $\Delta ntrBC$ was tested for its ability to use nitrate as an end-terminal electron acceptor by growing the deletion strain under denitrification conditions to observe its involvement in Nar expression.

Figure 3.18 shows that the NtrBC regulatory system most probably does not participate in regulating the Nar pathway, as the mutant culture was capable of efficiently using nitrate as a respiratory electron acceptor during anoxic conditions (Figure 3.18). Cultures achieved an OD_{max} of ~1.8 in both strains with no impaired growth observed, indicating *narKGHJI* is not under regulation by the general nitrogen regulators or the nitrogen-responsive sigma factor, RpoN (Figure 3.14B). Previous studies have instead demonstrated the bacterial *nar* pathway is under Fnr control during oxygen-limiting conditions (Li & DeMoss 1988; Takahashi et al. 1994).

Finally, the expression of *nasTS* and *nasABGHC* was tested in this deletion strain using

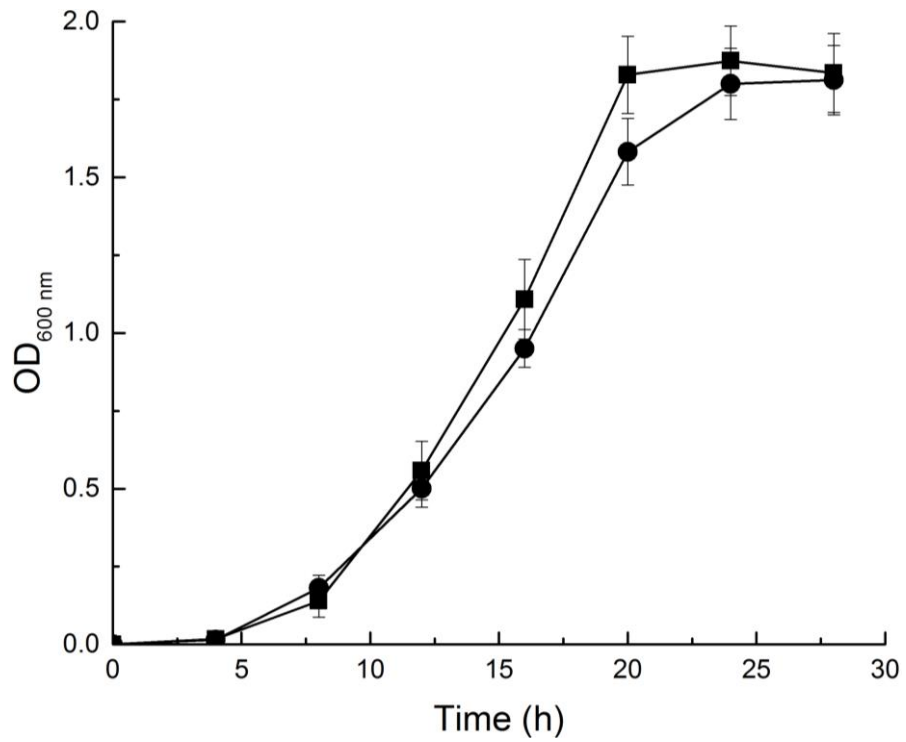


Figure 3.18 Growth under denitrification conditions of *P. denitrificans* deficient in genomic *NtrBC*. WT (squares) and $\Delta ntrBC$ (circles) were grown at 30 °C in batch minimal salt media cultures supplemented with 30 mM succinate as a carbon source. Anaerobic denitrification was performed with 20 mM nitrate as an electron acceptor and 10 mM ammonium as a nitrogen source.

transcriptional gene-reporter *lacZ*-fusion plasmids, as previous reports found the structural genes required for import and reduction of nitrate are activated by Ntr in heterotrophic bacteria. In addition, the ability of Ntr to upregulate the *nifR3-ntrBCYX* operon was tested using a *nifR3-lacZ* fusion plasmid (see Section 2.17 for construction details).

In Section 3.2, it was shown that *nasTS* and *nasABGHC* comprise individual operons to enable the assumption *nasT-lacZ* and *nasA-lacZ* gene-reporter fusions are indicative of their downstream genes. The *nifR3-ntrBCYX* cluster is proposed to form a single operon (Foster-Hartnett et al. 1993) which we demonstrated here by analysis of the transcriptional architecture of this locus, as performed for *nasT* and *nasA*. The presence of contiguous bands generated between each of the 5 genes in the *nifR3-ntrBCYX* gene cluster confirmed they are expressed together as a single transcriptional unit. Therefore, the measured activity of the *nifR3-lacZ* fusion plasmid is representative of the downstream genes.

Gene-reporter fusion vectors for *nasT-lacZ*, *nasA-lacZ* and *nifR3-lacZ* were conjugated into $\Delta ntrBC$ and assayed for levels of transcription under various nitrogen conditions in defined minimal media, grown aerobically and harvested at a late-exponential phase (Figure 3.20).

The transcriptomic data presented in Figure 3.20 reports regulatory roles for NtrBC in activation of the *nasABGHC* genes, and the *nifR3-ntr* operon. Upregulation of both these gene clusters was majorly attenuated in the $\Delta ntrBC$ strain during nitrate-dependant growth when compared to WT, as activity levels decreased from ~1250 Mu to ~500 Mu. However, expression was not completely abolished, when compared to the negative control, and $\Delta ntrBC$ was still capable of growing with nitrate as a sole nitrogen source (Figure 3.17), suggesting other regulatory participants may be active. Expression of *NasTS* was unresponsive to NtrBC where activity levels of ~3500 Mu was recorded for both strains during nitrate-dependent growth. This assay demonstrated the general nitrogen regulators activate gene expression of the structural *Nas* machinery, and additionally upregulates the *NifR3* gene in addition to itself.

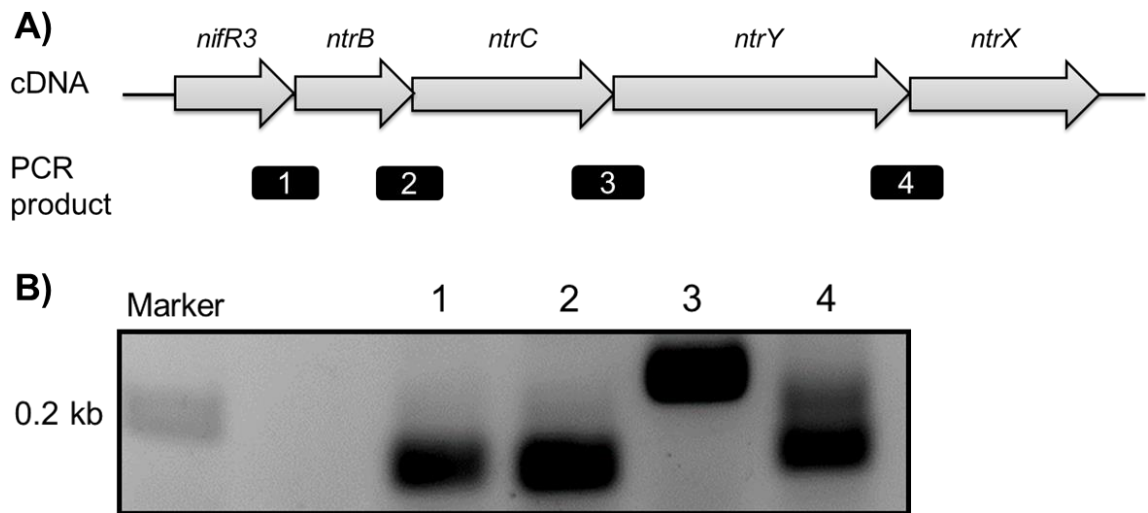


Figure 3.19. Defining the transcriptional architecture of the *nifR3-ntnBCYX* gene cluster of *P. denitrificans*. RNA was harvested at a mid-exponential phase from *P. denitrificans* cultures grown aerobically at 30 °C in minimal media with 30 mM succinate and 10 mM nitrate as a sole nitrogen source. RNA was reverse-transcribed to cDNA and set up in separate PCRs containing the appropriate primer pairs. A) The *nifR3-ntn* gene cluster of *P. denitrificans*, where PCR-generated fragments spanning adjacent genes are represented as black boxes. B) Agarose gel analysis of the PCR. Lanes 1-4 correspond to the appropriate fragments and the sizes (bp) are as follows: 1; 130, 2; 123, 3; 261, 4; 144. Marker indicates 1 kb Hyperladder.

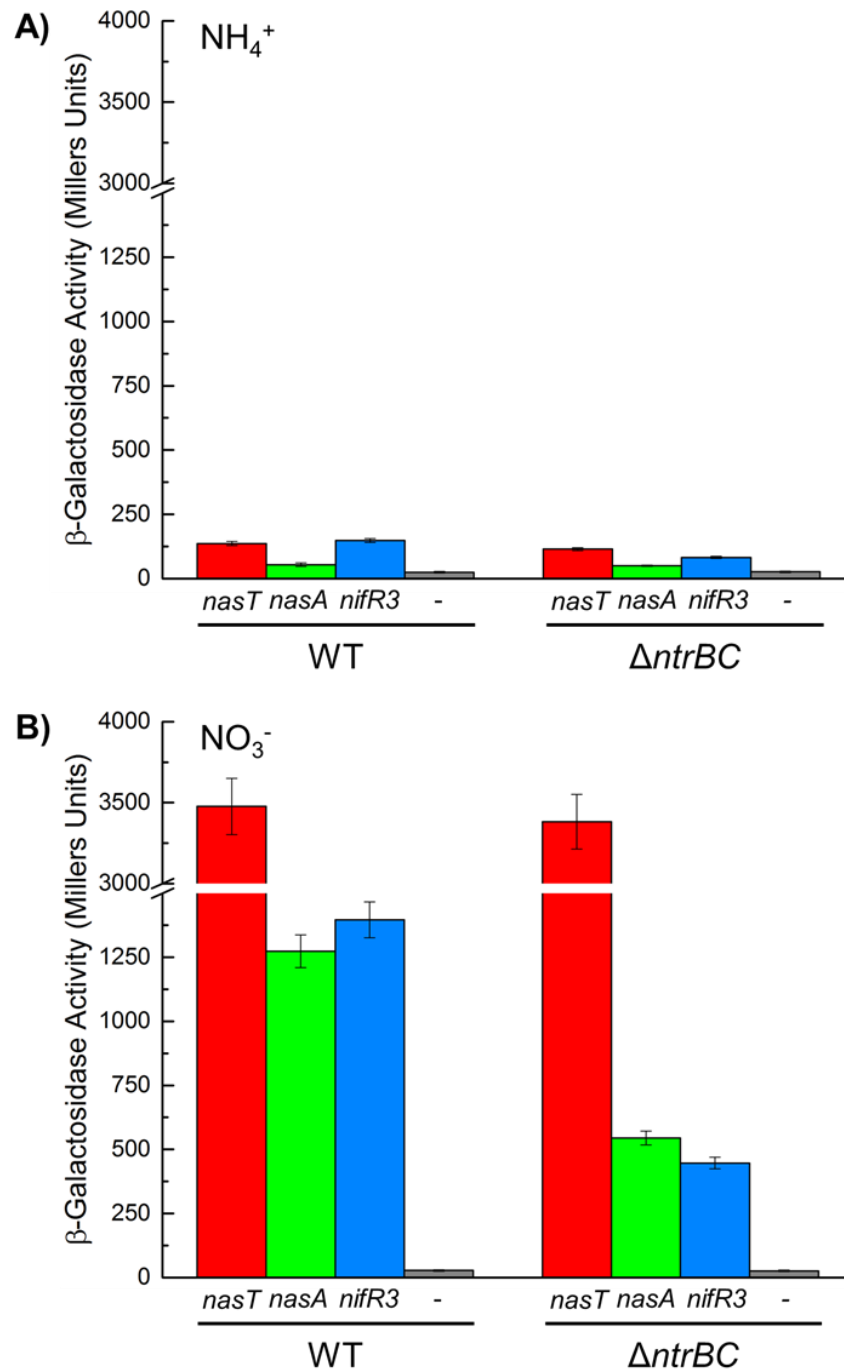


Figure 3.20. β -galactosidase activities for the *nasT-lacZ*, *nasA-lacZ* and *nifR3-lacZ* fusion plasmids in *P. denitrificans* strains. Transcriptional activity of *nasT* (red), *nasA* (green), *nifR3* (blue) fusion plasmids and pMP220 containing no promoter (grey) during aerobic growth of *P. denitrificans* strains at 30 °C supplemented with A) 10 mM ammonium or B) nitrate as a sole nitrogen source. Gene reporter activity was measured in WT and $\Delta ntrBC$ at a late-exponential phase.

3.7 Growth of $\Delta ntrBC$ on Various Carbon Substrates Exhibits an Altered Dependence

To further investigate the contribution of the Ntr system in regulating both the carbon/nitrogen interface, and the link between supplemented carbon source and the ability to assimilate nitrate through Nas regulation, experiments performed on WT in Section 3.2 were carried out here on $\Delta ntrBC$. Growth of the strain was monitored over a range of supplemented carbon concentrations for butyrate, pyruvate, succinate and malate (Figure 3.21).

P. denitrificans deficient for the *ntrBC* system showed a marked difference in carbon dependence when compared to WT in Section 3.3, where the growth rates and CFU of $\Delta ntrBC$ strain plateaued consistently at much lower values. Figure 3.9 showed growth on 10 mM butyrate in WT reaches a maximum growth rate of $\sim 0.16 \text{ h}^{-1}$ and cell count of $16 \times 10^7 \text{ CFU/mL}$ when assimilating nitrate, which was attenuated by half to $\sim 0.08 \text{ h}^{-1}$ and $\sim 9 \times 10^7 \text{ CFU/mL}$ in the $\Delta ntrBC$ strain.

For nitrate-dependant growth of WT on pyruvate and succinate, Figure 3.8 and 3.6 respectively, cultures displayed a linear increase of growth output with increasing carbon, reaching a maximum of $\sim 16 \times 10^7$ and $14 \times 10^7 \text{ CFU/mL}$, respectively, at 50 mM carbon. However, $\Delta ntrBC$ only reaches $\sim 9 \times 10^7$ and $8 \times 10^7 \text{ CFU/mL}$, for pyruvate and succinate respectively, which plateaus far lower at 30 mM carbon.

Furthermore, growth with ammonium as a sole nitrogen source showed attenuated growth compared to WT, though not as significant, being $\sim 10\%$ reduction in both growth rates and OD_{max} reached. This growth data suggests that in the absence of the NtrBC system, cells are ineffectively metabolising carbon and nitrogen which leads to loss of biomass formation and growth. This may be due to cells being unable to utilise the full carbon and nitrogen provided, possibly as GDH is incapable of integrating the entire quantity of ammonium, from uptake or nitrate reduction, into biosynthetic structures.

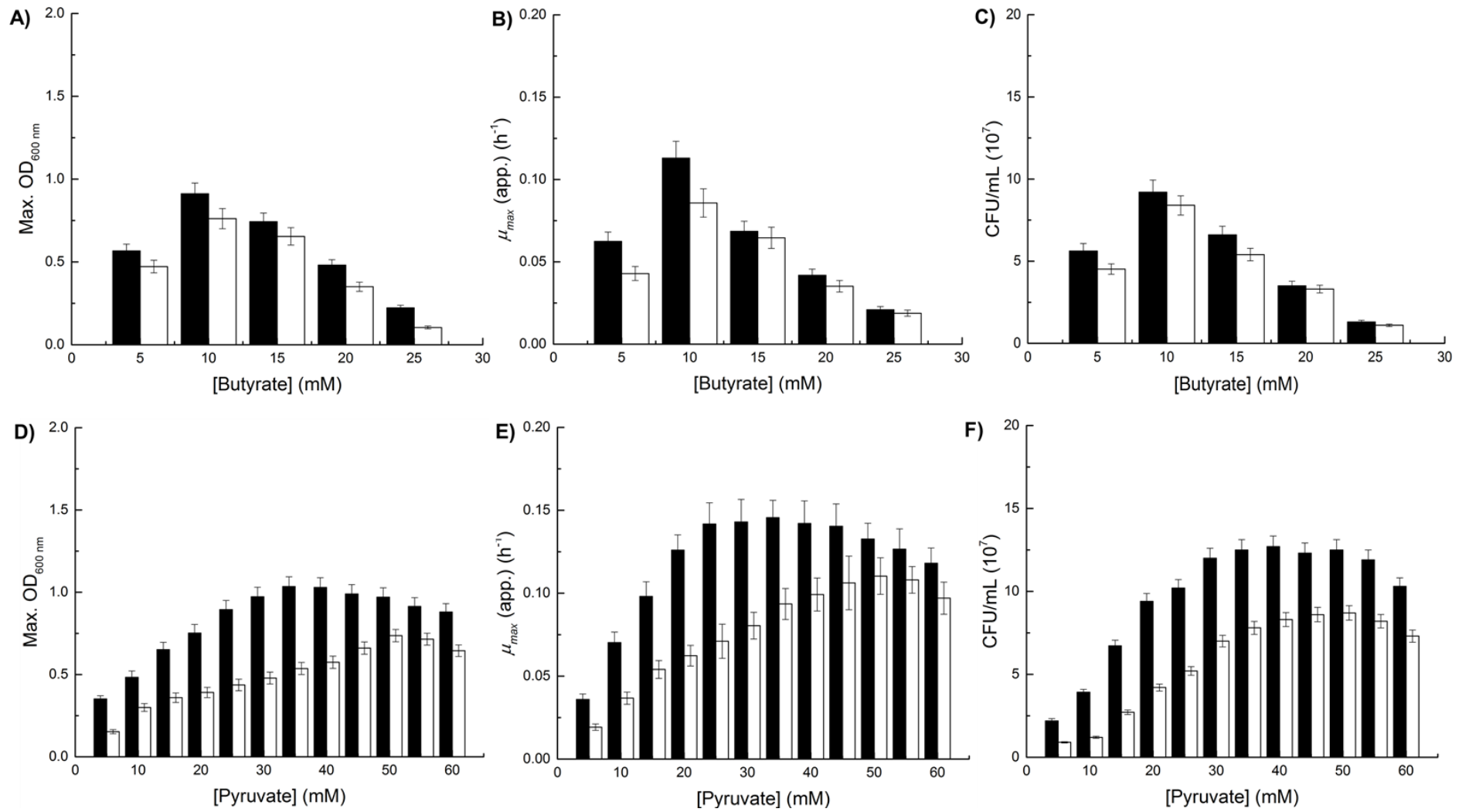
To explore the effect NtrBC has towards heterotrophic growth with limited nitrogen, the data accumulated in Figure 3.21 was formatted in Figure 3.22 and Table 3.4. Here, the maximum growth parameters of *P. denitrificans* when cultured on various carbon substrates using a C:N ratio of 4:1 and 16:1 is displayed.

At a 4:1 C:N ratio using butyrate as the carbon source, Figure 3.10A showed WT actually preferred to use nitrate as the nitrogen source, as it helps to alleviate excess energy by reducing nitrate for biomass. However, Figure 3.22B shows that this preference is swapped in the $\Delta ntrBC$ strain as growth yield on nitrate drops by $\sim 40\%$ from 15.6 to 8.4

CFU/mL. The cell count on ammonium was 9.2 CFU/mL and so is now greater than nitrate-dependent growth in the mutant. This swap in preference is also present at a 16:1 C:N with pyruvate as the carbon source, where 16.1 CFU/mL in WT was attenuated to 8.4 CFU/mL for nitrate-dependent growth. Due to this, we believe Nas functions as an NADH:nitrate/nitrite oxidoreductase to dissipate excess energy during nitrate assimilation instead of Nap. NasABGHC expression is attenuated in $\Delta ntrBC$ (Figure 3.20) but Nap is not, during nitrate-dependant growth.

When Figure 3.22B is compared to Figure 3.10B, it can be seen that the dependence of *P. denitrificans* upon the oxidation state of the carbon source to grow with nitrate is lost when NtrBC is absent. WT (Figure 3.10) exhibits a clear link between the NADH yield of a carbon source and the growth yield on nitrate as a sole nitrogen source. WT growth with pyruvate, succinate and malate achieved maximum cell counts of 15×10^7 , 9×10^7 and 5×10^7 CFU/mL, correlating with most NADH/carbon to the least NADH produced per carbon atom. However, for the $\Delta ntrBC$ strain (Figure 3.22B), both pyruvate and succinate as a carbon source only resulted in maximum cell counts $\sim 8 \times 10^7$ CFU/mL. This showed there was no increased biomass production with pyruvate compared to succinate, even though pyruvate produces a greater quantity of reducing equivalents, carbon for carbon, which can be utilised for nitrate-assimilation. The data presented demonstrates NtrBC is important in regulating the assimilation of inorganic nitrogen into organic cellular material for optimal growth under various environmental conditions. This may be due to attenuated expression of Nas and the GS-GOGAT system (Figure 3.20 and 12, respectively) in the absence of the transcriptional activator, NtrC, which leads to restricted growth due to inefficient metabolism of carbon and nitrogen.

Furthermore, the cell count and growth rates of $\Delta ntrBC$ on 10 mM butyrate with nitrate (Figure 3.22A) are $\sim 60\%$ that of WT (Figure 3.6), and $\Delta ntrBC$ found ammonium to be preferential for growth as opposed to nitrate in WT. This may show that under normal circumstances, Nas can use excess cellular energy, as a result of carbon-rich conditions, to enhance biosynthesis of key cellular structures when nitrate is present. This alleviates excess reductant and thus offers a growth advantage over ammonium-dependent cultures. Nas expression is reduced in $\Delta ntrBC$ (Figure 3.20) which coincides with its attenuated growth on butyrate when using nitrate as a sole nitrogen source, suggesting the inability of cultures to achieve WT growth is due to Nas ineffectively coupling oxidation of surplus reducing equivalents with assimilation of nitrate.



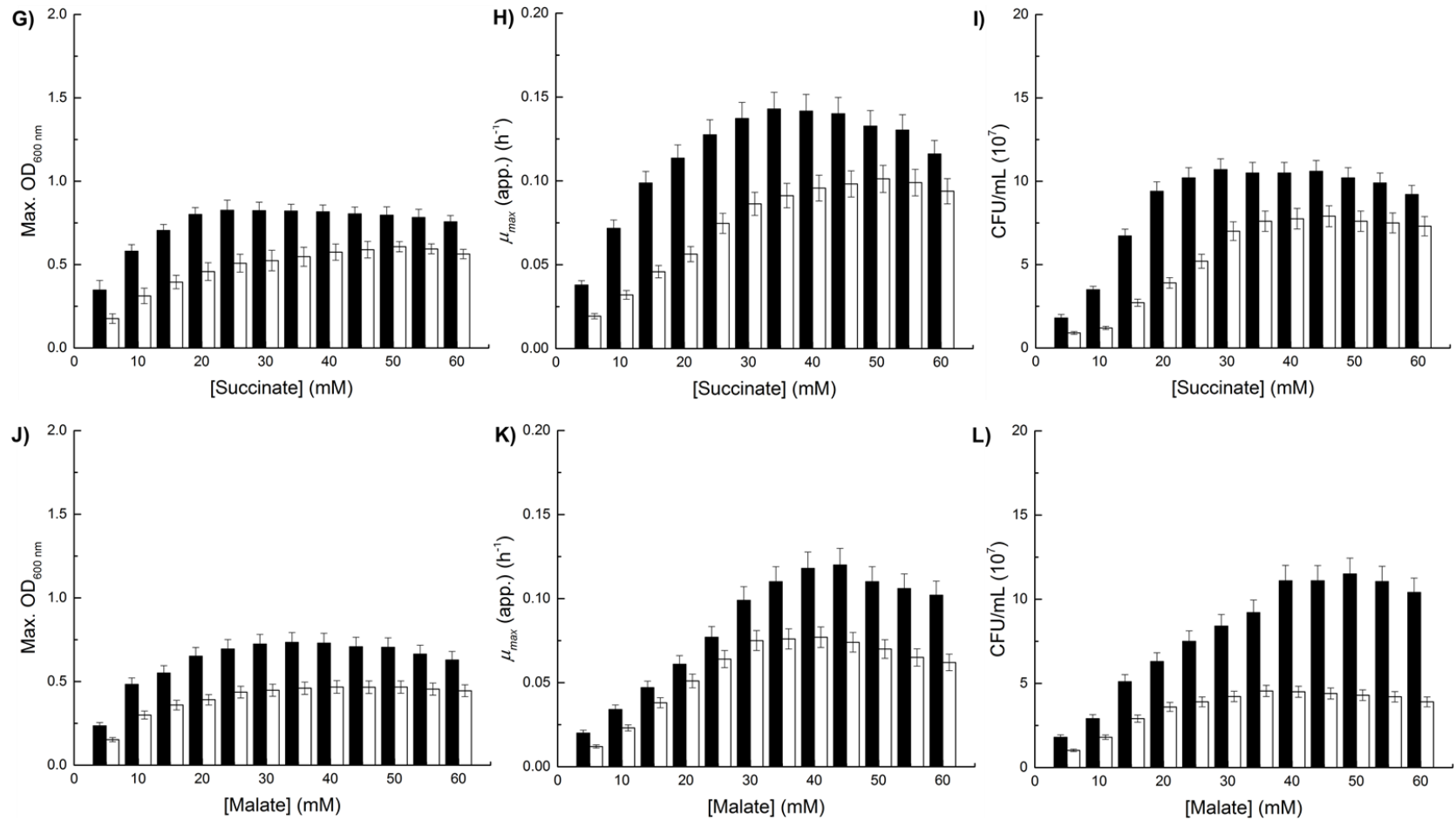


Figure 3.21. Growth analysis of $\Delta ntrBC$ cultured with various carbon sources. Aerobic growth of $\Delta ntrBC$ in minimal salt media at 30 °C supplemented with 10 mM ammonium (black) or nitrate (white) as a sole nitrogen source. Max. OD_{600 nm}, μ_{max} (app.) and CFU are shown when grown on a variety of concentrations of the supplied carbon source. A-C) Butyrate. D-F) Pyruvate. G-I) Succinate. J-L) Malate.

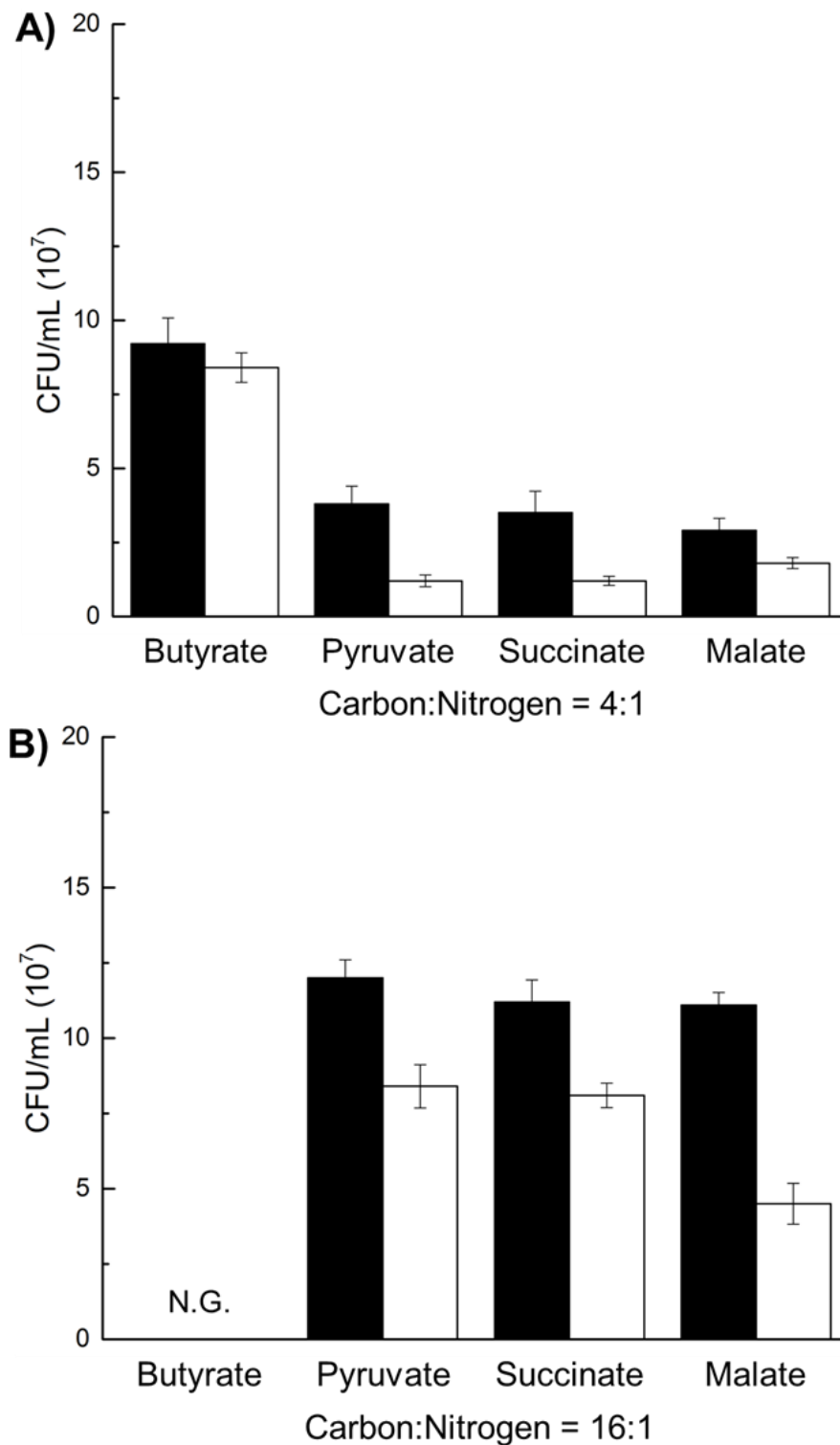


Figure 3.22. Maximum growth yield of $\Delta ntrBC$ at separate carbon:nitrogen ratios using various carbon sources. $\Delta ntrBC$ was grown aerobically in minimal media, 30 °C, with 10 mM ammonium (black) or nitrate (white) as sole nitrogen sources. The maximum CFU of cultures grown using butyrate, pyruvate, succinate or malate at a A) 4:1 and B) 16:1 carbon: nitrogen ratio are shown. N.G. represents no growth.

Table 3.4. Relevant growth parameters of *ΔntrBC* grown at separate C:N ratios on distinct carbon substrates.

Compound	Total Carbon Oxidation Number	NADH/molecule FADH ₂ /molecule	NADH/carbon FADH ₂ /carbon	C:N	mM	<i>μ</i> _{max} (app.) (h ⁻¹)			CFU/ mL (10 ⁷)	Dry Mass (mg/mL)	C:N	mM	<i>μ</i> _{max} (app.) (h ⁻¹)			CFU /mL (10 ⁷)	Dry Mass (mg/mL)
						NH ₄ ⁺	NH ₄ ⁺	NO ₃ ⁻					NH ₄ ⁺	NH ₄ ⁺	NO ₃ ⁻		
Butyrate	-4	7	1.75	4:1	10	0.11	9.2	1.02	16:1	40	N.G.	N.G.	N.G.				
		3	0.75			0.09	8.4	0.87									
Pyruvate	+2	4	1.33	4:1	13.3	0.07	3.8	0.54	16:1	53.3	0.14	12.0	1.08				
		1	0.33			0.04	1.2	0.36						0.12	8.4	0.82	
Succinate	+2	5	1.25	4:1	10	0.07	3.5	0.38	16:1	40	0.13	11.2	0.91				
		2	0.5			0.03	1.2	0.21						0.10	8.1	0.62	
Malate	+4	5	1.25	4:1	10	0.03	2.9	0.23	16:1	40	0.12	11.1	0.83				
		1	0.25			0.02	1.8	0.19						0.08	4.5	0.54	

This role is previously thought to be performed by the periplasmic Nap system in *Paracoccus* sp. (Richardson et al. 1988) which is still functional in $\Delta ntrBC$. In order to investigate the contribution of both Nap and Nas towards cellular redox balancing during growth on highly reduced carbon compounds, similar growth analyses were performed on an available *P. pantotrophus* $\Delta napD$ strain, where NapA is known to not be functional. Relevant growth parameters of *P. denitrificans* WT, *P. denitrificans* $\Delta ntrBC$ and *P. pantotrophus* $\Delta napD$ on various butyrate concentrations during ammonium-dependent and nitrate-dependent growth are shown below (Figure 3.23).

As discussed previously, WT cells prefer to grow using nitrate as a sole nitrogen source in the presence of excess reductant, where higher colony counts were recorded on nitrate for 5-20 mM butyrate, with 10 mM achieving maximum growth with a CFU/mL of $\sim 1.5 \times 10^7$ (Figure 3.23A). This value was attenuated to $\sim 8 \times 10^7$ in the $\Delta ntrBC$ strain when Nas is not highly expressed, consistent with its role in a biomass-linked reductant vent during energy rich conditions. Additionally, Figure 3.23C showed a similar growth phenotype for $\Delta napD$ when compared to $\Delta ntrBC$, where cultures achieved a maximum CFU/mL of $\sim 8.5 \times 10^7$ on nitrate at 10 mM butyrate, with ammonium again being the preferential nitrogen source for use.

Therefore, cells deficient in a Nap system were clearly unable to achieve maximum WT growth, most likely due to an unfavourable redox status and accumulation of excess reducing equivalents. This data indicates that both Nap and Nas are highly involved in regulating the cellular redox potential during heterotrophic growth. Nap is known to dissipate excess energy at the cell membrane through dissimilatory nitrate reduction during energy-rich growth. As opposed to this, the Nas system appears to be a biomass-linked reductant vent which couples anabolism of organic nitrogen containing structures with alleviation of excess cellular energy during nitrate assimilation.

3.8 Discussion

3.8.1 The influence of external carbon compounds upon microbial growth

When nitrate is the only bioavailable source of environmental nitrogen, we demonstrated via gene-reporter *lacZ*-fusion assays that *P. denitrificans* expresses the NasTSABGHC machinery to import and reduce the highly oxidised anion to the reduced ammonium cation. This is subsequently incorporated, by GS-GOGAT, with 2-oxoglutarate to produce the pivotal metabolic precursor glutamate. During such conditions, transcriptomic analysis identified upregulation of the TRAP dicarboxylate transporters system, Dct.

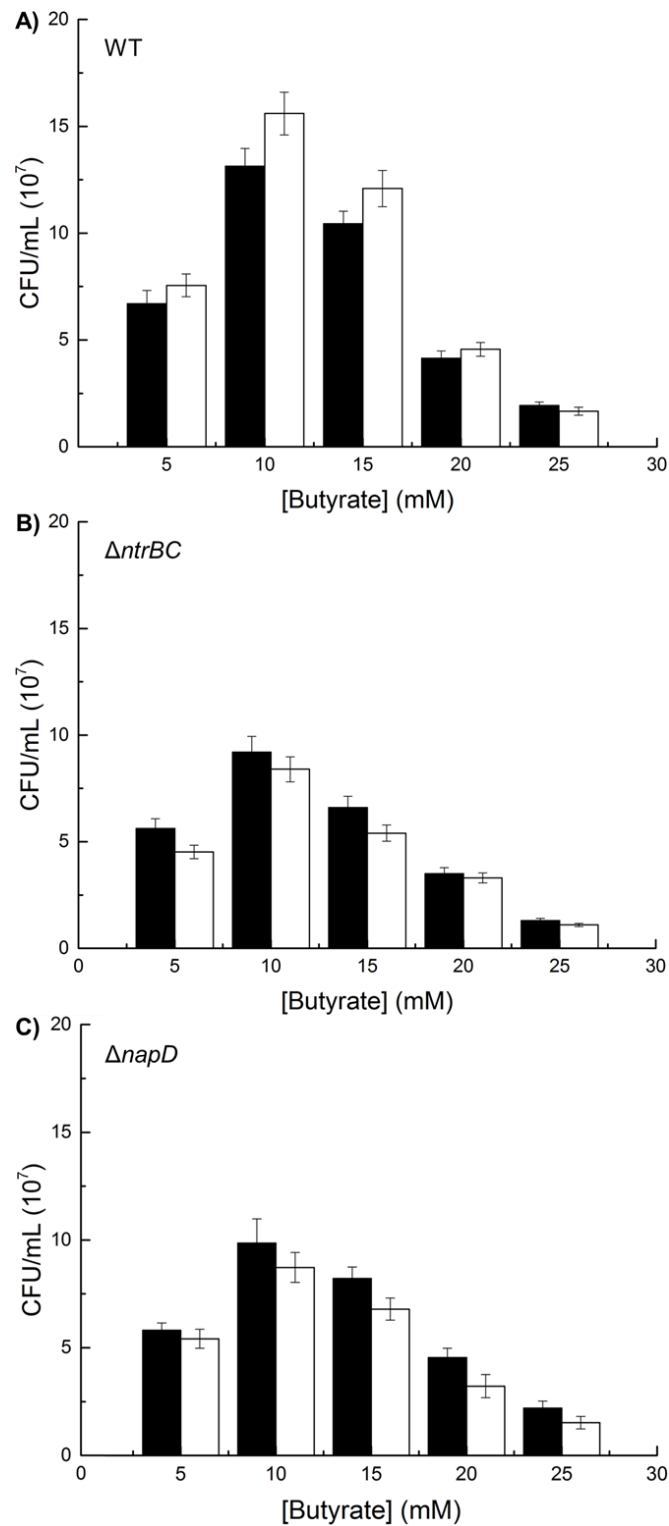


Figure 3.23. Growth of various *Paracoccus* strains on butyrate to investigate the contribution of Nap and Nas towards cellular redox balancing. Aerobic growth of *P. denitrificans* WT (A), *P. denitrificans* $\Delta ntrBC$ (B), and *P. pantotrophus* $\Delta napD$ in minimal salt media, 30 °C, with various concentrations of butyrate. 10 mM ammonium (black) or nitrate (white) were supplemented as a sole nitrogen source. Colony counts (CFU/mL) were taken at the maximum point of growth for each culture.

The necessity for increased respiration of organic acids to fuel NADH production for nitrate assimilation was analysed in this chapter by subjecting *P. denitrificans* to various concentrations of butyrate, pyruvate, succinate and malate, each having different redox statuses. For each carbon source, the data concluded a greater dependence of cells on the external carbon levels when grown with nitrate as opposed to ammonium, due to a longer linear increase of growth output with increasing supplemented carbon concentration. Whereas ammonium-dependant cultures reached consistent maximal growth at ~30 mM pyruvate, succinate and malate, nitrate-assimilating cells didn't achieve this point until ~50 mM carbon, as they required the NADH produced from carbon oxidation for nitrate reduction in addition to other energetic metabolic pathways and ATP generation.

To fully explore this redox link between organic acid respiration and nitrate assimilation for growth, carbon compounds of varying oxidation states were tested. As hypothesised, butyrate, the most reduced of the substrates tested and yielding the most NADH equivalents when fully oxidised, gave greater growth yields of *P. denitrificans* at lower C:N ratios. Furthermore, both growth rates and biomass yields of cultures assimilating nitrate were subsequently found to be highest to lowest in order of the most reduced carbon compound to most oxidised: butyrate, pyruvate, succinate and malate.

This data characterised a link between bioavailability of environmental carbon substrates, the oxidation state of the substrate, and nitrate assimilation for growth. Here, we showed more reduced carbon compounds at greater concentrations are preferential for cells to assimilate nitrate with during aerobic heterotrophic growth, due to their dependence on the reduced nucleotide pyridine pool as a physiological electron donor to NasC and NasB. We conclude Nas, the NADH:nitrate/nitrite oxidoreductase, acts as a reductant vent which couples dissipation of excess cytoplasmic reducing equivalents with reduction of nitrate to ammonium. Doing so allows subsequent incorporation into pivotal organic structures to offer a selective growth advantage, as opposed to Nap, ubiquinol:nitrate oxidoreductase, which dissipates free energy at the inner-membrane.

3.8.2 Regulating transcriptional activation of nitrogen-responsive genes

Activation of genes involved in nitrogen metabolism typically requires functional NtrC to bind a consensus promoter sequence, which is recognised by sigma 54 associated with an RNA-polymerase, thus guiding the enzyme to the appropriate gene for transcription. We initially believed both those systems were required for expression of *nas* and the GS-GOGAT system to fully metabolise and integrate nitrate into organic structures.

3.8.2.1 The nitrogen-responsive sigma 54 factor

Sigma 54 has been well characterised as the bacterial sigma factor regulating transcriptional activation of genes whose encoded products function in nitrogen metabolism (Rappas et al. 2007; Jones 2009). Importantly, recent work has emerged which determined NtrBC is capable of activating gene expression in a sigma 54-independent manner, binding to a DNA promoter sequence and catalysing formation of the active RNA polymerase isoform in the absence of the sigma factor.

Though it has previously been shown to regulate the genes for respiratory nitrate reduction and nitrate assimilation in several organisms such as *E. coli* and *A. vinelandii*, respectively (Studholme & Buck 2000; Kustu et al. 1989), construction of a deletion strain deficient in genomic *rpoN* displayed no significant growth phenotype. The ability of *P. denitrificans* to grow with nitrate as a sole inorganic nitrogen source for biomass assimilation or anaerobically as an end-terminal electron acceptor was not impaired in the absence of sigma 54. qRT-PCR transcriptomic data concluded there was no attenuated expression of *ntr* or *nas* genes during aerobic nitrate assimilation.

Here, we experimentally confirmed that sigma 54 is not implicated in regulating expression of nitrate assimilation, denitrification or the Ntr system in *P. denitrificans*, contrary to other bacterial systems. However, we cannot rule out the existence of functional complementation between sigma factors, as the genome of *P. denitrificans* harbours 5 in total, and a further putative 4. Whilst a deletion of the heat-shock sigma factor *rpoH* and double deletion of *rpoN/rpoH* gave no effect on the cultures ability to grow with nitrate, regulation of *nas* and *nar* genes may fall into a role of another sigma factor.

3.8.2.2 General nitrogen regulatory complex – NtrBC

The general nitrogen regulators, Ntr, are known to control expression of nitrogen-responsive genes in heterotrophic bacteria, such as nitrogenase and the GS-GOGAT system (Stadtman 2001; Reitzer 2004; Merrick & Edwards 1995). Here, we confirmed the latter by demonstrating NtrBC is necessary for transcription of GS-GOGAT using gene-reporter fusion assays in a *P. denitrificans* strain deficient for genomic *ntrBC*. This was further supported by phenotypic growth data of batch cultures which exhibited attenuation of biomass and growth rates, attributed to the inability of GDH to fully scavenge the low levels of cytoplasmic ammonium assimilated due to its low k_m compared to GS-GOGAT.

We were primarily interested in the role NtrBC performs concerning expression of the *nas* gene cluster and *nifR3-ntr*. Using gene-reporter fusion assays, a regulatory role was identified for NtrBC in transcriptional activation of both the *nasABGHC* gene cluster and

the *nifR3-ntr* operon, but not *nasTS*. *nasABGHC* has previously been stated to be under Ntr control (Luque-Almagro et al. 2011), experimentally reported previously for several bacteria (Wu et al. 1999; Toukdarian & Kennedy 1986) and proved here for *P. denitrificans*. However, *nasABGCH* expression was not completely abolished and $\Delta ntrBC$ is still capable of growing with nitrate as a nitrogen source, albeit attenuated. We hypothesised this is attributable to the structurally and functionally similar NtrYX system, lying clustered downstream of NtrBC, examined in the next chapter.

In this chapter, we conclusively validate that Ntr is essential for transcriptional upregulation of the *nifR3-ntr* operon, *nasABGHC* and genes encoding the GS-GOGAT cycle in a sigma 54-independent manner in *P. denitrificans*. These proteins are all upregulated during nitrate-dependant growth whilst GDH expression drastically decreases, validated by the previous microarray analysis (Figure 1.12). As the sigma factor characteristically involved in regulating nitrogen-metabolism was not found to function here, we believed other regulators may be contributing to gene expression in a coordinated manner with NtrBC. To identify other participants controlling expression of nitrogen-responsive genes in heterotrophic proteobacteria, the following chapters explored the involvement of the conserved, hypothetical *nifR3* gene and its encoded putative tRNA-dihydrouridine synthase product.

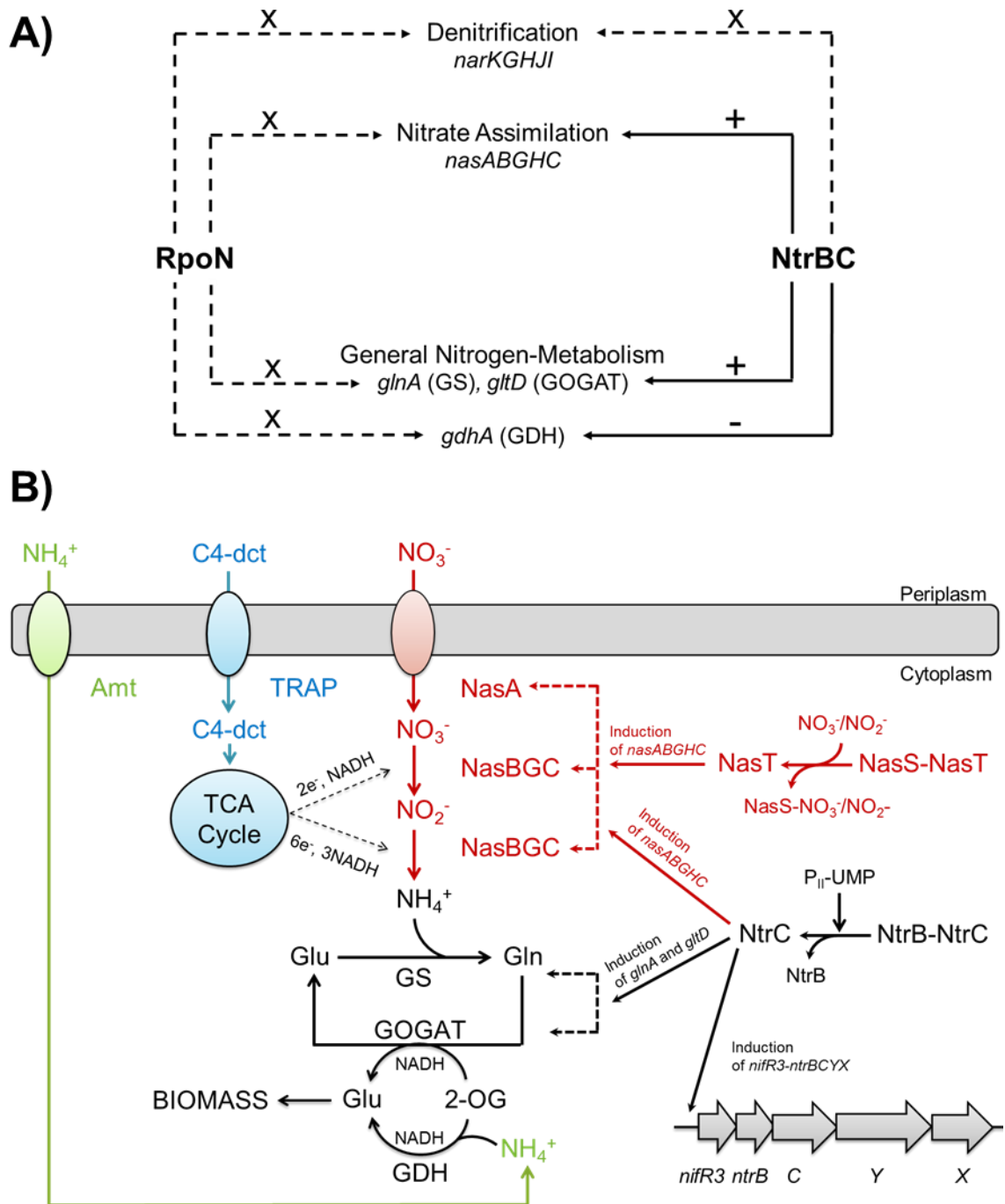


Figure 3.24. Overview depicting the regulation of inorganic nitrogen-metabolism and assimilation into organic biomass in *P. denitrificans*. A) Schematic showing the regulation of various nitrogen-responsive systems by NtrBC and RpoN. “+” indicates a regulatory role and “-” indicates no participation. B) Ammonium cations are imported through Amt transporters (green) and integrated with 2-oxoglutarate (2-OG) by glutamate dehydrogenase to produce glutamate (Glu). Nitrate/nitrite are reduced to ammonium by the cytoplasmic Nas pathway (red) which relies on the respiration of organic acids (blue) to provide required electrons. Nas is known to be under dual-control and its transcription is induced by NtrC following detection of low ammonium and NasT in the presence of cytoplasmic nitrate. The produced ammonium is integrated with glutamate to produce biomass through the GS-GOGAT cycle which is also under NtrBC control.

Chapter 4: Establishing the Role of *dusN* for Nitrogen Assimilation in *Paracoccus denitrificans*

4.1 Introduction

Assimilation of nitrate into cellular organic nitrogen is controlled by key nitrogen regulatory proteins, NtrB and NtrC, ubiquitous in Gram-negative bacteria (as reviewed in Section 1.2.2 and studied in Chapter 3). This anabolic process requires both the NasABGHC structural proteins and the GS-GOGAT system to create nitrogen-containing organic compounds from inorganic nitrate. When bioavailable ammonium is present in the environment, cells can bypass these pathways and incorporate ammonium directly into organic compounds (glutamate) using GDH. Recently, the first global transcriptional analyses of *P. denitrificans* grown using ammonium or nitrate as sole nitrogen sources was performed to compare changes in whole cell gene expression (Luque-Almagro et al. 2016). This microarray revealed significant upregulation of the regulatory and structural genes for the assimilatory nitrate/nitrite reductase system, in addition with genes encoding the glutamine synthetase and glutamate synthase systems (GS-GOGAT) required for biosynthesis of the pivotal metabolic precursor, glutamate. Importantly, the *ntr* operon was upregulated to coordinate the nitrogen-limitation response (Figure 4.1).

This chapter focuses on the gene coded by open reading frame Pden_4131, termed *nifR3*, which is present on chromosome II of *P. denitrificans* and forms a transcriptional operon with *ntrBCYX* that is upregulated during nitrate assimilation (Figure 3.19). The *nifR3* gene is predicted to encode a nitrogen-responsive, tRNA-Dihydrouridine synthase (DUS). DUS proteins form a flavin-dependent superfamily of RNA modifying enzymes. These proteins reduce uridine to dihydrouridine in an NAD(P)H-dependent reaction at specific positions in the D-loop of distinct tRNA transcripts (Kasprzak et al. 2012). This process is important for protein biosynthesis by forming a key post-transcriptional modification of tRNA to increase translational fidelity, as discussed in Section 1.9.

The presence of the *nifR3* gene immediately upstream of *ntrB-ntrC* is tightly conserved across α -proteobacteria and homologue systems are identified in other classes of proteobacteria, such as *dus-fis* in γ -proteobacteria. We propose renaming NifR3 to DusN as its genomic presence is not conserved with the ability of nitrogen fixation by the

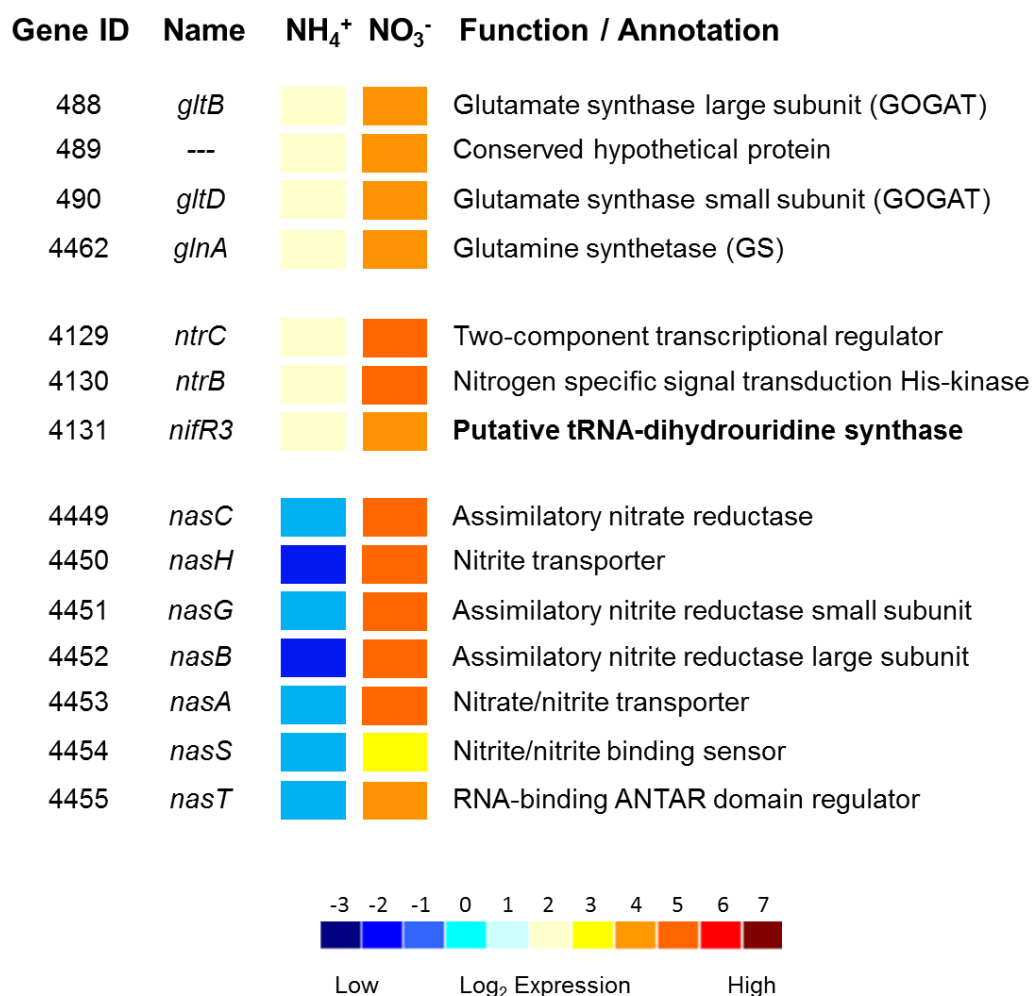


Figure 4.1. Microarray analysis of *P. denitrificans* WT comparing expression of key nitrogen-responsive genes during ammonium-dependant and nitrate-dependent growth. Heatmap depicting comparative gene expression levels of GS-GOGAT, *ntr* and *nas* from *P. denitrificans* grown aerobically in minimal salt media at 30 °C with 30 mM succinate using either 10 mM ammonium (left column) or nitrate (right column) as a sole nitrogen source. RNA was harvested at a mid-exponential phase and subject to a type-II microarray. Colours indicate average log₂ normalised expression values between three biological replicates. ID represents unique locus tag of each gene in the *P. denitrificans* genome (Accession: NC_008686–008688). Figure adapted from Luque-Almagro *et al* (Luque-Almagro et al. 2016).

microorganism, for which the *nifR3-ntrB(nifR2)-ntrC(nifR1)* cluster was originally named. Instead, the protein is predicted to encode a nitrogen-responsive, tRNA-DUS.

Based upon its strict evolutionary conservation with the nitrogen-regulatory system, we believe the gene gives rise to a functional DUS which plays an important role in the bacterial nitrogen-response, possibly in tandem with Ntr. However, the function of this gene, the physiological role of tRNA-DUS and the function of specific dihydrouridine formation are currently unknown. As this system is upregulated during nitrate-dependent growth, the hypothesis here is that DusN is required for regulating expression and translation of the Nas proteins, and possibly other nitrogen-responsive systems. The molecular and genetic characteristics of *dusN* were explored in this chapter.

4.2 Construction and Phenotypic Characterisation of a *P. denitrificans* strain deficient in *dusN*

4.2.1 Constructing a suicide vector for genomic deletion of *dusN*

A single previous investigation was performed by Foster-Hartnett and coworkers in *R. capsulatus* where they demonstrated that a deletion in *dusN* led to a loss of *nif* gene expression causing cells to be unable to fix dinitrogen to ammonium (Foster-Hartnett et al. 1993). However, this deletion was a polar mutation which disrupted expression of the downstream *ntrBC* genes and nitrogen fixation was restored when *ntrBC* was genetically complemented. Therefore, DusN isn't stringently required for *nif* expression and the authors inferred it might participate in signalling of the nitrogen status instead.

To initiate our investigation, a non-polar deletion of *dusN* in *P. denitrificans* was produced (see Section 2.16). Briefly, a pair of fragments identical to the forward and reverse regions of *dusN* were PCR-amplified and cloned into pK18*mobsacB* to construct suicide vector pBP005. This plasmid was conjugated into *P. denitrificans* where a double homologous recombinant event yielded a Δ *dusN* strain (Figure 4.2).

4.2.2 Phenotypic characterisation of a Δ *dusN* strain

Given that *dusN* is clustered, transcribed as a single unit (Figure 3.19) and conserved with the key *ntr* nitrogen regulatory genes, we tested the ability of this strain to respond to growth during various growth modes dependent upon nitrogen-metabolism. Cultures of WT and Δ *dusN* were grown aerobically in batch minimal salt media to examine its capacity to utilise a range of organic and inorganic nitrogen-sources for biomass formation. In addition, the strains were cultured anaerobically to stimulate denitrification and establish any regulatory function within this nitrate-reducing pathway (Figure 4.3).

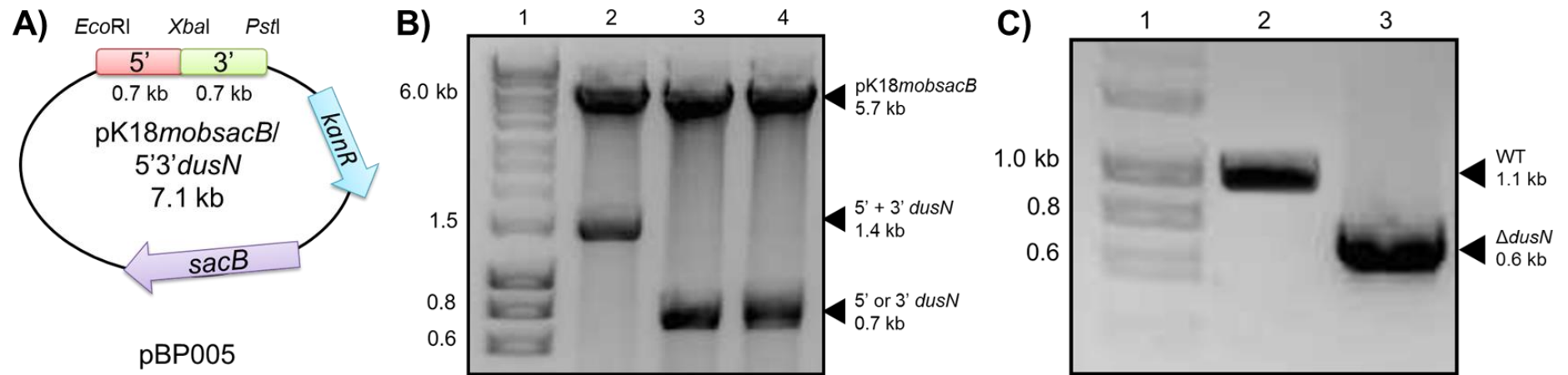


Figure 4.2. Generation of a mobilisation vector for the deletion of *dusN* from *P. denitrificans*. A) Suicide vector pBP050, pK18*mobsacB* derivative harbouring 5' and 3' fragments of *dusN*. B) Digestion analysis of pBP005. Lane 1; 1 kb Hyperladder, 2; *EcoRI/PstI* digestion of the 5'3' fragment, 3; *EcoRI/XbaI* digestion of the 5' fragment and 4; *XbaI/PstI* digestion of the 3' fragment. C) MyTaq PCR confirmation for the removal of 500 bp of genomic DNA coding for *dusN*. Lane 1; 1 kb Hyperladder, 2; WT, 3; Δ *dusN*.

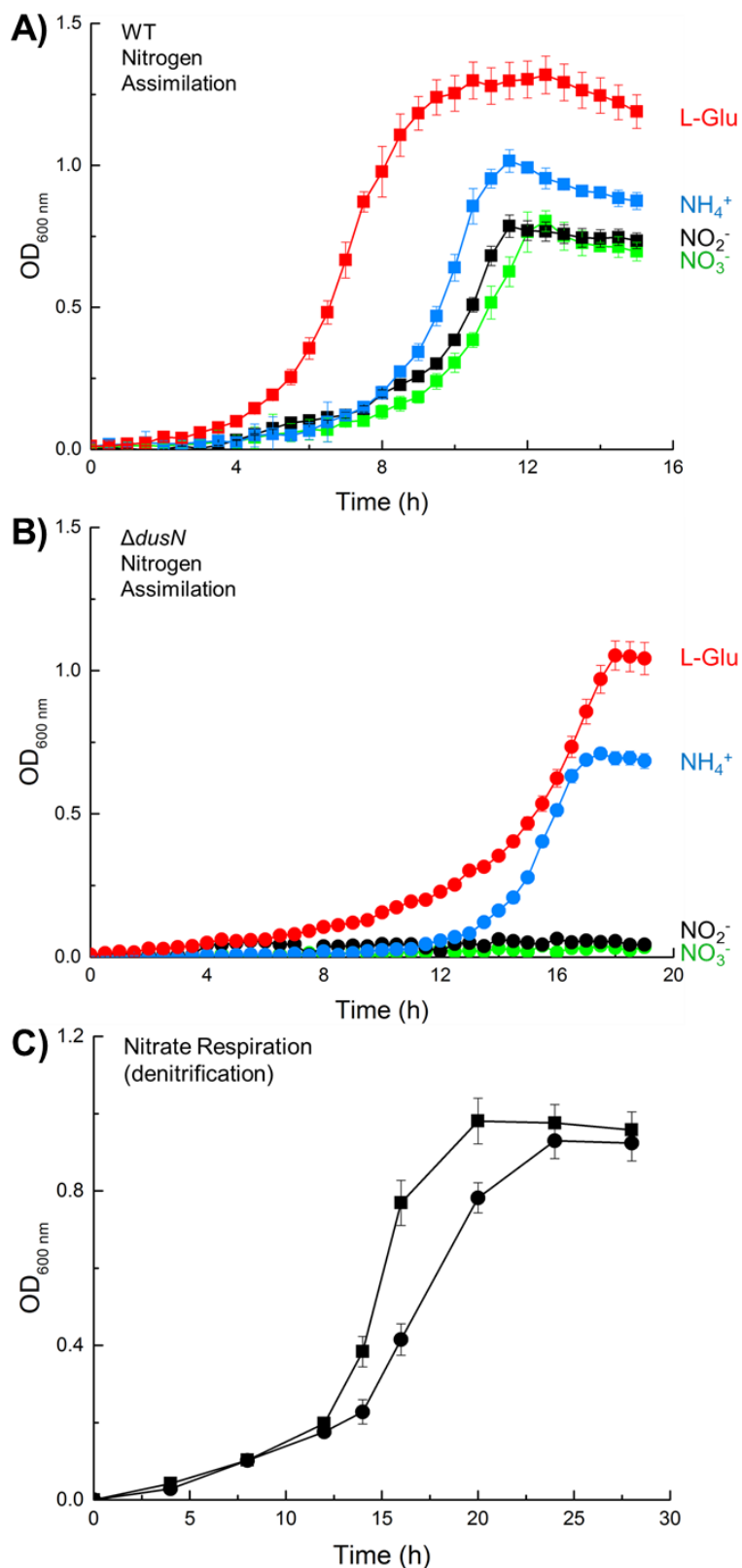


Figure 4.3. Bacterial growth curves showing the growth of $\Delta dusN$ on various nitrogen sources. *P. denitrificans* WT (squares) and $\Delta dusN$ (circles) were grown in minimal media at 30 °C with 30 mM succinate. A) Aerobic growth of WT using 10 mM of sole nitrogen sources: red; L-Glutamate, blue; ammonium, green; nitrate, black; nitrite. B) Aerobic growth of $\Delta dusN$. C) Anaerobic growth of WT and $\Delta dusN$ with 20 mM nitrate for respiration and 10 mM ammonium

Table 4.1. Summary of relevant growth parameters derived from Figure 4.3A & B.

Nitrogen Source	OD _{max} (at 600 nm)		μ_{max} (app.) (h ⁻¹)	
	WT	$\Delta dusN$	WT	$\Delta dusN$
10 mM NH ₄ ⁺	1.02 ± 0.04	0.71 ± 0.02	0.19 ± 0.02	0.15 ± 0.01
10 mM NO ₃ ⁻	0.81 ± 0.04	n.g.	0.14 ± 0.01	n.g.
10 mM NO ₂ ⁻	0.79 ± 0.03	n.g.	0.14 ± 0.02	n.g.
10 mM L-Glu	1.32 ± 0.07	1.05 ± 0.05	0.25 ± 0.03	0.17 ± 0.04

n.g. represents no growth.

Figure 4.3A shows *P. denitrificans* WT can effectively utilise ammonium, nitrate and nitrite as sole inorganic nitrogen sources for biomass synthesis as shown and discussed in Section 3.2. In addition, glutamate can be used individually as an organic nitrogen source, which, judging by the OD_{max} and μ_{max} (app.) values, is preferential for cells as these cultures recorded the greatest OD_{max} values and growth rate (Table 4.1) This is presumably due to the energy required to assimilate and integrate the inorganic nitrogen compounds with 2-oxoglutarate to form organic structures by the GS-GOGAT and GDH systems. Glutamate bypasses these prior processes donates its amine group directly into anabolic pathways, making it far more bioavailable. This bioavailability is reflected in the μ_{max} (app.) of 0.25 h⁻¹ which is almost double that for both nitrate and nitrite and is 30% greater than the value recorded for ammonium.

The absence of genomic *dusN* from *P. denitrificans* does not interfere with the bacterium's ability to use nitrate as an end-terminal electron acceptor for denitrification, as both strains achieved OD_{max} values of ~1.0 by 25 h (Figure 4.3C). This is consistent with data in Figure 3.18 where $\Delta ntrBC$ was observed to have no impact on denitrification and implies these regulators do not control this pathway.

However, a clear aerobic growth phenotype exists in $\Delta dusN$ (Figure 4.3B) where the ability to assimilate nitrate and nitrite was completely abolished and cells were unable to grow when supplemented with either nitrogen source. This key finding suggests that *DusN* is vital for nitrate/nitrite assimilation at some level of *Nas* expression and synthesis. Furthermore, attenuated growth was recorded during ammonium-dependent and glutamate-dependent growth of $\Delta dusN$. These cultures reached ~70% OD_{max} achieved by WT and experienced an increased lag time, reflected by the μ_{max} (app.) values. This suggests an effect in general nitrogen-metabolism as these sources are used ineffectively for biomass synthesis. This impact was further investigated by growing strains with varying external nitrogen concentrations.

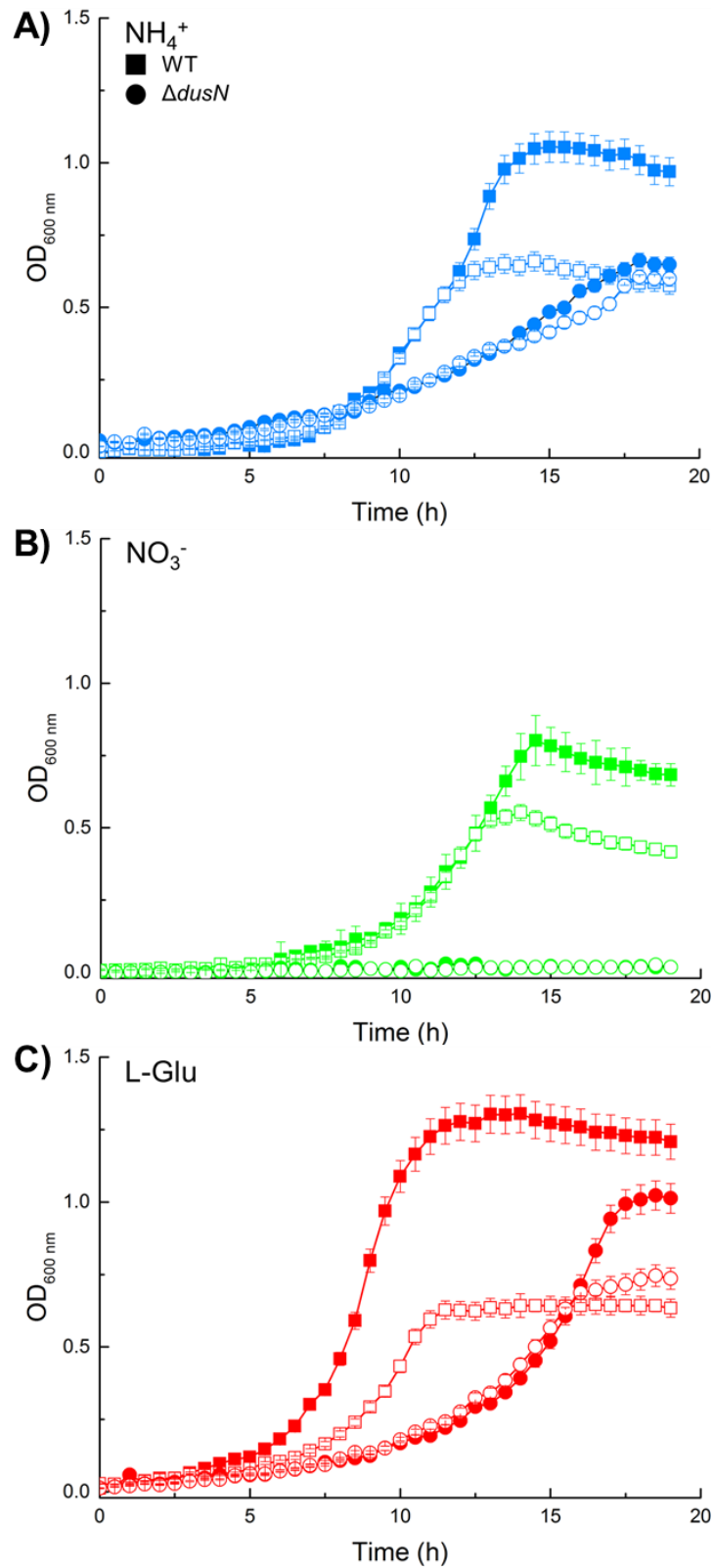


Figure 4.4. Aerobic growth of *P. denitrificans* strains using different concentrations of selected inorganic and organic nitrogen sources. Minimal salt media cultures of WT (squares) and $\Delta dusN$ (circles) grown aerobically at 30 °C using 30 mM succinate. Cultures were supplemented with either 5 mM (open symbol) or 10 mM (closed symbol) of the provided sole nitrogen source. A) ammonium (blue). B) nitrate (green). C) L-glutamate (red).

Figure 4.4 displays how *P. denitrificans* grows in response to various concentrations of a supplemented nitrogen source at a set carbon concentration (30 mM succinate). For ammonium-, nitrate- and glutamate-dependent growth, WT exhibits increased biomass output when more nitrogen was made available to the culture, reflected by the OD_{max} values. Ammonium-dependent and glutamate-dependent growth recorded ~100% greater OD_{max} when increasing the sole nitrogen source from 5 to 10 mM, matching the doubled input with a doubled output of biomass in a clear linear manner. Though not too as great an extent, the OD_{max} reached during nitrate-dependent growth still increased from ~0.5 to ~0.8 when 10 mM nitrate was made available to cultures. These values reflect increased biomass formation as a result of greater nitrogen availability for cells.

However, $\Delta dusN$ does not follow this pattern of matching increased growth output with increased nitrogen input. Though $\Delta dusN$ experiences an increase of ~35% OD_{max} values, reaching ~1.1, when grown with 10 mM glutamate as opposed to ~0.7 on 5 mM, this is nowhere near the 100% increase observed in WT where cultures reached an OD_{max} value of ~1.25 (Figure 4.4C). Furthermore, ammonium-dependent growth of $\Delta dusN$ showed a near complete lack of increased biomass formation upon doubling the nitrogen supplemented from 5 mM to 10 mM. OD_{max} values of ~0.65 and ~0.7 were recorded when grown with 5 mM and 10 mM ammonium, respectively (Figure 4.4A), reaching the same level of growth achieved by WT on 5 mM ammonium.

Due to the failure of $\Delta dusN$ to attain WT levels of growth, it is concluded that *P. denitrificans* is unable to effectively metabolise a range of nitrogen sources. The deletion has a lethal impact upon the cells ability to assimilate nitrate and nitrite, but also affects how the cells utilise ammonium as a sole nitrogen source. This may possibly be due to interference with the GS-GOGAT cycle as observed for $\Delta ntrBC$ in Figure 3.12, which resulted in ineffective incorporation of ammonium into organic compounds by GDH. This enzyme functions at the carbon/nitrogen interface to compensate the loss of GS-GOGAT and therefore loses optimal growth as GDH is unable to utilise the complete quantity of ammonium available due to its high K_m (Magasanik 1982).

To determine whether the phenotype observed is caused by deletion of *dusN* or disruption to the promoter region of the operon, qRT-PCR analysis was performed to ensure correct transcription of all remaining genes of the operon (Figure 4.5).

As $\Delta dusN$ is unable to grow with nitrate, all experiments requiring nitrate assimilation growth conditions used 10 mM L-alanine supplemented alongside the standard 10 mM nitrate. *P. denitrificans* uses this amino acid as a nitrogen source which feeds into

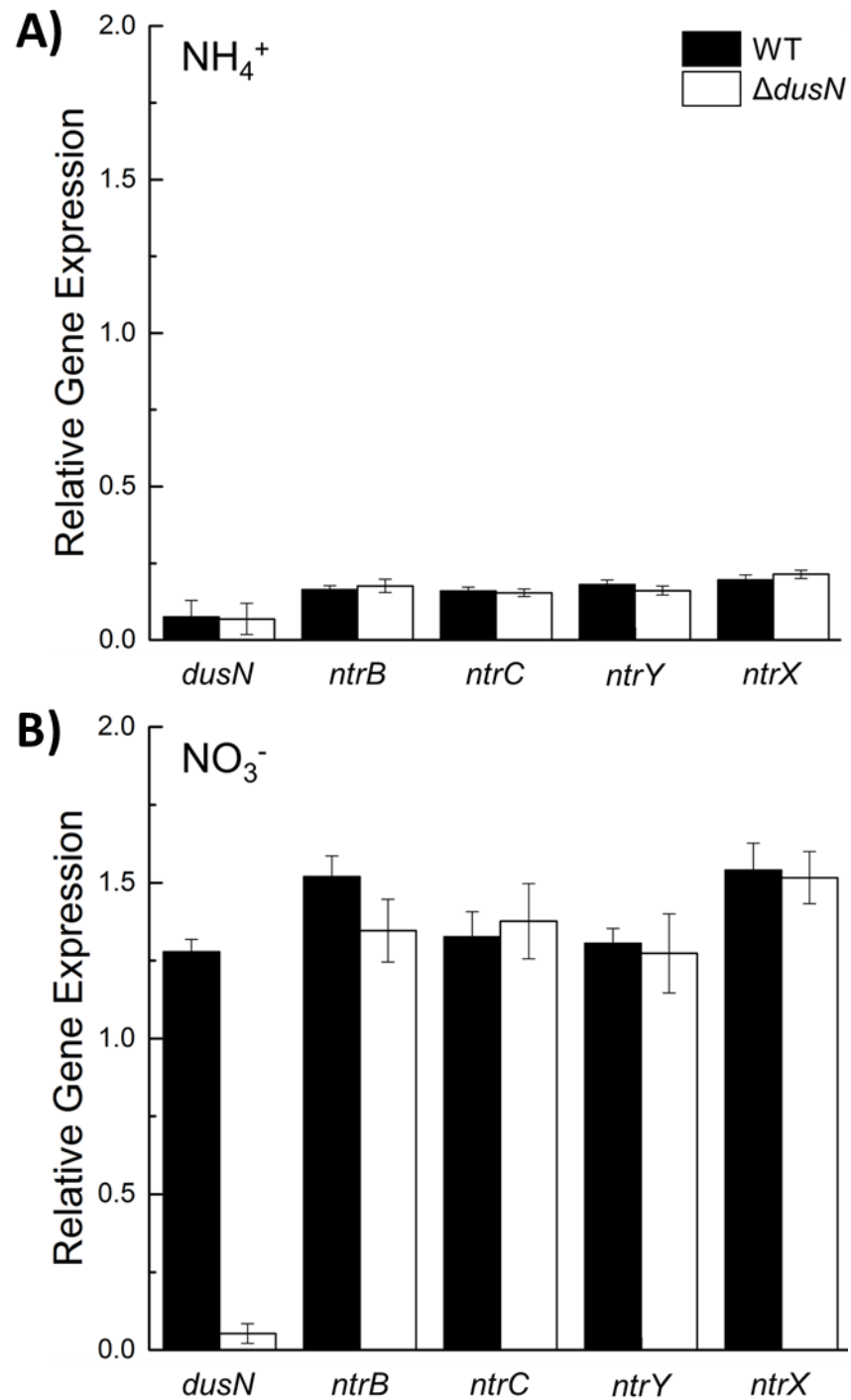


Figure 4.5. qRT-PCR analysis of the *dusN-ntrBCYX* operon in *P. denitrificans* strains. qRT-PCR data monitoring the gene expression of the *ntr* operon in WT (black) and $\Delta dusN$ (white) cultures. Cells were grown aerobically in minimal salt media supplemented with 30 mM succinate for carbon and either 10 mM ammonium or nitrate as a sole nitrogen source. RNA samples were harvested at a mid-exponential phase and gene expression was normalised to *dnaN*, a housekeeping gene.

biosynthesis of organic-nitrogen containing compounds without interfering with nitrogen-responsive systems under investigation such as Nas, GS-GOGAT and GDH.

qRT-PCR measures the transcription of individual genes during a defined mode of growth. As known from previous analysis and reports, the *ntr* genes are not expressed during ammonium-dependent growth which is in agreement with the data recorded in Figure 4.5A where the operon is transcribed at a very low level in both strains.

As expected, and consistent with previous reports and transcriptomic analysis (Figure 3.15 and Figure 4.1), the *dusN-ntrBCYX* genes are upregulated in WT during nitrate-dependant growth. In this case, expression increases by roughly an order of magnitude greater than in ammonium conditions. Furthermore, each of the genes reach a highly similar expression value of ~1.4 which is indicative of them forming a single transcriptional unit as proposed by data in Figure 3.19. Importantly, the transcription of *ntrBCYX* during nitrate-dependent growth was not attenuated in Δ *dusN* as each gene reached a comparable expression level with those recorded for WT (Figure 4.5B). From this it can be stated the genomic deletion of *dusN* causes no disruption to the promoter region of the operon and the loss of nitrate-assimilation capacity in Δ *dusN* is not due to interference with NtrBC or NtrYX. Instead, it shows the impact upon nitrogen-metabolism recorded by the Δ *dusN* phenotype is solely due to the loss of DusN and therefore it may be a novel regulator of nitrate/nitrite assimilation.

Upregulation of *dusN* during nitrate-dependent growth is not observed in the mutant due to the lack of the gene to produce mRNA for primers to anneal too during qRT-PCR, giving further confidence the genetic deletion was successful. Instead, to examine whether the deletion affects the expression of *dusN* by playing a positive self-regulatory role, the transcriptional *dusN-lacZ* fusion plasmid, pBP046, was used to quantify *dusN* transcription in WT and Δ *dusN* (see Section 2.17 for plasmid details).

As expected, the expression of *dusN-lacZ*, ~120 Mu, in the presence of ammonium is low. However, despite the low levels of β -galactosidase activity observed for ammonium grown cells, transcription of *dusN* is clearly not absent. By contrast, expression during nitrate-dependent growth increases by roughly an order of magnitude, consistent with the 10-fold increase observed by qRT-PCR in Figure 4.5, reaching ~1300 Mu. Importantly, no impact on the transcription of *dusN* is recorded in Δ *dusN* as no statistical difference was observed for β -galactosidase activity between the strains. This data suggests that DusN is not playing a regulatory role over the *dusN-ntrBCYX* operon at the level of expression and therefore coordinates nitrogen-responses in other manners.

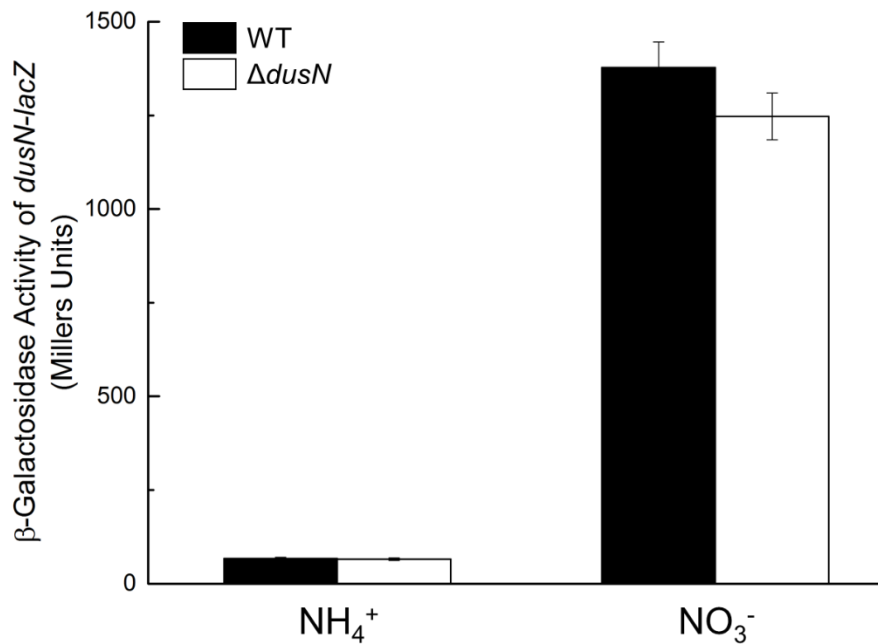


Figure 4.6. Expression of *dusN* from the *dusN-lacZ* fusion plasmid during the growth of *P. denitrificans* strains. WT (black) and $\Delta dusN$ (white) were grown in minimal media aerobically at 30 °C with 30 mM succinate and 10 mM of either ammonium or nitrate a sole nitrogen source. Gene reporter activity was measured for the transcription of *dusN* at a late-exponential phase and made relative to activity measured from a pMP220 vector containing no inserted promoter.

4.3 Genetic Restoration of Wild-Type Phenotype in $\Delta dusN$ Cells

To confirm the role of DusN in the expression of Nas and other nitrogen-responsive systems, *dusN* was genetically restored in the deletion strain to reinstate WT growth.

pLMB509 is a taurine-inducible expression vector capable of replication in a broad range of α -proteobacteria (Tett et al. 2012) and was used throughout this study to express recombinant proteins in *P. denitrificans* for complementation or purification purposes. The *dusN* gene of *P. denitrificans* was PCR-amplified and ligated as an *NdeI/NdeI* restriction fragment into pLMB509 to construct pBP006 (Figure 4.7B). Genes inserted at this restriction site lie downstream of a taurine inducible promoter and genetic elements to allow controllable expression of recombinant proteins. A stop codon was introduced in *dusN* to prevent incorporation of a C-terminal 6-His tag within the plasmid sequence.

Following construction and sequence confirmation, pBP006 was conjugated into $\Delta dusN$ to produce the strain denoted “*complement*” ($\Delta dusN$ + pBP006). Batch cultures were grown aerobically in minimal salt medium where addition of taurine stimulated recombinant DusN expression off the ectopic taurine promoter and thus used to screen for the restoration of WT phenotype.

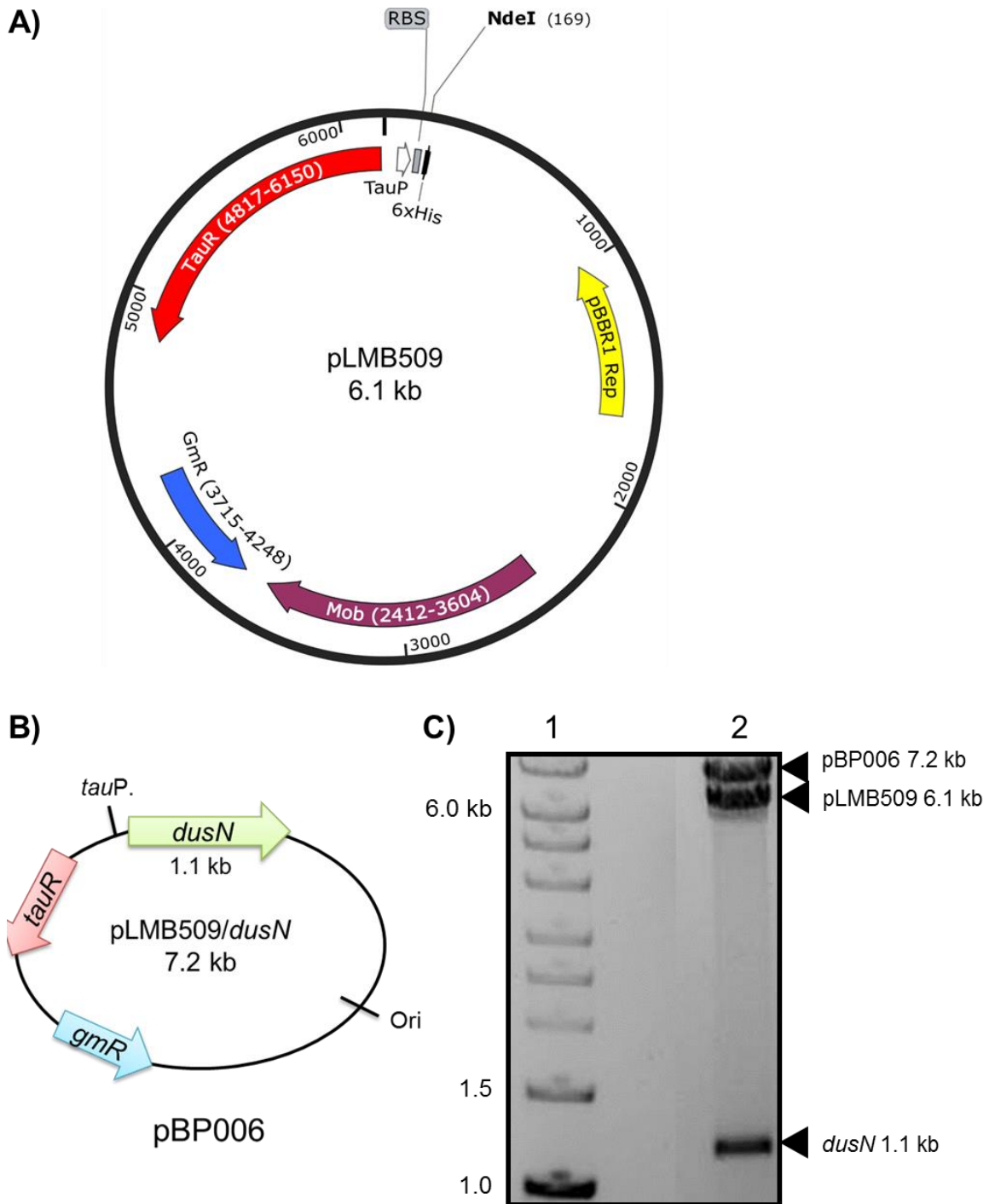


Figure 4.7. Generation of a *dusN* expression vector for genetic complementation of Δ *dusN*.

A) Plasmid map depicting key features of pLMB509: A taurine promoter and ribosome binding site (RBS) lay upstream of *NdeI* used to insert genes as *NdeI* restriction fragments. Also encoded is: taurine regulator (TauR), gentamycin resistance (GmR) and the mobilisation genes for conjugation (*mob*). Vector map drawn using SnapGene Viewer software. B) Schematic representing pBP006, the pLMB509 derivative harbouring the 1.1 kb *dusN* gene from *P. denitrificans*, inserted at an *NdeI* site. C) Agarose gel analysis of pBP006. Lane 1; 1 kb Hyperladder, 2; pBP006 digested with *NdeI* to cut the 1.1 kb *dusN* gene.

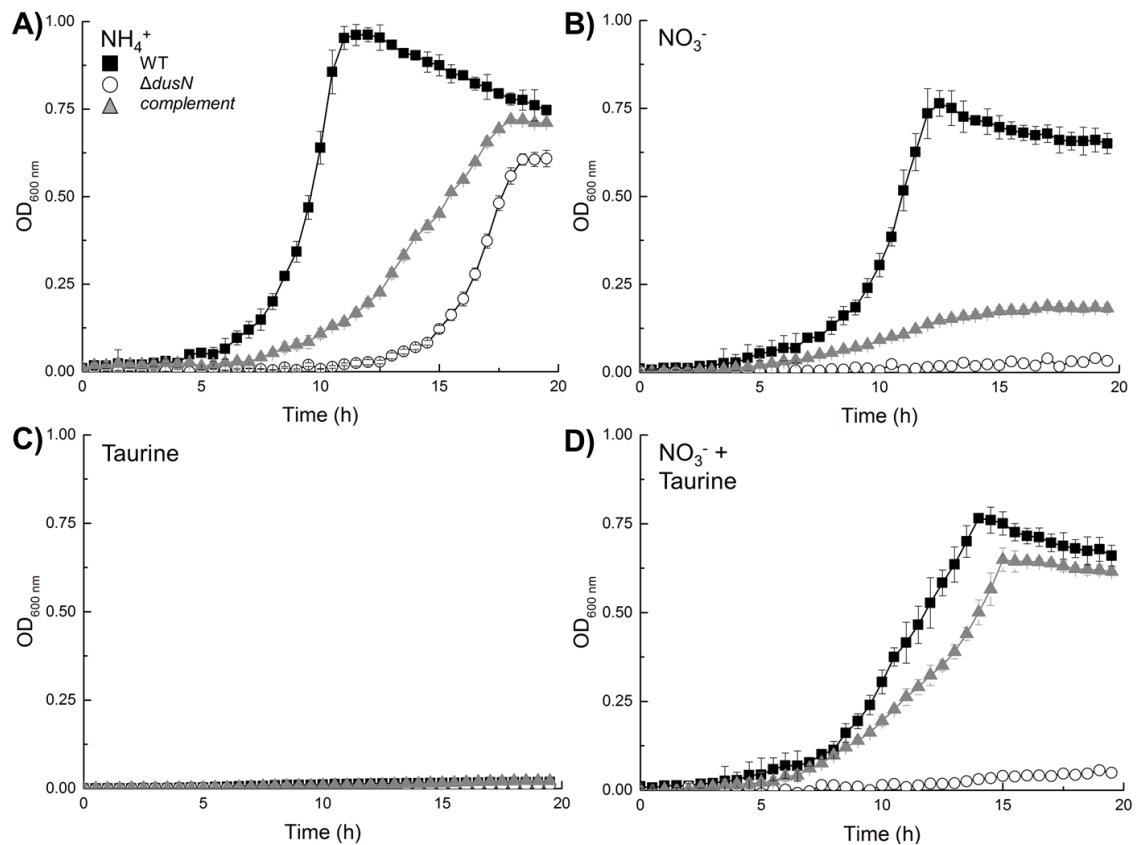


Figure 4.8. Genetic complementation of $\Delta dusN$ to restore wild-type phenotype. WT (black), $\Delta dusN$ (white) and complement ($\Delta dusN + pBP006$, grey) were grown aerobically in minimal salt media at 30 °C containing 30 mM succinate as a carbon source. A) 10 mM ammonium, B) 10 mM nitrate or C) 1 mM taurine were supplemented as sole nitrogen sources. D) 1 mM taurine was used to stimulate the expression of *DusN* from *pBP006* in complement ($\Delta dusN + pBP006$) with 10 mM nitrate.

Figure 4.8 shows the aerobic growth of WT, $\Delta dusN$ and $\Delta dusN + pBP006$ (*complement*) when supplemented with different nitrogen sources. All three strains were capable of growth using ammonium for nitrogen, with WT and $\Delta dusN$ displaying the same phenotypes as recorded and discussed previously in Figure 4.3. $\Delta dusN + pBP006$ grew to an OD_{max} of ~ 0.75 which is slightly, yet significantly, greater than $\Delta dusN$, ~ 0.63 , though not at a comparable level to ~ 1.0 achieved by WT (Figure 4.8A). A similar observation is present during nitrate-dependent growth where, although $\Delta dusN + pBP006$ was not capable of generating a great quantity of biomass, it does reach an OD_{max} of ~ 0.2 which represents some growth, especially when compared to $\Delta dusN$ as a negative control (Figure 4.8B). These phenotypes suggest that pLMB509 gives low levels of constitutive background expression and that *dusN* transcription is not completely repressed by the taurine repressor (TauR). Therefore, even in the absence of taurine, leaky expression of pBP006 gives rise to low levels of cellular DusN that begin to restore the WT phenotype.

Taurine is an amino acid derivative which contains carbon, nitrogen and sulfur atoms and can potentially be used by *P. denitrificans* as an organic nitrogen source. To check cells were unable to grow sufficiently with taurine, which would interfere with results when used later as an inducer, control cultures were supplemented with 1 mM taurine as a sole nitrogen source. However, none of the strains were capable of growth using this metabolite at such a low concentration (Figure 4.8C).

Figure 4.8D shows the nitrate-dependent growth of the strains when 1 mM taurine was present to stimulate *dusN* transcription from the ectopic plasmid promoter present in $\Delta dusN + pBP006$. Importantly, $\Delta dusN + pBP006$ observed a highly similar growth phenotype as WT where OD_{max} and μ_{max} (app.) values of ~ 0.65 and 0.12 were recorded, respectively. These growth measurements are comparable to the OD_{max} and μ_{max} (app.) of ~ 0.75 and 0.14 recorded for WT and allow the mutant strain to grow efficiently with nitrate as the sole nitrogen source (Figure 4.8D). From this, we confirm plasmid-borne DusN acts *in trans* to genetically restore WT phenotype in $\Delta dusN$ and reinstates the cells ability to express Nas for biomass formation and ultimately growth. To investigate how DusN functions and obtain a broad insight into its role in *P. denitrificans*, several transcriptomic techniques were performed, particularly with a view on Nas expression.

4.4 Global Transcriptomic Analysis of WT vs $\Delta dusN$ during Nitrate-Induced Growth

A type-II comparative microarray of WT vs $\Delta dusN$ was employed to visualise the whole cell changes in transcription patterns caused by the loss of DusN. RNA was harvested at a mid-exponential phase from aerobic batch cultures of WT and $\Delta dusN$ during nitrate-

induced growth. Once the RNA had been reversed transcribed to cDNA, it was used to quantify transcription of each gene in the genome of *P. denitrificans* to compare individual expression between the strains (Section 2.21). Genes which underwent a significant change in their transcriptional levels were highlighted by the microarray and presented as a heat-map (Figure 4.9). This heat map depicts the log₂ normalised gene expression as a colour where more intense red indicates greater transcription. 63 genes (not including *dusN*) out of 5134 total genes of *P. denitrificans* changed significantly between WT and Δ *dusN*, representing 1.25% of the total genome. Complete data set available on the CD attached with this thesis.

Genes presented in Figure 4.9A undergo a significant decrease in transcription in the Δ *dusN* strain. A number of these encode proteins which are involved in nitrogen- and amino acid-metabolism: urease (Pden_1208) catalyses the cleavage of ammonium from organic urea (Mobley & Hausinger 1989). Ureidoglycolate hydrolases (2103) breaks down ureidoglycolate to organic glyoxalate and ammonium (Winkler et al. 1988). 3-hydroxyisobutyrate dehydrogenase (3216) is involved in the catabolism of valine, leucine and isoleucine to carbon skeletons with the release of amine groups (Rougraff et al. 1988). Nicotinamide-nucleotide amidase (3665) breaks down nicotinamide D-ribonucleotide structures to release ammonium (Imai 1973). Asparaginase/glutaminase (4244) hydrolyses amine groups from the side chains of either amino acid to produce aspartate and glutamate (Imada et al. 1973). These enzymes are associated with producing inorganic nitrogen for the cell by scavenging ammonium from organic structures. These genes are presumably upregulated in WT during nitrate-dependent growth as bioavailable nitrogen is limiting and these encoded products provide a source of cellular ammonium for growth. However, these genes are transcribed to a significantly less extent in the mutant strain which may, therefore, determine that DusN is involved with the regulation of enzymes that can produce a useable, cytoplasmic, inorganic nitrogen source during nitrogen-limiting conditions, i.e. nitrate assimilation.

DusN may further be involved in general nitrogen-metabolism as several other genes downregulated in Δ *dusN* participate in the nitrogen-response. Phosphoserine phosphatase (812) dephosphorylates phosphoserine to serine which then feeds into biosynthesis of nucleic acids and amino acids (Chiba et al. 2012). Both the branched-chain amino acid transporter (3931) and urea ABC transporter (4020) are upregulated during nitrate-dependent growth in WT to scavenge useable organic nitrogen sources during limitation. Again, their decrease in transcription in the mutant suggests DusN is required to regulate their expression during the nitrogen-response.

A)	Gene ID	Name	WT	Δ dusN	Function / Annotation
	333	<i>trpA</i>	Orange	Light Blue	Tryptophan synthase
	429	<i>azlC</i>	Yellow	Light Blue	Branched chain amino acid efflux pump
	545	<i>glmM</i>	Red	Yellow	Phosphoglucosamine mutase
	552	<i>sucC</i>	Red	Yellow	Inner membrane protein
	652	<i>hisC</i>	Yellow	Light Blue	Histidinol-phosphate aminotransferase
	727	<i>exbB</i>	Red	Light Blue	MotA/TolQ/ExbB Proton channel
	790	<i>psuA</i>	Orange	Yellow	Pseudouridine synthase
	812	<i>serB</i>	Red	Light Blue	Phosphoserine phosphatase
	951	<i>nrdA</i>	Yellow	Light Blue	Ribonucleoside-diphosphate reductase
	1208	<i>ureC</i>	Orange	Yellow	Urease
	1260	<i>furA</i>	Yellow	Light Blue	Ferric-uptake regulator
	1553	<i>nusB</i>	Red	Orange	Transcription antitermination factor (NusB)
	1742	<i>dtd1</i>	Red	Light Blue	Tyrosyl-tRNA hydrolase
	1744	<i>tdkA</i>	Yellow	Light Blue	Thymidine kinase
	1862	<i>DksA</i>	Yellow	Light Blue	DksA/TraR family transcriptional regulator
	1913	<i>tyrS</i>	Red	Yellow	Tyrosyl-tRNA synthetase
	1948	---	Yellow	Light Blue	Hypothetical protein
	1997	<i>hemY</i>	Red	Orange	Uroporphyrinogen-III synthase
	2039	<i>argF</i>	Yellow	Light Blue	Ornithine carbamoyltransferase
	2041	<i>argD</i>	Yellow	Light Blue	Acetylornithine aminotransferase
	2044	<i>nudH</i>	Red	Light Blue	Nucleoside diphosphate hydrolase
	2103	<i>allA</i>	Yellow	Light Blue	Ureidoglycolate hydrolase
	2148	<i>mdcF</i>	Yellow	Light Blue	Malonate transporter
	2321	<i>odc1</i>	Yellow	Light Blue	Ornithine decarboxylase
	2384	<i>entA</i>	Yellow	Light Blue	2,3-dihydroxybenzoate dehydrogenase
	2425	---	Red	Yellow	Hypothetical protein
	2506	<i>gpml</i>	Red	Yellow	Phosphoglycerate mutase
	2525	<i>cbtA</i>	Yellow	Light Blue	Hypothetical metal binding protein
	2530	<i>cobZ</i>	Red	Light Blue	Hypothetical metal binding protei
	2543	---	Yellow	Light Blue	Hypothetical protein
	2572	<i>rpeA</i>	Red	Light Blue	Ribulose-phosphate 3-epimerase
	2577	<i>rumA</i>	Yellow	Light Blue	Uracil-5-methyltransferase
	2593	<i>rpIG</i>	Red	Yellow	Ribosomal protein 50s L7/L12
	2859	<i>lysR</i>	Yellow	Light Blue	LysR transcriptional regulator
	2956	<i>nspC</i>	Yellow	Light Blue	Carboxynorspermidine decarboxylase
	3014	---	Yellow	Light Blue	NtaA/SnaA/SoxA monooxygenase family
	3216	<i>garR</i>	Light Blue	Light Blue	3-hydroxyisobutyrate dehydrogenase
	3652	---	Orange	Light Blue	Hypothetical protein - ABC transporter related
	3665	<i>pncC</i>	Yellow	Light Blue	Nicotinamide-nucleotide amidase
	3880	<i>aroF</i>	Yellow	Light Blue	Chorismate mutase
	3931	<i>braF</i>	Red	Light Blue	Branched-chain amino acid ABC transporter
	3952	<i>hmt1</i>	Orange	Light Blue	Homo-cysteine S-methyltransferase
	3967	<i>sufD</i>	Red	Yellow	FeS assembly protein
	3970	<i>surS</i>	Yellow	Light Blue	Cysteine desulfurase
	3993	<i>pyrH</i>	Red	Orange	Uridylate kinase
	4020	<i>urfD</i>	Yellow	Light Blue	Urea ABC Transporter
	4050	<i>icm1</i>	Light Blue	Light Blue	Isoprenylcysteine carboxyl methyltransferase
	4063	<i>cvsS</i>	Yellow	Light Blue	CysteinyI-tRNA synthetase
	4131	<i>dusN</i>	Red	Light Blue	DusN
	4132	<i>sdaA</i>	Red	Yellow	Serine dehydratase
	4244	<i>ansA</i>	Red	Yellow	Asparaginase/glutaminase
	4313	<i>rimJ</i>	Yellow	Yellow	Ribosomal-protein-alanine N-acetyltransferase
	4366	<i>dbpA</i>	Red	Light Blue	ATP-dependent RNA helicase
	4377	<i>nrdE</i>	Yellow	Light Blue	Ribonucleotide diphosphate reductase, α
	4378	<i>nrdF</i>	Yellow	Light Blue	Ribonucleotide diphosphate reductase, β

B)

Gene ID	Name	WT	$\Delta dusN$	Function / Annotation
1444	--			Hypothetical protein
1594	<i>ppkB</i>			Polyphosphate kinase
1613	--			Acyl-CoA dehydrogenase, type 2
2024	<i>tag1</i>			DNA-3-methyladenine glycosylase I
2811	<i>sqdB</i>			UDP-sulfoquinovose biosynthesis protein
3196	<i>trbB</i>			Conjugal transfer protein (TrbB)
3456	<i>yjgH</i>			Endoribonuclease L-PSP
3872	<i>gdhA</i>			Glutamate dehydrogenase
4108	<i>ssuC</i>			Sulfonate transporter permease
4363	<i>ribD</i>			Bifunctional deaminase

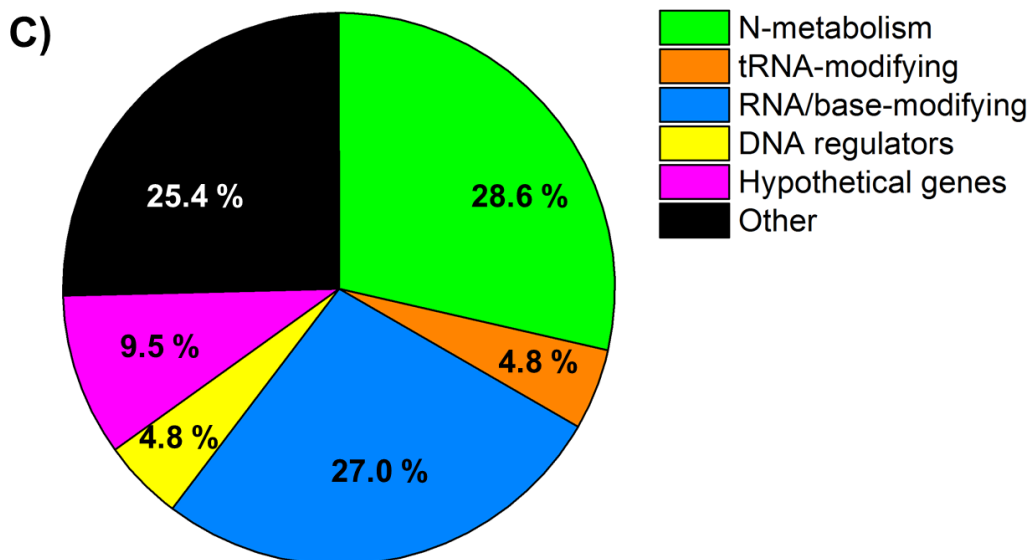


Figure 4.9. Microarray transcriptomic analysis of WT vs $\Delta dusN$ during nitrate-dependant growth. Heat map representing the expression levels of selected genes from WT (left) and $\Delta dusN$ (right). Cultures were grown aerobically in minimal media at 30 °C supplemented with 30 mM succinate, 10 mM nitrate and 10 mM L-alanine. RNA was harvested at a mid-exponential phase and subject to a type-II microarray. Colours indicate average log₂ normalised expression values between three biological replicates. ID represents unique locus tag of each gene in the *P. denitrificans* genome (Accession: NC_008686–008688). Panel A shows genes downregulated in $\Delta dusN$ and panel B shows the genes which are upregulated in the $\Delta dusN$ strain. C) Pie chart quantifying the various types of genes and pathways which underwent significantly altered expression in the $\Delta dusN$ strain. Colours are as follows: green; enzymes involved in nitrogen metabolism, orange; tRNA-modifying proteins, blue; RNA/base-modifying proteins, yellow; DNA regulators, pink; hypothetical proteins, black; other.

Intriguingly, two additional tRNA-modifying enzymes recorded an altered transcription when *dusN* was removed from the genome of *P. denitrificans*. The expression of tyrosyl-tRNA synthetase (1913) and cysteinyl-tRNA synthetase (4063) was majorly downregulated in Δ *dusN*. Both proteins belong to the aminoacyl-tRNA synthetase (AATS) family of enzymes which load their specific amino acid onto the correct tRNA compound (Woese et al. 2000). As discussed in Section 1.9.1.3, the D-loop, which DUS modify, serves as a recognition site for AATS to target their specific tRNA substrate (Hardt et al. 1993; Smith & Yarus 1989). Furthermore, individual DUS subgroups target different tRNA compounds and may provide stereochemical fine-tuning of the D-loop to allow AATS recognition. Therefore, as a combined effort of DUS and AATS may be required to correctly charge mature tRNA transcripts with their respective amino acids, a regulatory mechanism encompassing the genes encoding the Dus and AATS which act on a specific tRNA might be plausible. Certainly, the decrease in expression of both tyrosyl- and cysteinyl-tRNA synthetase in Δ *dusN* would support this hypothesis and be consistent with DusN modifying tRNA encoding tyrosine and cytosine. The tRNA for tyrosine has been previously reported to be a target for DUS activity in *S. cerevisiae* (Xing et al. 2004) and the interaction between DusN and whole cell tRNA will be studied further in Chapter 5 in order to identify specific RNA substrates.

Several genes exhibiting decreased transcription in the mutant compared to WT may be caused as a side effect of no nitrate assimilation instead of direct DusN regulation. Nas requires a total of 5 [Fe-S] clusters within the NasBGC three-component system. The ferric-uptake regulator (1260), 2,3-dihydroxybenzoate dehydrogenase (involved in synthesising siderophores, 2384), the Fe-S assembly protein (3967) and cysteine desulfurase (provides sulfur for Fe-S synthesis, 3970) are downregulated in Δ *dusN* as less [Fe-S] clusters are required in the absence of Nas. Additionally, uroporphyrinogen-III-synthase (1997) is transcribed to a lower extent as this protein is involved in siroheme synthesis, the catalytic cofactor of NasB (Raux et al. 2000).

Interestingly, many enzymes which modify RNA and nucleobases underwent significant decrease in their expression when *dusN* was removed: phosphoglucosamine mutase (545) converts glucosamine-6-phosphate to glucosamine 1-phosphate which is subsequently uridylated using UTP (Mengin-Lecreulx & van Heijenoort 1996). Pseudouridine synthase (790) catalyses the formation of pseudouridine from uridine in RNA transcripts (Kammen et al. 1988). Thymidine kinase (1744) converts thymidine to dTMP thus committing them to DNA synthesis (Kit 1985). Uracil-5 methyltransferase (2577) adds a methyl group onto C5 of uracil's pyrimidine structure to produce thymine (Hurwitz et al. 1964) and ribonucleotide reductase (4377/8) catalyses ribonucleotide

reduction to deoxyribonucleotides (Kolberg et al. 2004). These enzymes all shuttle nucleobases away from a metabolic route which could result in dihydrouridine synthesis. By decreasing the transcription of these genes in $\Delta dusN$, the cells are conserving the cytoplasmic stock of uridine/uracil which could participate in dihydrouridine formation. We believe, possibly, the cell is misinterpreting the deficiency of RNA-dihydrouridine with a lack of precursor compounds rather than an absence of cellular DusN and therefore attempts to compensate for the loss of this post-transcriptional modification by downregulating the genes which may remove uridine/uracil.

Figure 4.9B shows the genes that underwent a significantly increased level of transcription in the $\Delta dusN$ deletion strain. UDP-sulfoquinovose biosynthesis protein (2811) is involved with the formation of sulfolipids from UDP-glucose and ultimately releases UDP groups (Essigmann et al. 1998). Another encodes endoribonuclease L-PSP (3456), an enzyme which degrades single-stranded mRNA to recycle ribonucleosides (Morishita et al. 1999). As proposed earlier, this might be upregulated as the cell attempts to increase the cytoplasmic stock of uridine to compensate for the lack of dihydrouridine present in the RNA.

GDH (3872) displays major upregulation when compared to WT which validates the conclusions drawn in Section 4.2.2 (Figure 4.4). There, it was postulated that the inability of $\Delta dusN$ to achieve the same OD_{max} as WT was due to a loss of GS-GOGAT function which resulted in GDH operating the carbon/nitrogen interface which is ineffective at incorporating low levels (less than ~ 1 mM) ammonium into biomass (Magasanik 1982). Interestingly, neither GS or GOGAT were highlighted by this microarray analysis as undergoing a significant decrease in transcription. In Section 3.6 we demonstrated that NtrBC is responsible for activating both *glnA* (GS) and *gltD* (GOGAT) and in $\Delta ntrBC$ these genes are not expressed but *gdhA* (GDH) is, during nitrate-dependent growth (Figure 3.12). However, the transcription of *glnA*, *gltD* and *ntr* is not attenuated in $\Delta dusN$ during nitrate-induced growth, yet GDH is the dominant mode for assimilating ammonium into organic biosynthetic compounds. Should DusN be operating by manipulating the activity of NtrBC, we would expect the genes for GS and GOGAT to be not transcribed in $\Delta dusN$. Furthermore, the transcription of *nas* is not attenuated significantly enough to be highlighted by this microarray, yet the growth data demonstrates Nas is not functional (Figure 4.3B). From this, we conclude that DusN acts independently to the function of NtrBC and regulates expression of target proteins directly at a post-transcriptional level. This is consistent with the DUS family modifying tRNA to regulate the appropriate cell response at the level of translation.

4.5 Deciphering the Physiological Function of DusN using qRT-PCR and Gene-Reporter Fusion Assays

4.5.1 qRT-PCR analysis of the *nas* gene cluster

The transcription of *nas* and *ntr* were not significantly altered in $\Delta dusN$ due to their absence in the heat-map (Figure 4.9). Figure 4.5 further confirmed *ntr* is transcribed in the mutant strain to the same extent as WT by using qRT-PCR, which was also employed to validate that *nas* is expressed in $\Delta dusN$. WT and $\Delta dusN$ were grown aerobically in batch cultures supplemented with either ammonium or nitrate as a nitrogen source. RNA was harvested at a mid-exponential phase for subsequent qRT-PCR analysis using the specific *nas* primers (Figure 4.10).

As shown in various previous data sets, the expression of *nas* is at low background levels during ammonium-dependent growth, where *nasTS* is transcribed to ~0.5 which is roughly double that recorded for *nasABGHC* (Figure 4.10A). As expected, during nitrate-induced growth the transcription of the *nas* gene cluster is substantially upregulated to enable cellular nitrate assimilation (Figure 4.10B). Expression of *nasTS* increases 3-fold to ~1.6 whilst *nasABGHC* is upregulated from ~0.25 to 1.25. These values are in agreement with those presented in Figure 3.15A where *nasTSABGHC* was subject to similar qRT-PCR analysis. Importantly, expression of *nas* genes were not significantly affected by the loss of DusN during nitrate-induced growth. This is consistent with the microarray analysis and reveals that DusN does not act at a transcriptional level as *nas* and *ntr* mRNA is still present in $\Delta dusN$. Instead, this indicates that DusN may act to modulate expression of the Nas and/or Ntr proteins, as is consistent with their role in post-transcriptional modification of RNA.

4.5.2 Transcriptional and translation β -galactosidase gene-reporter fusion assays

Given that qRT-PCR and microarray techniques can only probe the presence of mRNA and thus provide information concerning gene transcription, the translation of Nas proteins was investigated using β -galactosidase gene-reporter fusion assays. Whereas in Chapter 3 these assays were performed in pMP220 to give a transcriptional fusion plasmid, here, the wide-host range pIJ1363 plasmid was used. This vector lacks a RBS which is present in pMP220 and genes are fused directly into the *lacZ* gene sequence in pIJ1363. Therefore, resulting *lacZ* expression from pIJ1363 and measured β -galactosidase activity is dependent upon, and proportional too, translation of the inserted region (see Figure 2.3).

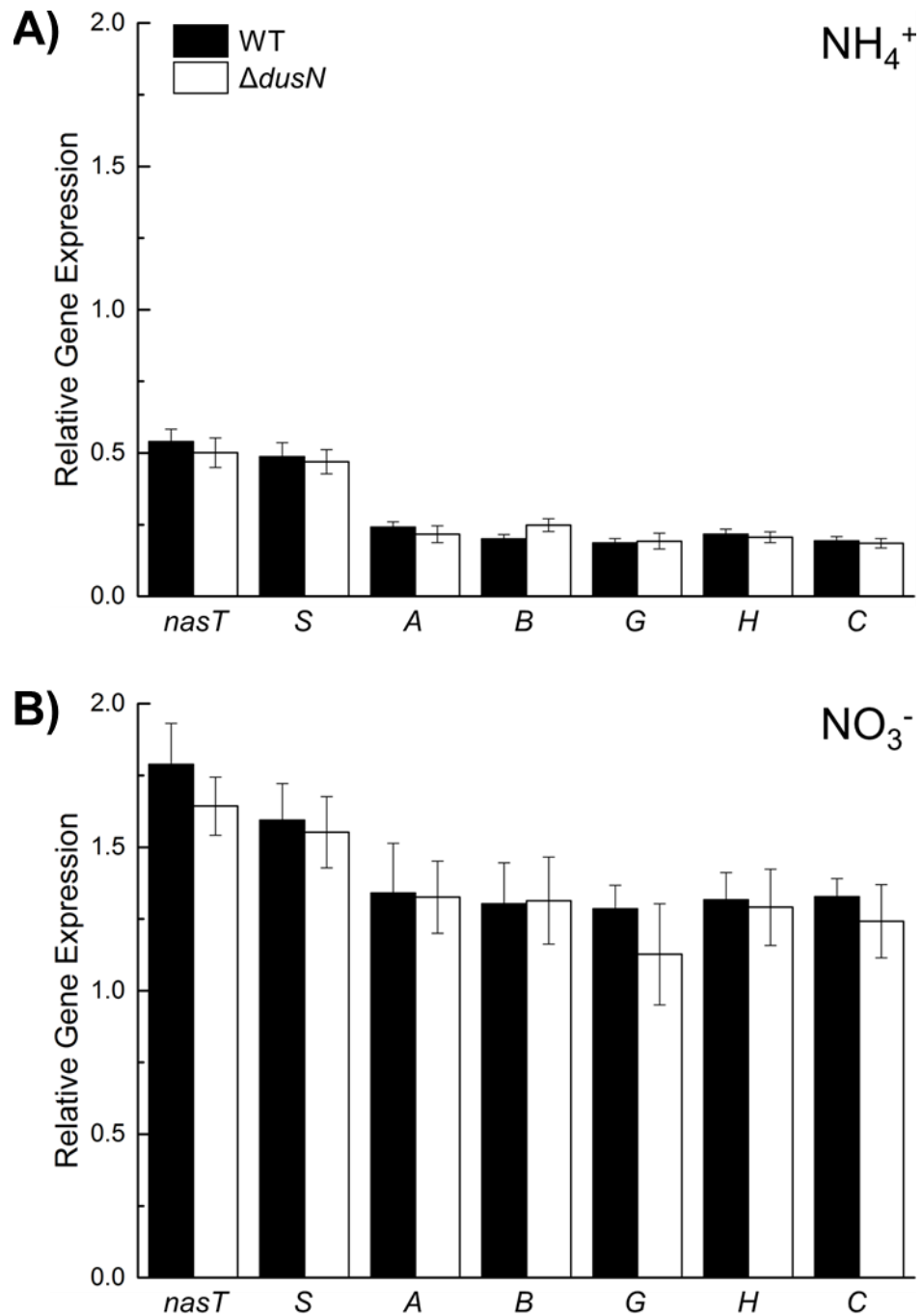


Figure 4.10. qRT-PCR analysis for the expression of the *nas* genes in *P. denitrificans* strains. Data showing the expression of each individual gene of *nasTSABGHC* in WT (black) and $\Delta dusN$ (white) cells monitored via qRT-PCR. Cultures were grown aerobically in minimal salt media at 30 °C supplemented with 30 mM succinate, 10 mM L-alanine and 10 mM ammonium or nitrate. RNA was extracted from cultures harvested at a mid-exponential phase and gene expression was normalised to *dnaN*, a housekeeping gene.

The same promoter regions of *nasA* and *nasT* which were cloned into pMP220 to construct pBP042 and pBP043 were cloned into pIJ1363 to construct translational gene-reporter fusion plasmids pBP044 and pBP045, respectively (see Section 2.17 for cloning details). Once these vectors had been conjugated into WT and $\Delta dusN$, the strains were grown in minimal salt media batch cultures to monitor the translation of the *nasTS* and *nasABGHC* operons during nitrate-induced growth (Figure 4.11).

The *nasT-lacZ* and *nasA-lacZ* activities shown in Figure 4.11A were measured from the pMP220-derived plasmids and thus represent transcription of the genes. The *nasT* and *nasA* genes were transcribed to ~3000 Mu and ~2000 Mu, respectively, and judged to be expressed at a very high level. Importantly, no variation was seen in these expression values for transcription of *nasTS* and *nasABGHC* in $\Delta dusN$, consistent with the microarray analysis and qRT-PCR data in Figure 4.9 and 11, respectively. This shows that the *nas* genes are transcribed correctly to mRNA during nitrate-dependent growth.

Figure 4.11B display the *nasT-lacZ* and *nasA-lacZ* translational gene-reporter fusion plasmids. In WT, β -galactosidase activities of ~1100 Mu and ~800 Mu were recorded, respectively, demonstrating both *nasTS* and *nasABGHC* are translated at a high level during nitrate-induced growth to enable nitrate import and reduction to ammonium. Whilst these expression values are around half that observed for transcription, the expression of β -galactosidase is dependent upon other factors such as copy-number of the plasmid. Importantly, both genes were clearly translated to a large extent when compared to the plasmid containing no insert which the *nasT-lacZ* and *nasA-lacZ* expression values were normalised too. Furthermore, the transcription of *nasA* is ~65% that of *nasT* and the translation of *nasA* is ~70% of *nasT*, both ratios being in good agreement between experiments.

The key finding of this experiment was the absence of *nasA-lacZ* β -galactosidase activity in $\Delta dusN$ from the pIJ1363-derived plasmid (Figure 4.11B). This diminished expression means that nascent *nasABGHC* mRNA is not translated to polypeptides in $\Delta dusN$. *NasTS* is translated in the deletion strain to the same extent as in WT, ~1100 Mu, therefore still acting as a regulator of *nasABGHC* transcription in $\Delta dusN$ which we have observed with multiple techniques. However, this lack of *nasABGHC* translation accounts for the inability of $\Delta dusN$ to perform nitrate-dependent growth (Figure 4.3B) as no Nas system is present to assimilate nitrate to ammonium for nitrogen assimilation.

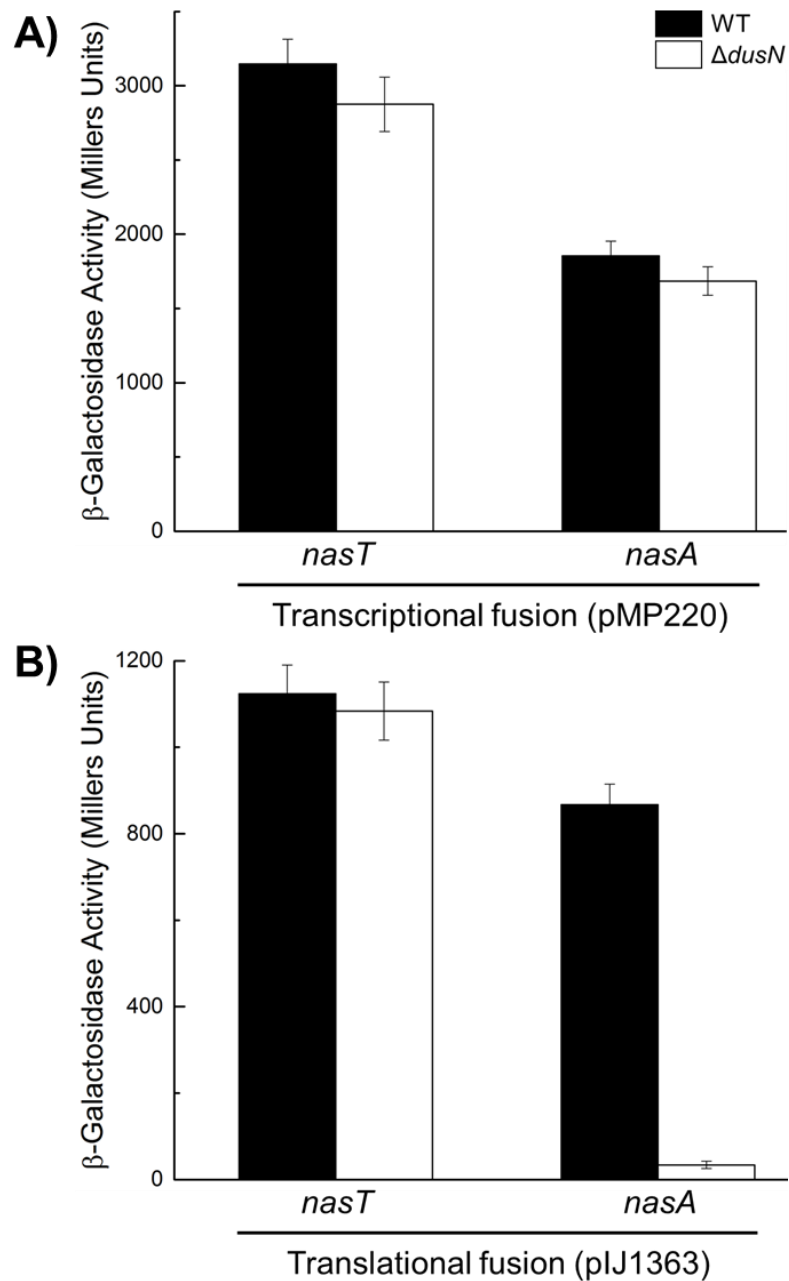


Figure 4.11. β -galactosidase activities of the *nasT-lacZ* and *nasA-lacZ* gene-reporter plasmids during nitrate-induced growth of *P. denitrificans* strains. WT (black) and $\Delta dusN$ (white) were grown in batch minimal media cultures aerobically at 30 °C supplemented with 30 mM succinate, 10 mM L-alanine and 10 mM nitrate. β -galactosidase activities were measured at an early-exponential stage to monitor the transcription and translation activity of *nasT* and *nasA*, made relative to activity measured from empty pMP220 and pIJ1363 vectors containing no inserted promoter.

This analysis concludes DusN is crucial for post-transcriptional regulation of Nas and is key for biosynthesis of the structural NasABGHC proteins by enabling translation of its mRNA. This investigation offered a new paradigm of Nas regulation and as such, complete *nas* expression was examined in several mutant strains deficient for various nitrogen-regulators to characterise molecular events pivotal for Nas synthesis.

4.6 Multiple Nitrogen-Responsive Regulators are Required for Complete *nasABGHC* Expression

The expression of Nas structural genes in heterotrophic bacteria requires a combined effort of Ntr transcriptional activation and NasTS/NasR transcriptional anti-termination (see Section 1.4 for review) (Luque-Almagro et al. 2011; Luque-Almagro et al. 2013).

To explore and confirm their contribution, in addition to DusN, for NasABGHC synthesis in *P. denitrificans*, the *nasT-lacZ* and *nasA-lacZ* gene-reporter fusion vectors were conjugated into deletion mutants of *P. denitrificans*: $\Delta dusN$, $\Delta nasT$, $\Delta ntrBC$ and $\Delta ntrBY$. The *ntrYX* genes lie immediately downstream of *ntrBC* within the operon and encodes another similar two-component system with a sensor-kinase (NtrY) and transcriptional activator (NtrB) involved in the nitrogen-response. A previous study in *Azospirillum brasilense* reported the NtrYX system activates the *nif* genes for nitrogenase expression, a role typically performed by NtrBC (Vitorino et al. 2001).

Furthermore, $\Delta ntrBC$ cultures can still assimilate nitrate and grow with it as the sole nitrogen source, but with attenuated growth (Figure 3.17). However, $\Delta ntrBY$ cannot grow via nitrate-dependent growth and therefore is unable to perform nitrate assimilation (data not shown). As the sensor-kinases of both these two-component systems is deleted in $\Delta ntrBY$, neither NtrC or NtrX can function as an activator of target gene transcription.

The various deletion mutants of *P. denitrificans* containing the transcriptional and translational *lacZ* fusion vectors of both *nasT* and *nasA* were grown under nitrate-induced conditions and subject to β -galactosidase assays at a mid-exponential growth phase (Figure 4.12).

Figure 4.12A shows the transcription of *nasTS* monitored from the *nasT-lacZ* pMP220-derived plasmid. A β -galactosidase activity of ~3500 Mu was recorded for WT which is consistent with values recorded previously (Figure 4.11A). Importantly, no significant decrease was observed in $\Delta dusN$, $\Delta ntrBC$ or $\Delta ntrBY$ which all reached ~3000 Mu. This agrees with previous results which showed NasTS expression is not attenuated by the deletion of DusN (Figure 4.11) or the Ntr system (Figure 3.20B). Interestingly, *nasTS*

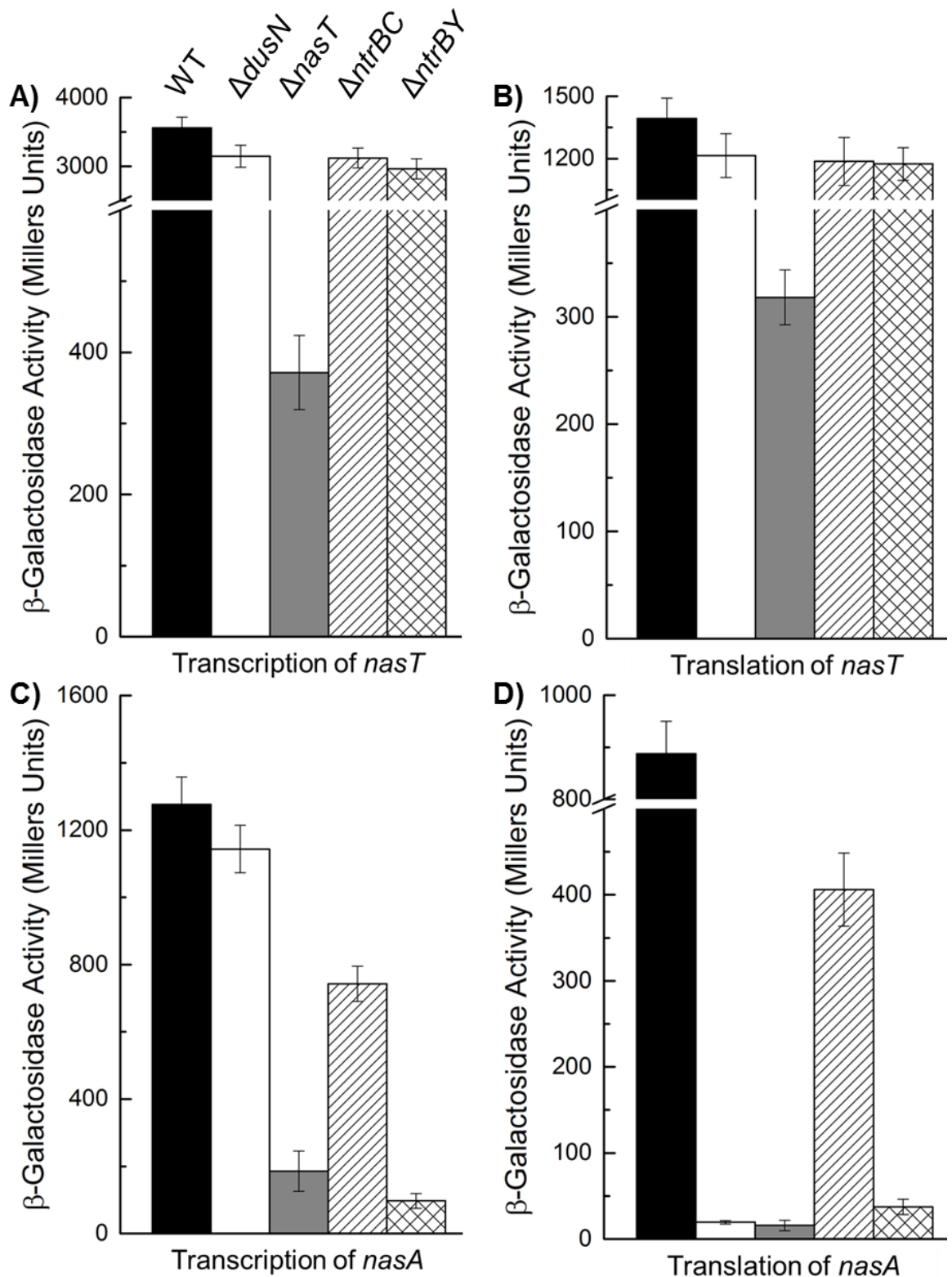


Figure 4.12. β-galactosidase activities of the *nasT-lacZ* and *nasA-lacZ* plasmids during nitrate-induced growth in *P. denitrificans* strains. WT (black), Δ*dusN* (white), Δ*nasT* (grey), Δ*ntrBC* (diagonal lines) and Δ*ntrBY* (gridded lines) were grown aerobically, 30 °C, with 30 mM succinate, 10 mM L-alanine and 10 mM nitrate. β-Galactosidase activity was measured at a late-exponential phase for the transcription (A and C) and translation (B and D) of *nasT* (A and B) and *nasA* (C and D). Activity was made relative to pMP220 and pIJ1363 vectors containing no insert.

transcription is attenuated by approximately an order of magnitude in the $\Delta nasT$ strain, reaching ~350 Mu. This data implies NasT may be performing a self-regulatory role by activating transcription of *nasTS* when induced by nitrate. However, *nasTS* expression is clearly not absent as β -galactosidase activity measured from *nasT-lacZ* is considerably more than the promoterless *lacZ* control which it was made relative too. This suggests *nasTS* transcription is additionally activated by a separate system, possibly a housekeeping regulator, which could account for its basal level of expression during ammonium-sufficient conditions.

The translation of NasTS is represented in Figure 4.12B by the β -galactosidase activity recorded from the pIJ1363-derived *nasT-lacZ* fusion plasmid. Here, the expression is ~1200 Mu which is consistent with the value recorded in Figure 4.11B. The translation of NasTS during nitrate-dependent growth is high in WT and not affected by the deletion of *dusN* or the Ntr system, as expected. Again, an activity of ~300 Mu was recorded for *nasT-lacZ* in $\Delta nasT$, being roughly an order of magnitude lower than the WT value. This will be a knock-on effect for attenuated transcription of *nasT*, as less mRNA will be available for translation.

By contrast, the expression of *nasABGHC* requires far more intricate control and the contribution of multiple regulators. The transcription of *nasABGCH* is represented in Figure 4.12C where a *nasA-lacZ* activity of ~1300 Mu is recorded in WT consistent with previous values measured from this plasmid (Figure 4.11A). However, this value is ~40% less in $\Delta ntrBC$ laying in agreement with the data in Figure 3.20B, but, transcription of *nasABGHC* is clearly not abolished in this strain. This attenuation in Nas expression accounts for the diminished growth output of $\Delta ntrBC$ recorded for nitrate-dependent growth (Table 3.3) and confirms the role of NtrBC in activating expression of the structural Nas genes, as demonstrated for other bacteria (Wu et al. 1999; Toukdarian & Kennedy 1986; Ishida et al. 2002). Interestingly, the strain lacking both *ntrB* and *ntrY*, and therefore deficient in NtrBC and NtrYX systems, showed complete loss of *nasABGHC* transcription. An activity of ~100 Mu was recorded for *nasA-lacZ* which indicates *NasABGHC* is not expressed in $\Delta ntrBY$ and explains why the strain is incapable of nitrate-dependent growth. Furthermore, this data indicates that NtrYX is indeed capable of functioning in the same capacity as NtrBC as it presumably is responsible for the partial transcription of *nasABGHC* in $\Delta ntrBC$, and thus the two nitrogen-responsive regulatory systems compensate for each other.

Furthermore, in the absence of NasT it is already known that *nasABGHC* is not expressed due to premature transcriptional-termination via inhibitory hairpin formation in

the *nasA* mRNA leader region (Luque-Almagro et al. 2013). This is consistent with the lack of activity recorded for *nasA-lacZ* transcriptional fusion (Figure 4.12B) and explains the inability of $\Delta nasT$ to grow when supplemented with nitrate as a sole nitrogen source (Luque-Almagro et al. 2013).

Finally, Figure 4.12D shows the β -galactosidase activity measured from *nasA-lacZ* dependent upon the translation of the inserted region. As seen in Figure 4.11B, the expression is ~900 Mu where NasABGHC is judged to be translated at a high level in WT during nitrate-dependent growth. In $\Delta ntrBC$, this level is approximately halved to ~400 Mu, agreeing with the observation in transcription and still leading to an appropriate level of Nas to allow nitrate assimilation. Also, the translation of *nasABGHC* is completely diminished in $\Delta dusN$ while transcription maintains WT levels of ~1200, as previously discussed for Figure 4.11. This pinpoints DusN operates at a post-transcriptional level to control target gene expression.

Here, gene-reporter fusion analysis concludes that in *P. denitrificans*, and perhaps other similar heterotrophic organisms, a combined effort of the NtrBC/NtrYX, NasTS/NasR and DusN is crucial for the complete expression of Nas to enable nitrate/nitrite import and reduction for growth during nitrogen-limiting conditions. The absence of either one of these regulators results in a loss of structural Nas proteins and the inability to grow by nitrate assimilation.

4.7 Discussion

4.7.1 *DusN is involved in regulating a multitude of nitrogen-responsive genes*

This chapter focused on characterising the role of *dusN* (Pden_4131) in *P. denitrificans*. This hypothetical gene is tightly conserved with the Ntr system across α -proteobacteria, with very few previous studies focused on it despite its genomic proximity and formation of a transcriptional unit containing key general nitrogen regulators. Here, we investigated this putative tRNA-DUS from a molecular perspective via a series of gene deletion studies, transcriptomic analysis and gene-reporter fusion assays.

One of the most significant findings of this thesis was the phenotypic growth data which reported the $\Delta dusN$ mutant strain was unable to grow with nitrate or nitrite as sole nitrogen sources (Figure 4.3B). Importantly, nitrate-dependent growth in the deletion strain was restored to WT levels upon genetically complementing DusN *in trans* using a plasmid-borne copy of the gene expressed from an inducible ectopic promoter (Figure 4.8). This, in tandem with the qRT-PCR data of *ntrBCYX*, demonstrated that the loss of nitrate assimilation is solely due to the removal of cellular DusN. Therefore, we show

that bacterial *dusN* is not hypothetical, but an ORF that translates to a functional protein, key for the bacterium's ability to import and reduce nitrate for biosynthetic metabolism.

Additionally, investigating the effect that supplementing various concentrations of different nitrogen sources has on the growth of strains indicated that DusN may also be involved more generally in nitrogen-responsive metabolism (Figure 4.4). The inability to reach WT levels of growth with ammonium or glutamate suggests that DusN may participate in controlling the expression of the GS-GOGAT cycle and other nitrogen-utilising pathways.

Strikingly, the microarray analysis (Figure 4.9) identified numerous genes that underwent transcriptional modulation in the absence of *dusN* during nitrate-induced growth. Many genes which were downregulated in Δ *dusN* compared to WT encode products that are involved in providing nitrogen for cells during nitrogen-limitation. These enzymes all act to catabolise various organic nitrogenous compounds leading to the release of amine groups, allowing the cell to scavenge a bioavailable nitrogen source. In addition, several amino acid transporters were downregulated in Δ *dusN*, presumably expressed in WT during nitrogen-limitation to use amino acids as an organic nitrogen source. As these genes are transcribed to a lesser extent in the mutant, we propose DusN regulates many processes involved in general nitrogen-metabolism, in addition to the Nas system. However, these changes recorded by the microarray are at a transcriptional level and we believe DusN acts directly at a post-transcriptional level to control expression of Nas proteins. Therefore, DusN possibly regulates these other nitrogen-responsive genes indirectly, maybe by controlling the expression of a separate transcriptional regulator. The presence of *dusN* with *ntr* genes throughout α -proteobacteria proceeds in *nas*-deficient bacteria, suggesting DusN does not solely act as a regulator of Nas expression. This transcriptomic analysis here further implies DusN operates in many nitrogen-responsive pathways and acts at a much broader scale of nitrogen-metabolism than initially postulated.

One of the genes which underwent significant upregulation in Δ *dusN* was GDH, supporting the conclusions drawn from growth data in Figure 4.4 concerning the cellular GS-GOGAT proteins. Their absence causes the expression of GDH to functionally compensate and inefficiently assimilate ammonium into organic biomass, causing attenuation in growth output in Δ *dusN*. However, the microarray analysis did not highlight the *nas* or GS-GOGAT genes as undergoing a significant decrease in transcription, which reports two key findings: NtrBC is active in Δ *dusN* to provide correct transcription of these genes, thus not requiring DusN for its maturation as previously suggested

(Foster-Hartnett et al. 1993). Additionally, it indicates DusN functions directly at a post-transcriptional level to target these genes, most likely regulating protein biosynthesis by catalysing post-transcriptional dihydrouridine modification of RNA.

To examine whether DusN regulates protein translation, both transcriptional and translational gene-reporter fusion assays were employed. The β -galactosidase activities determined that *nasT* was transcribed and translated correctly in both WT and $\Delta dusN$ whilst *nasA* was transcribed to a high level in both strains, consistent with microarray analysis. Perhaps the key finding of this chapter was that the translation of *nasABGHC* was completely diminished in the mutant strain deficient for cellular DusN (Figure 4.11B).

To our knowledge, this is the first study which has identified a clearly defined regulatory role of DusN in bacteria where its absence causes stalling of nitrate assimilation at nascent *nasABGHC* mRNA. We conclude that DusN is crucial in the translation of genes to proteins by regulating some aspect of protein biosynthesis, and that it monitors Nas expression in addition to other pathways of nitrogen-metabolism. This novel regulatory function will be explored from a biochemical view-point in the next chapter and aim to investigate how the DUS family operate to control protein expression.

4.7.2 *Nas* expression requires the concerted effort of multiple regulatory proteins

This finding added a new paradigm to the molecular events required for complete Nas expression during nitrate-dependent growth, which was studied here using both transcriptional and translational gene-reporter fusion assays in a variety of *P. denitrificans* deletion strains. The expression of *nasTS* was insensitive to the absence of the nitrogen-regulators NtrBC, NtrYX or DusN (Figure 4.12A). However, it appears to be positively self-upregulating during nitrate-induced growth due to the attenuation of *nasTS* transcription in the $\Delta nasT$ strain. But, expression was not completely abolished in the mutant and *nasTS* was still transcribed to a relatively high level. This suggests another regulator is capable of activating *nasTS* expression, responsible for basal *nasTS* transcription during nitrogen-sufficient conditions (Figure 4.10A).

The expression of the structural Nas enzymes in heterotrophic bacteria is more complex and requires two regulatory systems: NtrBC/NtrYX and NasTS/NasR (see Sections 1.4.3 and 1.4.4 for respective reviews). These have both been experimentally characterised as essential for transcription of *nasABGHC* during nitrate-dependent growth and confirmed here in *P. denitrificans* as a lack of *nasA-lacZ* activity was reported in the $\Delta nasT$ and $\Delta ntrBY$ deletion strains (Figure 4.12C). Interestingly, *nasABGHC* transcription was still observed in $\Delta ntrBC$ which allows this mutant strain to assimilate nitrate. This demonstrated the nitrogen-regulatory Ntr two-component systems are

functionally similar and able to complement each other, both being able to work in tandem with NasT for transcription of *nasABGHC*. However, the new additional participant, DusN, was shown to be essential in the translation of *nasABGHC* mRNA into the structural, cytoplasmic Nas system (Figure 4.11B). A schematic depicting the regulation of *nasABGHC* expression in *P. denitrificans* is shown in Figure 4.13 below.

Briefly, ammonium-limiting conditions are detected through low glutamine/high 2-oxoglutarate levels by uridylyltransferase to initiate a regulatory cascade. Active uridylyltransferase uridylylates P_{II} which subsequently stimulates the kinase domain of NtrB leading to phosphorylated NtrB homodimers. This forms a heterotetrameric complex with an NtrC dimer where a phosphate group is donated from NtrB to the accepting NtrC. Active homodimers of NtrC bind to their nucleotide-consensus element upstream of *nasA* to initiate promotion, found in Chapter 3 to be σ^{54} -independent in *P. denitrificans* (Figure 3.15). An inhibitory hairpin forms in the leader region of *nasA* mRNA which disrupts RNA polymerase binding and prematurely terminates transcription.

Secondly, when nitrate is present in the cell it is coordinated by NasS which subsequently releases dimeric NasT from the inactive heterotetrameric complex. Active homodimeric NasT use their ANTAR domain to bind to the nascent mRNA at a *cis*-regulatory element in the 5'-UTR of the transcript to promote transcriptional anti-termination. This alleviation of "default" transcriptional repression now allows the RNA-polymerase to successfully transcribe *nasABGHC* mRNA without stalling.

It is at this point in gene expression where DusN functions, as it is essential in regulating the link between mRNA and cytoplasmic Nas proteins. However, its precise role concerning controlling translation of mRNA in response to stimuli remains unknown, as is that for the ubiquitous DUS superfamily, although the role of DUS proteins are believed to be achieved through alteration of tRNA and to an extent, translational fidelity. The biochemical aspects underpinning the regulatory role of DusN and how this protein coordinates dihydrouridine synthesis with cellular response will be explored in detail over the following chapter.

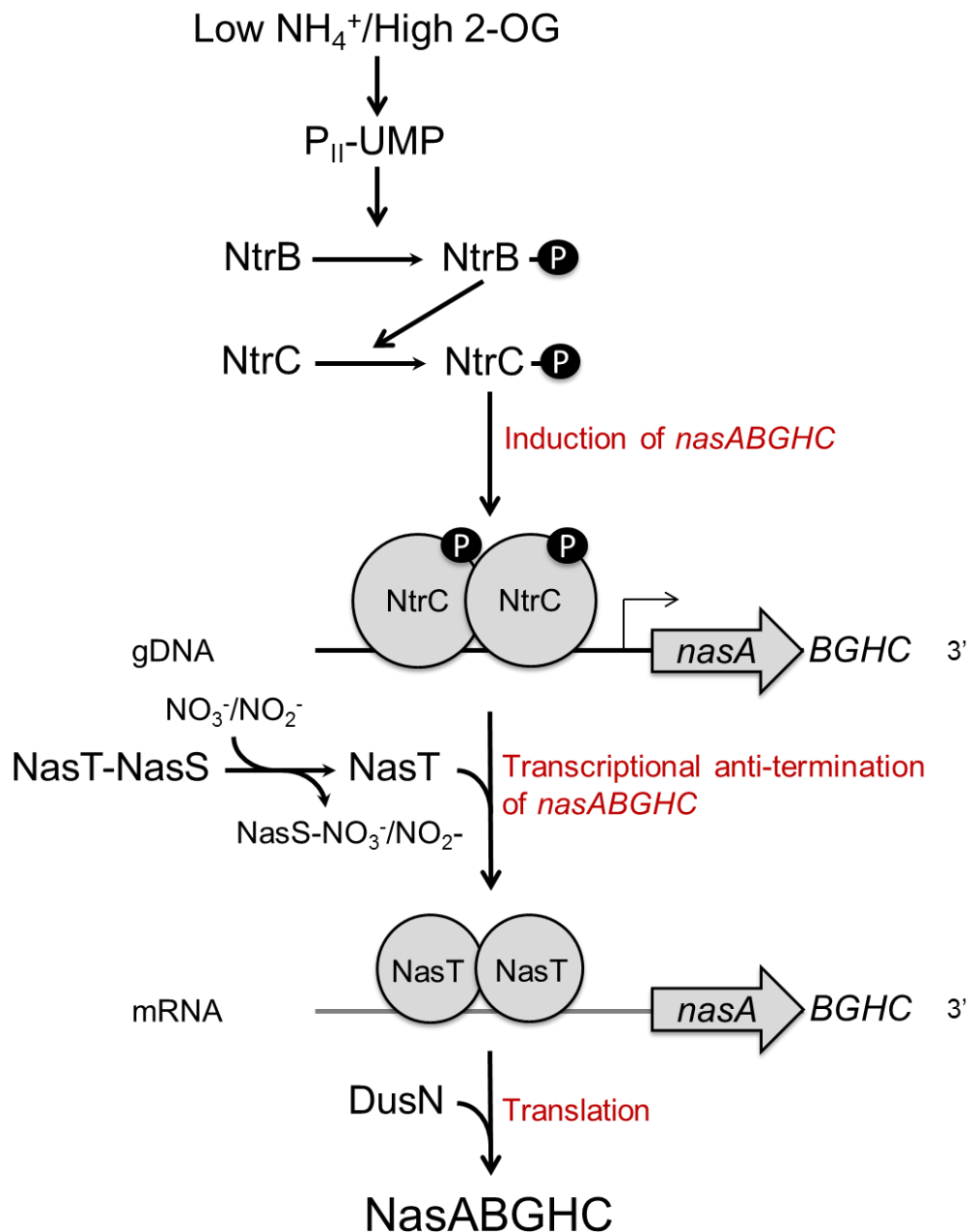


Figure 4.13. Schematic showing the regulatory events required for complete expression of Nas structural proteins. In the absence of intracellular ammonium, P_{II} is uridylylated by uridylyltransferase. $\text{P}_{\text{II}}\text{-UMP}$ subsequently activates NtrB kinase domains resulting in transautophosphorylation of NtrB homodimers. The newly acquired phosphate group is donated to a receiving NtrC cognate partner which stimulates dimerisation. Functional NtrC dimers recognise and bind to its target DNA sequence upstream of *nasABGHC* to promote transcription. NasS coordinates intracellular nitrate/nitrite releasing NasT from the inhibitory NasT-NasS complex. Active NasT dimers bind a *cis*-acting stretch of RNA in the 5'-UTR of *nasA* mRNA to negate inhibitory hairpin formation and allow elongation of complete *nasABGHC* mRNA. Finally, DusN offers a crucial regulatory role in ensuring successful translation to cytoplasmic Nas structural proteins for nitrate import and assimilation.

Chapter 5: Characterisation of DusN as a Nitrogen-Responsive tRNA-Dihydrouridine Synthase

5.1 Introduction

As identified in the previous chapter, DusN plays a critical post-transcriptional regulatory role in the bacterium's ability to assimilate nitrate to support growth by controlling translation of *nasABGHC* mRNA. The DUS protein family alter protein expression by reduction of distinct uridines to dihydrouridine in specific tRNA transcripts during post-transcriptional modification (see Section 1.9 for review). However, little is currently known about the link connecting this pivotal biochemical process with modulated gene expression. It is thought that introduction of dihydrouridine alters D-loop stereochemistry and as a result influences tRNA interactions with amino-acyl tRNA synthetases and ribosomes to affect translation. To elucidate the fundamental basis of how dihydrouridine synthesis leads to alteration of global proteomic changes, and how DusN specifically alters nitrogen-metabolism, further biochemical studies of the protein were performed. In this chapter, an overexpression system was constructed to enable purification of large quantities of DusN for subsequent analysis investigating biochemical traits such as catalytic activity, RNA interactions, substrate targets and cognate partners.

5.2 Construction of an Overexpression and Purification System for DusN

Recent advances in recombinant protein technology have enabled the construction of molecular systems to overexpress a target protein of interest containing an affinity tag to allow fast and efficient large-scale purification (Gräslund et al., 2008; Terpe, 2003). Such vector systems were utilised in this study to construct a number of overexpression strains for recombinant DusN of *P. denitrificans* containing a poly-His affinity tag (6His-tag) to aid purification by affinity chromatography.

Commonly used expression vectors are the specifically engineered pET- based plasmids (*Novagen*, Figure 5.1) which are highly tailored for recombinant protein overexpression in specialised *E. coli* strains (Baneyx, 1999; Rosano & Ceccarelli, 2014). Genes inserted into the MCS of these plasmids are under IPTG-inducible control via LacI repression, and lay downstream of a T7 promoter and ribosome binding site (RBS)

necessary for activating transcription. These plasmids encode 6His-tag sequences at either the N- or C-terminus of the inserted gene.

5.2.1 Overexpression trials for various tagged forms of recombinant *DusN*

To purify *DusN*, 5 unique plasmids were constructed for overexpression by cloning the *dusN* gene of *P. denitrificans* into pET24a and pET28a for *E. coli* hosts, and pLMB509 for use in *P. denitrificans* (see Figure 4.7 for vector map). Each construct gives rise to a unique form of recombinant *DusN* when induced, as outlined in Figure 5.2 below.

Firstly, *dusN* was cloned without a stop codon into pET24a as an *NdeI/HindIII* fragment to produce pBP022 expressing C-terminal 6His-tagged *DusN*. A separate construct was made in pET24a with a stop codon, cloned *NdeI/XhoI*, to give pBP023 expressing untagged *DusN*. Finally, *dusN* containing a stop codon was cloned into pET28a with *NdeI/XhoI* constructing pBP024 which produces an N-terminal 6His-tagged *DusN*. These pET- derived plasmids were expressed in *E. coli* BL21 (DE3), a specially engineered strain containing the required T7 RNA polymerase for protein expression when induced by IPTG (Studier et al., 1990). As the introduction of a foreign tag sequence may have detrimental effects on the integrity and folding of the recombinant protein (Carson et al., 2007), pBP023 was also constructed to produce untagged *DusN*.

Though *E. coli* BL21 (DE3) and pET- vector series have been highly tailored for simple and efficient large-scale protein purification, the bacterium may be lacking necessary expression components and chaperones required for production of functional protein. Therefore, two separate plasmid constructs were cloned to overexpress *dusN* in *P. denitrificans* using pLMB509 as discussed previously (Figure 4.7) via taurine stimulation. There, pBP006 was used to complement the Δ *dusN* strain (Figure 4.7) which gives rise to an untagged *DusN*. The stop codon of this gene was modified to incorporate an intrinsic C-terminal 6His-tag within the plasmid sequence resulting in pBP025 (see Figure 5.3 for details).

Following construction and sequence confirmation, pBP025 was conjugated into *P. denitrificans*. Overexpression trials were performed by growing *P. denitrificans* + pBP025 in LB media for 24 h, supplemented with taurine to induce recombinant *DusN*_6His expression. Whole cells were solubilised by heating at 95 °C for 20 mins in SDS (see Section 2.24.1) and proteins were resolved by size using SDS-PAGE (Figure 5.4).

Figure 5.4 shows the size-resolved protein profile of *P. denitrificans* harvested at stationary phase which appears consistent throughout all 4 conditions. However, when pBP025 was induced with 10 mM taurine, a distinct band was present at ~37 kDa which

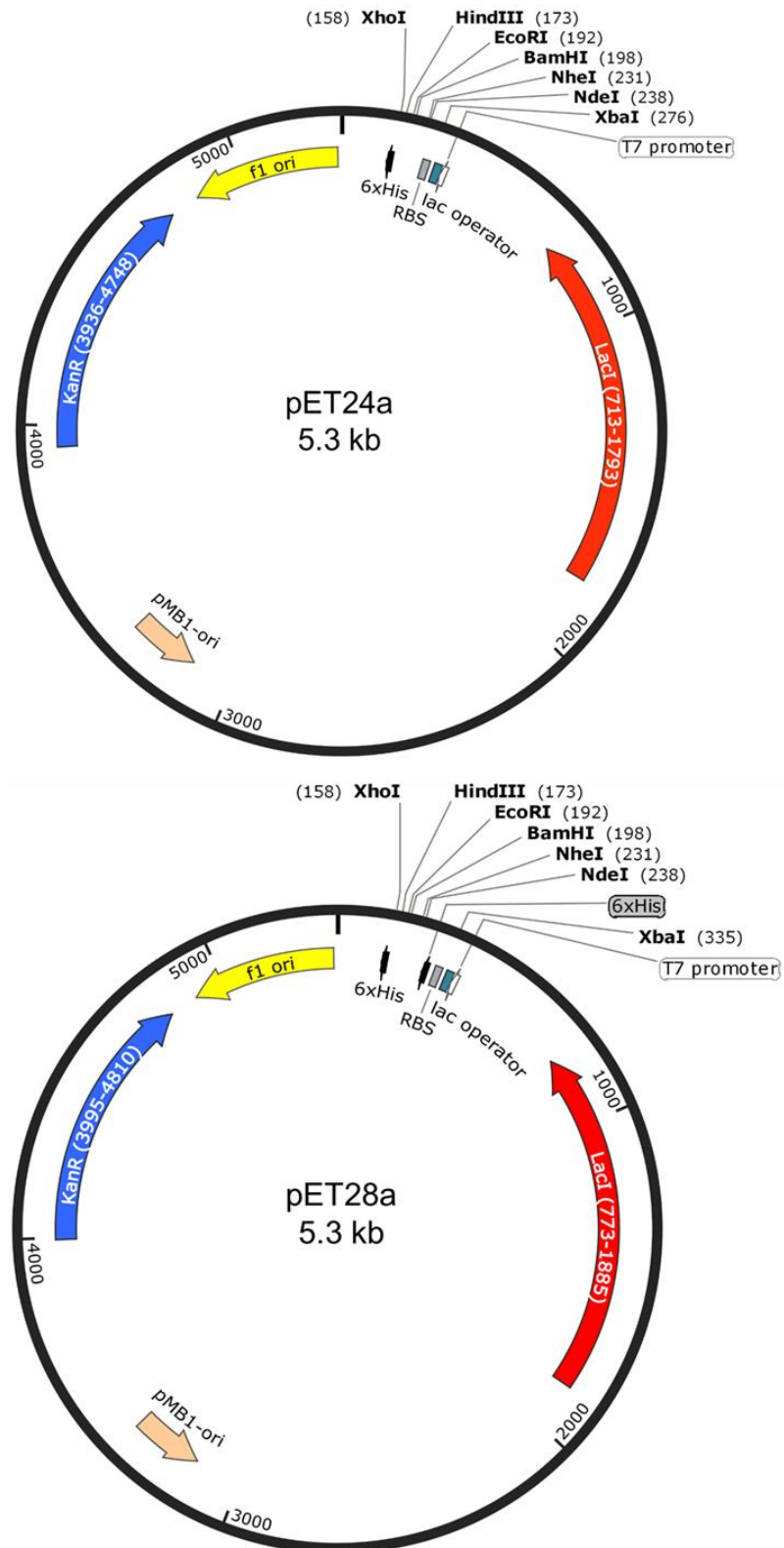


Figure 5.1. Plasmid maps for the overexpression pET24a and pET28a vectors used in this study. Vector maps depicting the key features of pET24a and pET28a used for overexpression of proteins in *E. coli* BL21 (DE3). Plasmids contain: *lac* repressor (LacI), kanamycin resistance (KanR), a MCS in close proximity to the T7 promoter, ribosome binding site (RBS), *lac* operator and 6His-tag sequence. Plasmids drawn using SnapGene Viewer software.

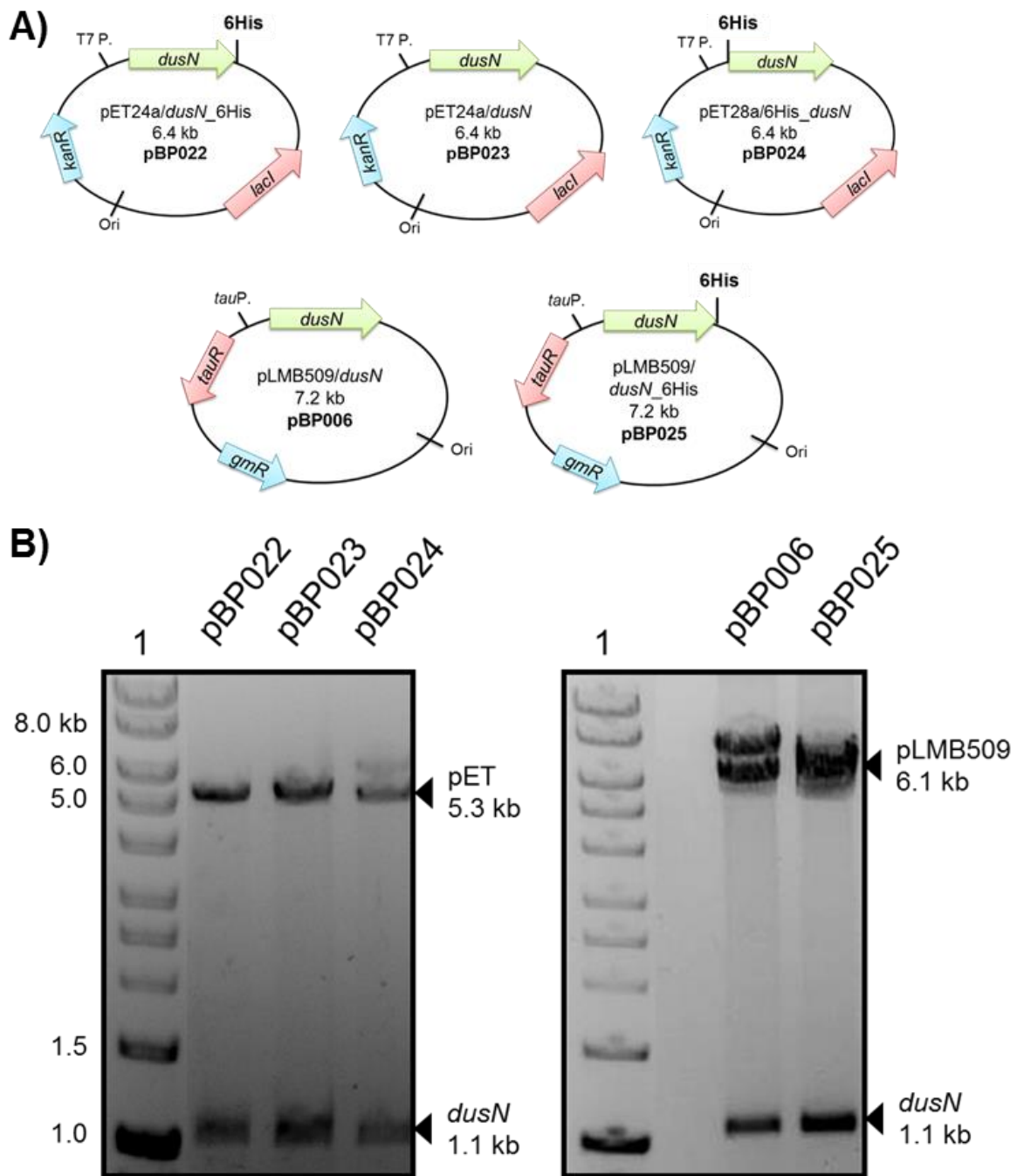


Figure 5.2. Construction of different overexpression systems for recombinant DusN. A) The individual plasmids for overexpression of *P. denitrificans* DusN. pBP022, pBP023 and pBP024 are pET-derived plasmids for expression in *E. coli* BL21 (DE3). pBP006 and pBP025 are pLMB509-derivatives used in the original host organism, *P. denitrificans*. B) Agarose gel electrophoresis of the constructs denoted in each lane digested with appropriate restriction enzymes to release *dusN* (1.1 kb). Lane 1 indicates 1 kb Hyperladder used as a molecular weights standard.

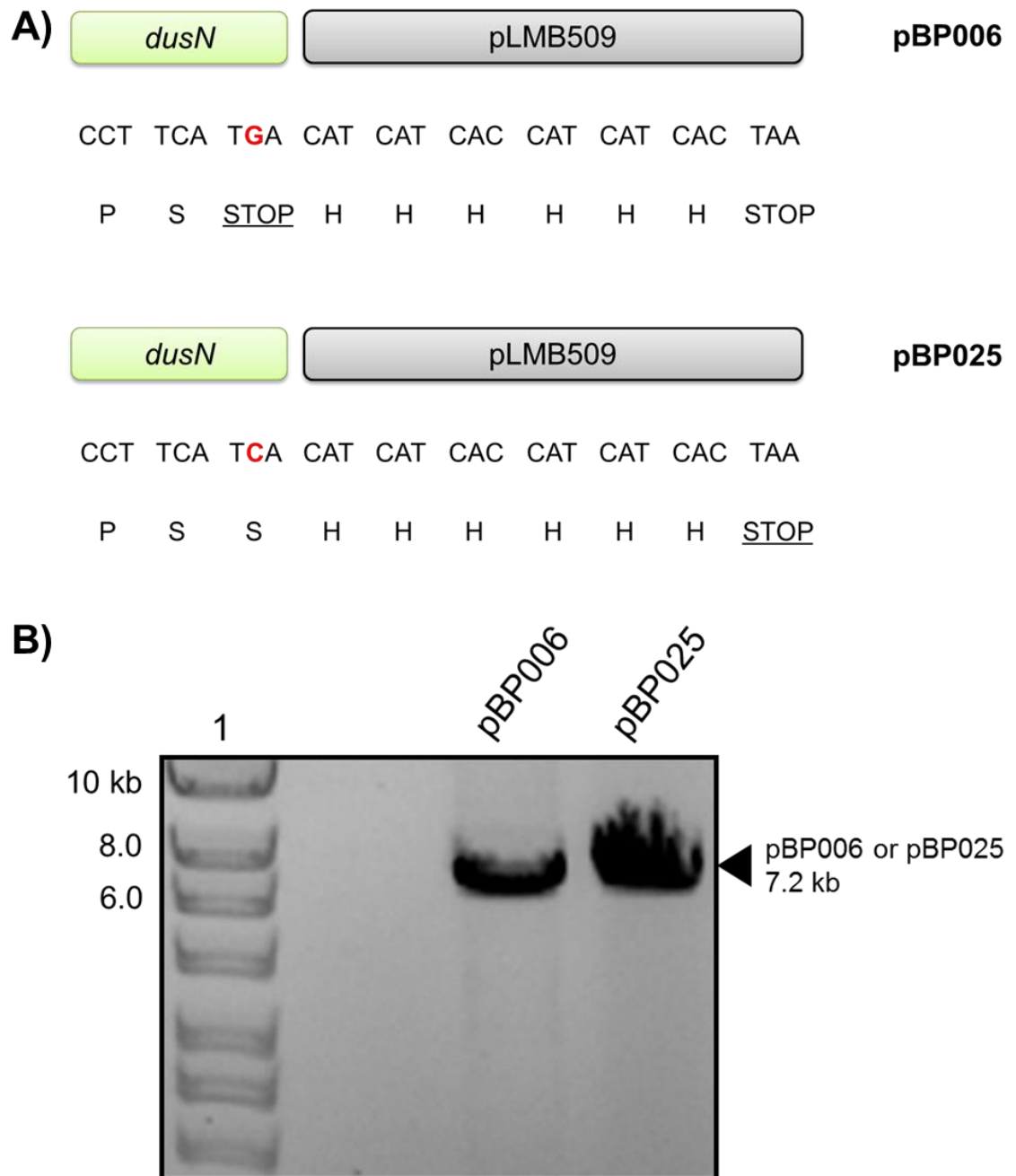


Figure 5.3. Site-directed mutagenesis of the *dusN* stop codon to construct pBP025 from pBP006. A) Primer pair F_6hisdusN/R1_6hisdusN was used to mutate the highlighted G to C resulting in incorporation of the vectors C-terminal 6His-tag and stop codon. B) Agarose gel analysis of the site-directed PCR. pBP006 was used as a template with the above primer pair to produce pBP025. Following completion, the pBP006 template was degraded with *DpnI*. Lane 1; 1 kb Hyperladder, 2; pBP006 template, 3; pBP025 following completion of PCR and restriction digestion.

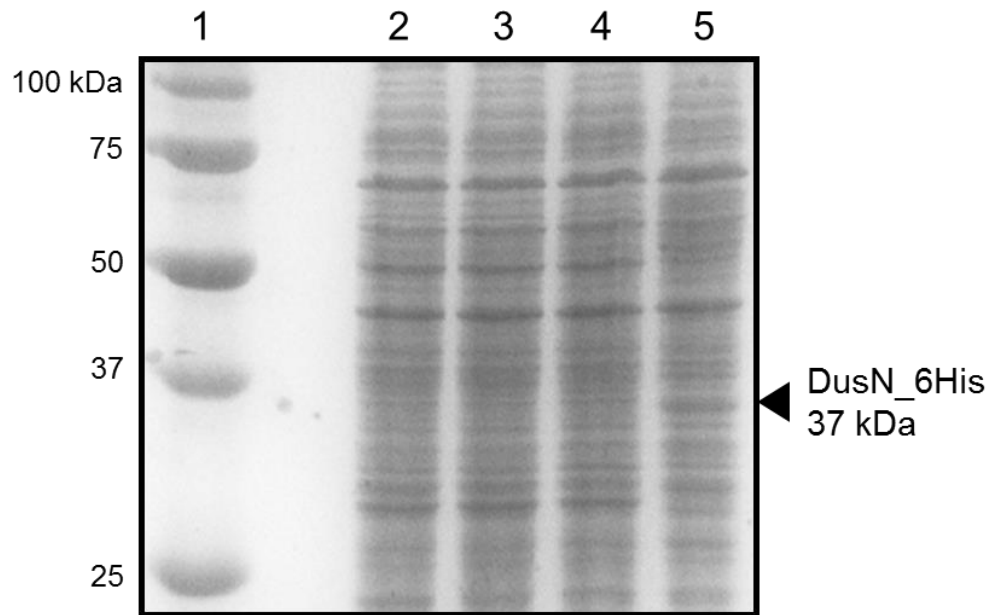


Figure 5.4. Overexpression of recombinant C-terminal tagged DusN_6His in *P. denitrificans*. SDS-PAGE analysis of pBP025 activity. *P. denitrificans* strains were grown aerobically in LB media at 30 °C for 24 h before being harvested, boiled and loaded onto the acrylamide gel. DusN_6His (37 kDa) was overexpressed from pBP025 in *P. denitrificans* using taurine supplemented with the inoculum. Lane 1; Precision Plus Protein™ marker, 2; *P. denitrificans* WT control, 3; *P. denitrificans* + pBP025 uninduced, 4; *P. denitrificans* + pBP025 + 1 mM taurine, 5; *P. denitrificans* + pBP025 + 10 mM taurine.

is in agreement with the molecular weight predicted for this recombinant DusN sequence (lane 4). Although this plasmid is functional and leads to target protein production, it is clearly observed to be at a very low quantity and deemed unsuitable for large-scale purification for use in multiple biochemical analysis. Due to this, the commonly used protein expression pET-based plasmids were employed to overexpress recombinant DusN in *E. coli* BL21 (DE3) cells.

The pBP023 construct produces untagged DusN following IPTG induction from the T7 promoter, as introduction of foreign tags may cause difficulties for protein folding. This system was initially tested using a range of IPTG concentrations to stimulate DusN expression. Cultures were grown aerobically in LB media at 37 °C until $OD_{600\text{ nm}} = \sim 0.7$, upon which appropriate amounts of IPTG was added and cultures were left to produce protein at 25 °C for a further 18 h (Figure 5.5A).

The SDS-PAGE gel shows the protein profile of *E. coli* is consistent throughout the expression trials, with the exception of a band at ~ 36 kDa. This large band is present when either 0.2 or 0.5 mM IPTG was added to the cultures and is in agreement with the native molecular weight of DusN. This analysis shows pBP023 is capable of yielding high quantities of untagged protein, even when stimulated with low levels of IPTG. Judging by band sizes, the pET-based systems in *E. coli* clearly leads to greater amounts of DusN than using pLMB509 vectors in *P. denitrificans* (Figure 5.4).

To aid the purification process, a 6His-tag sequence was introduced into the protein to enable affinity chromatography. In order to do this, a C-terminal and N-terminal 6His-tagged DusN expression system were constructed and tested for: pBP022 and pBP024 respectively. *E. coli* BL21 (DE3) strains containing these vectors were grown in LB medium and induced with IPTG as outlined for pBP023 above. This time, harvested cultures were lysed and separated to visualise the soluble and insoluble fractions individually (Figure 5.5B). DusN is predicted to be cytoplasmic and similar bacterial DUS proteins have previously been purified from the cytoplasm (Yu et al., 2011). Identification of this protein in the insoluble fraction would indicate protein misfolding and aggregation.

The pBP022 vector in *E. coli* produced C-terminal 6His-tagged DusN, visualised at ~ 37 kDa, in larger quantities than that seen for DusN_6His in *P. denitrificans* (Figure 5.4). However, the protein was located within the insoluble fraction, perhaps indicative of precipitation as inclusion bodies following protein misfolding. As no DusN was present in the soluble fraction, this expression system was discontinued due to the likelihood of potentially misfolded DusN.

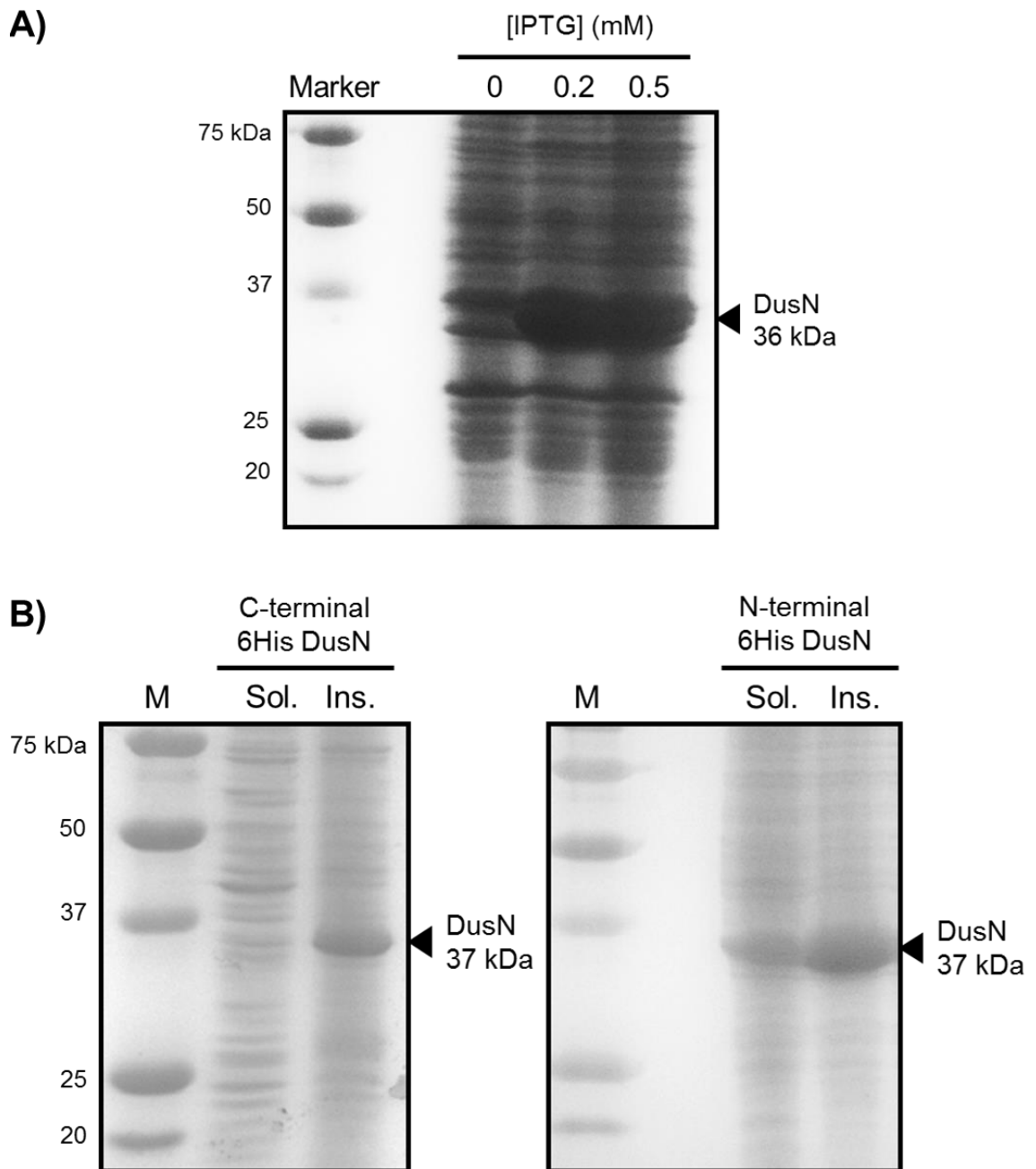


Figure 5.5. Overexpression analysis of various recombinant DusN proteins in *E. coli* BL21 (DE3). A) *E. coli* BL21 (DE3) harbouring pBP023 was grown aerobically in LB media to a mid-exponential phase at 37 °C, upon which IPTG was added to a final concentration of 0, 0.2 or 0.5 mM. Cultures were left for 18 h at 25 °C to express untagged DusN (36 kDa) before loading whole cells onto the polyacrylamide gel. B) SDS-PAGE analysis of pBP022 and pBP024 activity which express a C-terminal and N-terminal 6His-tagged DusN, respectively. *E. coli* strains were grown aerobically in LB media to a mid-exponential phase at 37 °C, upon which 0.2 mM IPTG was added. Cultures were left for 18 hours at 25 °C to express DusN (37kDa) before harvesting, and preparing cell extract. The soluble (Sol.) and insoluble (Ins.) fractions were ran separately on an SDS-PAGE gel. “Marker indicates Precision Plus Protein™ standard.

The expression of N-terminal 6His-tagged DusN from pBP024 also results in large quantities of recombinant protein in the insoluble fraction, observed as a large band at ~37 kDa. But, unlike its C-terminal counterpart, a relatively large quantity of the protein was additionally located within the soluble cell lysate. This suggests the N-terminus is more amenable to manipulation and does not interfere completely with folding of mature protein. The result of pBP024 expression is production of correctly folded, recombinant DusN within the cytoplasm of *E. coli* BL21 (DE3). As such, this pET28a/6His_*dusN* expression system was employed for large-scale purification of DusN for downstream biochemical and biophysical characterisation.

5.2.2 Purification of 6His_*DusN* for downstream analysis

Once overexpressed, DusN was purified from the *E. coli* cells using affinity chromatography as outlined in Section 2.22.1. Briefly, this was achieved using immobilised metal affinity chromatography (IMAC), where the column matrix is charged with Ni²⁺ which coordinates strong interactions with the imidazole ring structure of histidine (Bornhorst & Falke, 2000; Porath et al., 1975). As such, IMAC columns tightly bind accessible 6His-tags which retains the tagged protein of interest while the whole cell lysate and cytoplasmic proteins are removed from the column with a low imidazole wash. Subsequently, the column is then subject to high imidazole concentrations which disrupt Ni²⁺:6His interactions, removing the isolated target protein in a separate fraction. The purification process for 6His_*DusN* is shown below in Figure 5.6.

Figure 5.6A shows a representative elution profile from an IMAC column loaded with *E. coli* soluble extract containing 6His_*DusN*. Initially, the imidazole concentration applied was low and the majority of cytoplasmic proteins were removed from the column over the first 5 mL buffer wash. The imidazole concentration was increased in a step-wise manner to 130 mM to remove contaminant proteins that exerted a moderate interaction to the column matrix/Ni²⁺, visualised as the peak in Abs_{280 nm} ~18 mL. The imidazole concentration was stepped up again, to 500 mM, which eluted 6His_*DusN* from the Ni-IMAC column observed as a raise in Abs_{280nm} over 5 mL, with the peak fraction eluting at ~27 mL. Furthermore, this peak overlays precisely when the Abs_{340 nm} sharply increases which was used to monitor the presence of flavin compounds, the predicted cofactor of the tRNA-DUS family.

The SDS-PAGE gel in Figure 5.6B contained these fractions of interest and shows large quantities of 6His_*DusN* eluted as a pure, cytoplasmic protein following this one-step purification process, visualised as a band at ~37 kDa. A semi-dry Western-blot was performed (see Section 2.25) using an anti-6his antibody with a conjugated horse radish

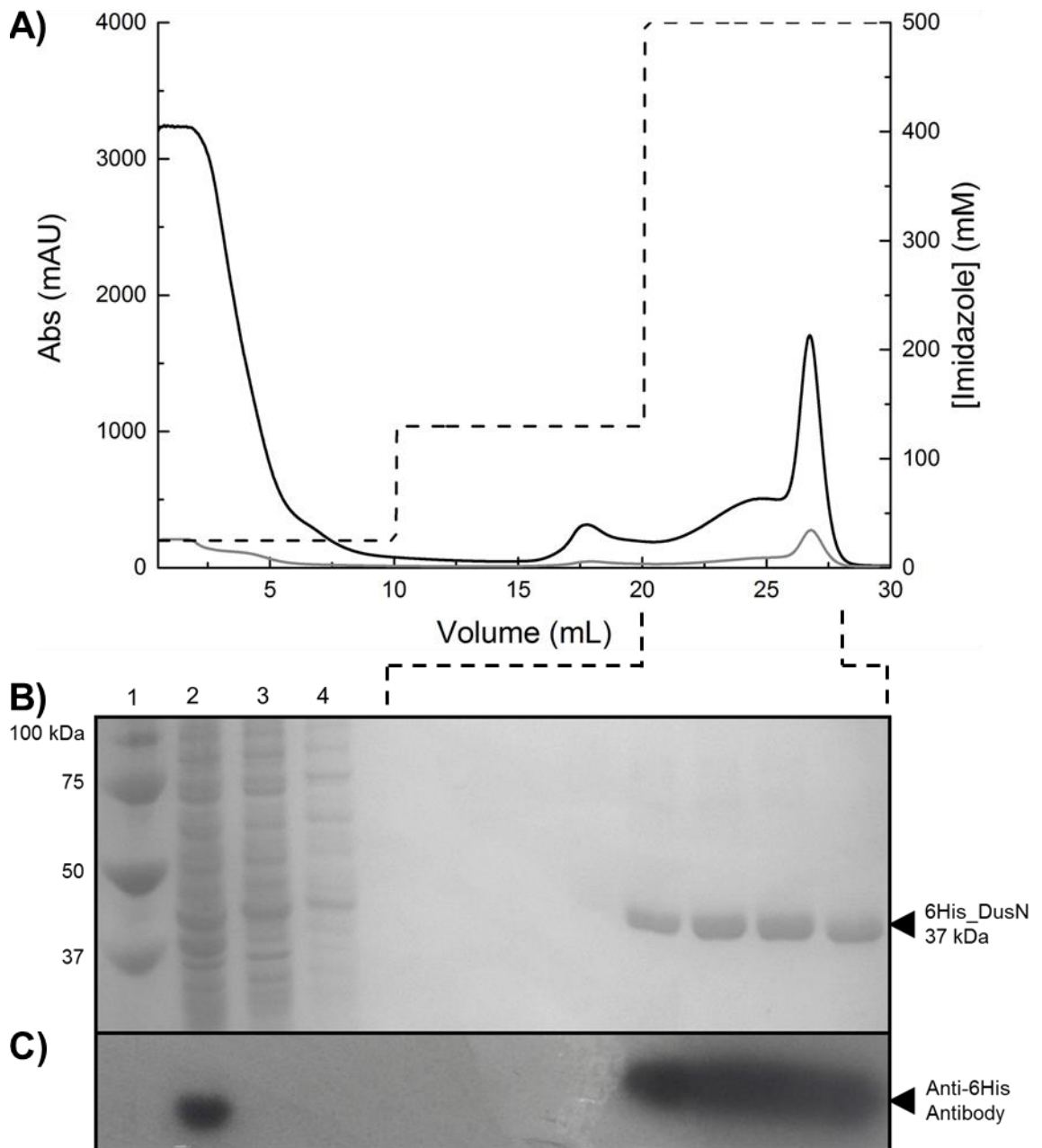


Figure 5.6. Affinity chromatography purification of 6His_DusN from *E. coli* BL21 (DE3). A) Chromatogram trace for the Ni²⁺-IMAC column: Abs_{280 nm}; black, Abs_{340 nm}; grey, concentration of imidazole; dotted. Cell lysate from IPTG-induced cultures containing pBP024 was loaded onto a column charged with Ni²⁺ and washed with buffer A (20 mM HEPES, 150 mM NaCl, 25 mM imidazole, pH 7.5). A step gradient of 25 %, followed by 100 % buffer B (buffer A with 500 mM imidazole) was applied to remove 6His_DusN. B) SDS-PAGE analysis of the purification. Lane 1; Precision Plus Protein™ marker, 2; whole cell lysate, 3; column flow-through whilst loading, 4; buffer A rinse. Dotted lines indicate the area of the trace loaded onto the gel. Pure 6His_DusN was visualised at 37 kDa. C) Corresponding semi-dry western-blot analysis of the gel using an anti-6His antibody conjugated with a horseradish peroxidase to chemiluminescently identify 6His-tagged proteins.

peroxidase (HRP) (Figure 5.6C). The 37 kDa band associated with 6His_DusN exhibited the observable chemiluminescent signal arising from HRP activity, indicating it contained the introduced 6His-tag sequence. The band was excised from the gel and sent for MALDI-TOF MS (see Section 2.26) which reported it to be DusN of *P. denitrificans* with a Mascot value of 196 and sequence coverage of 64 % (Table 2.12).

5.3 Identification and Quantification of FMN as a Cofactor of DusN

The tRNA-DUS family are known to be flavin-dependent enzymes, where a previous report identified the presence of an FMN cofactor in DUS of *T. thermophilus* through X-ray crystallography (Yu et al., 2011). The DusN protein sequence of *P. denitrificans* contains a predicted FMN-binding domain and Figure 5.6A revealed an increase in the Abs_{340 nm} (potentially arising from flavin absorbance) simultaneously with the peak elution of DusN. To investigate whether DusN of *P. denitrificans* harbours a flavin-based cofactor and if recombinant 6His_DusN purified as a holoprotein complete with its cofactor, spectrophotometric techniques were employed (Bessey, et al., 1949).

5.3.1 Fluorescence spectroscopy identification of FMN

Flavin compounds have an intrinsic fluorescence due to the existence of multiple π -bonds within the fused tricyclic ring of the isoalloxazine moiety (Islam et al., 2003; Koziol, 1971). This chromophoric feature was exploited to identify the presence of flavin within the purified DusN. Many various flavin compounds exist but DusN is believed to bind its cofactor in the form of FMN, a phosphorylated version of vitamin B₂ (riboflavin) (Figure 5.7C) (Michaelis, et al., 1986; Nelson & Cox, 2013). As such, a solution of 6His_DusN and an FMN control were analysed by fluorescence spectroscopy (Figure 5.7).

The spectrum of FMN in Figure 5.7A gives the characteristic features of flavin fluorescence (Beinert, 1956; Gordon-Walker et al., 1970). When excited at 365 nm, it results in fluorescence emission with a peak at 525 nm. When subject to emission at 525 nm, flavins record peaks at 365 nm and 450 nm. The FMN standard here exhibited these features distinctive to this class of compounds, and importantly, so did DusN. The protein spectrum followed a pattern identical to the FMN control, observing the three key absorbance signals and is in agreement with previous fluorescence analysis characterising flavoproteins (Mukherjee et al., 2013; Munro & Noble, 1999). As Figure 5.7B demonstrates, purified recombinant DusN exhibits an intense yellow colour which is typical of flavin compounds (flavin stems from Latin where “flavus” means yellow). This initial spectrophotometry indicates DusN of *P. denitrificans* contains an FMN cofactor which is retained during purification, signifying a relatively strong interaction.

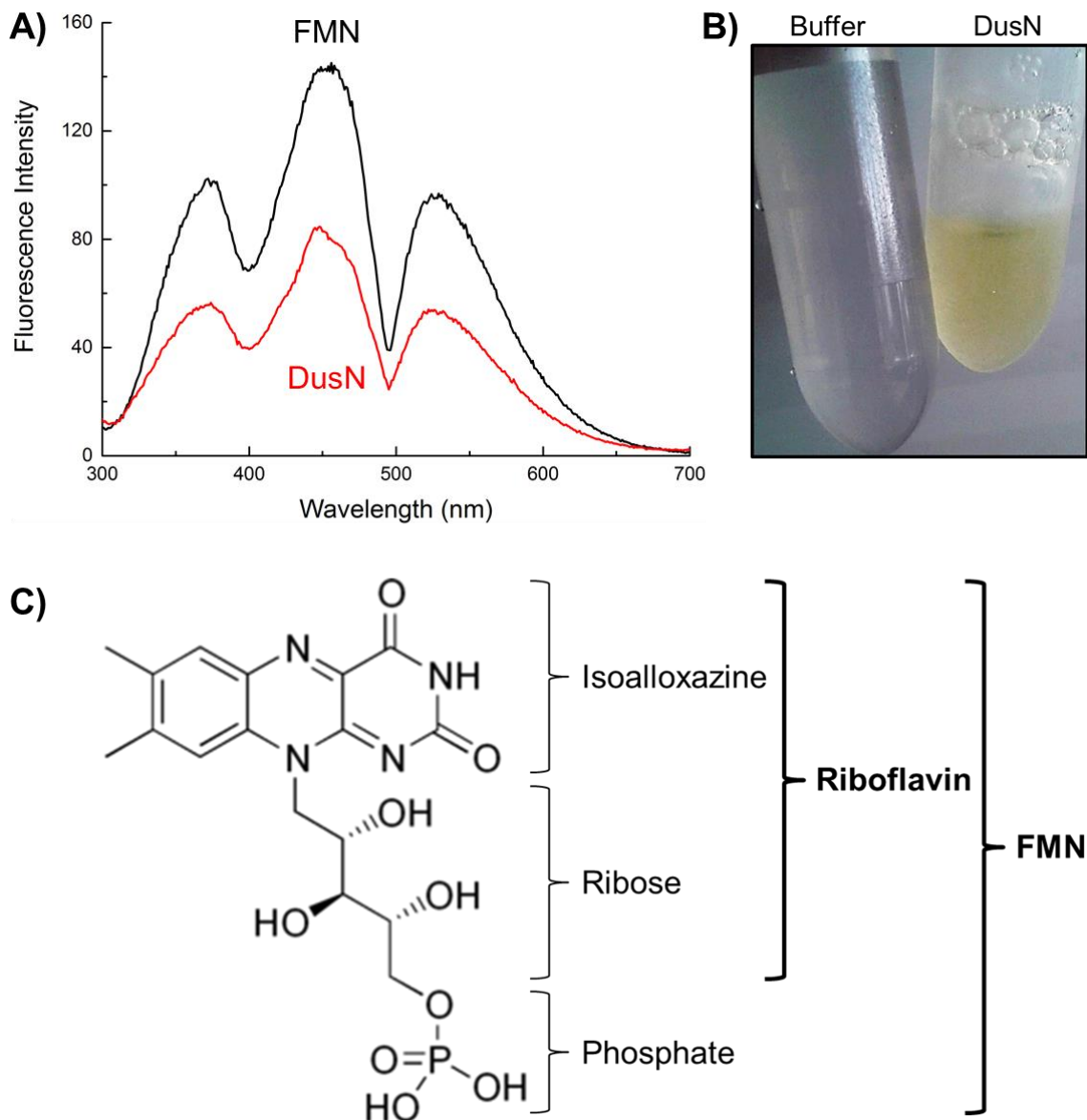


Figure 5.7. Fluorescence spectroscopy identification of an FMN cofactor within DusN. A) Pure 6His_DusN, 130 μ M (5 mg/mL, red), was analysed by fluorescence spectroscopy alongside an FMN standard, 100 μ M (black). Samples prepared in 20 mM HEPES, 150 mM NaCl, 10 % (v/v) glycerol, pH 7.5. Solutions were excited at 365 nm and emitted at 525 nm using a Cary Eclipse fluorescence spectrophotometer. B) A solution of pure 6His_DusN, 5 mg/mL, compared to a solution of buffer. C) The structure of FMN showing the various functional groups. The isoalloxazine tricyclic ring is core for all flavin compounds which joins with ribose to form vitamin B₂/riboflavin. This group is phosphorylated at the 5' hydroxyl group of ribose to give FMN.

5.3.2 Quantification of FMN:DusN stoichiometry

Though fluorescence spectroscopy identified the presence of FMN, this technique isn't quantitative, typically due to the quenching of fluorescence by the local protein environment. For example, 100 μM FMN fluoresces to nearly double the intensity as that recorded for 130 μM protein (Figure 5.7A). To accurately determine the concentration of cofactor within a known quantity of DusN, the protein was unfolded to release free FMN into the solution and thus prevent its quenching (Aliverti, Curti, & Vanoni, 1999). The subsequent absorbance at 444 nm (the peak absorbance of FMN) in conjugation with its extinction coefficient allowed calculation of FMN to quantify stoichiometry. Pure DusN was unfolded by the addition of 10 % (v/v) final amount of SDS and the sample was monitored at 444 nm over time by a UV-Visible spectrophotometer.

In Figure 5.8A below, a pure sample of DusN was unfolded following addition of SDS to denature the protein. As expected, an increase in $\text{Abs}_{444 \text{ nm}}$ was observed overtime, corresponding to the peak absorbance of free FMN as a consequence of its release from the protein. Bovine serum albumin (BSA) was used as a control as it contains no cofactors and demonstrated protein unfolding doesn't cause residual absorbance changes or light-scattering effects. Following this procedure, DusN UV-visible absorbance spectra of before and after SDS treatment revealed the emergence of peaks at wavelengths of 365 and 444 nm (Figure 5.8B).

When the difference spectrum between these initial and final wavelength scans of DusN was presented, these spectroscopic features became more prominent (Figure 5.8C). The FMN control followed the distinctive absorbance trace characteristic of flavin compounds, exhibiting peaks at 365 and 444 nm where the latter reaches the greatest intensity of the two (Oprian & Coon, 1982). As expected, the protein sample assumed a trace identical in pattern to the FMN standard and thus confirmed that the purification procedure does not disrupt protein integrity or cofactor binding and DusN is obtained as an FMN-containing holoenzyme.

With the absorbance at 444 nm accurately quantified for the sample, the concentration of cofactor was calculated using an extinction coefficient at this wavelength of $12,200 \text{ M}^{-1} \text{ cm}^{-1}$ for FMN (Macheroux, 1999). The absorbance change at 444 nm was 0.983 which corresponds to 73.2 μM FMN within the sample. Pure DusN was at 78.8 μM and therefore this calculation strongly indicates DusN coordinates an FMN cofactor in a 1:1 stoichiometry which is in agreement with studies performed on other purified DUS (Yu et al., 2011) and the presence of a single FMN binding domain within DusN.

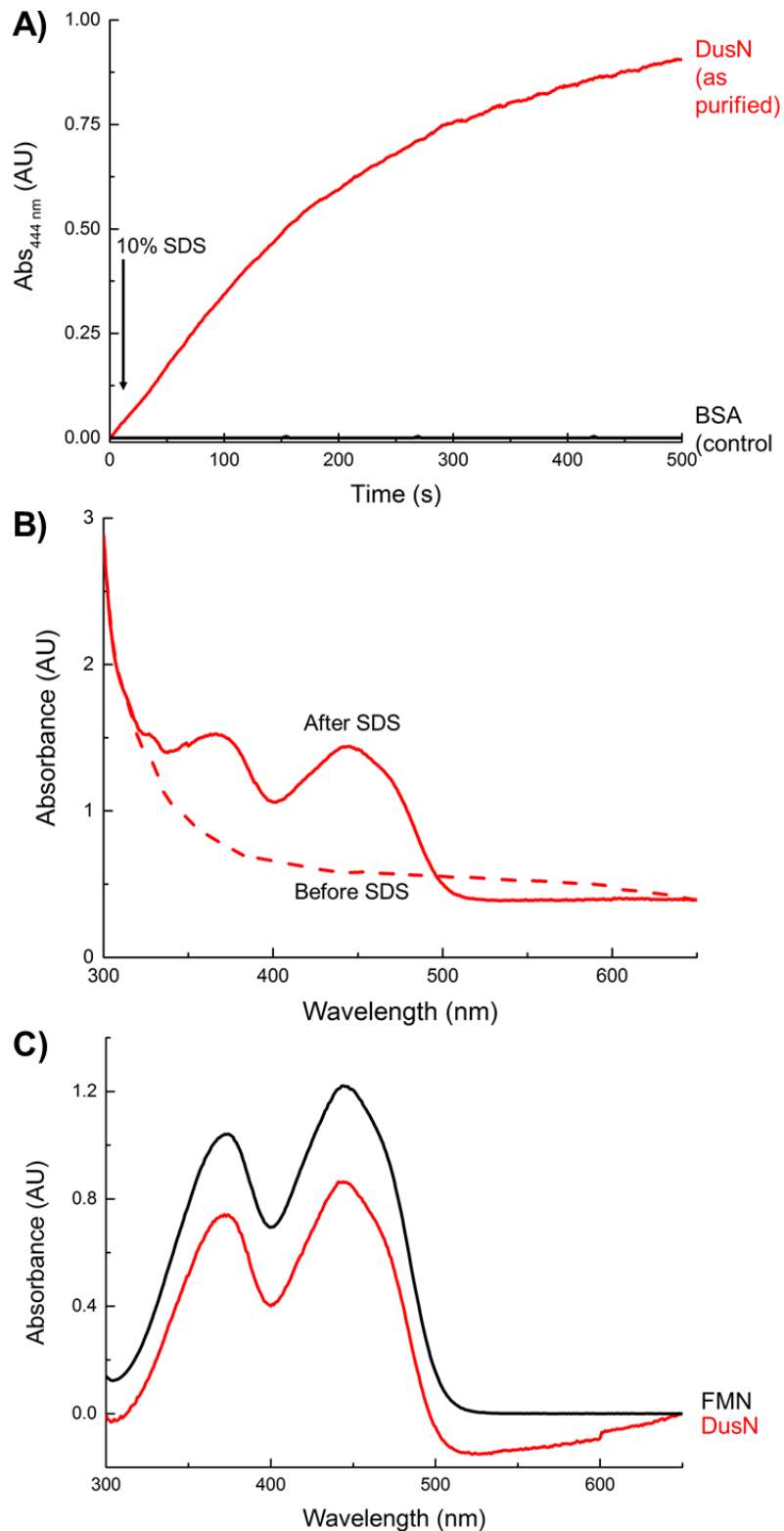


Figure 5.8. Quantifying FMN within 6His_DusN. A) A 3mg/mL solution of pure DusN (red) in 20 mM HEPES, 150 mM NaCl, 10 % (v/v) glycerol, pH 7.5 was measured at 444 nm following addition of 10 % (w/v) SDS to unfold the protein. Bovine serum albumin (BSA, black) was used as a negative control. B) UV-visible wavelength scans of 6His_DusN solution before (dashed line) and after (unbroken line) the unfolding reaction with SDS. C) Difference spectrum of DusN sample between the final and initial trace (red) compared to 100 μ M FMN (black).

5.4 Chemical Synthesis of Dihydrouridine for DUS-based Experiments

Dihydrouridine was required for investigating catalytic activity of DusN in addition to being required as a standard for quantifying whole cell dihydrouridine content. However, this compound is not commercially available and so was synthesised in this study by chemically reducing uridine as described previously (Hanze, 1967). Briefly, the precursor compound was reacted over 24 h in an anaerobic atmosphere saturated with hydrogen and in the presence of rhodium on activated alumina, which acted as a catalyst. The C5-C6 double bond in the pyrimidine structure was hydrogenated to produce dihydrouridine and the reaction was analysed using thin-layer chromatography (TLC) (Section 2.29).

Figure 5.9B shows the results of the TLC where the initial reaction material (uridine) and a sample of the final reaction mixture after 24 h was separated. Though the two compounds are very similar in structure, the lack of a planar ring in dihydrouridine is a key intrinsic property enabling differentiation between the base precursor and product. Uridine exhibits UV activity when excited due to the π -bond in the pyrimidine ring which is absent in dihydrouridine (Figure 5.9A).

When visualised under a UV lamp, the precursor uridine was clearly observed as a dark spot in both the initial and combined reaction mixtures but is absent following the reaction, suggesting uridine had been reduced to completion. A second technique to follow the reaction was achieved by staining the TLC slide with vanillin, a phenolic aldehyde that reacts with certain compounds to produce a visible colour (Burns, 1971; Price, et al., 2002). Vanillin reacts with dihydrouridine, but not uridine, on the TLC plate, as observed by the dark brown spot in the lane corresponding to the final reaction mixture. This stain was absent in the initial material thus confirming dihydrouridine was successfully synthesised. Following this, the base was purified from the mixture for downstream applications. This reaction was shown to synthesise pure dihydrouridine with a 99.1% yield, as judged by H^1 -NMR analysis (data not shown).

5.5 Probing the Catalytic Properties of DusN

Based on its primary amino acid sequence, DusN is a putative tRNA-DUS, a family of post-transcriptional modifying enzymes that reduce uridine to dihydrouridine in an NAD(P)H-dependant reaction. So far, we have reported DusN is critical for nitrate-dependent growth of *P. denitrificans* (Figure 4.3) by regulating translation of the structural Nas genes (Figure 4.11) and that it purifies as a holoenzyme complete with an FMN cofactor (Figure 5.8). To conclusively establish that the *dusN* gene encodes a functional enzyme, initial *in vitro* NADH catalytic analysis was performed with uridine.

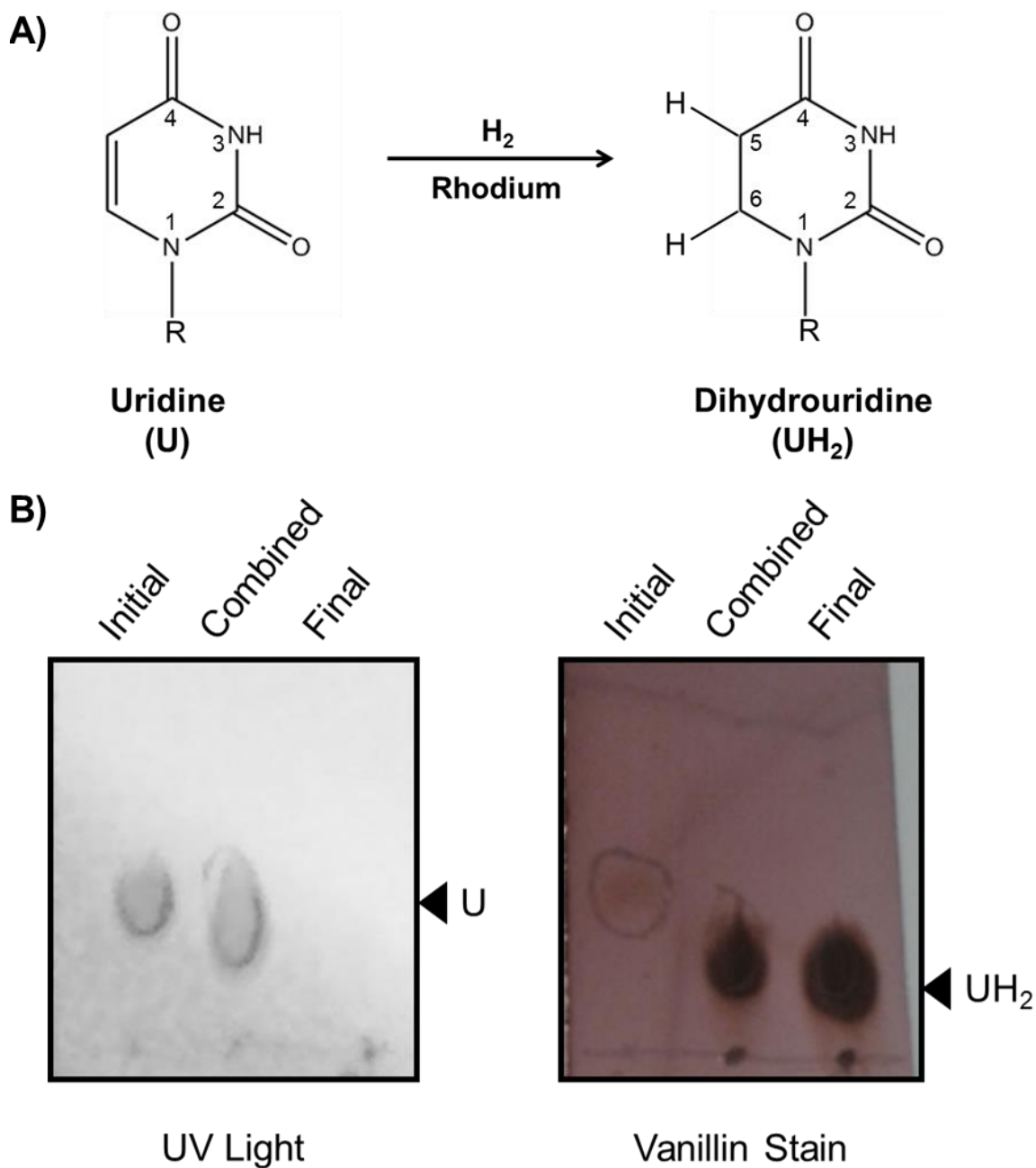


Figure 5.9. Thin-layer chromatography for the chemical synthesis of dihydrouridine. A) Uridine was placed in an anaerobic atmosphere saturated with dihydrogen in the presence of 5 % rhodium on activated alumina for 24 hours to reduce the C5-C6 double bond to produce dihydrouridine. B) Thin-layer chromatography to analyse the reaction progress was visualised under UV light or by a vanillin stain. Lane 1; initial reaction mixture (uridine, U), 2; solution mixture of both initial and final samples, 3; final reaction mixture (predominantly dihydrouridine, UH₂).

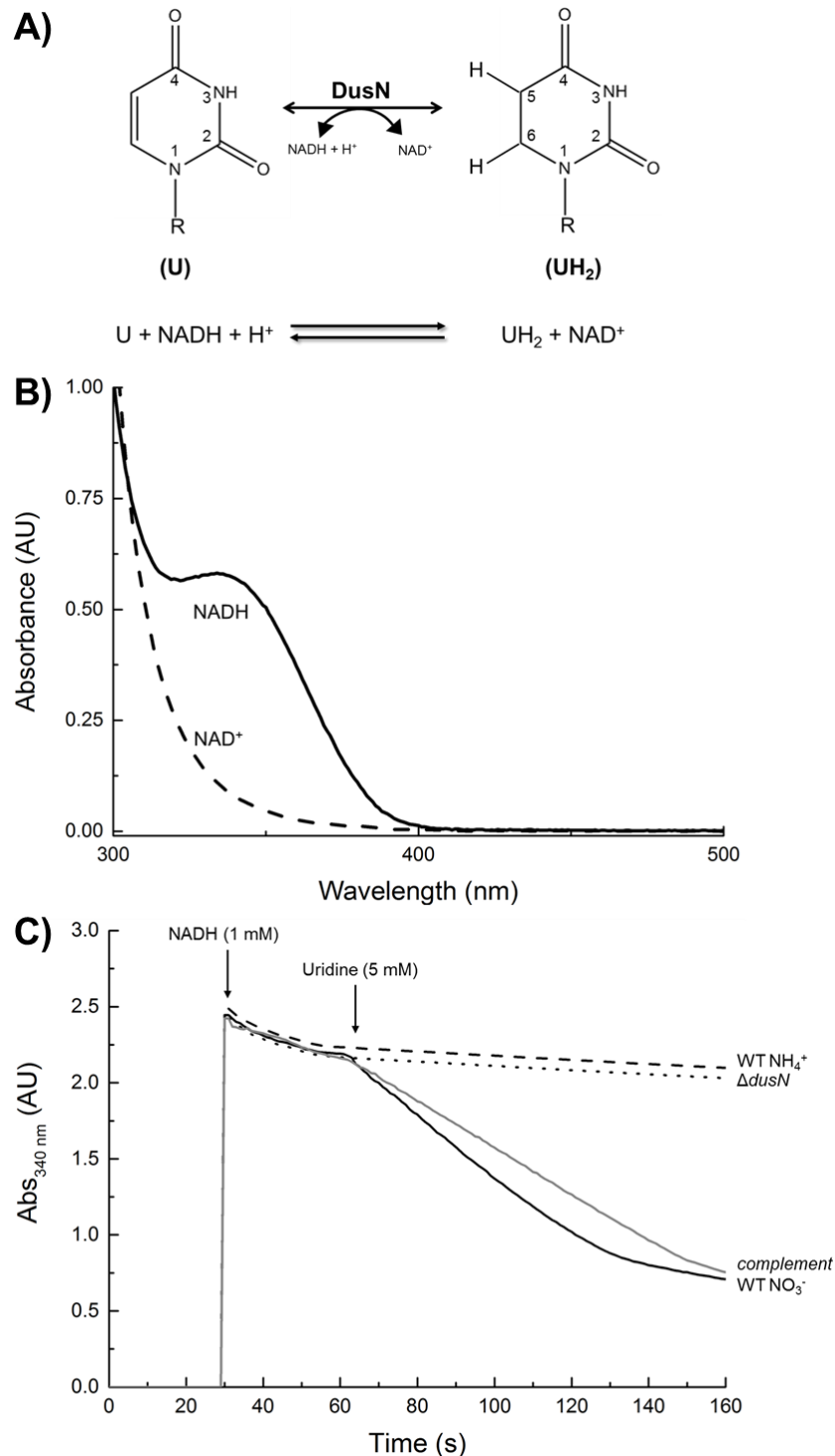
P. denitrificans strains were grown aerobically in batch cultures of defined minimal salt media during nitrate-dependent growth, where *dusN* is known to be expressed to a high level (Figure 1.12). Stationary phase cultures were harvested and cells were lysed to enable access of the substrates (NADH and uridine) to the soluble cytoplasmic proteins. NADH and uridine were sequentially added to the cell lysate reaction mixture and turnover was monitored spectrophotometrically due to a peak difference in absorbance at 340 nm between NADH and NAD⁺ (Figure 5.10B) (see Section 2.32.1).

The NADH-dependent reduction of uridine to dihydrouridine catalysed by DusN is presented in Figure 5.10A, where NADH donates the necessary hydrogens to reduce the double bond of uridine. In doing so, NADH is oxidised to NAD⁺ which causes a clear change at 340 nm (Figure 5.10B). The decrease in absorbance at this wavelength allows turnover of uridine by DusN to be monitored where an observed decrease at 340 nm over time is consistent with catalytic activity.

Dihydrouridine synthase activity of various *P. denitrificans* strains is presented in Figure 5.10C as monitored by NADH oxidation at 340 nm. Cell lysate obtained from WT grown using ammonium as a sole nitrogen source acted as a negative control for DusN catalysis as *dusN* expressed is minimal. Here, the trace recorded showed only a background decrease in Abs_{340 nm} of ~0.2 AU following NADH addition. However, WT under nitrate-dependent growth observed a clearly greater decrease in Abs_{340 nm}, ~1.5 AU over 100 s, succeeding uridine addition. This sizeable change was attributed to NADH turnover and was only present following uridine addition, indicating NADH-dependent dihydrouridine formation by DusN.

The cell lysate obtained from Δ *dusN* during nitrate-induced growth was unable to perform this nitrate-dependent reaction and displayed a near identical profile to that recorded for WT during ammonium-dependent growth. The key difference between WT and Δ *dusN* grown with nitrate is the absence of cytoplasmic DusN. Importantly, significant levels of NADH oxidation was observed in Δ *dusN* expression *dusN* from pBP006 (*complement*), where WT activity was restored to near completion. Here, expression of *dusN in trans* from a plasmid provides the DusN protein in the deletion mutant following taurine addition.

This catalytic data is the first report to show the *dusN* gene conserved across α -proteobacteria encodes a functional DUS flavoprotein and presents novel evidence for its role as a post-transcriptional modifier of nucleotides. Subsequently, *in vitro* catalytic assays were performed with pure 6His_DusN to determine kinetic parameters for enzyme activity. Here, colourimetric reactions were performed as described above, for



F igure 5.10. *In vitro* assay for DusN-catalysed reduction of uridine in *P. denitrificans* strains. A) NADH-dependent reduction of uridine by DusN. B) UV-visible spectrum of NADH (solid) and NAD⁺ (dashed) at 100 μ M to observe the peak difference at 340 nm. C) Enzyme assay of soluble *P. denitrificans* cell lysate at 340 nm. WT (black), Δ *dusN* (dotted) and *complement* (Δ *dusN* + pBP006) (grey) were grown aerobically at 30 $^{\circ}$ C in minimal media with 30 mM succinate, 10 mM nitrate and 1 mM taurine as a plasmid inducer. Cells were lysed in 20 mM HEPES, 150 mM NaCl, pH 7.5 and 1 mL lysate was placed in a cuvette. 1 mM NADH and 5 mM uridine were added. WT grown with 10 mM ammonium acted as a negative control (dashed).

both the forward and reverse reaction over a range of substrate concentrations.

The initial reaction rates were plotted against the concentrations to create Michaelis-Menten curves for each substrate (Figure 5.11) The Michaelis-Menten graphs for each of the four substrates assume the typical profile where the rates of reaction exhibit a sharp increase when initially increasing substrate concentration as the enzyme is in excess. This is followed eventually by a plateau as the enzyme reaches its maximum velocity and the rate is no longer dependent upon substrate concentration.

Subsequent inversion of the data set was performed to plot a reciprocal Lineweaver-Burke graph which allowed calculation of relevant kinetic data for DusN (Figure 5.12). The Lineweaver-Burke plots were used to accurately quantify the K_m (measure of affinity) of DusN for its individual substrates where $K_m = 1/X$ intercept, and the V_{max} (maximum velocity of reaction) of the enzyme where $V_{max} = 1/Y$ intercept.

Table 5.1 displays the kinetic parameters of recombinant 6His_DusN of *P. denitrificans* at 24 °C. DusN catalyses uridine reduction and dihydrouridine oxidation with similar maximum velocities of ~ 90 nmol.min⁻¹.mg protein⁻¹. Unfortunately, very few previous enzymology has been performed on this family making comparison of our data difficult. A single study reported a turnover number of 3.5×10^{-5} s⁻¹ for dihydrouridine oxidation by Dus2 of *S. cerevisiae*, highly similar to ours obtained here of 4.73×10^{-5} s⁻¹ (assuming the enzyme has one active site) (Rider et al., 2009). Whilst V_{max} values for the forward and reverse reaction of 94.38 and 91.02 nmol.min⁻¹.mg protein⁻¹, respectively, are not overly high for an enzyme, intense modifying activity and excess RNA alteration could be counterproductive for increasing fidelity of protein synthesis.

The K_m is a measure of affinity an enzyme holds for its substrate where a low K_m is indicative of high affinity. Interestingly, the K_m exhibited for the bases is roughly an order of magnitude higher than that of NADH/NAD⁺. Whereas the latter substrate pair recorded K_m values of 160 and 150 μ M, respectively, those for the nucleotides were over 1 mM. We propose the active site of DusN recognises a consensus sequence on its target tRNA, accommodating multiple protein:nucleotide interactions necessary to ensure specificity of uridine modification at distinct D-loop sites. This exhibited low affinity will thus prevent the enzyme from modifying the cytosolic pool of free uridine, as well as those it would encounter in non-specific RNA. We therefore suggest that a greater affinity/smaller K_m would be observed if the target oligomer was introduced as the ligand (analysis performed in Section 5.9).

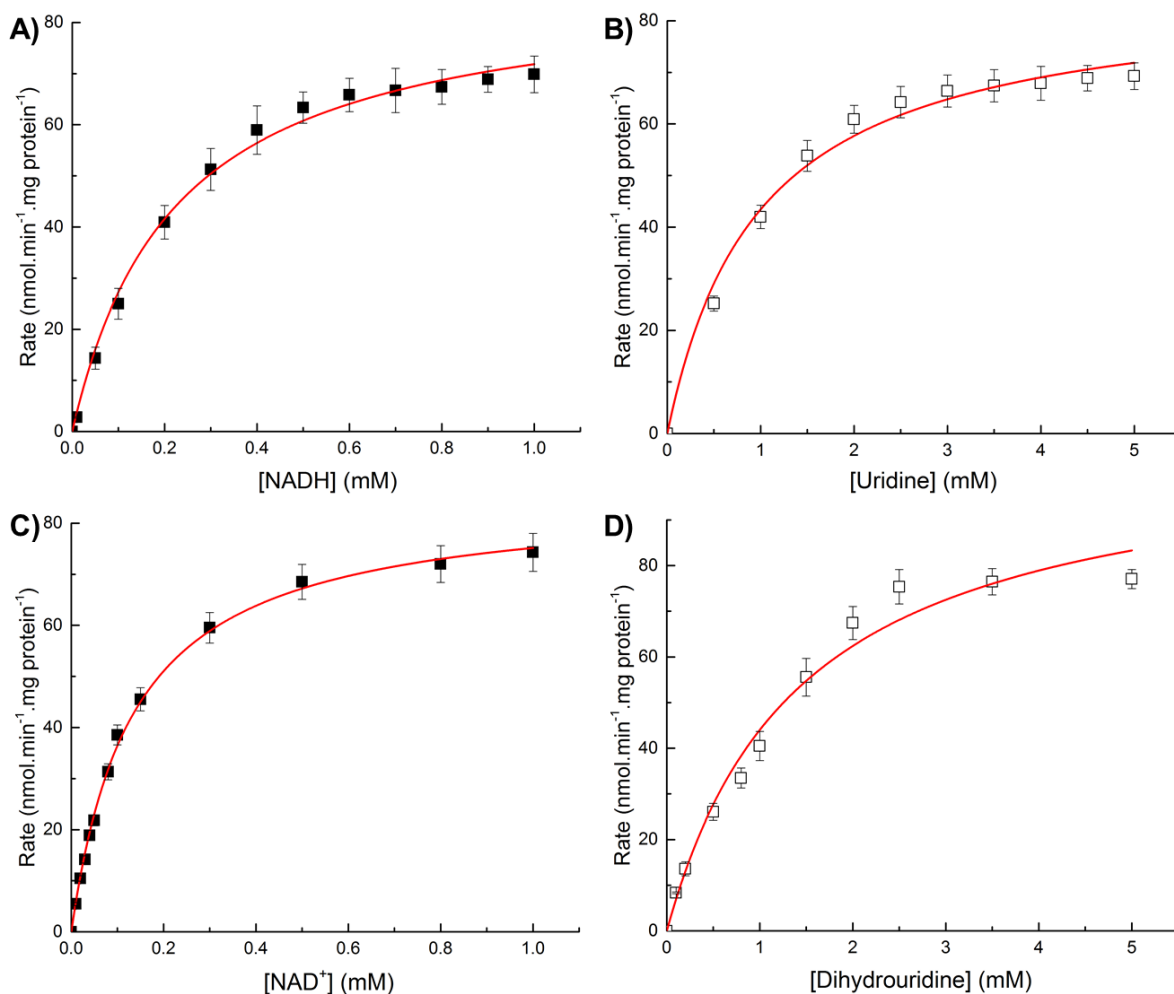


Figure 5.11. Michaelis-Menten plots for the forward and reverse reactions catalysed by DusN. Independent enzyme assays were performed on purified DusN (20 mM HEPES, 150 mM NaCl, 10 % (v/v) glycerol, pH 7.5) over a broad range of substrate concentrations (NADH/NAD⁺; black, uridine/dihydrouridine; white). A) Variation of NADH concentration against 5 mM uridine. B) Various concentrations of uridine against 1 mM NADH. C) Variation of NAD⁺ concentration against 5 mM dihydrouridine. D) Various concentrations of dihydrouridine against 1 mM NAD⁺. Red line indicates the Michaelis-Menten fit.

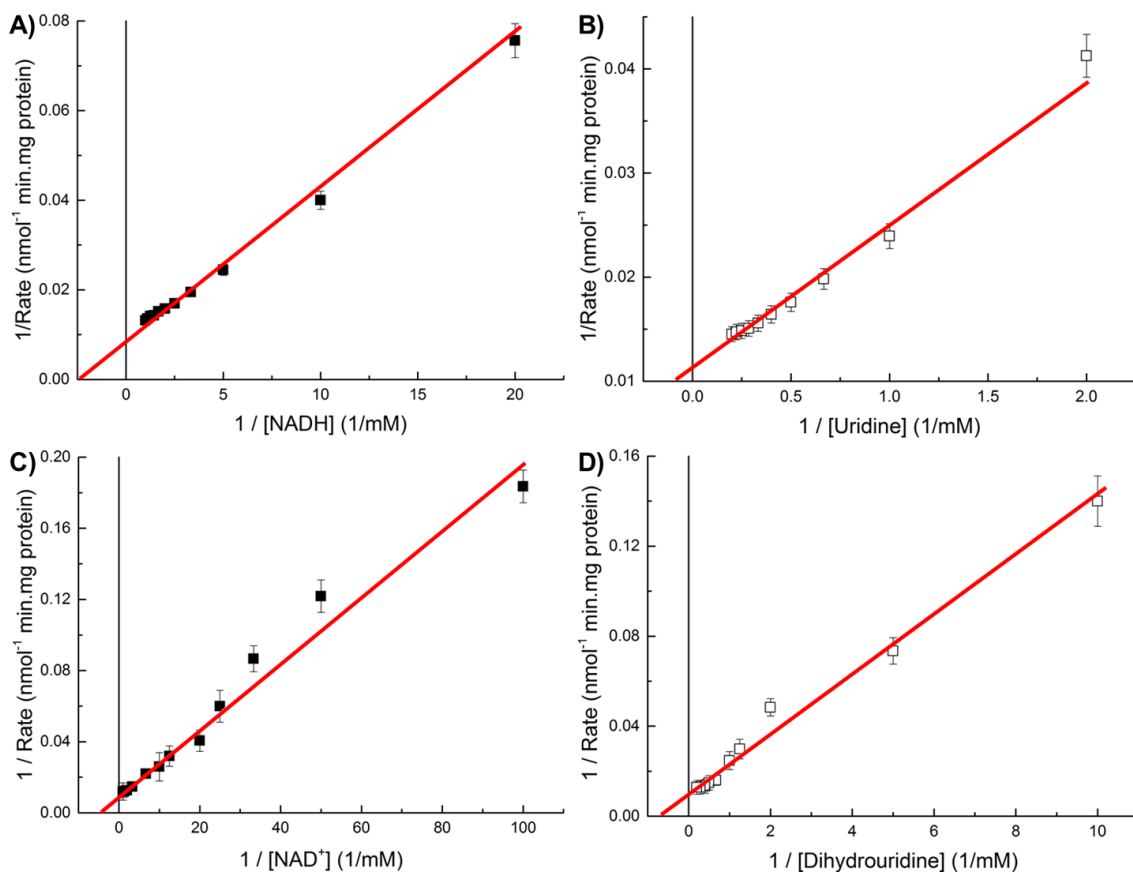


Figure 5.12. Lineweaver-Burke plots to determine parameters for the catalytic activity of DusN. Inversion of the data sets shown in Figure 5.11 was used to construct Lineweaver-Burke plots for accurate quantification of enzyme constants. Independent enzyme assays were performed on purified DusN (20 mM HEPES, 150 mM NaCl, 10 % (v/v) glycerol, pH 7.5) over a broad range of substrate concentrations (NADH/NAD⁺; black, uridine/dihydrouridine; white). A) Variation of NADH concentration against 5 mM uridine. B) Various concentrations of uridine against 1 mM NADH. C) Variation of NAD⁺ concentration against 5 mM dihydrouridine. D) Various concentrations of dihydrouridine against 1 mM NAD⁺.

Table 5.1. Relevant kinetic parameters for DusN Catalysis derived from the Lineweaver-Burke plots.

Reaction Orientation	V_{max} (nmol.min ⁻¹ .mg protein ⁻¹)
Forward	94.66 ± 3.4
Reverse	90.06 ± 6.2
Substrate	K_m (mM)
NADH	0.16 ± 0.01
Uridine	1.31 ± 0.12
NAD ⁺	0.15 ± 0.01
Dihydrouridine	1.26 ± 0.10

Furthermore, individual reactions were setup where adenosine, guanosine, cytidine or thymidine were added to pure DusN with either NADH or NAD⁺. No spectrophotometric activity was recorded (data not shown) reporting the enzyme can scrutinise between highly similar structures to a great degree of accuracy for specific catalysis of uridine and dihydrouridine.

5.6 Site-Directed Mutagenesis Identified Key Catalytic Residues

Following the calculation of kinetic parameters, the catalytic mechanism was investigated in more detail with a view on key residues. Prior studies exploring the mechanism of DUS proteins at a molecular level concluded 3 key amino acids are required for catalysis: C110, K150 and H180, which are fully conserved throughout the protein superfamily (Figure 1.16) and lie within close proximity to the active site (Figure 5.13) (Rider et al., 2009; Yu et al., 2011).

Here, individual DusN variants were constructed by mutating these three residues. Expression plasmid pBP006, pLMB509/*dusN*, was used as a template with appropriate primer pairs to construct three individual plasmids, pBP026, pBP027 and pBP028. These express a copy of DusN containing glycine, methionine and leucine instead of cysteine 110, lysine 150 and histidine 180, respectively.

Following construction and sequence confirmation for the correct substitutions of base pairs, the three plasmids harbouring the separate amino acid mutants were conjugated into Δ *dusN*. The lack of a genomic *dusN* copy certifies any detectable dihydrouridine synthase activity will be due to the mutant DusN. The Δ *dusN* strains harbouring pBP026, pBP027 and pBP028 (denoted C110G, K150M and H180L, respectively) were grown aerobically in minimal salt media under ammonium-dependent growth. Taurine (1 mM final) was added to induce plasmid-borne *dusN* expression resulting in the cytoplasmic presence of the specific mutant DusN. *In vitro* NADH-dependent assays were performed on the harvested cell lysate of the strains to monitor dihydrouridine synthase activity and made relative to activity recorded for Δ *dusN* + pBP006 which expresses native DusN (Table 5.2).

Mutations of cysteine and lysine to non-polar amino acids of similar size greatly attenuated the enzyme rate where they only exhibited ~10% activity relative to WT. This is consistent with values recorded by Yu and coworkers who proposed a catalytic mechanism outlining these as vital for hydrogen movement between NADH, FMN, and uridine (Yu et al., 2011).

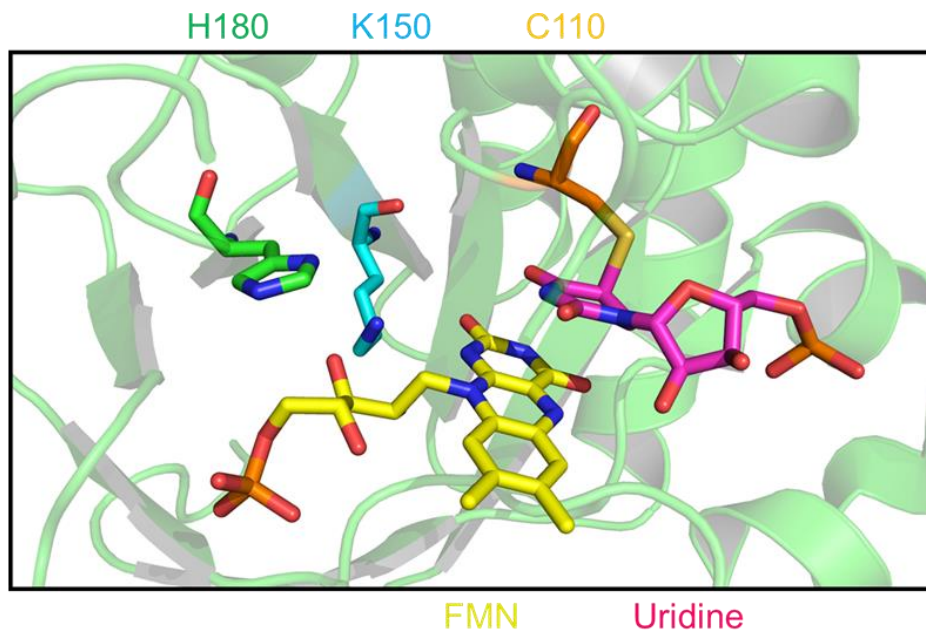


Figure 5.13. Analysis of the proposed key catalytic residues required for NADH-dependent dihydrouridine in DUS proteins. Structure of the active site configuration of a tRNA-DUS (Yu et al., 2011). The FMN (yellow) lays in close proximity with uridine (pink) and is surrounded closely by the three residues; C110 (orange), K150 (blue) and H180 (green). PDB-3B0V, manipulated using PyMOL.

Table 5.2. Relative activity of DusN mutants compared to the native WT protein.

DusN	Relative Activity (%)
WT	100
C110G	12.53
K150M	8.46
H180L	74.1

Interestingly, though histidine 180 is strictly conserved throughout the family, and lies within close proximity to the active site, ~ 70 % relative activity to WT was recorded upon mutation to leucine. This value informs us that a mutation of this residue isn't detrimental for DusN and the enzyme is still capable of dihydrouridine synthesis. Histidine 180 is implicated in coordination of the FMN cofactor through hydrophobic and planar interactions, which seemingly can be maintained in the H180L mutant.

This data is consistent with the requirement of C110 and K150 within the catalytic cycle of DUS proteins, and the partial involvement of the conserved H180. Next, catalysis and interactions between DusN and physiologically relevant tRNA was explored.

5.7 Isolating tRNA from *Paracoccus denitrificans* for Interaction Studies

With DusN able to catalyse the reduction of free uridine and dihydrouridine, the aim was to identify and investigate interactions between the protein and mature tRNA transcripts. Several studies have been performed previously upon tRNA-DUS which all concluded an ability of the enzyme to modify the dihydrouridine content of tRNA, either through *in vivo* or *in vitro* techniques (Rider et al., 2009; Xing et al., 2004; Yu et al., 2011).

In order to examine the impact of DusN on physiological substrate pools, a protocol was designed for specific purification of tRNA from *P. denitrificans*, outlined in Section 2.33. Essentially, whole cell RNA was extracted from batch cultures of *P. denitrificans* cultures grown to a mid-exponential phase in defined minimal salt media. A lithium chloride (LiCl) salt gradient was applied to separate the tRNA from rRNA and mRNA (Cathala et al., 1983; Walker, 2013).

5.7.1 Monitoring purity and integrity using an Experion bioanalyser

An *Experion* automated electrophoresis platform (*BioRad*) was used in tandem with an *Experion RNA StdSens* kit (*BioRad*) to provide a size-resolved, high resolution, virtual gel image of denatured RNA samples. This technique was used throughout this study to monitor the purity and integrity of harvested RNA where clear, sharp bands are indicative of high quality RNA.

Figure 5.14A presents a gel showing the resolution of whole cell RNA obtained from *P. denitrificans*, and the separated fractions of rRNA and tRNA. The whole cell RNA pool contained distinctive bands corresponding to the bacterial rRNA: 23s and 5s constitute the large ribosomal subunit whilst 16s rRNA comprises the small subunit (Yusupov et al., 2001). An additional, relatively weak band is observed at ~75 bp which is the average length of tRNA transcripts. This whole cell RNA was fractionated into rRNA and tRNA

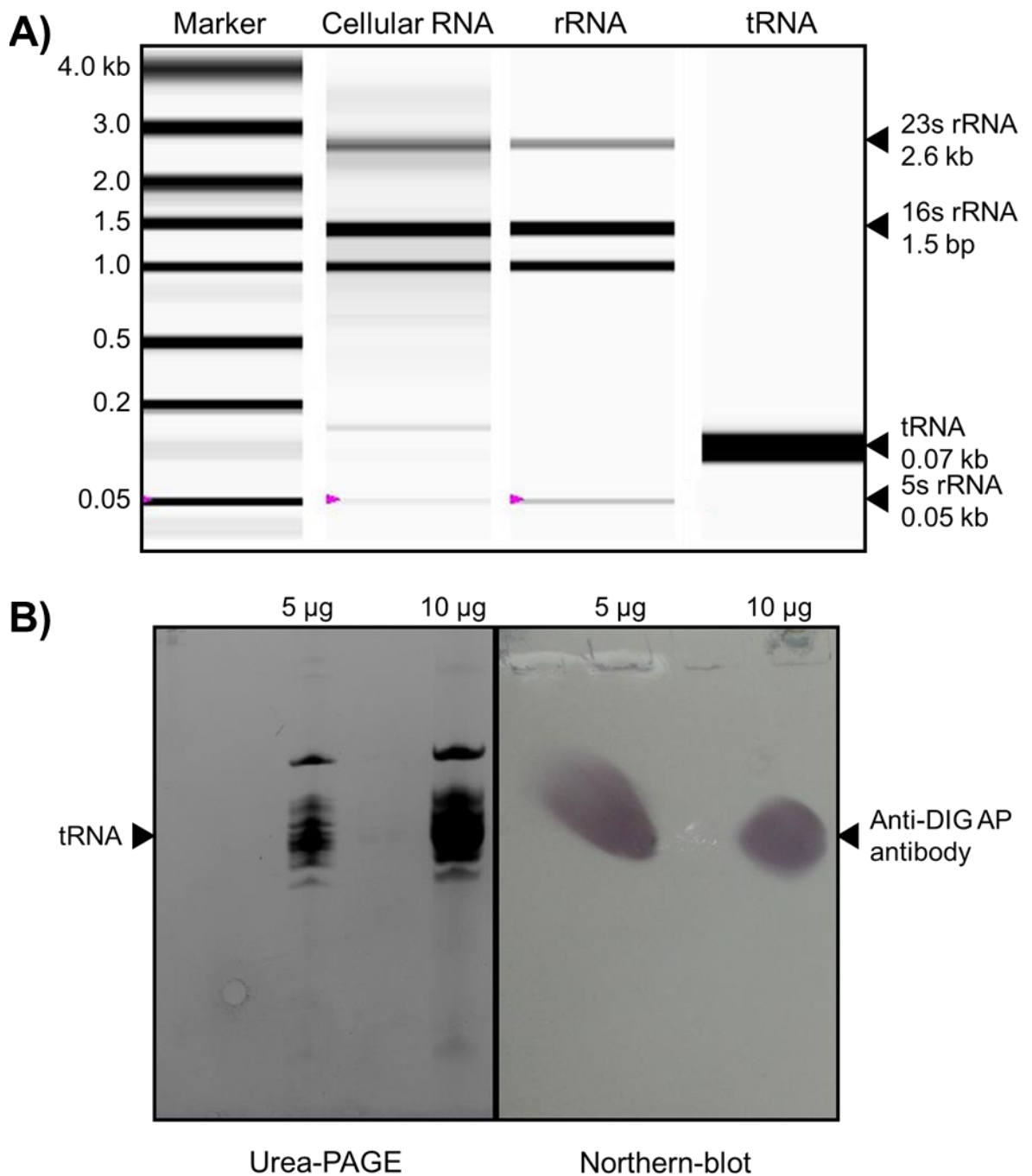


Figure 5.14. Analysis and identification of tRNA isolation from *P. denitrificans*. A) Automated gel electrophoresis using *BioRad Experion* to visualise RNA harvested from *P. denitrificans* at a mid-exponential phase, grown aerobically in minimal media at 30 °C with 30 mM succinate and 10 mM nitrate. The whole cell RNA was fractionated into pools of tRNA and rRNA by centrifugation using a 0.8 M LiCl salt gradient. The rRNA contains distinct bands for 23s, 16s and 5s rRNA while tRNA has one band ~75 bp. RNA ladder (*BioRad*) was used as a marker. B) Northern-blot identification of tRNA following resolution on a 4 M urea-PAGE. The gel was blotted to a nitrocellulose membrane followed by addition of tRNA_Probe labelled with DIG. Anti-DIGAP antibody was added where the conjugated alkaline phosphatase (AP) yielded coloured reaction products when its substrates were added. 5 µg and 10 µg tRNA was loaded onto the gel.

subpopulations, where the rRNA fraction contained all the distinct bands mentioned above. Importantly, the RNA fraction isolated via the LiCl gradient which was believed to be tRNA observed an enriched, single band at ~75 bp which is consistent with tRNA. The absence of smearing in the lane indicated great integrity of this RNA population.

5.7.2 Identification of tRNA via Northern-blot analysis

To confirm that the RNA pool obtained and the band at ~75 bp corresponds to tRNA, Northern-blot analysis was performed following size separation of the sample by denaturing urea-PAGE (see Section 2.34). Once the gel had been blotted to a nitrocellulose membrane, tRNA was exposed to a tRNA probe (i.e. ssDNA complimentary to tRNA sequence) labelled with digoxigenin (DIG) where the two complimentary sequences hybridised to form ssDNA:tRNA. This was subject to an anti-DIG antibody conjugated to an alkaline phosphatase (AP) to specifically target this complex labelled with DIG. The substrates of AP were introduced resulting in a colourimetric reaction catalysed by the enzyme yielding an observable band on the membrane (Figure 5.14B).

Following completion, a single dark purple spot was visualised at the region corresponding to the tRNA band on the urea-PAGE gel. The sole detectable AP activity over this specific point of the membrane confirmed the presence of tRNA. We therefore conclude the LiCl method of RNA extraction reliably and specifically purifies large yields of intact tRNA from *P. denitrificans*.

5.8 Contribution of tRNA-Dihydrouridine Modification by DusN

With *P. denitrificans* tRNA harvested, containing potential DusN substrates, the dihydrouridine content of samples isolated from different strains under various growth modes was calculated. In order to do this, a quantitative colourimetric assay specific for measuring solely dihydrouridine was performed, as outlined in Section 2.30. Briefly, dihydrouridine was hydrolysed by NaOH in a ring-opening reaction to yield N-ribosyl-3-ureidopropionic acid, which when subject to FeCl₃ produced a red colour (Figure 5.15A). Abs_{489 nm} values were measured to quantify the concentration of dihydrouridine within samples. Furthermore, this technique was carried out on the other bases in control experiments where no Abs_{489 nm} was measured, even for the structurally similar uridine and thymidine (data not shown).

5.8.1 Designing an assay to specifically quantify dihydrouridine concentrations

This colourimetric assay was initially performed on a series of dihydrouridine standards at a known concentration to construct a calibration curve and calculate an extinction coefficient for dihydrouridine to enable quantification of this modified base in RNA.

The calibration curve presented in Figure 5.15C demonstrates a positive, linear correlation where a clear, uniform increase in $Abs_{489\text{ nm}}$ was recorded with the incremental increase in dihydrouridine. The calibration curve was deemed reliable as judged by the line of best fit lying within close proximity to all data points. Using this calibration curve in tandem with the Beer-Lambert law, $A = \epsilon \cdot c \cdot l$, the extinction coefficient of dihydrouridine post-assay at 489 nm was calculated as $6413.67\text{ M}^{-1}\text{ cm}^{-1}$.

5.8.2 Quantifying the dihydrouridine content of *P. denitrificans* RNA

With this method for quantifying dihydrouridine established, the assay was used to investigate the physiological effect of DusN on cellular RNA pools, and how this alters in response to nitrogen-metabolism. Here, WT, $\Delta dusN$ and $\Delta dusN + pBP006$ (*complement*) strains were grown in batch cultures of defined minimal salt media to a mid-exponential phase upon which the RNA was harvested, fractionated and subject to the dihydrouridine assay (Figure 5.16).

Figure 5.16 reports the dihydrouridine levels determined in whole cell RNA and the separate tRNA and rRNA fractions (panels A, B and C respectively) obtained from *P. denitrificans* strains grown with either ammonium or nitrate as the sole nitrogen source. The cytoplasmic tRNA pool was the fraction of RNA demonstrated to be affected by both the nitrogen source and DusN (Figure 5.16B). tRNA obtained from WT cells grown with ammonium as a sole nitrogen source had a basal level of $\sim 3\ \mu\text{g}$ dihydrouridine. Interestingly, when cells were grown with nitrate as the sole nitrogen source, a significant 3-fold increase in tRNA-dihydrouridine to $\sim 9\ \mu\text{g}$ was detected. DusN is known to be expressed during nitrate-induced growth to coordinate the nitrogen response and this expression profile correlates well with this significant increase of dihydrouridine formation in tRNA. Furthermore, the levels of modification in $\Delta dusN$ was not affected by the presence of nitrate, where basal levels of $\sim 3\ \mu\text{g}$ dihydrouridine was recorded for both ammonium-dependent and nitrate-dependent growth. Importantly, WT levels of $\sim 9\ \mu\text{g}$ tRNA-dihydrouridine was observed in the complemented strain during nitrate-dependent growth when DusN was reintroduced. This attributed DusN directly as the regulator catalysing this increase in tRNA-dihydrouridine during nitrate assimilation, as predicted.

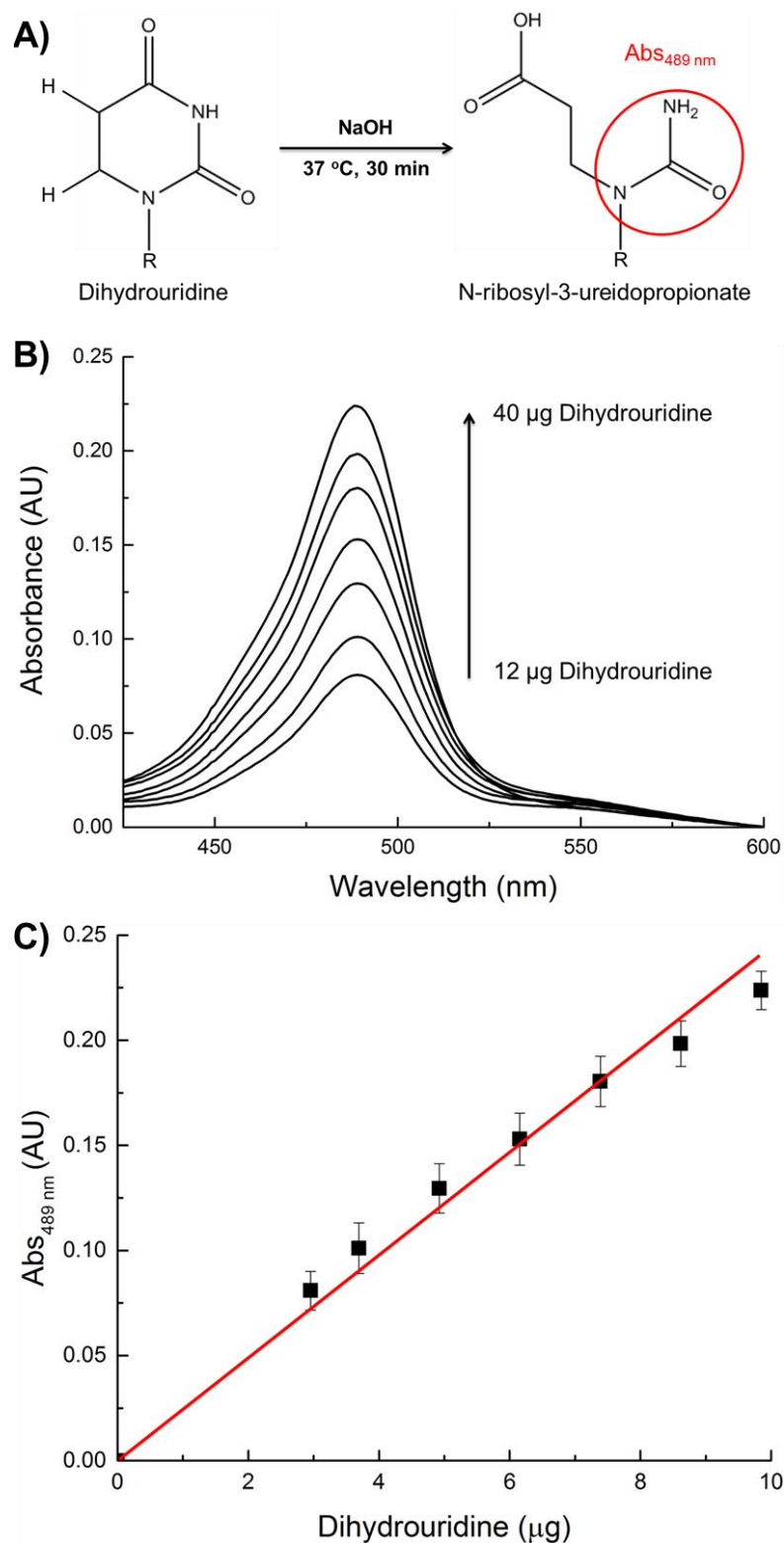


Figure 5.15. Construction of a calibration curve for dihydrouridine using a colourimetric assay. A) Reaction schematic: 30 min hydrolysis of dihydrouridine with NaOH, 37 °C, yields N-ribosyl-3-ureidopropionic acid. Supplemented FeCl_3 binds the chromophore (red) to produce a peak absorbance at 489 nm. B) UV-Visible wavelength spectra for a set of known dihydrouridine standards. C) Calibration curve plotting the $\text{Abs}_{489\text{ nm}}$ against dihydrouridine concentrations to calculate the extinction coefficient and construct a calibration curve.

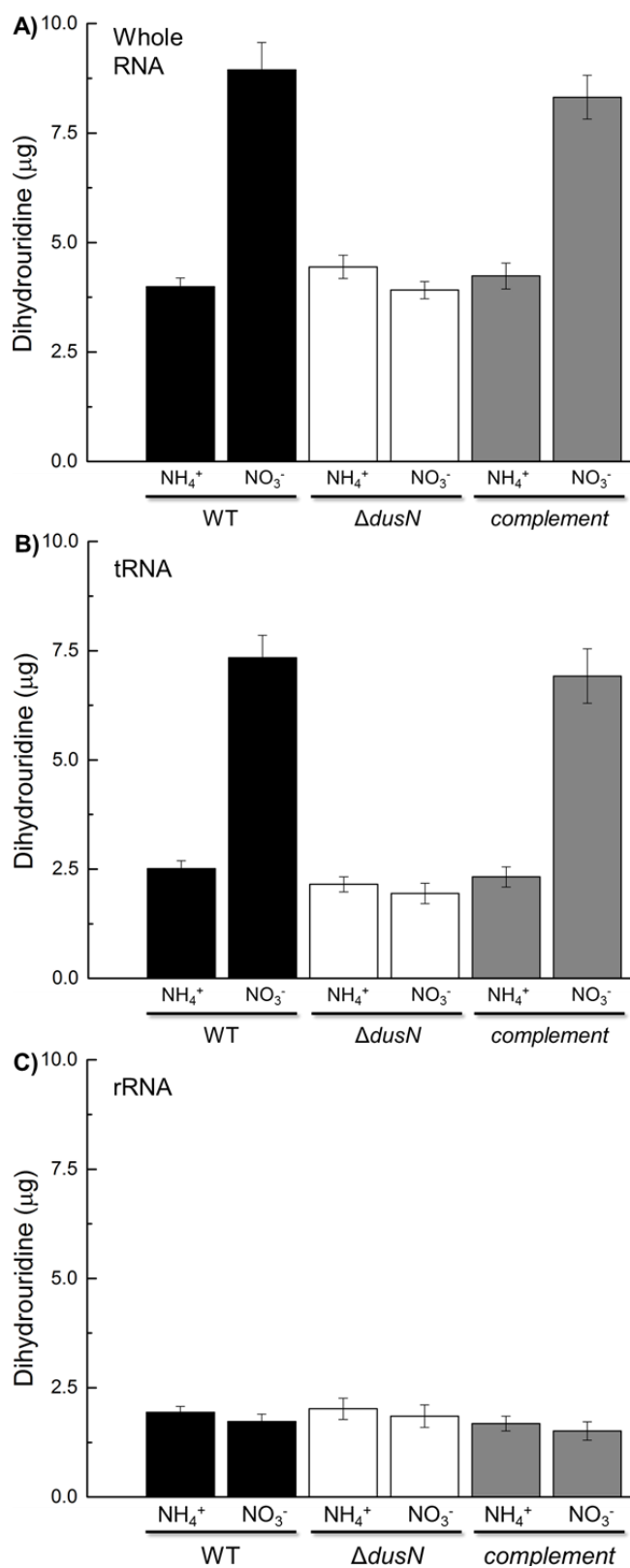


Figure 5.16. Dihydrouridine content of various RNA pools in *P. denitrificans* strains. WT (black), $\Delta dusN$ (white) and *complement* (grey) were grown in minimal media aerobically at 30 °C with 30 mM succinate and either 10 mM ammonium or nitrate as a sole nitrogen source. RNA was harvested at a mid-exponential phase and separated into distinct pools. Dihydrouridine assays were performed on 100 μg of whole cell RNA, tRNA and rRNA (panels, A, B and C).

The level of dihydrouridine in rRNA was consistently determined to be ~2 µg for either nitrogen source or strain (Figure 5.16C). The presence of dihydrouridine in rRNA is not as high as for tRNA, ~30% less, but has previously been reported (Kowalak et al. 1995) and maintains a steady level. Finally, the levels of dihydrouridine in the whole cell RNA pool is roughly the sum of the dihydrouridine present in rRNA and tRNA for each corresponding condition (Figure 5.16A), suggesting only these two RNA pools contain dihydrouridine, consistent with literature.

This data shows the ability of *P. denitrificans* DusN to specifically modify tRNA-uridine during nitrate assimilation when the gene is upregulated from the genome. Next, the activity of plasmid-borne *P. denitrificans* DusN in both *P. denitrificans* and *E. coli* was explored by performing similar analysis on cultures harbouring a plasmid containing a copy of the *dusN* gene.

P. denitrificans containing pBP006 (taurine inducible promoter for *dusN*) and *E. coli* BL21 (DE3) containing pBP024 (IPTG inducible vector for 6His_DusN) were grown in LB media batch cultures to a late-exponential phase (see Figure 5.2). Whole cell RNA was harvested and isolated tRNA was subject to dihydrouridine assays between uninduced and induced cultures to observe the effect of recombinant DusN (Figure 5.17).

LB media is rich in nutrients and contains a plethora of organic and inorganic nitrogen sources, resulting in low expression of *dusN-ntrBCY*. Therefore, dihydrouridine modification can be attributed to plasmid-borne DusN activity. Uninduced *P. denitrificans* grown aerobically in LB media had a tRNA-dihydrouridine content of ~4.5 µg, double the basal level for ammonium-dependent growth in minimal media (Figure 5.16B). Following induction of *dusN* expression, the quantity of dihydrouridine increased 120% to ~9 µg, a significant increase. This is consistent with DusN playing key role in modulating cellular dihydrouridine levels.

Interestingly, a similar increase in cellular dihydrouridine was also observed when the recombinant *P. denitrificans* DusN protein was overexpressed in *E. coli* using a pET-based vector. This organism had a similar basal level of ~5 µg tRNA-dihydrouridine as recorded for *P. denitrificans*, perhaps a housekeeping trait common across bacteria necessary to ensure correct folding and functioning of tRNA for translation. This level raised ~50% from 5 to 7.5 µg following IPTG induction of the DusN protein. The observed increase suggests that DusN from *P. denitrificans* is capable of modifying uridine in the tRNA pool of *E. coli*, most likely at D-loops of selected tRNAs. This may be a functional degeneracy shared amongst the DUS family where each subclass recognises its target sequence irrespective of the organism from which the tRNA originated from.

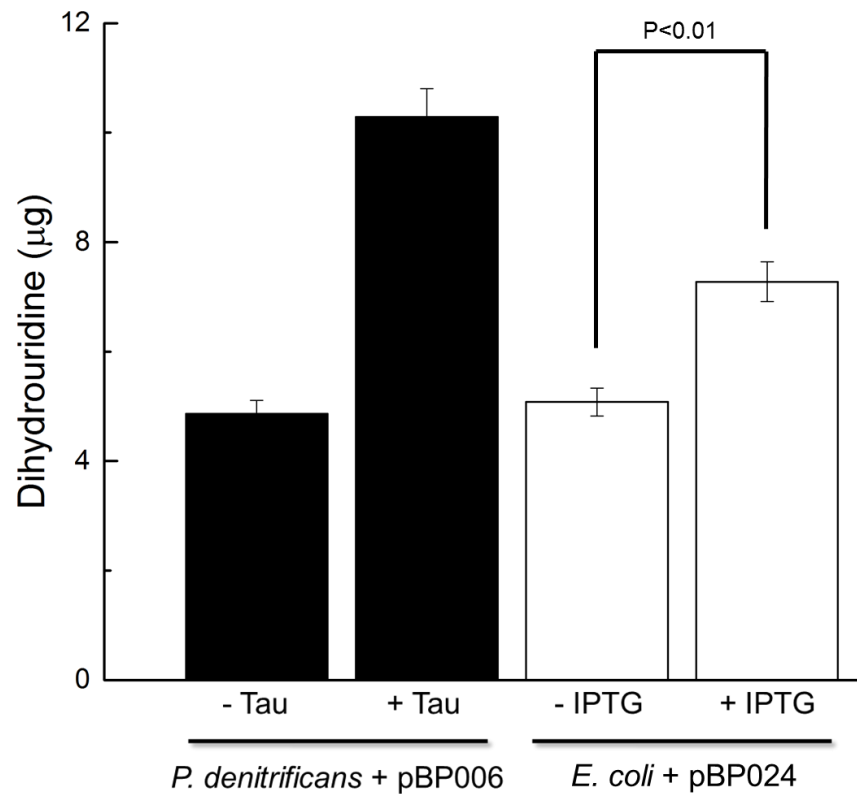


Figure 5.17. Quantification of dihydrouridine content in tRNA isolated from bacteria following induction of recombinant DusN. *P. denitrificans* + pBP006 (pLMB509/*dusN*, black) and *E. coli* BL21 (DE3) + pBP024 (pET28a/6His_*dusN*, white) were grown aerobically in LB media at 30 and 37 °C, respectively. Plasmid-borne DusN expression was stimulated from the ectopic promoters using 10 mM taurine or 0.2 mM IPTG, respectively. Whole cell RNA was extracted from batch cultures at a late-exponential phase following which 100 µg tRNA was isolated and subject to a dihydrouridine assay. P values were calculated from three independent biological replicates.

Noteably, Rider and coworkers have also observed a similar phenomenon where they reported the dihydrouridine levels of tRNA harvested from *E. coli* was sensitive to Dus2 of *S. cerevisiae* (Rider et al., 2009).

While Figure 5.16 and 5.19 both demonstrate DusN leads to increased dihydrouridine modification during nitrate-induced growth or following plasmid stimulation, the levels are never completely abolished in its absence. This is likely due to the presence of a second DUS family protein within *P. denitrificans*, *dusA*, which may provide a housekeeping role to provide necessary levels of dihydrouridine in both tRNA and rRNA.

5.8.3 Activity of *DusA*, a housekeeping dihydrouridine synthase

Bacteria encode at least one housekeeping DUS of class A, B or C, with many genomes typically containing several classes (see Section 1.9.1.1 for review). *P. denitrificans* encodes a second, housekeeping DUS; *dusA*, located on chromosome I of the published genome (Pden_1420). Despite both *DusA* and *DusN* belonging to the DUS family, only 32% sequence identity exists between them. To investigate the contribution of *dusA* towards both tRNA and rRNA modification, a deletion mutant of *P. denitrificans* defective in *dusA* was constructed (see Section 2.16). Suicide vector pBP016 was engineered with front and rear sections homologous to the regions flanking *dusA* in the genome. This plasmid was conjugated into *P. denitrificans* to allow a double homologous recombination event between the fragments and genome, ultimately excising *dusA*.

Following construction and sequence confirmation of the mutant strain, Δ *dusA* was grown aerobically in defined minimal salt media to phenotype *P. denitrificans* deficient in a housekeeping DUS. Figure 5.19 shows the growth of Δ *dusA* during ammonium-dependent and nitrate-dependent growth, where it was capable of using both as sole nitrogen sources for biosynthesis of key cellular structures to support growth. When supplemented with ammonium, Δ *dusA* followed the typical growth profile of WT throughout the lag and exponential phase which is reflected by similar μ_{max} (app.) values of 0.18 and 0.19, respectively. However, the late exponential stage of Δ *dusA* trails off at ~9 hours where it reaches an OD_{max} value of 0.84, as opposed to a greater 1.05 value recorded for WT. The mutant strain was capable of using nitrate effectively as a sole nitrogen source suggesting unlike *DusN*, *DusA* isn't essential for nitrate assimilation and both play separate cellular roles. Only a minor impact of *dusA* deletion towards biomass formation

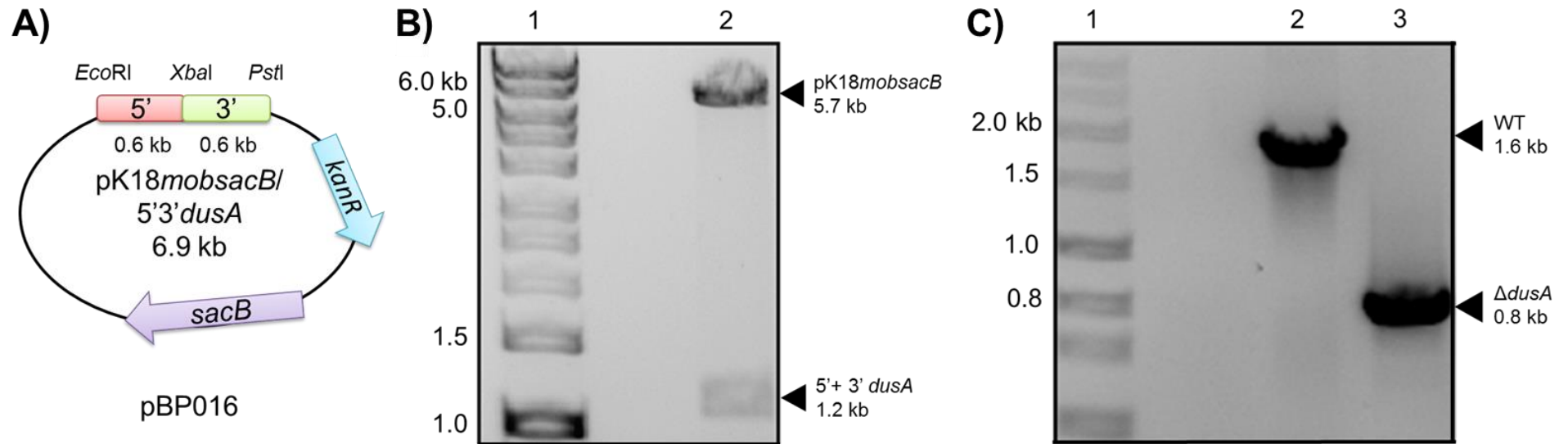


Figure 5.18. Cloning Procedure for the deletion of *dusA* from *P. denitrificans*. A) Suicide-vector pBP016, a *pK18mobsacB*-derivative harbouring 5' and 3' fragments of *dusA* used for deletion. B) Digestion analysis of pBP016, lane 1; 1kb Hyperladder, 2; *EcoRI/PstI* digestion of the 5'3' fragment (1.2 kb) from *pK18mobsacB* (5.7 kb). C) Colony MyTaq PCR confirmation for the removal of a 0.8 kb section of genomic DNA coding for *dusA*. Lane 1; 1 kb Hyperladder, 2; Δ *dusA*, 3; WT.

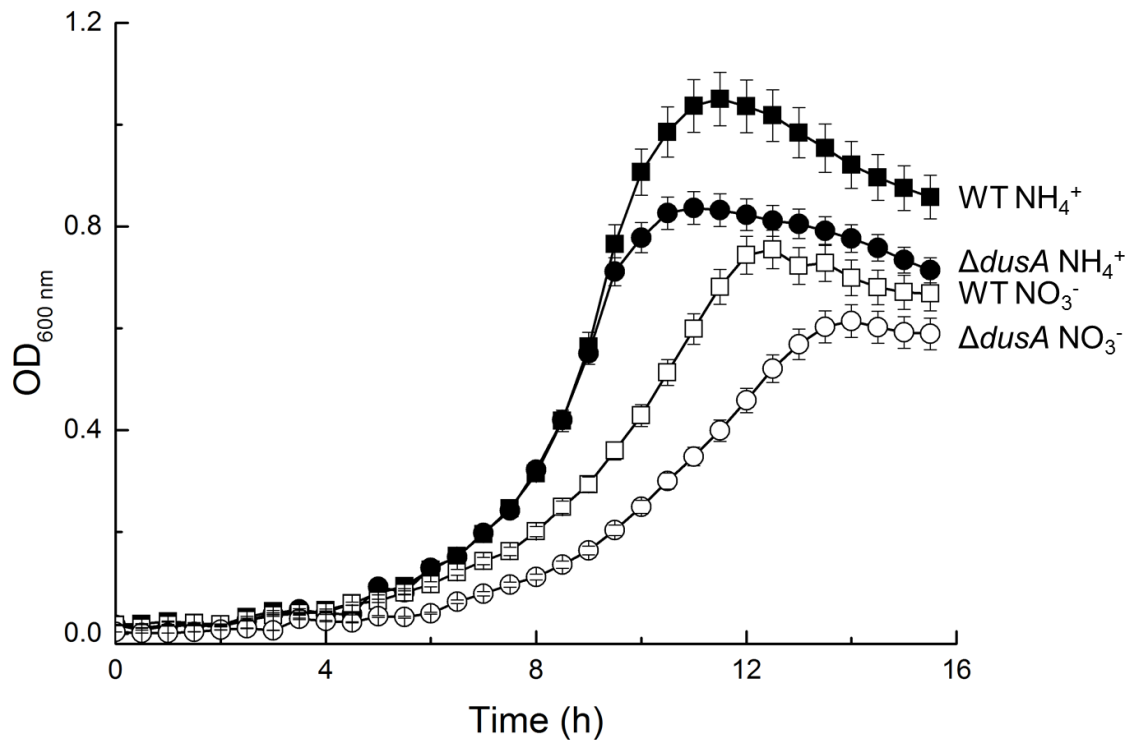


Figure 5.19. Aerobic growth of a *P. denitrificans* strain deficient in *dusA*. WT (squares) and $\Delta dusa$ (circles) were grown aerobically in minimal salt media batch cultures at 30 °C. Cultures were supplemented with 30 mM succinate as a carbon and energy source and 10 mM ammonium (black) or nitrate (white) as a sole nitrogen source.

Table 5.3. Relevant growth parameters calculated from Figure 5.19.

Strain	Nitrogen Source (10 mM)	OD _{max} (AU)	μ_{max} (app.) (h ⁻¹)
WT	NH ₄ ⁺	1.05 ± 0.05	0.19 ± 0.02
	NO ₃ ⁻	0.76 ± 0.04	0.15 ± 0.01
$\Delta dusa$	NH ₄ ⁺	0.84 ± 0.03	0.18 ± 0.02
	NO ₃ ⁻	0.61 ± 0.03	0.12 ± 0.01

and growth rate was observed during nitrate-dependent growth. Values for μ_{max} (app.) of 0.12 and an OD_{max} of 0.61 were determined for $\Delta dusA$ which is modestly attenuated with respect to values for μ_{max} (app.) of 0.15 and OD_{max} of 0.76 observed for WT.

Interestingly, $\Delta dusA$ reached an OD_{max} value of 80% compared to WT with both ammonium or nitrate as the sole nitrogen source. This could suggest a basal level of bacterial growth where the function of DusA is required for complete growth, possibly by optimising translational fidelity. Whilst DusN is crucial for Nas expression to enable nitrate assimilation, this growth data indicates the housekeeping DUS of an organism is not essential but does make an important contribution to biomass formation.

To further explore the function of DusA at the level of RNA, the $\Delta dusA$ strain was grown in defined minimal salt media and RNA was extracted for dihydrouridine quantification of the separate fractions as before in Section 5.8.2.

Figure 5.20 shows the dihydrouridine levels in the RNA pools of $\Delta dusA$ and compares them to WT and $\Delta dusN$ measured in Figure 5.16. Consistent with previous analysis for, the whole cell dihydrouridine content of $\Delta dusA$ was the sum of that found in tRNA and rRNA. In the $\Delta dusA$ strain an increase in tRNA-dihydrouridine from ~1 to ~5 μg was observed when switching from nitrogen sufficient to limiting growth (Figure 5.20B). WT displays a similar increase from 2.5 to 7.5 μg and this significant raise during nitrate-dependent growth is courtesy of DusN, as previously discussed for Figure 5.16.

However, the role of DusA became apparent upon analysing dihydrouridine quantity in RNA pools, where $\Delta dusA$ displayed lower absolute levels of dihydrouridine modification during both ammonium-dependent and nitrate-dependent growth. Despite the increase during nitrate assimilation, the concentration of tRNA-dihydrouridine in $\Delta dusA$ was ~1.5 μg lower than WT during either growth scenario, representing a significant diminishment. Additionally, rRNA-dihydrouridine was at a constant concentration of ~1.5 μg in both WT and $\Delta dusN$ irrespective of nitrogen-metabolism, whereas rRNA in $\Delta dusA$ was completely deficient in dihydrouridine (Figure 5.20C). This data is consistent with a housekeeping role for DusA of *P. denitrificans* for the production of the necessary dihydrouridine in both tRNA and rRNA populations, and is likely similar between organisms.

From this data, we believe DusA catalyses background levels of dihydrouridine formation in both tRNA and rRNA while DusN is involved in tRNA post-transcriptional modification during the nitrogen-stress response. It is highly likely these separate enzymes have distinct RNA targets they act upon to achieve their individual cellular role.

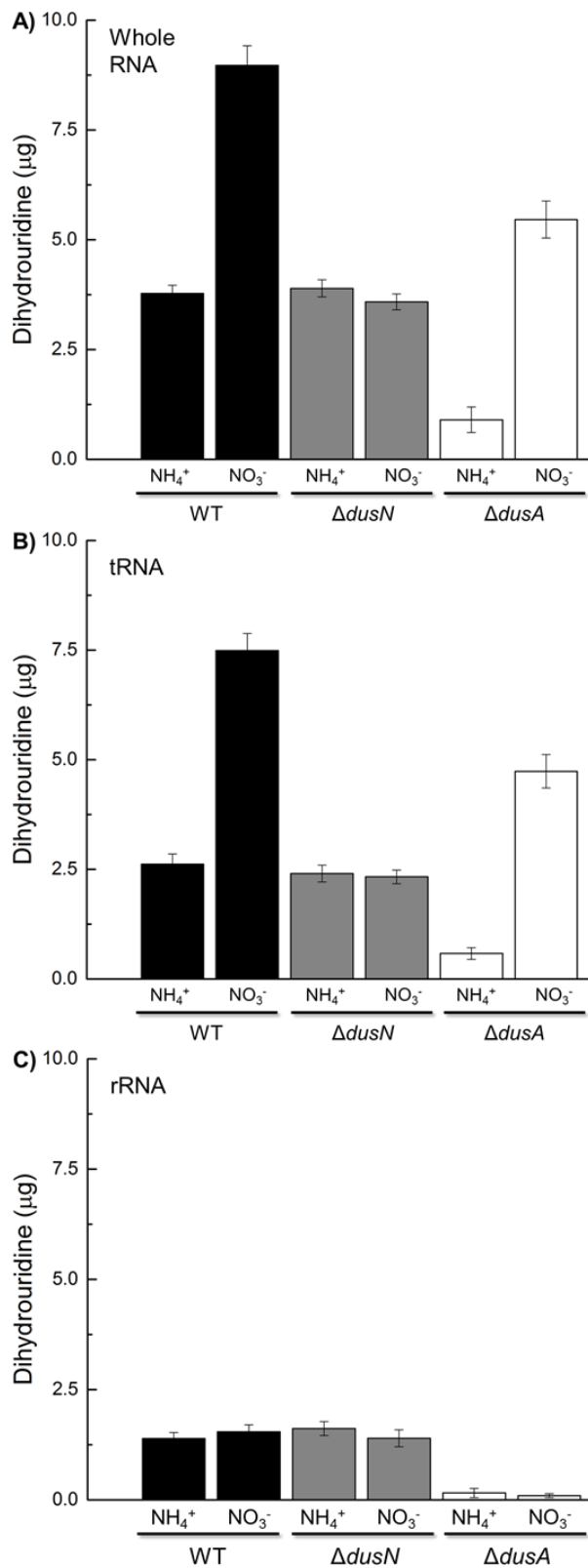


Figure 5.20. Dihydrouridine quantification in RNA harvested from *P. denitrificans* strains. WT (black), $\Delta dusN$ (grey) and $\Delta dusA$ (white) were grown in minimal salt media aerobically at 30 °C with 30 mM succinate and 10 mM ammonium or nitrate as a sole nitrogen source. Whole cell RNA was harvested at a mid-exponential phase, separated into respective RNA pools and dihydrouridine assays were performed on 100 μg of substrate.

5.9 Isolation of Physiological tRNA Targets of DusN

Analysis performed so far had highlighted the necessity of DusN for *nasABGHC* translation by providing a nitrate-induced increase in tRNA-dihydrouridine. The subsequent objective was to capture *in vitro* interactions using pure DusN and tRNA samples to isolate specific tRNA targets of the enzyme.

5.9.1 *In vitro catalytic DusN activity with pure tRNA substrate*

Section 5.6 demonstrated the dihydrouridine synthase capacity of DusN in catalysing the reduction of free uridine bases. However, the physiological role of DusN is performed at uridine moieties within tRNA, ostensibly at a consensus ribonucleotide sequence which increases the specific enzyme affinity. So far, this interaction has only been reported indirectly by investigating tRNA from $\Delta dusN$ mutants following growth and extraction of RNA pools, rather than probing direct contact between enzyme and tRNA substrates. In order to test whether DusN could turnover uridine in tRNA, initial NADH assays were performed with soluble cell extract of *P. denitrificans* strains grown with nitrate, and pure tRNA isolated from the bacterium (Figure 5.21).

Previously, total tRNA containing potential substrates for DusN was purified from *P. denitrificans* WT under ammonium-dependent growth to increase the likelihood that specific uridine targets of DusN were not already modified *in vivo* during growth, as *dusN* expression is low under these conditions.

Enzyme reduction of uridine in tRNA was monitored at 340 nm to follow NADH catalytic turnover to NAD⁺. In a control experiment, a background decrease of ~0.02 AU was recorded for $\Delta dusN$ following tRNA addition (Figure 5.21). This activity may be due to DusA as the substrate contained the whole tRNA population. WT cultured on nitrate is known to upregulate *dusN* expression leading to a sizeable increase of enzyme in the cell lysate. When the tRNA was added to this sample, a much greater decrease in the Abs_{340 nm}, ~0.2 AU, was recorded, an amplification of almost an order of magnitude compared to $\Delta dusN$. This significant increase of NADH oxidation in WT compared to the mutant strain is attributable solely to activity of DusN. Thus, we show for the first time *in vitro* dihydrouridine formation on mature tRNA transcripts by the bacterial nitrogen-responsive DusN.

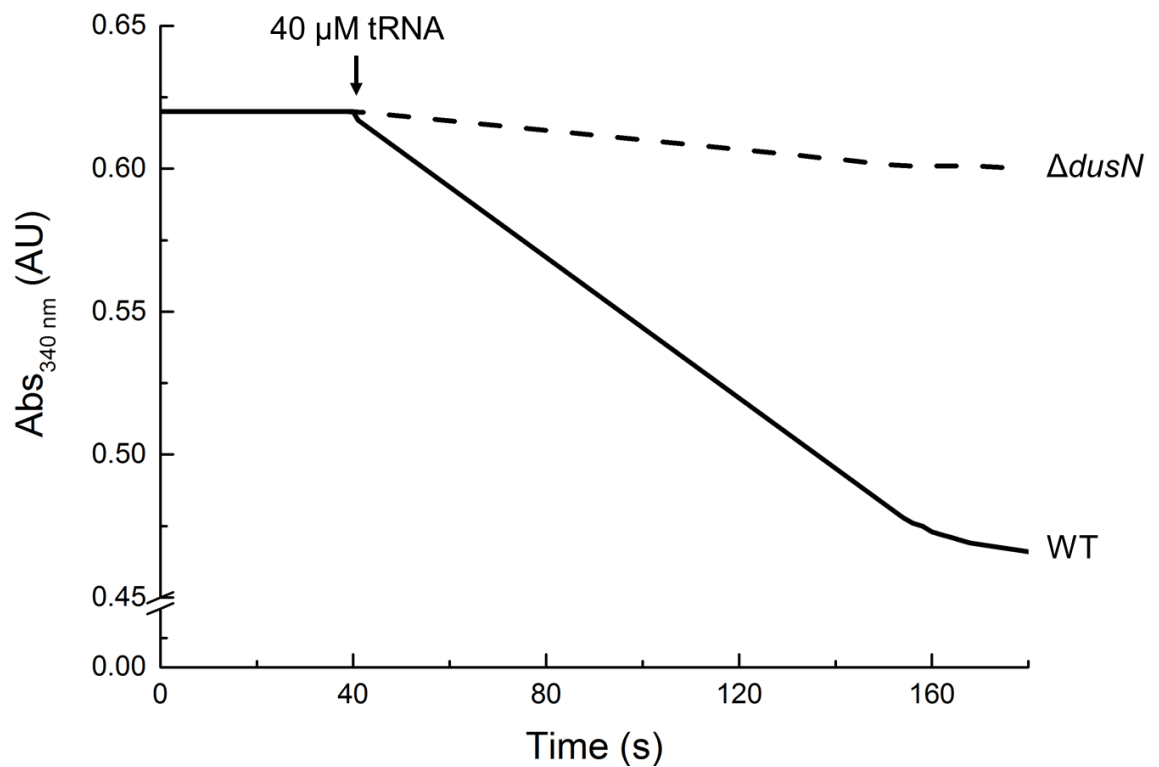


Figure 5.21 *In vitro* NADH assay for DusN catalysis of pure tRNA substrate using *P. denitrificans* strains. WT (solid line) and $\Delta dusN$ (dashed line) were grown aerobically in minimal salt media batch cultures at 30 °C, supplemented with 30 mM succinate and 10 mM nitrate. Cells were harvested and lysed in 20 mM HEPES, 150 mM NaCl, pH 7.5. 1 mL lysate was placed in a cuvette monitored at 340 nm, followed by addition of 1 mM final NADH. Pure tRNA harvested previously from *P. denitrificans* was subsequently added to the sample to 40 μ M final concentration and the absorbance was followed over time.

5.9.2 Band shift assays to visualise DusN:tRNA interactions

As DusN has the capacity to catalyse NADH-dependent uridine reduction on mature tRNA transcripts, we can conclude that DusN is a nitrogen-responsive member of the tRNA-DUS family. The next objective was to determine the identity of specific DusN substrates in the tRNA pool. Electrophoretic mobility shift assays were performed to observe interactions between DusN and tRNA molecules as a means of identifying substrates. Pure DusN and tRNA samples were incubated together and loaded onto a native-PAGE which was size-resolved using a low current at 4 °C. The gel was stained with ethidium bromide to visualise nucleic acids and observe tRNA migration. A disruption in this distance is characteristic of protein:polynucleotide where the complex gains increased weight which mitigates migration (Fried, 1989; Garner & Revzin, 1981).

The gel presented in Figure 5.22 displays the negative controls, which show the typical distance migrated by tRNA molecules where it was observed as a uniform band around halfway on the gel. Importantly, in both lanes where DusN was incubated with the substrate prior to gel loading, mobility of a subset of tRNA molecules was significantly lower (lanes 2 and 4). Here, separate bands appeared in addition to the native tRNA band which were observed closer to the starting position of the lane and thus displayed attenuated migration in the presence of DusN. Protein:nucleic acid complexes migrate slower through an acrylamide gel compared to linear free polynucleotides, implying the slower running band represented specific tRNA molecules in complex with DusN.

The shifted bands (labelled with an asterisk) were excised from the gel and the tRNA recovered was subsequently reverse transcribed to cDNA using degenerate primers. These double stranded cDNA fragments formed were blunt-end cloned into vector pJET/1.2 at an *EcoRV* cut site and transformed into *E. coli* JM101. Successfully ligated plasmids were isolated from clones and sequenced to identify the tRNA molecules bound by DusN (see Section 2.35 for detailed method).

Sequencing of clones derived from DusN:tRNA complexes identified three separate tRNA molecules from *P. denitrificans* 1222 which code for: Lysine (TTT), Phenylalanine (GAA) and Tryptophan (CCA). This band shift analysis demonstrates that the cognate targets of DusN are tRNA^{Lys}_{UUU}, tRNA^{Phe}_{GAA} and tRNA^{Trp}_{CCA} which can undergo dihydrouridine formation during nitrate-dependent growth. These are plausible targets as tRNA^{Phe} has been shown to be a target of DUS in *S. cerevisiae* and *T. thermophilus* (Xing et al., 2002; Yu et al., 2011), and very recently tRNA^{Trp} was found to be a target of DusC in *E. coli* (Byrne et al., 2015). Interestingly, when these three tRNA sequences

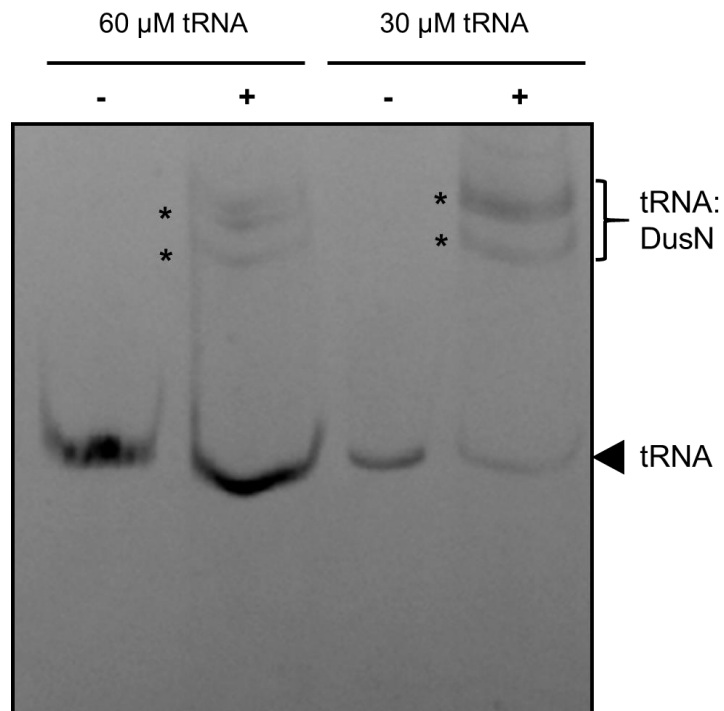


Figure 5.22. Electrophoretic mobility shift assay to evaluate complex formations between DusN and tRNA. Approximately 60 μM or 30 μM tRNA purified from *P. denitrificans* were subjected to electrophoretic mobility shift assays. tRNA samples denoted “+” were preincubated for 10 mins at room temperature with 20 μM pure DusN in a reaction buffer of 20 mM HEPES, 150 mM NaCl, 10 % (v/v) glycerol, pH 7.5. Lanes marked “-” were not subject to DusN. RNA was resolved on a 15 % acrylamide native-PAGE gel at 4 °C and visualised with ethidium bromide staining. Asterisks denote bands excised for sequencing.

were overlaid, a region of conservation was found around the D-loop which is absent in other tRNA, not resolved in DusN:tRNA complexes (Figure 5.23). Furthermore, all have uridines at position 16, 17 and 20, the most commonly targeted sites of dihydrouridine synthesis (Xing et al., 2004).

Figure 5.23 shows the ribonucleotide sequences for tRNAs encoding Lys_{UUU}, Phe_{GAA} and Trp_{CCA} from *P. denitrificans* which are highly similar, a trait uncommon amongst the tRNA. Even more uncommon is a conserved 19 base region which constitutes the D-loop on folded tRNA transcripts. This nucleotide sequence comprises uridines at commonly modified sites 16, 17 and 20: 5'-UAGCUCAGUUGGUAGAGCA-3'. This may thus represent the region of tRNA which forms the consensus sequence for DusN which undergoes modification during nitrogen-limited growth.

The genetic code is known to contain redundancy, where many amino acids may have multiple tRNAs with different anticodons, the most being arginine with 6 codons. Interestingly, lysine, phenylalanine and tryptophan are amongst the few which do not have this feature. Organisms contain two codons for lysine, AAA (DusN targets the corresponding tRNA) and AAG, and two for phenylalanine, TTC (DusN targets the corresponding tRNA) and TTT. Tryptophan is the only amino acid, besides methionine, that is encoded by a sole codon, i.e. TGG, which makes it a logical metabolic choice to modify as DusN only has to deal with one tRNA isoform.

5.9.3 Kinetic parameters of DusN with its target consensus RNA sequence

Section 5.5 investigated the enzymology of DusN with free uridine and dihydrouridine substrates which reported high K_m values of 1310 and 1260 μM , respectively. As discussed previously, this low affinity is most likely because the active site of DusN requires multiple nucleotide:amino acid interactions to enable specific targeting of its recognised motif on its tRNA substrates. To investigate the kinetic parameters of DusN with its physiologically relevant substrate, 5'-UAGCUCAGUUGGUAGAGCA-3' was synthesised (*Eurofins MWG*) and subject to catalytic experiments, as before in Section 5.5. The K_m values for the NADH-dependent reduction of uridine on the RNA substrate (referred to as "D-loop") are displayed below.

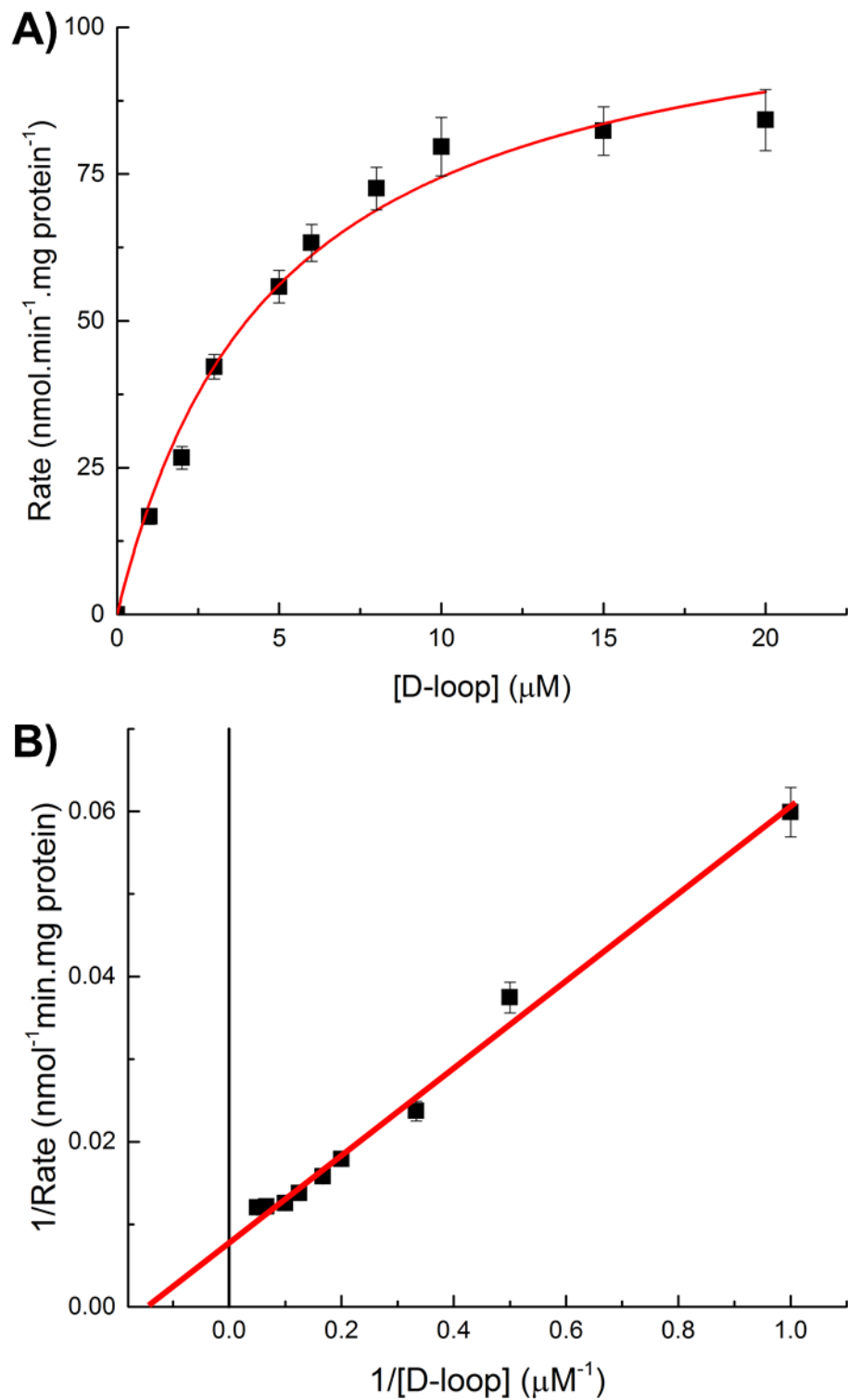


Figure 5.24 Enzyme kinetics for the NADH-dependent reduction of uridine in the RNA consensus sequence of DusN. Independent enzyme assays were performed on purified DusN (20 mM HEPES, 150 mM NaCl, 10 % (v/v) glycerol, pH 7.5) over a broad range of RNA substrate (D-loop) concentrations when using 1 mM NADH. Initial rates of reaction versus D-loop concentration was plotted as a Michaelis-Menton (A) and Lineweaver-Burke plot (B).

Table 5.4. Relevant kinetic parameters for DusN Catalysis of uridine on its target RNA consensus sequence

Substrate	K_M (μM)
Uridine	1310 ± 120
D-loop	4.85 ± 0.13

Catalytic experiments performed on pure DusN using the target RNA sequence as a substrate followed the typical Michaelis-Menton plot characteristic of enzyme catalysed reactions (Figure 5.24A). Upon using the synthesised D-loop as a physiologically relevant substrate, the affinity of DusN towards this substrate greatly increased compared to uridine. A K_M value of $4.85 \mu\text{M}$ was calculated for 5'-UAGCUCAGUU GGUAGAGCA-3', a significant decrease from 1.31 mM calculated for free uridine. This high substrate affinity is consistent with this nucleotide sequence forming a recognised D-loop on tRNA^{Lys}_{UUU}, tRNA^{Phe}_{GAA} and tRNA^{Trp}_{CCA} for DusN modification of specific uridine bases during nitrate-dependent growth.

5.10 Discussion

5.10.1 Exploring the dihydrouridine synthases of *P. denitrificans*

5.10.1.1 Purification and biochemical analysis of DusN catalysis

The protein overexpression and purification data showed recombinant 6His_DusN is a cytoplasmic, monomeric flavoprotein of 37 kDa, containing an FMN cofactor in a 1:1 stoichiometry, as reported for previous purification of DUS members (Yu et al., 2011). Additionally, the release of FMN upon unfolding the protein (Figure 5.8) indicates the cofactor is non-covalently bound. This is in agreement with the solved X-ray crystal structure of *T. thermophilus* DUS (Figure 1.18) where no covalent bonds were found, instead it appears to be coordinated through hydrophobic and planar interactions with multiple residues.

Colourimetric NADH-dependent enzyme assays on cell lysate of various *P. denitrificans* strains concluded the conserved *dusN* gene of α -proteobacteria encodes a functional, nitrogen-responsive, tRNA-DUS capable of turning over free uridine *in vitro* when cultured through nitrate-dependent growth. Catalytic activity was not observed in the Δ *dusN* strain but was recovered upon expression of a recombinant, plasmid-borne copy of the *dusN* gene in the Δ *dusN*.

In vitro spectrophotometry was performed to quantify catalytic kinetic properties at 24 °C, pH 7.5, of this NADH-dependent oxidoreductase. We experimentally determined DusN is capable of catalysing both the reduction and oxidation of uridine and dihydrouridine, respectively, with similar V_{max} values of $\sim 90 \text{ nmol}\cdot\text{min}^{-1}\cdot\text{mg protein}^{-1}$. The capacity for DUS to perform this modification reversibly enables metabolic flexibility as it allows the tRNA to return to its pre-modified state circumventing the necessity to synthesise a new transcript following termination of the initial signal. This physiological ability has been demonstrated by Rider and coworkers on mature tRNA by Dus2 in *S. cerevisiae* (Rider et al., 2009).

There have been no previous investigations reporting kinetic constants for bacterial DusN and a limited amount of studies performed on the DUS family, thus we cannot state if the values calculated for DusN are consistent. A single previous study reported a turnover number of $3.5 \times 10^{-5} \text{ s}^{-1}$ for dihydrouridine oxidation by Dus2 of *S. cerevisiae*, which was similar to that obtained for DusN here of $4.73 \times 10^{-5} \text{ s}^{-1}$ (assuming one active site per enzyme) (Rider et al., 2009). We can, however, speculate the V_{max} values for the forward and reverse reaction of 94.66 and 90.06 $\text{nmol}\cdot\text{min}^{-1} \text{ mg protein}^{-1}$, respectively, are not overly high for an enzyme. For example, respiratory enzymes typically catalyse with a maximum velocity an order of magnitude greater. Due to the nature of DUS as a post-transcriptional modifier regulating the whole-cell tRNA pool, intense activity and excess RNA alteration could be detrimental for the cell. Intriguingly, elevated DUS and dihydrouridine levels in tRNA^{Phe} have been identified in mammalian cancer tissue (Kato et al., 2005; Kuchino & Borek, 1978).

The K_m values of DusN from *P. denitrificans* were calculated as 0.16 and 1.31 mM for NADH and uridine, and 0.15 and 1.26 mM for NAD⁺ and dihydrouridine, respectively. Whilst these values for the physiological electron donor/acceptor are roughly in a range expected, those for the bases are ~ 10 -fold greater. We believe the active site recognises a consensus RNA sequence, accommodating multiple protein:nucleotide interactions necessary to ensure specificity of uridine at distinct sites. The exhibited low affinity will inhibit the enzyme from modifying the general cytosolic pool of free uridine, as well as those it would encounter in non-specific RNA. As expected, a greater affinity was observed for DusN when the specific consensus RNA sequence was introduced as the substrate, recording a K_m value of 4.85 μM . This was consistent with 5'-UAGCUCAGUU GGUAGAGCA-3' forming the physiological recognition site on the D-loop of target tRNA.

A catalytic mechanism previously suggested by Yu and coworkers propositioned a critical role of cysteine 110 acting as a proton donor to the pyrimidine double bond (Yu

et al., 2011). In addition, lysine 150 and histidine 180 are also strictly conserved throughout DUS and believed to aid catalysis. Site-directed mutagenesis here deduced the cysteine and lysine residues are indispensable for activity of *P. denitrificans* DusN due to the abolishment of substrate turnover, consistent with previous reports (Rider et al., 2009; Yu et al., 2011). However, DusN altered for histidine 180 retained ~70% relative enzyme activity, concluding this residue is not crucial despite strict sequence conservation. It is instead believed to contribute hydrophobic and planar interactions for FMN coordination to the protein where various other residues offer interactions enabling cofactor retention in the absence of histidine 180.

5.10.1.2 Cellular function of a housekeeping DusA protein

Each bacterium, archaea and eukaryote contains at least one DUS for catalysing required dihydrouridine formation in post-transcriptional processing of RNA. In addition to the nitrogen-responsive DusN, the genome of *P. denitrificans* encodes *dusA*, the housekeeping DUS distributed largely amongst α -proteobacteria (Kasprzak et al., 2012).

A *P. denitrificans* mutant deficient in genomic *dusA* displayed a detrimental impact on the ability to achieve WT growth formation and rates when cultured with either ammonium or nitrate. The deletion was not lethal, unlike *dusN* which could not utilise nitrate, and cells could still synthesise key cellular material. However, the reduction of biomass in the absence of a housekeeping DUS concludes an important role in maintaining appropriate dihydrouridine for optimal microbial growth.

Dihydrouridine quantification in distinct RNA fractions from *P. denitrificans* reported DusA is responsible for synthesising background levels of dihydrouridine in both ribosomal and transfer RNA. We propose that the ubiquitous housekeeping DUS in bacteria are not critical for cell survival, but do contribute towards optimal growth under a diverse array of environmental conditions. This could be due to ensuring high fidelity of gene translation through optimising tRNA and rRNA secondary structures by enabling complex loop-region folding. However, their function may vary between kingdoms as excess expression of hDus2 has been linked to the development of several human cancers and coincides with elevated tRNA-dihydrouridine (Kato et al., 2005; Mittelstadt et al., 2008). Therefore, it is believed that one function of eukaryotic DUS is as a tumour-suppressor protein amongst mammalian organisms.

Additionally, the data reports the two independent DUS can not crosstalk and fail to compensate for each others biochemical role as clear growth and metabolic phenotypes exist in Δ *dusA* and Δ *dusN*. Previous investigations suggest separate classes of DUS recognise specifically positioned uridines on distinct tRNA transcripts, backed up by the

data obtained here. Only 32% primary sequence identity exists between DusA and DusN of *P. denitrificans* which presumably confers separate consensus sequences and tRNA targets. This, in addition to their differential regulation – *dusN* is upregulated during nitrogen-limitation – possibly allocates their individual physiological functions.

5.10.2 DusN binds specific tRNA transcripts to catalyse dihydrouridine formation

The tRNA-dihydrouridine content of *P. denitrificans* underwent a 3-fold increase when nitrate was used as a sole nitrogen source, compared to ammonium. The levels in rRNA were non-responsive to the cellular nitrogen status. Importantly, this increase was non-existent in Δ *dusN* where background levels of ~3 μ g dihydrouridine were recorded for either cultures. Nitrate-induced increase in dihydrouridine was restored when DusN was introduced into the mutant strain off an ectopic promoter. We conclude from this *in vivo* RNA analysis that DusN is solely responsible for physiologically forming dihydrouridine in mature tRNA transcripts during nitrate assimilation.

Furthermore, tRNA-dihydrouridine modification could be stimulated by inducing plasmid-borne *dusN* expression in *P. denitrificans*, where levels approximately doubled from 4 to 8 μ g. This was performed in LB media which is rich in a multitude of nitrogen sources which should ensure *dusN-ntr* is expressed at low levels. Induced DusN is functional and modifies the tRNA pool, relaying the activity is not nitrogen-responsive, only transcriptional activation of the gene.

The key finding of this chapter was provided by a protein:tRNA interaction assay which identified three tRNA targets of DusN, coding for: Phe_{GAA}, Lys_{UUU} and Trp_{CCA}. These three share an identical 19 base-pair region around the D-loop, a trait highly uncommon amongst tRNA. This region harbours uridines at positions 16, 17 and 20, the most commonly reported sites for dihydrouridine synthesis (Xing et al., 2004).

We propose 5'-UAGCUCAGUUGGUAGAGCA-3' forms a 19 ribonucleotide consensus sequence encompassing the D-loop of these tRNA compounds and is recognised by DusN where the three potential uridine targets come within close proximity of the active site. Bioinformatic analysis was performed on tRNA sequences coding for Phe_{GAA}, Lys_{UUU} and Trp_{CCA} from a range of organisms encoding *dusN*, and those that do not (Figure 5.25). Additionally, a comparison of these sequences between bacteria able to assimilate nitrate (*P. denitrificans*, *B. japonicum* and *R. capsulatus*) and those unable to do so (*E. coli* and *R. sphaeroides*) was performed. This bioinformatic analysis aimed to decipher consistency between DusN, Nas, and target tRNA consensus sequences. Finally, tRNA encoding Met_{CAU} and Gln_{UUG} were chosen as negative controls.

Sequences of Trp_{CCA}, Phe_{GAA} and Lys_{UUU} tRNA in DusN Positive Organisms

** *

<i>E. coli</i>	Trp	AGGGGCGUAGCUCAGUUGGUAGAGCACCGGUCUCCAAAAACGGGUGUUGGGAAGUUCGAGU
<i>B. japonicum</i>	Trp	AGGAGUGUAGCUCAGUUGGUAGAGCACCGGUCUCCAAAAACGGGGGUCGCAGGUUCGAGC
<i>R. sphaeroides</i>	Trp	AGGGGUUAGCUCAGUUGGUAGAGCAUCGGUCUCCAAAAACGAGGGUCGUGGGUUCGAGU
Pd1222	Trp	AGGGGUUAGCUCAGUUGGUAGAGCAUCGGUCUCCAAAAACGAGGGUCGUGGGUUCGAGU
<i>R. capsulatus</i>	Trp	AGGAGUUAGCUCAGUUGGUAGAGCAUCGGUCUCCAAAAACGAGGGUCGUGGGUUCGAGU
<i>B. japonicum</i>	Phe	GCCCAGGUAGCUCAGUUGGUAGAGCAUGCGACUGAAAAUCCGAGUGUCGGUGGUUCGAIU
<i>E. coli</i>	Phe	GCCCAGGUAGCUCAGUUGGUAGAGCAGGGCAUUGAAAAUCCCGUGUCUUGGUUCGAIU
Pd1222	Phe	GCCCAGGUAGCUCAGUUGGUAGAGCAGCGCAUUGAAAAUCCGCGUGUCGGUGGUUCGAIU
<i>R. sphaeroides</i>	Phe	GCCCAGAUAGCUCAGUUGGUAGAGCAGCGCAUUGAAAAUCCGCGUGUCGCUGGUUCGAIU
<i>R. capsulatus</i>	Phe	GCCCAGAUAGCUCAGUUGGUAGAGCAGCGCAUUGAAAAUCCGCGUGUCGCUGGUUCGAIU
<i>R. sphaeroides</i>	Lys	GGGCGGGUAGCUCAGUUGGUAGAGCAGCUCACUUUUAAUCAGCUGUCGUGGGUUCGAIU
<i>B. japonicum</i>	Lys	GGGCGCAUAGCUCAGUUGGUAGAGCAGCUCACUUUUAAUCAGCGGGUCCAGGUUCGAGC
<i>E. coli</i>	Lys	GGGUCGUUAGCUCAGUUGGUAGAGCAGUUCACUUUUAAUCAAUUGUCGCAGGUUCGAIU
Pd1222	Lys	GGGCCCGUAGCUCAGUUGGUAGAGCAACUCACUUUUAAUCAGUGGUCACAGGUUCGAIU
<i>R. capsulatus</i>	Lys	GGGCCGUUAGCUCAGUUGGUAGAGCAGCUCACUUUUAAUCAGCGGGUCGCAGGUUCGAIU

Sequences of Trp_{CCA}, Phe_{GAA} and Lys_{UUU} tRNA in DusN Negative Organisms

** *

Pd1222	Trp	AGGGGUUAGCUCAGUUGGUA-GAGCAUCGGUCUCCAAAAACGAGGGUCGUGGGUUCGAG
<i>M. tuberculosis</i>	Trp	AGGGGCGUAGCUCAACUGGCA-GAGCAGCGGUCUCCAAAAACGCGAGGUUCAGGUUCAAG
<i>T. thermophilus</i>	Trp	GGGCCGUUAGCUCAACUGGCA-GAGCACCGGUCUCCAAAAACGGGGGUUGGAGGUUCGAG
<i>N. europaea</i>	Trp	AGGCCAGUAGCUCAAUUGGCA-GAGCGUCGGUCUCCAAAAACGAAGGUUGGGGUUCGAIU
<i>P. stutzeri</i>	Trp	AGGCCAGUAGCUCAAUUGGCA-GAGCGCGGGUCUCCAAAAACGCGAGGUUGGGGUUCGAIU
<i>M. tuberculosis</i>	Lys	GCCCCUAGCUCAGUUGGUA-GAGCUACGGACUUUUAAUCGCGAGGUCCAGGUUCGAG
<i>P. stutzeri</i>	Lys	GGGUCGUUAGCUCAGUUGGUA-GAGCAGUUGGCUUUUAAUCAAUUGGUCGUAAGGUUCGAA
<i>N. europaea</i>	Lys	GGGUCGUUAGCUCAGCUGGUA-GAGCAGCGACUUUUAAUCGCUUGGUCGCGGUUCGAA
Pd1222	Lys	GGGCCCGUAGCUCAGUUGGUA-GAGCAACUGACUUUUAAUCAGUUGGUCACAGGUUCGAA
<i>T. thermophilus</i>	Lys	GGGCCGUUAGCUCAGCUGGCA-GAGCAACCGACUUUUAAUCCGCUAGGUCGCAGGUUCGAA
<i>M. tuberculosis</i>	Phe	GGCCAGGUAGCUCAGUCGGUAUGAGCGUCGCCUGAAAACGGGAAGGUCGGCGUUCGAIU
Pd1222	Phe	GCCCAGGUAGCUCAGUUGGUA-GAGCAGCGGAUUGAAAAUCCGCGUGUCGGUGGUUCGAA
<i>T. thermophilus</i>	Phe	GCCGAGGUAGCUCAGUUGGUA-GAGCAUGCGACUGAAAAUCCGAGUGUCGGCGUUCGAIU
<i>N. europaea</i>	Phe	GGCCAAGUAGCUCAGUCGGUA-GAGCAGAGGACUGAAAAUCCUUGUGUCGGUGGUUCGAIU
<i>P. stutzeri</i>	Phe	GCCCAGGUAGCUCAGUCGGUA-GAGCAGGGGAUUGAAAAUCCCGUGUCGGCGGUUCGAIU

Sequence of Met_{CAU} tRNA in DusN Positive Organisms

** *

Pd1222	CGCGGGGUAAGCAGCCCGGUAGCUCGUCAGGCUCAUAACCUGAAGGUCGUAAGGUUCAAA
<i>R. sphaeroides</i>	CGCGGGGUGGAGCAGCCCGGUAGCUCGUCAGGCUCAUAACCUGAAGGCGCAGGUUCAAA
<i>E. coli</i>	-GGCCCUUAGCUCAGUGGUUAGAGCAGGCGACUCAUAACGCUUGGUCGUGGUUCGAG
<i>B. japonicum</i>	-UGGCCUGUAGCUCAAUGGUUAGAGCCGGCCGUCUCAUAACGGUCUGGUUCGAGGUUCGAG
<i>R. capsulatus</i>	-GGGCCUGUAGCUCAAUGGUCAGAGCCGGCCGUCUCAUAACGCCUUGGUUGGGGUUCGAG

Sequence of Gln_{UUG} tRNA in DusN Positive Organisms

** *

<i>E. coli</i>	GCGGGAAUAGCUCAGUUGGUAGAGCACGACCUUUUGAAGGUCGGGGUCGCGAAGUUCGAGU
<i>B. japonicum</i>	UGGGGAUUGG-UGUAACGGUAGCACAACAGACUUUGACUC-UGUUUGUCUUGGUUCGAIU
<i>R. capsulatus</i>	UGGGGUUUCG-CCAAGCGGUAAGGCAGCGUUUUUGGUUACCGCCAUUCUAGGUUCGAIU
Pd1222	UGGGGCGUGG-CCAAGUGGUAAGGCACCGUUUUUGGUUACCGUGUACCGUAGGUUCGAIU
<i>R. sphaeroides</i>	UGGGGCGUCG-CCAAGUGGUAAGGCAGCGUUUUUGGUUACCGCCAUUCGUUGGUUCGAIU

Figure 5.25. Comparative sequence alignment for various tRNA's across multiple bacteria.

The tRNA sequences for Phe_{GAA}, Lys_{UUU}, Trp_{CCA}, Met_{CAU} and Gln_{UUG} from *P. denitrificans*, *B. japonicum*, *R. capsulatus*, *R. sphaeroides*, *E. coli*, *M. tuberculosis*, *T. thermophilus*, *P. stutzeri* and *N. europaea* were gathered from GtRNAdb, aligned via Clustal Omega (EMBL-EBI) and shaded based on sequence conservation using BoxShade Server (ExPASy). Asterisks denote uridine at position 16, 17 and 20.

The data presented in Figure 5.25 conveys several key pieces of information. Firstly, the 19 nucleotide consensus sequence is present and strictly conserved in the tRNA sequences for Phe_{GAA}, Lys_{UUU}, Trp_{CCA} from organisms containing a copy of DusN or predicted homologue: *P. denitrificans*, *B. japonicum*, *R. capsulatus*, *R. sphaeroides* and *E. coli*. Conservation of ribonucleotide stretches is an uncommon characteristic and omitted from other tRNA's of these organisms, as exemplified by Met_{CAU} and Gln_{UUG}.

Secondly, whilst the consensus sequence was conserved in the tRNA's of interest from non-assimilating organisms, e.g. *R. sphaeroides* and *E. coli*, this was lost in organisms not encoding DusN: *M. tuberculosis*, *T. thermophilus*, *P. stutzeri* and *N. europaea*. Though the sequences display partial conservation, it is clear the strictness is lost in these species, where uridine 16 and 17 are not consistently found. Of note, uridine 20 is completely absent in tRNA^{Trp}_{CCA} from these organisms. This analysis highlights a link between not only the consensus sequence and the presence of genomic *dusN*, but also the co-conservation with uridine 20 of tRNA^{Trp}_{CCA}. This was discussed earlier (Figure 5.23) as being a sensible option for modification due to the existence of a single codon for tryptophan, where only one tRNA isoform would need regulating.

Finally, the identification of this sequence conserved with the presence of genomic *dusN* accounts for the observed increase in tRNA-dihydrouridine in *E. coli* when DusN from *P. denitrificans* was induced off a vector (Figure 5.17), in addition to the previous report observing this phenomenon with *S. cerevisiae* Dus2 (Rider et al., 2009). Therefore, members from the same DUS subgroup are non-specific to the organism lineage, so long as the recognised RNA consensus sequence is present within the transcript.

From this bioinformatic data, we conclude that no apparent relationship exists between the DusN consensus sequence on tRNA for Phe_{GAA}, Trp_{CCA} or Lys_{UUU} and the ability to assimilate nitrate in bacteria. However, this tRNA sequence does completely correlate with the presence of genomic *dusN*, as it was absent in *dusN* negative bacteria. The identification of this sequence across DusN positive organisms, irrespective of Nas, implies the function is much more widespread in nitrogen-signalling than we initially proposed. In addition to enabling NasABGHC biosynthesis, DusN may participate in a variety of nitrogen-metabolic processes (such as those discussed in Section 4.4) throughout a range of bacteria. We believe DusN achieves the appropriate cellular responses by monitoring translation in a novel mode of regulation based around stimuli-induced, rapid post-transcriptional modification of tRNA.

To investigate how this 19 base-pair sequence may function as a consensus site for DusN recognition at a molecular level, with a specific viewpoint on contact sites between

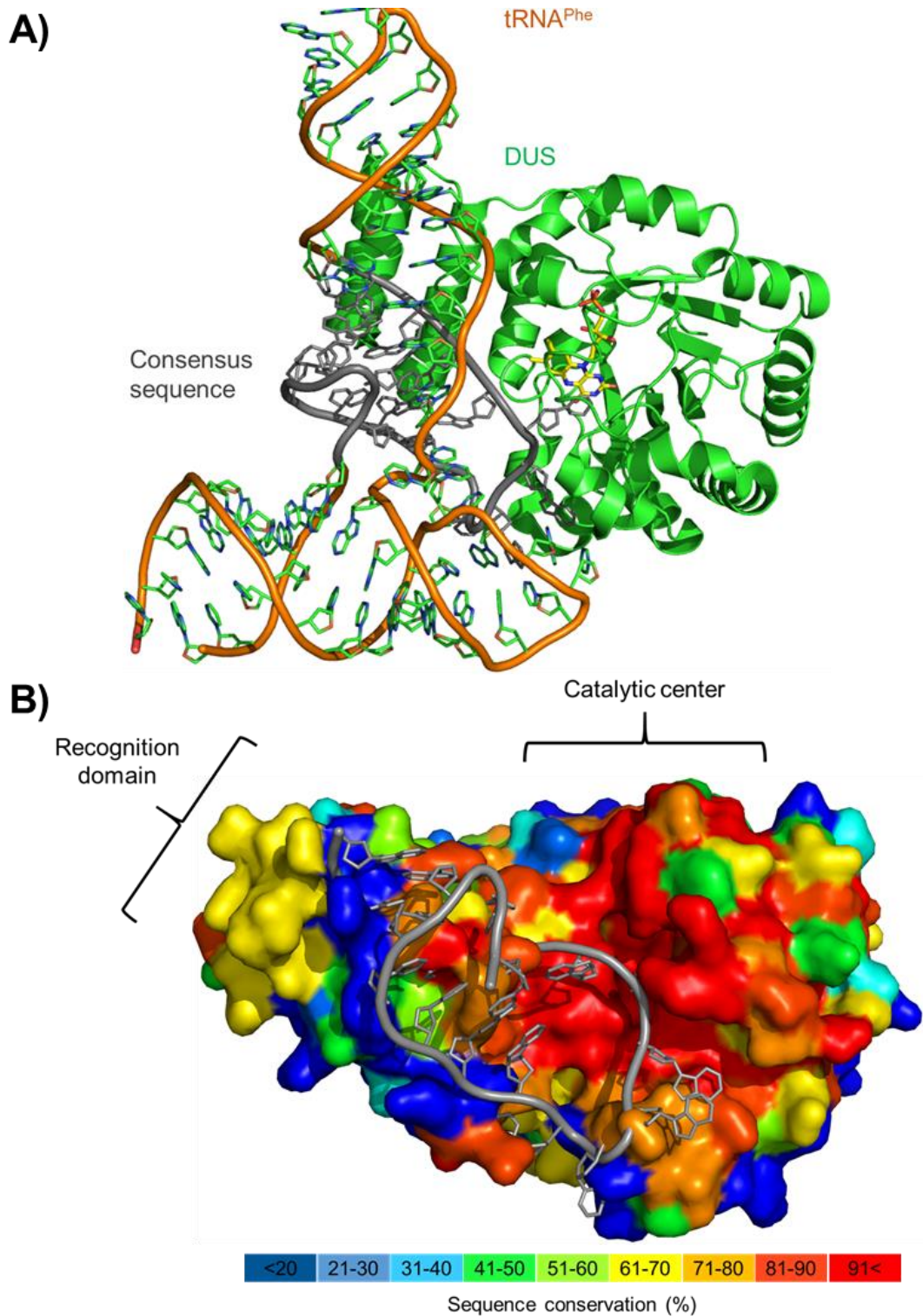


Figure 5.26. Structural regions of DUS necessary for recognition of their physiological target sequence. A) Crystal structure of the *T. thermophilus* DUS in complex with tRNA^{Phe}, PDB 3B0V, manipulated using PyMOL (Yu et al., 2011). The FMN cofactor (yellow) and ribonucleotide consensus sequence (grey) of DusN are highlighted. B) Surface representation of the DUS coloured by conservation of each residue as judged by alignment of the top 50 identical primary sequences. The ConSurf Server (Ashkenazy et al., 2010) rendered each amino acid based on its conservation strength and mapped it onto the 3D protein structure.

protein and nucleotides, the solved quaternary protein:RNA complex was studied (Figure 5.26A). Furthermore, the conservation of folded motifs was visualised by shading individual residues based on conservation strength (Figure 5.26B).

When the DusN consensus sequence was highlighted on the tRNA transcript in Figure 5.26A, it became apparent how this region serves as a recognition site for the enzyme. The target ribonucleotides are in contact with the FMN-containing active site which offers multiple interactions to ensure distinct uridine specificity, in addition to the C-terminal domain which is believed to act as a dsRNA-recognition domain (Whelan et al., 2015). Rendering of the folded protein scaffold based upon residue conservation highlighted conserved domains (Figure 5.26B). The catalytic center displays a strong red colour signifying high conservation, as expected, due to conserved catalytic residues. However, the C-terminal dsRNA-binding motif is not extremely preserved between distinct DUS. This domain variation could account for discrimination of highly similar tRNA compounds, enabling accurate targeting of a specific DUS to its cognate consensus sequence. Furthermore, we propose the separate subgroups of the DUS family exhibit greater dsRNA-binding domain conservation to recognise the same consensus sequence. This creates a molecular system where the dsRNA-binding region assigns the individual DUS members to their specific set of tRNA substrates to produce the desired cellular response, which is most likely similar across the bacterial kingdom.

From this chapter, we believe 5'-UAGCUCAGUUGGUAGAGCA-3' forms the consensus sequence for DusN to target tRNA^{Lys}_{UUU}, tRNA^{Phe}_{GAA} and tRNA^{Trp}_{CCA} for dihydrouridine formation during nitrogen-limiting conditions. This post-transcriptional modification ultimately leads to the multiple transcriptomic, proteomic and cellular effects upon various nitrogen-metabolic pathways observed throughout Chapter 4 and 5. Clearly, future work is required to fully understand the molecular link between tRNA-dihydrouridine synthesis and appropriate changes in translation, as discussed in Section 7.3

Chapter 6: Investigating NarJ as a Chaperone for Nitrate Reductases

6.1 Introduction

Whilst the previous chapters investigated regulatory requirements necessary for *nasABGHC* expression, a separate extension of this thesis was exploring maturation of active nitrate reductases. *P. denitrificans* expresses three functional, biochemically distinct nitrate reductases: NarG, NapA and NasC (Richardson et al., 2001). These are encoded at separate genomic loci and differentially expressed in response to various conditions (see Section 1.3.2). Two of these have active sites in the cytoplasmic compartment; the membrane-anchored NarGHI functions in anaerobic respiration (Betlach, 1982), and cytoplasmic NasC is involved in the incorporation of inorganic nitrogen into biomass (Pino et al., 2006; Ramos et al., 1993). Though NarG reduces nitrate in the cytoplasm, NarGHI draws the two electrons for nitrate reduction from the membrane-confined ubiquinol pool (Berks et al., 1995) whilst the Nas system obtains necessary electrons from the cytoplasmic NADH pool (Cammack, et al., 1982).

narG is part of the *narKGHJI* operon which encodes a nitrate/nitrite antiporter (NarK), the quinol:nitrate oxidoreductase NarGHI complex, and an assembly protein (NarJ). This system is induced by the homodimeric, [4Fe-4S]²⁺ isoform of FnrP in *P. denitrificans* under anaerobic conditions (Hutchings et al., 2002; Li & DeMoss, 1988). Nitrate reduction to nitrite is coupled to generation of a trans-membrane electrochemical potential for ATP synthesis and the nitrite generated is sequentially reduced to dinitrogen gas (as reviewed in Section 1.2.2) (Hochstein & Tomlinson, 1988).

The *nasC* gene belongs to *nasAHBGC* which encodes a nitrate/nitrite transporter (NasA), a nitrite transporter (NasH), an assimilatory nitrite reductase (NasB), a Rieske-type ferredoxin (NasG) and the assimilatory nitrate reductase (NasC). This system is expressed during nitrogen-limiting conditions as explored in Chapters 3 and 4. The nitrite produced from NasC is further reduced by NasB to ammonium which is subsequently incorporated into biomass via transamination reactions (Ramos et al., 1993).

Whilst both enzymes reduce nitrate to nitrite in the cytoplasm, they only share ~25% identity and NarG is much larger (~141 kDa) than NasC (~92 kDa). Despite this, both coordinate Fe-S clusters which shuttle electrons from the oxidation site to a bis-molybdopterin guanine dinucleotide (Mo[MGD]₂) active site cofactor for nitrate reduction, as exemplified by NarGHI in Figure 6.1.

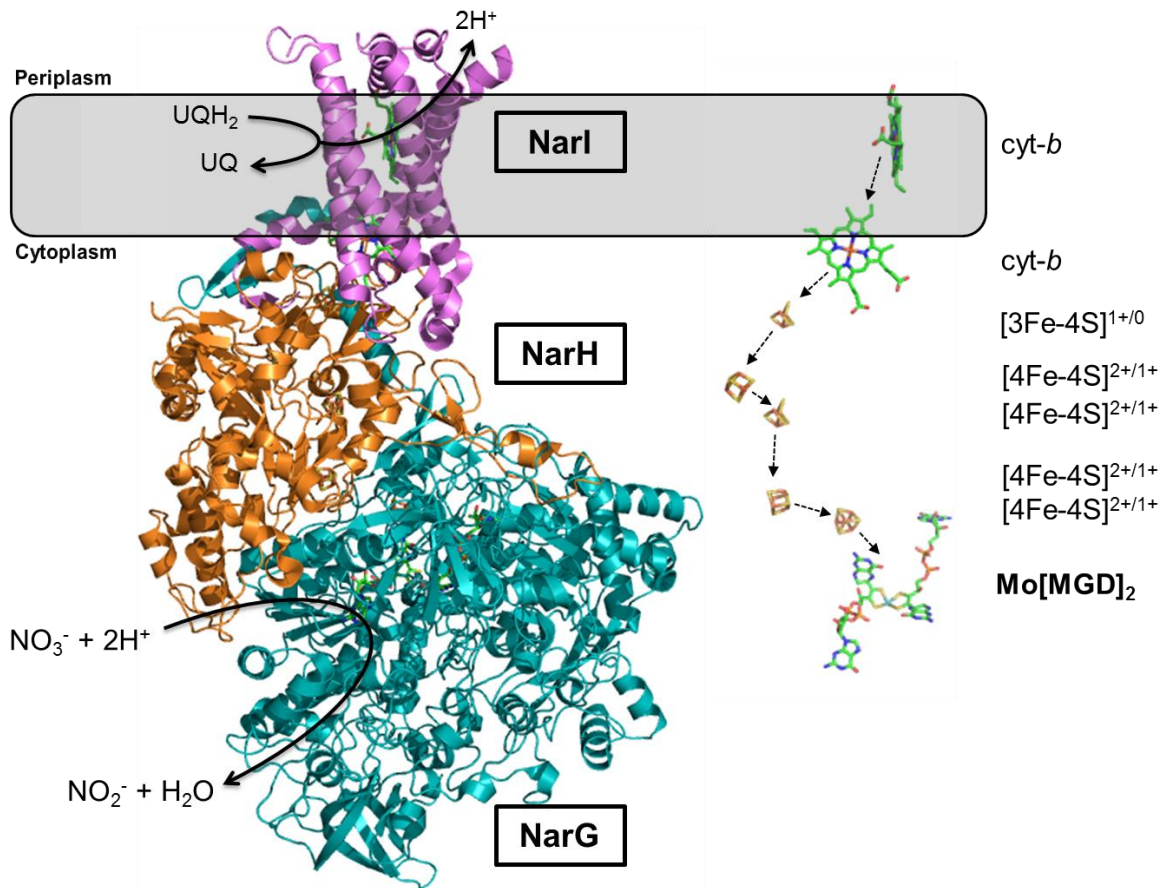


Figure 6.1. Crystal structure representing the cofactor architecture and electron movement in the NarGHI complex. The respiratory nitrate reductase complex, NarGHI, of *E. coli*. PDB-1Q16 (Bertero et al., 2003), modelled using PyMOL. Protein structures are displayed as cartoons and cofactors are shown as sticks. Dashed lines indicate electron movement, initiating with ubiquinol oxidation at the bi-heme NarI to move two protons across the membrane. Electrons subsequently are passed through a series of Fe-S clusters of NarH and NarG until they reach the Mo[MGD]₂ active site for cytoplasmic nitrate reduction.

The molybdenum atom is key for activity, making the insertion of Mo[MGD]₂ crucial. Post-translational folding and introduction of required cofactors is carried out by cytoplasmic chaperone proteins. Nitrate reductases are matured by redox enzyme maturation proteins (REMPs), a family of prokaryotic chaperones dedicated to biogenesis of complex iron sulfur molybdoenzymes (Bay et al., 2015; Turner et al., 2004).

In *P. denitrificans*, the dissimilatory nitrate reductase is encoded by *napABCDE* situated on the plasmid of the published genome (Pden_4719-23). Maturation of the NapABC ubiquinol:nitrate oxidoreductase complex requires the chaperone activity of NapD (Berks et al., 1995; Berks et al., 1994). This cytoplasmic protein is known to be the REMF of NapA and transient heterodimers of NapAD have been observed within the cytoplasm (Dow et al., 2014; Nilavongse et al., 2006). NapD aids formation of holoenzyme prior to its secretion as a folded complex into the periplasm (Natale et al., 2008).

It is known that maturation of the respiratory nitrate reductase, NarG, is performed by the REMF NarJ, a small cytoplasmic protein that doesn't form part of the final functional complex (see Section 1.8 for review). In *P. denitrificans*, *narJ* (Pden_4234) is situated in the *narKGHJI* gene cluster on chromosome II of the published genome, a genetic organisation conserved amongst NarG-encoding organisms. NarJ interacts with NarGH and matures the polypeptides prior to their association with NarI in the membrane to form the complete membrane-bound NarGHI complex (Blasco et al., 1998; Liu & DeMoss, 1997). NarJ is a member of the TorD subfamily of REMFs and displays strict sequence conservation across bacterial species.

Unlike the NAR and NAP systems, there is no gene that putatively encodes a REMF within the assimilatory *nas* gene cluster, and no other obvious candidates can be found in the genome. This poses the question of how the assimilatory nitrate reductase, NasC, forms a cytoplasmic holoenzyme complete with its two Fe-S clusters and Mo[MGD]₂ cofactor. Interestingly, global transcriptomic analysis reported *narJ* was majorly upregulated in *P. denitrificans* grown with nitrate as a sole nitrogen source when compared to ammonium, even in the presence of oxygen (Figure 1.12). Here, the possibility that NarJ is a uniquely dual-functional REMF, chaperoning maturation of both NarG and NasC during aerobic and anaerobic nitrate assimilation was explored.

6.2 Nitrate and Nitrite Reduction Capacity of *Paracoccus denitrificans* in Molybdenum-deplete Media

Initial experiments investigated the metabolic importance of molybdenum as the catalytic center for nitrate reduction under different growth conditions. *P. denitrificans* was grown

in minimal salt media supplemented with the standard Vishniac-Santer trace elements cocktail (Table 2.2) in which molybdenum is present at 1.8 μM (Mo-H) and in a medium in which a Vishniac-Santer solution was prepared containing no detectable molybdenum (Mo-L). Cultures were grown under nitrate-dependent and nitrite-dependent assimilatory and denitrificatory conditions. NasC is synthesised under aerobic nitrate assimilation for biomass production, whilst NarG is synthesised during anaerobicity for respiration.

As expected, *P. denitrificans* was capable of growing with nitrate as an end terminal electron acceptor, $\text{OD}_{\text{max}} \sim 0.9$, and as a sole nitrogen source to support biosynthesis of cellular material, $\text{OD}_{\text{max}} \sim 0.8$, when molybdenum was present in the media (Figure 6.2A and C respectively). Growth with nitrite in Mo-H conditions achieved comparable biomass formation and growth rates as recorded for nitrate. However, the absence of molybdenum in the media (Mo-L conditions) abolished growth in both metabolic modes when nitrate was used, where OD_{max} values of ~ 0.1 were recorded (Figure 6.2B and D). Nitrite was still used efficiently by the cells as a respiratory electron acceptor or a sole nitrogen source, observing an OD_{max} of ~ 0.8 for both conditions. Nitrite bypasses the molybdenum-requiring nitrate reductases and feeds directly into iron-dependent NirS in the denitrification pathway and the siroheme-containing NasB during assimilation.

This growth data indicates that the only step in denitrification and assimilation that is dependent on molybdenum at the concentrations studied are those catalysed by the two nitrate reductases, NarG and NasC. This points towards some efficiency of function if a mutual chaperone were available to mature these separate enzymes.

6.3 Expression of the *nar* Gene Cluster during Nitrate-Dependent Growth

The *P. denitrificans narKGHJI* gene cluster is known to be expressed under anaerobic conditions by the oxygen responsive FnrP regulator (Hutchings et al., 2002). By contrast, *nasAHBGC* is expressed under anaerobic or aerobic conditions in response to the cellular nitrogen status. In order for NarJ to chaperone the incorporation of Mo[MGD]₂ during aerobic synthesis of NasC, *narJ* expression would have to overcome the aerobic inactivation of the *narK* promoter. Previous microarray analysis highlighted the upregulation of *narJ* during aerobic nitrate-dependent growth (Figure 1.12) (Gates and coworkers, unpublished data). Intriguingly, inspection of the DNA region around the stop site of *narH* and the start site for *narJ* revealed that both a predicted promoter and ribosome binding site (RBS) are located immediately upstream of the *narJ* start ATG (Figure 6.3B). Expression of the *narKGHJI* genes was therefore investigated using qRT-PCR analysis on RNA harvested under a range of growth conditions (Figure 6.3A).

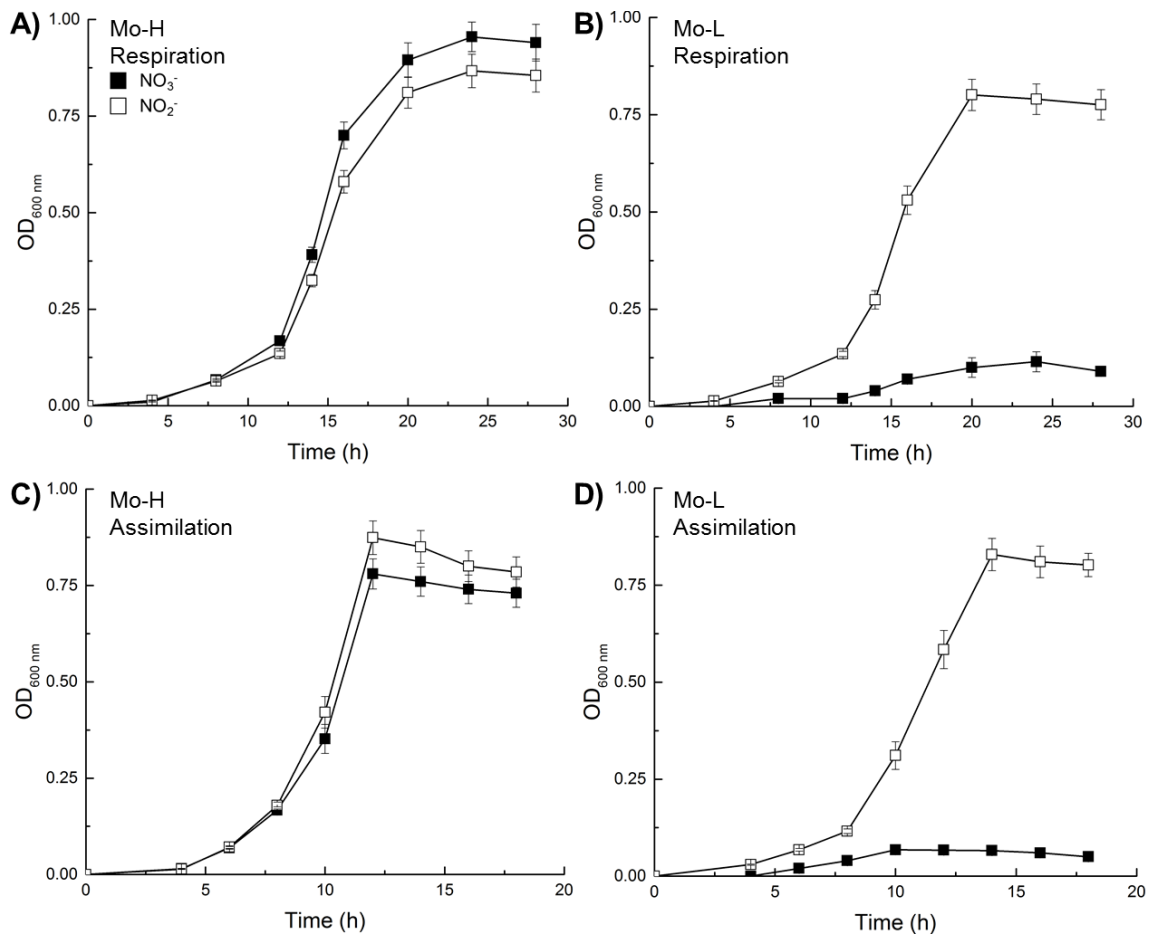


Figure 6.2. The involvement of molybdenum for nitrate-dependent growth in *P. denitrificans*. *P. denitrificans* was grown in batch cultures of minimal salt media supplemented with 30 mM succinate at 30 °C. A) and B) show anaerobic conditions with 10 mM ammonium as a nitrogen source, and 20 mM nitrate (black) or nitrite (white) as an electron acceptor for denitrification. C) and D) represent aerobic assimilation with 10 mM nitrate or nitrite as a lone nitrogen source. Cultures were supplemented with either a molybdenum containing (Mo-H) Vishniac-Santer solution (A and C) or molybdenum low (Mo-L) solution (B and D).

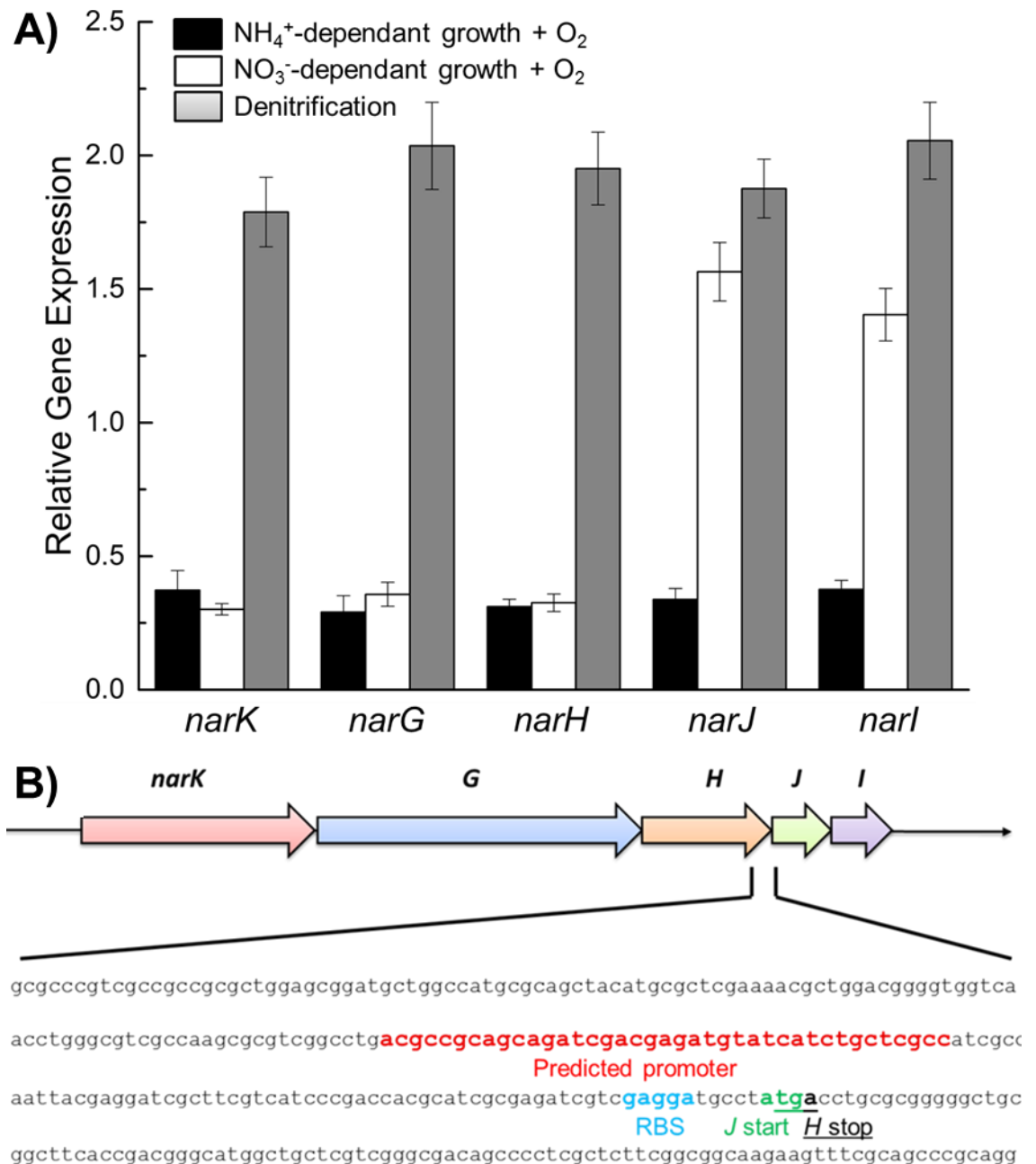


Figure 6.3. qRT-PCR investigation of *narKGHJI* expression in *P. denitrificans* during nitrate-dependent growth. A) *P. denitrificans* was grown in batch cultures of minimal salt media at 30 °C with 30 mM succinate. Aerobic growth was supplemented with 10 mM ammonium (black) or nitrate (white) as sole nitrogen sources. Denitrification was achieved anaerobically with 20 mM nitrate and 10 mM ammonium (grey). RNA was harvested at a mid-exponential phase and measured expression was made relative to *dnaN*. B) Bioinformatic analysis of the DNA around the end of *narH* and start of *narJ*. *narJ* start codon; green, *narH* stop codon; underlined, ribosome binding site (RBS); blue and predicted promoter; red. Promoter was predicted by Neural Network Promoter Prediction (*Fruitley*) with a score of 0.77.

As expected, qRT-PCR data indicated that *P. denitrificans* grown aerobically with ammonium as a sole nitrogen source expressed the *nar* gene cluster to a very low level, as the active FnrP homodimer dissociates in the presence of oxygen. This transcription drastically increased around 5-fold, to an expression value of ~2, during anaerobic growth by denitrification.

When grown aerobically under nitrate-dependent growth, and so requiring functional cytoplasmic NasC to support biomass synthesis, *narKGH* exhibited the same low level base expression as observed during ammonium-dependent aerobic growth. Notably though, *narJ* and *narI* were upregulated 4-fold compared to these conditions and reached comparable expression levels of ~2 to those observed under anaerobic nitrate-respiratory conditions (Figure 6.3A). This transcriptomic data concludes aerobic expression of *narJ* when *P. denitrificans* is cultured under nitrate-dependent growth, presumably from a specific promoter downstream of the anaerobically sensitive *narK* promoter. The transcription of *narJ* coinciding with a requirement for functional NasC points to a chaperone capacity for NarJ during both anaerobic and aerobic metabolism for maturation of NarG and NasC.

6.4 Construction of a *Paracoccus denitrificans* strain deficient in *narJ*

6.4.1 Assembling a suicide vector for gene deletion

To begin elucidating the involvement of NarJ towards maturation of the assimilatory nitrate reductase, a non-polar *narJ* deletion mutant of *P. denitrificans* was constructed (see Section 2.16 for details). Forward (5') and reverse (3') fragments of *narJ* were PCR-amplified and subsequently ligated into pK18*mobsacB* to construct suicide vector pBP011 (Figure 6.4). This plasmid was mobilised into *P. denitrificans* to produce a $\Delta narJ$ deletion strain via allelic exchange between plasmid and genome.

6.4.2 Nitrate- and nitrite-dependent respiratory growth of $\Delta narJ$

As NarG requires the chaperone capacity of NarJ, *P. denitrificans* deficient in *narJ* should be unable to use nitrate as an end-terminal electron acceptor. Strains were grown in minimal salt media under anaerobic conditions with a variety of inorganic nitrogen compounds for biomass formation and respiration (Figure 6.5).

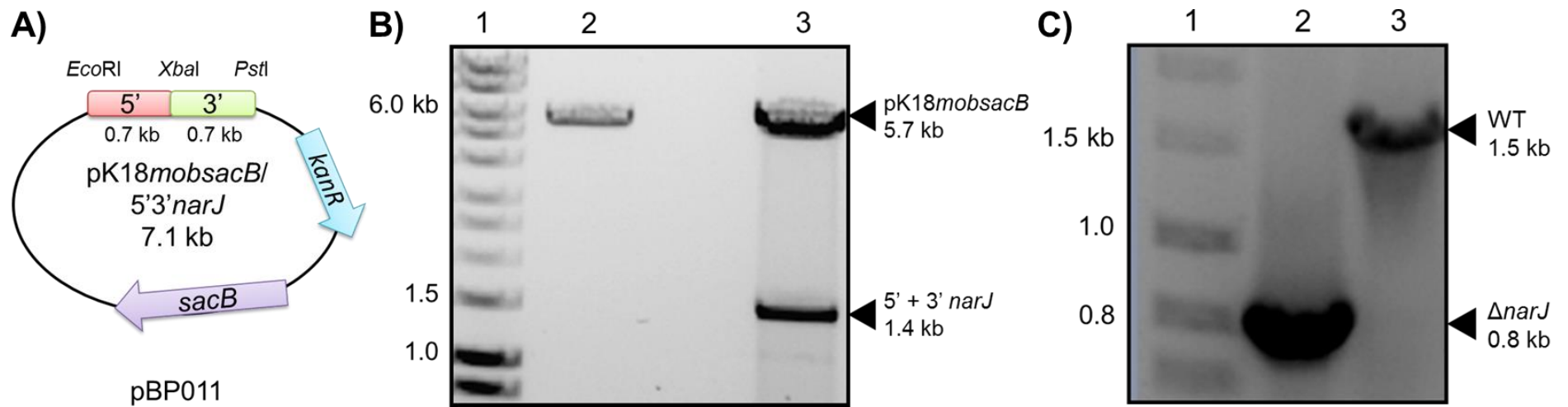


Figure 6.4. Cloning strategy for the genomic deletion of *narJ* from *P. denitrificans*. A) Suicide-vector pBP011, a *pK18mobsacB* derivative harbouring 5' and 3' fragments of *narJ* used for deletion. B) Digestion analysis of pBP011, lane 1; 1 kb Hyperladder, 2; *pK18mobsacB*, 3; *EcoRI/PstI* digestion of the 5'3' fragment. C) Colony MyTaq PCR confirmation for the removal of 0.7 kb section of genomic DNA coding for *narJ*. Lane 1; 1 kb Hyperladder, 2; $\Delta narJ$, 3; WT.

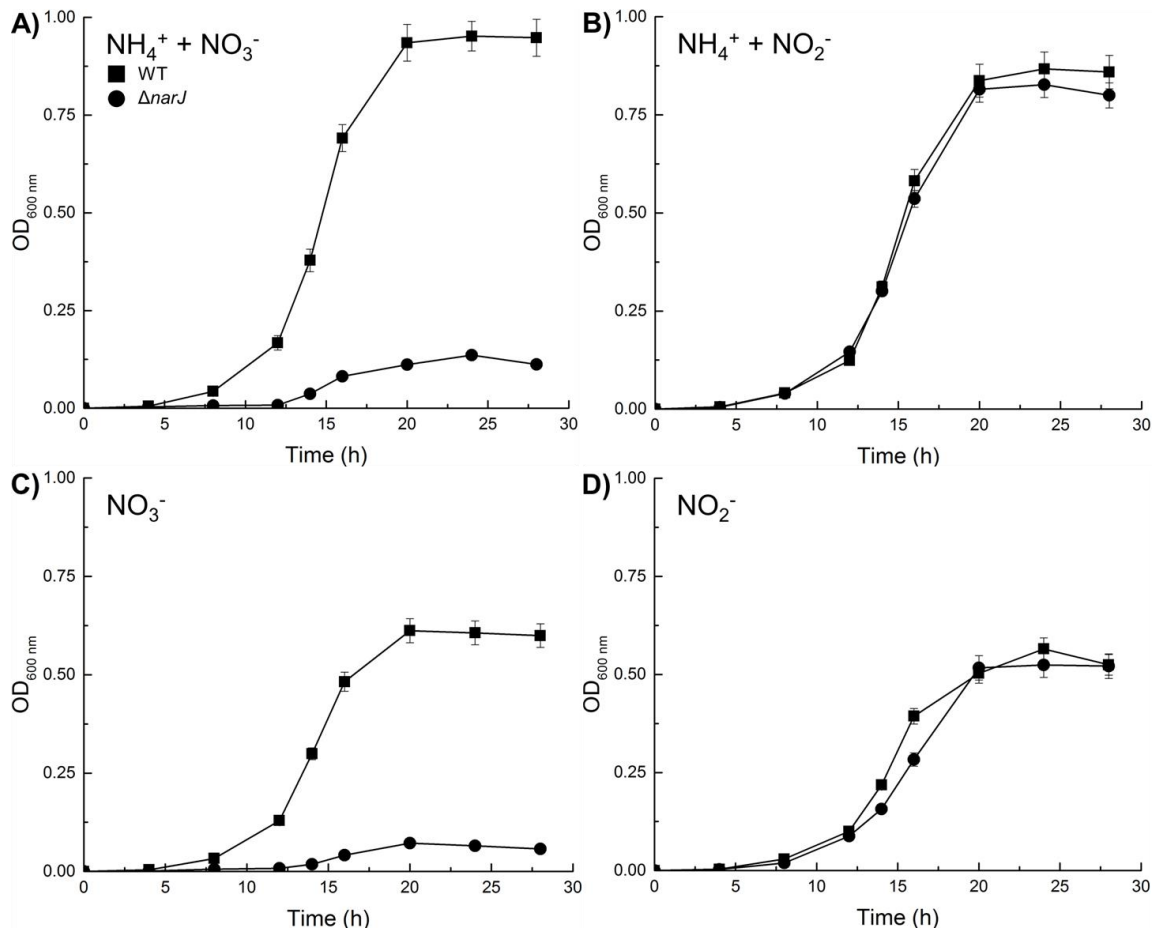


Figure 6.5. The impact of *narJ* deletion towards anaerobic growth of *P. denitrificans*. WT (squares) and $\Delta narJ$ (circles) were grown in anaerobic batch cultures of minimal salt media at 30 °C supplemented with 30 mM succinate as a carbon source. Cells were grown using various combinations of inorganic nitrogen sources and end-terminal electron acceptors; A) 10 mM ammonium and 20 mM nitrate, B) 10 mM ammonium and 20 mM nitrite, C) 30 mM nitrate or D) 30 mM nitrite.

Figure 6.5 demonstrates anaerobic growth with nitrite as a respiratory electron acceptor was not impaired in the *narJ* mutant, where both strains reached an OD_{max} value of ~0.9 at 20 h when ammonium was supplemented as a nitrogen source (Figure 6.5B). Whilst growth in both strains was still observed when using solely nitrite for both denitrification and biomass synthesis, it was clearly impaired as judged by OD_{max} values of ~0.6, a 30% decrease compared to before as the nitrite is required for both metabolic pathways (Figure 6.5D). The growth of $\Delta narJ$ with nitrite is consistent with the molybdenum studies in Figure 6.2, where nitrite bypasses the molybdenum-dependent nitrate reductases.

WT was capable of effectively growing with nitrate as an end-terminal electron acceptor when ammonium was supplemented for biosynthesis of organic nitrogenous material, achieving an OD_{max} 0.9 (Figure 6.5A). When cultures were supplemented solely with nitrate for both metabolic routes, the growth was attenuated to an OD_{max} 0.6, an effect discussed for nitrite above. However, the $\Delta narJ$ strain lost the capacity for anaerobic growth using nitrate as a respiratory electron acceptor (Figure 6.5A and C).

This observed phenotype is as predicted and in agreement with the literature as the loss of NarJ results in inactive NarG, where Blasco and coworkers reported a cytoplasmic accumulation of insoluble NarG polypeptides in NarJ deficient cells (Blasco et al., 1992).

6.4.3 Phenotyping $\Delta narJ$ growth during aerobic nitrate assimilation

The capacity of the $\Delta narJ$ strain to assimilate organic biomass using inorganic nitrate or nitrite as sole nitrogen sources via the Nas pathway was assessed. *P. denitrificans* strains were grown aerobically in minimal salt media supplemented with either ammonium, nitrate or nitrite as sole nitrogen sources (Figure 6.6).

Both strains achieved high levels of growth when using ammonium for biosynthesis of key cellular material, reaching OD_{max} values of ~0.9 at ~14 h (Figure 6.6A). Ammonium is a bioavailable inorganic nitrogen source and bypasses the Nas system. Additionally, both WT and $\Delta narJ$ could effectively use nitrite as a sole nitrogen source where they achieved comparable OD_{max} values of ~0.75. As discussed for the molybdenum data in Figure 6.2, nitrite enters assimilation downstream of the molybdenum-dependent nitrate reductase, and so NasC is not required for nitrite reduction to ammonium by NasB.

Importantly, the $\Delta narJ$ deletion strain was unable to grow aerobically using nitrate as a sole nitrogen source for biosynthesis of cellular material (Figure 6.6B). This data infers that NasC is inefficiently functioning and unable to catalyse nitrate reduction for assimilation. Furthermore, the lack of growth measured for nitrate-dependent aerobic

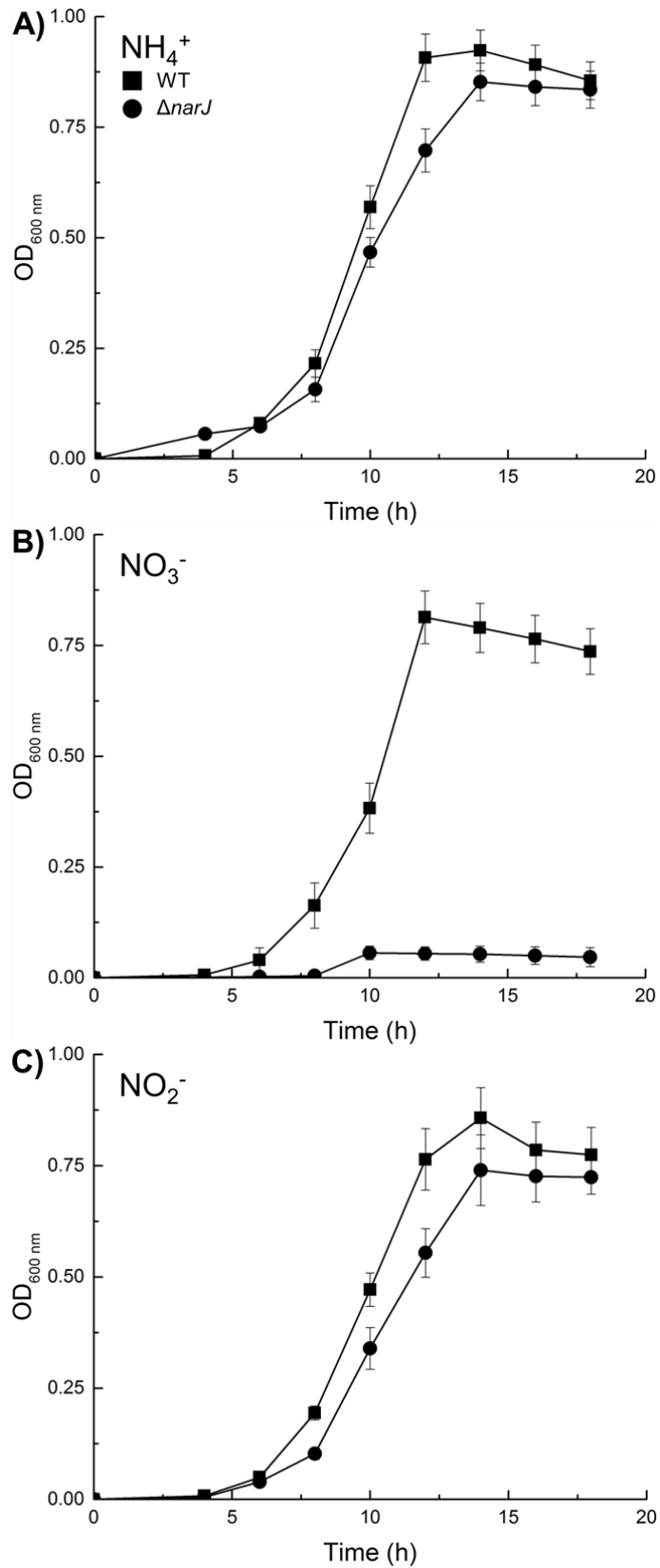


Figure 6.6. Aerobic growth phenotype of a $\Delta narJ$ mutant strain. WT (squares) and $\Delta narJ$ (circles) were grown aerobically in minimal media batch cultures at 30 °C with 30 mM succinate as a carbon source. Cells were supplemented with 10 mM of ammonium, nitrate or nitrite as a sole inorganic nitrogen source in panels A), B) and C), respectively.

conditions in media containing no detectable molybdenum is consistent with inactive NasC being attributable for the phenotype (Figure 6.2).

A similar phenotype of $\Delta narJ$ during nitrate-dependent anaerobic and aerobic growth supports the initial hypothesis that NarJ plays a role in maturation of both NarG and NasC. The loss of REMP to chaperone formation of these active nitrate reductases would account for the loss of nitrate respiration and nitrate assimilation (Figure 6.5A and 6.6B, respectively).

6.5 Genetic Restoration of the $\Delta narJ$ Mutant Strain

6.5.1 Constructing a *NarJ* expression system for $\Delta narJ$ complementation

To link the inability of nitrate-dependent growth with the loss of NarJ, the protein was introduced into the $\Delta narJ$ strain by expression from an ectopic promoter to attempt genetic restoration. The *narJ* gene from *P. denitrificans* was PCR-amplified and inserted into pLMB509 with *NdeI/NdeI* to construct overexpression vector pBP012 (Figure 6.7). The gene was cloned immediately downstream of a taurine inducible promoter to allow expression of recombinant NarJ by supplementing growth media with taurine. Additionally, *narJ* was cloned *NdeI/NdeI* into pLMB509 without a stop codon to produce pBP030 which results in incorporation of a C-terminal 6His tag in the recombinant protein for use in purification, discussed later (Section 6.7).

6.5.2 Restoration of nitrate-dependent growth in $\Delta narJ$

Following construction and sequence confirmation, pBP012 was conjugated into $\Delta narJ$ to test if anaerobic and aerobic nitrate-dependent growth could be restored using a recombinant NarJ acting *in trans*. WT, $\Delta narJ$ and *complement* ($\Delta narJ$ + pBP012) were grown under denitrifying and assimilatory conditions in the presence of taurine.

Figure 6.8A displays growth of the strains during nitrate-dependent respiration where *complement* was capable of using nitrate as an end-terminal electron acceptor when NarJ was expressed. This strain achieved an $OD_{max} \sim 0.75$ after 24 h and consumed the complete 20 mM of supplemented nitrate as revealed by HPLC analysis of the external nitrate concentration (Figure 6.8B). This significant increase in cell growth compared to the lack observed for $\Delta narJ$ concludes nitrate reduction by NarG has been recovered following introduction of NarJ.

Importantly, nitrate assimilation and associated nitrate consumption was recovered when the *narJ* gene was re-introduced and expressed in the deletion strain (Figure 6.8C

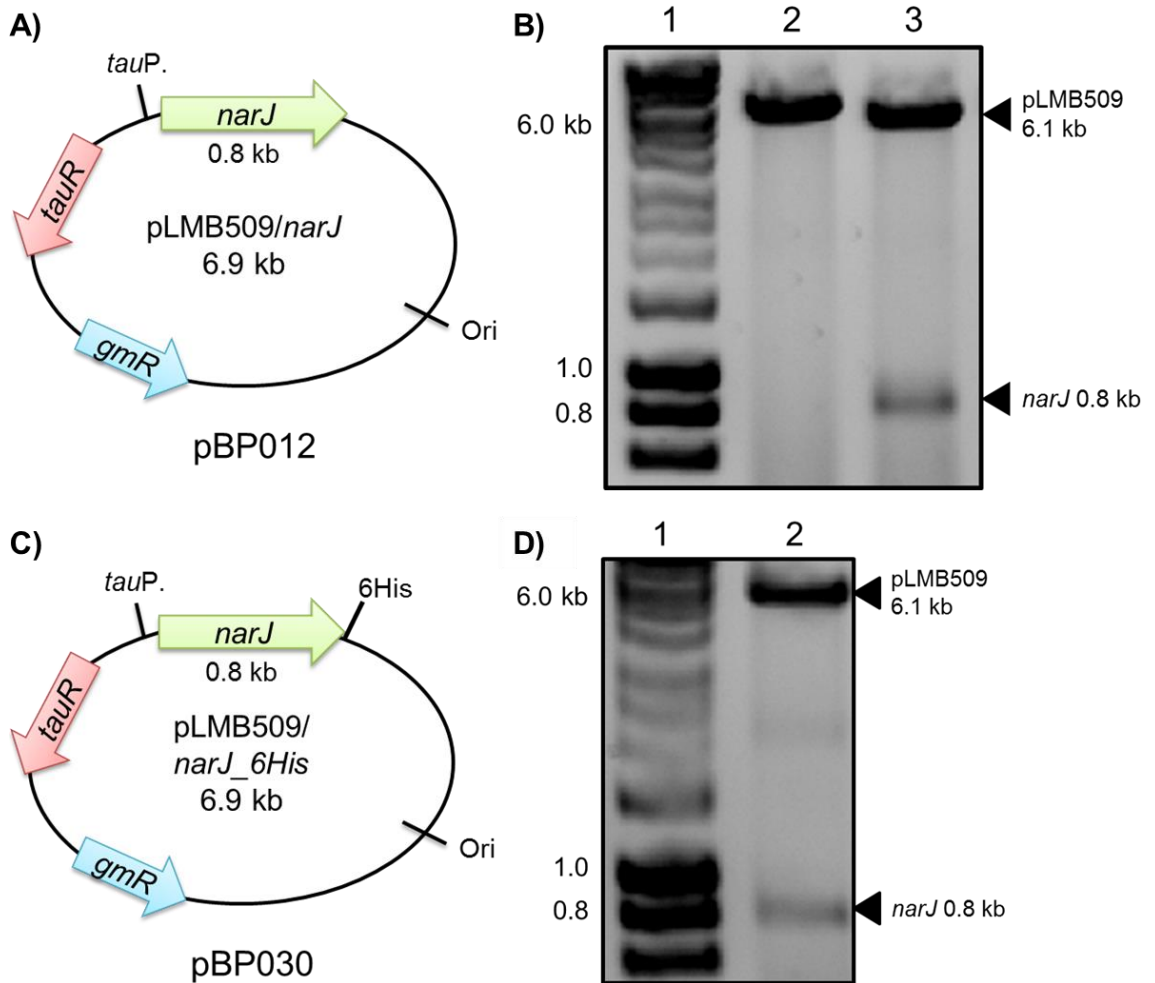


Figure 6.7. Cloning procedure for distinct pLMB509-derived, NarJ expression vectors. A) Diagram depicting pBP012, a pLMB509-derivative containing a copy of *P. denitrificans narJ* inserted at an *NdeI* cut site for genetic complementation of $\Delta narJ$. B) Agarose gel analysis of the pBP012 vector. Lane 1; 1 kb Hyperladder, 2; pLMB509 cut with *NdeI*, 3; *NdeI* digestion of pBP012 to release the *narJ* fragment (0.8 kb). C) pBP030, a pLMB509-derivative containing a copy of *P. denitrificans narJ* inserted at an *NdeI* cut site without a stop codon to incorporate a plasmid-borne C-terminal 6His-tag. D) Agarose gel analysis of pBP030. Lane 1; 1 kb Hyperladder, 2; *NdeI* digestion of pBP030 to release the *narJ* fragment (0.8 kb) from pLMB509 (6.1 kb).

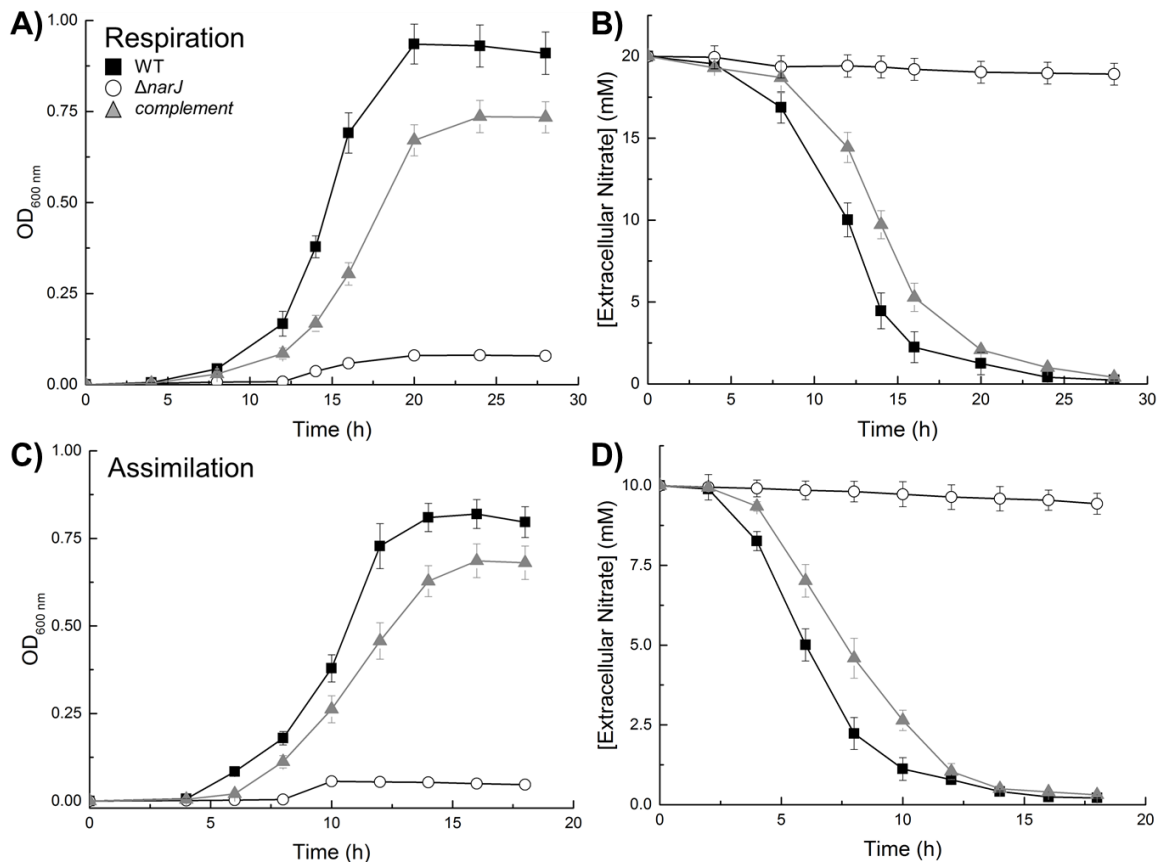


Figure 6.8. Genetic complementation of the $\Delta narJ$ strain during nitrate-dependent growth. WT (black), $\Delta narJ$ (white) and *complement* (grey, $\Delta narJ$ + pBP012) were grown in minimal salt media batch cultures at 30 °C with 30 mM succinate and 1 mM taurine to induce NarJ expression off pBP012. A) Denitrification was performed anaerobically with 10 mM ammonium as a nitrogen source and 20 mM nitrate as an electron acceptor. C) Aerobic nitrate assimilation with 10 mM nitrate as a lone nitrogen source. B) and D) display HPLC analysis of the external nitrate concentrations recorded for A) and C), respectively.

and D, respectively). The ability to grow aerobically using nitrate as a sole nitrogen source was fully recovered as observed by an $OD_{max} \sim 0.65$ by 15 h. Growth of *complement* both anaerobically and aerobically only achieved $\sim 80\%$ of the OD_{max} value recorded for WT. This is possibly due to the use of 1 mM taurine to stimulate *narJ* expression instead of the recommended 10 mM, which would have been used by the cells as a carbon and nitrogen source, hence 1 mM was selected.

Despite this, Figure 6.8 clearly demonstrated that reintroduction of NarJ in the $\Delta narJ$ strain restored the cultures ability to use nitrate as an end-terminal electron acceptor and a sole nitrogen source for biosynthetic pathways. This reinstated biological nitrate reduction is consistent with formation of functional NarG and NasC for catalysis which appears to be dependent upon the presence of cellular NarJ.

6.6 Catalytic *in vitro* Nitrate and Nitrite Reductase Assays

Following growth analysis, metabolic phenotypes were examined by directly assessing the levels of active nitrate and nitrite reductase synthesised in WT and $\Delta narJ$. This was achieved using colourimetric assays with reduced methyl viologen (MV) (NarG and NirS) or NAHD (NasC and NasB) as the artificial electron donors for nitrate and nitrite reduction. Enzyme assays were performed on cell extracts of cultures grown under appropriate nitrite-dependent conditions and rates of reactions for impure enzymes with saturating substrate concentrations (1 mM MV, 100 μ M NADH and 1 mM NO_3^-/NO_2^-) are given in Table 6.1.

6.6.1 Methyl-Viologen enzyme assays to measure NarG catalysis

MV is a commonly used redox indicator for monitoring enzyme activity due to changes in the UV-visible wavelength spectra exhibited by its various oxidation states. This compound acts as an *in vitro* electron donor for NarG to reduce nitrate to nitrite, during which it is oxidised from MV^{1+} to MV^{2+} and turns colourless to deep blue/violet as it gains a peak absorbance at 600 nm (see Section 2.32.2 for details).

P. denitrificans strains were grown under anaerobic conditions with nitrite as a respiratory electron acceptor to upregulate expression of genes involved in denitrification. Once at a mid-exponential phase, cells were lysed to expose the cytoplasmic-facing active site for MV access, as it cannot permeate the inner cell membrane (Jones et al., 1976). The *in vitro* assays were performed by addition of MV^{1+} and either nitrate or nitrite to observe activity of NarG and NirS, respectively.

The MV:nitrite-reductase profiles were comparable in both WT and $\Delta narJ$ cell extracts, where large decreases in the $Ab_{600\text{ nm}}$ were recorded following substrate addition,

consistent with reaction turnover (Figure 6.9B). As discussed for the above data, NirS does not require NarJ and is active in its absence, where nitrite reductase activities of $\sim 400 \text{ nmol}\cdot\text{min}^{-1}\cdot\text{mg protein}^{-1}$ were calculated here for all strains.

By contrast, the nitrate reductase activity (NarG) was abolished in the *narJ* deletion strain ($<10 \text{ nmol}\cdot\text{min}^{-1}\cdot\text{mg protein}^{-1}$) compared to WT ($\sim 700 \text{ nmol}\cdot\text{min}^{-1}\cdot\text{mg protein}^{-1}$), where the trace assumed the same trend as the negative buffer control. As predicted, the absence of NarJ results in a loss of active respiratory nitrate reductase and supports its known role in maturation of NarG. The nitrate reductase activity was reinstated in the *narJ* complemented strain when recombinant NarJ was expressed from the ectopic promoter, where a large absorbance decrease was recorded and quantified as a comparable rate to WT ($\sim 650 \text{ nmol}\cdot\text{min}^{-1}\cdot\text{mg protein}^{-1}$). This metabolic phenotype is consistent with the previous growth data.

6.6.2 NADH catalytic assays for monitoring NasC activity

Direct assays of the assimilatory nitrate and nitrite reductase activities (NasC and NasB) were conducted using NADH as the electron donor in soluble extracts prepared from cells grown under aerobic conditions with nitrite as the sole nitrogen source. The presence of oxygen represses *narG* expression (as validated by qRT-PCR data in Figure 6.3) and neither NarG or NapA can use NADH as an electron donor, ensuring measured NADH-dependent nitrate reduction is due to NasC.

Figure 6.10 displays the catalytic activity of NasC and NasB in WT and $\Delta narJ$ strains, where an identical metabolic phenotype was observed as compared to NarG and NirS in Figure 6.9. The NADH:nitrite reductase (NasB) activity profile was similar in the WT and $\Delta narJ$ strains with a quantified activity of $\sim 30 \text{ nmol}\cdot\text{min}^{-1}\cdot\text{mg protein}^{-1}$ (Figure 6.10B).

By contrast, the WT NADH:nitrate reductase (NasC) activity ($\sim 13 \text{ nmol}\cdot\text{min}^{-1}\cdot\text{mg protein}^{-1}$) was lost in the soluble extract prepared from $\Delta narJ$, but fully recovered when *narJ* was expressed *in trans* in the mutant strain (Figure 6.10A). This data therefore directly linked NarJ with the presence of fully functional assimilatory nitrate reductase in the cytoplasm as hypothesised.

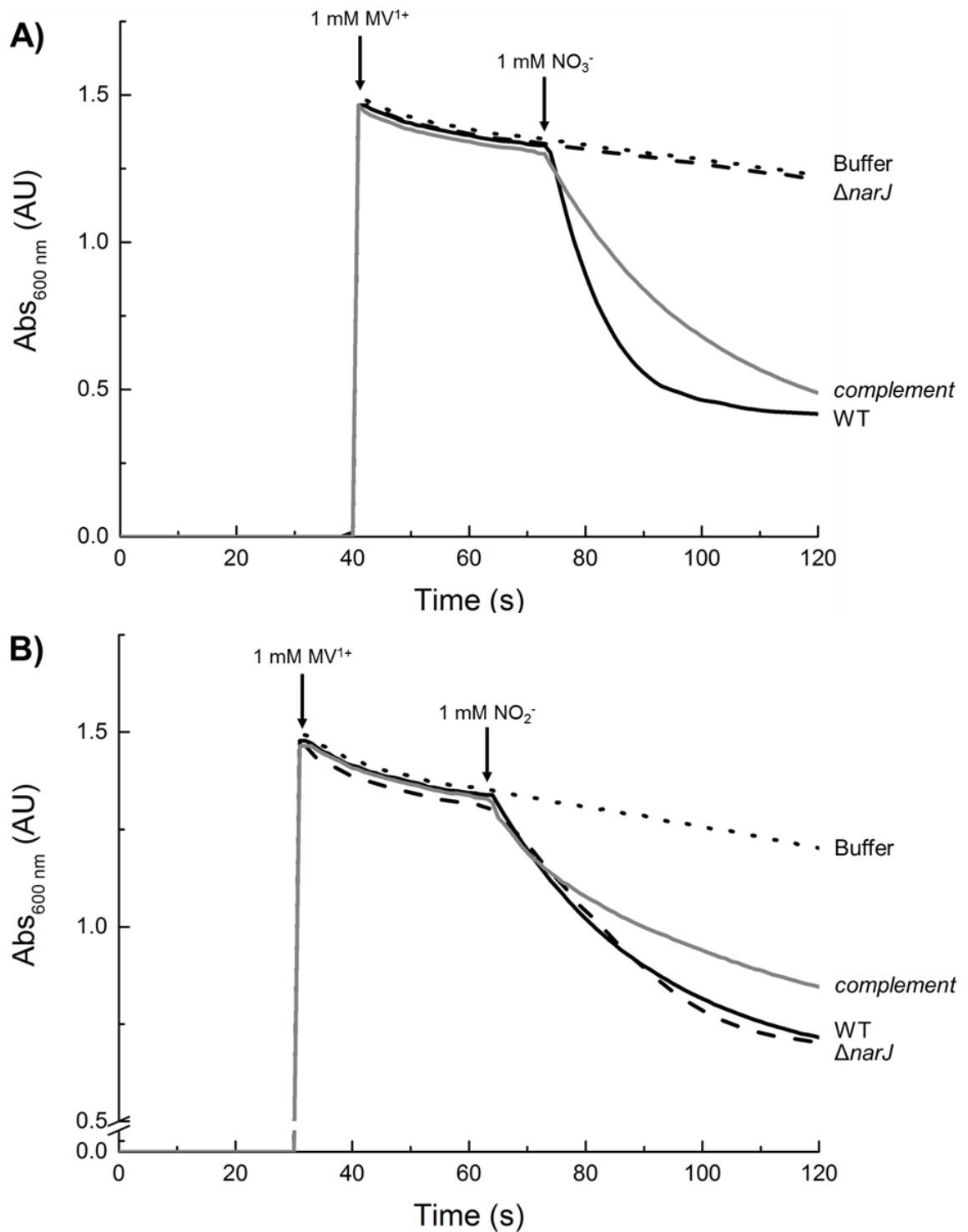


Figure 6.9. MV-dependent assays to monitor the respiratory nitrate and nitrite reductase in *P. denitrificans* strains. WT (solid line), $\Delta narJ$ (dashed line) and *complement* (grey) were grown anaerobically in minimal media at 30 °C with 30 mM succinate, 20 mM nitrite, 10 mM ammonium and 1 mM taurine to stimulate plasmid-borne NarJ expression in *complement*. Cells were lysed in a buffer of 20 mM HEPES, 150 mM NaCl, pH 7.5. 1 mL lysate was placed in a cuvette followed by 1 mM MV¹⁺ and 1 mM nitrate (panel A) or nitrite (panel B). Reactions were monitored at 600 nm over time and performed on a buffer (dotted line) control.

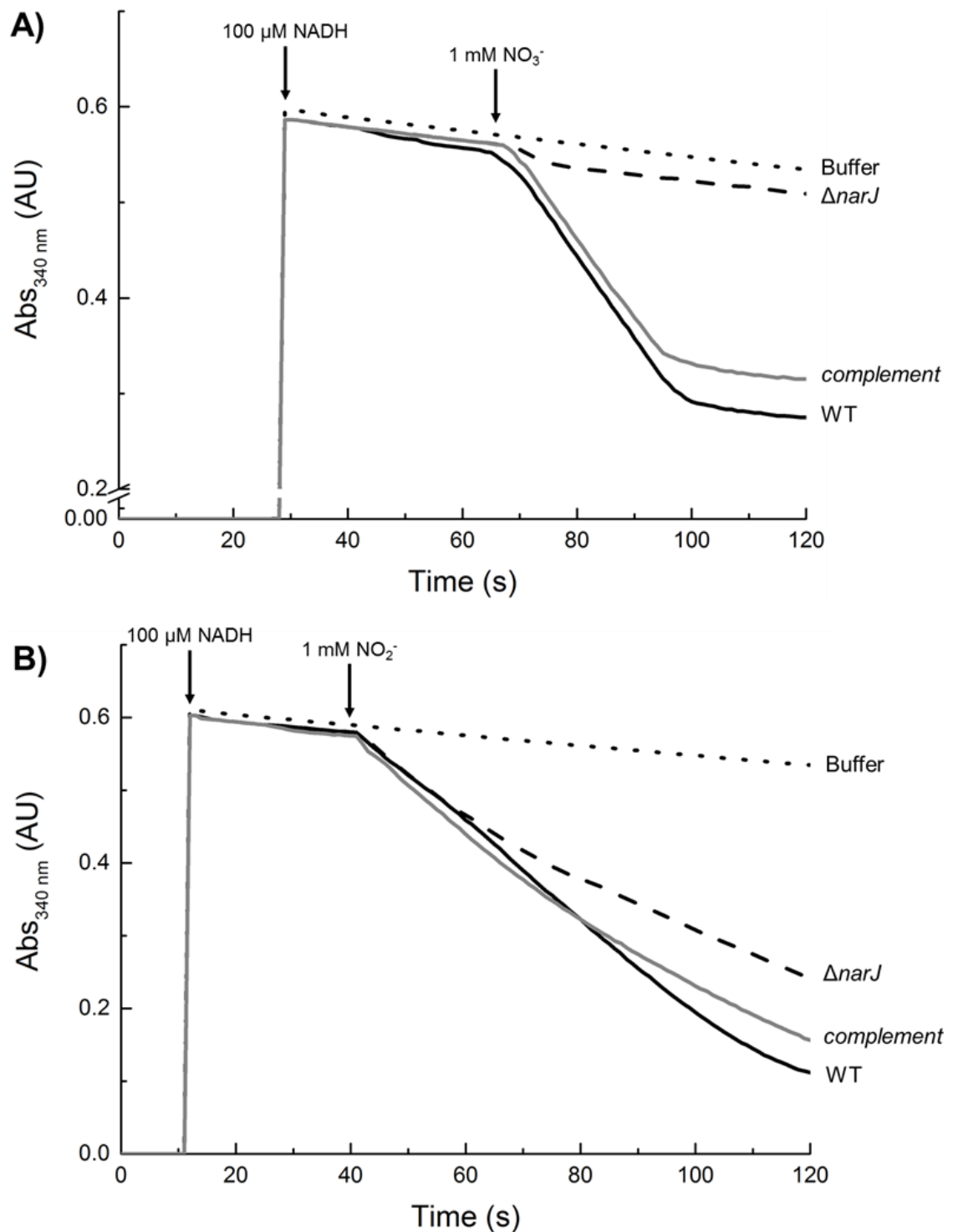


Figure 6.10. Colourimetric NADH assays to investigate a NarJ requirement for maturation of the assimilatory nitrate reductase. WT (solid line), $\Delta narJ$ (dashed line) and *complement* (grey) were grown aerobically in minimal media at 30 °C with 30 mM succinate, 10 mM nitrite as a sole nitrogen source and 1 mM taurine for NarJ expression in *complement*. Cells were lysed in a buffer of 20 mM HEPES, 150 mM NaCl, pH 7.5. 1 mL cell lysate was placed in a cuvette followed by 100 μ M NADH and 1 mM nitrate (panel A) or nitrite (panel B). Reactions were monitored at 340 nm over time and performed on a buffer (dotted line) negative control.

Table 6.1. Reduced MV- and NADH-dependant nitrate and nitrite reductase activities of *P. denitrificans* strains.

Strain	Electron Acceptor	Electron Donor	
		MV ¹⁺	NADH
WT	NO ₃ ⁻	727 ± 36	13 ± 3
	NO ₂ ⁻	391 ± 18	34 ± 4
<i>ΔnarJ</i>	NO ₃ ⁻	n.d.	n.d.
	NO ₂ ⁻	374 ± 19	27 ± 3
<i>complement</i>	NO ₃ ⁻	654 ± 33	11 ± 2
	NO ₂ ⁻	356 ± 18	31 ± 4

Activity was measured in nmol.min⁻¹.mg protein⁻¹. n.d., not detectable.

Table 6.1 above contains the quantified reaction velocities for impure NarG, NirS, NasC and NasB in soluble cell extracts with the appropriate electron donor and nitrogen compound. The values recorded for the Nas pathway are consistent with those previously reported for NasC and NasB, ~13 and ~35 nmol.min⁻¹.mg protein respectively, from *P. denitrificans* lysate with NADH as an electron donor (Gates et al., 2011). Nitrite reductase functions with a rate ~3-fold greater than nitrate reductase which is in agreement with the electron stoichiometry of each reduction, i.e. 2e⁻/NO₃⁻ and 6e⁻/NO₂⁻. In contrast, reaction velocities for the denitrification proteins were far greater than the assimilatory apparatus, as is usual for respiratory enzymes which function at high rates of reaction. Furthermore, the value of NarG recorded here is approximately double that for NirS, ~700 and ~400 nmol.min⁻¹.mg protein⁻¹, consistent with the electron stoichiometry of these reactions, i.e. 2e⁻/NO₃⁻ and 1e⁻/NO₂⁻.

Taken together, the metabolic data in this section demonstrated synthesis of active NarG or NasC is dysfunctional in the absence of NarJ and implements a role for this molecular REMP in biogenesis of these nitrate reductases.

6.7 Overexpression and Purification of Recombinant NarJ

To visualise and characterise contacts between the molecular chaperone and nitrate reductase targets, pure NarJ was required for interaction studies. An overexpression system was constructed by cloning the *narJ* gene of *P. denitrificans* into pLMB509 at *NdeI/NdeI* cut sites to produce expression vector pBP030 (Figure 6.7C). This method placed *narJ* immediately downstream of a taurine inducible promoter and was designed to incorporate a C-terminal 6His-tag into the recombinant protein sequence to ease the purification procedure.

Following sequencing, the plasmid was conjugated into *P. denitrificans* where taurine supplementation in the growth media stimulated overexpression of NarJ_6His. Target protein was purified by loading the soluble cell extract of lysed cultures onto a Ni²⁺-IMAC column and applying a linear imidazole gradient to disrupt 6His:Ni²⁺ interactions and remove tightly bound proteins (see Section 2.22.1 for methodology).

Figure 6.11A shows a representative elution profile from an IMAC column loaded with *P. denitrificans* soluble extract containing 6His_DusN which monitored the absorbance at 280nm. Initially, the imidazole concentration was low and the majority of cytoplasmic proteins were removed over the first 10 mL wash. The imidazole concentration gradually increased overtime in a linear manner to reach 500 mM after 90 mL buffer had been applied. NarJ_6His eluted from the column at ~250 mM imidazole as observed by the minor raise in Abs_{280 nm} between 50 and 60 mL on the trace.

The SDS-PAGE gel image presented in Figure 6.11B contained a sample of this eluted region and shows the presence of a single band between 25 and 37 kDa markers, consistent with monomeric NarJ_6His at 28 kDa. Western-blot analysis using an anti-6his antibody and conjugated HRP visualised a chemiluminescent signal corresponding specifically to this region, indicating a 6His-tagged protein. The band was excised and sent for MALDI-TOF MS which reported it as NarJ of *P. denitrificans* with a Mascot value of 183 and sequence coverage of 67 % (Table 2.12).

As observed here, pLMB509 vectors do not generate high quantities of recombinant protein compared to the pET- overexpression systems which are specifically tailored for this purpose (see Section 5.2). In addition, *P. denitrificans* is not engineered for protein expression like various *E. coli* strains, i.e. BL21 (DE3), used for DusN overexpressed. These facts account for the relatively low yield of NarJ visualised in the SDS-gel compared to that seen for DusN in Section 5.2.2. However, this system does enable purification of NarJ_6His in one chromatographic step to enable downstream studies.

6.8 NarJ Pull-Down Assays to Isolate and Identify Binding Partners

The growth and metabolic phenotypes of $\Delta narJ$ suggested a role for NarJ in the assembly of active NarG and NasC during appropriate conditions. To assess the molecular interaction between NarJ and these nitrate reductases, binding assays were performed to capture transient contacts (see Section 2.36 for detailed methodology).

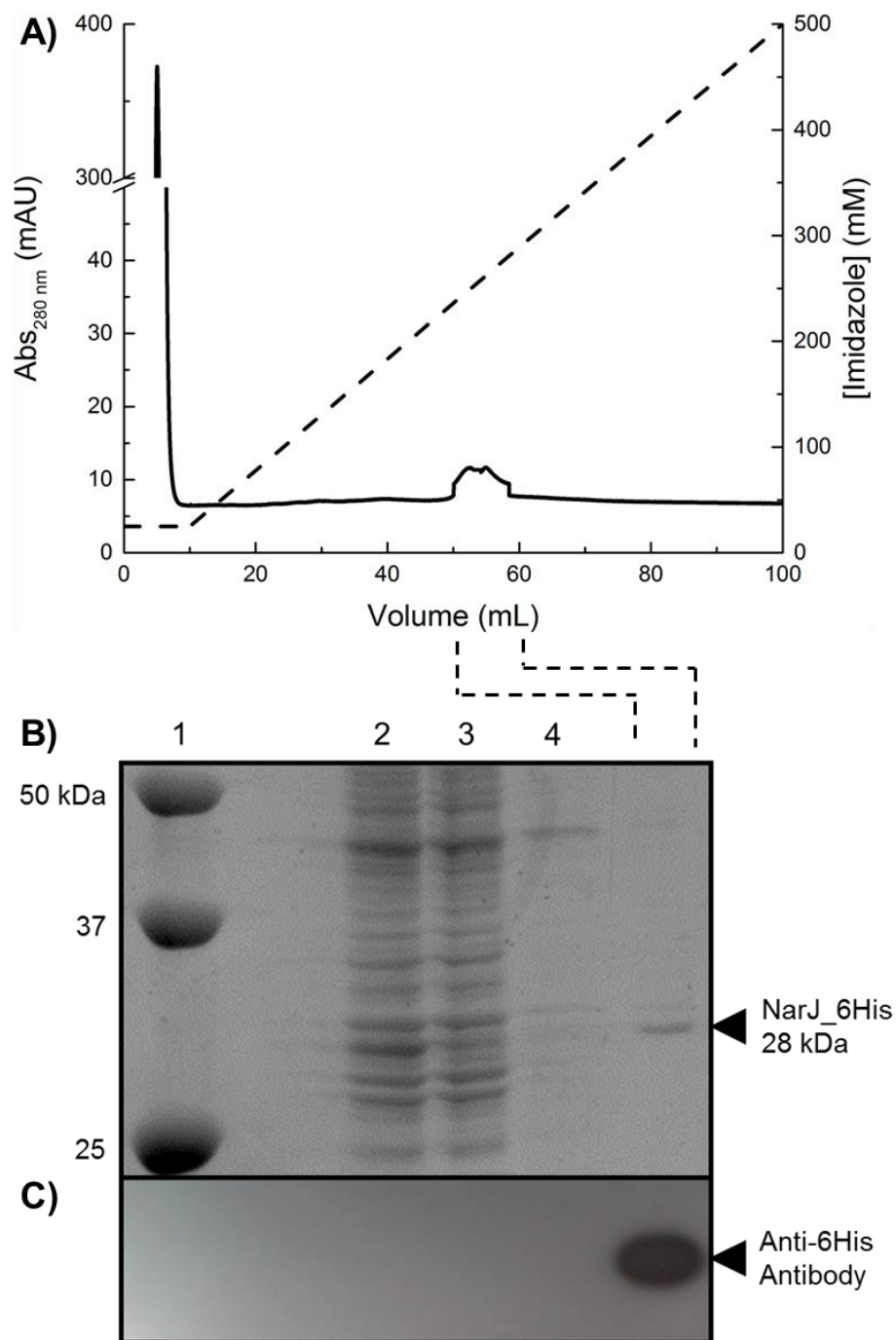


Figure 6.11. Purification of recombinant NarJ_6His from *P. denitrificans*. A) Chromatogram for Ni²⁺-IMAC column purification. Abs_{280 nm}; black, concentration of imidazole; dotted. Cell lysate was loaded onto a column charged with Ni²⁺ and washed with buffer A (20 mM HEPES, 150 mM NaCl, 25 mM imidazole, pH 7.5). A linear gradient from 0-100% buffer B (buffer A with 500 mM imidazole) was applied to remove NarJ_6His. B) SDS-PAGE analysis of the purification. Lane 1; Precision Plus Protein™ dual colour standard, 2; cell lysate, 3; buffer A rinse. Dotted lines indicate the area of the trace which were pooled together into one sample and loaded onto the gel. Pure NarJ_6His was visualised at ~28 kDa. C) Corresponding semi-dry western-blot analysis of the gel using an Anti-6His antibody conjugated with a horseradish peroxidase to chemiluminescently identify 6His-tagged proteins.

Briefly, NarJ_6His was immobilised on magnetic molecular sepharose beads charged with Ni²⁺ which function with the same principle as a Ni²⁺-IMAC column. These NarJ-beads were subject to soluble cell extracts prepared from *P. denitrificans* grown under aerobic ammonium-dependent and nitrate-dependent conditions. Should NarJ interact with any target molecules in the cytoplasmic compartment, it would be retained throughout the low imidazole washes and co-elute with NarJ following a high imidazole exposure. In addition to the native extracts, separate samples were heat treated prior to incubating with immobilised NarJ. Chaperones typically recognise specific secondary epitopes in the partially unfolded state of their target protein to help correctly fold them. Heat treatment of cell lysate promoted protein unfolding to potentially aid formation of NarJ target sequences. NarJ_6His and bound material was released from the beads following the high imidazole wash and size-resolved using SDS-PAGE (Figure 6.12).

Control experiments in which the NarJ-beads were exposed to water rather than cell extracts confirmed that the pure NarJ_6His was released from the beads with high imidazole exposure. In non-heat treated samples, weak non-specific binding to the beads was observed, as judged by the presence of multiple bands. This is most likely due to the low concentration of NarJ coating the sepharose beads which therefore offer many vacant sites for coordination of cellular proteins. This observation was lost following heat treatment of lysate due to disruption of protein tertiary structure and interference of any negatively charged domains binding the Ni²⁺.

Instead, in these heat-treated cell extract samples, a strong band ~92 kDa was retained by NarJ-beads from the cytoplasm of cells grown by nitrate assimilation that was absent in ammonium-dependent cultures, where *nasC* is not expressed. This band was excised and sequenced via MALDI-TOF MS analysis which confirmed it as NasC (Significance score = 139, coverage = 49%, E = 3.4 x 10⁻¹⁰). This result demonstrated the ability of the NarJ chaperone to tightly and specifically interact with the assimilatory nitrate reductase.

To further explore this broader chaperone nature of NarJ for molybdenum-dependant nitrate reductases, *P. denitrificans* was grown anaerobically with 20 mM nitrate as an end-terminal electron acceptor and a further 10 mM nitrate as a sole nitrogen source. This growth condition stimulated denitrification and nitrate assimilation simultaneously in the cultures, leading to both *narG* and *nasC* expression. The harvested cell lysate was heat treated as before and subject too NarJ-beads in a bid to capture chaperone interactions with both nitrate reductases concurrently (Figure 6.13).

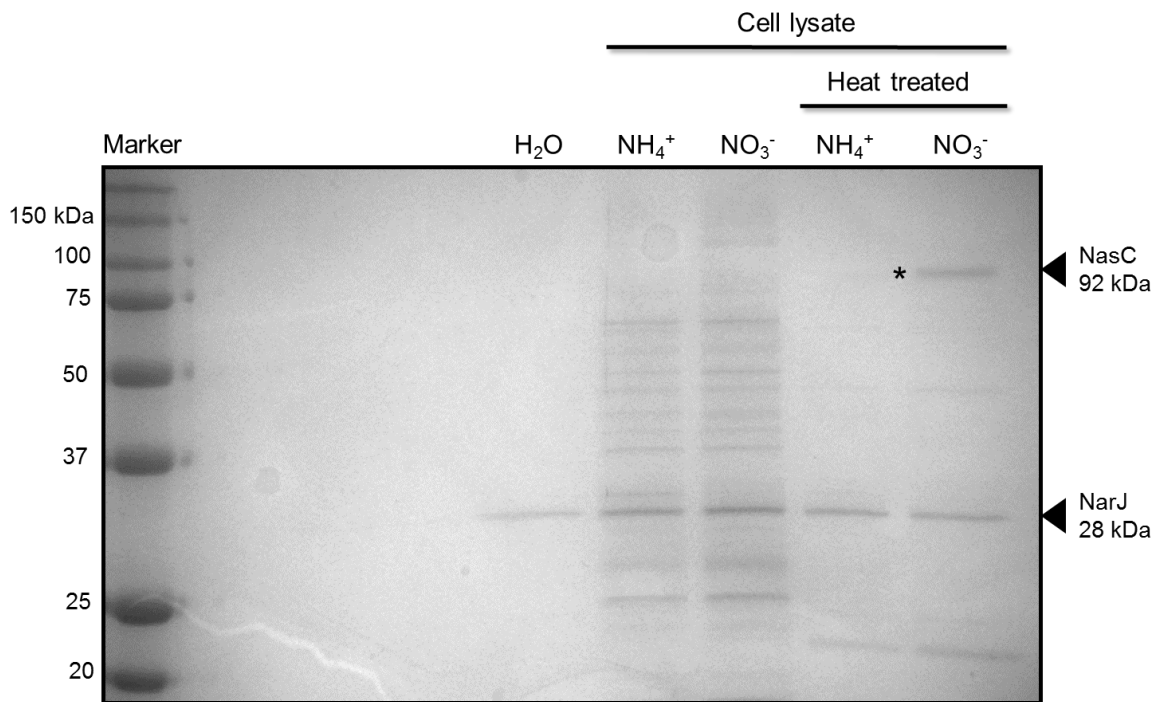


Figure 6.12. SDS-PAGE analysis for the pull-down assay of the assimilatory nitrate reductase by the NarJ chaperone. Approximately 5 μ M pure NarJ_{6His} (20 mM HEPES, 150 mM NaCl, pH 7.5) was subject to each pull-down assay via immobilisation on magnetic sepharose beads coated with Ni²⁺ (*GE Healthcare*). Beads-NarJ were incubated with either a water control, “H₂O”, or cell extracts harvested from *P. denitrificans* grown aerobically at 30°C in minimal media with 30 mM succinate and either 10 mM ammonium or nitrate as the sole nitrogen source, “NH₄⁺” or “NO₃⁻”, respectively. Separate cell extracts were incubated at 80 °C for 2 mins prior to assay: “heat treated”. Beads were washed with 25 mM imidazole to remove unbound protein and then 500 mM imidazole to elute NarJ and any bound molecules, which were resolved on a 12.5 % acrylamide gel. “Marker” indicates Precision Plus Protein™ dual colour molecular weight standards. Asterisk indicates band sent for sequencing via MALDI-TOF Mass spectrometry.

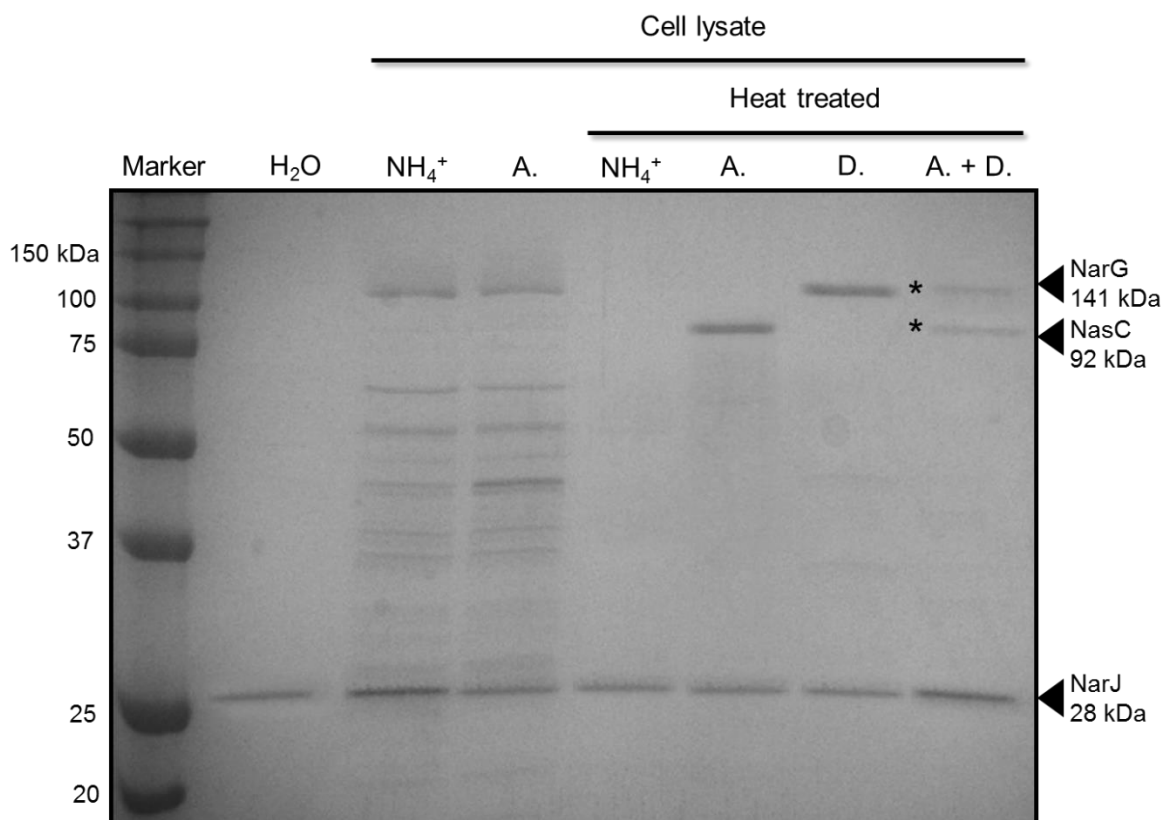


Figure 6.13. Pull-down assays monitoring interactions between NarJ and the nitrate reductases of *P. denitrificans*. Approximately 5 μ M pure NarJ_{6His} (20 mM HEPES, 150 mM NaCl, pH 7.5) was subject to each assay via immobilisation on magnetic sepharose beads charged with Ni²⁺ (*GE Healthcare*). Beads+NarJ were incubated with either a water control, “H₂O”, or cell extracts harvested from *P. denitrificans* grown at 30 °C in minimal salt media with 30 mM succinate. Cultures were grown aerobically with 10 mM ammonium, “NH₄⁺”, or nitrate, “A.” (assimilation) as a sole nitrogen source. Additional cultures were grown anaerobically with 20 mM nitrate and 10 mM ammonium, “D.” (denitrification), or 30 mM nitrate, “A. + D.” (assimilation and denitrification). Separate samples were incubated at 80 °C for 2 mins prior to assay (“heat treated”). Beads were washed with 25 mM imidazole to remove unbound protein and then 500 mM imidazole to elute NarJ and bound molecules which were separated on a 12.5 % SDS-PAGE gel. Marker indicates Precision Plus Protein™ dual colour standards. Asterisks indicates band sent for sequencing via MALDI-TOF Mass spectrometry.

The first five lanes on the gel image are identical to those displayed previously in Figure 6.12, reproducing the interaction between NarJ and NasC following partial unfolding of cell extract from nitrate-dependent cultures. In addition to the previous assay, the gel presented in Figure 6.13 contains proteins retained from the pull-down assay using heat-treated extract from cultures grown under denitrifying conditions, “D.”. This NasC band was not pulled down by NarJ when *P. denitrificans* was grown anaerobically with 20 mM nitrate as an end-terminal electron acceptor and 10 mM ammonium as a nitrogen source. Instead, a much larger band at ~141 kDa was bound by the NarJ-beads, which MALDI-TOF analysis confirmed as NarG (Significance score = 154, coverage = 55%, $E = 2.3 \times 10^{-9}$). In both cases the staining intensities of the NarJ:NasC bands or the NarJ:NarG bands washed off the beads were similar suggesting formation of a 1:1 complex.

Finally, cells were grown anaerobically with nitrate as a respiratory electron acceptor and a sole nitrogen source, “D. + A.”. In this case, NarJ recovered both the 92 kDa NasC and 141 kDa NarG bands simultaneously. Interestingly, the NarJ band was around twice the intensity of the individual NasC and NarG bands, which is consistent with 50% of NarJ being bound in a 1:1 complex with NasC and 50% being bound in a 1:1 complex with NarG. The results therefore suggest comparable specificity of NarJ for both types of nitrate reductase and no bias towards NarG as might have been expected. This interaction study concludes an ability for NarJ to interact specifically with NasC to aid formation of mature holoenzyme in a previously unprecedented chaperone function.

6.9 Discussion

Recent bioinformatic analyses of the taxonomically diverse NarJ subfamily members revealed that a close association exists between each chaperone and a specific complex iron-sulfur molybdoenzyme respiratory system. Here, however, we present new insights that extend the specificity of NarJ to assimilatory as well as respiratory nitrate reductase in *P. denitrificans*. These two enzymes are quite divergent, being very different sizes (92 and 141 kDa) and sharing only ~25 % similarity despite both being Mo[MGD]₂ containing nitrate reductases. However, there must be sufficient similarity in the NarJ recognition motifs of the two proteins to enable these interactions to take place.

An experiment modulated the molybdenum supplemented to *P. denitrificans* to study its role as a catalytic site for nitrate reduction. Growth data showed cultures were unable to perform nitrate-dependent growth aerobically or anaerobically in the absence of molybdenum. Cultures retained the capacity to grow when supplemented with nitrite, indicating molybdenum is a vital cofactor for nitrate reduction by NasC and NarG

In order for a REMP to be utilised by a system, it needs to be co-expressed with the relevant target redox enzyme. NarJ proteins are known to be expressed under anaerobic growth conditions to mature the respiratory nitrate reductase. However, for nitrate assimilation, aerobic expression of *narJ* is needed to help synthesise active NasC. Here, qRT-PCR analysis found that *narJ* and *narI* are upregulated during aerobic nitrate-dependent growth and that a separate promoter exists immediately upstream of *narJ* to enable relevant expression for NasC biogenesis.

A $\Delta narJ$ deletion strain deficient in genomic *narJ* followed the pattern displayed in molybdenum-deplete media, where cultures were unable to assimilate or denitrify nitrate but could use nitrite effectively as a sole nitrogen source or respiratory electron acceptor. Wild-type growth of both conditions with nitrate was restored when plasmid-borne NarJ was expressed *in trans* within the mutant strain. This demonstrated a role for NarJ in *P. denitrificans* for maturation of the respiratory nitrate reductase, consistent with literature (Blasco et al., 1998; Liu & DeMoss, 1997), and importantly hinted an essential physiological requirement in the biogenesis of functional assimilatory nitrate reductase.

Metabolic phenotyping explored the catalytic activity of NarG and NasC in cell extracts of *P. denitrificans* strains. Both of these molybdenum-dependant nitrate reductases recorded a lack of nitrate reduction in the absence of *narJ*, and only exhibited catalysis in WT and *complement* strains where NarJ was present. These assays showed that the function of NarG and NasC are dependent on NarJ under denitrifying and assimilatory conditions, respectively.

Protein:protein pull-down assays exposing NarJ to *P. denitrificans* cell extract resulted in interactions with NarG from extract prepared under denitrification and NasC from extract prepared from cultures grown by aerobic assimilation. Band intensities of each interaction suggested a 1:1 stoichiometry of chaperone to enzyme. Both nitrate reductases were pulled out from the soluble extract prepared from *P. denitrificans* grown with nitrate as both an end terminal electron acceptor and sole nitrogen source, with comparable specificity of NarJ for both types of nitrate reductase. Furthermore, associations were only observed following heat-treatment to promote polypeptide unfolding, consistent with chaperone recognition of unfolded epitopes on target proteins.

The research presented here proves the initial hypothesis stating NarJ is the REMP in *P. denitrificans* required for biogenesis of mature NarG and NasC complete with cofactors under appropriate physiological conditions. This paradigm represents a previously unprecedented cross-talking capacity of NarJ with other non-Nar nitrate reductases of cells, even during aerobic growth when *nar* is thought to be repressed.

Chapter 7: General Discussion

7.1 Nitrate Assimilation Provides a Biomass-Linked Reductant Vent during Carbon Rich Conditions

Chapter 3 focused on exploring heterotrophic growth of *P. denitrificans* with various nitrogen and carbon sources. Through HPLC analysis and gene-reporter fusion assays, we showed ammonium is the preferential inorganic nitrogen source for cultures to incorporate into cellular material, followed by nitrate, and that *nas* is repressed by millimolar levels of ammonium. Utilisation of ammonium for biosynthesis of pivotal organic structures is energetically advantageous to cells as nitrate requires processing prior to carbon integration.

Complete cytoplasmic reduction of a single nitrate molecule to ammonium requires 4 NADH molecules to supply a total of 8 electrons to the active sites of the assimilatory nitrate and nitrite reductases. The reduced nucleotide pyrimidine pool is generated, in part, by oxidation of carbon compounds in the Krebs cycle. We believed an upregulation of dicarboxylate transporters observed in *P. denitrificans* during nitrate assimilation served to increase organic acid import to fuel necessary NADH production. Furthermore, we proposed greater quantities of environmental carbon compounds may lead to higher levels of growth when assimilating nitrate, as under normal laboratory growth conditions the NADH generated from 30 mM succinate maybe limiting biomass formation.

This study demonstrated a greater dependence of cultures on the external carbon source when assimilating nitrate as opposed to ammonium-sufficient conditions, which achieved maximum biomass and growth rates at far lower concentrations of supplemented carbon source. For example, while ammonium-dependent cultures observed maximum growth at ~30 mM carbon, those grown with nitrate did not match similar output until ~50 mM carbon. Furthermore, the results demonstrate organic acids yielding greater NADH equivalents per molecule oxidised are preferential for *P. denitrificans* to use for nitrate-dependent growth. Here, we tested butyrate, pyruvate, succinate and malate (ranked most reduced to most oxidised) which enter respiration at various points and differ in quantities of reducing equivalents produced. Cultures grown with organic acids providing more NADH (i.e. butyrate and pyruvate) grew to higher levels than the more oxidised substrates (i.e. succinate and malate) with nitrate as the sole nitrogen source compared to ammonium.

These observations are consistent with cells being dependant upon their reduced cytoplasmic nucleotide pyrimidine pool during nitrate-dependant growth, and a clear redox link exists between biomass output and carbon respiration. Here, Nas, the NADH:nitrate/nitrite-oxidoreductase, acts as a reductant vent during nitrate assimilation by coupling the dissipation of excess energy stored in NADH and FADH₂ with accumulation of biomass. Nas oxidises the reduced nucleotide pyrimidine compounds to reduce nitrate to ammonium for subsequent incorporation into organic cellular structures, offering a selective growth advantage under energy-rich, nitrogen-limiting physiological conditions. This redox system is an alternative to Nap, the ubiquinol:nitrate oxidoreductase, which functions in a membrane-confined Q-loop to dissipate excess cellular energy at the inner-membrane.

To test this redox balancing capacity of Nas, future work could explore alteration of the carbon:nitrogen levels made available to bacteria. We observed 30 mM supplemented butyrate, a highly reduced carbon compound, was toxic to *P. denitrificans* cultures whereas other organic acids tested did not become lethal until above 60 mM. This is possibly due to accumulation of excess energy and reducing equivalents, as complete oxidation of butyrate produces 7 NADH and 3 FADH₂. It would be interesting to test whether increasing nitrate input could alleviate butyrate toxicity by offering dissipation of this excess energy via the Nas system. Furthermore, we showed that cultures consumed ammonium first, followed by nitrate, when supplemented with both nitrogen sources and succinate as the carbon source. However, due to this newly defined reductant vent capability of Nas, *P. denitrificans* may consume nitrate first when supplemented with butyrate as it offers this selective growth advantage over ammonium.

Defining this link between carbon respiration and nitrogen assimilation is important as carbon and nitrogen are typically stoichiometrically balanced in ecosystems due to syntrophic microbial interactions. Anthropogenic manipulation of their bioavailability can have significant ecological and environmental consequences. Johnson and coworkers previously showed artificial addition of organic respiratory substrates caused accelerated microbial biomass formation (“blooms”) in nitrate-polluted watercourses, consistent with data gathered here in bacterial batch cultures (Johnson et al. 2012). This can have positive bioremediation implications by removing toxic nitrate/nitrite from water reservoirs upon enhancing dissolved organic carbon levels. However, this metabolic system is detrimental in agriculture as use of nitrate/nitrite fertilisers stimulates increased uptake of organic compounds by soil bacteria which leaves the landscape nutrient deficient and barren. Furthermore, in the presence of a carbon sink, microbial communities enhance consumption of these soluble nitrogen oxyanions thus detracting

from intended crop growth. The work conducted here may have potential for aiding development of alternative methods for supplying bioavailable nitrogen to crops, possibly by inhibiting bacterial Nas pathways to circumvent these problems.

7.2 Exploring Regulators Required for Expression of Nitrogen-Responsive Genes

Bacterial expression of nitrogen-responsive genes typically requires stimuli-induced responses achieved by protein cascades stemming from P_{II}, as outlined in Section 1.2. In Gram-negative heterotrophic bacteria, a combination of the general nitrogen regulators, NtrBC/NtrYX, and sigma 54 (RpoN) characteristically activates gene transcription where encoded products are implicated in nitrogen-metabolism. Both transcriptional and translational gene-reporter fusion assays and qRT-PCR transcriptomic analysis were employed to investigate several regulatory proteins concerning expression of nitrogen-responsive genes in *P. denitrificans*. We initially proposed NtrBC was involved in transcription of such genes in coordination with sigma 54, following detection of low cellular nitrogen.

As a result of investigating the carbon:nitrogen interface, gene-reporter fusion assays revealed that the GS-GOGAT cycle is the dominant mode for ammonium integration with carbon during nitrate assimilation, as previously proposed (Helling 1998). This was found to be under NtrBC control where an $\Delta ntrBC$ deletion mutant of *P. denitrificans* failed to transcribe the genes encoding GS-GOGAT, resulting in GDH expression for necessary biosynthesis of organic-nitrogenous structures. NtrBC regulation of GS-GOGAT has previously been reported in heterotrophic bacteria (Merrick & Edwards 1995).

The Ntr system was also observed to govern upregulation of its own *dusN-ntrBCYX* operon, in addition to activating transcription of *nasABGHC* in *P. denitrificans*, as demonstrated in other bacteria such as *A. vinelandii* (Toukdarian & Kennedy 1986). Ntr is not involved in *nasTS* expression and therefore the NtrC-responsive promoter must lie in the 5'-UTR of *nasA*, downstream of *nasS*. Interestingly, an $\Delta ntrBC$ strain retained the capacity for nitrate assimilation and *nasABGHC* transcription was not fully abolished until the structurally and functionally similar NtrYX system was additionally deleted in an $\Delta ntrBY$ double mutant. This finding highlights an overlap between Ntr where functional complementation is performed by these two-component systems.

Gene-reporter fusion assays performed here demonstrated the role of NasT in the expression of *nasABGHC* due to an absence of *nasA* transcription recorded in $\Delta nasT$, consistent with previous investigations (Luque-Almagro et al. 2013). The work here

showed that a combined role of Ntr and NasT is required for transcription of *nasABGHC* mRNA in *P. denitrificans* during nitrate assimilation.

Interestingly, this study concluded sigma 54 does not participate in regulating the transcription of various nitrogen-responsive systems tested here: *nas*, *nar*, *dusN-ntr* and the GS-GOGAT/GDH pathway. Studies in other heterotrophic bacteria confirmed a role for sigma 54 in activating expression of systems for denitrification and assimilation. However, no such role was identified in *P. denitrificans* as judged by a lack of growth phenotype or genetic phenotype observed by qRT-PCR in $\Delta rpoN$. Importantly, other studies have reported a similar finding which conveys this sigma factor may not be as heavily implicated in regulating nitrogen-responsive genes as believed (Foster-Hartnett et al. 1994). The heat shock sigma factor, sigma 32, was our second candidate for regulating expression of such genes, but a double deletion mutant of $\Delta rpoN\Delta rpoH$ was still capable of nitrate-dependent anaerobic and aerobic growth where *nas* and *nar* transcription was not attenuated. Future work requires investigation of the other three identifiable sigma factors in the genome of *P. denitrificans* to assign regulatory control. Additionally, global microarray analysis on the $\Delta rpoN$ strain will allow visualisation of whole cell transcriptomic changes, if any, caused as a result of deletion, offering valuable insight into gene regulation in *P. denitrificans* where relatively little is currently known.

Exploration of sigma factors, NtrBC/YX and NasT in Chapters 3 and 4 investigated regulatory requirements necessary for transcriptional control of *nasABGHC*. To thoroughly probe the complete synthesis of the structural Nas proteins, a key aspect of this study examined their expression from a post-transcriptional perspective. Through this, a novel, pivotal role for a conserved *dusN* gene was identified. Through gene-reporter fusion assays, qRT-PCR and microarray analysis it was confirmed that DusN critically regulates nitrate assimilation by enabling translation of *nasABGHC* mRNA, forming a key link between mRNA and polypeptide synthesis.

7.3 Bacterial DusN is a Post-Transcriptional Regulator of Protein Biosynthesis

7.3.1 DusN controls expression of a multitude of nitrogen-responsive proteins

Bacterial *dusN* was initially an uncharacterised hypothetical gene with very few studies performed previously on it. This gene is clustered with the Ntr system in *P. denitrificans*, a genetic organisation strictly conserved across α -proteobacteria and additionally in some other Gram-negative heterotrophic and autotrophic bacteria. Homologues of *dusN* are also present in the genomes of many β - and γ -proteobacteria, not necessarily

conserved with an assimilatory nitrate reductase, where *dusB-fis* is believed to have arisen via horizontal gene-transfer of *dusN-ntr* during evolutionary divergence (Xu & Johnson 1995). The conservation and proximity of this gene with key regulatory proteins suggests that it may potentially play an important cellular role which we explored here.

Potentially the most exciting finding of this research was that this putative, nitrogen-responsive tRNA-DUS is a crucial regulator controlling nitrate assimilation, as a *P. denitrificans* mutant strain deficient in genomic *dusN* was unable to grow with nitrate or nitrite as the sole nitrogen source. Restoration of nitrate-dependent growth was achieved when DusN was reintroduced in to the deletion strain from a plasmid, showing that DusN is critical for Nas biosynthesis. DUS members are known to modulate protein expression by catalysing post-transcriptional modifications in tRNA compounds and synthesise dihydrouridine at specific sites (Xing et al. 2002; Sprinzl et al. 1998). Introduction of dihydrouridine in tRNA is known to influence structural conformation by increasing dynamic motion due to impaired stacking with neighbouring nucleotides, important in forming loop regions (Dalluge et al. 1996; Emerson & Sundaralingam 1980). Once a role for DusN had been established, this research sought to understand how DUS couple dihydrouridine formation with the associated influence on protein biosynthesis.

Using RT-PCR analysis, we found *dusN-ntrBCYX* comprises one nitrogen-responsive operon, the encoded products of which are key in regulating many metabolic pathways concerning the nitrogen status of the cell, such as *nas* and GS-GOGAT. As discussed above, the Ntr regulatory systems bind DNA to active transcription of a target gene. However, transcriptomic analysis performed here demonstrated that *nasABGHC* mRNA was still transcribed in Δ *dusN* and that this regulator isn't involved in transcription. Instead, gene-reporter fusion assays showed this nascent mRNA was not translated to the structural Nas genes, hence the inability of the mutant strain to assimilate nitrate or nitrite into biomass. Therefore, DusN functions to regulate target protein expression at a post-transcriptional level, consistent with the family's function to modify RNA.

Comparative microarray analysis between WT and Δ *dusN* was conducted to probe global transcriptomic changes in response to DusN absence in *P. denitrificans*. This highlighted a multitude of genes (63 out of 5134 genes) which underwent attenuated expression, the majority of which encode proteins involved in nitrogen-metabolism to scavenge bioavailable nitrogen sources or recycle amine groups. The whole-cell data implicates a broader regulatory role of DusN than initially believed due to the plethora of enzymatic pathways exhibiting altered expression. This is consistent with the conservation of genomic *dusN* in organisms lacking a Nas system, such as *R.*

sphaeroides, where DusN may participate in regulating other nitrogen-metabolism possibly in coordination with the Ntr system. Future studies are required to identify proteins under DusN control, such as GS-GOGAT, which was not highlighted in the microarray and is thus transcribed unsuccessfully as *nasABGHC* is.

The transcriptional and translational techniques performed on $\Delta dusN$ concluded bacterial DusN functions at the post-transcriptional level to regulate expression and is required for ensuring the correct translation of NasABGHC in *P. denitrificans*, and most likely other bacteria. This data shows a novel mode of regulation, where nitrogen-responsive synthesis of dihydrouridine in tRNA transcripts may alter protein biosynthesis for a metabolic response. To explore the biochemical and biophysical aspects of DusN and investigate how DUS couple stimuli-induced modification of tRNA with regulation of specific target proteins, DusN was examined.

7.3.2 Characterising DusN as a tRNA-dihydrouridine synthase

Through overexpression and biochemical analysis of recombinant DusN from *P. denitrificans*, we confirmed it is a functional, RNA-modifying, NADH-dependent oxidoreductase complete with an FMN molecule. We showed the protein and cofactor exist in a 1:1 stoichiometry and is held through non-covalent interactions as it was released upon protein unfolding (Yu et al. 2011).

Analysis of RNA from *P. denitrificans* strains found a significant increase of tRNA-dihydrouridine extracted from nitrate-dependent cells compared to ammonium-dependent cultures. This modification was absent in $\Delta dusN$ and assigned the nitrate-induced formation of dihydrouridine to the post-transcriptional activity of DusN. Previous reports have concluded similar findings, where a deficiency of dihydrouridine was observed in bacteria where a *dus* was removed (Bishop et al. 2002; Xing et al. 2002).

Despite identifying this global cellular function, few studies have investigated kinetic properties of DUS members or bacterial DusN to determine catalytic constants. Two previous reports have performed biophysical analysis to probe the enzyme mechanism at a molecular level. Rider and coworkers used $^1\text{H-NMR}$ to resolve sequential binding of substrates by Dus2 in *S. cerevisiae*, which deduced NAD(P)H associates and reduces DUS-FMN in a reductive-half reaction, following by tRNA docking and subsequent oxidation of protein-cofactor (Rider et al. 2009). Furthermore, Yu and colleagues proposed a catalytic mechanism implicating FMN and cysteine 110 as hydride and proton donors, respectively, to the pyrimidine ring of uridine (Figure 1.19) (Yu et al. 2011).

In this study, we used *in vitro* colourimetric assays with NADH/NAD⁺ and uridine/dihydrouridine to quantify the kinetic parameters of DusN from *P. denitrificans* at 24 °C, pH 7.5. V_{max} values of 94.66 and 90.06 nmol.min⁻¹ mg protein⁻¹ for uridine reduction and dihydrouridine oxidation, respectively (turnover numbers of 4.73 x 10⁻⁵ s⁻¹ and 4.57 x 10⁻⁵ s⁻¹), were calculated. Whilst these are not necessarily high for enzymes, such as nitrate reductases (Section 6.6), they are comparable with a single previous report quantifying a turnover number of 3.5 x 10⁻⁵ s⁻¹ for dihydrouridine synthesis by Dus2 in *S. cerevisiae* (Rider et al. 2009). K_m values of 160 and 1310 μM for NADH and uridine, and 150 and 1260 μM for NAD⁺ and dihydrouridine, respectively, were calculated here, though no previous values have been reported for comparison. This relatively low affinity of uridine and dihydrouridine will impede the enzyme from modifying the cytosolic pool of free uridine, as well as those it would encounter in non-specific RNA. Finally, *in vivo* analysis of site-directed mutant DusN proteins found the conserved cysteine 110 and lysine 150 are key for catalysis as previously found for DUS from *T. thermophilus* and *S. cerevisiae* (Yu et al. 2011; Xing et al. 2002).

P. denitrificans additionally encodes a housekeeping *dusA* on chromosome I which we also investigated here. The growth phenotype of $\Delta dusA$ and contribution of DusA to RNA-dihydrouridine levels was examined, and we conclude a housekeeping function of this DUS necessary for optimal growth under various physiological conditions by forming basal tRNA- and rRNA-dihydrouridine levels. Though it is not stringently required as the genomic deletion is not lethal, it does enable increased growth rates and biomass formation, presumably by increasing translational fidelity for efficient protein biosynthesis. The presence of clear growth and metabolic phenotypes in $\Delta dusN$ and $\Delta dusA$ indicates the specificity of separate DUS classes towards distinct uridine positions and individual tRNA transcripts as the enzymes do not complement one another, though it may be due to a lack of expression under the physiological conditions. Therefore, genetic complementation using plasmid-borne *dusN* and *dusA* in $\Delta dusA$ and $\Delta dusN$, respectively, would confirm whether the different DUS subfamilies can carry out the same physiological role.

A significant finding from this research was the identification, from protein:RNA pull-down assays, of three cognate tRNA targets for bacterial DusN, coding for: Phe_{GAA}, Lys_{UUU} and Trp_{CCA}. Interestingly, each comprise a 19 base-pair ribonucleotide sequence absent in other tRNA of *P. denitrificans* and strictly conserved in these three tRNA in *dusN* positive organisms, but absent amongst those lacking *dusN*. We propose 5'-UAGCUCAGUUUGGUAGAGCA-3' forms a DusN consensus sequence surrounding the

D-loop of these folded tRNA transcripts, offering uridines at positions 16, 17 and 20, the most commonly reported sites for dihydrouridine formation.

To explore this, catalytic experiments were performed on pure DusN using this RNA sequence (synthesised by *Eurofins MWG*) as a substrate instead of free uridine as described above. Upon doing so, the affinity of DusN towards this sequence greatly increased compared to uridine. A K_M value of 4.85 μM was calculated for 5'-UAGCUCAGUUGGUAGAGCA-3', a significant decrease from 1310 μM for uridine. Therefore, the enzyme displays great affinity for its target tRNA sequence to enable specific dihydrouridine formation on distinct tRNA compounds. Additionally, this identical sequence was identified in tRNA for Phe_{GAA}, Lys_{UUU} and Trp_{CCA} of *E. coli*. Overexpression of plasmid-borne DusN from *P. denitrificans* in *E. coli* stimulated an increase in tRNA-dihydrouridine levels, indicating this is the correct consensus sequence of DusN.

Mapping of this sequence onto the solved crystal structure of *T. thermophilus* DUS:tRNA^{Phe_{GAA}} identified contacts largely arise between the active site and the D-loop region during tRNA docking for catalysis, as expected (Yu et al. 2011). Importantly, additional interactions are observed between this ribonucleotide consensus region and the C-terminal dsRNA binding domain, proposed to govern protein:RNA interactions of DUS. We believe a combined effort between the FMN-containing active site and this dsRNA binding domain allows DUS discrimination between highly similar tRNA structures for specific targeting of distinct uridines. Furthermore, the flexibility in primary sequences of this C-terminal dsRNA binding motif (Figure 5.26) programmes the separate DUS classes to recognise different uridine positions and a specific subset of tRNA compounds, hence negating functional complementation between the separate classes (Byrne et al. 2015). Preliminary crystallography of pure DusN has been undertaken and yellow protein crystals have formed under various conditions (Figure 2.5). X-ray crystallographic resolution of DusN in complex with tRNA will be a valuable insight into biophysical properties such as interactions and contact sites.

From this study, we propose DusN modifies tRNA compounds for Phe_{GAA}, Lys_{UUU} and Trp_{CCA} to regulate translation of *nasABGHC*, and presumably other nitrogen-responsive systems due to identification of this consensus sequence in organisms containing DusN but do not encode Nas. We conclude the DUS superfamily act as specific post-transcriptional regulators by influencing RNA-dihydrouridine levels which governs their folding and formation of secondary structures. DusN governs a rapid, stimuli-response

alteration of protein expression patterns based upon tRNA modification, the first such finding, to our knowledge, of this novel regulatory mechanism in nitrogen metabolism.

However, it is still unclear how dihydrouridine formation directly produces the changes in protein biosynthesis or how distinct uridine alteration of individual tRNA compounds modulates specific cellular output. Thermodynamic and structural investigations using NMR demonstrated dihydrouridine enhances molecular fluidity and promotes folding of loop regions in secondary RNA structures (Dalluge et al. 1996). This modification is critical for fine-tuning protein production and increasing fidelity of translation by altering and optimising RNA secondary structure, though how a precise regulatory response is fashioned from rapid dihydrouridine formation still requires future work.

7.3.3 Hypothetical models for *DusN* regulation over *Nas* translation

We propose two separate hypothetical models underpinning *DusN* regulation of *nasABGHC* translation in *P. denitrificans*, though this function may differ for other DUS subfamilies or between distinct species.

Our first model is based around the GS-GOGAT cycle at the carbon/nitrogen interface, where the pivotal metabolic precursors glutamate and glutamine are formed (see Section 1.5 for review). Both amino acids may exit this pathway and flow into protein synthesis instead of other biosynthetic pathways, detracting from potential organic biomass. During nitrate-dependant growth, scarce concentrations of ammonium are assimilated and it is essential these produce all critical cellular nitrogenous structures. Should the amino acids prematurely depart the GS-GOGAT cycle for protein biosynthesis unchecked, it could prove detrimental in generating other organic compounds, such as nucleotides and protein cofactors. Post-transcriptional introduction of dihydrouridine in tRNA increases flexibility, where excess formation destabilises the secondary structure. This would disrupt interactions between tRNA:ribosomes and production of amino-acyl tRNA to result in failed protein biosynthesis. Due to observing ~3-fold amplification in tRNA-dihydrouridine during nitrate assimilation, we postulate *DusN* may regulate glutamate and glutamine incorporation into proteins by heavily modifying tRNA transcripts. Exacerbated structural fluidity will stall translation and recover glutamate and glutamine to assure sufficient nitrogen delivery to key organic structures and thus *DusN* may affect the bias between protein synthesis and other biosynthetic pathways (Figure 7.1).

Future work required to confirm or dismiss this hypothetical model will involve techniques such as whole cell proteomics to profile protein expression and the concentration of

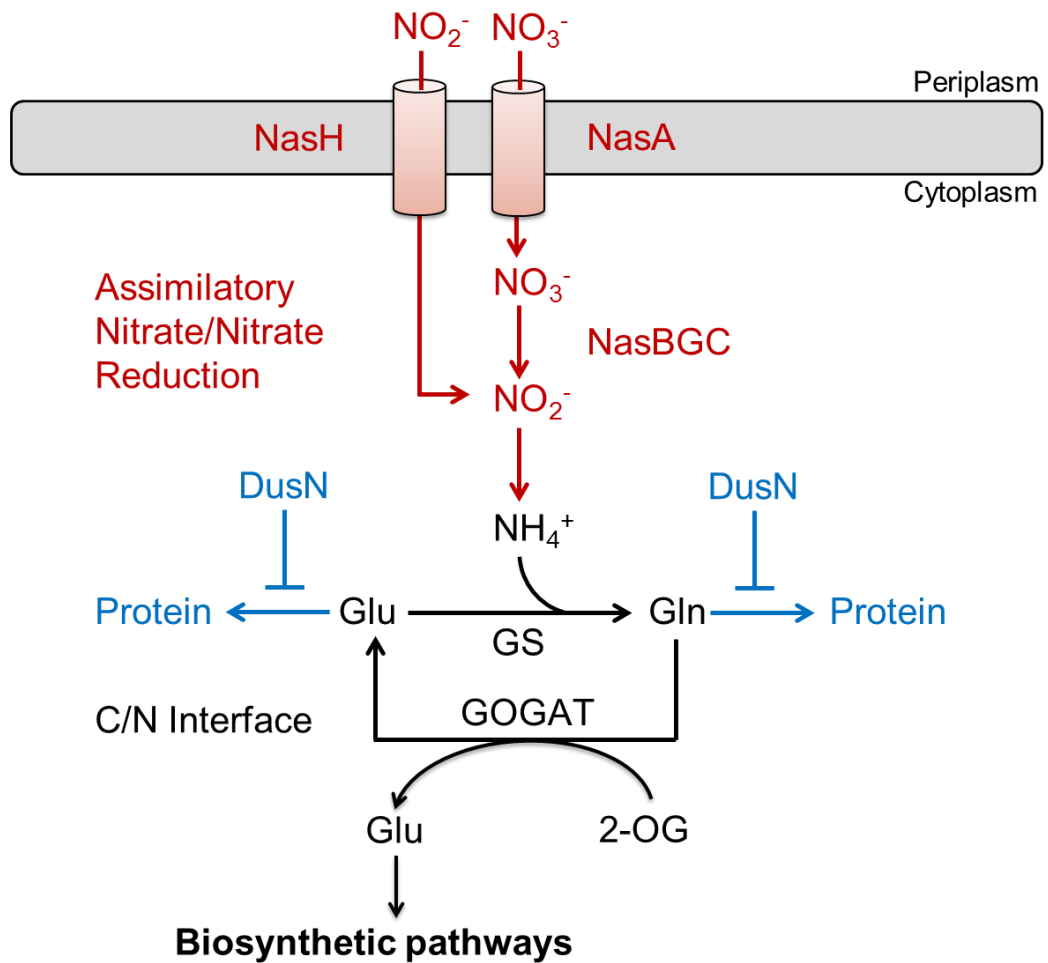


Figure 7.1. Hypothetical scheme detailing how DusN may regulate protein biosynthesis during nitrate assimilation. NasA and NasH import nitrate and nitrite into the cell for cytoplasmic reduction to ammonium by NasBGC. Ammonium cations are integrated with L-glutamate (Glu) to produce L-glutamine (Gln) via glutamine synthetase (GS). Transamination between the glutamine donor and an accepting 2-oxoglutarate (2-OG) by glutamine:2-oxoglutarate amidotransferase (GOGAT) yields two glutamate compounds, one of which is recycled whilst the second flows into biomass production. Glutamate and glutamine can prematurely exit this cycle and enter protein biosynthesis, detracting from production of other pivotal nitrogen-containing structures. DusN may possibly regulate this metabolism by attenuating protein translation to retain the amino acids for nitrogen-donation in various biosynthetic pathways.

individual amino acids, e.g. glutamate and glutamine, between wild-type and $\Delta dusN$. Additionally, translation rates may be quantified to investigate if DusN acts as a repressor of protein biosynthesis, using assays described for similar analysis in other bacteria (Li et al. 2014). However, this does not, yet, account for the observed lack specifically of *nasABGHC* translation observed in $\Delta dusN$.

The second hypothetical model for DusN control over *NasABGHC* expression stems from the alignment of tRNA^{Trp}_{CCA} sequences between DusN-encoding and DusN-negative organisms (Figure 5.25). Whilst uridine 16, 17 and 20 was present in tRNA for Phe_{GAA} and Lys_{UUU} regardless of organism, uridine 20 is only identified in tRNA^{Trp}_{CCA} from bacteria encoding a *dusN* or homologue. Furthermore, organisms harbour two codons each for phenylalanine (UUU and UUC) and lysine (AAA and AAG) but only one for tryptophan (UGG). This makes Trp_{CCA} a simple and energetically-beneficial choice for regulating translation due to a lack of redundancy, as modulation of just one tRNA type will produce a global change of protein biosynthesis.

Initial bioinformatics exploring this concept seemed promising, where examination of tryptophan content found a consistently greater level in the structural *Nas* proteins when compared to various housekeeping proteins or nitrogen-responsive proteins outside *NasABGHC* (Table 7.1). We propose a second, distinct hypothetical model where DusN specifically synthesises dihydrouridine at conserved position 20 in tRNA^{Trp}_{CCA} to ultimately affect tryptophan incorporation into polypeptides. Fine-tuning of this tRNA compound may allow increased fidelity of translation for proteins abundant in tryptophan, such as *Nas*, though clearly future work is needed to explore this hypothesis further.

Table 7.1. Tryptophan content in various housekeeping and *Nas* proteins.

Protein	Amino acid length	% Tryptophan content
RecA	356	0.3
DnaN	372	0
GyrA	892	0.4
RBS12	123	0
RpoD (σ^{70})	664	0.8
RpoN (σ^{54})	396	1.0
NtrB	385	0.5
NtrC	485	0.4
NasT	196	0
NasS	390	1.8

NasA	402	2.5
NasB	810	1.5
NasG	111	1.8
NasH	285	1.4
NasC	870	1.8

The next stage for investigating this proposal would be developing HPLC separation of pure tRNA to isolate specific populations of amino-acyl tRNA. With this, analysis on individual tRNAs will be enabled, such as LC-MS to identify nucleotide modifications. Importantly, reverse-transcriptase primer extension assays, described previously (Xing et al. 2004), will allow mapping of dihydrouridine positions in the tRNA and resolve the position 20 identity in Trp_{CCA}. Identifying additional DusN controlled nitrogen-metabolising pathways, potentially in other organisms, and quantifying tryptophan content in the involved proteins may help assess this theory.

Expanding this study to DusN from Nas-positive and Nas-negative α -proteobacteria, such as *B. japonicum* and *R. sphaeroides*, respectively, will enable greater characterisation of DUS enzymes and the contribution of dihydrouridine synthesis towards influencing global protein translation and whole cell changes.

7.4 NarJ is the Chaperone Responsible for Maturation of Respiratory and Assimilatory Nitrate Reductases

The main focus of this study explored regulatory events encompassing gene expression of nitrogen-responsive participants. However, a separate subproject examined the post-translational requirements necessary to produce fully assembled nitrate reductases.

NarJ is known to be the redox enzyme maturation protein (REMP) for formation of the functional NarG holoenzyme complete with cofactors during anaerobic denitrification (Liu & DeMoss 1997). But, there were no clear candidates in the *nas* gene cluster for maturation of Nas during aerobic nitrate assimilation in *P. denitrificans*. We hypothesised NarJ is the molecular chaperone for biogenesis of both NarG and NasC under appropriate physiological circumstances.

Blasco and coworkers previously identified an absence of molybdenum as a catalytic center in NarG extracted from a *narJ* deletion mutant of *E. coli* (Blasco et al. 1998). We used molybdenum deplete minimal media to show this metal is crucial for nitrate reduction during denitrification and assimilation in *P. denitrificans*. Furthermore, a $\Delta narJ$ strain constructed here was unable to perform anaerobic or aerobic growth with nitrate,

consistent with non-functional NarG and NasC. The metabolic phenotype supported this observation as enzyme assays found nitrate reductase activity was dependent upon the presence of the NarJ chaperone. Cell lysate from $\Delta narJ$ grown by denitrification or assimilation was unable to reduce nitrate, as opposed to the WT, relaying both NarG and NasC are inactive in the absence of NarJ.

Significantly, interactions between NarJ and the distinct nitrate reductases NarG and NasC were visualised using pull-down assays where they appeared to form 1:1 stoichiometries of protein:REMP. This was only observed when the cell lysate had been heat treated prior to the assay, suggesting NarJ recognises the unfolded polypeptides as is consistent with the chaperone function. Interestingly, when both nitrate reductases were pulled-out together from cultures simultaneously denitrifying and assimilating nitrate, the populations on the gel appeared equal, suggesting comparable specificity of NarJ for both types of nitrate reductase. This data indicates a chaperone capacity of NarJ in biogenesis of the respiratory nitrate reductase and the assimilatory nitrate reductase, NasC, during aerobic nitrate assimilation.

In order for a chaperone to be utilised by a system, it needs to be co-expressed with the relevant redox enzyme. Gene clusters encoding *nar* are typically under Fnr regulation and widely known to be expressed under anaerobic growth conditions to mature the respiratory nitrate reductase. However, for nitrate assimilation, aerobic expression of *narJ* is needed. Here we have shown how a separate nitrogen-responsive promoter embedded in *narKGHJI* exists to enable *narJ* expression under aerobic, nitrate-dependent growth conditions so it can mature NasC. This novel regulatory mechanism is most likely governed in an Fnr-independent manner, with prime suspects being NtrBC and NasT which would enable expression of NarJ when NasC requires assembly. qRT-PCR analysis and gene-reporter fusion assays investigating the transcription of *nar* in various deletion mutants of *P. denitrificans* may help decipher the participants involved in the aerobic transcription of *narJ*. Additionally, 5'-RACE could ascertain the precise transcriptional start site of the *narJ* promoter within the end sequence of *narH* during aerobic expression.

Though the interaction between chaperone and enzyme was demonstrated here, few studies were performed to assess this newly defined relationship. Full biochemical characterisation via studies of pure NarJ with NarG, and NasC such as isothermal titration calorimetry, gel filtration and analytic ultracentrifugation would gain insight into many biophysical properties such as binding stoichiometry, how the folding is accomplished and identification of a recognised target epitope. Crystallography of the

chaperone:protein complex may help deduce further understanding of these questions, particularly the recognised motif for NarJ. Interactions between NarJ and NarG so far have been found at the N-terminal signal sequence (Li & Turner 2009; Zakian et al. 2010; Chan et al. 2014) as is common for REMP's, though cytoplasmic NasC does not comprise this feature. Identifying common residues in NarG and NasC responsible for recognition by NarJ should be performed, where mutations of the target region would result in an unfolded apoprotein. These two classes of nitrate reductase, despite both being Mo[MGD]₂, are actually quite divergent, sharing only ~20% similarity. However, there must be sufficient similarity in the NarJ recognition motifs of the two proteins to enable these interactions to take place. The findings here represents an unprecedented cross-talking capacity of NarJ with the assimilatory nitrate reductase.

7.5 Concluding Remarks

The research performed for this thesis reported three key findings relating to nitrogen-metabolism in *P. denitrificans*, mainly concerning the cytoplasmic assimilatory nitrate/nitrite reducing Nas pathway. Firstly, we show that Nas, the NADH:nitrate/nitrite-oxidoreductase, acts as a reductant vent during nitrate assimilation by coupling the dissipation of excess energy with biomass formation. Nas oxidises NADH during nitrate reduction to ammonium for subsequent incorporation into organic cellular structures, offering a growth advantage under energy-rich, nitrogen-limiting conditions.

Secondly, we found that bacterial DusN is a nitrogen-responsive, tRNA-DUS flavoprotein which catalyses NADH-dependent tRNA-dihydrouridine synthesis on tRNA^{Phe}_{GAA}, tRNA^{Lys}_{UUU} and tRNA^{Trp}_{CCA}. Importantly, this activity is key for nitrate assimilation within the cell, as nascent *nasABGHC* mRNA was not translated in the absence of genomic *dusN*. The data collected in this study imply a novel post-transcriptional regulation in response to external stimuli, underpinned by rapid nucleotide modification of tRNA.

Finally, the results here indicate a previously unprecedented cross-talking capacity of NarJ with other non-Nar nitrate reductases of cells, even during aerobic growth when *nar* is thought to be repressed. Both growth and metabolic phenotypes of a $\Delta narJ$ deletion strain implicate NarJ in biogenesis of functional NasC holoenzyme.

These last two are particularly interesting as DusN had not been implicated in biogeochemical nitrogen-cycle processes, and NarJ had not been considered outside of the denitrification pathway. However, both seem to be critical in assembling the nitrate assimilatory machinery in *P. denitrificans*, and presumably, other heterotrophic bacteria. This thesis highlights that even genes distant from core gene clusters may often have

an essential role in enabling that clusters cellular function, and that regulatory pathways and control of both the transcriptome and proteome is often more complex than initially believed. Although decades of intense microbial, molecular and biochemical studies by countless research teams upon a plethora of microorganisms have been performed, numerous cellular functions, metabolic pathways and protein roles remain elusive. The potential and implications of such findings could be vast in development of superior bioremediation, bioenergetic, and pharmaceutical technologies in an ever-changing world, and thus future work is key in this field of biogeochemistry.

References

- Addiscott, T.M. & Benjamin, N.** (2006). Nitrate and human health. *Soil Use and Management*, **20**: pp.98–104.
- Ahmadian, M.R., Ghozlan, H. A., Sabry, S., Kleiner, D.** (1993). Characterization of a *Paracoccus denitrificans* mutant pleiotropically impaired in nitrogen metabolism. *Arch. Microbiol.*, **160**: pp.166–8.
- Aliverti, A., Curti, B. & Vanoni, M.A.** (1999). Identifying and quantitating FAD and FMN in simple and in iron-sulfur-containing flavoproteins. *Methods in Mol. Biol.*, **131**: pp.9–23.
- Allen, A.E., Booth, M.G., Frischer, M.E., Verity, P.G., Zehr, J.P., Zani, S.** (2001). Diversity and detection of nitrate assimilation genes in marine bacteria. *Appl. and Env. Microbiol.*, **67**: pp.5343–8.
- Ashkenazy, H. Erez, E., Martz, E., Pupko, T., Ben-Tal, N.** (2010). ConSurf 2010: calculating evolutionary conservation in sequence and structure of proteins and nucleic acids. *Nucl. Acids Res.*, **38**: pp.529–33.
- Austin, S. & Dixon, R.** (1992). The prokaryotic enhancer binding protein NTRC has an ATPase activity which is phosphorylation and DNA dependent. *EMBO*, **11**(6), pp.2219–28.
- Baneyx, F.** (1999). Recombinant protein expression in *Escherichia coli*. *Curr. Op. Biotechnol.*, **10**: pp.411–21.
- Bay, D.C., Chan, C.S. & Turner, R.J.** (2015). NarJ subfamily system specific chaperone diversity and evolution is directed by respiratory enzyme associations. *BMC Evol. Biol.*, **15**: p.110.
- Beckham, K.S.H., Potter, J.A. & Unkles, S.E.** (2010). Formate-nitrite transporters: optimisation of expression, purification and analysis of prokaryotic and eukaryotic representatives. *Protein Expression and Purification*, **71**: pp.184–9.
- Bedzyk, L., Wang, T. & Ye, R.W.** (1999). The periplasmic nitrate reductase in *Pseudomonas* sp. strain G-179 catalyzes the first step of denitrification. *J. Bacteriol.*, **181**, pp.2802–6.
- Beevers, L. & Hageman, R.H.** (1969). Nitrate Reduction in Higher Plants. *Annu. Rev. of Plant Physiology*, **20**: pp.495–522.

- Beinert, H.** (1956). Spectral Characteristics of Flavins at the Semiquinoid Oxidation Level. *JACS*, **78**: pp.5323–8.
- Bender, R.A.** (1991). The role of the NAC protein in the nitrogen regulation of *Klebsiella aerogenes*. *Mol. Microbiol.*, **5**: pp.2575–80.
- Bender, R.A. & Friedrich, B.** (1990). Regulation of assimilatory nitrate reductase formation in *Klebsiella aerogenes* W70. *J. of Bacteriol.*, **172**: pp.7256–9.
- Bennett, B.D. Kimball, E. H., Gao, M., Osterhout, R. van Dien, S.J. Rabinowitz, J. D.** (2009). Absolute metabolite concentrations and implied enzyme active site occupancy in *Escherichia coli*. *Nature Chem. Biol.*, **5**: pp.593–9.
- Beringer, J.E. & Hopwood, D.A.** (1976). Chromosomal recombination and mapping in *Rhizobium leguminosarum*. *Nature*, **264**: pp.291–3.
- Berks, B.C., Ferguson, S.J., Moir, J.W., Richardson, D.J.** (1995). Enzymes and associated electron transport systems that catalyse the respiratory reduction of nitrogen oxides and oxyanions. *Biochimica et Biophysica acta*, **123**: pp.97–173.
- Berks, B.C., Robinson, C., Reilly, A.A., Robin, T. Ferguson, S.J.** (1994). Purification and characterization of the periplasmic nitrate reductase from *Thiosphaera pantotropha*. *European J. of Biochem.* **220**: pp.117–24.
- Berks, B.C., Page, M.D., Richardson, D.J., Reilly, A., Cavill, A., Outen, F., Ferguson, S. J.** (1995). Sequence analysis of subunits of the membrane-bound nitrate reductase from a denitrifying bacterium: the integral membrane subunit provides a prototype for the dihaem electron-carrying arm of a redox loop. *Mol. Microbiol.*, **15**: pp.319–31.
- Bertero, M.G. Rothery, R.A., Palak, M., Hou, C., Lim, D., Blasco, F., Weiner, J.H. Strynadka, Natalie C.J.** (2003). Insights into the respiratory electron transfer pathway from the structure of nitrate reductase A. *Nature Structural Biology*, **10**: pp.681–7.
- Bessey, O.A., Lowry, O.I. & Love, R.I.** (1949). The Fluoremetric Measurement of the Nucleotides of Riboflavin and Their Concentration in Tissues. *JBC*, **180**: 755-79.
- Betlach, M.R.** (1983). Evolution of bacterial denitrification and denitrifier diversity. *Antonie van Leeuwenhoek*, **48**: pp.585–607.
- Bird, C. & Wyman, M.** (2003). Nitrate/nitrite assimilation system of the marine picoplanktonic cyanobacterium *Synechococcus* sp. strain WH 8103: effect of nitrogen source and availability on gene expression. *Appl. and Env. Microbiol.*, **69**: pp.7009–18.
- Bishop, A.C. Xu, J., Johnson, R.C. Schimmel, P. de Crécy-Lagard, V.** (2002).

Identification of the tRNA-dihydrouridine synthase family. *J Biol. Chem.*, **277**: pp.25090–5.

Blasco, F., Pommier, J., Augier, V., Chippaux, M., Giordano, G. (1992). Involvement of the *narJ* or *narW* gene product in the formation of active nitrate reductase in *Escherichia coli*. *Mol. Microbiol.*, **6**: pp.221–30.

Blasco, F., Dos Santos, J.P., Magalon, A., Frixon, C., Guigliarelli, B., Santini, C.L., Giordano, G. (1998). NarJ is a specific chaperone required for molybdenum cofactor assembly in nitrate reductase A of *Escherichia coli*. *Mol. Microbiol.*, **28**: pp.435–47.

De Boer, W., Kowalchuk, G. (2001). Nitrification in acid soils: micro-organisms and mechanisms. *Soil Biol. and Biochem.*, **33**: pp.853–66.

Bornhorst, J.A., Falke, J.J. (2000). Purification of proteins using polyhistidine affinity tags. *Methods in Enzymology*, **326**: pp.245–54.

Botman, D., Tigchelaar, W., Van Noorden, C.J.F. (2014). Determination of glutamate dehydrogenase activity and its kinetics in mouse tissues using metabolic mapping (quantitative enzyme histochemistry). *The J. of Histochemistry and Cytochemistry*, **62**: pp.802–12.

Boudes, M., Lazar, N., Graille, M., Durand, D., Gaidenko, T.A., Stewart, V., van Tilbeurgh, H. (2012). The structure of the NasR transcription antiterminator reveals a one-component system with a NIT nitrate receptor coupled to an ANTAR RNA-binding effector. *Mol. Microbiol.*, **85**: pp.431–44.

Boundless. (2015). Nitrate Reduction and Denitrification.

Bradford, M.M. (1976). A rapid and sensitive method for the quantitation of microgram quantities of protein utilizing the principle of protein-dye binding. *Analy. Biochem.*, **72**: pp.248–54.

Bremner, J.M. & Blackmer, A.M. (1978). Nitrous Oxide: Emission from Soils During Nitrification of Fertilizer Nitrogen. *Science*, **199**: pp.295–6.

Buck, M., Gallegos, M.T., Studholme, D.J., Guo, Y., Gralla, J.D. (2000). The bacterial enhancer-dependent sigma(54) (sigma(N)) transcription factor. *J. Bacteriol.*, **182**: pp.4129–36.

Burns, R.C. & Hardy, R.W. (1975). Nitrogen fixation in bacteria and higher plants. *Mol. Biol., Biochem., and Biophys.*, **21**: pp.1–189.

Burns, R.E. (1971). Method for estimation of tannin in grain sorghum. *Agronomy J.*, **63**:

pp. 511-2.

Byrne, R.T., Jenkins, H.T., Peters, D.T., Whelan, F., Stowell, J., Aziz, N., Kasatsky, P., Rodnina, M.V., Koonin, E.V., Konevega, A.L., Antson, A.A. (2015). Major reorientation of tRNA substrates defines specificity of dihydrouridine synthases. *PNAS*, **112**: pp.6033–7.

Caballero, A., Esteve-Núñez, A., Zylstra, G.J., Ramos, J.L. (2005). Assimilation of nitrogen from nitrite and trinitrotoluene in *Pseudomonas putida* JLR11. *J. Bacteriol.*, **187**: pp.396–9.

Cabello, P., Roldán, M.D. & Moreno-Vivián, C. (2004). Nitrate reduction and the nitrogen cycle in archaea. *Microbiol.*, **150**: pp.3527–46.

Cali, B.M., Micca, J.L. & Stewart, V. (1989). Genetic regulation of nitrate assimilation in *Klebsiella pneumoniae* M5a1. *J. Bacteriol.*, **171**: pp.2666–72.

Camarena, L., Poggio, S., García, N., Osorio, A. (1998). Transcriptional repression of *gdhA* in *Escherichia coli* is mediated by the Nac protein. *FEMS Microbiol. Letters*, **167**: pp.51–6.

Cammack, R., Jackson, R.H., Cornish-Bowden, A., Cole, J.A. (1982). Electron-spin-resonance studies of the NADH-dependent nitrite reductase from *Escherichia coli* K12. *Biochem. J.*, **207**: pp.333–9.

Candau, P., Manzano, C., Losado, M. (1976). Bioconversion of light energy into chemical energy through reduction with water of nitrate to ammonia. *Nature*, **262**: pp.715–7.

Canfield, D.E., Glazer, A.N., Falkowski, P.G. (2010). The evolution and future of Earth's nitrogen cycle. *Science (New York, N. Y.)*, **330**: pp.192–6.

Carlson, C.A., & Ingraham, J.L. (1983). Comparison of denitrification by *Pseudomonas stutzeri*, *Pseudomonas aeruginosa*, and *Paracoccus denitrificans*. *Appl. and Env. Microbiol.*, **45**: pp.1247–53.

Carson, M., Johnson, D.H., McDonald, H., Brouillette, C., Delucas, L.J. (2007). His-tag impact on structure. *Acta Crystallographica.*, **63**: pp.295–301.

Cathala, G., Savouret, J.F., Mendez, B., West, B.L., Karin, M., Martial, J.A., Baxter, J.D. (1983). A method for isolation of intact, translationally active ribonucleic acid. *DNA*, **2**: pp.329–35.

Chan, C.S., Bay, D.C., Leach, T.G.H., Winstone, T.M.L, Kuzniatsova, L., Tran, V.A.,

- Turner, R.J.** (2014). "Come into the fold": A comparative analysis of bacterial redox enzyme maturation protein members of the NarJ subfamily. *Biochim. et Biophysica Acta*, **1838**: pp.2971–84.
- Chandrangsu, P., Helmann, J.D.** (2014). Sigma Factors in Gene Expression, Chichester, UK: John Wiley & Sons, Ltd.
- Chavez, S., Lucena, J.M., Reyes, J.C., Florencio, F.J., Candau, P.** (1999). The Presence of Glutamate Dehydrogenase Is a Selective Advantage for the Cyanobacterium *Synechocystis* sp. Strain PCC 6803 under Nonexponential Growth Conditions. *J. Bacteriol.*, **181**: pp.808–13.
- Chiba, Y., Oshima, K., Arai, H., Ishii, M., Igarashi, Y.** (2012). Discovery and Analysis of Cofactor-dependent Phosphoglycerate Mutase Homologs as Novel Phosphoserine Phosphatases in *Hydrogenobacter thermophilus*. *JBC*, **287**: pp.11934–41.
- Cole, J.A., Brown, C.M.** (1980). Nitrite reduction to ammonia by fermentative bacteria: A short circuit in the biological nitrogen cycle. *FEMS Microbiol. Letters*, **7**: pp.65–72.
- Conroy, M.J., Durand, A., Lupo, D., Li, X.D., Bullough, P.A., Winkler, F.K., Merrick, M.** (2007). The crystal structure of the *Escherichia coli* AmtB-GlnK complex reveals how GlnK regulates the ammonia channel. *PNAS*, **104**: pp.1213–8.
- Craske, A., Ferguson, S.J.** (1986). The respiratory nitrate reductase from *Paracoccus denitrificans*. Molecular characterisation and kinetic properties. *European J. of Biochem.*, **158**: pp.429–36.
- Crawford, N.M., Arst, H.N.** (1993). The molecular genetics of nitrate assimilation in fungi and plants. *Annu. Rev. of Genetics*, **27**: pp.115–46.
- Crutzen, P.J., Mosier, A.R., Smith, K.A., Winiwarter, W.** (2008). N₂O release from agro-biofuel production negates global warming reduction by replacing fossil fuels. *Atmospheric Chem. and Phys.*, **8**: pp.389–95.
- Cullen, P.J., Bowman, W.C., Hartnett, D.F., Reilly, S.C., Kranz, R.G.** (1998). Translational activation by an NtrC enhancer-binding protein. *J. Molecul. Biol.*, **278**: pp.903–14.
- Dalluge, J.J., Hashizume, T., Sopchik, A.E., McCloskey, J.A., Davis, D.R.** (1996). Conformational flexibility in RNA: the role of dihydrouridine. *Nucl. Acids Res.*, **24**: pp.1073–9.
- Dalluge, J.J., Hamamoto, T., Horikoshi, K., Morita, R.Y., Stetter, K.O., McCloskey,**

- J.A.** (1997). Posttranscriptional modification of tRNA in psychrophilic bacteria. *J. Bacteriol.*, **179**: pp.1918–23.
- Di, H.J., Cameron, K.C., Shen, J.P., Winefield, C.S., O’Callaghan, M., Bowatte, S., He, J.Z.** (2009). Nitrification driven by bacteria and not archaea in nitrogen-rich grassland soils. *Nature Geoscience*, **2**: pp.621–4.
- Dixon, R., Kahn, D.** (2004). Genetic regulation of biological nitrogen fixation. *Nature Revs. Microbiol.*, **2**: pp.621–31.
- Dow, J.M., Grahl, S., Ward, R., Evans, R., Byron, O., Norman, D.G., Palmer, T., Sargent, F.** (2014). Characterization of a periplasmic nitrate reductase in complex with its biosynthetic chaperone. *The FEBS J.*, **281**: pp.246–60.
- Dubourdieu, M., DeMoss, J.A.** (1992). The *narJ* gene product is required for biogenesis of respiratory nitrate reductase in *Escherichia coli*. *J. Bacteriol.*, **174**: pp.867–72.
- Durand, A., Merrick, M.** (2006). In vitro analysis of the *Escherichia coli* AmtB-GlnK complex reveals a stoichiometric interaction and sensitivity to ATP and 2-oxoglutarate. *JBC*, **281**: pp.29558–67.
- Ebner, E., Wolf, D., Gancedo, C., Elsässer, S., Holzer, H.** (1970). ATP: glutamine synthetase adenylyltransferase from *Escherichia coli* B. Purification and properties. *European J. Biochem./FEBS*, **14**: pp.535–44.
- Eisenberg, D., Almasy, R.J., Janson, C.A., Chapman, M.S., Suh, S.W., Cascio, D., Smith, W.W.** (1987). Some evolutionary relationships of the primary biological catalysts glutamine synthetase and RuBisCO. *Symposia on Quantitative Biol.*, **52**: pp.483–90.
- Ellington, M.J.K., Sawers, G., Sears, H.J., Spiro, S., Richardson, D.J., Ferguson, S.J.** (2003). Characterization of the expression and activity of the periplasmic nitrate reductase of *Paracoccus pantotrophus* in chemostat cultures. *Microbiol.*, **149**: pp.1533–40.
- Ellington, M.J.K., Bhakoo, K.K., Sawers, G., Richardson, D.J., Ferguson, S.J.** (2002). Hierarchy of carbon source selection in *Paracoccus pantotrophus*: strict correlation between reduction state of the carbon substrate and aerobic expression of the nap operon. *J. Bacteriol.*, **184**: pp.4767–74.
- Ellis, R.J.** (2006). Molecular chaperones: assisting assembly in addition to folding. *Trends in Biochem. Sci.*, **31**: pp.395–401.
- Emerson, J., Sundaralingam, M.** (1980). Structure of the potassium salt of the modified nucleotide dihydrouridine 3'-monophosphate hemihydrate: correlation between the base

pucker and sugar pucker and models for metal interactions with ribonucleic acid loops. *Acta Crystallographica*, **36**: pp.537–43.

Essigmann, B., Güler, S., Narang, R.A., Linke, D., Benning, C. (1998). Phosphate availability affects the thylakoid lipid composition and the expression of SQD1, a gene required for sulfolipid biosynthesis in *Arabidopsis thaliana*. *PNAS*, **95**: pp.1950–5.

Farnham, P.J., Platt, T. (1981). Rho-independent termination: dyad symmetry in DNA causes RNA polymerase to pause during transcription in vitro. *Nucl. Acids Res.*, **9**: pp.563–77.

Feklistov, A., Darst, S.A. (2009.) Promoter recognition by bacterial alternative sigma factors: the price of high selectivity? *Genes & Development*, **23**: pp.2371–5.

Ferguson, S.J. (1998). Nitrogen cycle enzymology. *Curr. Opinion in Chem. Biol.*, **2**: pp.182–93.

Figurski, D.H., Helinski, D.R. (1979). Replication of an origin-containing derivative of plasmid RK2 dependent on a plasmid function provided in trans. *PNAS*, **76**: pp.1648–52.

Firestone, M.K. (1982). Nitrogen in Agricultural Soils, *American Society of Agronomy, Crop Science Society of America*.

Flores, E., Frías, José E., Rubio, L.M., Herrero, A. (2005). Photosynthetic nitrate assimilation in cyanobacteria. *Photosynthesis Res.*, **83**: pp.117–33.

Forchhammer, K. (2008). P(II) signal transducers: novel functional and structural insights. *Trends in Microbiol.*, **16**: pp.65–72.

Forward, J.A., Behrendt, M.C., Wyborn, N.R., Cross, R., Kelly, D.J. (1997). TRAP transporters: a new family of periplasmic solute transport systems encoded by the *dctPQM* genes of *Rhodobacter capsulatus* and by homologs in diverse gram-negative bacteria. *J. Bacteriol.*, **179**: pp.5482–93.

Foster-Hartnett, D., Cullen, P.J., Gabbert, K.K., Kranz, R.G. (1993). Sequence, genetic, and lacZ fusion analyses of a *nifR3-ntrB-ntrC* operon in *Rhodobacter capsulatus*. *Mol. Microbiol.*, **8**: pp.903–14.

Foster-Hartnett, D., Cullen, P.J., Monika, E.M., Kranz, R.G. (1994). A new type of NtrC transcriptional activator. *J. Bacteriol.*, **176**: pp.6175–87.

Francis, C.A., Beman, J.M., Kuypers, M.M.M. (2007). New processes and players in the nitrogen cycle: the microbial ecology of anaerobic and archaeal ammonia oxidation. *ISME*, **1**: pp.19–27.

- Fried, M.G.** (1989). Measurement of protein-DNA interaction parameters by electrophoresis mobility shift assay. *Electrophoresis*, **10**: pp.366–76.
- Frieden, C.** (1959). Glutamic dehydrogenase. II. The effect of various nucleotides on the association-dissociation and kinetic properties. *JBC*, **234**: pp.815–20.
- Fuerst, J.A., Sagulenko, E.** (2011). Beyond the bacterium: planctomycetes challenge our concepts of microbial structure and function. *Nature Rev. Microbiol.*, **9**: pp.403–13.
- Galloway, J.N.** (2003). *Treatise on Geochemistry*, **8**.
- Garcia, E., Bancroft, S., Rhee, S.G., Kustu, S.** (1977). The product of a newly identified gene, *glnF*, is required for synthesis of glutamine synthetase in *Salmonella*. *PNAS*, **74**: pp.1662–6.
- Garner, M.M., Revzin, A.** (1981). A gel electrophoresis method for quantifying the binding of proteins to specific DNA regions: application to components of the *Escherichia coli* lactose operon regulatory system. *Nucl. Acids Res.*, **9**: pp.3047–60.
- Gates, A.J. Luque-Almagro, V.M., Goddard, A.D., Ferguson, S.J., Roldán, M.D., Richardson, D.J.** (2011). A composite biochemical system for bacterial nitrate and nitrite assimilation as exemplified by *Paracoccus denitrificans*. *Biochem. J.*, **435**: pp.743–53.
- Gates, A.J., Richardson, D.J., Butt, J.N.** (2008). Voltammetric characterization of the aerobic energy-dissipating nitrate reductase of *Paracoccus pantotrophus*: exploring the activity of a redox-balancing enzyme as a function of electrochemical potential. *Biochem. J.*, **409**: pp.159–68.
- Glaser, P., Danchin, A., Kunst, F., Zuber, P., Nakano, M.M.** (1995). Identification and isolation of a gene required for nitrate assimilation and anaerobic growth of *Bacillus subtilis*. *J. Bacteriol.*, **177**: pp.1112–5.
- Goldman, B.S., Lin, J.T, Stewart, V.** (1994). Identification and structure of the *nasR* gene encoding a nitrate- and nitrite-responsive positive regulator of *nasFEDCBA* (nitrate assimilation) operon expression in *Klebsiella pneumoniae* M5a1. *J. Bacteriol.* **176**: pp.5077–85.
- González, P.J., Correia, C., Moura, I., Brondino, C.D., Moura, J.J.G.** (2006). Bacterial nitrate reductases: Molecular and biological aspects of nitrate reduction. *J. Inorganic Biochem.*, **100**: pp.1015–23.
- Gordon-Walker, A., Penzer, G.R., Radda, G.K.** (1970). Excited States of Flavins Characterised by Absorption, Prompt and Delayed Emission Spectra. *European J.*

Biochem., **13**: pp.313–21.

Gräslund, S., et al. (2008). Protein production and purification. *Nature Methods*, **5**: pp.135–46.

Griffiths, S., Byrne, R.T., Antson, A.A., Whelan, F. (2012). Crystallization and preliminary X-ray crystallographic analysis of the catalytic domain of human dihydrouridine synthase. *Acta crystallographica. Section F*, **68**., pp.333–6.

Gruber, T.M., Gross, C.A. (2003). Multiple Sigma Subunits and the Partitioning of Bacterial Transcription Space. *Annu. Rev. Microbiol.*, **57**, pp. 441-66.

Guerrero, M.G., Vega, J.M., Losada, M. (1981). The Assimilatory Nitrate-Reducing System and its Regulation. *Annu. Rev. Plant Physiol.*, **32**: pp.169–204.

Gunka, K., Commichau, F.M. (2012). Control of glutamate homeostasis in *Bacillus subtilis*: a complex interplay between ammonium assimilation, glutamate biosynthesis and degradation. *Mol. Microbiol.*, **85**: pp.213–24.

Gustilo, E.M., Vendeix, F.A., Agris, P.F. (2008). tRNA's modifications bring order to gene expression. *Curr. Opinion in Microbiol.*, **11**: pp.134–40.

Gutierrez, J.C., Ramos, F., Ortner, L., Tortolero, M. (1995). *nasST*, two genes involved in the induction of the assimilatory nitrite-nitrate reductase operon (*nasAB*) of *Azotobacter vinelandii*. *Mol. Microbiol.*, **18**: pp.579–91.

Hanahan, D. 1983. Studies on transformation of *Escherichia coli* with plasmids. *J. Mol. Biol.*, **166**: pp.557–80.

Handley, K.M., VerBerkmoes, N.C., Steefel, C.I., Williams, K.H., Sharon, I., Miller, C.S., Frischkorn, K.R., Chourey, K., Thomas, B.C., Shah, M.B., Long, P.E., Hettich, R.L., Banfield, J.F. (2013). Biostimulation induces syntrophic interactions that impact C, S and N cycling in a sediment microbial community. *ISME*, **7**: pp.800–16.

Hanson, R. (1990). Oxidation states of carbon as aids to understanding oxidative pathways in metabolism. *Biochemical Education*, **18**: pp.194–6.

Hanze, A.R. (1967). Nucleic acids. IV. The catalytic reduction of pyrimidine nucleosides (human liver deaminase inhibitors). *JACS*, **89**., pp.6720–5.

Hardt, W.D., Schlegl, J., Erdmann, V.A., Hartmann, R.K. (1993). Role of the D arm and the anticodon arm in tRNA recognition by eubacterial and eukaryotic RNase P enzymes. *Biochem.*, **32**: pp.13046–053.

- Helling, R.B.** (1998). Pathway choice in glutamate synthesis in *Escherichia coli*. *J. Bacteriol.*, **180**: pp.4571–5.
- van den Heuvel, R.H.H., Svergun, D.I., Petoukhov, M.V., Coda, A., Curti, B., Ravasio, S., Vanoni, M.A., Mattevi, A.** (2003). The active conformation of glutamate synthase and its binding to ferredoxin. *J. Mol. Biol.*, **330**: pp.113–28.
- Hillard, E.A., et al.** (2008). Electrochemical parameters and techniques in drug development, with an emphasis on quinones and related compounds. *Chem. Comm.*, **69**: p.2612.
- Hochstein, L.I., Tomlinson, G.A.** (1988). The enzymes associated with denitrification. *Annu. Rev. Microbiol.*, **42**: pp.231–61.
- Hu, B., Shen, L., Xu, X., Zheng, P.** (2011). Anaerobic ammonium oxidation (anammox) in different natural ecosystems. *Biochem. Soc. Transactions*, **39**: pp.1811–6.
- Hurwitz, J., Gold, M., Anders, M.** (1964). The Enzymatic Methylation of Ribonucleic Acid and Deoxyribonucleic Acid. 3. Purification of Soluble Ribonucleic Acid-Methylating Enzymes. *JBC*, **239**: pp.3462–73.
- Hutchings, M.I., Crack, J.C., Shearer, N., Thompson, B.J., Thomson, A.J., Spiro, S.** (2002). Transcription Factor FnrP from *Paracoccus denitrificans* Contains an Iron-Sulfur Cluster and Is Activated by Anoxia: Identification of Essential Cysteine Residues. *J. Bacteriol.*, **184**: pp.503–8.
- Ilbert, M., Méjean, V., Iobbi-Nivol, C.** (2004). Functional and structural analysis of members of the TorD family, a large chaperone family dedicated to molybdoproteins. *Microbiol.*, **150**: pp.935–43.
- Imada, A., Igarasi, S., Nakahama, K., Isono, M.** (1973). Asparaginase and glutaminase activities of micro-organisms. *J. General Microbiol.*, **76**: pp.85–99.
- Imai, T.** (1973). Purification and properties of nicotinamide mononucleotide amidohydrolase from *Azotobacter vinelandii*. *J. Biochem.*, **73**: pp.139–53.
- Ishida, M.L., Assumpção, M.C., Machado, H.B., Benelli, E.M., Souza, E.M., Pedrosa, F.O.** (2002). Identification and characterization of the two-component NtrY/NtrX regulatory system in *Azospirillum brasilense*. *Brazilian J. Med. and Biol. Res.*, **35**: pp.651–61.
- Islam, S.D.M., Susdorf, T., Penzkofer, A., Hegemann, P.** (2003). Fluorescence quenching of flavin adenine dinucleotide in aqueous solution by pH dependent isomerisation and photo-induced electron transfer. *Chem. Phys.*, **295**: pp.137–49.

- Jacobson, M., Hedgcoth, C.** (1970). Determination of 5,6-dihydrouridine in ribonucleic acid. *Anal. Biochem.*, **34**: pp.459–69.
- Jepson, B.J.N., Mohan, S., Clarke, T.A., Gates, A.J., Cole, J.A., Butler, C.S., Butt, J.N., Hemmings, A.M., Richardson, D.J.** (2007). Spectropotentiometric and structural analysis of the periplasmic nitrate reductase from *Escherichia coli*. *JBC*, **282**: pp.6425–37.
- Jepson, B.J.N., Anderson, L.J., Rubio, L.M., Taylor, C.J., Butler, C.S., Flores, E., Herrero, A., Butt, J.N., Richardson, D.J.** (2004). Tuning a nitrate reductase for function. The first spectropotentiometric characterization of a bacterial assimilatory nitrate reductase reveals novel redox properties. *JBC*, **279**: pp.32212–8.
- John, P., Whatley, F.R.** (1975). *Paracoccus denitrificans* and the evolutionary origin of the mitochondrion. *Nature*, **254**: pp.495–8.
- Johnson, L.T., Royer, T.V., Edgerton, J.M., Leff, L.G.** (2012). Manipulation of the Dissolved Organic Carbon Pool in an Agricultural Stream: Responses in Microbial Community Structure, Denitrification, and Assimilatory Nitrogen Uptake. *Ecosystems*, **15**: pp.1027–38.
- Johnston, A.W.B., Setchell, S.M., Beringer, J.E.** (1978). Interspecific Crosses between *Rhizobium leguminosarum* and *R. meliloti*: Formation of Haploid Recombinants and of R-primes. *J. General Microbiol.*, **104**: pp.209–218.
- Jones, R.W., Gray, T.A., Garland, P.B.** (1976). A Study of the Permeability of the Cytoplasmic Membrane of *Escherichia coli* to Reduced and Oxidized Benzyl Viologen and Methyl Viologen Cations: Complications in the Use of Viologens as Redox Mediators for Membrane-Bound Enzymes. *Biochem. Soc. Trans.*, **4**: pp. 671-3.
- Jones, S.** (2009). Bacterial transcription: Sigma 54 minds the gap. *Nature Rev. Microbiol.*, **7**: pp.3.
- Kadenbach, B.** (2003). Intrinsic and extrinsic uncoupling of oxidative phosphorylation. *Biochimica et Biophysica Acta*, **1604**: pp.77–94.
- Kammen, H.O., Marvel, C.C., Hardy, L., Penhoet, E.E.** (1988). Purification, structure, and properties of *Escherichia coli* tRNA pseudouridine synthase I. *JBC*, **263**: pp.2255–63.
- Kanamori, K., Weiss, R.L., Roberts, J.D.** (1989). Ammonia assimilation pathways in nitrogen-fixing *Clostridium kluyverii* and *Clostridium butyricum*. *J. Bacteriol.*, **171**: pp.2148–54.

- Kapanidis, A.N., Margeat, E., Laurence, T.A., Doose, S., Ho, S.O., Mukhopadhyay, J., Kortkhonja, E., Mekler, V., Ebright, R.H., Weiss, S.** (2005). Retention of transcription initiation factor sigma70 in transcription elongation: single-molecule analysis. *Mol. Cell*, **20**: pp.347–56.
- Kasprzak, J.M., Czerwoniec, A., Bujnicki, J.M.** (2012). Molecular evolution of dihydrouridine synthases. *BMC Bioinformatics*, **13**: p.153.
- Kato, T., Daigo, Y., Hayama, S., Ishikawa, N., Yamabuki, T., Ito, T., Miyamoto, M., Kondo, S., Nakamura, Y.** (2005). A novel human tRNA-dihydrouridine synthase involved in pulmonary carcinogenesis. *Cancer Res.*, **65**: pp.5638–46.
- Kazmierczak, M.J., Wiedmann, M., Boor, K.J.** (2005). Alternative sigma factors and their roles in bacterial virulence. *Microbio. and Mol. Biol. Rev.* **69**: pp.527–43.
- Kelley, L.A., Mezulis, S., Yates, C.M., Wass, M.N., Sternberg, M.J.E** (2015). The Phyre2 web portal for protein modeling, prediction and analysis. *Nature Protocols*, **10**: pp.845–58.
- Kelly, D.J., Thomas, G.H.** (2001). The tripartite ATP-independent periplasmic (TRAP) transporters of bacteria and archaea. *FEMS Microbiol. Rev.*, **25**: pp.405–24.
- Khoroshilova, N., Popescu, C., Münck, E., Beinert, H., Kiley, P.J.** (1997). Iron-sulfur cluster disassembly in the FNR protein of *Escherichia coli* by O₂: [4Fe-4S] to [2Fe-2S] conversion with loss of biological activity. *PNAS*, **94**: pp.6087–92.
- Kiley, P.J., Beinert, H.** (1998). Oxygen sensing by the global regulator, FNR: the role of the iron-sulfur cluster. *FEMS Microbiol. Rev.*, **22**: pp.341–52.
- Kit, S.** (1985). Thymidine kinase. *Microbiol. Sciences*, **2**: pp.369–75.
- Kolberg, M., Strand, K.R., Graff, P., Kristoffer, A.K.** (2004). Structure, function, and mechanism of ribonucleotide reductases. *Biochimica et Biophysica Acta (BBA) - Proteins and Proteomics*, **1699**: pp.1–34.
- Koropatkin, N.M., Pakrasi, H.B., Smith, T.J.** (2006). Atomic structure of a nitrate-binding protein crucial for photosynthetic productivity. *PNAS*, **103**: pp.9820–5.
- Kowalak, J.A., Bruenger, E., McCloskey, J.A.** (1995). Posttranscriptional modification of the central loop of domain V in *Escherichia coli* 23 S ribosomal RNA. *JBC*, **270**: pp.17758–64.
- Kozioł, J.** (1971). [132] Fluorometric analyses of riboflavin and its coenzymes. *Methods in Enzymology*, **18**: pp.253–85.

- Kuchino, Y., Borek, E.** (1978). Tumour-specific phenylalanine tRNA contains two supernumerary methylated bases. *Nature*, **271**: pp.126–9.
- Kuenen, J.G.** (2008). Anammox bacteria: from discovery to application. *Nature Revs. Microbiol.*, **6**: pp.320–6.
- Kuenen, J.G., Robertson, L.A.** (1994). Combined nitrification-denitrification processes. *FEMS Microbiol. Rev.*, **15**: pp.109–17.
- Kustu, S., Santero, E., Keener, J., Popham, D., Weiss, D.** (1989). Expression of sigma 54 (ntrA)-dependent genes is probably united by a common mechanism. *Microbiol. Rev.*, **53**: pp.367–76.
- Letunic, I., Bork, P.** (2007). Interactive Tree Of Life (iTOL): an online tool for phylogenetic tree display and annotation. *Bioinformatics*, **23**: pp.127–8.
- Li, G.W., Burkhardt, D., Gross, C., Weissman, J.S.** (2014). Quantifying absolute protein synthesis rates reveals principles underlying allocation of cellular resources. *Cell*, **157**: pp.624–35.
- Li, H., Turner, R.J.** (2009). In vivo associations of *Escherichia coli* NarJ with a peptide of the first 50 residues of nitrate reductase catalytic subunit NarG. *Canadian J. Microbiol.*, **55**: pp.179–88.
- Li, S.F., DeMoss, J.A.** (1988). Location of sequences in the nar promoter of *Escherichia coli* required for regulation by Fnr and NarL. *JBC*, **263** pp.13700–5.
- Li, W., Lu, C.D.** (2007). Regulation of carbon and nitrogen utilization by CbrAB and NtrBC two-component systems in *Pseudomonas aeruginosa*. *J. Bacteriol.*, **189**: pp.5413–20.
- Li, Y., Bali, S., Borg, S., Katzmann, E., Ferguson, S.J., Schüler, D.** (2013). Cytochrome *cd1* nitrite reductase NirS is involved in anaerobic magnetite biomineralization in *Magnetospirillum gryphiswaldense* and requires NirN for proper d1 heme assembly. *J. Bacteriol.*, **195**: pp.4297–309.
- Li, Y., Katzmann, E., Borg, S., Schüler, D.** (2012). The periplasmic nitrate reductase Nap is required for anaerobic growth and involved in redox control of magnetite biomineralization in *Magnetospirillum gryphiswaldense*. *J. Bacteriol.*, **194**: pp.4847–56.
- Liaw, S.H., Kuo, I., Eisenberg, D.** (1995). Discovery of the ammonium substrate site on glutamine synthetase, a third cation binding site. *Protein science*, **4**: pp.2358–65.
- Lin, J.T., Goldman, B.S., Stewart, V.** (1994). The nasFEDCBA operon for nitrate and nitrite assimilation in *Klebsiella pneumoniae* M5al. *J. Bacteriol.*, **176**: pp.2551–9.

- Lin, J.T., Stewart, V.** (1996). Nitrate and nitrite-mediated transcription antitermination control of *nasF* (nitrate assimilation) operon expression in *Klebsiella pneumoniae* M5a1. *J. Mol. Biol.*, **256**: pp.423–35.
- Lin, J.T., Stewart, V.** (1998). Nitrate assimilation by bacteria. *Advances in Microbial Physiol.*, **39**: pp.1–30
- Liu, X., DeMoss, J.A.** (1997). Characterization of NarJ, a system-specific chaperone required for nitrate reductase biogenesis in *Escherichia coli*. *JBC*, **272**: pp.24266–71.
- Lü, W., Du, J., Schwarzer, N.J., Wacker, T., Andrade, S.L.A., Einsle, O.** (2013). The formate/nitrite transporter family of anion channels. *Biol. Chem.*, **394**: pp.715–27.
- Luque-Almagro, V.M., Gates, A.J., Moreno-Vivián, C., Ferguson, S.J., Richardson, D.J., Roldán, M.D.** (2011). Bacterial nitrate assimilation: gene distribution and regulation. *Biochem. Soc. Trans.*, **39**: pp.1838–43.
- Luque-Almagro, V.M., Lyall, V.J., Ferguson, S.J., Roldan, M.D., Richardson, D.J., Gates, A.J.** (2013). Nitrogen Oxyanion-dependent Dissociation of a Two-component Complex That Regulates Bacterial Nitrate Assimilation. *JBC*, **288**: pp.29692–702.
- Macheroux, P.** (1999). UV-visible spectroscopy as a tool to study flavoproteins. *Methods in Mol. Biol.*, **131**: pp.1–7.
- Magasanik, B.** (1982). Genetic control of nitrogen assimilation in bacteria. *Annu. Rev. of Genetics*, **16**: pp.135–68.
- Malm, S., Tiffert, Y., Micklinghoff, J., Schultze, S., Joost, I., Weber, I., Horst, S., Ackermann, B., Schmidt, M., Wohlleben, W., Ehlers, S., Geffers, R., Reuther, J., Bange, F.C.** (2009). The roles of the nitrate reductase NarGHJI, the nitrite reductase NirBD and the response regulator GlnR in nitrate assimilation of *Mycobacterium tuberculosis*. *Microbiol.*, **155**: pp.1332–9.
- Manzano, C., Candau, P., Gomez-Moreno, C., Relimpio, A.M., Losada, M.** (1976). Ferredoxin-dependent photosynthetic reduction of nitrate and nitrite by particles of *Anacystis nidulans*. *Mol. Cell. Biochem.*, **10**: pp.161–9.
- Martienssen, M., Schöps, R.** (1999). Population dynamics of denitrifying bacteria in a model biocommunity. *Water Res.*, **33**: pp.639–46.
- Mauri, M., Klumpp, S.** (2014). A Model for Sigma Factor Competition in Bacterial Cells *PLoS Comp. Biol.*, **10**: p.e1003845.
- McDevitt, C.A., Hugenholtz, P., Hanson, G.R., McEwan, A.G.** (2002). Molecular

analysis of dimethyl sulphide dehydrogenase from *Rhodovulum sulfidophilum*: its place in the dimethyl sulphoxide reductase family of microbial molybdopterin-containing enzymes. *Mol. Microbiol.*, **44**: pp.1575–87.

Mengin-Lecreux, D., van Heijenoort, J. (1996). Characterization of the essential gene glmM encoding phosphoglucosamine mutase in *Escherichia coli*. *JBC*, **271**: pp.32–9.

Merrick, M.J. (1993). In a class of its own--the RNA polymerase sigma factor sigma 54 (sigma N). *Mol. Microbiol.*, **10**: pp.903–9.

Merrick, M.J. (1992). Regulation of nitrogen fixation genes in free - living and symbiotic bacteria. *Biol.Nitrogen Fixation*. pp. 835–76.

Merrick, M.J., Edwards, R.A. (1995). Nitrogen control in bacteria. *Microbiol. Rev.*, **59**: pp.604–22.

Messing, J. (1979). A multipurpose cloning system based on the single-stranded DNA bacteriophage M13. *Recomb. DNA Tech. Bull.*, **3**: pp.43–8.

Michaelis, L., Schubert, M.P., Smythe, C.V. (1936). Potentiometric Study of the Flavins. *JBC*, **116**: pp.587-607.

Mikes, V., Chválová, H., Mátlová, L. (1991). Assimilation of ammonia in *Paracoccus denitrificans*. *Folia Microbiologica*, **36**: pp.35–41.

Miller, J.H. (1972). Experiments in Molecular Genetics. *Cold Spring Harbor Laboratory Press, NY*.

Miller, R.E. (1974). Glutamate synthase from *Escherichia coli*—An iron-sulfur flavoprotein. *Biochimica et Biophysica Acta (BBA) - Enzymology*, **364**: pp.243–9.

Mittelstadt, M., Frump, A., Khuu, T., Fowlkes, V., Handy, I., Patel, C.V., Patel, R.C. (2008). Interaction of human tRNA-dihydrouridine synthase-2 with interferon-induced protein kinase PKR. *Nucl. Acids Res.*, **36**: pp.998–1008.

Mobley, H.L., Hausinger, R.P. (1989). Microbial ureases: significance, regulation, and molecular characterization. *Microbiol. Rev.*, **53**: pp.85–108.

Moir, J.W., Wood, N.J. (2001). Nitrate and nitrite transport in bacteria. *CMLS*, **58**: pp.215–24.

Moreno-Vivián, C., Cabello, P., Martínez-Luque, M., Blasco, R., Castillo, F. (1999). Prokaryotic nitrate reduction: molecular properties and functional distinction among bacterial nitrate reductases. *J. Bacteriol*, **181**: pp.6573–84.

- Moreno-Vivián, C., Ferguson, S.J.** (1998). Definition and distinction between assimilatory, dissimilatory and respiratory pathways. *Mol. Microbiol.*, **29**: pp.664–6.
- Morett, E., Segovia, L.** (1993). The sigma 54 bacterial enhancer-binding protein family: mechanism of action and phylogenetic relationship of their functional domains. *J. Bacteriol.*, **175**: pp.6067–74.
- Morishita, R., Kawagoshi, A., Sawasaki, T., Madin, K., Ogasawara, T., Oka, T., Endo, Y.** (1999). Ribonuclease activity of rat liver perchloric acid-soluble protein, a potent inhibitor of protein synthesis. *JBC*, **274**: pp.20688–92.
- Mothes, G., Ackermann, J.U., Babel, W.** (2004). Mole Fraction Control of Poly([R]-3-hydroxybutyrate-co-3-hydroxyvalerate) (PHB/HV) Synthesized by *Paracoccus denitrificans*. *Engineering in Life Sci.*, **4**: pp.247–51.
- Motohara, K., Kobayashi, M., Ishimoto, M.** (1976). Assimilatory nitrate reductase in a chlorate-resistant mutant of *Escherichia coli*. *Zeitschrift für allgemeine Mikrobiologie*, **16**: pp.543–50.
- Mukherjee, A., et al.** (2013). Characterization of Flavin-Based Fluorescent Proteins: An Emerging Class of Fluorescent Reporters. *PLoS ONE*, **8**: p.e64753.
- Mulligan, C., Geertsma, E.R., Severi, E., Kelly, D.J., Poolman, B., Thomas, G.H.** (2009). The substrate-binding protein imposes directionality on an electrochemical sodium gradient-driven TRAP transporter. *PNAS*, **106**: pp.1778–83.
- Mulligan, C., Fischer, M., Thomas, G.H.** (2011). Tripartite ATP-independent periplasmic (TRAP) transporters in bacteria and archaea. *FEMS Microbiol. Rev.*, **35**: pp.68–86.
- Mulligan, C., Kelly, D.J., Thomas, G.H.** (2007). Tripartite ATP-independent periplasmic transporters: application of a relational database for genome-wide analysis of transporter gene frequency and organization. *J. Mol. Microbiol. Biotech.*, **12**: pp.218–26.
- Munro, A.W., Noble, M.A.** (1999). Fluorescence Analysis of Flavoproteins. *Flavoprotein Protocols*. New Jersey: Humana Press, pp. 25–48.
- Murphy, M.J., Siegel, L.M., Tove, S.R., Kamin, H.** (1974). Siroheme: a new prosthetic group participating in six-electron reduction reactions catalyzed by both sulfite and nitrite reductases. *PNAS*, **71**: pp.612–6.
- Murray, D.S., Chinnam, N., Tonthat, N.K., Whitfill, T., Wray, L.V., Fisher, S.H., Schumacher, M.A.** (2013). Structures of the *Bacillus subtilis* glutamine synthetase dodecamer reveal large intersubunit catalytic conformational changes linked to a unique

feedback inhibition mechanism. *JBC*, **288**: pp.35801–11.

Nakano, M.M., Yang, F., Hardin, P., Zuber, P. (1995). Nitrogen regulation of *nasA* and the *nasB* operon, which encode genes required for nitrate assimilation in *Bacillus subtilis*. *J. Bacteriol.*, **177**: pp.573–9.

Nakano, S., Takahashi, M., Sakamoto, A., Morikawa, H., Katayanagi, K. (2012). The reductive reaction mechanism of tobacco nitrite reductase derived from a combination of crystal structures and ultraviolet-visible microspectroscopy. *Proteins*, **80**: pp.2035–45.

Natale, P., Brüser, T., Driessen, A.J.M. (2008). Sec- and Tat-mediated protein secretion across the bacterial cytoplasmic membrane—Distinct translocases and mechanisms. *Biochimica et Biophysica Acta (BBA) - Biomembranes*, **1778**: pp.1735–56.

Nelson, D.L., Cox, M.M. (2013). Lehninger, Principles of Biochemistry, 6th edition. *W H Freeman*.

Nilavongse, A., Brondijk, T.H.C., Overton, T.W., Richardson, D.J., Leach, E.R., Cole, J.A. (2006). The NapF protein of the *Escherichia coli* periplasmic nitrate reductase system: demonstration of a cytoplasmic location and interaction with the catalytic subunit, NapA. *Microbiol.*, **152**: pp.3227–37.

Ninfa, A.J., Magasanik, B. (1986). Covalent modification of the *glnG* product, NRI, by the *glnL* product, NRII, regulates the transcription of the *glnALG* operon in *Escherichia coli*. *PNAS*, **83**: pp.5909–13.

O'Connor, M., Lee, W.M., Mankad, A., Squires, C.L., Dahlberg, A.E. (2001). Mutagenesis of the peptidyltransferase center of 23S rRNA: the invariant U2449 is dispensable. *Nucl. Acids Res.*, **29**: pp.710–5.

O'Hara, B.P., Norman, R.A., Wan, P.T., Roe, S.M., Barrett, T.E., Drew, R.E., Pearl, L.H. (1999). Crystal structure and induction mechanism of AmiC-AmiR: a ligand-regulated transcription antitermination complex. *EMBO*, **18**: pp.5175–86.

Ogawa, K., Akagawa, E., Yamane, K., Sun, Z.W., LaCelle, M., Zuber, P., Nakano, M.M. (1995). The *nasB* operon and *nasA* gene are required for nitrate/nitrite assimilation in *Bacillus subtilis*. *J. Bacteriol.*, **177**: pp.1409–13.

Ohashi, Y., Shi, W., Takatani, N., Aichi, M., Maeda, S., Watanabe, S., Yoshikawa, H., Omata, T. (2011). Regulation of nitrate assimilation in cyanobacteria. *J. Exp. Botany*, **62**: pp.1411–24.

Omata, T. (1991). Cloning and Characterization of the *nrtA* Gene That Encodes a 45-kDa

Protein Involved in Nitrate Transport in the *Cyanobacterium Synechococcus* PCC 7942. *Plant Cell Physiol.*, 32:pp.151–157.

Opran, D.D., Coon, M.J. (1982). Oxidation-reduction states of FMN and FAD in NADPH-cytochrome P-450 reductase during reduction by NADPH. *JBC*, **257**: pp.8935–44.

Oron, A. (2001). Encyclopedia of Life Sciences. *Chichester, UK: John Wiley & Sons, Ltd.*

Paget, M.S.B., Helmann, J.D. (2003). The sigma70 family of sigma factors. *Genome Biol.*, **4**: p.203.

Palmer, T., Santini, C.L., Iobbi-Nivol, C., Eaves, D.J., Boxer, D.H., Giordano, G. (1996). Involvement of the *narJ* and *mob* gene products in distinct steps in the biosynthesis of the molybdoenzyme nitrate reductase in *Escherichia coli*. *Mol. Microbiol.* **20**: pp.875–84.

Pao, S.S., Paulsen, I.T., Saier, M.H. (1998). Major facilitator superfamily. *Microbiol. Mol. Biol. Rev.*, **62**: pp.1–34.

Patriarca, E.J., Riccio, A., Taté, R., Colonna-Romano, S., Iaccarino, M., Defez, R. (1993). The *ntrBC* genes of *Rhizobium leguminosarum* are part of a complex operon subject to negative regulation. *Mol. Microbiol.*, **9**: pp.569–77.

Pawlowski, K., Klosse, U., de Bruijn, F.J. (1991). Characterization of a novel *Azorhizobium caulinodans* ORS571 two-component regulatory system, NtrY/NtrX, involved in nitrogen fixation and metabolism. *Mol. & General Genetics*, **231**: pp.124–38.

Pino, C., Olmo-Mira, F., Cabello, P., Martínez-Luque, M., Castillo, F., Roldán, M.D., Moreno-Vivián, C. (2006). The assimilatory nitrate reduction system of the phototrophic bacterium *Rhodobacter capsulatus* E1F1. *Biochem. Soc. Trans.*, **34**: pp.127–9.

Pomowski, A., Zumft, W.G., Kroneck, P.M.H., Einsle, O. (2011). N₂O binding at a [4Cu:2S] copper-sulphur cluster in nitrous oxide reductase. *Nature*, **477**: pp.234–7.

Porath, J., Carlsson, J., Olsson, I., Belfrage, G. (1975). Metal chelate affinity chromatography, a new approach to protein fractionation. *Nature*, **258**: pp.598–9.

Postgate, J. (1998). Nitrogen Fixation. *Cambridge University Press.*

Postgate, J. (2012). The Chemistry and Biochemistry of Nitrogen Fixation. *Springer Science.*

Price, M.L., Scoyoc, S., Butler, L.G. (2002). A critical evaluation of the vanillin reaction as an assay for tannin in sorghum grain. *J. Agric. Food Chem.*, **26**: pp. 1214-8.

- Quigley, G.J., Rich, A.** (1976). Structural domains of transfer RNA molecules. *Science*, **194**: pp.796–806.
- Radchenko, M. V, Thornton, J., Merrick, M.** (2013). P(II) signal transduction proteins are ATPases whose activity is regulated by 2-oxoglutarate. *PNAS*, **110**: pp.12948–53.
- Ramesh, A., DebRoy, S., Goodson, J.R., Fox, K.A., Faz, H., Garsin, D.A., Winkler, W.C.** (2012). The mechanism for RNA recognition by ANTAR regulators of gene expression. *PLoS Genetics*, **8**: p.e1002666.
- Ramos, F., Blanco, G., Gutiérrez, J.C., Luque, F., Tortolero, M.** (1993). Identification of an operon involved in the assimilatory nitrate-reducing system of *Azotobacter vinelandii*. *Mol. Microbiol.*, **8**: pp.1145–53.
- Rappas, M., Bose, D., Zhang, X.** (2007). Bacterial enhancer-binding proteins: unlocking sigma54-dependent gene transcription. *Curr. Op. Structural Biol.*, **17**: pp.110–6.
- Raux, E., Schubert, H.L., Warren, M.J.** (2000). Biosynthesis of cobalamin (vitamin B12): a bacterial conundrum. *CMLS*, **57**: pp.1880–93.
- Ravishankara, A.R., Daniel, J.S., Portmann, R.W.** (2009). Nitrous oxide (N₂O): the dominant ozone-depleting substance emitted in the 21st century. *Science*, **326**: pp.123–5.
- Redelberger, D., Seduk, F., Genest, O., Méjean, V., Leimkühler, S., Iobbi-Nivol, C.** (2011). YcdY protein of *Escherichia coli*, an atypical member of the TorD chaperone family. *J. Bacteriol*, **193**: pp.6512–6.
- Reitzer, L.** (2004). Biosynthesis of Glutamate, Aspartate, Asparagine, L-Alanine, and D-Alanine. *EcoSal Plus*, **1**.
- Richardson, D., Felgate, H., Watmough, N., Thomson, A., Baggs, E.** (2009). Mitigating release of the potent greenhouse gas N(2)O from the nitrogen cycle - could enzymic regulation hold the key? *Trends in Biotech.*, **27**: pp.388–97.
- Richardson, D.J.** (2000). Bacterial respiration: a flexible process for a changing environment. *Microbiol.*, **146**: pp.551–71.
- Richardson, D.J., Berks, B.C., Russell, D.A., Spiro, S. Taylor, C.J.** (2001). Functional, biochemical and genetic diversity of prokaryotic nitrate reductases. *CMLS*, **58**: pp.165–78.
- Richardson, D.J.** (2008). *Structural and Functional Flexibility of Bacterial Respiromes*. Springer Berlin Heidelberg.

- Richardson, D.J., King, G.F., Kelly, D.J., McEwan, A.G., Ferguson, S.J., Jackson, J.B.** (1988). The role of auxiliary oxidants in maintaining redox balance during phototrophic growth of *Rhodobacter capsulatus* on propionate or butyrate. *Arch. Microbiol.*, **150**: pp.131–137.
- Richardson, D.J., Ferguson, S.J.** (1992). The influence of carbon substrate on the activity of the periplasmic nitrate reductase in aerobically grown *Thiosphaera pantotropha*. *Arch. Microbiol.*, **157**: pp.535–537.
- Richardson, D.J., Watmough, N.J.** (1999). Inorganic nitrogen metabolism in bacteria. *Curr. Op. Chem. Biol.*, **3**: pp.207–19.
- Rider, L.W., Ottosen, M.B., Gattis, S.G., Palfey, B.A.** (2009). Mechanism of dihydrouridine synthase 2 from yeast and the importance of modifications for efficient tRNA reduction. *JBC*, **284**: pp.10324–33.
- Rodríguez, R., Kobayashi, M., Omata, T., Lara, C.** (1998). Independence of carbon and nitrogen control in the posttranslational regulation of nitrate transport in the cyanobacterium *Synechococcus* sp. strain PCC 7942. *FEBS Letters*, **432**: pp.207–12.
- Roldan, M.D., Sears, H.J., Cheesman, M.R., Ferguson, S.J., Thomson, A.J., Berks, B.C., Richardson, D.J.** (1998). Spectroscopic Characterization of a Novel Multiheme-Type Cytochrome Widely Implicated in Bacterial Electron Transport. *JBC*, **273**: pp.28785–90.
- Rosano, G.L., Ceccarelli, E.A.** (2014). Recombinant protein expression in *Escherichia coli*: advances and challenges. *Frontiers in Microbiol.*, **5**: p.172.
- Rossen, L., Shearman, C.A., Johnston, A.W, Downie, J.A.** (1985). The *nodD* gene of *Rhizobium leguminosarum* is autoregulatory and in the presence of plant exudate induces the *nodA,B,C* genes. *EMBO*, **4**: pp.3369–73.
- Rougraff, P.M., Paxton, R., Kuntz, M.J., Crabb, D.W., Harris, R.A.** (1988). Purification and characterization of 3-hydroxyisobutyrate dehydrogenase from rabbit liver. *JBC*, **263**: pp.327–31.
- Rozenski, J., Crain, P.F., McCloskey, J.A.** (1999). The RNA Modification Database: 1999 update. *Nucl. Acids Res.*, **27**: pp.196–7.
- Ruiz, J.** (1998). NAD-specific glutamate dehydrogenase from *Thermus thermophilus* HB8: purification and enzymatic properties. *FEMS Microbiol. Letters*, **159**: pp.15–20.
- Sanders, D.A., Gillece-Castro, B.L., Burlingame, A.L., Koshland, D.E.** (1992).

Phosphorylation site of NtrC, a protein phosphatase whose covalent intermediate activates transcription. *J. Bacteriol.*, **174**: pp.5117–22.

Schäfer, A., Tauch, A., Jäger, W., Kalinowski, J., Thierbach, G., Pühler, A. (1994). Small mobilizable multi-purpose cloning vectors derived from the *Escherichia coli* plasmids pK18 and pK19: selection of defined deletions in the chromosome of *Corynebacterium glutamicum*. *Gene*, **145**: pp.69–73.

Schwacha, A., Bender, R.A. (1993). The product of the *Klebsiella aerogenes nac* (nitrogen assimilation control) gene is sufficient for activation of the *hut* operons and repression of the *gdh* operon. *J. Bacteriol.*, **175**: pp.2116–24.

Sears, H., Little, P.J., Richardson, D.J., Berks, B.C., Spiro, S., Ferguson, S.J. (1997). Identification of an assimilatory nitrate reductase in mutants of *Paracoccus denitrificans* GB17 deficient in nitrate respiration. *Arch. Microbiol.*, **167**: pp.61–6.

Sears, H.J., Sawers, G., Berks, B.C., Ferguson, S.J., Richardson, D.J. (2000). Control of periplasmic nitrate reductase gene expression (*napEDABC*) from *Paracoccus pantotrophus* in response to oxygen and carbon substrates. *Microbiol.*, **146**: pp.2977–85.

Seefeldt, L.C., Hoffman, B.M., Dean, D.R. (2009). Mechanism of Mo-dependent nitrogenase. *Annu. Rev. Biochem.*, **78**: pp.701–22.

Seitzinger, S., Harrison, J.A., Böhlke, J.K., Bouwman, A.F., Lowrance, R., Peterson, B., Tobias, C., Van Drecht, G. (2006). Denitrification across landscapes and waterscapes: a synthesis. *Ecological applications*, **16**: pp.2064–90.

Senior, P.J. (1975). Regulation of nitrogen metabolism in *Escherichia coli* and *Klebsiella aerogenes*: studies with the continuous-culture technique. *J. Bacteriol.*, **123**: pp.407–18.

Shao, Z., Gao, J., Ding, X., Wang, J., Chiao, J., Zhao, G. (2011). Identification and functional analysis of a nitrate assimilation operon *nasACKBDEF* from *Amycolatopsis mediterranei* U32. *Arch. Microbiol.*, **193**: pp.463–77.

Sharma, U.K., Chatterji, D. (2010). Transcriptional switching in *Escherichia coli* during stress and starvation by modulation of sigma activity. *FEMS Microbiol. Rev.*, **34**: pp.646–57.

Shi, W., Lu, W., Liu, Q., Zhi, Y., Zhou, P. (2014). The identification of the nitrate assimilation related genes in the novel *Bacillus megaterium* NCT-2 accounts for its ability to use nitrate as its only source of nitrogen. *Functional & Integrative Genomics*, **14**: pp.219–27.

- Shiro, Y.** (2012). Structure and function of bacterial nitric oxide reductases: nitric oxide reductase, anaerobic enzymes. *Biochimica et biophysica acta*, **1817**: pp.1907–13.
- Short, J.M., Fernandez, J.M., Sorge, J.A., Huse, W.D.** (1988). Lambda ZAP: a bacteriophage lambda expression vector with in vivo excision properties. *Nucl. Acids Res.*, **16**: pp.7583–600.
- Shu, C.J., Zhulin, I.B.** (2002). ANTAR: an RNA-binding domain in transcription antitermination regulatory proteins. *Trends in Biochem. Sci.*, **27**: pp.3–5.
- Simon, J., van Spanning, R.J.M., Richardson, D.J.** (2008). The organisation of proton motive and non-proton motive redox loops in prokaryotic respiratory systems. *Biochimica et biophysica acta*, **1777**: pp.1480–90.
- Smith, D., Yarus, M.** (1989). Transfer RNA structure and coding specificity. *J. Mol. Biol.*, **206**: pp.489–501.
- Sodergren, E.J., Hsu, P.Y., DeMoss, J.A.** (1988). Roles of the *narJ* and *narI* gene products in the expression of nitrate reductase in *Escherichia coli*. *JBC*, **263**: pp.16156–62.
- Solomonson, L.P., Barber, M.J.** (1990). Assimilatory Nitrate Reductase: Functional Properties and Regulation. *Annu. Rev. Plant Phys.* **41**: pp.225–53.
- Spaink, H.P., Okker, R.J., Wijffelman, C.A., Pees, E., Lugtenberg, B.J.** (1987). Promoters in the nodulation region of the *Rhizobium leguminosarum* Sym plasmid pRL1JI. *Plant Mol. Biol.*, **9**: pp.27–39.
- Spanaki, C., Plaitakis, A.** (2012). The role of glutamate dehydrogenase in mammalian ammonia metabolism. *Neurotoxicity Res.*, **21**: pp.117–27.
- Sprinzi, M., Horn, C., Brown, M., loudovitch, A., Steinberg, S.** (1998). Compilation of tRNA sequences and sequences of tRNA genes. *Nucl. Acids Res.*, **26**: pp.148–53.
- Stadtman, E.R.** (2001). The story of glutamine synthetase regulation. *JBC*, **276**: pp.44357–64.
- Stewart, V., Lu, Y., Darwin, A.J.** (2002). Periplasmic nitrate reductase (NapABC enzyme) supports anaerobic respiration by *Escherichia coli* K-12. *J. Bacteriol.*, **184**: pp.1314–23.
- Stewart, V., van Tilbeurgh, H.** (2012). Found: the elusive ANTAR transcription antiterminator. *PLoS Genetics*, **8**: p.e1002773.
- Studholme, D.J., Buck, M.** (2000). The biology of enhancer-dependent transcriptional

regulation in bacteria: insights from genome sequences. *FEMS Microbiol. Letters*, **186**: pp.1–9.

Studier, F.W., Rosenberg, A.H., Dunn, J.J., Dubendorff, J.W. (1990). Use of T7 RNA polymerase to direct expression of cloned genes. *Methods in Enzymology*, **185**: pp.60–89.

Suck, D., Saenger, W., Zechmeister, K. (1971). Conformation of the tRNA minor constituent dihydrouridine. *FEBS Letters*, **12**: pp.257–9.

Sullivan, M.J., Gates, A.J., Appia-Ayme, C., Rowley, G., Richardson, D.J. (2013). Copper control of bacterial nitrous oxide emission and its impact on vitamin B12-dependent metabolism. *PNAS*, **110**: pp.19926–31.

Swanson, R. V., Alex, L.A., Simon, M.I. (1994). Histidine and aspartate phosphorylation: two-component systems and the limits of homology. *Trends in Biochem. Sci.*, **19**: pp.485–490.

Szeto, W.W., Nixon, B.T., Ronson, C.W., Ausubel, F.M. (1987). Identification and characterization of the *Rhizobium meliloti* ntrC gene: *R. meliloti* has separate regulatory pathways for activation of nitrogen fixation genes in free-living and symbiotic cells. *J. Bacteriol.*, **169**: pp.1423–32.

Takahashi, K., Hattori, T., Nakanishi, T., Nohno, T., Fujita, N., Ishihama, A., Taniguchi, S. (1994). Repression of in vitro transcription of the *Escherichia coli* *fnr* and *narX* genes by FNR protein. *FEBS Letters*, **340**: pp.59–64.

Takaya, N., Catalan-Sakairi, M.A.B., Sakaguchi, Y., Kato, I., Zhou, Z., Shoun, H. (2003). Aerobic denitrifying bacteria that produce low levels of nitrous oxide. *Appl. and Env. Microbiol.*, **69**: pp.3152–7.

Tate, R., Riccio, A., Iaccarino, M., Patriarca, E.J. (1997). A *cysG* mutant strain of *Rhizobium etli* pleiotropically defective in sulfate and nitrate assimilation. *J. Bacteriol.*, **179**: pp.7343–50.

Tempest, D.W., Meers, J.L., Brown, C.M. (1970). Synthesis of glutamate in *Aerobacter aerogenes* by a hitherto unknown route. *Biochem. J.*, **117**: pp.405–7.

Terpe, K. (2003). Overview of tag protein fusions: from molecular and biochemical fundamentals to commercial systems. *Appl. Microbiol. Biotechnol.*, **60**: pp.523–33.

Tett, A.J., Rudder, S.J., Bourdès, A., Karunakaran, R., Poole, P.S. (2012). Regulatable vectors for environmental gene expression in Alphaproteobacteria. *Appl. and Env.*

Microbiol., **78**: pp.7137–40.

Thomas, D., Surdin-Kerjan, Y. (1997). Metabolism of sulfur amino acids in *Saccharomyces cerevisiae*. *Microbiol. and Mol. Biol. Rev.*, **61**: pp.503–32.

Tolman, W.B. (2010). Binding and activation of N₂O at transition-metal centers: recent mechanistic insights. *Angewandte Chemie*, **49**: pp.1018–24.

Toukdarian, A., Kennedy, C. (1986). Regulation of nitrogen metabolism in *Azotobacter vinelandii*: isolation of *ntr* and *glnA* genes and construction of *ntr* mutants. *EMBO*, **5**: pp.399–407.

Tripathy, B.C., Sherameti, I., Oelmüller, R. (2010). Siroheme: an essential component for life on earth. *Plant Signaling & Behavior*, **5**: pp.14–20.

Turner, R.J., Papish, A.L., Sargent, F. (2004). Sequence analysis of bacterial redox enzyme maturation proteins (REMPs). *Canadian J. Microbiol.*, **50**: pp.225–38.

Tyler, B. (1978). Regulation of the assimilation of nitrogen compounds. *Annu. Rev. Biochem.*, **47**: pp.1127–62.

Uden, G., Achebach, S., Holighaus, G., Tran, H.G., Wackwitz, B., Zeuner, Y. (2002). Control of FNR function of *Escherichia coli* by O₂ and reducing conditions. *J. Mol. Microbiol. and Biotech.*, **4**: pp.263–8.

Uden, G., Bongaerts, J. (1997). Alternative respiratory pathways of *Escherichia coli*: energetics and transcriptional regulation in response to electron acceptors. *Biochimica et biophysica acta*, **1320**: pp.217–34.

Urbonavicius, J., Stahl, Gu., Durand, J.M.B., Ben Salem, S.N., Qian, Q., Farabaugh, P.J., Björk, G.R. (2003). Transfer RNA modifications that alter +1 frameshifting in general fail to affect -1 frameshifting. *RNA*, **9**: pp.760–8.

US EPA, C.C.D. (2011). Carbon Dioxide Capture and Sequestration.

Vishniac, W., Santer, M. (1957). The thiobacilli. *Bacteriol.Rev.*, **21**: pp.195–213.

Vitorino, J.C., Steffens, M.B., Machado, H.B., Yates, M.G., Souza, E.M., Pedrosa, F.O. (2001). Potential roles for the *glnB* and *ntrYX* genes in *Azospirillum brasilense*. *FEMS Microbiol. Letters*, **201**: pp.199–204.

de Vries, G.E., Harms, N., Hoogendijk, J., Stouthamer, A.H. (1989). Isolation and characterization of *Paracoccus denitrificans* mutants with increased conjugation frequencies and pleiotropic loss of a (nGATCn) DNA-modifying property. *Arch. Microbiol.*,

152: pp.52–7.

Walker, S.E. (2013). RNA Purification – Precipitation Methods. *Methods in Enzymology*. pp. 337–43.

Wang, H., Gunsalus, R.P. (2000). The *nrfA* and *nirB* nitrite reductase operons in *Escherichia coli* are expressed differently in response to nitrate than to nitrite. *J. Bacteriol.*, **182:** pp.5813–22.

Wawrik, B., Boling, W.B., Van Nostrand, J.D., Xie, J., Zhou, J., Bronk, D.A. (2012). Assimilatory nitrate utilization by bacteria on the West Florida Shelf as determined by stable isotope probing and functional microarray analysis. *FEMS Microbiol. Eco.*, **79:** pp.400–11.

Weiss, V., Magasanik, B. (1988). Phosphorylation of nitrogen regulator I (NRI) of *Escherichia coli*. *PNAS*, **85:** pp.8919–23.

Whelan, F., Jenkins, H.T., Griffiths, S.C., Byrne, R.T., Dodson, E.J., Antson, A.A. (2015). From bacterial to human dihydrouridine synthase: automated structure determination. *Acta crystallographica. Section D*, **71:** pp.1564–71.

Wilson, K.S., von Hippel, P.H. (1995). Transcription termination at intrinsic terminators: the role of the RNA hairpin. *PNAS*, **92:** pp.8793–7.

Winkler, R.G., Blevins, D.G., Randall, D.D. (1988). Ureide Catabolism in Soybeans : III. Ureidoglycolate Amidohydrolase and Allantoate Amidohydrolase Are Activities of an Allantoate Degrading Enzyme Complex. *Plant Phys.*, **86:** pp.1084-8.

Woese, C.R., Olsen, G.J., Ibba, M., Söll, D. (2000). Aminoacyl-tRNA synthetases, the genetic code, and the evolutionary process. *Microbiol. and Mol. Biol. Rev.*, **64:** pp.202–36.

Wood, N.J., Alizadeh, T., Richardson, D.J., Ferguson, S.J., Moir, J.W.B. (2002). Two domains of a dual-function NarK protein are required for nitrate uptake, the first step of denitrification in *Paracoccus pantotrophus*. *Mol. Microbiol.*, **44:** pp.157–70.

Wood, W.B. (1966). Host specificity of DNA produced by *Escherichia coli*: bacterial mutations affecting the restriction and modification of DNA. *J. Mol. Biol.*, **16:** pp.118–33.

Wu, Q., Stewart, V. (1998). NasFED proteins mediate assimilatory nitrate and nitrite transport in *Klebsiella oxytoca (pneumoniae)* M5a1. *J. Bacteriol.*, **180:** pp.1311–22.

Wu, S.Q., Chai, W., Lin, J.T., Stewart, V. (1999). General nitrogen regulation of nitrate assimilation regulatory gene *nasR* expression in *Klebsiella oxytoca* M5a1. *J. Bacteriol.*,

181: pp.7274–84.

Xing, F., Hiley, S.L., Hughes, T.R., Phizicky, E.M. (2004). The specificities of four yeast dihydrouridine synthases for cytoplasmic tRNAs. *JBC*, **279**: pp.17850–60.

Xing, F., Martzen, M.R., Phizicky, E.M. (2002). A conserved family of *Saccharomyces cerevisiae* synthases effects dihydrouridine modification of tRNA. *RNA*, **8**: pp.370–81.

Xu, J., Johnson, R.C. (1995). Identification of genes negatively regulated by Fis: Fis and RpoS comodulate growth-phase-dependent gene expression in *Escherichia coli*. *J. Bacteriol.*, **177**: pp.938–47.

Yang, X.F., Ji, Y., Schneider, B.L., Reitzer, L. (2004). Phosphorylation-independent dimer-dimer interactions by the enhancer-binding activator NtrC of *Escherichia coli*: a third function for the C-terminal domain. *JBC*, **279**: pp.36708–14.

Yu, F., Yanaka, Y., Yamashita, K., Suzuki, T., Nakamura, A., Hirano, N., Suzuki, T., Yao, M., Tanaka, I. (2011). Molecular basis of dihydrouridine formation on tRNA. *PNAS*, **108**: pp.19593–8.

Yusupov, M.M., Yusupova, G.Z., Baucom, A., Lieberman, K., Earnest, T.N., Cate, J.H., Noller, H.F. (2001). Crystal structure of the ribosome at 5.5 Å resolution. *Science*, **292**: pp.883–96.

Zakian, S., Lafitte, D., Vergnes, A., Pimentel, C., Sebban-Kreuzer, C., Toci, R., Claude, J., Guerlesquin, F., Magalon, A. (2010). Basis of recognition between the NarJ chaperone and the N-terminus of the NarG subunit from *Escherichia coli* nitrate reductase. *FEBS*, **277**: pp.1886–95.

Zumft, W. (1997). Cell biology and molecular basis of denitrification. *Microbiol. Mol. Biol. Rev.*, **61**: pp.533–616.

Zumft, W.G., Kroneck, P.M.H. (2007). Respiratory transformation of nitrous oxide (N₂O) to dinitrogen by Bacteria and Archaea. *Advances in Microb. Phys.*, **52**: pp.107–227.